CRANFIELD UNIVERSITY

ALA H. M. KHODIER

CO-FIRING FOSSIL FUELS AND BIOMASS: COMBUSTION, DEPOSITION AND MODELLING

SCHOOL OF APPLIED SCIENCES

PhD THESIS
Academic Year: 2010 - 2011

Supervisor: Dr. Nigel J. Simms
January 2011

CRANFIELD UNIVERSITY

SCHOOL OF APPLIED SCIENCES

PhD THESIS

Academic Year 2010 - 2011

ALA H. M. KHODIER

Co-firing fossil fuels and biomass: combustion, deposition and modelling

Supervisor: Dr. Nigel J. Simms

January 2011

This thesis is submitted in partial fulfilment of the requirements for the degree of Doctor of Philosophy

ABSTRACT

The application of advanced technologies employing combustion/co-firing of coal and biomass is seen as a promising approach to minimising the environmental impact and reducing CO_2 emissions of heat/power production. The existing uncertainties in the combustion behaviour of such fuel mixes and the release of alkali metals with other elements during the combustion (or co-firing) of many bio-fuels are some of the main issues that are hindering its application. The potential presence of high levels of alkali chlorides and low levels of sulfates in the deposits formed on heat exchanger can cause enhanced corrosion and/or limit the heat transfer between the hot combustion gases and the water/steam system within the process plant.

This work has investigated the detailed gas compositions and deposition characteristics of the combusted gas streams produced from fossil and biomass fuels pure and/or blend in a pilot-scale combustors (PF and FBC) at Cranfield University. Combustion gas analysis were obtained on-line by a high resolution multi-component Fourier Transform Infra-Red (FTIR) gas analyser and deposits samples were collected from the flue gas using air-cooled probes with surface temperatures of about 500, 600, 700 ^{o}C and analysed using SEM-EDX and XRD techniques. Fuels included several biomass fuels (cereal co-product (CCP) straw, miscanthus (pulverised), oil seed rape straw (against stored pellets), miscanthus (pellets), willow, fast pyrolysis bio-oil) and two commercially-used coals (El-cerrejon and Daw Mill). The results of the experimental studies have been compared with thermodynamic equilibrium predictions.

High combustion efficiency was maintained throughout the range of fuel mixes. The SO_2 and HCl levels were low in pure biomass combustion and increased as the biomass fraction of the fuel decreased when co-fired with these coals. However, the NO_x output remained stable except for Miscanthus:Daw Mill mixtures and OSR stored pellet combustion. The deposition flux was highest on the coolest probes for each fuel. The lowest deposition fluxes were found for the combustion of either fast pyrolysis bio-oil or coppiced willow. There is evidence of significant differences deposition fluxes between El-cerrejon coal and Daw Mill coal mixed with CCP and/or miscanthus. The

presence of chlorine was identified in deposits produced from combustion of pure biomass or high biomass mixes. The lowest levels found here in fast pyrolysis bio-oil combustion and only detected at higher shares (≥ 80 %) of biomass co-fired with Daw Mill coal, whereas, mixed biomass with El-cerrejon coal produced Cl in deposits at a low % biomass share.

The application of thermodynamic equilibrium modelling has been found to be useful tool for providing a qualitative understanding of elements present and/or control by hot gas in modern combustion processes.

ACKNOWLEDGEMENTS

I gratefully acknowledge the EPSRC and SUPERGEN agreed across RCUK for the financial support provided.

I would like to express my great gratitude to Dr. Nigel Simms (Director of studies) and Dr. Paul Kilgallon for their guidance and moral support of my research. I also thank Professor John Oakey the Head of the Center for Energy & Resource Technology, (SAS) for solving problems and guidance. Acknowledgement and thanks are also extended to the staff of the department, in particular Miss Jessica Greenwood (Secretary/Administrator) for her help and support of organising meetings and conferences during my study.

Special thanks are offered to the technical staff at Cranfield University; Dr Matthew Kershaw, Mr. Peter West and especially my friend Mr. Nigel Legrave for their exceptional guidance, the hours they put in to get my tests running and the many useful discussions that took place over the years of this study.

I would finally like to express my deepest gratitude to my whole family Mum, Dad, brothers and sisters for their encouragement and support throughout every step of my university career. In particular, a special mention to my mum for her early support that led me to begin this study.

Last, but definitely not least, I wish to express my love and gratitude to my wife (Amal) for all her understanding, strength and loving support, and my lovely children (Khalid, Abeer and Hamood). I would like to dedicate this thesis to them.

TABLE OF CONTENTS

ABSTRACT i

ACKNOWLEDGEMENTS iii

LIST OF FIGURES ix

LIST OF TABLES xvii

LIST OF NOMENCLATURE xviii

CHAPTER 1 GENERAL INTRODUCTION, AIMS AND OBJECTIVES 1
1.1 Introduction and Background 1
1.2 Aims, Objectives and Scope of Study 6
1.3 Thesis structure 7

CHAPTER 2 LITERATURE REVIEW 9
2.1 Introduction 9
2.2 Biomass: a general overview 9
2.3 Biomass conversion technologies 13
2.3.1 Introduction 13
2.3.2 Gasification 16
2.3.3 Pyrolysis 16
2.3.4 Torrefaction 17
2.3.5 Hydro thermal upgrading (HTU) and liquefaction 18
2.3.6 Fermentation 18
2.3.7 Anaerobic digestion (AD) 18
2.3.8 Mechanical extraction 19
2.3.9 Combustion, co-combustion (co-firing) 19
2.3.9.1 Grate bed combustion 21
2.3.9.2 Pulverised fuels combustion (PF) 21
2.3.9.3 Fluidised bed combustion (FBC) 22
2.3.9.4 Combustion, co-firing studies 23
2.4 Gaseous emissions from combustion and co-combustion of biomass 26
2.5 Ash formation from combustion and co-combustion of biomass 29
2.5.1 Ash fractions formed in biomass combustion plants 33
2.5.2 The behaviour of biomass ash in combustion plants 34
2.5.2.1 Ash behaviour in fluidised bed combustors 34
2.5.2.2 Ash behaviour in pulverised fuel combustion systems 35
2.5.3 Deposition 37
2.6 Thermodynamic modelling biomass combustion 39
2.6.1 Overview of MTDATA 43
2.6.2 Thermodynamic equilibrium calculation studies 46
2.7 Deposition formation/mechanisms 49
2.7.1 Inertial impaction 50
2.7.2 Condensation 51
2.7.3 Thermophoresis 52
2.7.4 Eddy impaction 53
2.7.5 Chemical reaction 53
2.7.6 Other mechanisms 53

2.7.7 Deposit growth rates 54
2.8 Concluding remarks 55
CHAPTER 3 METHODOLOGY 57
3.1 Modelling 57
3.1.1 Prediction of combustion products 57
3.1.2 Heat generation prediction 59
3.1.3 Thermodynamic equilibrium 62
3.1.3.1 The application of MTDATA 62
3.1.3.2 Calculation protocol 62
3.1.3.3 Validation 64
3.1.4 Preliminary study 66
3.1.4.1 Prediction of combustion products and database on biomass fuel characteristics 66
3.1.4.2 Predictions of thermodynamic equilibrium compositions 67
3.1.4.2.1 Eight elements system 69
3.1.4.2.2 Fifteen elements system 76
3.1.4.2.3 Seventeen elements system 80
3.1.4.2.4 MTDATA model sensitivity (effect of excess air) 83
3.2 Experimental pilot-scale combusting rig 85
3.2.1 Test programme 85
3.2.1.1 Coal biomass co-firing 87
3.2.1.2 Pelletised/lump fuels combustion 87
3.2.1.3 Liquid fuel combustion 88
3.2.2 Rig description 94
3.2.3 Liquid feeding system 96
3.2.4 Solid feeding system for pelletised/lump fuels 97
3.2.5 Solid feeding system for pulverised fuels 97
3.2.6 Flue gas analysis 98
3.2.7 Deposit collection/ analysis 99
3.2.8 Quality assurance (QA) & control 105
3.2.9 Preliminary study 106
3.2.9.1 Optimisation of liquid feeding system operating conditions 106
3.2.9.2 Optimisation of solid feeding systems performance 114
3.2.9.3 Operating procedure of combustion rig 120
3.3 Test matrix/combustion conditions 126
3.4 Summary 129
CHAPTER 4 PULVERISED FUELS STUDIES RESULTS & DISCUSSION 131
4.1 Introduction 131
4.2 Modelling 132
4.2.1 Pure fuels 132
4.2.1.1 El-cerrejon coal 132
4.2.1.2 Daw Mill coal 135
4.2.1.3 CCP biomass 138
4.2.1.4 Miscanthus biomass 140
4.2.2 Blend mixtures fuels 143
4.2.2.1 Co-firing CCP: El-cerrejon coal (20, 40, 60 and 80 %, wt) 143
4.2.2.2 Co-firing CCP: Daw Mill coal (20, 40, 60 and 80 %, wt) 149

4.2.2.3 Co-firing Miscanthus: Daw Mill coal (20, 40, 60 and 80 %, wt) 155
4.2.2.4 Co-firing Miscanthus: El-cerrejon coal (60:40 %, wt) 161
4.3 Experimental pilot-scale combustion rig exposures 164
4.3.1 Co-firing CCP: El-cerrejon coal (0, 20, 40, 60 and 80 %, wt) 164
4.3.2 Co-firing CCP: Daw Mill coal (0, 20, 40, 60 and 80 %, wt) 174
4.3.3 Co-firing Miscanthus: Daw Mill coal (0, 20, 40, 60 and 80 %, wt) 184
4.3.4 Co-firing Miscanthus: El-cerrejon coal (60:40 %, wt) 194
4.4 General comments 198

CHAPTER 5 PELLETISED/LUMP FUELS STUDIES RESULTS & DISCUSSION 201
5.1 Introduction 201
5.2 Modelling 201
5.2.1 Oil seed rape straw (OSR) pellets 201
5.2.2 Miscanthus pellets 209
5.2.3 Coppiced willow 212
5.3 Experimental pilot-scale combustion rig exposures 215
5.3.1 Oil seed rape straw (OSR) pellets 215
5.3.2 Miscanthus pellets 231
5.3.3 Coppiced willow 244
5.4 General comments 253

CHAPTER 6 BIO-OIL FUEL STUDIES RESULTS & DISCUSSION 255
6.1 Introduction 255
6.2 Modelling 255
6.2.1 Combustion product prediction 255
6.2.2 Heat generation prediction 255
6.2.3 MTDATA calculations 256
6.3 Experimental pilot-scale combustion rig exposures 259
6.3.1 Combustion behaviour/efficiency 259
6.3.2 Deposition fluxes, compositions and analysis 263
6.4 General comments 271

CHAPTER 7 GENERAL DISCUSSION 273
7.1 Introduction 273
7.2 Gaseous emissions model validation 273
7.3 Deposition model validation 277
7.4 General comments 278

CHAPTER 8 CONCLUSIONS AND SUGGESTIONS FOR FURTHER WORK 281
8.1 Conclusions 281
8.1.1 Experimental 281
8.1.2 Modelling 284
8.2 Technological implications 285
8.3 Suggestions for further work 286

REFERENCES 289

APPENDICES 303
APPENDIX A 303
A.1 Reported excess air, O_2 and CO_2 in flue gas for fossil fuels combustions 304
A.2 Prediction of combustion products & spreadsheet example 305

A.3 Combustion product prediction of three fuels combustion/co-firing (using PF & FBC) 308
A.4 Heat generation prediction (HP) spreadsheet example of three fuels combustion/co-firing 311
A.5 Molar composition input in MTDATA for each fuel combustion/co-firing . 314
APPENDIX B 320
APPENDIX C 323
APPENDIX D 325
APPENDIX E 344

LIST OF FIGURES

Figure 2.1 Example of biomass resources converted to bio-energy carriers 15
Figure 2.2 Influence of co-firing various bio-fuels on SO_2 emissions 27
Figure 2.3 Effect on NO_x emissions when a) co-firing switchgrass and b) wood with coal in pulverised fuel combustor (FBC) 28
Figure 2.4 Influence of mixed combustion of wood (wood chips & sawdust) and coal on N_2O emissions in a fluidised bed boiler 29
Figure 2.5 Mechanisms involved in ash formation in biomass combustion 30
Figure 2.6 SEM images of a) coarse fly ash and b) fine-mode fly ash (aerosol particles) upon wood combustion in a grate furnace 31
Figure 2.7 Ash fractions collected from a biomass fixed-bed combustion plant 33
Figure 2.8 Variation in Cl and S content of coals and biomass fuels 36
Figure 2.9 Deposition rates (from cooled target of constant probe surface temperature of ~ 540 ^oC) for various fuels in g deposit per kg fuel 38
Figure 2.10 Inertial impaction mechanism 50
Figure 2.11 Condensation mechanism 51
Figure 2.12 Thermophoresis mechanism 52
Figure 3.1 Screenshot of MTDATA for Windows with calculated MULTIPHASE speciation diagram under “15 elements system” 68
Figure 3.2 Calculated values for gaseous & condensed species produced during the cooling of combustion products from (a) El-cerrejon coal and (b) CCP fuel (based on “8 elements system”) 71
Figure 3.3 Calculated values for gas phase species (in terms of volume %) produced as combustion gases are cooled for (a) El-cerrejon coal and (b) CCP (for “8 elements system”) 72
Figure 3.4 Calculated flue-gas gaseous species upon combustion of, a) CCP:El-Cerrejon coal (20:80 %, wt) and b) CCP:El-cerrejon coal (40:60 %, wt) blend mixtures fuels ... 73
Figure 3.5 Calculated flue-gas condensed species upon combustion of El-cerrejon coal (100 %, wt) of a) Na element and b) K element (under “8 elements system”) 74
Figure 3.6 Calculated flue-gas condensed species upon combustion of CCP (100 %, wt) of a) Na element and b) K element (under “8 elements system”) 75
Figure 3.7 Calculated flue-gas emissions (gaseous & condensed) upon combustion of CCP (100%, wt) fuel, under “15 elements system” study 77
Figure 3.8 Calculated flue-gas emissions (gaseous & condensed species) of K element upon combustion of, a) El-cerrejon coal (100 %, wt) and b) CCP (100 %, wt), (for “17 elements system” study) 81
Figure 3.9 Calculated flue-gas emissions (gaseous & condensed species) of C element upon combustion of, a) El-cerrejon coal (100 %, wt) and b) CCP (100 %, wt), (for “17 elements system” study) 82
Figure 3.10 Calculated flue-gas emissions (gaseous & condensed species) of El-cerrejon coal (100 %, wt) combustion at excess air of, a) O_2 (6 %, vol.), b) O_2 (8 %, vol.) and C) O_2 (10 %, vol.) output (under “15 elements system”) 84
Figure 3.11 Diagram of selected fuel combustion studies 86
Figure 3.12 Schematic diagram of the FBC (left) PF rig facility 94
Figure 3.13 Close up view showing optical access and data collection positions of FBC, PF rig facility 95

Figure 3.14 Schematic showing bio-oil feeding system fitted to the combustor chamber 96
Figure 3.15 Schematic showing solid feeding system for pelletised/lump fuel combustion 97
Figure 3.16 Schematic showing solid feeding system for pulverised fuel combustions 98
Figure 3.17 Detail of FTIR gas analyser operation 99
Figure 3.18 Schematic drawing diagram of the deposit collection probe in the combustion chamber..... 100
Figure 3.19 Drawing diagram of the ceramic deposition ring..... 102
Figure 3.20 SEM image map of pure OSR straw deposit 104
Figure 3.21 Factorial design hypercube 106
Figure 3.22 A central composite design hypercube 107
Figure 3.23 A straight-line plots to deduce ± 1 of the 3 variables 110
Figure 3.24 Solid feeding systems used in preliminary study..... 115
Figure 3.25 Pulverised feeding system feed calibration..... 118
Figure 3.26 Consistency of feed rate of pulverised feeding system over period of time 119
Figure 3.27 Pelletised/lump feeding system feed calibration..... 120
Figure 3.28 Deposit probe of coal: CCP (80:20 %, wt) co-firing, initial run..... 121
Figure 3.29 Extracted bio-oil deposit probe after combustion, initial run 121
Figure 3.30 Cross section of combustion chamber body showing conventional and altered fuel particles at co-firing..... 122
Figure 3.31 Broken deposit ceramic sample after extraction under wrong fitting/type 123
Figure 3.32 Bio-oil nozzle feeder (burner) after extraction under wrong fitting/treatment 124
Figure 4.1 Calculated (MTDATA) major gaseous from pure El-cerrejon coal combustion 134
Figure 4.2 Calculated (MTDATA) gaseous & condensed species from pure El-cerrejon coal combustion..... 134
Figure 4.3 Calculated (MTDATA) major gaseous species from pure Daw Mill coal combustion 137
Figure 4.4 Calculated (MTDATA) gaseous & condensed species from pure Daw Mill coal combustion..... 137
Figure 4.5 Calculated (MTDATA) major gaseous species from pure CCP biomass combustion 139
Figure 4.6 Calculated (MTDATA) gaseous & condensed species from pure CCP biomass combustion 140
Figure 4.7 Calculated (MTDATA) major gaseous species from pure miscanthus biomass combustion 142
Figure 4.8 Calculated (MTDATA) gaseous & condensed species from pure miscanthus biomass combustion 142
Figure 4.9 Calculated (MTDATA) major gaseous species from co-firing mixed fuels of a) CCP:El-cerrejon coal (20:80 %, wt) and b) CCP:El-cerrejon coal (40:60 %, wt)... 145
Figure 4.10 Calculated (MTDATA) gaseous & condensed species from co-firing mixed fuels of a) CCP:El-cerrejon coal (20:80 %, wt) and b) CCP:El-cerrejon coal (40:60 %, wt)..... 147
Figure 4.11 Calculated (MTDATA) major gaseous species from co-firing mixed fuels of a) CCP:Daw Mill coal (20:80 %, wt) and b) CCP:Daw Mill coal (40:60 %, wt).... 151

Figure 4.12 Calculated (MTDATA) gaseous & condensed species from co-firing mixed fuels of a) CCP:Daw Mill coal (20:80 %, wt) and b) CCP:Daw Mill coal (40:60 %, wt) 153
Figure 4.13 Calculated (MTDATA) major gaseous species from co-firing mixed fuels of a) Miscanthus:Daw Mill coal (20:80 %, wt) and b) Miscanthus:Daw Mill coal (40:60 %, wt) 157
Figure 4.14 Calculated (MTDATA) gaseous & condensed species from co-firing mixed fuels of a) Miscanthus:Daw Mill coal (20:80 %, wt) and b) Miscanthus:Daw Mill coal (40:60 %, wt) 159
Figure 4.15 Calculated (MTDATA) major gaseous species from co-firing mixed fuels of Miscanthus:El-cerrejon coal (60:40 %, wt) 163
Figure 4.16 Calculated (MTDATA) gaseous & condensed species from co-firing mixed fuels of Miscanthus:El-cerrejon coal (60:40 %, wt) 163
Figure 4.17 Major gaseous emissions from combustion of a) pure El-cerrejon coal (100 %, wt), b) pure CCP (100 %, wt) and c) CCP: El-cerrejon coal (80:20 %, wt) 166
Figure 4.18 Minor gaseous emissions from combustion of a) pure El-cerrejon coal (100 %, wt), b) pure CCP (100 %, wt) and c) CCP: El-cerrejon coal (80:20 %, wt) 167
Figure 4.19 Deposition rates on the surface temperatures of the three probes (on each side) for three of the fuels mixtures 168
Figure 4.20 Deposition fluxes for probe 3 (~ 500 °C) on top and side deposits from CCP:El-cerrejon coal (pure and mixed) pulverised fuels combustion 169
Figure 4.21 Elemental concentrations of the three probes deposits (top & side) from a) pure El-cerrejon coal (100 %, wt), b) pure CCP (100 %, wt) and c) CCP:El-cerrejon coal (80:20 %, wt) 172
Figure 4.22 Elemental concentrations of the three probes deposits (top & side) from a) CCP:El-cerrejon coal (20:80 %, wt), b) CCP:El-cerrejon coal (40:60 %, wt) and c) CCP:El-cerrejon coal (60:40 %, wt) 173
Figure 4.23 Major gaseous emissions from combustion of a) pure Daw Mill coal (100 %, wt), b) CCP:Daw Mill (20:80 %, wt), c) CCP:Daw Mill (40:60 %, wt) and d) CCP:Daw Mill (80:20 %, wt) 176
Figure 4.24 Minor gaseous emissions from combustion of a) pure Daw Mill coal (100 %, wt), b) CCP:Daw Mill (20:80 %, wt), c) CCP:Daw Mill (40:60 %, wt) and d) CCP:Daw Mill (80:20 %, wt) 177
Figure 4.25 Mean concentrations of gaseous emissions (major & minor) from CCP:Daw Mill mixed fuels combustion 178
Figure 4.26 Deposition rate from probes 1, 2 and 3 (~ 700, 600, 500 ^{o}C, surface temperature) with deposits formed on top, side and underside from CCP:Daw Mill mixed fuels combustion 179
Figure 4.27 Elemental concentrations of the three probes (1, 2 and 3, ~ 700, 600, 500 ^{o}C) deposits (on top, side and underside) from co-firing of a) CCP: Daw Mill (20:80 %, wt), b) CCP: Daw Mill (40:60 %, wt), c) CCP: Daw Mill (60:40 %, wt) and d) CCP: Daw Mill (80:20 %, wt) 183
Figure 4.28 Major gaseous emissions from combustion of a) Miscanthus:Daw Mill (40:60 %, wt), b) Miscanthus:Daw Mill (60:40 %, wt), c) Miscanthus:Daw Mill (80:20 %, wt) and d) pure Miscanthus (100 %, wt) 186
Figure 4.29 Minor gaseous emissions from combustion of a) Miscanthus:Daw Mill (40:60 %, wt), b) Miscanthus:Daw Mill (60:40 %, wt), c) Miscanthus:Daw Mill (80:20 %, wt) and d) pure Miscanthus (100 %, wt) 187

Figure 4.30 Deposition rate from probes 1, 2 and 3 (~ 700, 600, 500 ^{o}C, surface temperature) with deposits formed on top, side and underside from Miscanthus:Daw Mill mixed fuels combustion 189
Figure 4.31 Elemental concentrations of the three probes deposits (1, 2 and 3, ~ 700, 600, 500 ^{o}C) deposits (on top, side and underside) from co-firing of a) pure Daw Mill coal (100 %, wt), b) Miscanthus:Daw Mill (20:80 %, wt) and c) Miscanthus:Daw Mill (40:60 %, wt) 192
Figure 4.32 Gaseous species emissions from co-firing of Miscanthus:El-cerrejon (60:40 %, wt) of a) major species and b) minor species 194
Figure 4.33 Deposition rates of the probes (top, side & underside) with surface temperatures of ~ 700, 600 and 500 ^{o}C from co-firing Miscanthus: El-cerrejon coal (60:40 %, wt) 196
Figure 4.34 Elemental concentrations of the three probes deposits (1, 2 and 3, ~ 700, 600, 500 oC) deposits (on top, side and underside) from co-firing Miscanthus: El-cerrejon coal (60:40 %, wt) 198
Figure 5.1 Calculated (MTDATA) major gaseous species from OSR combustion of a) 1 months of pellets storage, b) 3 months of pellets storage 205
Figure 5.2 Calculated (MTDATA) gaseous & condensed species from OSR combustion of a) 1 months of pellets storage, b) 3 months of pellets storage 207
Figure 5.3 Calculated (MTDATA) major gaseous from miscanthus pellet combustion 211
Figure 5.4 Calculated (MTDATA) gaseous & condensed species from miscanthus pellet combustion 211
Figure 5.5 Calculated (MTDATA) major gaseous from coppiced willow combustion214
Figure 5.6 Calculated (MTDATA) gaseous & condensed species from coppiced willow combustion 214
Figure 5.7 Fluidised bed behaviour during the combustion of OSR straw pellets after 1, 3, 6 and 12 months storage 215
Figure 5.8 Figure 5.8 Major gaseous emissions species from the combustion of OSR straw pellets after 1, 3, 6 and 12 months storage 218
Figure 5.9 Minor gaseous emissions species from the combustion of OSR straw pellets after 1, 3, 6 and 12 months storage 218
Figure 5.10 Deposition rates of the probes (top & side) with surface temperatures of ~ 500 ^{o}C from the combustion of OSR straw pellets after 1, 3, 6 and 12 months storage 219
Figure 5.11 Photographs of the deposits formed on probes with surface temperatures of ~ 500 ^{o}C from the combustion of OSR straw pellets after 1, 3, 6 and 12 months storage 220
Figure 5.12 SEM images of the top deposits from probes with surface temperatures of ~ 500 ^{o}C from the combustion of OSR straw pellets after 1, 3, 6 and 12 months storage 221
Figure 5.13 SEM images of the side deposits from probes with surface temperatures of ~ 500 ^{o}C from the combustion of OSR straw pellets after 1, 3, 6 and 12 months storage 222
Figure 5.14 EDX analysis of deposits (top & side) from probes with surface temperature of ~ 500 ^{o}C exposed to combustion gases from combustion of OSR straw pellets after 1, 3, 6 and 12 months storage 223

Figure 5.15 XRD patterns of the top deposits from probes with surface temperatures of ~ 500 ^{o}C exposed to combustion gases from combustion of OSR straw pellets after 1, 3, 6 and 12 months storage 224
Figure 5.16 XRD patterns of the side deposits from probes with surface temperatures of ~ 500 ^{o}C exposed to combustion gases from combustion of OSR straw pellets after 6 months storage 225
Figure 5.17 SEM images map of elements of top deposits (~ 500 ^{o}C) from combustion of OSR straw after 1 month storage 227
Figure 5.18 Close-up view of bed material after subtracted from FBC from the combustion of OSR straw pellets after 1 and 12 months storage 228
Figure 5.19 SEM images (with varying magnification) of bed material after subtracted from FBC from the combustion of OSR straw pellets after 12 months storage 229
Figure 5.20 SEM images of fly ash from the combustion of OSR straw pellets after 12 months storage 229
Figure 5.21 EDX analysis of bed materials (from the combustion of OSR straw pellets after 1, 3, 6 and 12 months storage) and fly ash (from the combustion of OSR straw pellets after 12 months storage) 230
Figure 5.22 Fluidised bed behaviour during the combustion of miscanthus pellets using Bed mater A (silica sand) and Bed material B(silica sand: limestone, 50:50, wt %) ... 231
Figure 5.23 Major gaseous emissions from combustion of (a) miscanthus using Bed material A and (b) miscanthus using Bed material B 234
Figure 5.24 Minor gaseous emissions from combustion of (a) miscanthus using Bed material A and (b) miscanthus using Bed material B 235
Figure 5.25 Photographs of the deposits formed on probes with surface temperatures of ~ 500 ^{o}C from a) miscanthus combustion using Bed A and b) miscanthus combustion using Bed B 236
Figure 5.26 SEM images of the top deposits formed on probes with surface temperatures of ~ 500 ^{o}C from a) miscanthus combustion using Bed A and b) miscanthus combustion using Bed B 236
Figure 5.27 Deposition rates of the probes (top & side) with surface temperatures of ~ 700, 600 and 500 ^{o}C from the combustion miscanthus pellets using Bed B 237
Figure 5.28 EDX analysis of the top surface deposits (using Bed A), top and side surface deposits (using Bed B) formed on probes with surface temperatures of ~ 500 ^{o}C from miscanthus pellet combustion 238
Figure 5.29 XRD patterns of the top deposits from probes with surface temperatures of ~ 500 ^{o}C exposed to gases from combustion of miscanthus using Bed B 239
Figure 5.30 SEM images map of elements of top surface deposit (~ 500 ^{o}C) from combustion of miscanthus pellets using Bed B 240
Figure 5.31 Close-up view of bed materials after subtracted from FBC from the combustion of miscanthus pellets 241
Figure 5.32 SEM images of bed materials after subtracted from FBC from the combustion of miscanthus pellets 242
Figure 5.33 Particle clump of hot spot of bed material A found after subtracted from FBC from the combustion of miscanthus pellets 242
Figure 5.34 EDX analysis of bed materials A of two bulk samples found after subtracted from FBC from the combustion of miscanthus pellets 243
Figure 5.35 Fluidised bed behaviour during the combustion of coppiced willow 244

Figure 5.36 Gaseous species emissions from combustion of willow a) major species and b) minor species 245
Figure 5.37 Close-up view of the deposits formed on probes with surface temperatures of ~ 500 ^{o}C from combustion of willow 246
Figure 5.38 SEM images of deposits formed on probes with surface temperatures of ~ 500 ^{o}C of a) top deposits and b) side deposits from combustion of willow 247
Figure 5.39 Deposition rates of the probes (top & side) with surface temperatures of ~ 700, 600 and 500 ^{o}C from the combustion coppiced willow 248
Figure 5.40 EDX analysis of the top and side deposits formed on probe with surface temperature of ~ 500 ^{o}C from willow combustion 249
Figure 5.41 XRD patterns of the top deposits from probes with surface temperatures of ~ 500 ^{o}C exposed to gases from combustion of willow 249
Figure 5.42 SEM images map of elements of top deposits (~ 500 ^{o}C) from combustion of coppiced willow 250
Figure 5.43 Close-up view of bed materials (a) and SEM images of the bed materials (b) after subtracted from FBC from the combustion of coppiced willow 251
Figure 5.44 EDX analysis of bed materials after subtracted from FBC from the combustion of coppiced willow 252
Figure 5.45 XRD patterns of bed material after subtracted from FBC from the combustion of coppiced willow 252
Figure 6.1 Calculated (MTDATA) major gaseous species from fast pyrolysis bio-oil combustion 257
Figure 6.2 Calculated (MTDATA) from fast pyrolysis bio-oil combustion of a) minor gaseous and condensed species (at fraction of 10^{-4}) and b) major, minor gaseous and condensed species (at fraction of 10^{-8}) 258
Figure 6.3 Major gaseous species emissions from bio-oil combustion continuously feeding at 0.23 l/min 261
Figure 6.4 Minor gaseous species emissions from bio-oil combustion continuously feeding at 0.23 l/min 261
Figure 6.5 Major gaseous species emissions from bio-oil combustion continuously at various feeding rate 262
Figure 6.6 Minor gaseous species emissions from bio-oil combustion continuously at various feeding rate 262
Figure 6.7 Close-up view of the deposits formed on probes (with various surface temperatures of ~ 700, 600 and 500 ^{o}C) from bio-oil combustion 263
Figure 6.8 SEM images of the top and side deposits formed on probes (with various surface temperatures of ~ 700, 600 and 500 ^{o}C) from bio-oil combustion 264
Figure 6.9 Deposition rate of the probes (with various surface temperatures of ~ 700, 600 and 500 ^{o}C) from bio-oil combustion 265
Figure 6.10 EDX analysis of deposits of the deposits produced from bio-oil combustion on the top and side of air cooled probes studied 267
Figure 6.11 XRD patterns of the top deposits from probe 3 with surface temperatures of ~ 500 ^{o}C exposed to combusted bio-oil flue gas stream 267
Figure 6.12 XRD patterns of the top deposits from probe 1 with surface temperatures of ~ 700 ^{o}C exposed to combusted bio-oil flue gas stream 268
Figure 6.13 XRD patterns (overnight run) of the top deposits from probe 1 with surface temperatures of ~ 700 ^{o}C exposed to combusted bio-oil bio-oil flue gas stream 268

Figure 6.14 SEM images map of elements of top deposits (probe 1, ~ 700 ^{o}C) from bio-oil combustion 269
Figure 6.15 SEM images map of elements of top deposits (probe 3, ~ 500 ^{o}C) from bio-oil combustion 270
Figure 7.1 Major gaseous emissions for T-series fuels combustions/co-firing: Model predictions and experimental data 275
Figure 7.2 Minor gaseous emissions for T-series fuels combustions/co-firing: Model predictions and experimental data 276
Figure 7.3 NO_2 and N_2O gaseous emissions for T-series fuels combustions/co-firing: Model predictions and experimental data 276

LIST OF TABLES

Table 2.1 Example of biomass within their characterised group 12
Table 2.2 Summary of biomass characteristics and impact on boiler performance 23
Table 2.3 Selected combustion studies 24
Table 2.4 Summary of functions of selected MTDATA modules 45
Table 3.1 Species selected for thermodynamic modelling after initial screening calculations (the MTDATA format of elements in chemical formula a has been retained) 65
Table 3.2 Total moles of major and minor elements total moles input in the equilibrium calculation for El-cerrejon coal, Cereal Co-product (CCP) and blends 68
Table 3.3 Species (gaseous & condensed) of thermodynamic equilibrium minor elements during the combustion of pure fuels (Coal, CCP) under “15 elements system” 78
Table 3.4 Species (gaseous & condensed) of thermodynamic equilibrium minor elements during the combustion of fuels (CCP:Coal (20:80 & 40:60 %, wt) under “15 elements system” 79
Table 3.5 Fuel analysis of coal for co-firing tests 89
Table 3.6 Fuel analysis of biomass for co-firing tests 90
Table 3.7 Fuel analysis of OSR biomass for pelletised/lump fuel combustion tests 91
Table 3.8 Fuel analysis of miscanthus and willow biomass for pelletised/lump combustion tests 92
Table 3.9 Fast pyrolysis bio-oil composition analysis for liquid combustion tests 93
Table 3.10 surface area calculation of cylinder ceramic deposit ring used in the combustion/co-firing exposures 103
Table 3.11 Coded design matrix 108
Table 3.12 Coded values against real values 109
Table 3.13 Design matrix 109
Table 3.14 Central Composite Design parameters for liquid feeding system 112
Table 3.15 Multi-linear regression on the results 113
Table 3.16 Results of feeding rate of different fuels using solid feeding systems 116
Table 3.17 matrix for experimental & modelling testing 126
Table 3.18 Combustion operating conditions 127
Table 4.1 Modelling of pure El-cerrejon coal combustion tests 133
Table 4.2 Modelling of pure Daw Mill coal combustion tests 136
Table 4.3 Modelling of pure CCP biomass combustion tests 139
Table 4.4 Modelling of pure miscanthus biomass combustion tests 141
Table 4.5 Modelling of co-firing mixed fuel of CCP:El-cerrejon tests 144
Table 4.6 Modelling of co-firing mixed fuel of CCP:Daw Mill tests 150
Table 4.7 Modelling of co-firing mixed fuel of Miscanthus:Daw Mill tests 156
Table 4.8 Modelling of co-firing mixed fuel of Miscanthus:El-cerrejon coal tests 162
Table 5.1 Modelling of OSR stored pellets for pelletised/lump combustion tests 204
Table 5.2 Modelling of miscanthus pellets for pelletised/lump combustion tests 210
Table 5.3 Modelling of coppiced willow for pelletised/lump combustion tests 213
Table 6.1 Modelling of bio-oil combustion tests 256

LIST OF NOMENCLATURE

Latin letters

Capital letters

D	diameter
ID	internal diameter
MW	molecular weight
N	number of species in the system
OD	outside diameter
P	pressure (Pa)
T	temperature (^{o}C)
ΔT	temperature change

Small letters

h	enthalpy
t	time
Δt	time step

Greek symbols

ρ	density
θ	inertial deposition angle
u_f	bulk gas velocity, m/s
η_I	local impaction efficiency
π	pi value

Subscripts

A	related to air
AR	as received
atm	atmospheric
<c>	condense phase species

daf	dry ash free
i, j	species
<g>	gas phase species
max	maximum
mix	related to mixture
pf	related to pulverised fuel
V	related to speed voltage transformer (volts)
Vol	volume

Abbreviations

AD	Anaerobic Digestion
A/F	Air to Fuel ratio
ASTM	American Society for Testing and Materials
CCD	Central Composite Design
CCP	Cereal Co-product
CFD	Computational Fluid Dynamics
CHP	Combined Heat and Power
CP	Combustion product Prediction
CV	Calorific Value
CVgross	Gross Calorific Value
CVnet	Net Calorific Value
DM	Daw Mill coal
EC	European Commission
EPA	US Environmental Protection Agency
EPRI	Electric Power Research Institute
EPSRC	Engineering and Physical Sciences Research Council
EU	European Union
FBC	Fluidised Bed Combustor
FC	Fixed Carbon
FTIR	Fourier Transform Infra Red
HHV	Higher Heating Value

HP	Heat generation Prediction
HTU	Hydro Thermal Upgrading
IEA	International Energy Agency
LHV	Lower Heating Value
MLR	Multi Linear Regression
MSW	Municipal Solid Waste
MTDATA	Metallurgical and Thermochemical Databank
NPL	National Physical Laboratory
NRV	None Return Valve
OSR	Oil Seed Rape straw
PAH	Polycyclic Aromatic Hydrocarbon
PCDD	PolyChlorinated Diebenzo-Dioxins
PCDF	PolyChlorinated Diebenzo-Furans
PF	Pulverised Fuel Combustor
PTFE	Polytetraflouroethylene
QA	Quality Assurance
R&D	Research & Development
RDF	Refuse Derived Fuel
RO	Renewable Obligation
RSD	Relative Standard Deviation
SD	Standard Deviation
SEM-EDX	Scanning Electron Microscopy-Energy Dispersive X-ray
SGTE	Scientific Group Thermodata Europe
SUPERGEN	Engineering and Physical Sciences Research Council, Sustainable Power Generation and Supply programme
VM	Volatile Matter
VOC	Volatile Organic Components
XRD	X-ray Diffraction

CHAPTER 1 GENERAL INTRODUCTION, AIMS AND OBJECTIVES

1.1 Introduction and Background

The international agreements such as Agenda 21 and the Kyoto Protocol focus on decreasing global environmental impacts and in particular greenhouse gas emissions where individual countries expressed their intention to contribute and establish their own commitment. The UK government enacted the Renewable Obligation (RO) on 1st April 2002 (and effective until 31st March 2027) to reduce CO_2 emissions via growth of renewable energy sources such as biomass, wind, solar, geothermal and hydrogen for electricity generation. It set a challenging target of reducing CO_2 emissions by 80 % by 2050 [CCC, 2008]. The latest announcement of the heat and energy saving strategy 2009 by the UK government [DECC, 2009] sets out the long-term ambition of how energy should be used in homes and business. It set out a carbon emission reduction target (CERT) of 20 % by 2020. This includes a biomass strategy with the following main aims:

- Increase use of biomass
- Develop a competitive, sustainable supply chain
- Promote innovation and low-carbon technology
- Take advantage of the environmental benefits of biomass and maximise the contributions towards the reduction in CO_2 emissions

The following alternatives of biomass use are proposed;

- Co-fired electricity in large fossil fuel plants
- Biomass combined heat and power (CHP)
- Bioenergy (particularly in industrial and commercial applications)
- Dedicated biomass power plant
- Transport biofuels

Biomass can be used in energy generation (i.e. electricity and/or heat) or alternatively converted into a transport fuel or chemical feedstock [Van Loo and Koppejan, 2008]. Biomass can be described as fuel of which at least 98 % of the energy content is derived from a plant or animal matter or substances. Researchers classify them mainly in the following types; lignite plant/woody, herbaceous, aquatic, derivatives, manures and wastes [Weather et al., 2000; McKendry, 2002; Williams, 2001].

The utilisation of different forms of biomass seems to be an opportunity to reduce CO_2 emissions and fulfil the demands of the Kyoto protocol [United Nations, 1997] and UK RO. Additional benefits, such as increasing the use of local resources and decreasing the demand for disposal of residues, can also be achieved. Straw is a by-product of growing commercial crops (especially cereal grain and oil seed rape). The European Renewable Energy Council [EREC, 2000] reported that every year more than 300 Mton of straw is produced within Europe, the amount being influenced by EU internal agricultural policies, weather during growth and harvest, etc. In the UK, miscanthus and willow are relatively easy to grow and harvest and have a high dry-matter yield, resulting in great interest in growing these plants as energy crops. The UK government offers financial support to farmers for the establishment of miscanthus and short rotation willow coppice through the Energy Crop Scheme [Defra website]. Further processing of biomass to give a liquid or pellets has the advantage over unprocessed biomass of being storable (under controlled conditions) and transportable (i.e. higher bulk density) [Bridgwater and Kuester, 1991; Bridgwater and Peacock, 2000].

Recent studies have demonstrated that co-firing (co-combustion) biomass with coal is among the less expensive alternatives for environmental benefits (CO_2 emissions reduction) and electric utilities [Bapat et al, 1997; Hein and Bemtgen 1998; Hughes and Tillman 1998; Baxter, 2005] with modifications to most existing coal-fired power plant boiler. In addition, co-firing biomass in existing coal power plants would not require a continuous supply of biomass as the plant would always have the primary coal fuel for 100 % combustion [NERL, 2005]. Also, there is far too little biomass to replace coal globally [Green, 1994; Baxter, 2005]. However, choices of bio-fuel and operating conditions are issues that have to be considered to prevent putting boiler plant at risk

[EUBIONET, 2005]. In general, biomass is characterised as having a higher volatile matter content, lower heating values, less carbon, less ash, more oxygen, higher moisture content, usually lower density, wider size distribution and higher volatile alkali content when compared with coal compositions [Easterly and Burnham, 1996]. This causes co-firing technology to face some critical issues, such as operating performance, ash deposition, flame stability, combustor slagging, fouling and/or corrosion.

Although there has been scientific agreement of the benefit of using biomass from co-firing programs carried out in Europe (under the European Union) and in the United States (under Department of Energy (DOE) and Electric Power Research Institute (EPRI)), relatively little research has been undertaken of a wide range of coal: biomass blends. Some typical biomass types currently being used for co-firing are cattle manure, sawdust, sewage sludge, wood chips, straw, refuse derived fuels and olive residues. At present, the maximum share of these biomasses with coal at most power plants has been very small, only using up to 5-10 % of biomass by mass for co-firing [European Commission, 2006]. The feedback from these power plants showed that co-firing could be practiced without encountering major problems (with respect to other issues such as fuel feeding, vermin, biomass storage, etc.) in terms of component lives and the efficiencies of boilers (or furnaces) were not reduced [European Commission, 2006; EUBIONET, 2005].

Combustion, co-firing biomass has been evaluated for a variety of boiler technologies e.g. pulverised combustion, grate bed combustion, fluidised bed combustion, etc [Tillman, 2000]. The choice of these combustion technologies depends on the biomass types/formations. For example, grate co-firing technology can handle untreated fuel with high moisture content, whereas pulverised fuel co-firing is based on a finely ground fuel as a feed. Fluidised bed technology offers great fuel flexibility [de Jong, 2005; Oniszk-Poplawska et al., 2003] and the implementation of the technology is growing fast with over 1200 FBC plants worldwide [McMullan, 2004; Cleve, 1999] and a total installed capacity of some 65 GW_{th} with most operating on coal. However, many issues still have to be investigated, understood and solved to identify which technology has the advantage over another to substitute coal fully or partially by biomass. For example, the amount and distribution of ash produced from biomass

combustion are greatly influenced by the combustion technology used. Also, ash from biomass such as straw has a much lower melting temperature than of other biomass resulting in serious slagging and fouling of the installations [van Loo and Koppejan, 2008]. This work tries to answer some of the questions and presents the influence of combustion/co-firing techniques on ash formation and deposition from a wide range of bio-fuels.

Recent studies reported that calculations carried out using software thermodynamic equilibrium such as a Metallurgical and Thermochemical Databank (MTDATA, available from NPL) were useful for predicting gaseous emission releases before combustion tests, and in interpreting experimental results [Miller et al, 2004]. Also, by combining modelling with experiments, an improved design of combustion and co-combustion fuel conversion systems is possible with respect to the reduction of emissions (flue gas) and/or corrosion, deposition. It can be seen from the following review of the literature (Chapter 2) that there is relatively little information in the open literature about the behaviour of trace elements in combustion for many available fossil/biomass fuels. Thermodynamic equilibrium modelling of elemental behaviour in combustion has received much less attention than experimental, and no attempts appear to have been published to validate these predictions by comparison with measurements.

The existing unknowns and uncertainties in the chemistry of the release of alkali metals (such as K, Na) and S, Cl during the combustion and/or co-combustion process for many bio-fuels are one of the main issues that is hindering its application in the energy production market. Therefore, extensive studies are needed into the effects of coal and biomass fuel blends and/or stand-alone biomass in order to determine combustion behaviour characteristics and to reduce emissions from coal-fired power plants to the minimum. The results of these efforts may aid in optimisation of fuel blends, plant reliability and performance.

This study focuses on the combustion and co-firing of several coals and biomass, both alone and/or in blends, in a pilot-scale combustion rig (pulverised fuel and fluidised bed) in terms of their combustion behaviour, resulting emissions, deposition rates and deposit compositions to assess the differences between such potential fuels. The results

of experimental combustion trials have been compared with modelling predictions (combustion product prediction (CP), heat generation prediction (HP) and thermodynamic equilibrium calculations (using MTDATA, NPL software)) over a range of feedstock combinations including: Colombian coal (El-cerrejon), British coal (Daw Mill), coppiced willow, miscanthus (mixed with coal in range 0-100 %, wt), cereal co-product (CCP, mixed with coal in range 0-100 %, wt), oil seed rape straw pellets and fast pyrolysis bio-oil were performed. The fuels selected for investigation were based on coal and biomass fuels available in the UK and being considered for use in new combustion processes.

This combination (experimental and modelling) of data helps define accurate and relevant models useful for predicting and understanding combustion gas compositions and deposition for coal/biomass combustion.

The project was funded by the UK Engineering and Physical Sciences Research Council which supports and leads the Sustainable Power Generation and Supply (SUPERGEN) initiative focused on “Powering the Future”. SUPERGEN was established in order to help UK meet the Renewables Obligation targets, as well as developing future options for power generation.

The Centre for Energy and Resource Technology at Cranfield University, where the work were based, was one of eight UK academic partners selected to take part in SUPERGEN consortium on “Biomass, Bio-fuels and Energy Crops”, which started its eight year research programme supported by a group of industrial companies. It co-ordinates work concerned with the minimisation of engineering risk in the co-firing and co-processing of biomass.

Several parts of this work have already been presented (as oral presentations, posters and papers at conferences) and published in journals (see list of publications in Appendix E).

1.2 Aims, Objectives and Scope of Study

Aims

The overall aim of the project is to support the use of biomass products (alone or co-fired) in combustion systems by generating experimental data on their performance and developing predictive models of this performance.

Objectives

Specific objectives are;

- Development of biomass, biomass/coal combustion models for combustion product, heat generation and MTDATA in terms of compositions of flue gases, condensed species and deposits
- Generation of pilot plant data on emissions (CO_2, O_2, H_2O, SO_2, CO, NO, NO_2, N_2O, HCl, HF), deposition flux and deposit compositions, as well as combustion product and heat generation predictions, for fuels selected for this research
- Comparison of pilot plant data and models to optimise/validate models, for biomass use
- Identify outstanding issues/errors and improvement in understanding

Scope of Study

In order to achieve these aims and objectives, the following scope of work was identified and is reported in this thesis:

- Experiments: carried out using a pilot-scale combustion rig with a ~ 50 kW_{th} capacity fluidised bed combustor (FBC) and a ~ 100 kW_{th} capacity pulverised fuel combustor (PF) with ~ 12-15 kg/hour feed rate [based at Cranfield University]. Solid and liquid feeding systems were designed and constructed to incorporate feeding the fuels selected for the study. Optimisations of the feeding systems on operating conditions were carried out by statistical/experimental design investigation. Combustion gas emission samples for CO_2, O_2, H_2O, SO_2, CO, NO, NO_2, N_2O, HCl, HF were measured on-line by

a high resolution multi-component Fourier Transform Infra-Red **(**FTIR) gas analyser. Deposits from the flue gas stream were collected using air cooled deposition probes with surface temperatures set to ~ 500 °C, 600 °C and 700 °C (to simulate conditions in the heat exchanger of fuel fired boilers). These deposits were analysed using a Scanning Electron Microscope (SEM) equipped with Energy Dispersive X-ray (EDX) analysis and a standalone X-ray Diffraction (XRD) system.

- Modelling: the selected fuel mixes composition were entered into a spreadsheet created for heat generation prediction (HP), combustion product prediction (CP, to indicate flue gas compositions of CO_2, H_2O, N_2, O_2, HCl, SO_2) and thermodynamic equilibrium calculations (using MTDATA, software available from NPL). The MTDATA has been validated and used to measure the levels of major elements (C, H, N, O, S, Cl), minor elements (Si, Al, Fe, Ca, Mg, K, Na, Ti, Ba, Mn, P) and their partitioning behaviour for selected fuels combustions system.
- The results of the experimental work have been compared with these models predictions under equivalent conditions of combustion and co-combustion trials.

1.3 Thesis structure

This thesis is divided into eight chapters and five appendices and is organised in the following:

CHAPTER 2 presents a review of literature biomass, biomass conversion technologies, combustion and co-combustion emissions (in term of gaseous and ash formation), deposition mechanisms and thermodynamic modeling combustion related to the research area.

CHAPTER 3 details the preliminary study of the modeling and experimental set-up methodology employed in this study. Optimisations/performances of feeding systems were also presented.

CHAPTER 4 presents the modeling predictions, experimental results and discussions on the results obtained from the pulverised fuels (El-cerrejon coal, Daw mill

coal, miscanthus, CCP biomass) combustions and co-combustion (at different fuel mixes ratio) in PF combustor.

CHAPTER 5 presents the modeling predictions, experimental results and discussions on the results obtained from the pelletised/lump fuels (oil seed rape straw, miscanthus, coppiced willow) combustion in fluidised bed combustor.

CHAPTER 6 presents the modeling predictions, experimental results and discussions on the results obtained from the fast pyrolysis bio-oil combustion.

CHAPTER 7 presents the general discussion to identify outstanding issues and improvement in understanding of combined modeling and experimental for biomass use in combustion and co-combustion in PF and FB combustors.

CHAPTER 8 lists the conclusions and suggestions for further study.

CHAPTER 2 LITERATURE REVIEW

2.1 Introduction

From the general literature, it has been found that there is a huge interest in using biomass as a renewable energy source. Combustion and co-combustion (co-firing) technologies are among the simplest and cheapest methods of converting any biomass into heat and/or power. Coal and biomass fuels are quite different in composition. Low levels of co-firing have been carried out by nearly all of the UK coal stations and various issues addressed. Co-firing at high levels with difficult biomass, 100 % biomass, as well as dust, storage etc, present more issues that are still to be addressed. Therefore, biomass combustion and/or co-firing a combination of biomass and coal needs significant R&D into combustion characteristics and the effect of deposit formation on heat exchanger among other topics. Biomass fuels require attention to their shape/form, particle sizes, feeding and storage to achieve efficient combustion performance. Using a computer model, such as MTDATA, thermodynamic equilibrium calculations can be carried out. These have been found to be a useful first step in predicting flue gas emissions and trace element release in combustion systems, however this topic has received little attention and no attempts appear to have been made to validate these predictions by comparison with measurements.

A literature review of biomass characteristics, conversion technologies, gaseous emissions and deposition formation measured and predicted from combustion systems supported by some research studies is presented below.

2.2 Biomass: a general overview

Biomass can be described as fuel of which at least 98 % of the energy content is derived from a plant or animal matter or substances [Weather et al., 2000; McKendry, 2002a; Hossain, 2005]. It can be harvested as energy crops (i.e. specially grown for energy generation purposes) or can be reclaimed as wastes from crops grown originally for food and/or manufacturing raw materials (known as co-product) subjected to different

processing (e.g. multi-product plants already exist in the form of large scale for commercial e.g. baggase in Thailand and rice husks in Egypt) as shown in Table 2.1. Biomass is mainly composed of carbohydrate compounds of which the elements carbon, hydrogen and oxygen are the building blocks [White and Plaskett, 1981]. Researchers classify them in various ways, mainly in following types [Weather et al., 2000; Williams et al., 2001]:

- lignite plant/woody - includes soft wood such as sawdust and hard wood such as wood chips
- herbaceous - can vary from grass and straws to seeds/grain
- aquatic - includes algae and kelp
- derivatives - include paper and food production residue
- manures - include cattle waste and poultry litter
- wastes - include municipal solid waste (MSW), refused-derived fuel (RDF) and sewage sludge (Tchobanoglous et al. 1977 defined solid wastes as all those wastes arising from human and animal activities that are normally solid in nature and are discarded as useless or unwanted)

Aquatic plants and manures can be further described as high moisture materials, while herbaceous plants and derivatives can have either high or low moisture contents. On the other hand, lignite/woody plants (slow growing) are described as ‘dry’ biomass [McKendry, 2002a].

All biomass contains cellulose, hemicellulose and lignin [White and Plaskett, 1981; McKendry, 2002a]. Cellulose is a crystalline glucose polymer and represents about 40 to 50 % of the biomass by weight. The hemicellulose is about 20 to 40 % of the material by weight with consisting of 5 or 6 carbon sugar. Lignin is an amorphous polymer with high molecular weight and random structure [Backreedy et al., 2004].

Weathering, geographic location, soil type and soil water content all have an impact on biomass growing conditions and properties [Palz and Chartier, 1980]. Photosynthesis, the process responsible for the capture of energy from sunlight and converting it into chemical energy, has an influence that differs between plant species. The process passes through a different route depending on the mass of carbon contained in the plant

material (e.g. C_4 or C_3 process (i.e. method of CO_2 uptake which forms a 4-carbon molecule instead of the two 3-carbon molecules)) [White and Plaskett, 1981]. In the C_3 process the compound fixed initially by enzyme action is 3-phosphoglyceric acid (which contains 3 carbon atoms), whereas C_4 different enzymes produce the four carbon acids. Crops like rice, beet and algae are an example of C_3 plants, whereas maize and sugar cane are believed to follow the C_4 path. In general, C_4 plants are more productive than C_3 plants because of their growing in lower latitudes as they can better use the high sunlight levels prevailing. Therefore, C_4 plants will have an advantage of higher biomass yields for energy conversion over C_3 plants [White and Plaskett, 1981; McKendry, 2002a]. However, the optimum growing conditions and the efficiency with which plants can use the photosynthetic process depends on the in having sufficient water and nutrients as well as the absence of disease. The overall productivity depends mainly on the length of the growing seasons. Therefore, many plants can achieve very high growth for limited periods [White and Plaskett, 1981].

The major biomass properties of concern are calorific value (CV), moisture content, proportions of fixed carbon/volatiles, ash, alkali metal content and cellulose/lignin ratio [Weather et al., 2000]. The CV of the material is a heat value measured in energy content per unit mass or volume (e.g. MJ/kg for solid). It is further subdivided into gross CV (CVgross), also known as higher heating value (HHV) and net CV (CVnet), also known as lower heating value (LHV). Moisture content can be classed as intrinsic or extrinsic moisture which is related to whether the water content was influenced by external factors e.g. weather effects. Moisture content differs significantly depending on the kind of biomass for example, 3 % in paper and 98 % in sludge [Shinya and Yukihiko, 2008]. Ash can also classified as intrinsic and extrinsic, consisting primarily of SiO_2. Intrinsic ash can be described as being naturally formed as the matrix of biomass, where as extrinsic ash is a solid residues produced by chemical breakdown of biomass [Livingston, 2009]. Woody biomass ash contents are much lower than coal and herbaceous biomass, and they vary widely (e.g. rice hulls 18 %, almond shell 5 %). Volatile matter (VM) of the biomass is the amount of matter driven-off as a gas by heating, whereas, the fixed carbon content (FC) is the mass left after volatiles releases [Weather et al., 2000]. Those are important factors for providing information of biomass

for ignition, gasification and oxidation. The trace metal content of biomass, such as Na, K, Ca, P an Mg, can react with silica present in the ash producing a slag and/or sticky mobile liquid phase forming an operating problem [Weather et al., 2000; McKendry, 2002a; Livingston, 2009]. The amount of cellulose/lignin ratio is important only in bio-chemical conversion, in which is not concern in this research.

Analyses of biomass are usually presented in termed the proximate and ultimate analyses. Proximate analysis consists of the determination of ash, moisture, and VM content, with the FC obtained by difference. The ultimate analysis of biomass presents the elemental composition as C, N, H, O and S. Other biomass properties can be important: for example, the bulk density of biomass can be an important parameter as it relates to transport and storage costs [White and Plaskett, 1981].

Table 2.1 Example of biomass within their characterised group
Source: [Frontline Bio-energy Inc]

Agricultural products	**Forestry products**	**Wastes**	**Energy crops**
Harvesting residues	**Harvesting residues**	**Domestic/industrial**	**Wood**
Cereal straws Oil seed rape and linseed Oil straws Flax straw Corn stalks	Forestry residues	Municipal solid waste (MSW) Refuse-derived fuels (RDF) Construction and demolition wood	Willow Poplar Cottonwood
Processing residues	**Primary processing wastes**	**Urban green wastes**	**Grasses and other crops**
Rice husks Sugarcane bagasse Olive residues Palm oil residues Citrus fruit residues	Sawdusts Bark Offcuts	Leaves Grass and hedge cuttings	Switchgrass Reed canary grass Miscanthus
Animal wastes	**Secondary processing wastes**		
Poultry litter Tallow Meat/bone meal	Sawdusts Offcuts		

Biomass availability is a major issue of concern. Residues from agriculture (e.g. cereal straw normally left in the field at harvest), plantation forests (e.g. wood, tree branches), food and fiber processing operations (required treatment or disposal) are available in large quantities [Livingston and Morris, 2009], and have been collected worldwide for use in a wide variety of processes (e.g. conversion plants). However, land use competition between forests, arable land, pasture and other lands (as these are the biomass recourses base) have become severe. Also competition between biomass uses (such as food, materials, energy) and its measurement become severe too. The amount of forested land has decreased (due to human activity) by 1.2 billion hectares since 1700. Thus, the deforestation caused the increase of arable land. On arable land, energy crops can be produced beside food. In countries, such as United States and Brazil they use their surplus arable land to produce energy crops and biofuel (such as bio-ethanol and bio-diesel) especially between years 2006-2007 when the oil price hit the historical record. In the UK, there is huge interest from the government to promote the use of arable land for growth of energy crops such as miscanthus and willow [Defra online website].

Although quantifying and obtaining accurate data on the biomass resource availability even in a local district, are difficult to achieve (as it varies from year to year and across seasons), with careful management (i.e. using biomass by-products), improved use of available land and/or plantation energy crops or forests can reduce the risk of limited biomass availability [IEA, 2007].

2.3 Biomass conversion technologies

2.3.1 Introduction

There are mainly three categories of process technologies for biomass conversion [Palz and Chartier, 1980; McKendry, 2002b; Demirbas and Demirbas, 2007]:

- Thermo-chemical
- Combustion
- Gasification

- Pyrolysis
- Torrefaction
- Hydro thermal upgrading (HTU)
- Liquefaction
- Bio-chemical
- Fermentation
- Anaerobic digestion
- Mechanical extraction (known as trans-estrification)

Techniques for solid materials upgrading (known also as physical conversion of biomass) like natural or processing drying, pelletising, briquetting, bailing are advancing [IEA, 2007; Shinya and Yukihiko, 2008], where pelletisation is now accepted practice before biomass fuels are burned in furnaces [Yang et al., 2005]. Drying biomass involves vaporisation of the moisture content to about 4-25 wt. % [Van Loo and Koppejan, 2008]. Pelletising compresses the material into the cylindrical shape of a pellet with typical dimensions between 6-12 mm in diameter and a length of 10-25 mm, or into briquettes typically with a diameter of 50-80 mm and a length of 250-300 mm. Pelletising produces a homogenous fuel with a high energy density and the advantage of a high bulk density, which has an impact on transportation costs and storage space compared to other biomass fuels. The pelletising process consists of drying (raw material must be ~12-17 wt % moisture before entering the pelletiser), milling (raw material particle size must be in a accordance with size of pellets), conditioning (e.g. addition of binding agents (such as natural paraffin, plant oil, lignin sulphate to improve the durability of the pellets and avoid dust emissions during transportation and storage), actual pelletising (i.e. desired pellet lengths) and cooling (to stabilise and harden pellets) [EBA, 2000; Van Loo and Koppejan, 2008]. Despite the benefits of utilising pellets, handling of pellets can be an issue as pellets may absorb moisture from the surrounding air and can swell and/or lose shape. Therefore, pellets should be stored in a dry condition (in closed halls or rooms) to prevent absorbing atmospheric moisture [Livingston, 2005].

Biomass can be used in combined power generation (i.e. electrical/heat energy) or alternatively converted into a transport fuel or chemical feedstock (see Figure 2.1). The selection of biomass depends on the type of energy conversion process. For example, high moisture content herbaceous biomass like sugarcane is more appropriate for biological conversion such as fermentation, whereas wood chips are more suitable for gasification, pyrolysis or combustion. However, biomass such as cereal crops can be fitted to both bio-chemical and thermo-chemical conversion processes. In Europe, most biomass selected for conversion processes are woody plants such as willow, poplar and forestry residues. While in the USA, herbaceous plants like cereal (corn based) are used for conversion to ethanol fuel [McKendry, 2002a]. Sugarcane is widely used in Brazil for alcohol fuel production and oil seed rape used for bio-diesel fuel production in Germany, France and Italy [Pahl, 2005]. Miscanthus is a C_4 herbaceous plant that has become of great interest in the UK as it is relatively easy to grow and harvest. Switchgrass is also a C_4 plant, which has recently been used in USA as a crop model for a bio-fuel feedstock program. Both give a high dry-matter yield suitable for the conversion processes.

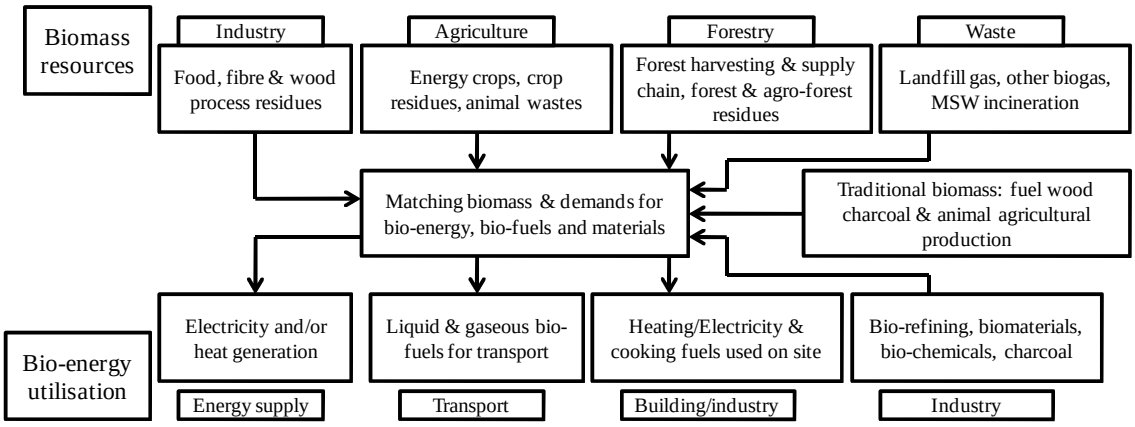

Figure 2.1 Example of biomass resources converted to bio-energy carriers
Source: [IEA, 2007]

The organic fraction of municipal solid waste (MSW), such as kitchen wastes or food residues from households, varies from one country to another depending on nature of the waste, habits and standard of living [White and Plaskett, 1981; Hossain, 2005]. In general, about 30-60 % of the MSW is an organic matter suitable as a renewable source.

Sewage sludge before treatment can be delivered in a liquid form having approximately 50 % of solid materials. It has been reported that mixing 5 % of sewage sludge to MSW gives good conversion performance, from higher practice achievement feedstock of 80:20 % weight mixture of MSW: sewage sludge [Demirbas and Demirbas, 2007].

A brief review of all the conversion processes (listed above) is presented below, with a more detailed description for combustion and co-combustion (co-firing) technologies as these are the main focus for this research.

2.3.2 Gasification

Biomass can be converted by gasification into a gaseous fuel mixture in the presence of limited amounts of oxygen or air. There are different types of gasification technology options operating in various conditions (e.g. temperature range from 800-900 °C for fludised bed gasifiers or ≥ 1200 °C, for entrained flow systems). The gas mixture produced (syngas) consists mainly of CO, H_2, CH_4, CO_2 and N_2. This can be used for chemical production such as methanol or as a fuel gas input into engines or turbines to generate power [Palz and Chartier, 1980]. The syngas needs to be cooled and passed through a cleaning train system to remove impurities such as tar and alkali metals. Larkin et al., [2004] investigated using a fuel based on wood and sugarcane bagasee in a pilot plant with electrical output range from 5-10 MW. They reported that the combined cycle gas turbine is the most efficient method to convert the gaseous fuel to electricity. McKendry, [2002b] reported that methanol and hydrogen production from gasification may present future options as fuels for transportation.

2.3.3 Pyrolysis

Pyrolysis of biomass produces liquid (bio-oil), solid and gaseous fractions in the absence of oxygen or air. Depending on the operating conditions, the technique types are conventional, flash and fast pyrolysis [Maschio et al. 1992]. Conventional pyrolysis can produce solid, liquid and gaseous under a slow heating rate range from 0.1-1 °C/sec at an operating temperature of 300-700 °C. Flash pyrolysis occurs under a faster heating

rate (≥ 1000 °C/sec) and produces liquid in significant proportions. Similar to the flash technique, fast pyrolysis is heating the biomass to a temperature of 450-550 °C but with a lower heating rate of 10-200 °C/sec with no air to vaporise followed by rapid cooling. Bridgwater and Peacocke, [2000] stated that fast pyrolysis is now an acceptable and viable method for bio-oil production. The elemental and chemical composition of the fast pyrolysis oil is dependent on the biomass feedstock [Bridgwater, 2009]. Pyrolysis oil consists of about 70 % oxygenated organics and 30 % water on a weight basis with very minimum ash content (by a proper design of pyrolysis process) [Jensen et al., 2001; European Commission, 2006].

Bio-oil has the advantage over other biomass of being easier to store (under controlled conditions) and transportable (i.e. higher bulk density). PyNe, [2005] mentioned that the cost is the big challenge for bio-oil as it is 10-100 % more expensive than fossil fuel. Successful studies have been carried out using bio-oil to run dual-fuel engines without any pre-treatment [Demirbas and Demirbas, 2007]. Ormrod diesel in the UK reported that bio-oil been successful used to operate a dual fuel engine at 250 kWe medium speed. Bio-oil has been used as boiler fuel at pilot and commercial scale for different energy organisations (e.g. Canmet Canada, MIT USA and Neste Finland). The high viscosity of bio-oil is reported as causing feeding problems, which have been overcome by preheating by Canmet and by the addition of alcohol by Neste [Bridgewater and Peacocke, 2000].

2.3.4 Torrefaction

Torrefaction of biomass produces solid as a final product (occasionally referred to as char) operated in the absence of oxygen at a temperature of 200-3000 °C and a typically one hour residence time. The most advantage of the technique is different types of feedstock will have a quite similar physical and chemical properties after the process. However, torreied biomass needs to be testing in scaling-up technology in order to be economical with alternate conversion technologies and hence a successful market [European Commission, 2006].

2.3.5 Hydro thermal upgrading (HTU) and liquefaction

Liquefaction and HTU are other processes for converting biomass into bio-oil. The processes are almost at the pilot stage, which create wet environments (hot compressed water of around 300 ^{o}C) for biomass conversion under high pressure (~ 10-20 MPa) to stable liquid. These processes are not currently favored for practical use as the reactors and fuel feeding system are more complex and expensive than those needed for pyrolysis [McKendry, 2002b; Shinya and Yukihiko, 2008].

2.3.6 Fermentation

Liquid fuels such as ethanol and methanol can be produced from biomass by distillation of the products from a fermentation process. Sugar crops, like sugar cane or sugar beet, contain a simple sugar form (i.e. glucose or fructose). These crops can be crushed and filtered to produce sugar juice, which can be further processed with yeast for complete conversion. Starch crops, like wheat or corn, can also be used to produce ethanol, but with an additional break down treatment, by enzymes as their structure is more complex [Palz and Chartier, 1980]. Recently, high-cellulose content materials, such as wood or grasses, have been used for methanol production. This is a more costly and complex method due to the large plant required to convert the raw materials into a gaseous intermediate from which methanol can be synthesized. Larkin et al., [2004] stated that alcohol can be used as a liquid fuel either on its own or blended with petroleum for power generation. Wereko-Broby and Hagen, [1996] concluded that a blended mixture of ethanol: gasoline (20:80 % weight volume) can be used in engines without adjustment. They also reported that combustion engines have been modified in Brazil for use with 100 % ethanol. Alcohol run engines produce less NO_x than gasoline engines because of their lower temperature burn and that NOx emissions drop with decreasing temperature [Demirbas and Demirbas, 2007].

2.3.7 Anaerobic digestion (AD)

Anaerobic digestion is widely used to convert high moisture biomass, such as manures from cattle, sewage sludge or MSW, by attacking them with bacteria in the absence of

oxygen to generate biogas. The gas mixture produced consists mainly of methane (CH_4) and carbon dioxide (CO_2) with small amount of other gases like H_2, N_2, NH_3 and H_2S, depending on the composition of the biomass feedstock. Anaerobic digestion can occur at temperatures ranging from < 20 °C, 20-40 °C or 50-65 °C based on the type of the bacteria digester. An Institute of Wastes Management report [IWM, 1998] concluded that in practice, the digestion reactor system operated better at 35 °C or 55 °C conditions and that the temperature should remain constant during operation. Biogas can be used for all applications developed for natural gas with lower NO_x emissions [IEA, 2003; Demirbas and Demirbas, 2007]. Higher CO emissions are problematic with biogas. However this can be improved by upgrading to higher quality removal of CO_2.

2.3.8 Mechanical extraction

Mechanical extraction is a process used to convert biomass seeds like oilseed rape or cotton into oil, with small amounts of residual solids suitable for animal fodder [Warren Spring Laboratory, 1993]. This process was applied in some European countries for bio-diesel (fatty acid methyl ester) production in which the bio-oil is subjected to an esterfication technique (where the oil is reacted with an alcohol). This helps to reduce the visco-elasticity and flash point to around 3-5 mm^2/s and 160 ^oC, respectively, which allows its use as an automobile fuel.

2.3.9 Combustion, co-combustion (co-firing)

Combustion is the simplest method of converting biomass (see formula) into heat or electricity by using air to oxidize the material into carbon dioxide and water [Demirbas and Demirbas, 2007; Van Loo and Koppejan, 2008].

$$CxHyO + O_2 \rightarrow CO_2 + H_2O + Heat \qquad \textbf{Eq. 2.1}$$

The combustion plant usually consists of fuel storage, feeding system, combustion system (combustor chamber or combustor bed boiler), heat exchanger, ash removal, flue gas clean-up and stack. This can range from domestic scale to large scale (i.e. 100-4000

MW range). In the combustion system the characteristics of the biomass will be changed by various physical and chemical mechanisms. When the biomass is introduced into the combustor, the particles will dry out due to the heat, then devolatilise, followed by ignition and burnout mechanisms. At the devolatilisation stage, most of the solid mass of the particles will be lost forming a gaseous volatile phase with residual char [Weather et al., 2000; Demirbas and Demirbas, 2007, Ma et al. 2007]. The volatile gas consists of an organic component (e.g. CO, CO_2, and CH_4) and inorganic component (e.g. Na, K) based on the biomass feedstock composition. At the burnout stage, the inorganic component may undergo sulphidation or chlorindation (etc.), whereas the organic will oxidize.

McGowin and Wiltse, [1996] reported that the Electric Power Research Institute (EPRI) in the USA initiated a strategic analysis of biomass for electric power generation. They stated that co-firing (co-combustion) with coal in industrial and utility boilers is the highest efficiency, lowest cost and lowest risk technology. Co-firing is the burning of more than one fuel, which can take place in any existing coal-fired power plant boiler. When co-firing biomass with coal in a power plant, a continuous supply of biomass would not be an issue, because the boiler plant would always have the primary coal fuel for 100 % combustion [NERL, 2005]. However, choices of bio-fuel and operating conditions are an issue that have to be considered to prevent putting boiler plant at risk [EUBIONET, 2005]. Also, there is far too little biomass to replace coal globally [Green, 1994; Baxter, 2005].

There are generally three different options for coal: biomass co-firing. Direct co-firing involves combustion of coal and biomass within the same combustion chamber, whereas indirect co-firing involves the burning of coal and biomass that have been gasified separately before being co-fired. Parallel co-firing is a more complex method involving at least two boilers where coal is burnt in one and biomass in the other. The direct co-firing approach is the most widely used in the UK and United States as it is the simplest approach and has the least cost. Coal and biomass can be supplied to a direct co-firing boiler by either co-milling together or feeding separately [EUBIONET, 2005; Van Loo and Koppejan, 2008].

The three most common combustion systems utilised in co-firing include the following, each of which has its unique characteristics and benefits when firing fuel alone or blends [Van Loo and Koppejan, 2008]:

- Grate bed combustion
- Pulverised fuel combustion
- Fluidised bed combustion

Brief descriptions of each are presented below;

2.3.9.1 Grate bed combustion

In grate-firing technology, fuel is distributed over a fixed or moving bed (with bed temperature of ~ 1000-1200 ^{o}C), where the combustion air is supplied from the base. Fixed grates can be level or sloping, whereas moving bed divided into combustion zone and sections after-combustion zone moves the grate gradually. In GBC, the intention is to keep the majority of the ash on the grate for removal (either manually or mechanically). However, a significant quantity of it will be released as fly ash entrained in the combustion gases or in the form of vapours and/or fine fumes. One of the major advantages of grate combustion technology is that it can be applied to a wide range of fuels from chip to block type, even untreated fuels (e.g. with high moisture content). Recent studies showed that the efficiency of electricity production is quite low when using biomass fuel due to formation of large ash agglomerates on the bed associated with poor fuel distribution which causes areas on the bed which are too deep and have poor air distribution and hence tend to run relatively hot [Obernberger, 1998; Hein and Bemtgen, 1998].

2.3.9.2 Pulverised fuels combustion (PF)

Pulverised firing technology is based on a finely ground fuel fed pneumatically into the boiler. Fuel feeding needs for pulverised combustion are much higher than fluidised and bed combustion [Mann and Spath, 2001]. The maximum particle size for coal and

biomass should not exceed ~ 100 µm, 10-20 mm respectively, as the residence time in combustion system is relatively short, so the fuel size must be small to achieve full conversion [Van Loo and Koppejan, 2008]. Because of high flue gas velocities, the fly ash is carried with the flue gas and is partially deposited on the combustion system components.

2.3.9.3 Fluidised bed combustion (FBC)

Fluidised bed boilers are widely used in power plants due to their low operating temperatures (~ 700-900 °C), which leads to limit the formation of thermal nitrogen oxide, simplification of the fuel feeding system and their ability to combust almost any solid, semi-solid or liquid with sufficient calorific value [de Jong, 2005; Oniszk-Poplawska et al., 2003]. In FBC systems, the fuel particles are suspended in a fluidising air stream, along with a coarse-grained bed material.

Fludised bed combustor performance depends on fuel properties [Tillman, 2000]. Table 2.2 shows a summary of the three key fuel properties and their effects on bed combustion performance [Howe and Divilio, 1993]. The higher the moisture and ash content the lower the bed temperature. This is due the amount of heat required to evaporate the fuel moisture and to heat up the ash and combustion air. The volatile parts of the fuel will affect the above bed combustor temperature when they are released as they tend to combust in the upper region of the combustion chamber. Also, the pattern for char and/or volatiles burn out may be carried directly out of the bed by the fraction of fuel particles [Howard, 1983]. This happens when their velocities are more than the upward gas velocity in the bed (i.e. function of shape, particle size and density).

When fuel size and composition vary over time, the rate of drying, devolatilisation and volatiles combustion will not be uniform [Weather et al., 2000]. Because of the speed at which the burning volatiles consume any available oxygen, there are periods of time when local regions of the combustor are running fuel rich versus fuel lean [Demirbas and Demirbas, 2007]. This causes the quantity of partially combusted fuel leaving the combustion chamber as CO to vary.

Table 2.2 Summary of biomass characteristics and impact on boiler performance

Fuel properties	Impact on performance
Basic fuel composition	
• Proximate analysis (ash and moister %, wt) • Ultimate analysis (C,H,N,O,S and Cl) • Heating value	• Combustor plan area heat release rate • Thermal combustion limit • Flow rates of air, ash and flue gas • Boiler efficiency
Particle mixing and combustion characteristics	
• Moisture (%, wt) • Particle size • Particle density • VM/FC ratio • O/FC ratio	• Particle heat-up and drying time • Develatilisation and volatile combustion time • Char combustion time • Particle mixing and segregation • Combustion stability
Ash and non-combustible impurities	
• Ash (%, wt) • Ash deposition • Chemical composition • Physical composition	• Melting/vaporisation temperature • Tramp/oversized material accumulation • Low melting point compound formation • Bed material

2.3.9.4 Combustion, co-firing studies

Recently, combustion and co-firing biomass with coal has received considerable attention worldwide [Livingston and Morris, 2009]. R&D studies were carried out using an experimental range from laboratory (bench-scale) up to industrial scale and has been evaluated for a variety of boiler technologies (e.g. pulverised combustion, grate bed combustion, fluidised bed combustion, etc) [Tillman, 2000]. Colombian, British and Polish coals were used as fossil fuels for a number of studies [Hansen et al. 1998; Sami et al., 2001; Savolainen, 2003; Fryda et al. 2006, Gulyurtlu et al., 2007; Lu et al. 2008], whereas sawdust, sewage sludge, RDF, switchgrass, wood chips, straw among the most used bio-fuels [Sami et al., 2001; EUBIONET, 2005; Zulfiqar, 2006; Hernandez-Atonal et al., 2007]. Table 2.3 provides a brief overview of some selected combustion studies.

Table 2.3 Selected combustion studies

System Description	Fuel Type	Experiments/ studies	Results	Issues	Remarks	Ref.
Bench-scale spray combustor of 5 kW capacity, fitted with pressurised (4 -10 psi) delivery tank & atomizer air. Feeding rate of 15-25 ml/min.	Pyrolysis oil & pyrolysis:ethanol (90:10 %,v) blend mixture. Ethanol used as an additive to reduce oil viscosity.	Evaluate the Feasibility of using pyrolysis oil to fire, flue gases, PAH & possible VOC emissions	Promising combustion achieved under preheat pyrolysis oil to 40 °C. Blend fuel without heating clog the atomizer. GC-MS indicated no pollutants above detection limit.	Stainless steel must use for all parts (i.e. tank, lines, atomizers, valves,filter) due to oil has a pH of 2-3 & moisture up to 20-30 %,wt.	Further research on atomization, burning dynamics will be necessary to apply the finding of this laboratory scale study to the design of an industrial scale energy conversion system.	Krum-dieck, & Daily [1998]
Pilot-scale single burner furnace, feeding rate of 6 M Btu/h.	Coal:switchgeass (90:10 %, wt)	Combustion & Handling	NOx emission reduction due to low sulphur of switchgrass	Burned well for both eastern & western coals	Handlin & feeding are the toughest problems due to low bulk density of switchgrass	Boylan et al. [2000]
Bench-scale single fluidised bed with conical bed, feeding rate of 100 kg/h.	Sawdust, rice husk and sugar cane bagasse, run at five excess air (ER) (20,40,60,80, 100 %)	Combustion efficiency and effects of fuel properties	Over 99 % combustion efficiency achieved for sawdust & bagasse at ER of 50-100 %. CO_{max} recorded for rice husk	Firing sawdust is the most emissions reduction, whereas, rice husk with high environmental impact	NO_{max} was highly effected by fuel nitrogen & weakly dependent on operating conditions	Permc-hart, & Koupr-ianov [2004]
Pilot-scale basic plant consists in supplying pre-heated air, feeding rate up to 2 g/sec.	Forest residues pellets (Eucalyptus, pine, pine bark)	Combustion capability and feeding systems	Feeding system consists of 200 mm wide belt conveyor gave regular feeding rate. Screw auger feeding system causes high segregation.	Pine bark is the most suitable product for co-firing as efficiency and viable due to lower price of the treatment.	Co-firing in basic plant only works with higher amount of air. Different burner suggested.	Granada et al. [2006]

Experience of commercial co-firing has been gained in over sixteen countries [Baxter, 2005]. For example, up to 10 %, wt were commercially co-fired with coal/switchgrass in USA [Boylan et al. 2000], and coal/sewage sludge in Germany (including trials with straw and wood) [Ekmann et al., 1996]. In Netherlands, experience with a higher blend mixtures of fuel (up to 40 %, wt, in ~ 1 MW_{th} pilot-scale plant) considered using coal with various biomass fuels such as wood, paper sludge, coco-shells, chicken litter, plastics and olive kernels [Meijer, 2005]. In the UK, 16 major coal power plants have been co-firing biomass (up to ~10 % on an energy basis). The feedback from these power plants shows that co-firing can be practiced without encountering major problems (with respect to other issues such as fuel feeding, vermin, biomass storage, etc.) in terms of component lives and that the efficiencies of boilers were not reduced [European Commission, 2006; Livingston and Morris, 2009]. Livingston and Morris, [2009] stated that the qualification of a range of fuels for commercial co-firing activities possibly dependent on the successful performance of a number of plant trials on a range of specific fuels. They concluded technical issues that have been experienced from co-firing biomass in large capacity boilers were the challenges of storage and handling of the biomass and in particular with the tendency of some biomass materials to generate significant dust levels. Also, included that the preferred approach for co-firing technology involve the direct injection of pre-milled biomass with coal and in principle biomass co-firing ratios up to 50 % (energy basis) can be achieved and the technical concern suitable for both retrofit and new build application.

It can be concluded from the worldwide research and commercial experience that the technical feasibility of biomass co-firing is largely proven. However, potentially serious problems from long term use still remain: e.g., effects on boiler efficiency, slagging, fuel feed control, combustion stability, fuel delivery, unsolved and/or unknown combustion chemistry for many bio-fuels, deposition etc. [European Commission, 2006; Van Loo and Koppejan, 2008]. Information on ash chemistry results in potential deposition issues in operational biomass and/or biomass: coal blend which combustion for many fuels is still very limited. Biomass and biomass:coal power plant operation and design depend strongly on deposition and corrosion [Van Loo and Koppejan, 2008; Livingston, 2009].

2.4 Gaseous emissions from combustion and co-combustion of biomass

The gaseous emissions of primary concern from the combustion and co-combustion of biomass and coal in power plant systems are CO_2, SOx, NO_x (NO and NO_2), N_2O, CO, particulate (fly ash), acid halides (e.g. HBr, HCl, HF), the organic compounds (such as VOCs, PAHs, chlorinated dioxins (PCDD), furans (PCDF)) and trace metals. Demirbas, [2003] stated that a biomass fuel fired in a combustion boiler behaves differently from coal. This is due to the fact that biomass in general is characterised as having a higher volatile matter content, lower heating values, less carbon, more oxygen, higher moisture content, usually lower density, wider size distribution and higher volatile alkali content when compared with coal compositions [Easterly and Burnham, 1996; Van Loo and Koppejan, 2008].

CO_2 is a major product from all biomass combustion, originating from the carbon content in the fuel. However, CO_2 emissions from biomass combustion are regarded as being CO_2-neutral with respect to the greenhouse gas effect and this is considered to be the main environmental benefit of biomass combustion [Hein, 1998; Klass, 1998].

Generally, SOx emissions decrease in line with the co-firing ratio due to the low sulphur (typically less than 0.5 % on a dry basis) in biomass materials. Figure 2.2 shows the influence of co-firing various bio-fuels (miscanthus, straw and sewage sludge) on SO_2 emissions. An additional reduction beyond the amount anticipated on the basis of fuel sulphur content is observed due to retention of sulphur in coal by alkali based compounds in biomass ashes [Montgomery and Larsen, 2002].

The combustion of most biomass materials can be expected to result in lower NO_x emissions due to the nitrogen contents of most biomass being very low (around 0.5-1.0 %, on a dry basis). Figure 2.3 shows the effects on NO_x emissions when co-firing switchgrass (N, content 331 g/GJ) and wood (N, content 77g/GJ) with coal (N, content 430–516 g/GJ). It can be seen that NO_x emissions of coal (at 3 % O_2) were greater than both biomass and blended fuels. However, other experimental analysis of NOx emissions during combustion of various blends of coal and biomass indicated that NO_x

emissions can increase or decrease when co-firing, in particular at low ratios. The possible reason to explain this is related to the type of biomass materials used and the impact of biomass growing conditions and properties (i.e. soil type, weathering). Other possible reasons are that biomass produces greater volatile yields than coals and this can create larger fuel rich regions in the burner region, which able to enhance the performance of NO_x burners.

In addition to NO_x, N_2O emissions can also be significantly reduced by co-firing of biomass (example of N_2O emissions of coal: wood firing in fluidised bed combustor can be seen in Figure 2.4).

The particulate emissions data available for combustion and co-firing biomass are conflicting. Some research data show no significant change, whereas some show a sharp increase in particulate emission. The possible reason to explain this is related to the performance of the installed particulate collection equipment [Van Loo and Koppejan, 2008].

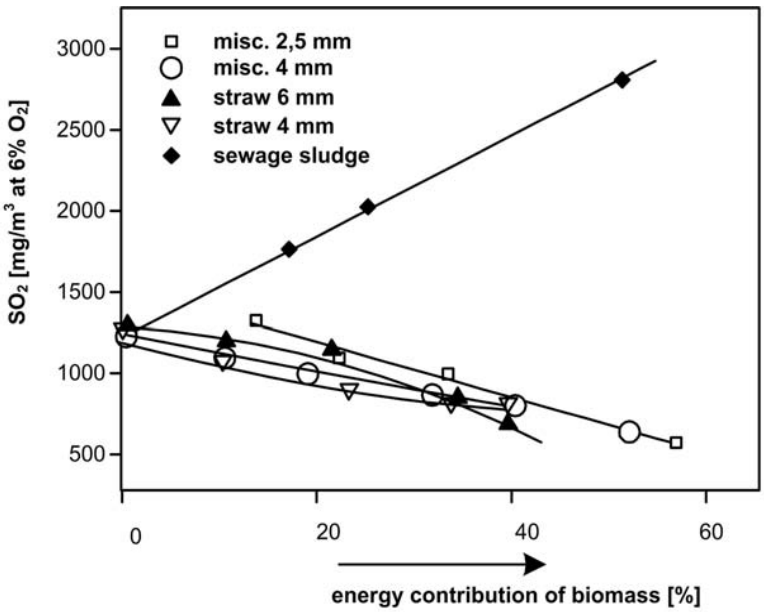

Figure 2.2 Influence of co-firing various bio-fuels on SO_2 emissions
Source: [Montgomery and Larsen, 2002]

The effect on HCl emission levels when co-firing biomass fuel vary. This is due to the fact that biomass materials can have low or relatively high chlorine which increase or decrease in the total chlorine input to the boiler and hence affect the HCl emissions levels.

The emission levels of CO and the organic pollutant species are dependent largely on the quality of the combustion process. Co-firing biomass data showed that the emissions of CO and the organic pollutant species were no higher than for coal firing if the system is operated properly and the particle size and moisture content of the biomass are at acceptable level [Van Loo and Koppejan, 2008].

Also, it should be pointed out that the measurement of the CO emission levels during combustion is a good indicator of the quality of the combustion, and provides a reasonably good indicator of the organic species. Analytical measurement of CO emission measurement is simpler than measurement of the more complex organic species.

(a)

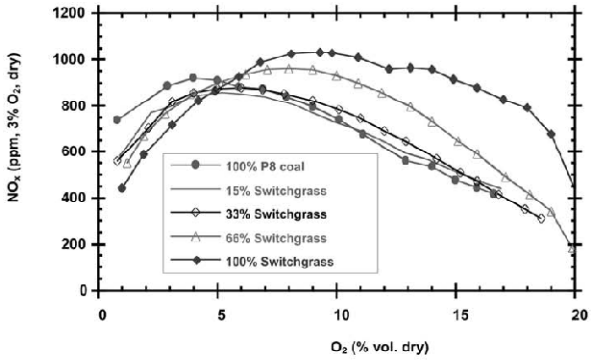

(b)

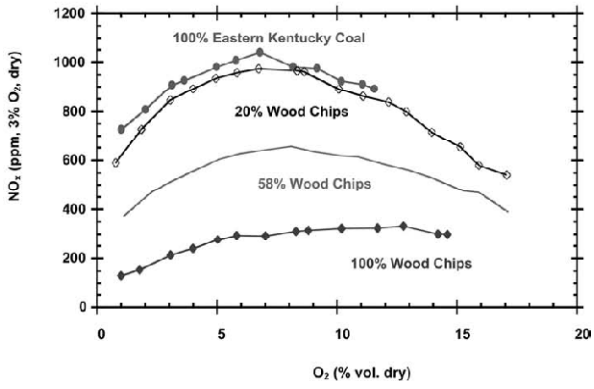

Figure 2.3 Effect on NO_x emissions when a) co-firing switchgrass and b) wood with coal in pulverised fuel combustor (FBC)
Source: [Montgomery and Larsen, 2002]

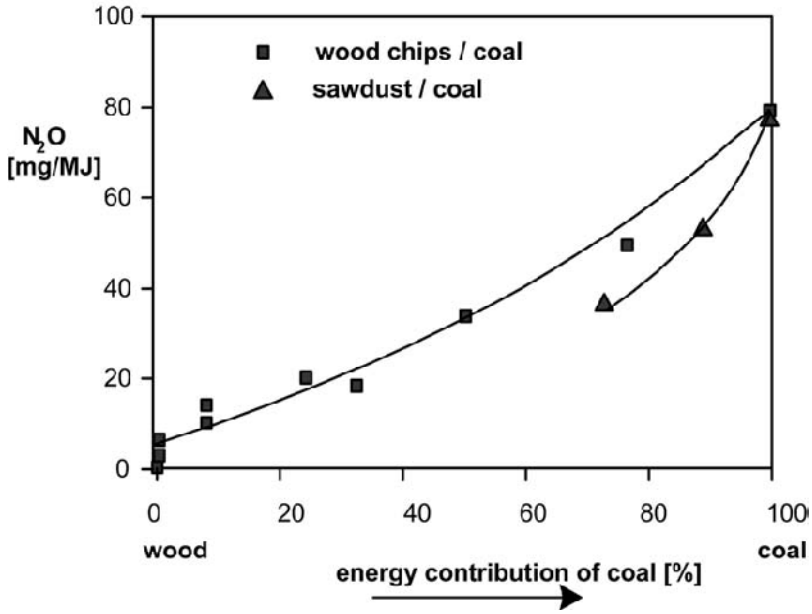

Figure 2.4 Influence of mixed combustion of wood (wood chips & sawdust) and coal on N_2O emissions in a fluidised bed boiler
Source: [Karlsvik et al, 1993].

Heavy metal (e.g. Cu, Pb, Cd, Hg) emissions from combusting biomass will be via either fly ash (i.e. fly-ash particles or attached to the surface of particles emitted to the atmosphere) or evaporation. The level of the heavy metal emissions will be related to their concentration in the biomass fuel as well as the presence of other elements, combustion operating conditions, gas cleanup equipment etc. Contaminated biomass fuels (e.g. painted wood) may contain significantly higher levels of heavy metals [Van Loo and Koppejan, 2008].

2.5 Ash formation from combustion and co-combustion of biomass

Ash is formed from inorganic elements present in biomass as salts bound in the carbon structure (known as inherent ash) and/or extraneous mineral particles (known as entrained ash) that enter with the fuel during harvest or transport, like rock, dirt or metals. The compounds in inherent ash are homogeneously distributed in the fuel and are much more mobile, volatile and available for reactions than the compounds in entrained ash during combustion [Obernberger and Brunnert, 1999; Livingston, 2009]. Figure 2.5 shows the mechanisms of ash formation in biomass combustion.

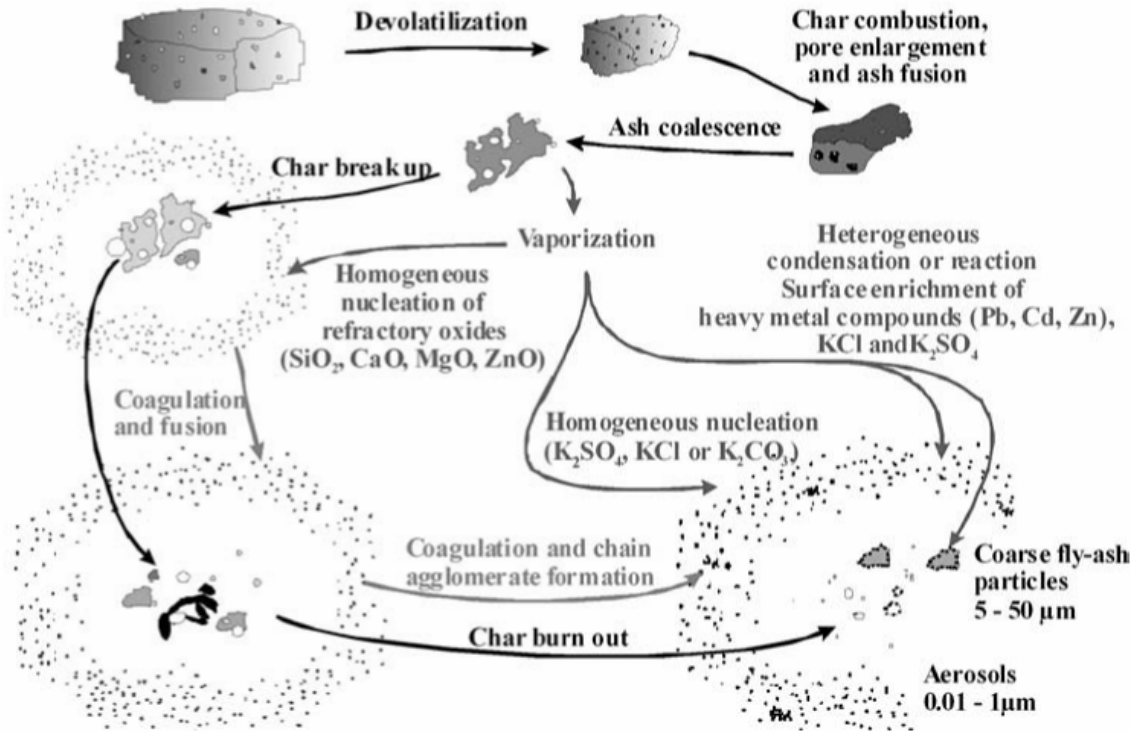

Figure 2.5 Mechanisms involved in ash formation in biomass combustion
Source: [Christensen, 1995]

Obernberger and Biedermann, [1998] reported that at high combustion temperatures, a reducing atmosphere can enhance the volatilisation of heavy metals such as Zn, Pb and Cd. When these metals are released, they will pass through the boundary layer and enter the surrounding furnace environment in their gaseous state to mix with other volatile elements such as Cl, S and K. Also, at this condition, even a small fraction present as refractory oxides, such as SiO_2, CaO and MgO, may convert to more volatile SiO, Ca and Mg when released from the char as vapours to form very small primary particles in the boundary layer of the burning char particles due to re-oxidation and subsequent nucleation [Kauppinen, 1998]. Primary particles are very small in size (about 5–10 nm), but when travelling in the flue gas they grow by coagulation, agglomeration and condensation to form the basis of the fine-mode fly ash (aerosols, a particle size of < 1 µm) [Kauppinen, 1998].

The non-volatile ash compounds remaining in the char may melt and coalesce inside and on the surface of the char to form a wide range of compositions, shapes and sizes, related to the characteristic of the parent mineral particles. Depending on the density and size of the residual ash particles, the combustion technology and the flue

gas velocity, a fraction of the residual ash will be entrained with the flue gas and form the coarse part of fly ash (a particle size of > 5μm), while the other fraction will stay in the combustor and form bottom ash [Lind et al. 1998, Brunner et al., 1998]. Figure 2.6 shows the SEM images of coarse fly ash and fine-mode fly ash (aerosol) particles from wood combustion in a grate furnace.

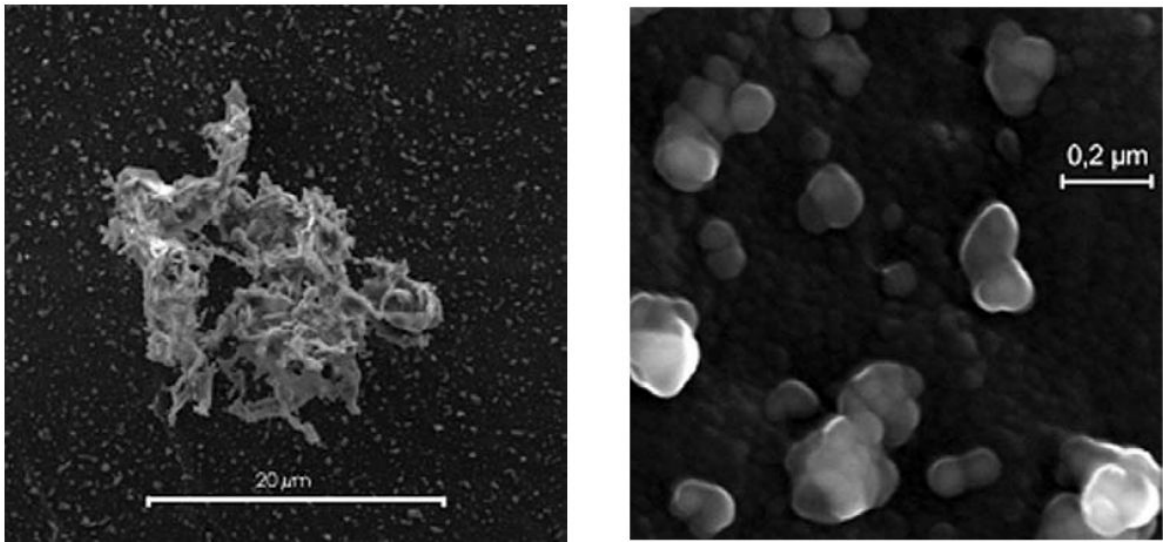

(a) **(b)**

Figure 2.6 SEM images of a) coarse fly ash and b) fine-mode fly ash (aerosol particles) upon wood combustion in a grate furnace
Source: [Obernberger and Brunnert, 1999]

When the flue gas is cooled within the convective heat exchanger section, vapours of volatilized compounds may condense or react on the surface of pre-existing ash particles in the flue gas. It is been reported that the rate of condensing or reacting ash-forming elements are much higher with fine-mode particles compared to the coarse fly-ash particles, due to the larger specific surface and small particle sizes. This explains some of the very high heavy-metal concentrations found in fine-mode (aerosol) particles from combustion plants [Lind et al. 1998; Obernberger and Brunnert, 1999].

If the cooling rate in the heat exchanger and the concentration of inorganic vapours in the flue gas are both high, supersaturation of these vapour compounds may occur, causing formation of new particles by nucleation. In biomass combustion, alkali metals sodium (Na) and potassium (K) generated from inherent ash play an important role in ash deposit formation, thickness and melting point (because of Na and K in the inherent

ash are typically present as thermally very stable mineral silicate compounds and will not vaporise). They react with chlorine from the fuel to form volatile chlorides NaCl and KCl capable of condensing onto cold metal surfaces as chloride salt deposits [Livingston, 2009].

Mainly, the actual forms of the inorganic materials that deposit include; clays/silicates, sulphides, sulphates, carbonates, phosphates and some oxides. Henderson et al., [2006] reported that sulphate salt deposits are less aggressive than chlorides salt deposits because of their higher melting point. However, hot corrosion can be increased rapidly if deposits form liquid phases on the surface of the components [Simms et al., 2008]. Zheng et al. [2006] concluded that alkali metals and Si, Al, Ca can decrease the volatile K in the ash from co-firing. They observe a partial removal of volatile K by adding a sufficient amount of Si and Ca with nearly complete removal of volatile K when both Si and Al are added. Miles et al. 1995 noticed the effect of Mg on lowering the temperature of the ash.

According to chemical equilibrium calculations, at high temperatures in the flue gas, the vaporised K is mainly present as gaseous KCl or KOH. When the flue gas temperature decreases, the chloride and hydroxide are converted to sulphate (K_2SO_4) by homogeneous gas-phase reactions. Gaseous K_2SO_4 usually forms with high numbers of new primary particles (by homogeneous nucleation) since it has a very low vapour pressure and becomes highly supersaturated as soon as it is formed. However, the formation of K_2SO_4 does not always follow equilibrium and only a part of the potassium in the gas phase may be converted according to gas phase kinetic considerations [Christensen, 1995]. It either nucleates as KCl or K_2CO_3 or condenses on pre-existing particles at significantly lower temperatures than the K_2SO_4. In addition, solid KCl or K_2CO_3 on the particles may undergo heterogeneous reactions with SO_2 and form solid K_2SO_4 as time proceeds in the flue gas. It is reported that the sulphation of KCl releases corrosive Cl that can react with the heat exchanger surface and promote corrosion. Other elements should also taken into account such as iron (Fe) which can react with sulphur gas species (i.e. SO_2, SO_3) and accumulate as iron sulphate, $Fe_2(SO_4)_3$, and hence participate in corrosion reactions [Brunner et al., 1998].

2.5.1 Ash fractions formed in biomass combustion plants

In biomass combustion plants three different ash fractions (bottom ash, cyclone fly ash and filter fly ash) are often collected [Van Loo and Koppejan, 2008]. Figure 2.7 shows the ash fractions collected from a biomass combustion plant.

The amounts of ash for the various fractions are different, depending on the combustion technology used. For example, in fluidised bed combustion plants, the fly-ash fractions are quantitatively dominant.

The bottom ash fraction formed on the grate and/or in the combustion chamber may be mixed with the mineral impurities contained in the biomass fuel (e.g. sand, stones) or with bed material in fluidised bed combustion plants to cause slag formation and sintered ash particles. The cyclone fly ashes mainly consist of coarse fly-ash particles, which were carried by the flue gas and separated out by the cyclone. Whereas, the filter fly ash fraction mainly consists of aerosol (fine-mode) particles collected by the filter unit (e.g. electrostatic filters or fibrous filters). In small-scale combustion plants (i.e. without efficient dust precipitation technology) this fine ash fraction remains in the flue gas and causes dust emissions [Obernberger et al., 1995].

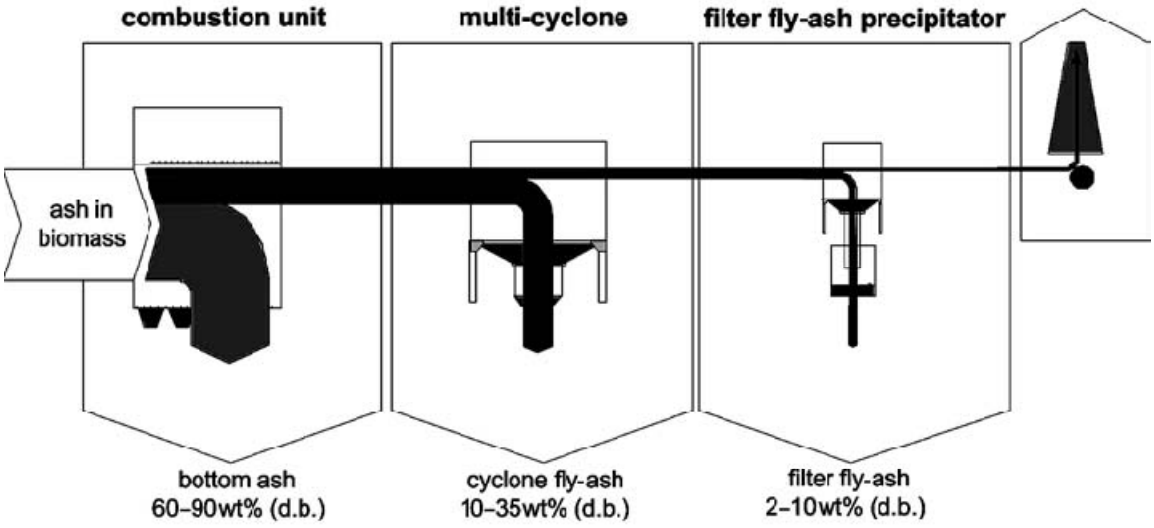

Key: (d.b.) dry base.

Figure 2.7 Ash fractions collected from a biomass fixed-bed combustion plant
Source: [Obernberger et al., 1995]

2.5.2 The behaviour of biomass ash in combustion plants

As mentioned above, the amount and distribution of the ashes forming will depend on the combustion technology used. In the following sections, the behaviour of the biomass ashes in fluidised bed and pulverised fuel combustion systems will be addressed, as these two combustion technologies are both used in this study.

2.5.2.1 Ash behaviour in fluidised bed combustors

The behaviour of biomass ash materials in fluidised bed systems has been the subject of several studies, in particular with waste products (e.g. pulp and paper industries) [Bain et al., 1998]. As mentioned above, in fluidised bed combustion systems, the fuel particles are suspended in a fluidising air stream, along with a coarse-grained bed material. This results in the majority of the ash leaving the fluidised bed combustor consisting of fly-ash particles (diameter, around 50–100 μm) and small fine particles of elutriated bed material (commonly quartz, or un-reacted limestone, with lime and calcium sulphate/sulphite) [Van Loo and Koppejan, 2008].

As the combustion temperatures that apply in fluidised beds tend to be less than 900 $^{\circ}$C, the inorganic constituents of the biomass and the bed material may undergo thermal decomposition reactions (e.g. calcium carbonate or calcium oxalate to calcium oxide, and the subsequent sulphation of the lime particles) causing sintering and forming agglomerates. The main sintering mechanism involves the low melting temperature ash components forming a liquid phase of low viscosity that, in turn, forms necks between the bed particles. This has been indicated for fuels with ash rich in alkali metals, phosphates and some of the heavy metals (e.g. Pb). Also, sintering may occur between solid ash and bed particles if silicates and/or alumino-silicate species are partially soluble in the liquid phase that forms on the surfaces of the bed material. This can sometimes create an environment for chemical reactions to occur at the surfaces of the bed particles, which can increase the strength of inter-particle bonds. For example, the reaction of lime on the surfaces of the bed particles with SO_2, to form calcium sulphate, is considered responsible for the sintering of bed

particles in fluidised bed combustors firing high calcium biomass materials [Skrifvars et al., 1996]. Agglomeration of the bed particles can lead to poor air distribution and eventually de-fluidisation of the bed. This is a key issue in operational fluidised bed combustors (FBC) that may make it necessary to bring the combustor off line and replace the bed material.

2.5.2.2 Ash behaviour in pulverised fuel combustion systems

Generally, pulverised fuel combustion systems are linked with very large solid fuel boilers for power generation. As mentioned above, it is quite rare for this technology to be fuelled with biomass alone. However, there are a small number of 100 % pulverised wood-fired boilers in operation, particularly in Scandinavia [Van Loo and Koppejan, 2008; Livingston and Morris, 2009].

Coals vary in ash content with wide variations of ash properties and composition. Rank is one type of coal classification that links with the degree of coalification (a process in which vegetable matter converts into coal with anthracite as the final product). The coals are quantitatively based on heating value and fixed carbon (i.e. the amount of organic residue upon pyrolysis at fixed temperature). The main coal ranks are lignite, subbituminous, bituminous and anthracite in increasing order of heating value or fixed carbon. The lowest rank coals (lignites) contain high moisture content and volatile matter and relatively large amounts of inorganic elements (such as Na, Mg, Ca, K and Sr) compared to the highest rank coals (anthracite). By contrast, high rank coals commonly contain more Cl, Fe and S than low-rank coals [Smith, 1994]. This variation of inorganic content changes the deposition and corrosion potential of coals, which make it as one of the most investigated issues in power generation. Figure 2.8 shows the extent variation in Cl and S contents of coals as well as biomass.

Ash behaviour from biomass combustion can be quite different compared to various coals. The principal concerns in co-firing are with the behaviour of the inorganic material associated with the biomass and the impact of the blends resultant ashes and deposits (i.e. with the characteristics of the mixed biomass–coal ashes and resulting

deposits). There is much known about ash deposition during coal and their behaviour in pulverised coal combustion systems (e.g. Erich Raask, 1985, presents a summary of the state of knowledge on coal ash characteristics and behaviour in pulverised combustors) compared to biomass. In coal, alkali metals are believed to be bound either with organic compounds (such as cations associated with carboxylic acids) or as inorganic compounds. In the inorganic form they may exist as: simple soluble salts; or as silicates (crystalline); or associated with alumino-silicates, such as $Na_2O \bullet Al_2O_3 \bullet [SiO_2]_6$, $K_2O \bullet [Al_2O_3]_3 \bullet [SiO_2]_6 \bullet [H_2O]$ and $K_2O \bullet Al_2O_3 \bullet [SiO_2]_6$, and hence not easily released to the gas phase during combustion [Raask, 1985, Hald, 1994]. In biomass, alkali metals together with Si, Cl, S, Ca and possibly phosphorous could react with the mainly alumino-silicate coal ash during co-firing and form lower melting point ashes. In general, there is an agreement that the organically bound potassium in biomass has a high mobility and can be easily released [Gottwald et al., 2002]. Miles, [1996] showed that over 90 % of the potassium in straw biofuels is available as either water soluble or ion exchangeable material under chemical fractionation experiments.

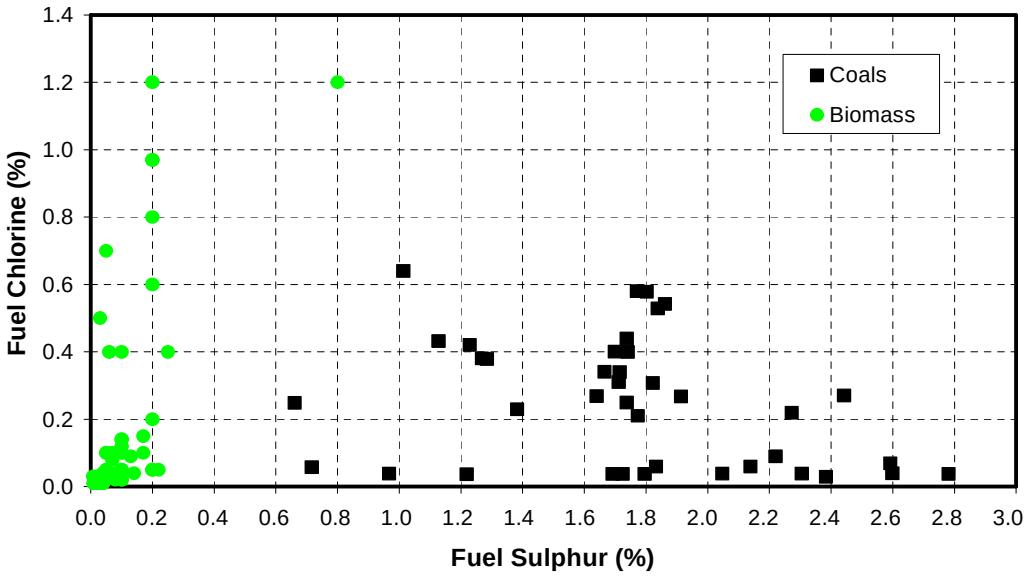

Figure 2.8 Variation in Cl and S content of coals and biomass fuels
Source: [Simms, 2009]

However, there have been few attempts at detailed test work on deposit formation during biomass co-combustion (most only consider 100 % biomass combustion). One important example [Skrifvars et al., 2004] describes the results of trials, firing 100 % pulverised wood fuels in an 80 MW_{th} down-shot fired boiler in Sweden. Interesting data on the fly-ash formation occurring in the milled biomass suspension flames and information on the deposit formation processes were obtained. Ash materials samples were collected from the combustion unit and the filter unit. The size fractions of fly-ash particles taken from the flue gas ductwork at temperatures around 400 $^{\circ}C$ were in the range up to 10 μm. Chemical analysis showed that the concentrations of the volatile inorganic elements (i.e. the K, Na, S and Cl) decreased with increasing particle size, whereas the concentrations of the less volatile species (i.e. the Si, Al, Fe, Ca, Mg, Mn, and P) tended to increase with increasing particle size. They concluded that the products of biomass combustion when co-fired with coal tend to have a higher level of sub-micron fume and vapour, and the fly-ash particles tend to be significantly smaller than those formed by the combustion of pulverised coal.

Generally, other literature reports that the key ash-related impacts of the co-firing of biomass with coal are on the slagging and fouling deposit formation potential of the mixed biomass–coal ash due to the relatively high “free” alkali and alkaline earth metals contents of biomass; the resulting compounds are effective fluxes for the alumino-silicate ashes from the coal [Weather et al., 2000; Klass, 1998; Tomeczek and Palugniok, 2002; Livingston, 2009].

2.5.3 Deposition

Deposition rates from biomass fuels combustion can be quite different compared to various coals. Co-firing biomass can lead to either decreases or increases in deposition rates relative to neat fuels. Figure 2.9 shows deposition rates for various combustion fuels. It can be seen that the deposition of herbaceous biomass (wheat straw) exceeds those of coal by a large margin, whereas those from wood materials tend to be lower [Baxter et al., 2003].

In general literature observed the following:

- Deposition rates should not be affected significantly when co-firing wood or similar low-ash, low-alkali and low-chlorine fuels even at elevated co-firing ratios.
- Deposition rates should increase when co-firing herbaceous and agricultural residue materials (because of high-chlorine, high-alkali and high-ash fuels).
- Deposition rates depend strongly on both individual fuel properties and interactions between the co-fired fuels.

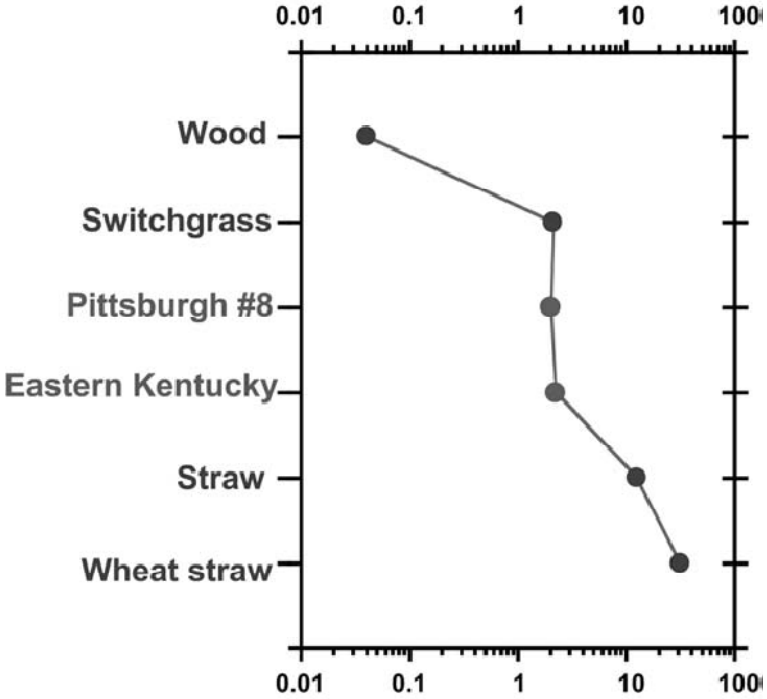

Figure 2.9 Deposition rates (from cooled target of constant probe surface temperature of ~ 540 ^{o}C) for various fuels in g deposit per kg fuel
Source: [Baxter et al., 2003]

2.6 Thermodynamic modelling biomass combustion

Modelling together with experimental studies enables improvements to the competitiveness of biomass combustion and a cost effective approach in future biomass combustion applications for heat and electricity generation. Modelling improves our understanding of the fundamental processes involved in biomass combustion. If advances are to be made in protecting components, and reducing deposition in combustion and co-combustion technology, then an understanding of ash formation and deposition processes is crucial [Hughes and Tillman, 1998].

Various types of modelling exist, ranging in complexity from simple heat and predition of combustion products models to larger computational fluid dynamics (CFD) programs using software such as FLUENT. The larger CFD models incorporate ash formation, combustion and deposition codes to provide a detailed picture of the coal combustion process. The type of inputs and models used often varies and outputs include deposition rate, deposition composition and impact efficiency. Most computer models are tailored to the specific needs of the operator [Yan et al., 2001].

Yan et al., [2001] detailed three processes involved in ash deposition:

- transformation of mineral matter into ash particles,
- transport of ash particles to heat transfer/deposit surfaces (impaction),
- retention of ash particles on surfaces.

Yan et al., [2001] noted that the main influence on all three of these processes is the mineral distribution in pulverised coal. Therefore, in order to model ash deposition accurately, details of the composition and size distribution of minerals in coal must be used to predict the resulting ash particle distribution [Wilemski et al., 1992]. The conventional method to characterise ash properties has involved the use of the empirical indices and standard analyses such as ASTM (American Society for Testing and Materials) and BSI standards [Wang and Harb, 1997]. This data is usually readily available and easy to reproduce. However, these methods have lately been proved inadequate as the data is derived from average properties of the coal and the ash fuel

and fails to account for the huge variation in composition and size of ash particles [Yan et al., 2001; Wilemski et al., 1992; Beer et al., 1992]. The complex chemistry that exists is not considered and these methods often produce misleading results that in turn cause problems when using the data for modelling purposes.

Analytical techniques such as computer controlled scanning electron microscopy (CCSEM) and chemical fractionation enable the inorganic constituents of coal to be better characterised. CCSEM allows a large amount of data to be collected on the composition of individual particles in a reasonable time period and at a similar cost. It provides detailed information on size, type and amount of the various minerals present [Wilemski et al., 1992; Wang and Harb, 1997; Yan et al., 2001].

Data from CCSEM analysis is then used as input for an ash transformation model. Ash transformation models are distinguished using three characteristics: 1) the type of input data used, 2) the method used to describe char combustion and 3) the mode of coalescence. There are three modes of coalescence – full coalescence, no coalescence and partial coalescence. Full coalescence assumes that all of the ash in a char particle coalesces to form a single ash particle. No coalescence assumes that no coalescence occurs and each mineral inclusion forms one ash particle. Partial coalescence provides predictions between the two extremes [Wang and Harb, 1997].

According to Wilemski et al., [1992] the full coalescence model gives generally reliable predictions of ash composition and size distribution but the no coalescence model underestimates ash size distribution in the smaller particle size range and also fails to identify several ash composition categories. Yan et al., [2001] present the view that neither of the extreme models perform satisfactorily and that the partial coalescence model presents more realistic data whereas, Wang and Harb, [1997] argue that the use of both full and partial coalescence models can adequately predict fly ash size and composition.

These predictions of particle size and composition distributions (PSCD) from ash transformation models are then used in ash deposition models to predict slagging and fouling.

Wang and Harb, [1997] list several issues that a fundamental deposition model must address;

- ash formation
- fluid dynamics and particle transport
- particle impaction and sticking
- deposit growth as a function of time
- deposit properties and strength development
- heat transfer through the deposit
- the effect of deposition on operating conditions
- deposit structure and its effect on flow patterns in the combustor

Deposition models are characterised by the way in which they deal with each of these issues.

Output data of deposition models can include deposition rate (upstream, inner and downstream deposits), deposit growth, strength development and loss of heat exchanger efficiency [Allan et al., 1996].

An example of a deposition model is LEADER (Low-temperature Engineering Algorithm of DEposition Risk), a computer code designed to predict low temperature fouling potential of coal (developed by the Energy and Environmental Research Centre (EERC) in North Dakota, USA) [Tomeczek et al., 2004].

The code requires specific input data regarding the inorganic components of the coal. This is provided by the analysis techniques mentioned above: CCSEM, chemical fractionation and ASTM. This data is used by a model called ATRAN (Ash TRANsformation) to predict PSCD data that is then used as input for the LEADER

model. LEADER determines deposition rate, strength development and loss of heat exchanger efficiency [Benson et al., 1993].

Most recent ash deposition models were developed to be user friendly and produce useful results in a short time period using minimum computational resources [Yan et al., 2001]. Ash deposition models like LEADER and its more advanced EERC developed relative FOULER do not have an incorporated combustion code making it difficult to predict deposition inside the boiler. Rushdi et al., [2005] states that gas temperature and flow field are the most important parameters in this area and modelled these with a CFD package, FLUENT, while Lee et al., [1996] used a CFD combustion code known as CINAR (developed by CINAR Ltd).

CFD modelling of ash deposition has proved to be an accurate method when applied to pulverised fuel systems. When using fouling coals, CFD may be useful in predicting potential problems regarding boiler operation [Huang et al., 1996]. However, the amount of computational time needed when combining flow calculations and chemical kinetics is currently very high, even with the most advanced computers.

Therefore, simplifications have to be made that reduce the reliability of the modelling results. There are other modelling tools that can be combined with experiments, such as simple heat and predition of combustion products models or chemical equilibrium models, enable to better decisions to be made with respect to the design and operational principles of the various parts of biomass conversion systems, such as furnaces, heat exchangers and dust precipitators [Van Loo and Koppejan, 2008].

Recent studies have reported that using chemical equilibrium models, such as Metallurgical and Thermodynamic Databank (MTDATA) equilibrium calculations software (produced by National Physical Laboratory (NPL), in the UK) to be a useful first step in predicting flue gases and trace element condensation release in combustion tests [Miller et al., 2004].

A brief review of MTDATA is presented below, with a detailed description of the type of calculations which can undertaken within the model and research studies that have used the software for investigating combustion technology as it is the main focus of modelling used in this research.

2.6.1 Overview of MTDATA

MTDATA is a general tool for calculating phase, chemical equilibria and thermodynamic properties with very high reliability [NPL, 1994]. It is used in the analysis of diverse problems in research sciences, including;

- energy conversion
- extraction and recycling
- alloy development
- ceramics, glasses and composites
- joining materials
- materials processing
- hot and aqueous corrosion
- coating, etching and crystal growth
- molten salt chemistry
- electronic and magnetic materials
- environmental control
- aqueous and gas chemistry

Generally, the similar problems in these areas involve many chemical components as well as many possible product phases (i.e. gaseous, liquid and crystalline). The concept behind MTDATA is that the mathematical models incorporated in the software enable equilibria to be calculated on the basis of critically assessed data for simpler systems, which are usually better established [Barry and Chart, 1989; Davies et al., 2002]. Thus using the facilities within MTDATA it is possible to explore compositions and conditions for which no direct experimental data exist.

MTDATA calculates chemical equilibrium using a robust true Gibbs energy minimisation [Dinsdale et al., 1989], which can identify the dominant species of each element in chemical system (for a given temperature and pressure) and can be determined by the following:

$$Minimise\ G = \sum_{j=1}^{N} n_j\, u_j \qquad \textbf{Eq. 2.2}$$

$$\sum_{j=1}^{N} a_{ij} * n_j = r_i \qquad \textbf{Eq. 2.3}$$

$$n_i \geq 0, \quad i = 1,2 \ldots M \leq N$$

Where,

G = Gibbs energy which is to be minimised by varying the values of the n_i, j = 1, 2,...N,

n_i = is the amount in moles of species j present in the system; each chemical substance with different phase designation being considered as a distinct chemical species,

N = number of species in the system,

u_j = the chemical potential of species *j*, which may be a function of some or all of the species amounts in the same phase and it also depends on temperature, pressure and model of the phase under consideration,

a_{ij} = number of units of component *i* per species *j*,

M = number of components in the system,

r_i = number of moles of component *i* in the system.

MTDATA consists of number of modules (including UTILITY, THERMOTAB, ACCESS, MULTIPHASE, UNARY, GPLOT, BINARY, TERNARY, APPLICATION, COPLOT, FITANDPLOT) that retrieve thermodynamic data from databases and perform specified calculations on the data. The specific modules used depends on the type of calculation being performed [NPL, 1994]. For example, the THERMOTAB module is used for thermodynamic calculations for individual substances or a chemical equation, whereas the TERNARY module calculates and plots ternary phase diagrams. A summary of the functions (descriptions and examples of use) of the selected MTDATA modules is shown in Table 2.4.

Table 2.4 Summary of functions of selected MTDATA modules

Modules/description	Examples of use
UTILITY	
Utility module is used for creating, loading and listing databases (include users own database as an option). Facilities are also incorporated for personalising access to particular databases and for customising graphics output.	Listing of the contents of a user's own database can be achieved as follows, *list databace = my_data formate = name!* where, name = e.g. Fe<LIQIUD>, C,Fe<LIQIUD>
ACCESS	
ACCESS module is designed to be used as a data retrieval system for MULTIPHASE, GPLOT, BINARY, TERNARY, APPLICATION and COPLOT, with which it shares common features. The components (which may be elements, compounds or charged species) are entered and the databases are searched for all the substances which might be present in the system at equilibrium. In a large system this could run to many hundreds of substances, many of which may not be very relevant to a particular application and may therefore be excluded. ACCESS allows the user to remove these substances from consideration completely, and to choose from which databases the data for the remaining substances are to be retrieved on an individual basis.	The Commands in ACCESS are; DEFINE LIST CLASSIFY SAVE RETURN Where, **Define system** = e.g. C,H,O **List** = e.g. my_data, and/or SGTE Substance Database - PHASE, GRAPHITE, DIMOND, GAS, CH4O, H2O - C<GRAPHITE, C<DIMOND, C3<g>, CH4<g>, C2H2<g>, C2H4<g>, C2H6<g>, C3H4_1<g>, C3H4_2<g>, CH40, CH40<g>, CO<g>, CO2<g>, H2<g>, HO<g>, H2O, H2O<g>, H2O2<g>, O<g>, O2<g>, O3<g> **Classify** = this command allows to delete any of substances (e.g. if calculations are to be made at high temperature and moderate pressure, it useful to delete volatile phases, dimond and substances corresponding to these phases). **Save** = complete the preparation of a datafile.
MULTIPHASE	
MULTIPHASE is a module for the calculation of multiphase, multicomponent equilibria. Phases may include alloys, molten salts, gases, aqueous solutions, slags, mattes and pure stoichiometric substances in combination. Equilibrium calculations state can be made at constant pressure or volume with a system (including composition and temperature (fixed or range) in terms of the distribution of components and species between the stable phases. Output results can be in the form of tabulated or graphical equilibrium presented in an amounts and/or mole fractions of each of the substances, allowing a large number of plots to be drawn for the same set of equilibrium calculations.	The graph shows the results output from a calculation of only species containing Potassium of the combustion of blend mixture fuel (Coal and CCP, 60:40, %wt) over a range of temperatures (between 200-1300 ^{o}C). 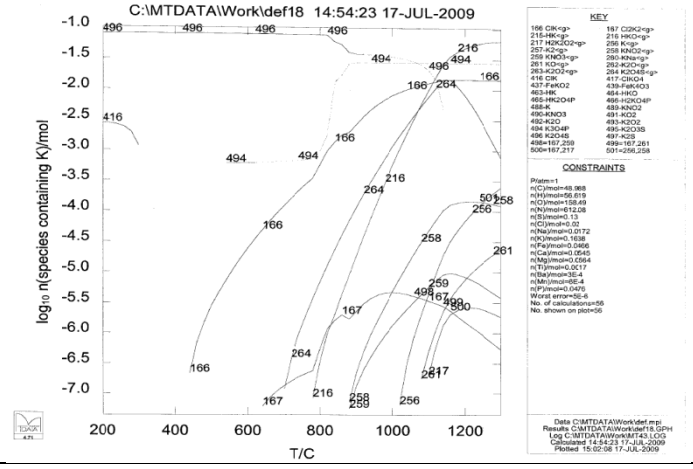

Several thermodynamic databases are supplied with MTDATA such as SGTE (contains around 78 elements), SGSOL (contains multicomponents), MTSOL (alloy solution database), MTAL (Al-base alloys), TCNI (Ni-base alloy), NPLOX (contains liquid oxides), MTOX (optimise model of silicate melt containing a range of oxides) and AQDATA (contains over 450 ionic and neutral complexes species), where the selection between them relates to the type of study. In addition, MTDATA allows users to link the programme with third party software like kinetics, fluid flow, plant simulation, databases and management packages [Davies et al., 2005]. Huang et al., [2008] demonstrated the computational interface to enable a linkage between MTDATA, MATLAB (mathematical) and COMSOL (multiphysics) software packages. They concluded that the routine calculations in MTDATA can be conducted within MATLAB, COMSOL and combined MATLAB-COMSOL environments.

2.6.2 Thermodynamic equilibrium calculation studies

There are ongoing research activities in the fields of biomass thermo-chemical conversions technologies using thermodynamic equilibrium calculations (e.g. modelling of the behaviour of alkali metals, the formation of low melting compounds as well as the behaviour of heavy metals), but they are very limited and almost no previous study has considered the interactions between major and multiple minor coal (or biomass) elements.

Coals contain: major elements (C, H, N, O, S, Cl), with a concentration range usually of >1000 ppmw; minor elements (Si, Al, Fe, Ca, Mg, K, Na, Ti, Ba, Mn, P), with a concentration range usually of 100-1000 ppmw; and trace elements (almost all the other elements of the Periodic Table), with a concentration range of < 100 ppmw [Miller et al., 2002; Ratafia-Brown 1994]. Frandsen et al., [1994] reported the interest in studying the behavior of minor coal elements during coal combustion is due to their effects on the ash formation, particle emission and on the partitioning of trace elements between flue gases and condensed phases. Yan et al., [1999] stated that most previous studies neglected the interactions between minor coal elements during combustion because of insufficient thermochemical data. They reported that in order to simulate the

coexistence of any element in the combustion zone and obtain its most reasonable speciation, it is necessary to consider a complex computation system involving all the important elements in coal and their major species, as well as to investigate the interactions between these elements. They used ALEX software [Baronet, 1983] (which includes thermochemical data for about 600 pure condensed, liquid, solid and gaseous components of 30 minor and trace elements) to study the behavior of 10 minor elements during coal combustion under oxidizing conditions in the temperature range 400-2000 K. It was found that the equilibrium calculation was strongly affected by the species initially considered in the system and so it was concluded that all the important chemical species present must be considered; otherwise the output of the equilibrium analysis might be misleading. Daniel, [1991] indicated an equilibrium flue-gas composition and molecular composition of condensate deposits on boiler tubes, for incinerating a refused-derived fuel (RDF). The thermodynamic calculation showed that sodium sulphate and sodium chloride were the predominant compounds to deposit on superheater tubes at 527 °C.

Bradshaw et al., [2008] used MTDATA to identify the volatile trace species produced by gasification of biomass and waste fuels and whether these species could pass through the hot fuel gas path of a gasification system to form surface deposits on hot components within gas turbines. These thermodynamic studies showed that some trace species could pass through the gasifier fuel gas path to produce deposits in the gas turbine. However, the locations of these deposits in the gas turbines were limited by their dewpoints at that point in this power system. Along with alkali metal sulphates/chlorides, they identified trace species of $CdSO_4$, $PbSO_4$ and SbO_2 at metal temperatures of 640-800 °C, 730-1020 °C, 700-910 °C respectively, as having the potential to initiate the hot corrosion at species locations in the gas turbines.

Goni et al., [2003] used the MTDATA program combined with the NPLOX database for coal ash oxides composition (SiO_2-Al_2O_3-CaO-FeO-MgO and K_2O) during work on coal blend combustion. They compared the model predictions to data from ash samples (bottom and fly ashes) obtained as outcomes from three power plants in Chile. Ash samples were observed mineralogically by X-ray diffraction (XRD) and

morphologically by scanning electron microscopy (SEM). According to their conclusion, the dominant crystalline phases detected by XRD of fly ashes and bottom ashes were similar (containing mullite, quartz, plagioclase, hematite and anhydrite) which agreed with results obtained in MTDATA modelling. Also MTDATA evaluations of the proportion of liquid phase generated by each type of coal (depending on the oxide composition) at 1250 °C gave the same results as obtained from SEM observations.

Gibbs et al., [2008] used MTDATA combined with the MTOX database to predict the formation of an oxide melt from the combustion of as-supplied Binungan coal, and as-supplied and cleaned Gascoigne Wood, El Cerrejon and Harworth coals. They studied the partitioning of the elements Ba, Be, Cd, Co, Mo, Nb, Sb, V, and W during combustion by model predictions and compared these with bottom and fly ash analysis results obtained from a pilot scale combustor (by PowerGen, in the UK). It was predicted that the amount of melt fell more rapidly with falling temperature for cleaned fuels than for as-supplied fuels. They concluded that the mobilities of the elements concerned agreed with those implied by the ratio of bottom ash and fly ash concentrations found in the experimental industrial pilot-scale combustor.

Miller et al., [2002] used MTDATA to predict the speciation of individual trace elements during the co-combustion of coal with biomass fuels and compared the predictions to experimental data. They used coal (Polish and Colombian) and biomass (wood-bark, straw, pulp sludge, paper sludge, agricultural waste, sewage sludge, and plastic waste) in bench-scale fluidised co-firing experiments. It was found that the emissions of trace elements associated with the ash constituents could increase or decrease from co-firing fuel mixtures based on the blends and it was concluded that MTDATA was useful for interpreting the experimental results. It was found that the most volatile trace elements were Hg and Se, followed by Cd, Ti, Pb, and As. For example, complete Se volatilisation (as SeO and SeO_2 in the gas phase) was predicted by the MTDATA model for all the fuels and blends used in the study. In another example, MTDATA predicted Pb would be partially volatilised (due to $PbSO_4$ formation) during combustion of Colombian coal, Colombian coal/straw, or Polish

coal/sewage sludge at 800 °C, but Pb would be completely volatilised (as Pb, PbO and $PbCl_2$ in the gas phase) for other fuel mixtures.

Otsuka, [2002] used the thermodynamic database MALT 2 software package developed by National Chemical Laboratory (in Japan) [Kagaku Gijutsu-Sha, 1992], to understand the fireside corrosion of tube materials for boilers firing dirty fuels. The flue-gas composition and deposition/condensation of fuel impurities, such as Na, K, Cl and S, on tube surfaces were estimated by thermodynamic equilibrium calculations. The results showed that for boilers firing municipal solid waste fuel, the flue-gases at 650-1000 °C and condensate deposit species formed on metal surface at 600 °C, contained NaCl and KCl along with ZnO The equilibrium calculations indicated sodium and potassium sulphates as deposit condensates for boilers firing high-Cl, high-S coal as with flue-gases at 1100-1200 °C and metal surfaces at 600 °C. Also for boilers firing black liquor fuel, mixtures of potassium and sodium chlorides, sulphates and carbonates were predicted for 600 °C metal surface temperatures and flue-gases at 1000 °C. It was concluded that the amount of Cl, S, K, Na, Pb and Zn in fuels together with other metals such as Ca, Mg must be examined by equilibrium calculation to interpret the deposit chemistry on boiler tubes surfaces. However, the programme used allows the calculation of thermodynamic equilibria containing up to 10 elements.

2.7 Deposition formation/mechanisms

Deposits formed were determined by model development studies by a number of researches (e.g. Baxter 1993; Baxter and Desollar, 1993; Rosner and Tandon 1995; Huang et al., 1996; Wessel and Righi 1988; Tomeczek et al., 2004; Zhou et al. 2007). Deposits form as a result of both physical and chemical processes and involve at least five mechanisms [Baxter, 1993]:

- Inertial impaction
- Condensation
- Thermophresis
- Eddy impaction
- Chemical reaction

Each mechanisms has a specific driving force in sequence of momentum, temperature gradient, vapour pressure of alkali salt vapours, turbulence intensity and species concentration gradients. This leads to a large variety of parameters controlling each mechanism.

2.7.1 Inertial impaction

Inertial impaction is the primary source of deposition on heat exchanger boiler tubes. At the start (i.e. when the probe is clean), vapours and fine particles which arrive at the probe surface in a sticky condition can contribute to the initial deposit formation [Zhou et al., 2007]. Inertial impaction contributes to the deposit build up following initial formation where large ash particles (≥ 10 μm) are most likely to be deposited. Large particles can gain enough momentum towards the tube to overcome the drag forces of the flow gas, which direct particles to pass through the boundary layer, stagnation zone and impact the tube on a coarse deposit form (as can be seen in Figure 2.10). The impaction capture efficiency depends on the propensity of these particles to stay on the surface once they impact and the surface properties (like roughness of metal surface, surface tension).

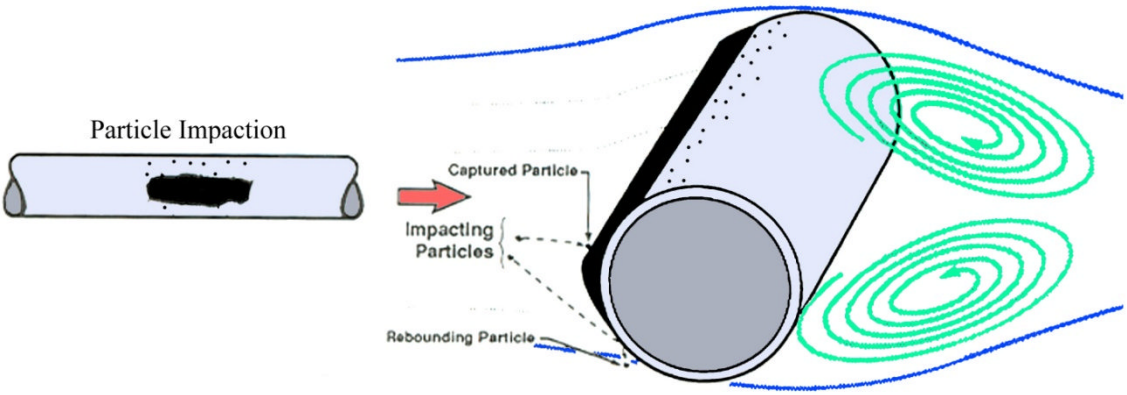

Figure 2.10 Inertial impaction mechanism
Source: [Baxter and DeSollar, 1993]

Zhou et al., [2007] used the following equation to model the large particle inertial impaction rate on the upstream side of the probe (which is a function of mass concentration of fly ash, gas velocity and fraction captured when collision on the surface occurred);

$$I_f\,(t,\theta) = u_f * C_{ash,\,I} * \eta_I * f_{stick} * s \qquad \textbf{Eq. 2.4}$$

Where,

$I_f\,(t,\theta)$= Inertial deposition rate,

u_f = the bulk gas velocity,

$C_{ash,\,I}$ = the mass concentration of the large fly ash particle,

f_{stick} = the total sticking coefficient,

s = surface area at the angle section $\Delta\theta$.

2.7.2 Condensation

The condensation mechanism is where vapours (often alkali compounds) are collected on heat transfer surfaces. Vapour will condense on the tube if the partial pressure of a vapour at the relatively cold temperature of a tube exceeds the vapour pressure (see Figure 2.11). Condensation contacts the metal surface more efficiently than inertial impacted deposits and is favoured at the leading edge of tubes because of the high degrees of heat and mass transfer compared to the trailing edge. The vapour pressure of alkali chlorides depends on the concentration of the chlorides in the gas phase, thus condensation of alkali salts also governed by the mass fraction of the salts in the fuel. The deposits formed were described as uniform and finely texture [Baxter and Desollar, 1993].

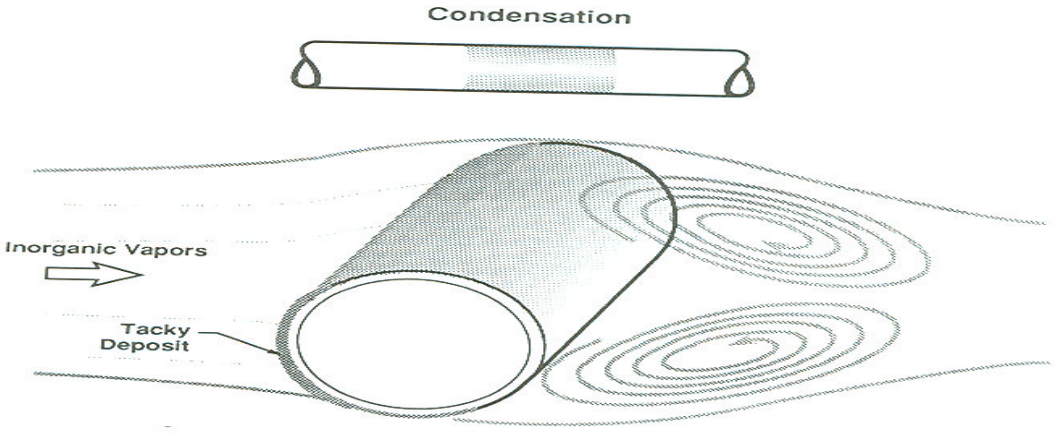

Figure 2.11 Condensation mechanism
Source: [Baxter and DeSollar, 1993]

2.7.3 Thermophoresis

The thermophoresis mechanism is the process of particle motion in the flue gas which relies on the local temperature gradient. When the temperature difference between the heat transfer surface and the flue gas is large enough, then the particles will be suspended in the direction opposite to that of temperature gradient (see Figure 2.12) [Baxter and Desollar, 1993]. Also, thermophoresis can act in the direction of the temperature gradient (under certain conditions) and in the particle itself [Baxter and Desollar, 1993; Tomeczek et al., 2004]. The deposits formed were described as finer grained (submicron particles) texture with more distribution capability around a tube surface than inertial impaction deposits and not tacky like condensation deposit [Baxter and Desollar, 1993]. Deposit accumulation on the tube surface decreases the temperature gradient between the flue gas and the tube surface, which decreases the thermophoresis deposition rate.

Zhou et al., [2007] stated that submicron particles such as KCl and K_2SO_4 may still be formed even under certain conditions which they presume not (e.g. when the flue gas temperature is higher than 1273 K) if a low temperature layer presents at the heat transfer surface (i.e. when the temperature difference between the heat transfer surface and the flue gas is huge).

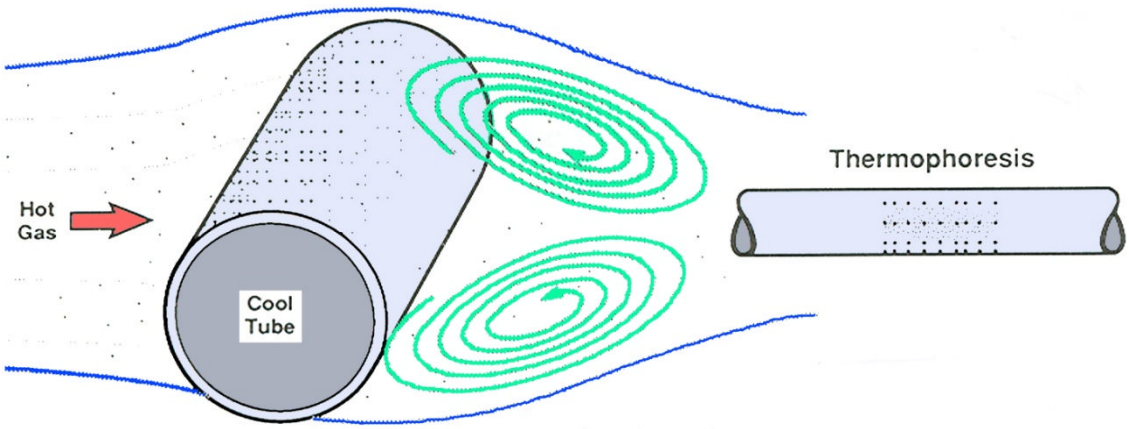

Figure 2.12 Thermophoresis mechanism
Source: [Baxter and DeSollar, 1993]

2.7.4 Eddy impaction

The eddy impaction mechanism involves fine ash particles that are entrained in turbulent eddies where these eddies have enough momentum to impact on tube surface, although they would be too small to impact (based on average gas velocities). Given that turbulent eddies are difficult to describe, the mechanism is less understood and it related mainly to empirical coefficient [Wood, 1981; Yang et al., 2008].

2.7.5 Chemical reaction

Various chemical reactions between the flue gas and either the existing deposits or the deposit surfaces can act to add or remove mass. The conversion rate depends on the chemical kinetics reactions employed and on mass transfer rates to the surface. The most important chemical reactions involved (with respect to deposition) are sulphation, alkali absorption (e.g. silica absorbs alkali material to form silicate (SiO_3^{-2}) in which can induce sintering and significant changes in the deposit properties) and oxidation. Reactions from alkali absorption are slow comparative to sulphation [Baxter, 1993].

2.7.6 Other mechanisms

There are several other mechanisms of deposit formation such as Photophoresis, Electrophoresis and Brownian motion, but there is not enough evidence that suggests these mechanisms contribute significantly in deposit growth in boiler heat exchanger tubes.

Kaufmann et al., [2000] examined Electrophoresis and Brownian motion mechanisms for their theoretical contribution to the deposit growth from combustion of herbage-grass, miscanthus and wood under two different levels of the excess air ratio. Brownian is a motion (diffusion) of small particles, which can reach the tube surface randomly through molecular diffusion. Electrophoresis is a motion of particles $\leq 0.1\mu m$

influenced by electrostatic forces of the surrounding particles (where particles in the flue gas of combustion system are only weakly charged due to the diffusion of ions to the particle surface and possibly to electron exchange at fluid-solid interfaces) and surfaces. They conclude that no important particle transport effect was contributed by Electrophoresis and Brownian motion.

2.7.7 Deposit growth rates

The deposit build up rate based on these mechanisms can be expressed as [Baxter, 1993; Lokare, 2008]:

$$\frac{dm}{dt} = I*G + C + T + E + R \qquad \textbf{Eq. 2.5}$$

Where,

m = deposit weight,

t = time,

I = inertial impaction rate,

G = capture efficiency,

C = condensation rate,

T = thermophoresis deposition rate,

E= eddy impaction rate,

R = chemical reaction rate.

Deposit build up was also classified into inner layer, upstream and downstream as a result of these mechanisms. Inner layer consists mainly of condensed matter at high temperature and flow velocities, whereas small particles of about $\leq$ 5μm dominate the layer composition at low temperature. Upstream deposits growth is mainly by inertial impaction (directly onto surface) of large particles with the inner layer formed by thermophoresis deposition. Downstream deposits enlargement by inertial impaction of small particles (due to recirculation of flow) with inner layer formed by thermophoresis deposition [Allan et al., 1996].

2.8 Concluding remarks

It is clear from the literature reviewed above that the fly ash and gaseous emissions that occur from biomass combustors, and biomass and coal co-firing, are complex phenomenon as they can be influenced by combustion technology, process conditions and fuel properties. Another major focus of R&D activities is on solving problems concerning deposit formation in the heat exchanger sections to ensure that biomass combustion and co-combustion with coal are realistic alternatives for large-scale power plant. Available data about these critical issues are still limited for various biomass fuels. Therefore it is necessary to thoroughly investigate emissions (ash and gaseous) data from a wide range of biomass fuel-combustion technology combinations.

By combining modelling with experiments (as suggested by Van Loo and Koppejan, 2008), improved designs of combustion and co-combustion systems can be achieved, making it is possible to get reductions in emissions (flue gas) and/or corrosion/deposition.

The use of models such as thermodynamic equilibrium calculations (e.g. the behaviour of alkali metals, the formation of low melting compounds) results in a deeper understanding of processes with regard to emissions and deposition, which may provide a basis for the development of appropriate technological prevention measures.

The available literature includes few thermodynamic research studies attempting to model deposition during thermo-chemical biomass conversions. In addition, there are still gaps in the information available on thermodynamic and physical properties of certain elements, interactions between elements, compounds and especially multi-component/multiphase systems. This complicates the simulation of chemical reactions and processes at high temperatures, as well as models of deposit forming elements in biomass conversion processes. Consequently, further expansion and improvement of basic data is necessary.

CHAPTER 3 METHODOLOGY

This chapter presents an outline of the methods and means used to carry out the modelling (which includes calculation procedures) and the experimental set-up work (which includes the combustor operating procedures, fuels selected, feeding systems and its performance, as well as methods of analysis of gaseous emissions and deposition) for coal/biomass combustion.

Details of the preliminary studies presented here for both modelling and experimental activities show that the methodology employed was well controlled.

3.1 Modelling

3.1.1 Prediction of combustion products

Combustion product predictions were prepared for each of the tests. Stoichiometric or theoretical combustion is the ideal combustion process where fuel is burned completely, but in reality excess air is used to ensure total combustion. Combustion product prediction for combustion can be based on the mass flow rates of air, gas and fuel, together with the air, gas compositions and fuel mass fractions of carbon (C), hydrogen (H), oxygen (O), nitrogen (N), sulphur (S), chlorine (Cl) (as these are the major elements in all fuels) along with ash (A) and moisture (W) content. For stable combustion conditions, fuel particles are in contact with air, and the ratio of air to fuel is an important parameter controlling the combustion atmosphere [Van Loo and Koppejan, 2008].

The combustion process can be expressed as:

$[C + H + O + N + S + Cl\ (fuel)] + [O_2 + N_2\ (Air)] + [C + H_4\ (Gas)] \rightarrow (Combustion\ Process) \rightarrow [CO_2 + H_2O + N_2 + O_2 + SO_2 + HCl + (Heat)]$ **Eq. 3.1**

In theory there is a specific amount of air is needed to completely burn a given amount of fuel, whereas in practice, burning conditions are never ideal. Therefore, more air than

ideal must be supplied to burn all the fuel completely. This amount of air more than the theoretical requirement is known as excess air**.** If an insufficient amount of air is supplied to the burner, then the results may indicate unburned fuel, soot, smoke, and carbon monoxide exhausted from the boiler. This may cause heat transfer surface fouling, pollution, lower combustion efficiency, excessive corrosion, safety issues (from CO), flame instability and a potential for explosion. Also, this excess air provides protection from insufficient oxygen conditions caused by variations in fuel composition and produces an acceptable range air to fuel ratio (A/F). It should be pointed that when the air content is higher than the stoichiometric ratio, the mixture is said to be fuel-lean, whereas if air content is less than the stoichiometric ratio, the mixture is fuel-rich.

Generally, power plant pulverised coal-fired boilers run at about 10-20 % excess air. Depending on the type of the fuels, excess air can be as high as 100 % in other types of combustion systems (e.g. stoker semi-anthracite coal-fired boilers) [Van Loo and Koppejan, 2008]. In practice, this can be controlled by knowing the amount of the percent volumes of oxygen in the output gas streams. Appendix A1 shows the approximate values for CO_2 and O_2 in the flue gas as result of excess air for different fossil fuels combustion.

For this project, in order to run the combustion experiments in an acceptable range (i.e. air to fuel ratio (A/F)), a spreadsheet was created for prediction of combustion products (CP – for combustion product prediction) calculations. An example of combustion calculation and spreadsheet created is described in Appendix A2. The main purpose for the spreadsheet was to quantitatively relate fuel flows to the major gas products of combustion (i.e. CO_2, H_2O, N_2, O_2, HCl and SO_2) and to determine the excess air. It was preferred to have the percent volumes of oxygen output of 4.0 – 5.0 % for pulverised fuels (e.g. coal/CCP) and fast pyrolysis bio-oil, whereas around $\leq$ 10.0 % volume of O_2 output for pellets fuels (e.g. oil-seed rape straw pellets).

An example of for combustion product predictions (CP) for fuels combustion/co-firing used in this project are given in Appendix A3.

3.1.2 Heat generation prediction

The first law of thermodynamics is used to balance the energy input and output of the combustor for the heat generation prediction model. For a steady state process, the first law of thermodynamics is simple stated as;

Energy input = Energy losses + Energy output **Eq. 3.2**

Each part of the foregoing equation is calculated for the combustor as following;

Energy input

- Energy input with combustion air: the temperature of the pre-heated air entering the combustor could be high and so a significant amount of energy could be added via this route. The preheated energy is an energy difference between air temperature and ambient conditions calculated by enthalpy expression (h) for each gas species air and the molecular mass. This amount of (heat) energy is then calculated as;

  $Q_a = m_a (h_{a@T} - h_{a@25\ oC})$ **Eq. 3.3**

- Energy input of the fuel: the energy input of each kilogram of fuel is equal to its higher heating value (it should be pointed out that this is based on the assumption of complete combustion and assumed also, that the water formed is in the liquid phase and it does not account for the energy requirement of vaporisation of the moisture content in the fuel). The total energy input of the fuel is then equal to:

  $Q_f = m_f\ HHV_{(as\ rec.)}$ **Eq. 3.4**

The total rate of energy input of the combustor is then calculated as;

$Q_{in} = Q_a + Q_f$ **Eq. 3.5**

Energy losses

The energy that is either lost to the environment or not used to increase the temperature of the flue gas is treated as energy loss. Such losses include radiation loss, energy used for the evaporation of water formed during combustion, energy used for the vaporisation of moisture content of the fuel, energy loss due to generation of carbon monoxide (instead of carbon dioxide), energy loss due to loss of fuel (unburned carbon), and energy used to heat the ash in the fuel [Van Loo and Koppejan, 2008].

- Radiation loss: A constant value of 2 % of the fuel energy input is assumed to lost by combustor radiation. Two percent is a value typical of industrial sized combustors.
- Energy loss due to unburned carbon: For each kilogram of carbon that is burnt to carbon dioxide, 34910 kJ of heat is released. For each kilogram of carbon that is not burnt (leaves the boiler as particulate or remains in the ash), this amount of energy is lost. The rate of energy loss due to unburned carbon is;

$$Q_{unburned} = m_{unburned\ c}\ (34910\ kJ/kg) \qquad \textbf{Eq. 3.6}$$

- Energy loss due to formation of carbon monoxide: Each kilogram of CO generated there is a loss of 10102 kJ. The heat loss rate due to generation of CO is then calculated as;

$$Q_{CO} = m_{CO}\ (10102\ kJ/kg) \qquad \textbf{Eq. 3.7}$$

- Energy loss due to heating of the ash: The amount of ash carried with the fuel into the combustor leaves the combustor with the ash and is discharged at approximately the same temperature as the flue gas. The energy consumed to heat the dirt is a loss since it is not used in raising the temperature of the flue gas. The energy loss is calculated as;

$$Q_{ash} = m_{ash}\ C_{ash}\ (T_{com}-T_{amb.(25oC)}) \qquad \textbf{Eq. 3.8}$$

- Energy used to vaporise the water formed during combustion: The higher heating value is the amount of heat released during the complete combustion of fuel. The heat of vaporisation of water at 25 ^{o}C at 1 bar pressure is approximately 2441.8 kJ/kg of water. Therefore, the rate of energy required to vaporise the water formed during the combustor is;

$$Q_{H2O} = m_{H2O} (2441 \text{ kJ/kg}) \quad \textbf{Eq. 3.9}$$

The total heat loss of combustion is obtained by adding all the aforementioned heat losses and then calculated as;

$$Q_{loss} = Q_{rad.} + Q_{unburned\ C} + Q_{CO} + Q_{ash} + Q_{vap.} \quad \textbf{Eq. 3.10}$$

Energy output

The flue gas leaving the combustor at high temperature is the only stream that carries useful heat outside the combustor. The rate of heat output is calculated as;

$$Q_{out} = m_{out} (h_{out@Tcom} - h_{ref.@25oC}) \quad \textbf{Eq. 3.11}$$

Where Q_{out} is the rate of heat content of the flue gas, m_{out} is the mass rate of flue gas; h_{out} is the enthalpy of the flue gas (calculated at flue gas temperature and composition).

Then the heat generation (HP) equation can be written as;

$$Q_a + Q_f = Q_{rad.} + Q_{unburned\ C} + Q_{CO} + Q_{ash} + Q_{vap.} + Q_{out} \quad \textbf{Eq. 3.12}$$

A spreadsheet has been constructed where the information and equations mentioned above were used to calculate the energy entering and leaving the combustor. An example of heat generation predictions for fuel (of pure, blend and pellets) combustion/co-firing used in this project are given in Appendix A4.

3.1.3 Thermodynamic equilibrium

3.1.3.1 The application of MTDATA

Thermodynamic equilibrium modeling of major elements (C, H, N, O, S, Cl) and minor elements (Fe, Ca, Mg, K, Na, Ti, Ba, Mn, P) to indicate their partitioning behaviour on a chemical equilibrium basis for the combustion of selected fuels (at the conditions of the pilot-scale experiments) has been carried out using MTDATA software package [National Physical Laboratory, Teddington, London, UK]. This software (which uses free energy minimisation) calculates the equilibrium species for a range of defined inputs (the gas phase was modeled as an ideal gas and the condensed phase as pure substance). The MULTIPHASE module in MTDATA combined with the SGTE (Scientific Group Thermodata Europe) database has been run to predict compositions over the temperature range from 200 to 1300 °C in steps of 20 °C at atmospheric pressure.

The stability of many of the species identified in the initial search was marginal, and the calculation time impracticably long. Judgement therefore needed to be exercised on whether to include each species. In the case of the major elements (C, H, N, O, S, Cl), the species included were known from prior knowledge to be present in the fuel gas of the combustion system. In the case of the minor elements (Na, K, Fe, Ca, Mg, Ti, Ba, Mn, P, Al, Si) there were few experimental data on speciation for many of them. The protocol adopted was therefore to assume a notional composition (for all the elements with the conditions of the experimental combustor used) and to perform a sensitivity analysis of the equilibrium composition. Element species found to be formed at all concentrations were included in a simplified database. The relevant simplified database was then used to calculate the equilibrium composition for specific element in each test.

3.1.3.2 Calculation protocol

In order to ensure that all relevant species were included in the calculation, an initial search of SGTE database for species containing one or more of the input components was conducted. Further study was to look at the sensitivity of the calculations to

changes in the input elements used, the predictions of the software with three different groups of elements was investigated:

- Firstly calculations were carried out to investigate the interactions between two minor elements, Na and K, with the six major elements (subsequently referred to as the "8 elements system"), in order to obtain a baseline for the major species predicted for a relatively simple idealized combustion system.
- Secondly, the outcome from a complex system was investigated by including the six major elements with nine minor elements i.e. Na, K, Fe, Ca, Mg, Ti, Ba, Mn, P (subsequently referred to as the "15 elements system"). This was carried out to find the predicted interactions between low levels of the minor elements during cooling of the combustion gases.
- Finally, calculations were carried out that included the six major and eleven minor elements, to find out how the inclusion of Si and Al affected the calculations outputs (subsequently referred to as the "17 elements system").

The results showed that inclusion of all the major and minor elements except Si and Al (i.e. "15 elements system") lead to realistic model outputs when considering prediction of fate of the trace elements (in terms of gas phase and condensed phases) present in fuel combustion. The Si and Al compounds in the fuels are believed to be generally more stable and so this is not an appropriate modelling route to use for them; they reach the heat exchanger surfaces by other deposition routes. Also, check calculations were done to perform a sensitivity analysis of the equilibrium composition to the parameter impact of the excess air (within the percent volumes of oxygen output of 4.0 – 11.0 %) change. This showed no significant impacts. Preliminary study section 3.1.4.2 explained in more details the results outcome of the predictions/sensitivity studies.

Also, it was found that including data on all possible compounds in the defined systems resulted in extremely large data-files and long computational times. Careful investigation of the generated outputs showed that this was due to the systems containing many possible compounds that are unlikely to form that required MTDATA to effectively calculate zero values for (in agreement with the study by Miller et al.

2002). Therefore, to reduce both the size of the data-files and the time taken for the calculations, the compounds that were found not to form in initial trial runs were eliminated as potential outputs from subsequent calculations. As a result of this, lists of potential compounds, in both the gaseous and condensed states, were created for each element included in the calculations (Table 3.1).

A molar composition for each test was defined next, based upon the pilot-scale experimental measured composition. For combustion/co-firing tests, the amounts of the major and minor elements are numerically equivalent to the hourly mass flow rate under predition of combustion products for each test. Full details of the molar compositions used are given in Appendix A5.

3.1.3.3 Validation

Where any significant proportion of trace elements had been detected experimentally in the gas phase, the predictions of MTDATA were validated by comparing the predicted amounts with the measured level. Species of the most abundant elements (in gaseous and condensed form) found to be formed above a fraction of 10^{-3} were identified. However, as the parameters were varied across the range of the experimental conditions/fuel compositions, the amount of species above a fraction of 10^{-6} were included for such exposures.

Table 3.1 Species selected for thermodynamic modelling after initial screening calculations (the MTDATA format of elements in chemical formula a has been retained)

Elements	Condensed species	Gaseous species
C	C, CNa_2O_3, CTi	C, CO, CO_2, CH, CHO
H	HK, HKO, H_2Mg, HNa, HNaO, H_2O, H_2O_2, H_2O_4S	HCl, H, H_2, HK, HKO, $H_2K_2O_2$, HMg, HMgO, H_2MgO_2, HMn, HMnO, HN, H_2N, H_3N, HNO, HNO_3, HNa, HNaO, $H_2Na_2O_2$, HO, HO_2, H_2O, H_2O_2, H_2O_4S, HP, HS, H_2S, H_2S_2, HSi, H_2Si, HP, HOP
O		O, O_2, OTi, OP
N		N, N_2, NO, NO_2, N_2O
S	S, STi, S_2Ti	S, SO, SO_2, SO_3
Cl	ClFeO, Cl_2FeO, ClHMgO, Cl_2H_2MgO, $ClKO_4$, Cl_2Mg, Cl_2Mn, $ClNaO_4$, Cl_2Fe, $ClKO_4$, $ClNaO_4$, ClOTi	Cl, ClFe, Cl_2Fe, Cl_3Fe, Cl_4Fe_2, ClFeO, ClHO, $ClHO_3S$, ClMg, Cl_2Mg, ClMn, Cl_2Mn, ClNO, ClO, ClTi, Cl_2Na_2
Si	Si, Si_2ON_2, SiO_2	Si, Si_2,Si_3, SiO, SiO_2, Si_2O_2
Al	$AlKO_4Si$, $AlKO_6Si$, $Al_2O_7Si_2$, AlO_4P, $AlNaO_4Si$, Al_2BaO_4, $AlCaO_4$, Al_2FeO_4, $AlKO_2$, Al_2O_3	Al, Al_2, AlC, AlC_2, AlCl,$AlCl_2$, AlClH, AlO, AlClO
Fe	Fe, $FeHO_2$, $Fe_2H_2O_2$, FeH_2O_2, FeH_3O_3, $Fe_2H_2O_4$, $FeKO_2$, $Fe_2K_2O_2$, FeK_4O_3, Fe_2MgO_4, Fe_2MnO_4, $FeNaO_2$, FeO, Fe_2O_3, Fe_3O_4, FeO_4S, FeO_4S, FeSi, $FeSi_2$, FeO_3Si, FeO_3Ti	Fe, Fe_2, FeH, FeHO, $FeHO_2$, FeH_2O_2, FeO, FeO_2, FeS
Ca	Ca, $CaCO_3$, $CaCl_2$, $CaCl_2O$, $CaFe_2O_4$, $Ca_2Fe_2O_5$, $CaMg_2$, $CaMgO_2$, CaO, CaO_2, CaS, $CaSO_3$, $CaSO_4$, CaO_3Ti	Ca, Ca_2, CaCl, $CaCl_2$, CaClHO, CaH, CaHO, CaH_2O_2, CaO, CaO_3, CaS
Mg	Mg, MgO, MgO_4S, MgO_3Ti, MgS, MgO_3Si	Mg, Mg_2, MgO
K	KCl, K, KNO_2, KNO_3, KO_2, K_2O, K_2O_2, K_3O_4P, K_2O_3S, K_2O_4S, K_2S, K_2O_3Si	KCl, K, K_2, K_2Cl_2, KNO_2, KNO_3, KNa, KO, K_2O, K_2O_2, K_2O_4S
Na	NaCl, Na, $NaPO_3$, Na_2CO_3, NaO_2, Na_2O, Na_2O_2, Na_2O_3S, Na_2O_4S, Na_2O3Ti, NaS, Na_2O_3Si, Na_3O_4P,	NaCl, Na_2Cl_2, Na, NaO, Na_2O, Na_2O_2, Na_2O_4S
Ti	Ti	Ti, Ti_2
Ba	BaC_2, $BaCO_3$, $BaCl_2$, BaH_2, BaH_2O_2, BaO, BaO_2,BaO_4S, BaO_3Ti, Ba_2O_4Ti, BaS	Ba, Ba_2, BaCl, $BaCl_2$, BaClHO, BaH, BaOH, BaH_2O_2, BaO, Ba_2O, Ba_2O_2, BaS
Mn	Mn, MnO, MnO_2, Mn_2O_3, MnO_4S, MnO_3Ti, MnS, MnS_2, Mn_2O_4Si	Mn, MnO, MnO_2, MnS
P	P, P<red>, P_2S_3	P, P_2

3.1.4 Preliminary study

3.1.4.1 Prediction of combustion products and database on biomass fuel characteristics

Data on the compositions of the fossil fuels selected for this project (e.g. El-cerrejon coal) and biomass (e.g. CCP) were obtained from the fuel supplier (E.ON). Combustion product prediction (CP) and MTDADA analysis used these data provided and hence can be directly compared to the pilot-scale combustion trials.

The IEA (International Energy Agency, Bioenergy Agreement), BIOBIB database (developed by the Institute of Chemical Engineering, Fuel and Environmental Technology at the University of Technology, Vienna, Austria), and Phyllis database (designed and maintained by the Netherlands Energy Research Foundation (ECN), research area Fuels, Conversion & Environment) also have extensive databases on the compositions of samples from biomass fuels and fossils fuels collected from literature and actual installations. The IEA database currently contains 1560 different biomass samples, whereas BIOBIB database contains 647 different biomass fuel samples (covering several minor and trace elements) and are accessible via the internet at www.ieabcc.nl. and www.vt.tuwien.ac., respectively. In addition to data from literature and from the BIOBIB database, Phyllis database contains data on fuels analysed at ECN and are about 2275 data records (updated and extended regularly) and also available on the internet (at: www.ecn.nl/Phyllis.). In Phyllis, the various materials are divided into groups and subgroups in which one type of fuel can be presented with various compositions (i.e. dependent on at, age, moisture content, etc.) and each data record has a unique ID number.

In this project, comparison between the data available on the Phyllis database for such fuels was carried out. For example, miscanthus biomass data were compared to the average of 10 data record at Phyllis (e.g. miscanthus fresh, miscanthus high K, miscanthus silage dried). The results on the average of miscanthus data (from Phyllis) indicated that the moisture content, ash content, S and Cl elements are the major variation with 83.3 % RSD, 49.7 % RSD, 31.5 % RSD, 93.5 % RSD respectively, when it compared to other elemental of C (0.8 % RSD), H (3.1 % RSD), O (1.4 % RSD). Similar behaviour was noticed on most other

biomass fuel (see the results on the average of 10 data recorded at Phyllis for wheat biomass, Appendix B). However, this information (from this type of website) may be helpful for a possible theoretical calculations and/or identify the major variation (in respect to fuels compositions), but missing data on either approximate/ultimate analysis or ash compositions for so many fuels inhibit full investigation. Results used for this purpose are given in Appendix B.

3.1.4.2 Predictions of thermodynamic equilibrium compositions

In the preliminary study, four fuels were selected to perform a sensitivity analysis of the equilibrium composition (under "8, 15 and 17 elements system"). The fuels selected were as follows;

- El-cerrejon coal (100 %, wt),
- CCP (100 %, wt),
- CCP:El-cerrejon coal (20:80 %, wt),
- CCP:El-cerrejon coal (40:60 %, wt)

The equilibrium calculations were performed by considering the elements given in the fuels compositions (Sec. 3.2.1) and the model was used to study the interactions between these elements under A/F ratio combustions of percent volumes with O_2 output of 4.0 %. Table 3.2 shows equilibrium calculations for each selected fuels in the preliminary study entered into the MTDATA module on molar basis.

Figure 3.1 shows a screenshot of MTDATA for Windows with calculated MULTIPHASE speciation diagram for a "15 elements system". Analysis of the output data generated from the modelling was further refined by careful study using spreadsheets.

Table 3.2 Total moles of major and minor elements total moles input in the equilibrium calculation for El-cerrejon coal, Cereal Co-product (CCP) and blends

Molar numbers	Fuel			
	Coal (100 %, wt)	**CCP (100 %, wt)**	**CCP: Coal (20:80 %, wt)**	**CCP: Coal (40:60 %, wt)**
C	57.6138	36.0502	53.3011	48.9884
H	50.0490	66.4748	53.3342	56.61937
O	177.6677	129.7049	168.0620	158.4957
N	723.7845	444.3885	667.8489	612.0825
S	0.1800	0.0500	0.1500	0.1300
Cl	0.0100	0.0500	0.0100	0.0200
Si	0.8686	0.3100	0.7377	0.6165
Al	0.3712	0.0229	0.2750	0.1921
Fe	0.0800	0.0129	0.0622	0.0466
Ca	0.0348	0.0582	0.0464	0.0545
Mg	0.0618	0.0412	0.0596	0.0564
K	0.0423	0.2204	0.1114	0.1638
Na	0.0294	0.0048	0.0229	0.0172
Ti	0.0033	0.0002	0.0024	0.0017
Ba	0.0006	0.0001	0.0004	0.0003
Mn	0.0006	0.0005	0.0006	0.0006
P	0.0025	0.0712	0.0280	0.0476

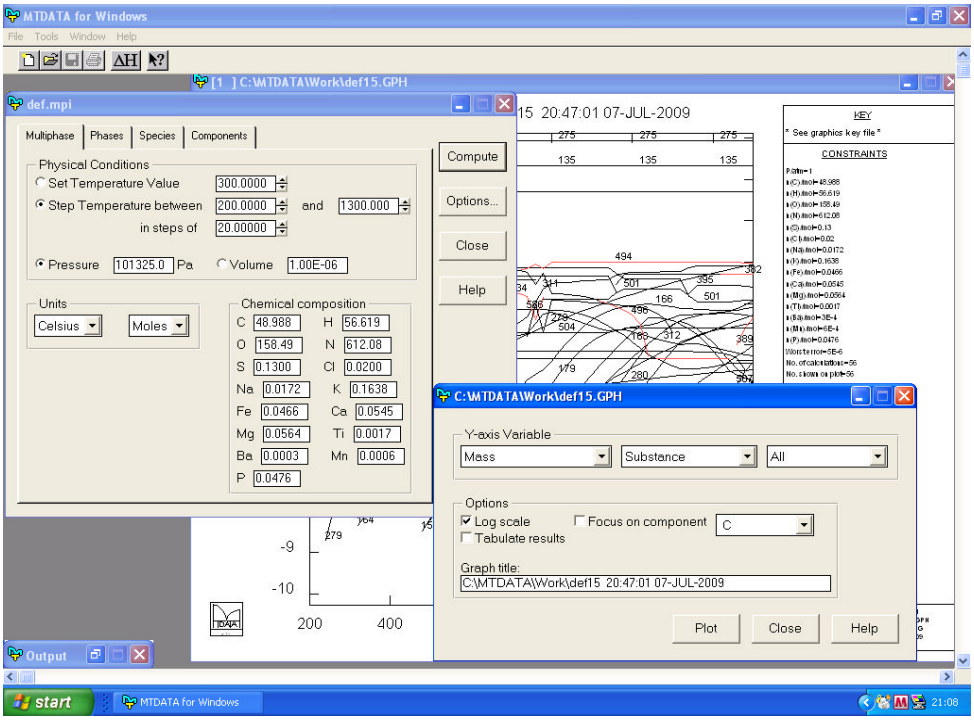

Figure 3.1 Screenshot of MTDATA for Windows with calculated MULTIPHASE speciation diagram under "15 elements system"

3.1.4.2.1 Eight elements system

For these calculations, the pure fuels and the two fuel mixtures were described in terms of two minor elements (Na, K) and the six major elements (C, H, N, O, S, Cl). Figure 3.2 gives example graphs of the outputs obtained for the two pure fuels in terms of the moles of the various compounds as a function of temperature for the combustion products. These graphs illustrate the complexity of the model outputs and so the data produced has been further analysed and split between major and minor gas phases and condensed phases. Flue gases consisted predominantly of CO_2, H_2O, N_2, O_2, HCl and SO_2 upon combustion of all fuels. Figures 3.3 and 3.4 show the percent volume of gaseous species for coal (100 %, wt), CCP (100 %, wt) and blend mixtures fuel of CCP:Coal (20:80 %, wt), CCP:Coal (40:60 %, wt), respectively. The calculated combustion predicted the flue gas composition coal (100 %, wt) of 12.4 volume % CO_2, 5.4 % H_2O, 78.2 % N_2, 4.0 % O_2, 0.001 % HCl and 0.04 % SO_2 (Fig. 3.3.a), whereas the calculation for CCP (100 %, wt) predicted 11.8 % CO_2, 10.9 % H_2O, 73.1 % N_2, 4.0 % O_2, 0.02 % HCl and 0.02 % SO_2 (Fig. 3.3.b). For the fuel blends, the prediction for CCP:Coal (20:80 %, wt) (Figure 3.4.a), was 12.3 % CO_2, 6.1 % H_2O, 77.4 % N_2, 4.0 % O_2, 0.001 % HCl and 0.04 % SO_2, and for CCP:Coal (40:60 %, wt) (Fig. 3.4.b) 12.2 % CO_2, 7.0 % H_2O, 76.6 % N_2, 4.0 % O_2, 0.01 % HCl and 0.03 % SO_2.

The concentration of CO_2, H_2O, N_2 and O_2 did not significantly change at 200-1300 °C for all fuels, but HCl concentration became lower at 820 °C for coal (100 %, wt) and both blend mixtures fuels, SO_2 became higher at 440, 480 and 500 °C for coal (100 %, wt), CCP:Coal (20:80 %, wt), CCP:Coal (40:60 %, wt), respectively. Flue gas concentrations of HCl and SO_2 for combustion of CCP (100 %, wt) start at 1080 °C and 1060 °C, respectively (shown in Figure 3.3.b). Concentration of NO, NO_2, OH, NaOH gaseous becomes higher at higher gas temperatures for all fuels at different dewpoints (e.g. NaOH dew-points at 800 °C and 1040 °C for CCP (100 %, wt) and coal (100 %, wt), respectively). It should be pointed out that concentration of gaseous NaCl and KCl increased at temperature around 820 °C (± 40 °C) for all fuels, except KCl increases at 560 °C for combustion of CCP (100 %, wt). Gaseous Na_2Cl_2 and K_2Cl_2 had a maximum concentration at around 860 °C, 720 °C of CCP (100 %, wt), and around 960 °C, 940 °C

of coal (100 %, wt) and the blend mixtures fuels, respectively. Vapour H_2SO_4 decreased drastically at 200 °C to around 960 °C (dewpoint) of coal (100 %, wt) (shown in Figure 3.2.a) and the blend mixtures fuels, whereas non formed of CCP (100 %, wt) combustion.

The molar quantity of condensed alkali metals (Na and K) in equilibrium with flue gas (200-1300 °C) for combustion of coal (100 %, wt) and CCP (100 %, wt) is shown in Figure 3.5 and 3.6, respectively. It can be seen that Na_2SO_4 and K_2SO_4 were the only condensed species found, being stable over most of the temperature range used (dewpoints of around 1160 °C and 1110 °C, respectively). Condensed Na_2SO_4 was not formed, but condensed sodium carbonate (Na_2CO_3) was found with CCP (100 %, wt) (as shown in Figure 3.6.a). Also, solid KCl (200-700 °C), KNO_3 (200-500 °C) and K_2SO_4 (200-1180 °C) have been predicted for with CCP (100 %, wt) combustion.

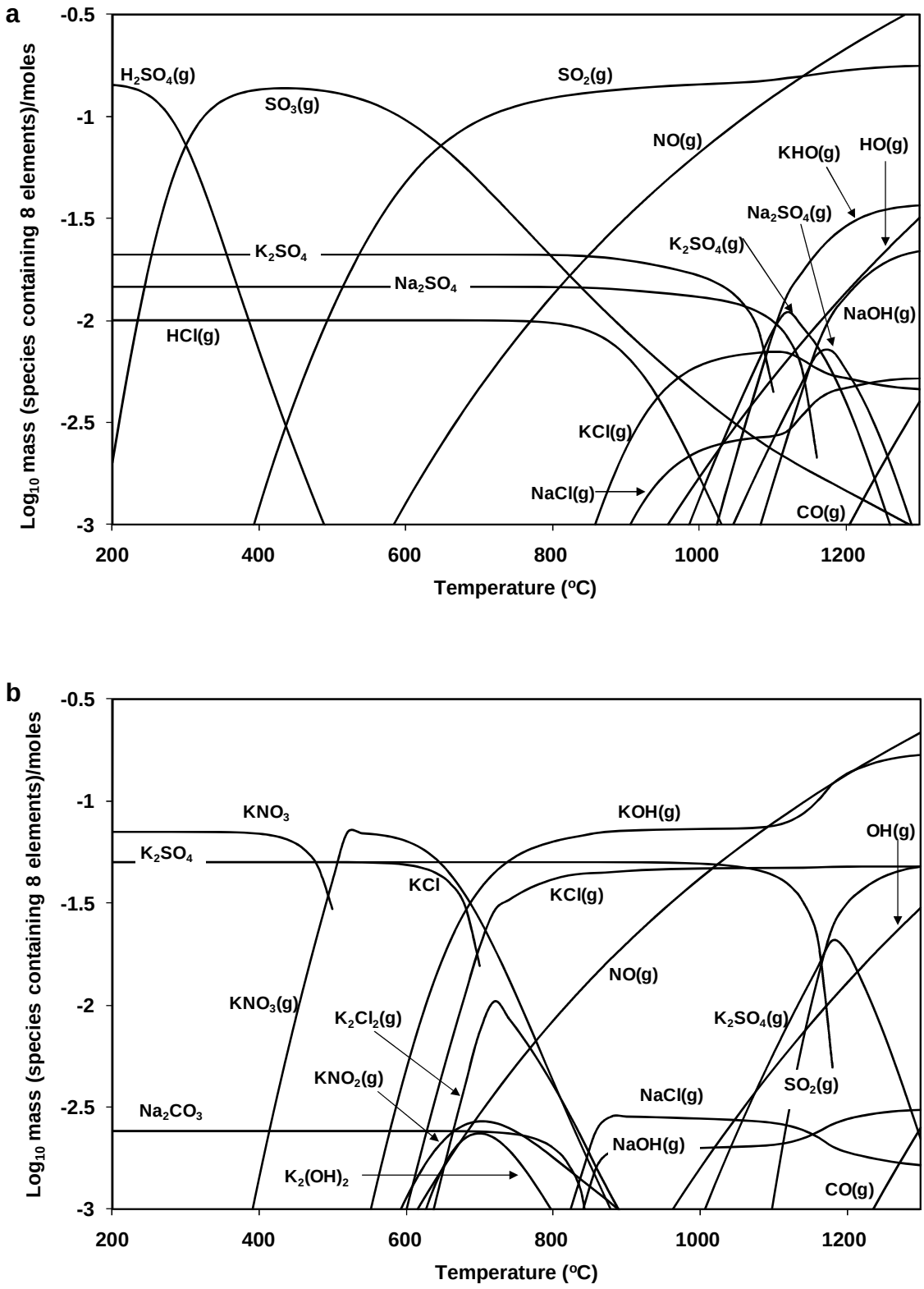

Figure 3.2 Calculated values for gaseous & condensed species produced during the cooling of combustion products from (a) El-cerrejon coal and (b) CCP fuel (based on "8 elements system")

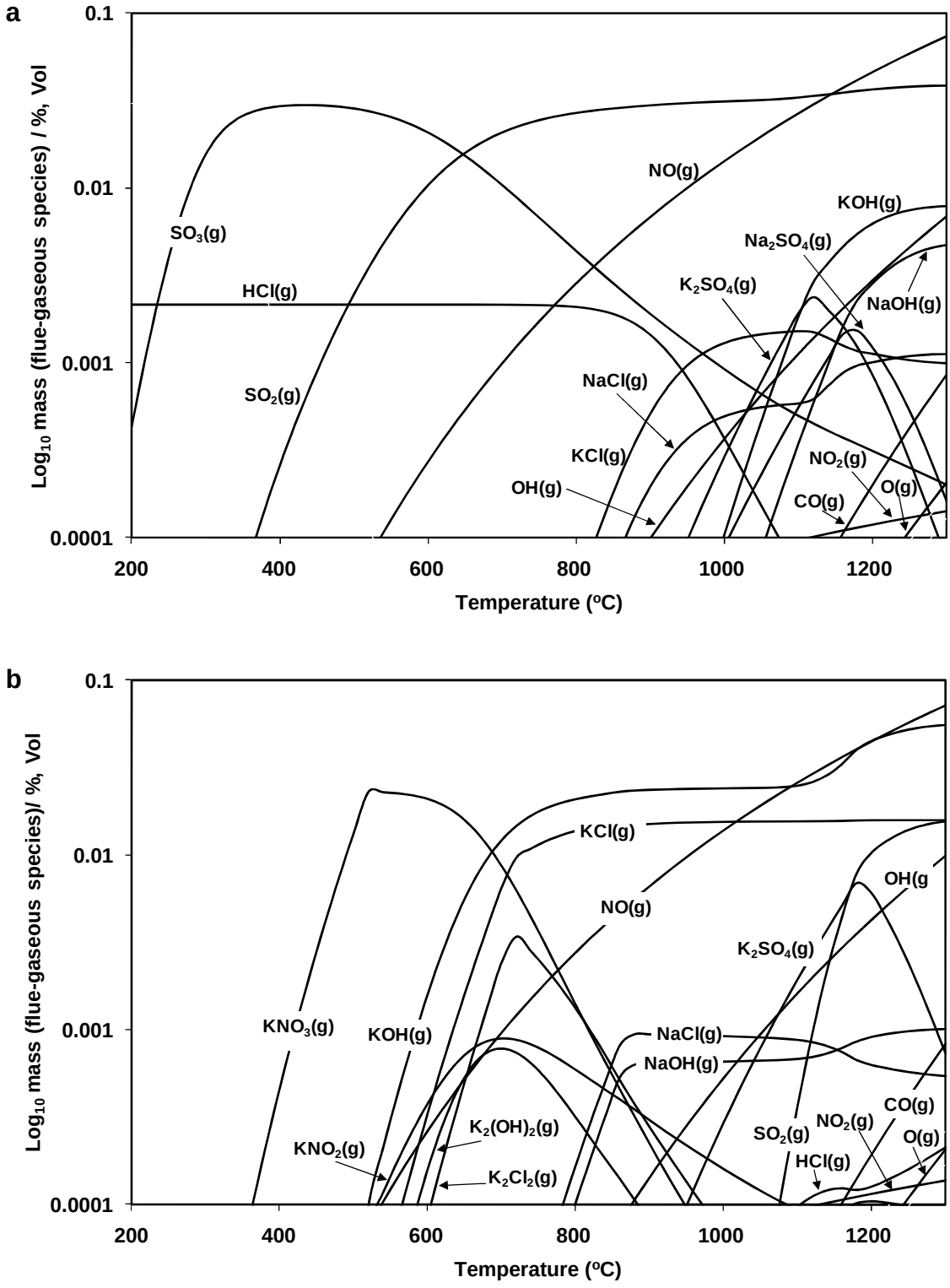

Figure 3.3 Calculated values for gas phase species (in terms of volume %) produced as combustion gases are cooled for (a) El-cerrejon coal and (b) CCP (for "8 elements system")

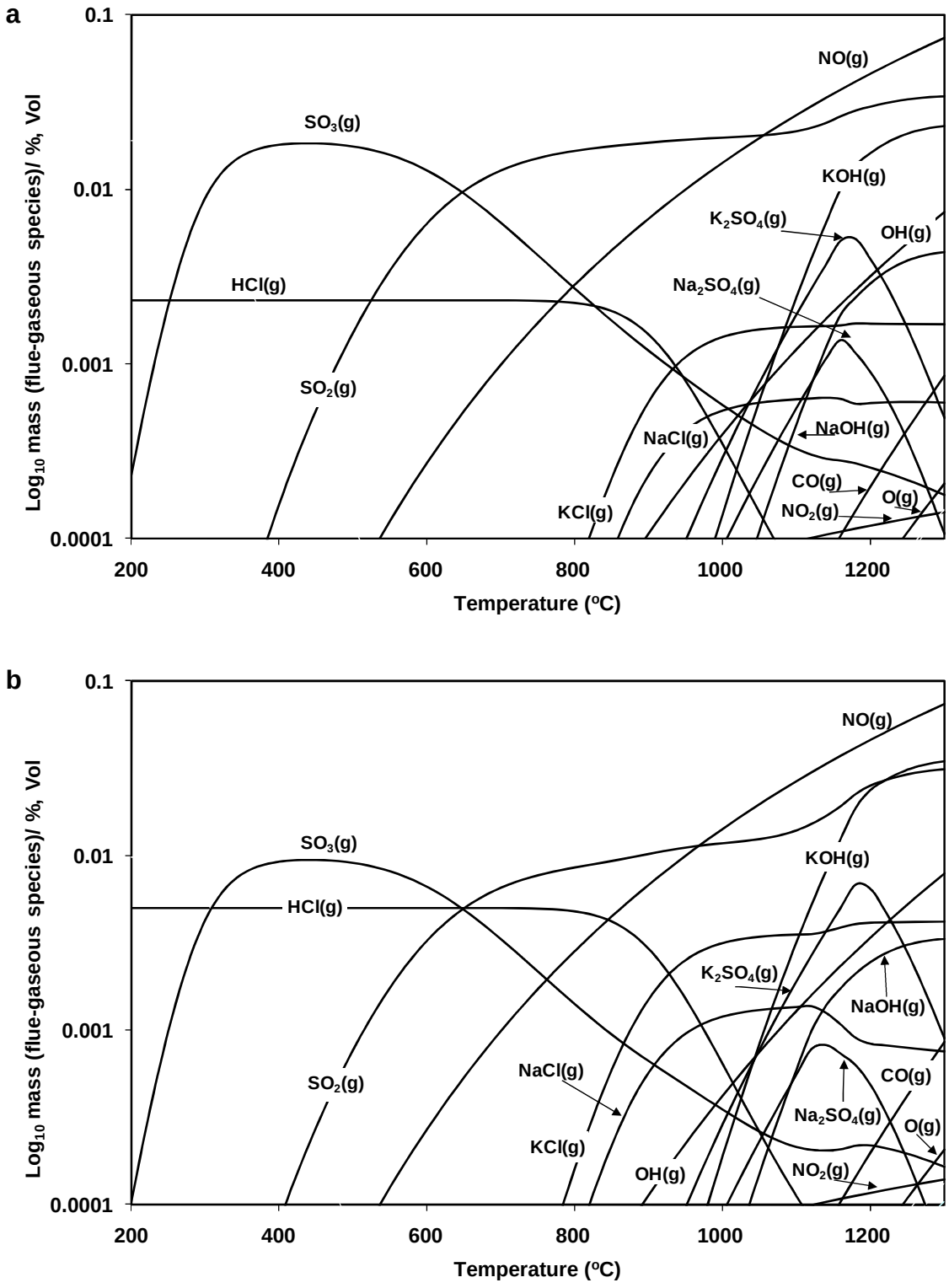

Figure 3.4 Calculated flue-gas gaseous species upon combustion of, a) CCP:El-Cerrejon coal (20:80 %, wt) and b) CCP:El-cerrejon coal (40:60 %, wt) blend mixtures fuels

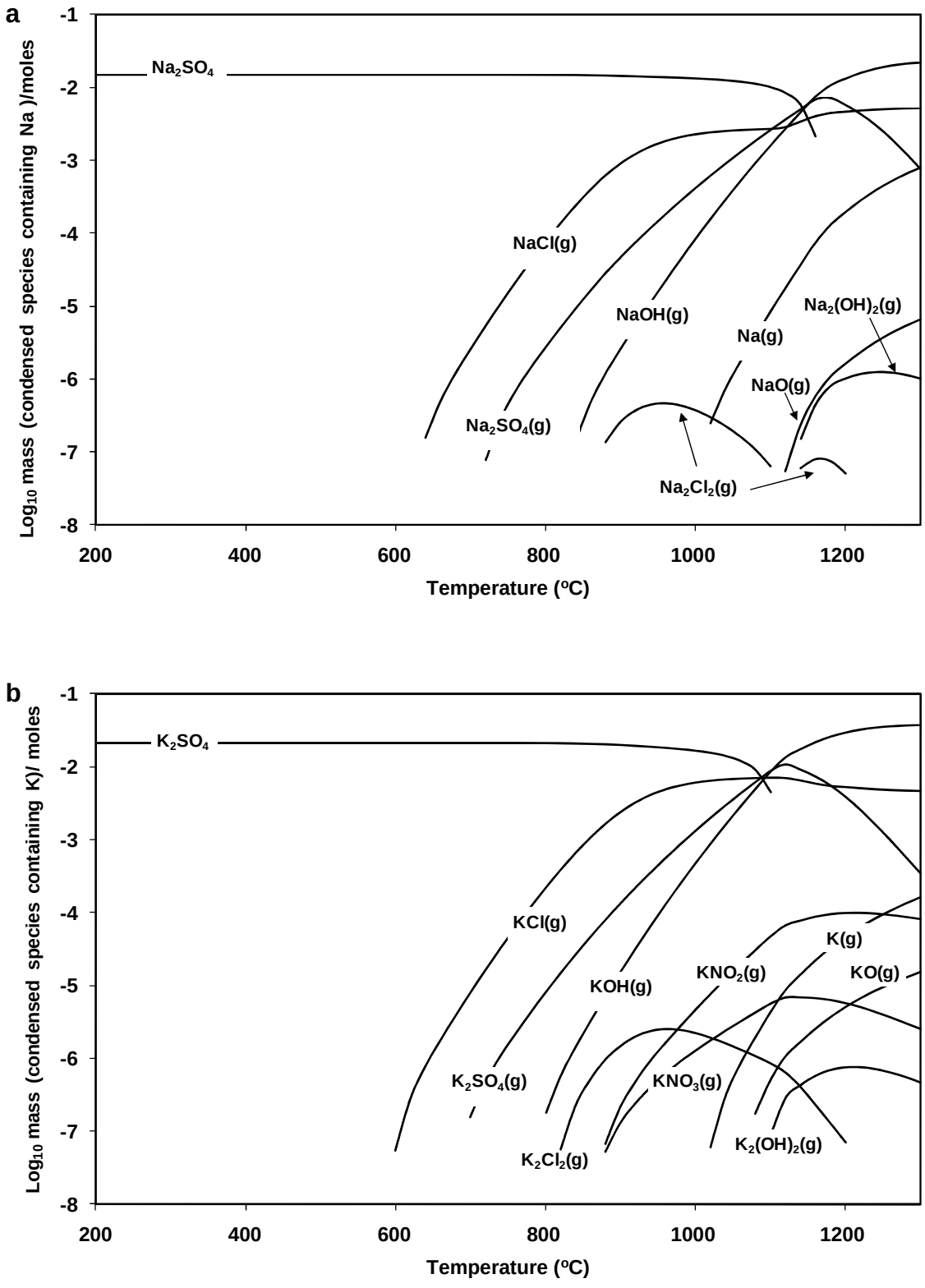

Figure 3.5 Calculated flue-gas condensed species upon combustion of El-cerrejon coal (100 %, wt) of a) Na element and b) K element (under "8 elements system")

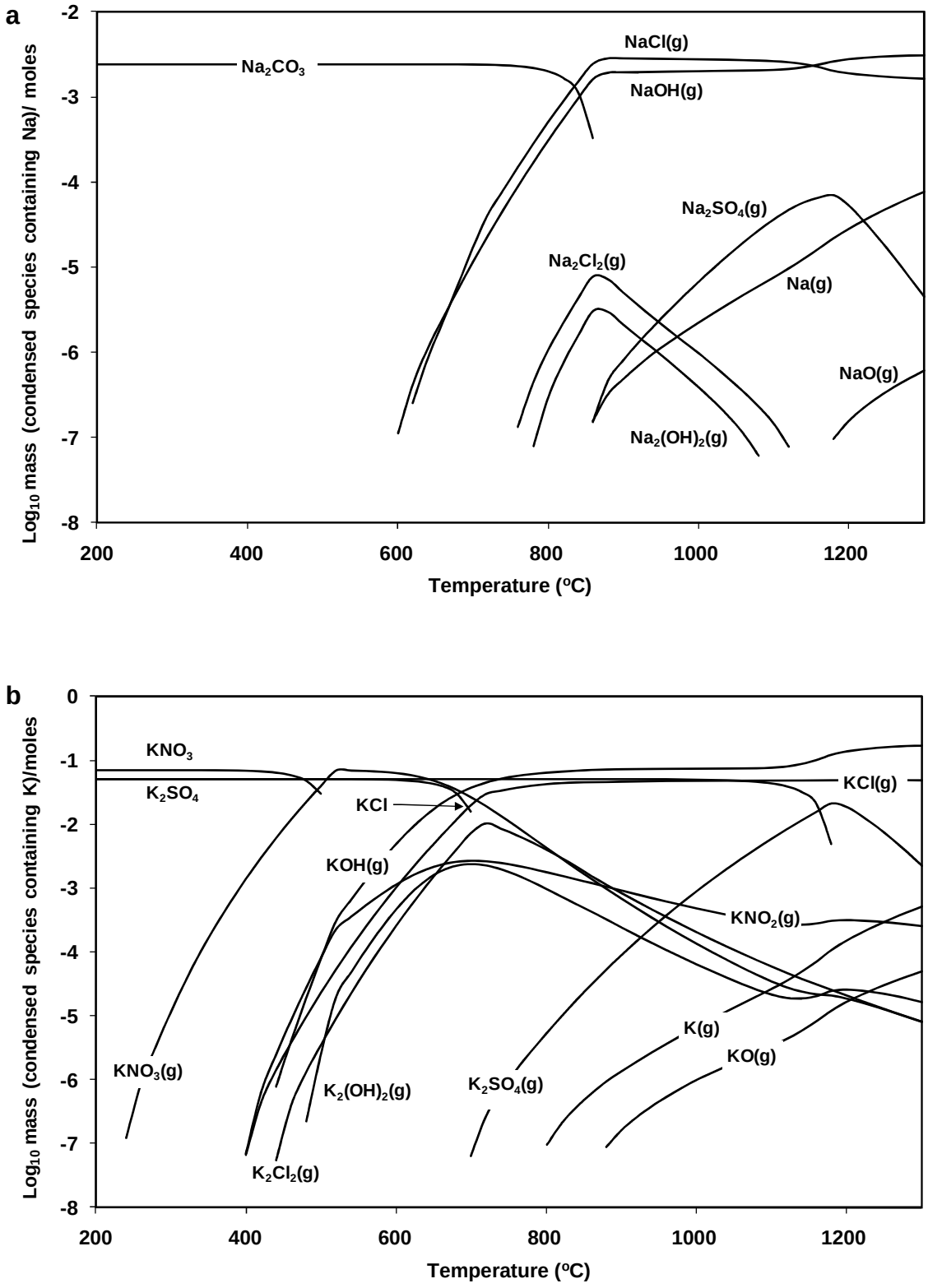

Figure 3.6 Calculated flue-gas condensed species upon combustion of CCP (100 %, wt) of a) Na element and b) K element (under "8 elements system")

3.1.4.2.2 Fifteen elements system

The behaviour of nine minor elements (Na, K, Fe, Ca, Mg,Ti, Ba, Mn, P) with all major elements (C, H, N, O, S, Cl) during coal and CCP co-firing (mixed with coal in range 0, 20, 40 and 100 %, wt) is described below. An example of the data produced by MTDATA for CCP (100 %, wt) combustion is shown in Figure 3.7.

The percent volume of predominantly gaseous species (i.e. CO_2, H_2O, N_2, O_2, HCl and SO_2) for all fuels combustion under fifteen elements system was the same as eight elements system so these figures are excluded for the sake of brevity. The calculated species (condensed and gaseous) of each minor element for each combustion fuel concern study in this system are listed in Tables 3.3 and 3.4.

As sodium and potassium were the two minor elements studied in both the eight and fifteen element systems their interactions in both systems can be compared. For example, with CCP (100 %, wt) combustion, species formed in the eight element system, such as gaseous KNO_3 (240-1300 °C) and condensed K_2SO_4 (200-1180 °C), KCl (200-700 °C) still exist in the fifteen element system, but at a different temperature range e.g. KNO_3 (560-980 °C) and condensed K_2SO_4 (1020-1200 °C), KCl (200-640 °C). As mentioned above, condensed Na_2SO_4 was not predicted in the eight element system, but was predicted in the fifteen element system in the temperature range of 820-1080 °C (shown in Table 3.3). In addition, condensed NaCl (200-660 °C) has been predicted in this system. However, for combustion of coal (100 %, wt) and the fuel blends no major variation between the systems was found.

Predictions produced using the fifteen element system helped to give a better understanding of the possible condensed species for each element due to their interactions and partitioning behaviour. For example, for coal (100 %, wt) combustion, condensed Na_2SO_4 (200-1160 °C), K_2SO_4 (200-1100 °C), $FeSO_4$ (200-320 °C), Fe_2O_3 (200-720 °C), Fe_2MgO_4 (> 710 °C), $CaFe_2O_4$ (> 980 °C), $CaSO_4$ (200-960 °C), $MgSO_4$ (> 720 °C), MgO (> 800 °C), MgO_3Ti (> 200 °C), BaO_4S (200-1080 °C), BaO_3Ti (> 1100 °C), MnO_3Ti (200-680 °C), Mn_2O_3 (700-1240 °C) and K_3PO_4 (200-1300 °C) were

all indicated. By comparing the condensed species predicted for coal (100 %, wt) to predictions for CCP fuel blends (CCP biomass 20:80 and 40:60 %, wt), it can be seen that almost the same condensed species are predicted with small variations in dewpoint temperatures (~ 20-40 °C) (as shown Table 3.4) and small variations in concentration (e.g. K_2SO_4 condensed content were -1.86, -1.98 moles for CCP:Coal (20:80 %, wt) and CCP:Coal (40:60 %, wt), respectively).

It should be pointed out that potassium phosphate (K_3PO_4) was predicted for the entire temperature range studied (200-1300 °C) for all the fuel combinations studied (along with others such as sulphates, chlorides, sulphides and oxides) under this system. This showed the significant of indicating added elements compared to the "8 elements system".

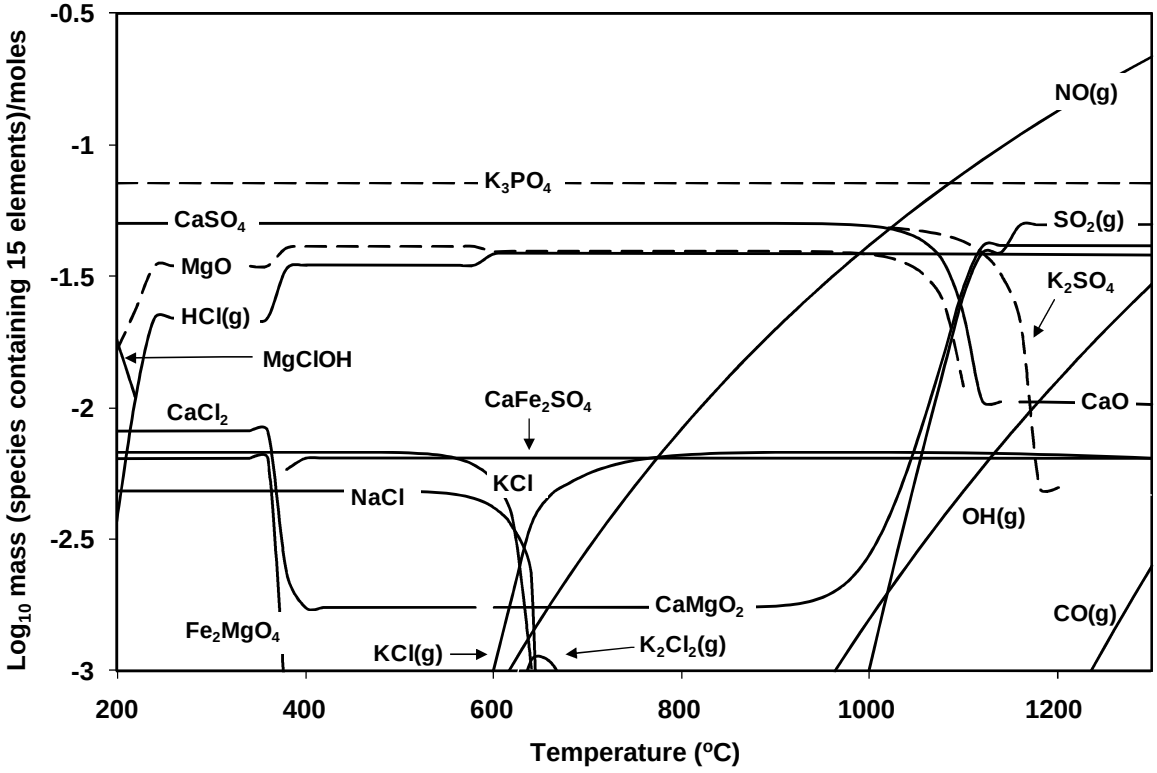

Figure 3.7 Calculated flue-gas emissions (gaseous & condensed) upon combustion of CCP (100%, wt) fuel, under "15 elements system" study

Table 3.3 Species (gaseous & condensed) of thermodynamic equilibrium minor elements during the combustion of pure fuels (Coal, CCP) under "15 elements system"

Elements	El-cerrejon coal (100 %, wt)	CCP (100 %, wt)
Na	Na_2SO_4 (c) (200-1160°C), Na_2SO_4 (g) (> 720°C), NaOH (g) (> 840°C), Na (g) (> 1020 °C), NaO (g) (> 1120°C), NaCl (g) (> 620°C), $H_2Na_2O_2$ (> 1120°C) and Na_2Cl_2 (> 860 °C)	NaCl (c) (200-660°C), Na_2SO_4 (c) (820-1080°C), Na_2SO_4 (g) (1020-1180°C), NaOH (g) (> 680°C), Na (g) (> 920°C), $H_2Na_2O_2$ (> 1100°C), NaO (g) (> 1080°C), NaCl (g) (> 420°C) and Na_2Cl_2 (> 440 °C)
K	K_2SO_4 (c) (200-1100°C), K_3PO_4 (c) (200-1300°C), KCl (g) (>600°C), K_2O_4S (g) (> 700°C), K_2O (g) (> 800°C), K_2Cl_2 (g) (> 820°C), KNO_2 (g) (> 880°C), KNO_3 (g) (> 880°C), K (g)(> 1020°C), KO (g) (> 1080°C) and $H_2K_2O_2$ (g) (> 1100°C)	K_3PO_4 (c) (200-1300°C), KCl (c) (200-640°C), KCl (g) (> 400°C), K_2Cl_2 (g) (> 440°C), KNO_2 (g) (> 760°C), KNO_3 (g) (560-980°C), K_2O_4S (s) (1020-1200 °C), KO (g) (at 1140°C) (g) and KOH (g) (> 640°C), K_2O_4S (g) (1040-1200 °C)
Fe	$FeSO_4$ (c) (200-320°C), Fe_2O_3 (c) (200-720°C), Fe_2MgO_4 (c) (> 740°C), $CaFe_2O_4$ (c) (> 980°C), FeH_2O_2 (g) (> 1040°C) and FeO_2 (g) (> 1260°C)	Fe_2MgO_4 (c) (200-380°C), $CaFe_2O4$ (c) (>380°C), FeH_2O_2 (g) (> 1080°C) and FeCl (g) (at 1300°C)
Ca	$CaSO_4$ (c) (200-960°C) and $CaFe_2O_4$ (c) (> 1260°C)	$CaSO_4$ (c) (200-1120°C), $CaCl_2$ (c) (200-580°C), $CaFe_2O_4$ (c) (> 380°C), $CaMgO_2$ (c) (> 600°C), CaO (c) (> 1140°C), $CaCl_2$ (g) (> 720°C), $CaClHO_3$ (g) (> 760 °C) and CaH_2O_2 (g) (> 960°C),
Mg	$MgSO_4$ (c) (> 720°C), Fe_2MgO_4 (c) (> 710°C), MgO (c) (> 800°C), MgO_3Ti (c) (> 200°C) and H_2MgO_2 (g) (> 1060°C)	MgO (c) (200-1100°C), ClHMgO (c) (200-220°C), Fe_2MgO_4 (c) (200-380°C), $CaMgO_2$ (c) (> 600°C), MgO_3Ti (c) (200-620°C), H_2MgO_2 (g) (> 1000°C) and Cl_2Mg (c) (> 1040°C)
Ti	MgO_3Ti (c) (> 200°C), MnO_3Ti (c) (200- 680°C) and BaO_3Ti (c) (> 1100°C)	MgO_3Ti (c) (200-620°C), MnO_3Ti (c) (> 1140°C) and BaO_3Ti (c) (> 620°C)
Ba	$BaSO_4$ (c) (200-1080°C), BaO_3Ti (c) (> 1100°C) and BaH_2O_2 (g) (> 1180°C)	$BaCl_2$ (c) (200-600°C), BaO_3Ti (c) (> 620°C), $BaCl_2$ (g) (> 820°C) and BaH_2O_2 (g) (> 1120°C) and BaClHO (g) (> 880°C)
Mn	MnO_3Ti (c) (200- 680°C), Mn_2O_3 (c) (700-1240°C), MnO (g) (> 1260°C) and MnO_2 (g) (at 1300°C)	MnO_2 (c) (200-420°C), Mn_2O_3 (c) (440-1240°C), MnO_3Ti (c) (> 1140°C), MnO (g) (> 1160°C), Cl_2Mn (g) (> 720°C), ClMn (g) (> 1140°C) and MnO_2 (g) (at 1260°C)
P	K_3PO_4 (c) (200-1300°C)	K_3PO_4 (c) (200-1300°C)

Table 3.4 Species (gaseous & condensed) of thermodynamic equilibrium minor elements during the combustion of fuels (CCP:Coal (20:80 & 40:60 %, wt) under "15 elements system"

Elements	CCP:Coal (20:80, % wt)	CCP:Coal (40:60, % wt)
Na	Na_2SO_4 (c) (200-1140°C), Na_2SO_4 (g) (> 720°C), NaOH (g) (> 840°C),), Na (g) (> 1020 °C) NaO (g) (> 1120°C), $H_2Na_2O_2$ (g) (> 1140°C) and Na_2Cl_2 (> 860 °C)	Na_2SO_4 (c) (200-1140°C), Na_2SO_4 (g) (> 720°C), NaOH (g) (> 840°C),), Na (g) (> 1020 °C) NaO (g) (> 1120°C), $H_2Na_2O_2$ (g) (> 1140°C) and Na_2Cl_2 (> 820 °C)
K	K_2SO_4 (c) (200-1080°C), K_3PO_4 (c) (200-1300°C), KCl (g) (>580°C), K_2SO_4 (g) (> 700°C), K_2O (g) (> 800°C), K_2Cl_2 (g) (> 820°C), KNO_2 (g) (> 880°C), KNO_3 (g) (> 880°C), K (g)(> 1020°C), KO (g) (> 1080°C) and $H_2K_2O_2$ (g) (> 1100 °C)	K_2SO_4 (c) (200-1040°C), K_3PO_4 (c) (200-1300°C), KCl (g) (> 540°C), K_2SO_4 (g) (> 700°C), K_2O (g) (> 800°C), K_2Cl_2 (g) (> 760°C), KNO_2 (g) (> 880°C), KNO_3 (g) (> 880°C), K (g)(> 1020°C), KO (g) (> 1020°C) and $H_2K_2O_2$ (g) (> 1100 °C)
Fe	$FeSO_4$ (c) (200-300°C), Fe_2O_3 (c) (200-720°C), Fe_2MgO_4 (c) (> 720°C), $CaFe_2O_4$ (c) (> 960°C), FeH_2O_2 (g) (> 1140°C) and FeO_2 (g) (> 1260°C)	Fe_2O_3 (c) (200-700°C), Fe_2MgO_4 (c) (> 660-960°C), $CaFe_2O_4$ (c) (> 960°C) and FeH_2O_2 (g) (> 1140°C)
Ca	$CaSO_4$ (c) (200-1140°C), $CaFe_2O_4$ (c) (> 960°C), $CaMgO_2$ (c) (> 1140°C), CaH_2O_2 (g) (> 1100°C) and $CaClHO_3$ (g) (> 1140°C)	$CaSO_4$ (c) (200-1140°C), $CaFe_2O_4$ (c) (> 960°C), $CaMgO_2$ (c) (> 1140°C), CaH_2O_2 (g) (> 1100°C) and $CaClHO_3$ (g) (> 1120°C)
Mg	$MgSO_4$ (c) (>200-780°C), Fe_2MgO_4 (c) (720-960°C), MgO (c) (> 800°C), MgO_3Ti (c) (> 200°C) and H_2MgO_2 (g) (> 1060°C)	$MgSO_4$ (c) (> 200-780°C), Fe_2MgO_4 (c) (660-960°C), MgO (c) (> 780°C), MgO_3Ti (c) (> 200°C) and H_2MgO_2 (g) (> 1060°C)
Ti	MgO_3Ti (c) (> 200°C), MnO_3Ti (c) (200- 640°C) and BaO_3Ti (c) (> 1080°C)	MgO_3Ti (c) (> 200°C), MnO_3Ti (c) (200- 580°C) and BaO_3Ti (c) (> 1080°C)
Ba	$BaSO_4$ (c) (200-1060°C), BaO_3Ti (c) (> 1080°C) and BaH_2O_2 (g) (> 1180°C)	$BaSO_4$ (c) (200-1060°C), BaO_3Ti (c) (> 1080°C), BaH_2O_2 (g) (> 1180°C) and BaClHO (g) (> 1220°C)
Mn	MnO_3Ti (c) (200-640°C), Mn_2O_3 (c) (700-1240°C), MnO (g) (> 1260°C) and MnO_2 (g) (at 1300°C)	MnO_3Ti (c) (200-580°C), Mn_2O_3 (c) (660-1240°C), MnO (g) (> 1260°C), MnO_2 (g) (at 1300°C) and Cl_2Mn (g) (860-900°C)
P	K_3PO_4 (c) (200-1300°C)	K_3PO_4 (c) (200-1300°C)

Keys: (c) condensed species and (g) gaseous species

3.1.4.2.3 Seventeen elements system

This system included all the elements in the 15 element system but with the addition of Si and Al. Figure 3.8 shows the thermodynamic study of minor element (K) species (gaseous and condensed) during coal (100 %, wt) and CCP (100 %, wt) combustion. From the graph, it can be noted that the predominant $KAlSiO_4$ was the only condensed species for coal (Fig. 3.8.a). Whereas the calculations of pure CCP combustion (Fig. 3.8.b) show that K_2SiO_3, $KAl(SiO_3)_2$ and K_3PO_4 were the condensed species accompanied by KCl and KOH gaseous species. This deviates from the calculations under "8 and 15 elements system" where a condensed K_2SO_4 and KCl formed. According to Christensen and Livbjerg, 1996, if chemical equilibrium is sustained, the amount of S increases during cooling of the flue gas and K_2SO_4(s) is the first potassium compound to become supersaturated (which may begin even above 1000 °C accompanied by the condensation of KCl(s) at lower temperatures, usually in the proximity of 700 °C). This may backup the calculations formed under 8 and 15 elements systems.

Also, observations (from a repeat run) was clearly preserved that gaseous species like H_2O, N_2, O_2 and all other emissions species in gaseous and condensed status were imperfectly predicted for this system. Figure 3.9 shows the calculations of major element (C) species (gaseous and condensed) during coal (100 %, wt) and CCP (100 %, wt) combustion. This showed that the predominant CO_2 gas were decreased drastically at temperature below 540 °C for coal (Fig. 3.9.a) and below 560 °C CCP biomass (Fig. 3.9.b) fuel combustion. It can be say that the MTDATA calculation did not correctly predicted the interactions between these elements studied under this system as repeatable modeling runs always gave different results. This agreed with Otsuka 2002 indicated of non importance of aluminum and silicon since are considered inert, in comparison to the corrosive elements.

This information is very helpful for understanding MTDATA software (combined with SGTE database) in term of its limitations. Therefore, it was decided that MTDATA calculations were carried out using "15 elements system" in this project.

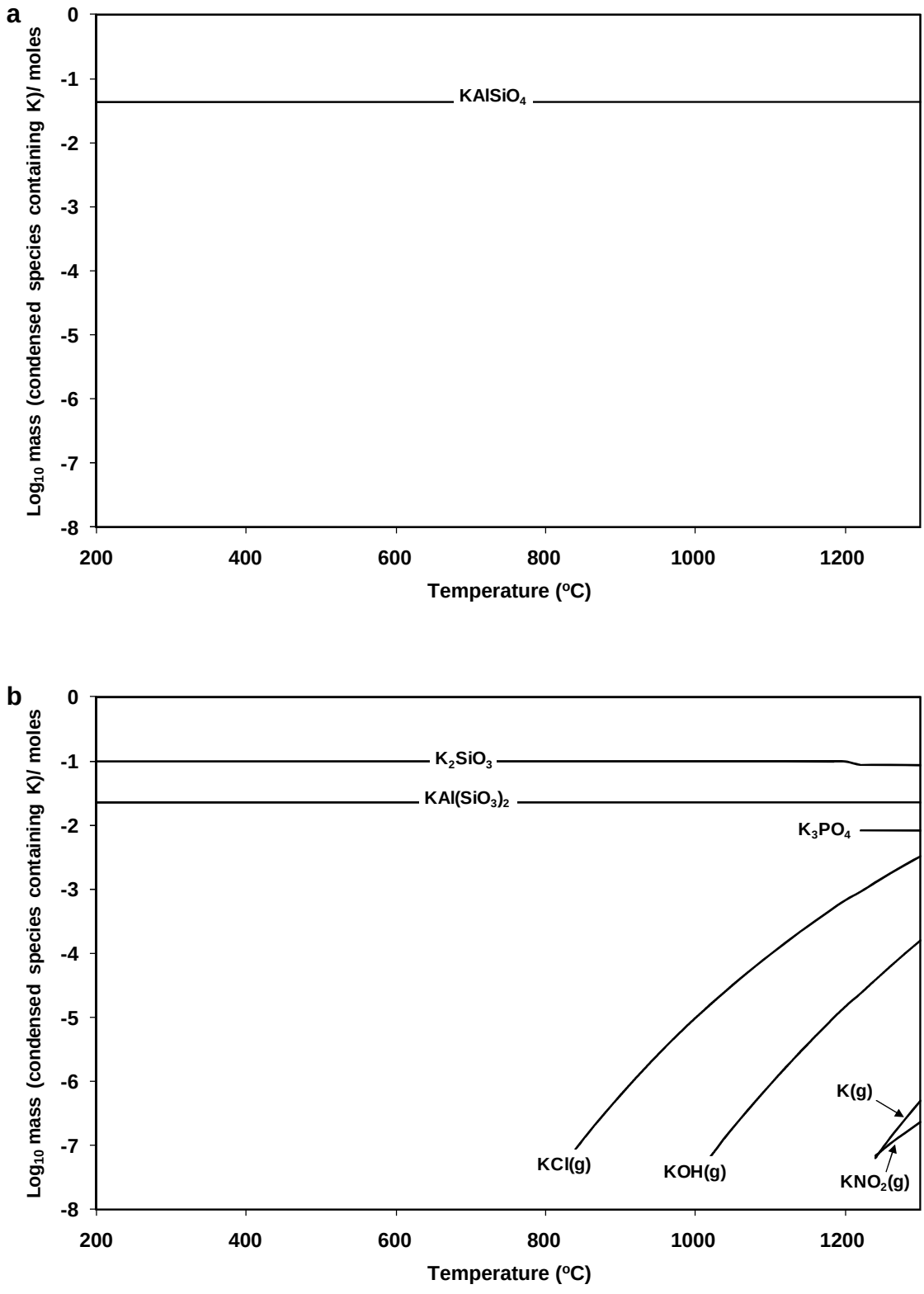

Figure 3.8 Calculated flue-gas emissions (gaseous & condensed species) of K element upon combustion of, a) El-cerrejon coal (100 %, wt) and b) CCP (100 %, wt), (for "17 elements system" study)

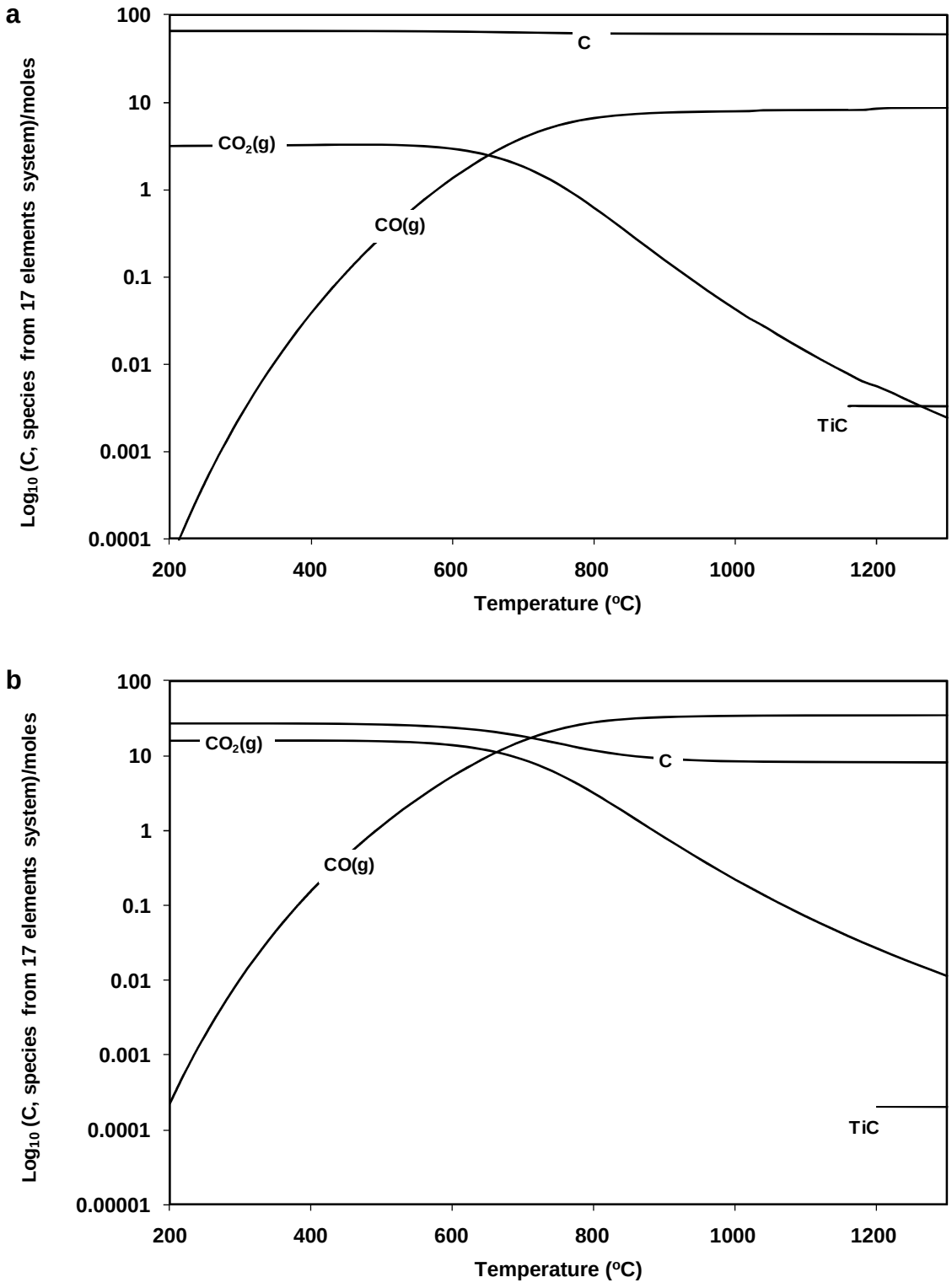

Figure 3.9 Calculated flue-gas emissions (gaseous & condensed species) of C element upon combustion of, a) El-cerrejon coal (100 %, wt) and b) CCP (100 %, wt), (for "17 elements system" study)

3.1.4.2.4 MTDATA model sensitivity (effect of excess air)

The influence of the excess air parameter on the results of the MTDATA calculations was investigated. The variations of excess air concentration (controlled by the amount of oxygen in combustion flue gas in this project) chosen for the study were in a range of 4-11 % O_2 by volume. At a coal feed rate of 1 kg/h, species emitted from the combustion of pure El-Cerrejon coal was calculated using the "15 elements system" for the chosen range of oxygen output. Figure 3.10 shows the species (gaseous and condensed) formed in terms of the moles at various excess air levels (6, 8 and 10 % O_2, vol.).

From the study, the results show that all the compounds in the MTDATA outputs were identical for all excess air values. The concentration of O_2 and NO_x increased at the higher excess air levels (which is expected [Van Loo and Koppejan, 2008]). For example, O_2 and N_2 concentrations were 1.50 and 2.62 moles at an excess air of 6 % O_2 by volume (Fig. 3.10.a), compared to 1.89 and 2.79 moles at an excess air of 10 % O_2 by volume (Fig. 3.10.c).

Therefore, it can be concluded that increasing the level of excess air showed no change in the equilibrium calculations for the compounds formed with respect to the concentrations of these species. This gives confidence when comparing the MTDATA calculations under the same target combustion conditions as the pilot-scale experiments, for data produced with O_2 levels measured in range 4-7 volume %.

Also, the study looked earlier (Sec. 3.1.3.2, Chapter 3) at the sensitivity of the calculations to changes in the input elements used (i.e. the effects of the major elements mixed with some and all minor elements on partitioning behaviour, flue gas composition and deposition) revealed 15 elements system lead to realistic model outputs. Emitted species in the gaseous and condensed states from the 17 element system were incorrectly predicted, whereas the 8 elements system which omitted some minor element species did not predict significant condensed species (e.g. phosphorus in the form of potassium phosphate (K_3PO_4) as found by the 15 elements system).

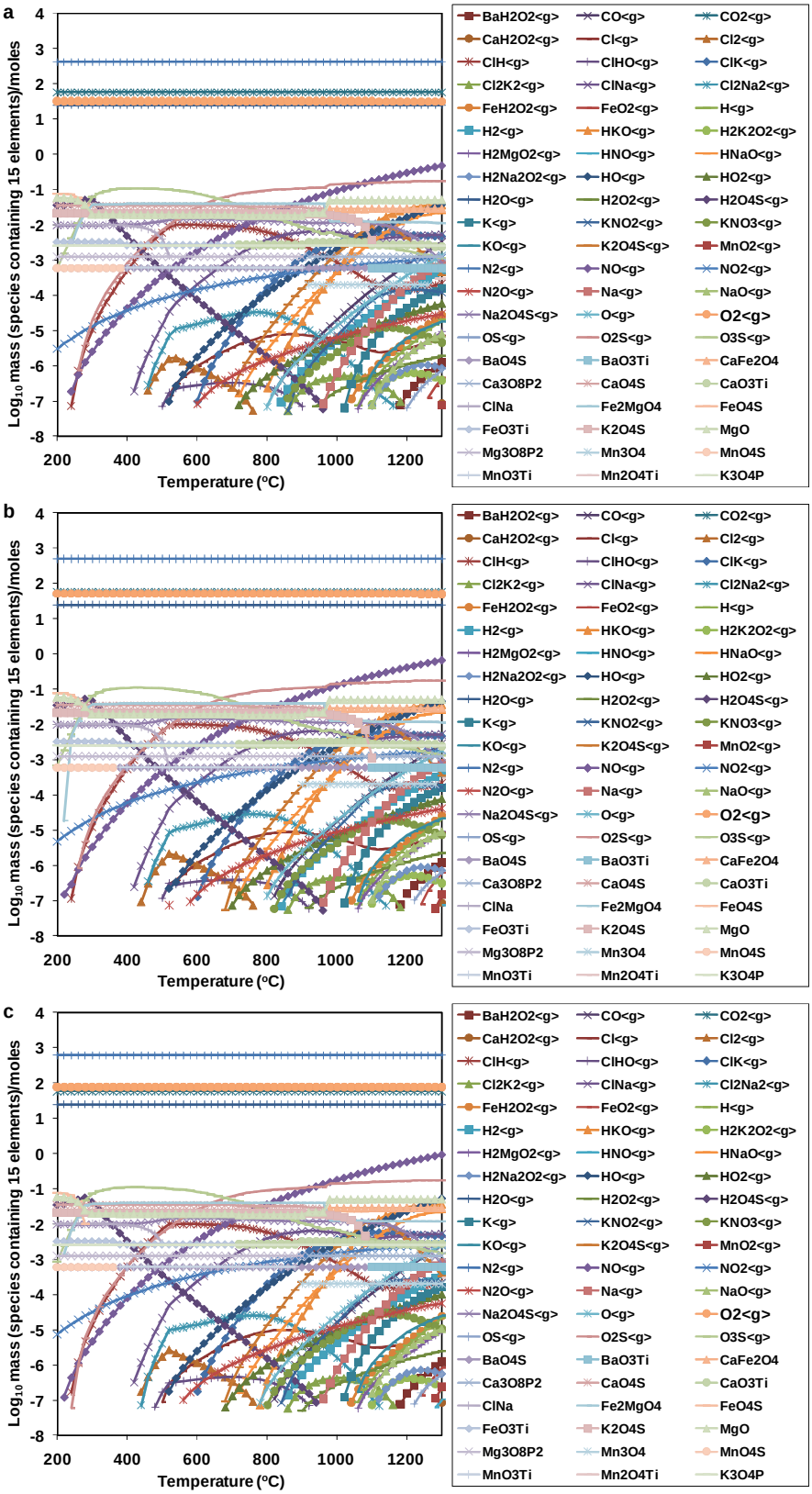

Figure 3.10 Calculated flue-gas emissions (gaseous & condensed species) of El-cerrejon coal (100 %, wt) combustion at excess air of, a) O_2 (6 %, vol.), b) O_2 (8 %, vol.) and C) O_2 (10 %, vol.) output (under "15 elements system")

3.2 Experimental pilot-scale combusting rig

3.2.1 Test programme

This research work consists of several groups of fuels associated with various combustion technologies/conditions: (1) Co-firing biomass with coal using pulverised fuels in PF combustor, (2) Combustion biomass using pelletised/lump fuels in FB combustor and (3) Liquid combustion using fast pyrolysis bio-oil.

As these fuels were a different physical forms, the installation and use of different feeding systems in the pilot rig unit was necessary for the combustion tests. These units were used to provide reliable and uniform feed rates with each fuel. A study of the factors influencing the operating feed systems was performed (explained in more details in Sec. 3.2.9). The following steps and the diagram (Figure 3.11) are the summary of the combustion experiments performed for the fuels selected:

- Using fuel of known composition, the fuel was fed to the combustion rig with known mass/volume and time feeding
- Using a robust feeding system method (under quality assurance and control) for combustion study
- Applying consistent operating conditions
- Flue gas emissions data were recorded on-line at the time of experiments
- After suitable periods of time, probes were extracted and samples of deposits were collected, measured and analysed
- Deposit samples were split into sub-samples, to determine any differences in the products that were formed on the probe.
- Analysis of samples of bed ash under only fluidised bed combustion and fly ash for all the combustions tests were performed.
- Sub-samples of deposits were then subjected to Scanning Electron Microscope (SEM) with Electron Dispersive X-ray (EDX) and/or X-ray Diffraction (XRD) analysis.

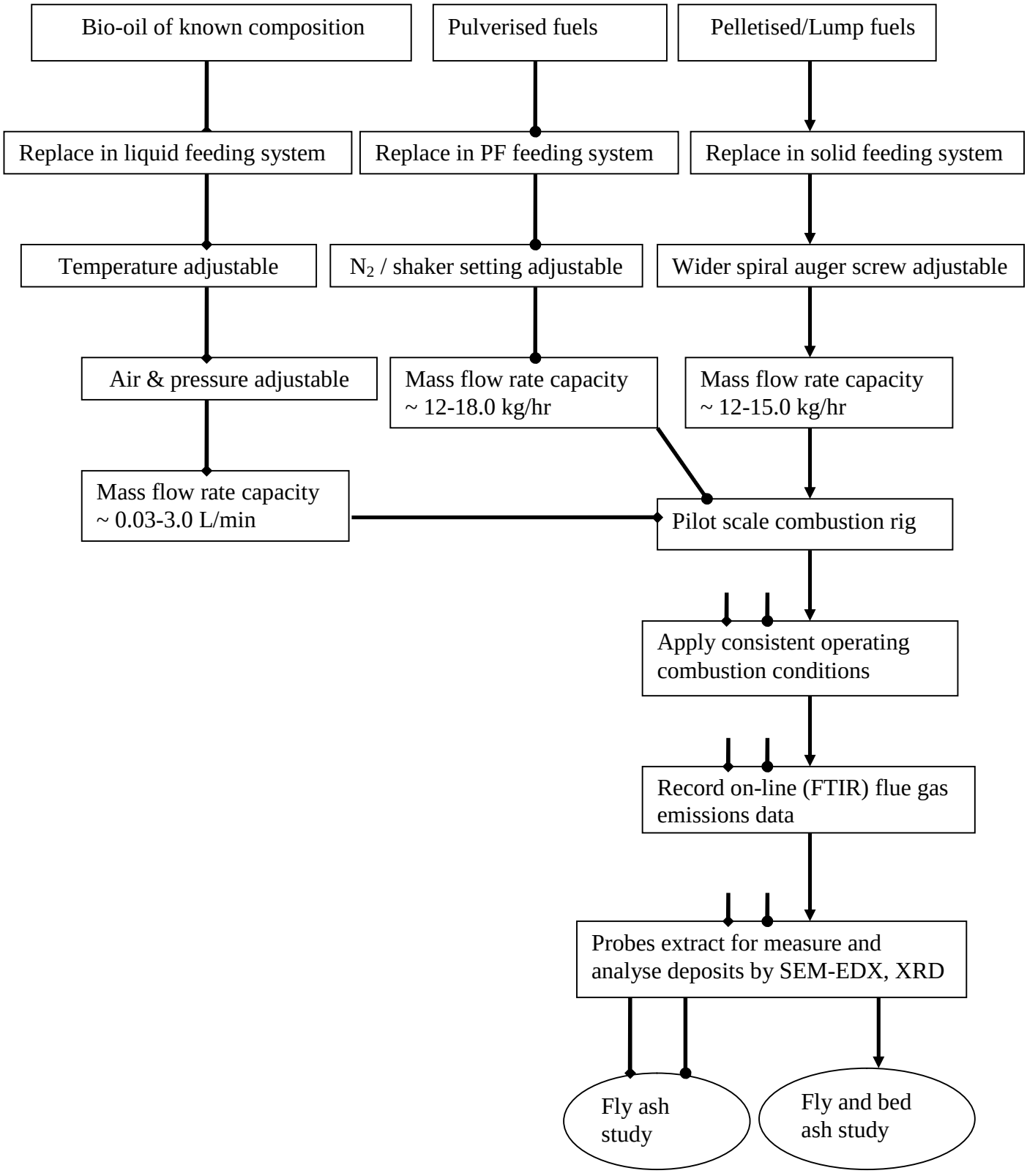

Figure 3.11 Diagram of selected fuel combustion studies

3.2.1.1 Coal biomass co-firing

Co-firing tests were performed with two coals: Colombian coal (El-cerrejon) and British coal (Daw Mill). Each of these coals was fired with air for a reference test and then under co-firing conditions with two type of biomass (cereal co-product (CCP) and miscanthus) mixed with coals in range 0-100 %, wt. The coal fuels were chosen according to the extent of their usage in E.ON power stations in the UK. The Daw Mill is a common UK power station fuel and around 6 % of the energy for UK power generation is produced from it. One of the crucial concerns when considering biomass co-firing is the availability of sufficient biomass to warrant undertaking plant modifications. Of the available potential fuels, wood and straw based products are distinct types that are available in large quantities [Van Loo and Koppejan, 2008]. Miscanthus was chosen based on the interest of UK government in promoting the growth of this plant through the Energy Crop Scheme [Defra online website] (by offering financial support to farmers for the establishment of miscanthus and willow) as an energy crop for use in conversion processes.

The coals and biomass used in this study were supplied by E. ON Engineering plc [Power Technology Centre, Ratcliffe-on-Soar, Nottingham, UK]. Their characterisations/analysis (in terms of proximate, ultimate and ash compositions) are presented in Tables 3.5 and 3.6, respectively.

3.2.1.2 Pelletised/lump fuels combustion

The fuels selected for this part of the project consists of 3 biomass fuels; Oilseed rape straw (OSR), miscanthus pellets and coppiced willow. In the UK, the total area of OSR harvested increased between 2000 and 2008 from 332,000 ha to 598,000 ha (representing 12 % of the total crop area) an example of an agricultural residue that could be used as a fuel for energy generation [DEFRA, 2009]. Currently there is not a significant market for OSR straw and a large amount of it is chopped and incorporated into the soil through ploughing. Densification into pellets increases the bulk density of biomass [Obernberger and Thek, 2004; McMullen et al., 2005] and as result, the net

calorific content per unit volume is increased [Bhattacharya et al. 1989] and storage, transport and handling of the material is easier and cheaper [Samson et al., 2000; Kaliyan and Morey, 2006]. A further concern is that storage of biomass can result in oxidative self-heating or spontaneous heating [Meijer and Gast, 2004] and can result in changes in the chemical constituents, dry matter losses and moisture content changes which reduce the value and quality of the end product [Assarsson, 1969]. Previous research investigated how storage of raw material effect the characteristics of pellets [Lehtikangas, 2000], but up to date, there is no awareness of research investigating the effect of storage on pellets. Therefore in addition of study the behaviour of OSR combustion in fluidised bed combustor, an investigation the effect of storage period on OSR pellets combustions were performed.

The OSR used in this study was provided by Harper Adams University College (UK). OSR bales were stored (under cover in a shed with roof and three open sides at ambient temperature) for 10 months prior to pelletisation. OSR pellets produced (individual cylinder of about 16.0 mm wide by 24.0 mm in length) were stored for 1, 3, 6 and 12 months under same conditions. At each storage time period following pelletisation, samples of OSR pellets were analysed by TES Bretby [Ashby Road, Burton Upon Trent, Staffordshire, UK]. Analysis of these OSR pellets fuels are shown in Table 3.7.

Miscanthus in form of pellets (individual cylinder of about 7.2 mm wide by 22.0 mm in length) and willow in the form of wood pieces (up to 5.4 cm in size) were supplied by E. ON Engineering plc [Power Technology Centre, Ratcliffe-on-Soar, Nottingham, UK]. Table 3.8 shows the fuel analysis of these two fuels.

3.2.1.3 Liquid fuel combustion

The bio-oil used in this study was a biomass fast pyrolysis oil (wood residues), supplied by [West Lorne Bio-oil, West Lorne, Ontario, Canada: via the Bio-energy Research Group, Chemical Engineering and Applied Chemistry, Aston University, Birmingham, UK]. The bio-oil composition is given in Table 3.9.

Table 3.5 Fuel analysis of coal for co-firing tests

	Daw Mill Coal	**El-cerrejon Coal**
Proximate analysis (% wt, AR)		
Moisture	4.60	5.80
Ash	4.20	8.60
Volatile matter	31.30	34.80
Calorific value (kJ/kg)		
Gross Calorific value	25260	27850
Net Calorific value	24107	27122
Ultimate analysis (% wt, AR)		
Carbon	74.15	69.20
Hydrogen	4.38	4.80
Nitrogen	1.17	1.42
Oxygen	10.49	9.98
Sulphur	1.28	0.58
Chlorine	0.20	0.02
Ash composition (% wt, of total ash)		
SiO_2	36.80	60.69
Al_2O_3	23.90	22.01
Fe_2O_3	11.20	7.43
TiO_2	1.10	0.92
CaO	12.00	2.27
MgO	2.50	2.90
Na_2O	1.50	1.06
K_2O	0.50	2.32
Mn_3O_4	0.40	0.06
P_2O_5	-	0.21
SO_3	-	-
BaO	-	0.11

Table 3.6 Fuel analysis of biomass for co-firing tests

	CCP	**Miscanthus**
Proximate analysis (% wt, AR)		
Moisture	8.10	10.80
Ash	4.20	4.60
Volatile matter	70.80	70.70
Calorific value (kJ/kg)		
Gross Calorific value	17610	17824
Net Calorific value	16340	16478
Ultimate analysis (% wt, AR)		
Carbon	43.30	43.59
Hydrogen	5.80	4.80
Nitrogen	2.70	0.58
Oxygen	35.57	35.52
Sulphur	0.16	0.11
Chlorine	0.17	0.09
Ash composition (% wt, of total ash)		
SiO_2	44.36	55.85
Al_2O_3	2.79	3.14
Fe_2O_3	2.47	2.12
TiO_2	0.12	0.19
CaO	7.78	8.77
MgO	3.96	3.76
Na_2O	0.36	0.50
K_2O	24.72	12.69
Mn_3O_4	0.10	0.15
P_2O_5	12.04	12.30
SO_3	-	-
BaO	0.05	0.03

Table 3.7 Fuel analysis of OSR biomass for pelletised/lump fuel combustion tests

	OSR 1[a]	**OSR 2[b]**	**OSR 3[c]**	**OSR 4[d]**
Proximate analysis (% wt, AR)				
Moisture	10.77	10.40	10.86	11.46
Ash	7.89	8.03	7.47	6.75
Volatile matter				
Calorific value (kJ/kg)				
Gross Calorific value	17840	17060	17180	17370
Ultimate analysis (% wt, AR)				
Carbon	42.71	43.64	43.98	44.34
Hydrogen	4.95	5.52	4.49	4.66
Nitrogen	0.70	0.84	0.83	0.77
Oxygen	32.35	30.97	31.69	31.36
Sulphur	0.43	0.37	0.45	0.44
Chlorine	0.17	0.19	0.21	0.2
Ash composition (% wt, of total ash)				
SiO_2	16.3	16.7	12.4	7.3
Al_2O_3	3.0	1.8	1.5	1.3
Fe_2O_3	1.7	0.8	1.0	0.7
TiO_2	0.2	0.1	0.1	0.1
CaO	26.5	23.4	24.9	25.7
MgO	1.6	1.3	1.3	1.3
Na_2O	1.5	1.7	1.1	1.2
K_2O	13.6	14.0	14.7	14.6
Mn_3O_4	0.1	0.1	0.1	0.1
P_2O_5	1.5	1.4	1.5	1.5
SO_3	9.2	9.3	9.3	10.0
BaO	-			

Keys;

(a): OSR raw material 10 month storage, pellets 1 month storage
(b): OSR raw material 10 month storage, pellets 3 month storage
(c): OSR raw material 10 month storage, pellets 6 month storage
(d): OSR raw material 10 month storage, pellets 12 month storage

Table 3.8 Fuel analysis of miscanthus and willow biomass for pelletised/lump combustion tests

	Miscanthus Pellets	**Willow coppiced**
Proximate analysis (% wt, AR)		
Moisture	13.00	15.10
Ash	6.30	1.30
Volatile matter	63.10	69.00
Calorific value (kJ/kg)		
Gross Calorific value	16033	16801
Net Calorific value	14755	15390
Ultimate analysis (% wt, AR)		
Carbon	39.93	42.02
Hydrogen	4.64	4.75
Nitrogen	0.58	0.56
Oxygen	35.50	36.20
Sulphur	0.06	0.03
Chlorine	0.06	0.01
Ash composition (% wt, of total ash)		
SiO_2	42.2	12.7
Al_2O_3	1.3	2.5
Fe_2O_3	0.9	1.2
TiO_2	<0.1	0.1
CaO	6.1	26.2
MgO	1.5	4.5
Na_2O	24.9	3.8
K_2O	12.6	15.5
Mn_3O_4	<0.1	0.6
P_2O_5	1.8	10.0
SO_3	2.8	4.2
BaO	<0.1	<0.1

Table 3.9 Fast pyrolysis bio-oil composition analysis for liquid combustion tests

Proximate Analysis (% wt, as received)	
Moisture (in emulsion)	20.00
Ash	0.09
Volatile	65.3
Calorific Value	
Gross Calorific value (Btu/lb)	7464
MJ/kg (Gross)	17.77
Physical & Chemical Properties	
Density (g/cm^3)	1.13
Viscosity 20°C (mm^2/s)	13.5
Viscosity 40°C (mm^2/s)	5.57
Viscosity 60°C (mm^2/s)	2.97
pH	2.5
Ultimate Analysis (% wt, as received)	
Carbon	34.53
Hydrogen	6.18
Oxygen	39.00
Nitrogen	0.11
Sulphur	0.02
Chloride	0.001
Ash composition (% wt, of total ash)	
SiO_2	52.0
Al_2O_3	6.1
Fe_2O_3	4.0
TiO_2	0.3
CaO	12.8
MgO	0.9
Na_2O	5.2
K_2O	4.8
Mn_3O_4	0.1
P_2O_5	1.5
SO_3	12.9
BaO	-

3.2.2 Rig description

A pilot scale combustion rig with ~ 50 kW_{th} capacity in a fluidised bed combustor (FBC) and ~ 100 kW_{th} capacity in a pulverised fuel combustor (PF) [based at Cranfield University] was used for the study. Figure 3.12 shows the layout of combustion rig.

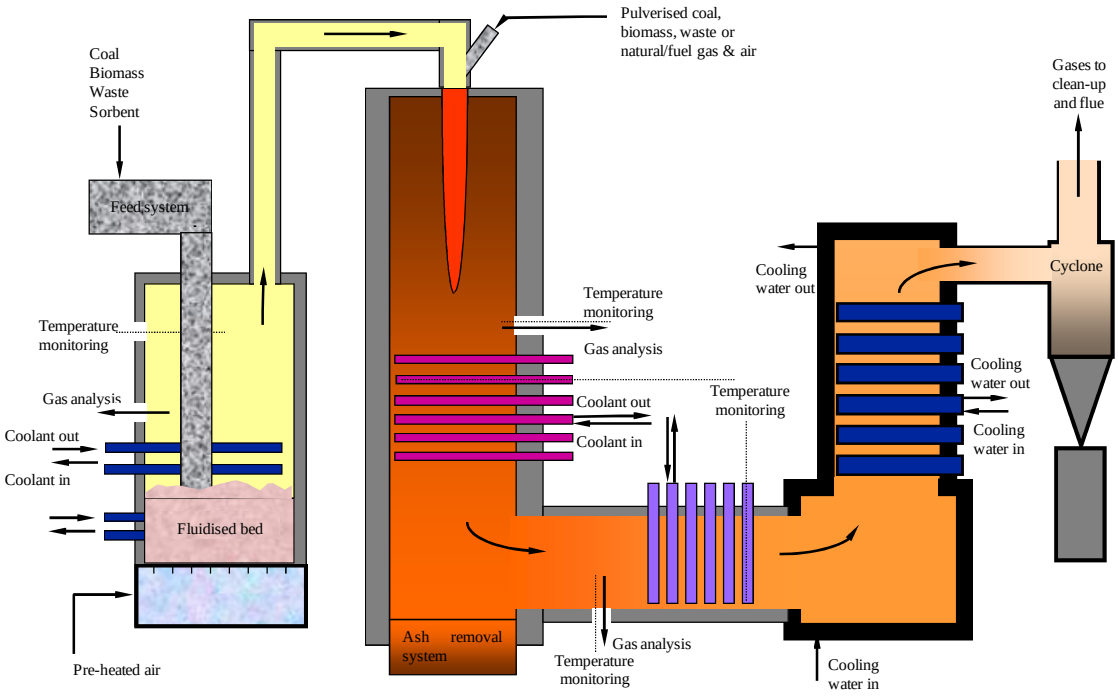

Figure 3.12 Schematic diagram of the FBC (left) PF rig facility

The rig consisted of a fluidised bed (operated at temperature up to ~ 900 ^{o}C with fluidised bed heights of up to 3 m and fluidising velocity in the range of 0.6-1.2 m/s) and a vertical combustion chamber (operated at temperature up to ~ 1400 ^{o}C with unit heights of up to 3 m) with fuels fed from the top. Air was pre-heated by a gas burner and passed through the fluidised bed before flowing into the vertical combustion chamber. The rig was run at negative pressure to prevent the gases escaping into the combustion hall. Sample ports (e.g. for fly ash) and observation windows (allowing optical access of combustion zone, particle shape/size during combustion, image acquisition, etc) (see Figure 3.13) were located in different positions along the rig. The flue gases leaving the combustor pass through water cooled heat exchanger assembly before entering a cyclone and then going through an extraction fan before exiting

through the stack. Gas and rig temperatures were measured at locations along the hot gas path (via sensors connected to a data logger [Pico Logger Unit-TC-08, 8 Channels with RS232 Connection to Hard Drive-Windows NT, ver. 4] and type "K" thermocouples (1.5 mm diameter and 20 cm long, [Farnell Components, Canal Road, Leeds, UK]). The most important temperature data generated from these thermocouples before and during experiments were situated: 1) between the preheater and fluidised bed; 2) in fluidised bed zone; 3) above the fluidised bed; 4) combustor chamber zone; and 5) combustor chamber gas temperature at deposition probes (explained later in more details in section 3.2.9). Banks of sample ports are located downstream of the combustion chamber in the rig to allow connection of gas analysis equipment and the introduction of deposition probes.

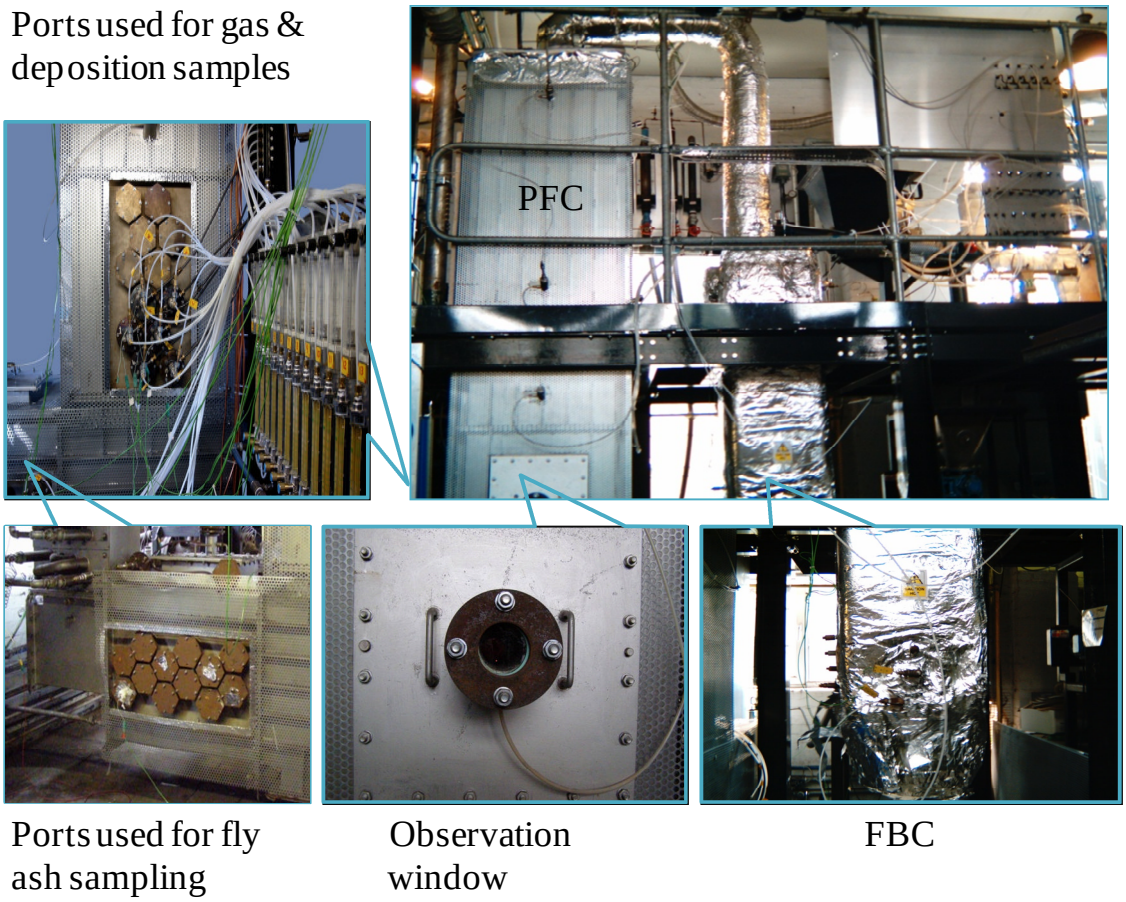

Figure 3.13 Close up view showing optical access and data collection positions of FBC, PF rig facility

3.2.3 Liquid feeding system

A bio-oil feeding system for the combustor was designed and constructed using a heated liquid feed to a spray nozzle as the basis of the design. Figure 3.14 shows a schematic diagram of the liquid feeding system. The fuel injector consisted of a central nozzle distributor device with an air inlet surrounding it. Liquid fuel (i.e. bio-oil) was supplied from a vented tank via a high pressure pump at 35 psi (1 psi = 6894.76 Pa) [Little Giant Pump Co., Oklahoma City, USA], controlled by a voltage transformer [Clairtronic, Elms Industrial Estate, Bedford, UK], through a PTFE tubes, stainless steel pipes, a manual needle valve and a non-return valve (NRV) into the spray nozzle [Legris (UK) Ltd, Hucclecote, Gloucester]. The swirling oil was then forced out through an orifice at the end of the nozzle as a spray of droplets. Air inlet to the nozzle was carefully designed to ensure mixing of the bio-oil at the orifice to form fine droplets, typically sized between 0.03 and 0.15 mm [Aircare (UK) Ltd, Glebe House, Corby, Northants]. All the bio-oil feed pipes were covered with trace heating (connected with a heater control) to allow the viscosity of the oil to be reduced during operation.

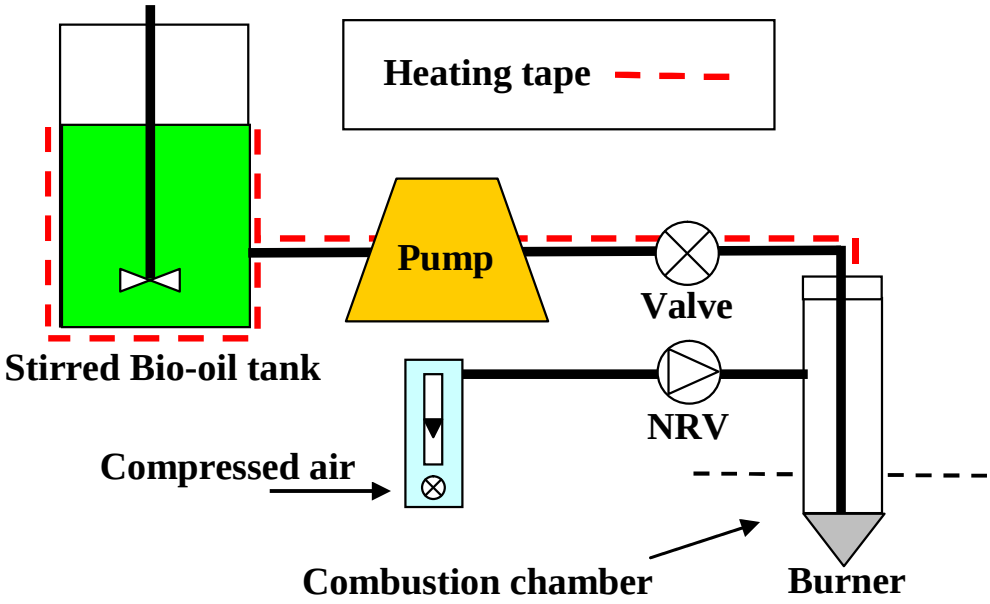

Figure 3.14 Schematic showing bio-oil feeding system fitted to the combustor chamber

3.2.4 Solid feeding system for pelletised/lump fuels

The solid feeding system for pelletised/lump fuels consisted of a sealed feed hopper with wider spiral horizontal auger feed screw (to prevent slumping, bridging and agglomeration of the material in the hopper) and gear unit driven by a DC motor. The drive motor was controlled by a speed controller (fitted in the rig control panel). A schematic of the feeder is shown in Figure 3.15.

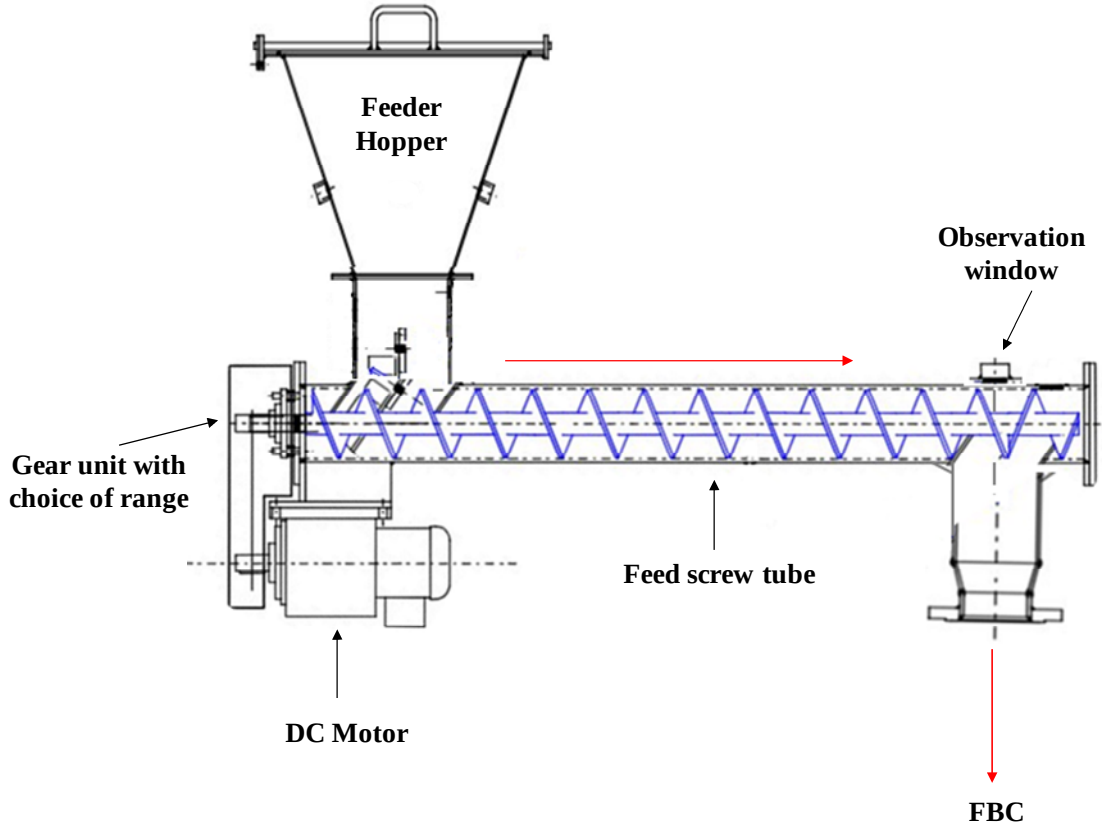

Figure 3.15 Schematic showing solid feeding system for pelletised/lump fuel combustion

3.2.5 Solid feeding system for pulverised fuels

A new solid feeding system for pulverised fuels (pf) co-firing studies has been designed and constructed (details of choice/reasons of this are explained in more details later in section 3.2.9). The system consisted of a fuel hopper attached to shaker device (with speed controller), stainless steel high flow vacuum pump for material transfer [Parker Hannifin Ltd., Parker KV Division, Milton Keynes, Buckinghamshire, UK] and a tube

feeding line leading to the combustor. Figure 3.16 shows a schematic diagram of the pf solid feeding system. The principle of operation is using the vacuum pump unit, where nitrogen is fed into an outer annular ring that has a number of orifices leading into the centre of the unit. There, the nitrogen flow rotates with a spiral motion (similar to a corkscrew) creates a powerful vacuum flow (i.e. cyclonic flow) capable of drawing materials into through, and out of the pump under force. The fuel hopper has a capacity of ~ 7 kg (fuel loading) and is placed on the shaker unit in a vertical position. The shaker unit is used to agitate the fuels to prevent slumping, bridging and agglomeration of the materials. Also, it can vibrate the fuel at various speeds which can be used to increase or decrease the fuel feeding rate injected to the vacuum pump unit and hence to the combustor chamber.

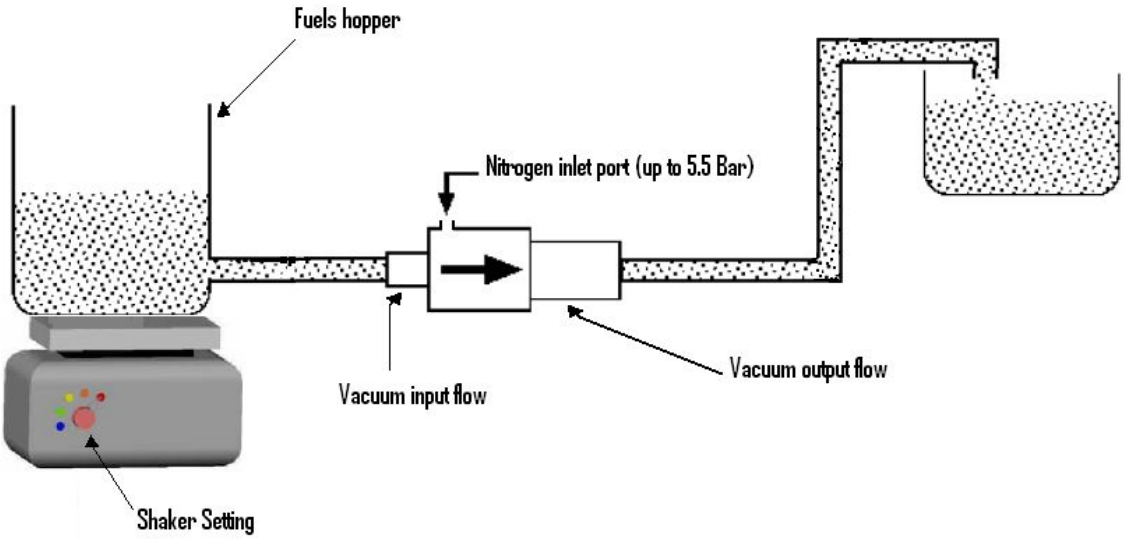

Figure 3.16 Schematic showing solid feeding system for pulverised fuel combustions

3.2.6 Flue gas analysis

Combustion gas samples for CO_2, O_2, H_2O, SO_2, CO, NO, NO_2, N_2O, HCl, HF, were obtained from a sampling port located at the side-access of the vertical chamber and analysed by a high resolution multi-component Fourier Transform Infra-Red (FTIR) on-line gas analyser [Protea-Protir 240M/C Mobile FTIR analyser, Protea Ltd., Cheshire, UK]. The analyser is fitted with an integral sampling control system (i.e. controlled

temperature and pressure) where the gases have to pass through a pipe (595 mm length, 12 mm internal pore size) bounded by glass wool, filter, and a heated line (~180 °C), in order to ensure that conditioned sample gases pass to the analyser. Figure 3.17 shows close up view of FTIR system and sampling control system (fitted into the vertical chamber sample port). The FTIR contains an on-board electrochemical (zirconia-based) oxygen sensor. This allowed the collection of oxygen results in parallel to the main combustion gas results and provides the system with the unique ability to actively correct for oxygen content online.

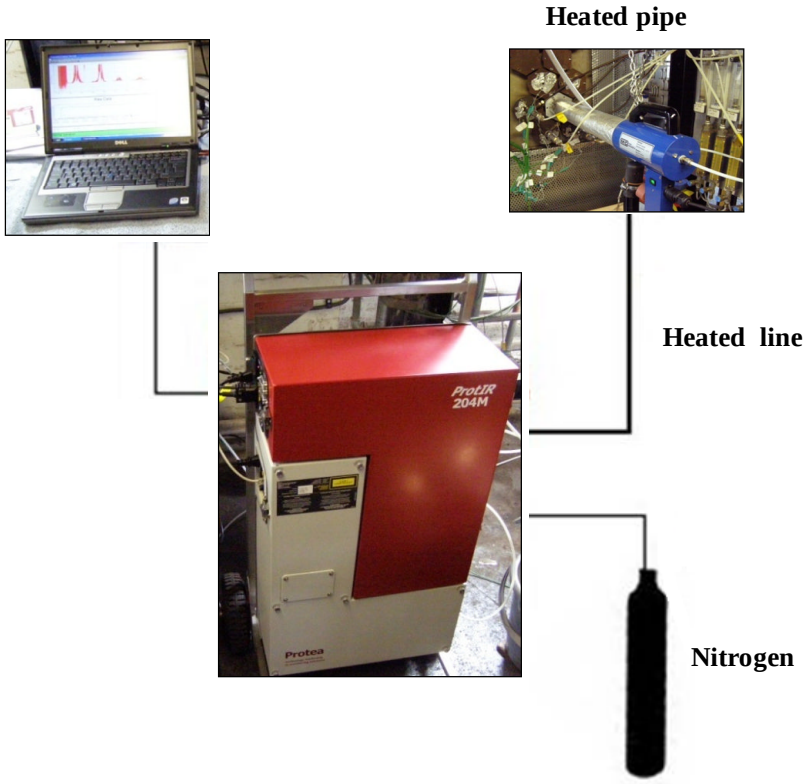

Figure 3.17 Detail of FTIR gas analyser operation

3.2.7 Deposit collection/ analysis

Deposits were collected using three deposition probes, an example of which is shown in Figure 3.18. Probe design, calculation and mathematical model used for heat transfer calculations are described in Coleman PhD dissertation (Coleman 2008). These probes have two stainless steel rings and a removable ceramic ring (OD = 39.05 mm, ID = 32.16 mm, length = 60 mm) on which the deposits were collected. The probes were

cooled by passing a controlled air flow through the probes using calibrated rotameters. When the cooling air flow reached the end of the probe it passed through holes in the inner tube to the outer tube formed by the ceramic and metal sections. It then flowed in the opposite direction back down the probe before exiting. The probes were fitted with two thermocouples, to evaluate the heat flux at the top and end surface of the tube wall. Thermocouples were referred to as T_{top} (top surface of the tube) and T_{end} (end surface of the tube) and temperatures were recorded throughout the test run. The three probe surface temperatures were chosen to represent the high range of typical heat exchanger surface temperatures, namely 700 °C (probe 1), 600 °C (probe 2) and 500 °C (probe 3). Probe cooling air supplies were adjusted throughout the tests to maintain constant surface temperatures. After the operating runs, the probes were allowed to cool down before being carefully extracted. To examine the ceramic section of the probe, its surface was divided into three areas which represented upstream, side-stream and downstream areas of the deposit build-up (named as top, side and underside deposit in this project (see Figure 3.19)). The deposit weight was assessed by carefully removing the deposit from each of the three areas of the ceramic section.

The temperature of the fuel particles in the PF and FBC around the deposition probes are approximately of 1000-1100 ^{o}C and 820 ^{o}C, respectively.

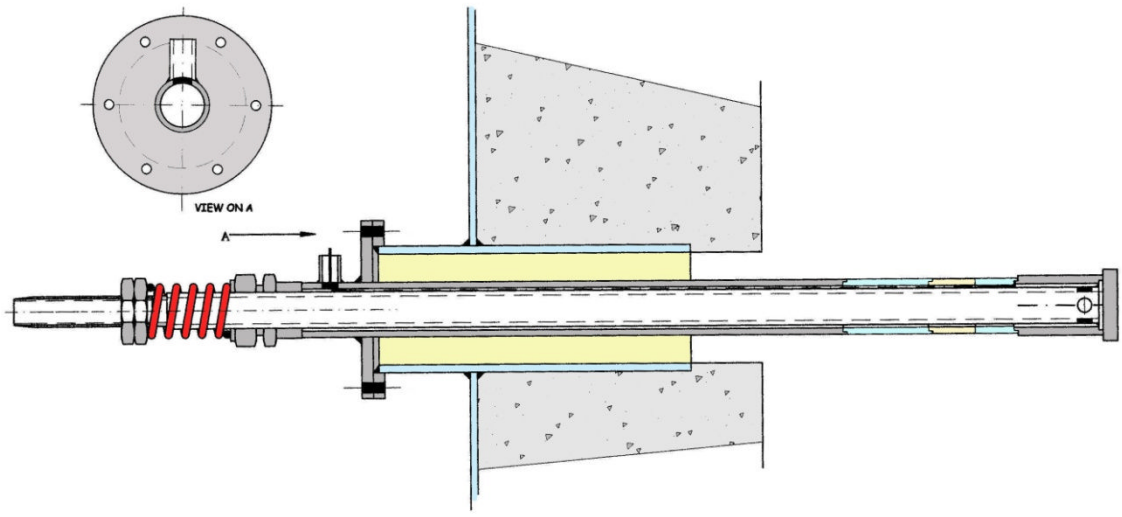

Figure 3.18 Schematic drawing diagram of the deposit collection probe in the combustion chamber

The velocity of the particles (which may strike the deposition probe) can be calculated by dividing the combustion gas flow (of air, gas and fuel composition) at the measured gas temperature by the combustion chamber cross-sectional area; a range of ~ 1.4 m/s (depends on fuel feeding conditions) was found. An example of this particle velocity calculation when feeding Daw Mill coal in the PF combustor is shown below.

Knowing the combustion gas flow rate of 1851.5 l/min, the temperature of the particles of ~ 1100 °C and combustion chamber cross sectional area of 300 × 300 mm, the particles velocity can be calculated as follows:

Particle velocity = [1.8515 (m^3/min) × (1100 + 273)/293 (m^3/min)] / 0.3 × 0.3 (m^2) / 60 (s) = 1.38 m/s.

The rate of deposit build up was defined as the amount of deposit collected per unit surface area of the probe per unit time [Theis et al. 2006]. Using the ceramic sample area (e.g. top surface) and deposit weight collected from that area during the exposure. The rate of the deposit formation (i.e. deposition flux) was calculated with then units mg/cm^2 h.

The original ceramic material was received in cylindrical form. The cylinder was machined and cut into 18 rings (with length mentioned above) and then area for each ceramic ring was calculated (using $2\pi rh$) by measuring height (h) and width (r) using a digital micrometer (with a resolution of ±0.001mm). The ring height was measured inside (ID) and outside (OD) at two different points so an average could be calculated for accuracy. The diagram of the ceramic ring is shown in Figure 3.19 and calculation of each ring is shown in Table 3.10. This calculation served as a reference (i.e. a known ceramic ring was used in a known deposition probe and combustion/co-firing test) of the different rings used for deposition measurement work.

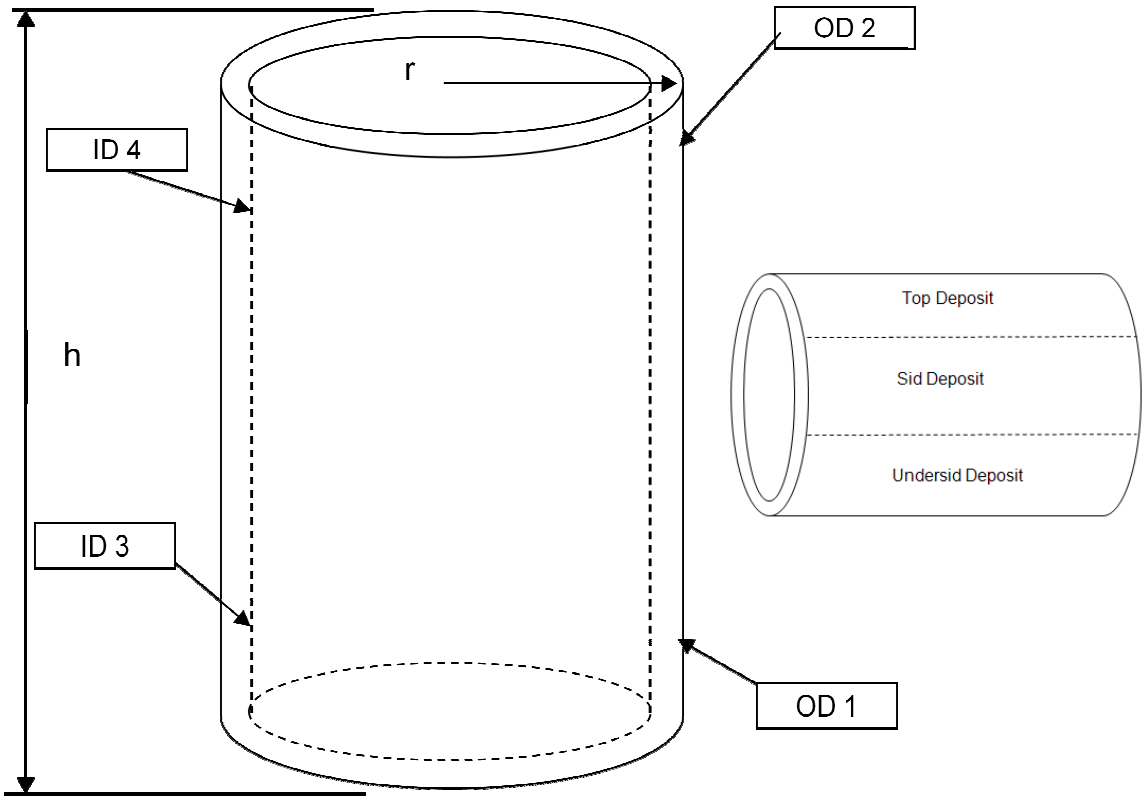

Figure 3.19 Drawing diagram of the ceramic deposition ring

Table 3.10 surface area calculation of cylinder ceramic deposit ring used in the combustion/co-firing exposures

Cylinder no	OD 1 (mm's)	OD 2 (mm's)	Average	ID 3 (mm)	ID 4 (mm)	Average	Cylinder no	OD 1 (mm's)	OD 2 (mm's)	Average	Radius (r)	r * height)	Total surface area (mm^2)
1	39.08	39.16	39.12	32.28	31.99	32.14	1	39.08	39.16	39.120	19.5600	1173.600	7374.90
2	38.86	39.15	39.01	32.14	32.07	32.11	2	38.86	39.15	39.005	19.5025	1170.150	7353.22
3	39.22	39.15	39.19	32.39	32.42	32.41	3	39.22	39.15	39.185	19.5925	1175.550	7387.16
4	39.29	39.03	39.16	32.08	32.13	32.11	4	39.29	39.03	39.160	19.5800	1174.800	7382.44
5	39.24	39.23	39.24	32.32	32.24	32.28	5	39.24	39.23	39.235	19.6175	1177.050	7396.58
6	39.21	39.13	39.17	32.11	32.04	32.08	6	39.21	39.13	39.170	19.5850	1175.100	7384.33
7	39.17	39.14	39.16	32.11	32.05	32.08	7	39.17	39.14	39.155	19.5775	1174.650	7381.50
8	38.96	39.15	39.06	32.35	32.31	32.33	8	38.96	39.15	39.055	19.5275	1171.650	7362.65
9	39.09	39.10	39.10	32.42	32.29	32.36	9	39.09	39.10	39.095	19.5475	1172.850	7370.19
10	39.33	39.20	39.27	32.31	32.45	32.38	10	39.33	39.20	39.265	19.6325	1177.950	7402.24
11	39.03	39.12	39.08	32.02	31.91	31.97	11	39.03	39.12	39.075	19.5375	1172.250	7366.42
12	39.65	39.38	39.52	32.24	32.44	32.34	12	39.65	39.38	39.515	19.7575	1185.450	7449.37
13	39.20	39.05	39.13	32.31	32.09	32.20	13	39.20	39.05	39.125	19.5625	1173.750	7375.85
14	38.95	39.10	39.03	32.15	32.22	32.19	14	38.95	39.10	39.025	19.5125	1170.750	7356.99
15	38.99	39.30	39.15	32.51	32.46	32.49	15	38.99	39.30	39.145	19.5725	1174.350	7379.62
16	39.10	39.29	39.20	32.92	32.35	32.64	16	39.10	39.29	39.195	19.5975	1175.850	7389.04
17	38.99	39.20	39.10	32.51	32.21	32.36	17	38.99	39.20	39.095	19.5475	1172.850	7370.19
18	39.27	39.33	39.30	32.47	32.50	32.49	18	39.27	39.33	39.300	19.6500	1179.000	7408.84

The deposit composition was analysed by using a Scanning Electron Microscope (SEM) equipped with Energy Dispersive X-ray (EDX) analysis [SEM XL30, FEI, Eindhoven, Netherlands]. This was attached to image processing software "imagic –images" and quantitative analysis was performed using the software INCA^{TM} [Oxford Instruments]. Deposit samples were prepared on the front face of 12.5 mm diameter, 6 mm pin length specimen stub [Agar Scientific Ltd., Stansted, Essex, UK] and then placed into specific sample holder for examination. Back-scattered electron detector (BSE) and secondary electron detector (SE) were then used to obtain the analysis from the specimen.

In SEM back scattered imaging was used so that the picture brightness depended on the density or atomic weight of elements present in the sample. The EDX mapping feature was used to produce maps of each element found over the scanned image area. If the element is present in very low concentrations, it is possible to produce only very weak signals or for the background noise to dominate the element map. Figure 3.20 shows an example of the EDX elemental mapping data for two selected elements (K and Cl) obtained for an OSR straw deposit sample. This shown the potassium and chlorine maps indicate fairly uniform brightness layers/structures association between them for presence of potassium chloride.

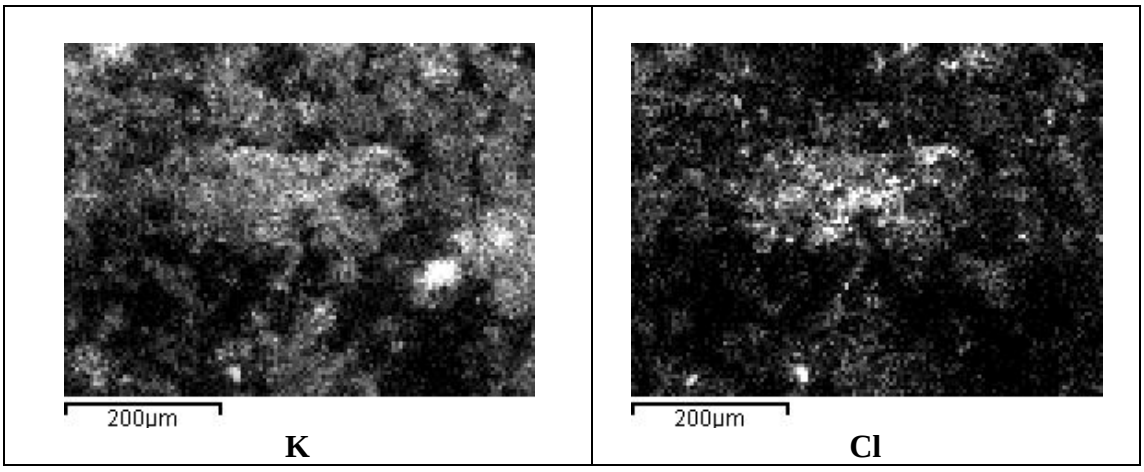

Figure 3.20 SEM image map of pure OSR straw deposit

X-ray Diffraction (XRD) analysis was carried out using a Siemens D5005 X-ray diffractometer. The deposit samples were presented in a powder for identification of the

various crystalline phases (using the characterisation diffraction patterns of each compound). The identification achieved by comparing the X-ray diffraction patterns obtained from the samples with the stored standard media in the XRD control computer (about 50,000 inorganic and 25,000 organic) by a search/match procedure.

3.2.8 Quality assurance (QA) & control

The high cost of performing this type of pilot-scale experimental exposure together with the analysis on a large number of samples precluded sufficient duplicate analysis to allow the estimation of variance for each sample. Also variations between identical exposures are mainly caused by the inherent variability of the fuel properties and the complexity of deposition and solid fuel combustion. However, duplicate exposures/analysis were performed on selected experiments/samples; these repeats showed the relative variability (or relative deviation) to be better than 5-10 %. To quantify variability it is defined here that the relative variability is the standard deviation divided by the average determined from a group of experiments/samples [Miller and Miller, 2000] using the same fuel. The analytical procedures used for deposit composition identification appeared to have no significant source of the experimental variability. However, a major obstacle to be overcome in the sampling procedure is the risk of introducing contamination. Sources of contamination, such as the environment in which the samples were kept, cross-contamination of samples by sampler collection and/or during transport between the combustor and the laboratory, were addressed by establishing a routine to eliminate contamination. Preparation and sample recovery were always conducted in a clean environment and the samples sealed with plastic bags and/or aluminium foil before being transported. Before each deposition probe use the connecting pipe-work was cleaned with dry film lubricant [TBA Industrial Products Ltd., Rochdale, Lanes, UK].

The combustor and feeding systems tools were monitored by analysis/optimisation achieved. The following preliminary study section explained the methods/techniques used.

3.2.9 Preliminary study

3.2.9.1 Optimisation of liquid feeding system operating conditions

Methods

An investigation was carried out of the effects of three independent variables of air flow (Air), temperature (T) and speed voltage transformer (V) on the feeding rate of the bio-oil (viscous liquid) via a liquid feeding system.

The most appropriate and efficient experimental design, a Central Composite Design (CCD), was selected and a design matrix derived in order to investigate the effects of the independent variables. A CCD allows estimation of the main, interactions and quadratic effects of the variables. This design can be considered as a 3^k factorial design with points deleted and modification of some of the remaining points.

In a non-linear 3^k design each of the 'k' variables was studied at three levels allowing quadratic effects to be estimated. This design is orthogonal hence, all the parameters can be estimated. Where 'k' = 3 a 3^3 design produces 27 experiments and can be defined by 8 cube points, 12 edge centre points, 6 face points and a centre point. This design is illustrated as a graphic known as a 'hypercube' shown in Figure 3.21.

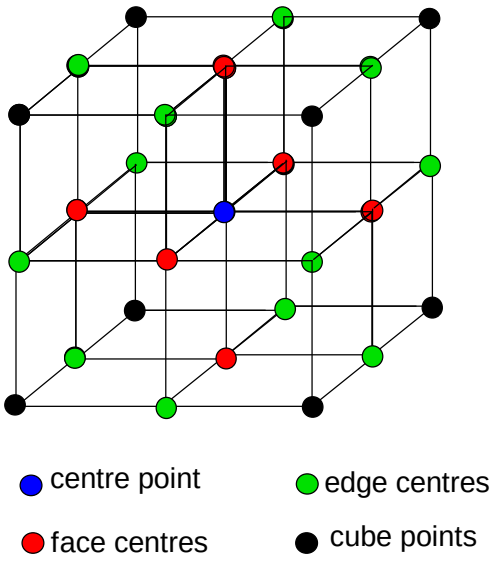

Figure 3.21 Factorial design hypercube

However, the full 3^3 factorial design does not contain replicates and so estimates of experimental error will require extra treatments. The CCD allows estimation of the main, interactions and quadratic effects and requires a smaller number of experiments. It involves removing the edge centre points of the 3^3 cubes and extending the face centres further from the centre to correspond to 'star points'. The CCD maintains the orthogonality of the 3^3 designs even when points are deleted providing the face centre points are extended to a specific distance from the centre and in addition sufficient replicates must be undertaken. A further advantage of the CCD is that it can confer rotability; suggesting that the accuracy of the design is constant at equal distances from the centre points [Miller and Miller, 2000]. Additional replicates were included in the design centre. This can be illustrated as a graphic (see Figure 3.22).

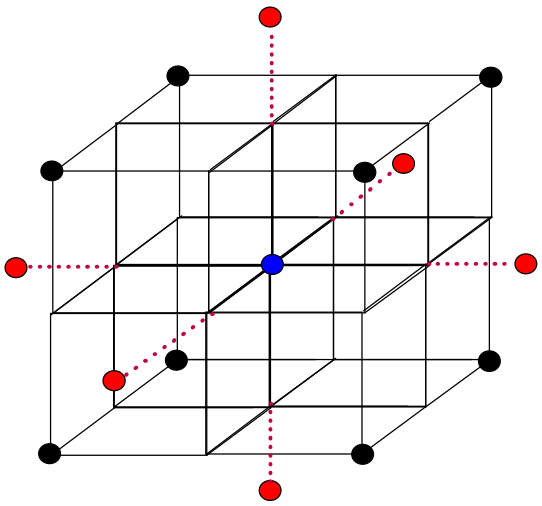

Figure 3.22 A central composite design hypercube

This design can now be seen to equate to a simplified 2^k design of cube points with the addition of the extended face centre points and centre.

Hence, when k= 3 the CCD has 15 treatment combinations and in addition 2 replicates at the design centres (centre points), in total 17 experiments. Each variable is therefore studied at 5 levels and hence, the CCD is more robust.

The 3 levels from the 3^k design **+1, - 1** and **0**. The remaining 2 levels were the 'star points' at a + α and - α distance from the centre. The coded value of α was governed by orthogonality and rotability requirements. In the CCD where the number of independent variables is 3 the value is specifically ± 1.682. The coded design matrix for the CCD was produced using the STATISTICA software package [CSS Statistica/W, Release 5.0 with Industrial units, Statsoft UK, Letchworth, UK] and is explained in Table 3.11. This illustrates the 17 experiments for the 3 variables to be undertaken in randomised blocks over 3 days.

Table 3.11 Coded design matrix

BLOCK	RANDOM EXPERIMENTS	AIR FLOW	TEMP	VOLTAGE
1	5 ©	0	0	0
1	1	-1	-1	-1
1	4	1	1	-1
1	3	-1	1	1
1	2	1	-1	1
2	8	1	1	-1
2	7	1	-1	-1
2	9	1	1	1
2	10 ©	0	0	0
2	6	-1	-1	1
3	14	1.682	0	0
3	11	0	-1.682	0
3	15	0	0	-1.682
3	13	-1.682	0	0
3	12	0	1.682	0
3	16	0	0	1.682
3	17 ©	0	0	0

The star points represent the extremes of variable's levels. Hence, they can be defined as the maximum and minimum values to be used in the design. Therefore, a suitable dataset containing real values at the 5 levels can be assigned, considering the fixed parameters of the feeding system instrument.

The maximum and minimum parameters for the independent variables air flow, temperature and speed voltage were determined to be in the ranges 10 – 100 l/min, 20 –

50 °C, and 100 – 250 volt respectively. The centre points were therefore, taken as 55 l/min, 35 °C and 175 volt, respectively.

The method selected to determine the real values of the cube points at ± **1** was to construct a plot in Excel of real values against coded values. This produced a straight-line plot (see Figure 3.23) allowing interpolation to deduce the values of the 3 variables at the cube points at ± **1** as stated in Table 3.12**.**

Table 3.12 Coded values against real values

	Air flow	Temperature	Voltage
Coded values	Real values	Real values	Real values
-1.682	10	20	100
-1	28	26	130
0	55	35	175
+1	82	44	220
+1.682	100	50	250

Then the calculated real values for the 5 levels of the CCD were tabulated in the design matrix in Table 3.13.

Table 3.13 Design matrix

BLOCK	RANDOM EXPERIMENTS	AIR FLOW	TEMP	VOLTAGE
1	5 ©	55	35	175
1	1	28	26	130
1	4	82	44	130
1	3	28	44	220
1	2	82	26	220
2	8	28	44	130
2	7	82	26	130
2	9	82	44	220
2	10 ©	55	35	175
2	6	28	26	220
3	14	100	35	175
3	11	55	20	175
3	15	55	35	100
3	13	10	35	175
3	12	55	50	175
3	16	55	35	250
3	17 ©	55	35	175

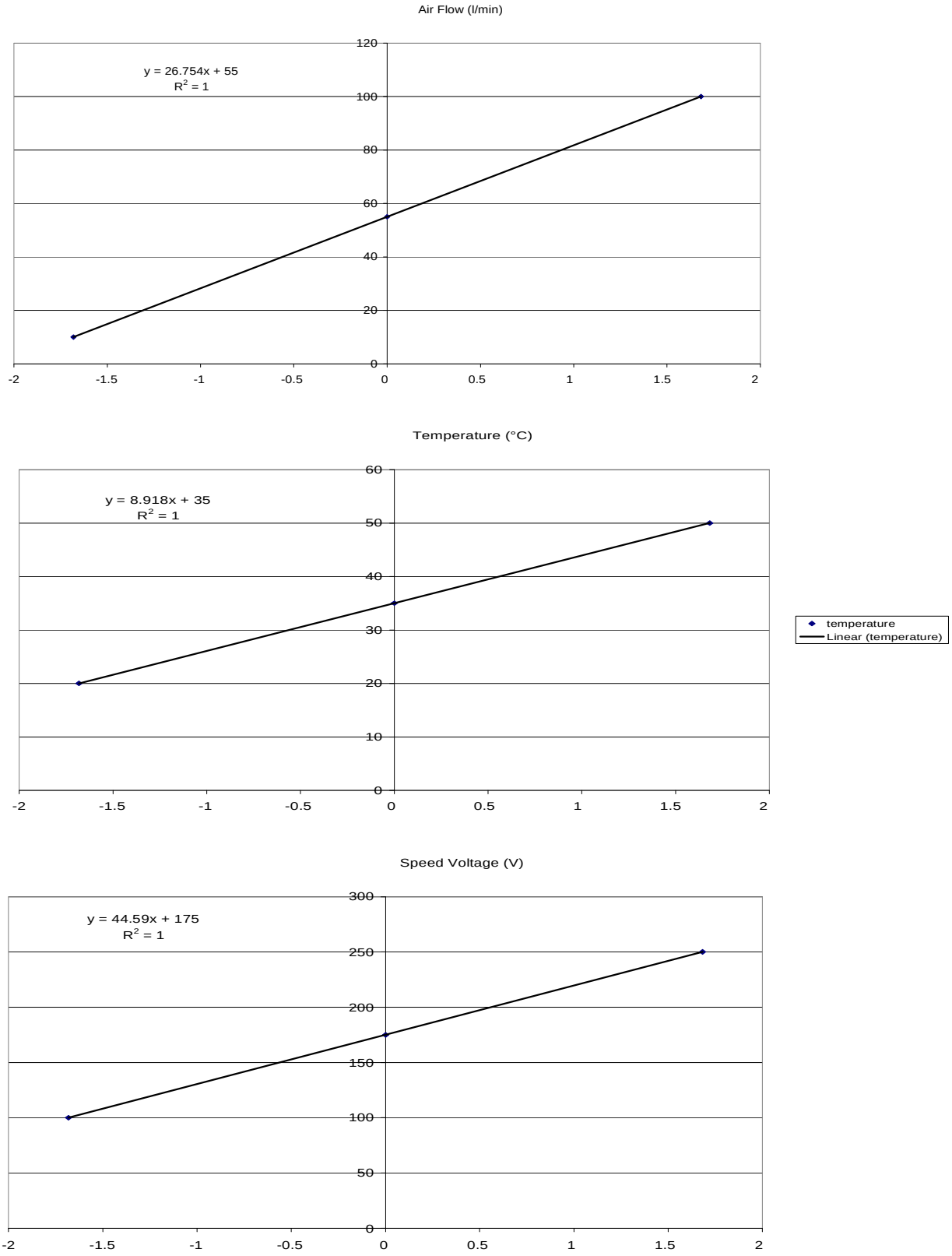

Figure 3.23 A straight-line plots to deduce ± 1 of the 3 variables

Optimisation/achievements

Water was used initially as a control standard to test the system with same conditions. The manual needle valve of the liquid feeding system was kept full open (i.e. maximum) for the seventeen experiments required for the CCD model. The operating parameters and the quantity of bio-oil that was removed from the feeding nozzle for each experiment are shown in Table 3.14.

Table 3.14 Central Composite Design parameters for liquid feeding system

Exp. No.	Air Flow (A) (l/min)	Temp. (T) (^{o}C)	Speed Voltage (V) (volts)	Air ^{2}	Temp.^{2}	Voltage ^{2}	A.T	A. V	T. V	A. T. V	Bio-oil (ml/min)
1	28	26	130	784	676	16900	728	3640	3380	94640	0
2	82	26	220	6724	676	48400	2132	18040	5720	469040	0
3	28	44	220	784	1936	48400	1232	6160	9680	271040	140
4	82	44	130	6724	1936	16900	3608	10660	5720	469040	0
5	55	35	175	3025	1225	30625	1925	9625	6125	336875	24
6	28	26	220	784	676	48400	728	6160	5720	160160	0
7	82	26	130	6724	676	16900	2132	10660	3380	277160	0
8	28	44	130	784	1936	16900	1232	3640	5720	160160	0
9	82	44	220	6724	1936	48400	3608	18040	9680	793760	162
10	55	35	175	3025	1225	30625	1925	9625	6125	336875	24
11	55	20	175	3025	400	30625	1100	9625	3500	182500	0
12	55	50	175	3025	2500	30625	2750	9625	8750	481250	25
13	10	35	175	100	1225	30625	350	1750	6125	61250	14
14	100	35	175	1000	1225	30625	3500	17500	6125	612500	58
15	55	35	100	0	1225	10000	1925	5500	3500	192500	0
16	55	35	250	3025	1225	62500	1925	13750	8750	481250	460
17	55	35	175	3025	1225	30625	1925	9625	6125	336875	25

Multi-linear regression (MLR) was then performed on the data using a mathematical package (Statistica). From the results of the MLR a model for the flow rate of bio-oil from the feeding system can be determined. The significant parameters at the 95 % confidence interval are highlighted in bold in Table 3.15.

Table 3.15 Multi-linear regression on the results from the CCD on bio-oil feeding rate

Variable	*Coefficient*	*P-value*
Intercept	4052.3132	0.0888
T	-21.7235	0.1638
A	-2.7538	0.1023
V	-295.4112	0.1415
T2	-0.0222	0.3790
V2	-3.0480	0.3670
A2	0.0003	0.3531
AT	0.0173	0.0552
TV	3.7158	**0.0296**
AV	0.2126	0.0683
ATV	-0.0022	**0.0258**

It can be seen that the combined temperature and speed voltage (TV), together with the 3 term interaction (ATV) were the most significant parameters at the 95 % confidence level. Individual and quadratic parameters were deemed not to be significant at the 95 % confidence level. The following general equation for the central composite design is:

$$y = b_0 + b_1.X_1 + b_2.X_2 + b_3.X_3 + b_4.X_1^2 + b_5.X_2^2 + b_6.X_3^2 + b_7.X_1.X_2 + b_8.X_1.X_3 + b_9.X_2.X_3 + b_{10}.X_1.X_2.X_3 \quad \textbf{Eq. 3.13}$$

Where y = ml/min of bio-oil flow rate capacity

b_0 = intercept

X_1 = Air Flow

X_2 = Temperature

X_3 = Speed Voltage

The r and r^2 correlation coefficients for this study were 0.9085 and 0.8253, respectively.

Using the above model, a plot of response (amount of bio-oil removed) vs. speed voltage and temperature was produced. This showed that the optimum conditions for the flow of bio-oil from feeding system were a trace heating temperature of 35 °C and speed voltage of 175 volts (air flow was fixed at 55 l/min). These conditions were used in bio-oil combustion work on bio-oil feeding to the combustion chamber to give ~ 24 ml/min feeding rate.

It was also found that this feeding rate can be decreased from 24 to 10 and 0 ml/min when the manual valve is used in the full open, half open or shut positions, respectively. This was taking into account in the work done on the effect of the bio-oil feed rates on flue gas composition (Chapter 6).

3.2.9.2 Optimisation of solid feeding systems performance

Pulverised fuels

Initially, to evaluate the suitability of existing/available feeding systems, three different solid feeding systems were used and coal/biomass flow rates measured: 1) Rospen feeding system [Rospen Industries (UK) Ltd., Stone-house, Gloucestershire]; 2) Accurate feeding system [Accurate Cutting Services (UK) Ltd., Redditich, Worcestershire]; 3) Hopper motorized feeding system [Energy Technology Centre Rig Lab Facilities, Cranfield University, Cranfield, UK].

Feeding systems 1 and 2 consisted of sealed feeders with a wider spiral and a narrow spiral horizontal auger screws respectively, which fed the fuel into a flow of pressurised air. The screws were an increasing pitch auger screws which were driven by a variable speed motor. Feeding system 3 was fitted with valve cylinder drive motor controlled by a speed controller. The hopper was purged with air intermittently which agitated the fuels to prevent slumping, bridging and agglomeration of the materials. Photographs of these feeding systems (includes feeder type) are shown in Figure 3.24. The solid fuels exited all feeding systems through an orifice and were pneumatically conveyed by a

controlled stream of air through a tube line leading to the combustor. The capacity of feeding systems 1, 2 and 3 provides fuel loading of 20, 10 and 10 kg of feedstock respectively. However feeding system 3 includes two hoppers attached to each other for switching and/or refilling for longer tests.

Feeding system 1 Feeding system 2 Feeding system 3

Figure 3.24 Solid feeding systems used in preliminary study

To evaluate the flow rate of pure or blend fuels performance on these feeding systems, the following work was undertaken;

- El-cerrejon coal (100 %, wt) and El-cerrejon coal: Cereal Co-product (80:20 %, wt) were sieved to 2 mm size (average size of 0.5 mm)
- The feeding systems were each filled with 2.0 kg of fuel (accurately weighed)
- Each feeding system was operated at low, middle and full speed
- Feed rate was determined as a function of time
- Repeat measurement were made

The average flow rate (n = 5) results for different feeding systems of both fuels used under full speed operation (as an example) are stated in Table 3.16.

Table 3.16 Results of feeding rate of different fuels using solid feeding systems

	El-cerrejon Coal (100 %, wt)			Coal :CCP (80:20 %, wt)		
	Rospen Feeding 1	Accurate Feeding 2	Hopper Feeding 3	Rospen Feeding 1	Accurate Feeding 2	Hopper Feeding 3
		Fuel Feed (kg)			Fuel Feed (kg)	
	2 (Flow Rate)	2 (Flow Rate)	2 (Flow Rate)	2 (Flow Rate)	2 (Flow Rate)	2 (Flow Rate)
Mean g/min (n = 5)	166	224	111	N/A [a]	179	104
SD	10.05	2.75	0.96	N/A	38.31	1.29
% RSD	6.0	1.2	0.9		21.3	1.2

a Not/Applicable

It can be seen that Hopper feeding system (3) gave average coal flow rate of 111 g/min (0.9 % RSD) and mixture coal: biomass flow rate of 104 g/min (1.2 % RSD). Feeding system 1 was not satisfactory for coal: biomass blend mixture fuel. The feeder could not deliver a consistent flow due to blockage or sticking in the feed pipe. Feeding system 2 gave poor precision and repeatability of fuel mixture flow rate with 21.3 % RSD.

However the hopper feeding system gave good precision but the amount of fuels delivered were too low (e.g. ~ 6.6 kg/hr Coal:CCP, 80:20 %,wt) and not suitable for co-firing tests in respect to the prediction of combustion products calculations (minimum feed ~ 8.1 kg/hr). Results from low and middle speed performance had difficulties in feeding blend fuels. These problems included: (1) feeding materials agglomerated and plugged the feed hopper and the valve cylinder feeder; (2) feed rates were not reproducible; and (3) feed rates were not consistent during a run.

In conclusion, these three feeding systems studied were not suitable for combustion/co-firing exposures.

These problems have been solved by designing and constructing a new feeding system (described in Sec. 3.2.5). The feeding system was designed after a literature review to determine the conditions required to feed materials into a combustor at a constant mass flow rate (and with appropriate quality assurance and control). This is briefly explained as following;

- Literature review: There are only a few literature references for feeding systems. Most laboratory and/or pilot-scale feeders can be classified as either mechanical (e.g. screw feeder), gravity (depend on a smooth flow of material through a controlled opening) or aspirated (feeder suspends the material particles in a gas). The problems encountered in feeding solid materials are formidable. Generally, the irregular shape of the individual solid particles leads to variations in bulk density (due to differences in practical orientation and compaction). Also, the rough surfaces of particles in contact with each other produce varying inter-particle friction so that smooth flow is difficult to maintain. These factors combine to cause common feeder problems such as bridging and slagging. Wilen and Rautalin, 1993 stated the technical requirement of feeder design are: smooth and continuous feed, suitability for handling a variety of bulk material, insensitivity to variation in fuel quality, a sufficient pressure seal against back feeding, accurate feed control, a construction suited to measuring the feed rate, durability and availability. Green et al. 1991 constructed a biomass feeder for use with co-firing biomass and natural gas in a modular incinerator. The system had three hoppers with different size of augers and rotation speed. The injection chute system was connected to the primary combustion chamber in an almost vertical position. A wind box and external fan provided overpressure so the materials were forced into the chamber. From their own experiences, they recommended the following steps when designing biomass feeders for small modular combustor:
  - Design hoppers with walls as close to vertical as possible (wherever possible have a negative slope)
  - Make the hopper walls as smooth as possible (use a low friction coating if necessary)
  - Avoid tight constrictions or conversion points

- Use vibrators on walls with sticking tendencies
- Use drag chains when the above procedures fail
- Use chutes with free fall for injection

- Quality assurance: the following studies/methods were used to ensure the quality of the designed pulverised solid feeding system performance:
  - Feed materials: A wide variety of samples were used. Preliminary feeder tests were conducted with different percentage shares of biomass with coal to study the effect of the fuel properties changes on feeding system. The CCP and miscanthus were blended with the El-cerrejon coal at 0, 20, 40, 60 and 80 %, wt. The samples were screened and the sizes were fine particles in the range less than 2 mm (miscanthus, CCP average size of 0.8 and 0.5 mm, respectively). Fuel mixtures were prepared by mixing the appropriate amount of each in a bucket.
  - Feeder calibration procedure/results: About 4 kg of sample was placed in the feed hopper (for each experiment) and the feed speed was controlled by adjusting the shaker setting (within a range 10-70 speed controller). The whole unit was placed on a weight balance to indicate the change in the weight of the solid fuel in the hopper with time in order to determine the actual feed flow rate of the solid fuel. The cumulative weight delivered (which was pneumatically conveyed by a constant flow of nitrogen, ~ 30 l/min at 2 bar) was measured at 10 minutes intervals during specific shaker setting speed controller (e.g. 10, 20, etc.) and then the procedure was repeated. The result of feeding pure El-cerrejon coal (100 %, wt) as an example is presented in Figure 3.25

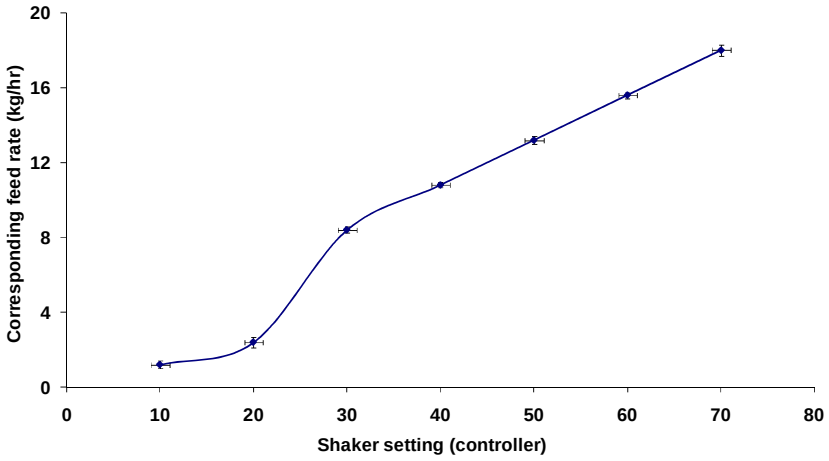

Figure 3.25 Pulverised feeding system feed calibration

It can be seen that increasing the speed of the feed (by the shaker setting controller) increased the feed rate linearly (however, no significant increase between speed of 10 to 20). The degree of reproducibility was very high (SD within a range of 0.15-0.30) as shown by scattering (error bar) data on the graph. The reproducibility decreased below speed control around 20 for such fuel (e.g. pure CCP biomass) indicated the feeding system set start speed at 20. Also, inspection revealed the type of fuel mixes influence the corresponding feeding rate signifying a necessary calibration procedure for each material samples.

- Consistency of feed rate: The consistency of feed rates was studied over a period time (30 minute). Figure 3.26 presents the constancy of feed rate at various sample tests under speed of feed shaking of 30. The results demonstrate that the pulverised feeding system was able to feed at a constant rate. As shown, feeding pure coal gave the highest feed rate (average of 8.3 kg/hr) while the lowest feed rate was from feeding higher shares (≥ 80 %) of biomass for El-cerrejon:CCP fuel mixes (average of 6.3 kg/hr) at the same speed of feed. It could be explained by the difference in density of materials, so the higher density of materials, the higher mass feed rate.

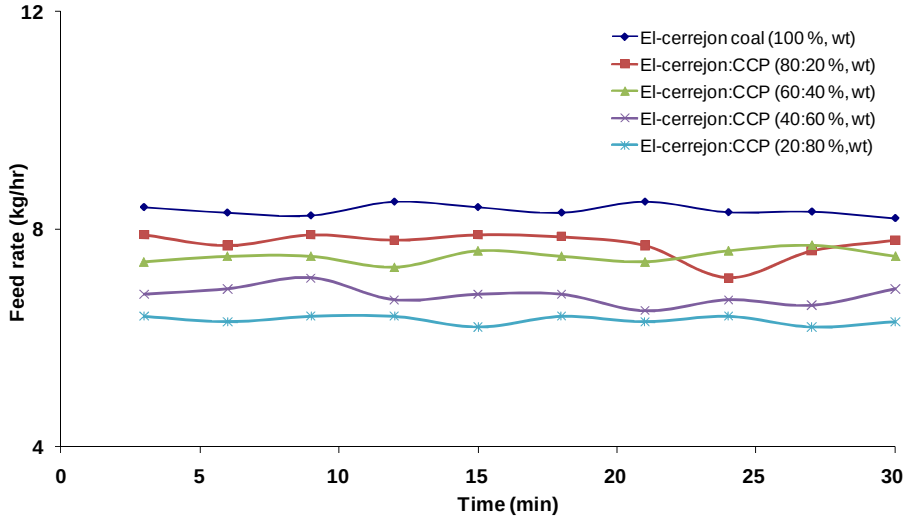

Figure 3.26 Consistency of feed rate of pulverised feeding system over period of time

Pelletised/lump fuels

The solid feeding system for pelletised/lump fuels (described in Sec. 3.2.4) was calibrated with wide variety of samples. The fuel feed was controlled by adjusting the

feed rate (e.g. 40 %, 50 %, etc.) and the corresponding mass flow rate was measured at 10 minutes time period. Figure 3.27 shows the feed rate calibration of coppiced willow fuel (woodchips, up to 5.4 in size) as an example. The results gave a linear straight-line relationship (corresponding feed rate vs. adjusting speed) with an equation of y = 0.1321x – 1.65 and a correlation coefficient of (R^2) 0.9549. Good precision and reproducibility were achieved (SD within a range of 0.7-0.1). Alternatively, the corresponding feed rate using pellets fuel (e.g. OSR straw) was higher (with % RSD significantly lower) than feeding woodchips at the same speed of feed. This can be explained by fuel in pellet form being homogenous than chopped willow, indicating that the larger solid particle size results in a lower feed rate. This proved that feeding miscanthus pellets (individual cylinders of about 7.2 mm long) gave higher feeding rate than OSR straw pellets (individual cylinders of ~ 16.0 mm long) at the same speed of feed.

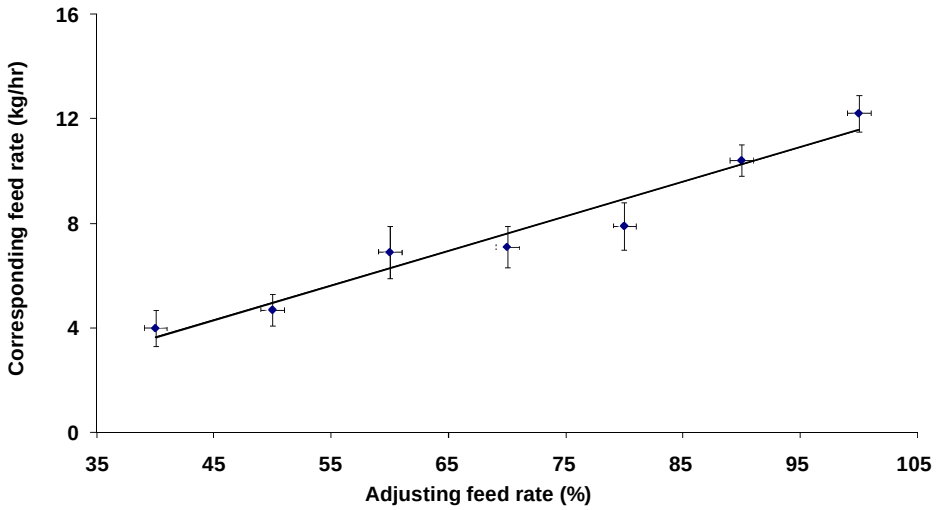

Figure 3.27 Pelletised/lump feeding system feed calibration

3.2.9.3 Operating procedure of combustion rig

In order to operate and control the combustor, different trials/conditions were validated with respect to precision and repeatability. A number of combustion/co-firing tests were carried out as preliminary studies for both solid and liquid fuels.

The observation/investigation work lead to a typical operating procedure. Some observations are recorded here.

Observations/investigations

An initial experiment run started-up the combustion rig with a natural gas-fired pilot burner (~ 55 l/min) and air (~ 1050 l/min) onto the silica bed surface for around 4 to 5 hours. El-cerrejon coal mixed with 20 % CCP biomass was then co-fired. Figures 3.28 and 3.29 show photos of the probe deposit (surface temperature ~ 700 ^{o}C) of the coal:biomass and bio-oil combustion (after ~ one hour test operation run), respectively.

Figure 3.28 Deposit probe of coal: CCP (80:20 %, wt) co-firing, initial run

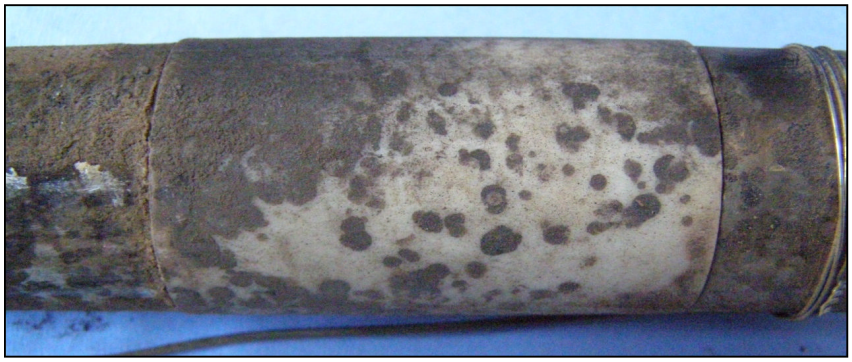

Figure 3.29 Extracted bio-oil deposit probe after combustion, initial run

This proved problematical in as much as can be seen from the ash deposit that the combustion was not complete (confirmed by SEM-EDX identify high concentration of carbon). The problem was identified to be due to the start-up time was not sufficient for the vertical combustion chamber to reach a target temperature of ~ 900 °C in the deposition probe zone. Also the internal construction of the vertical chamber with

concrete side walls could have an effect. If the temperature of the walls is higher than the bulk gas, the passage of the most fuel particles will be altered to the side wall. Figure 3.30 shows the regular (conventional) and altered situations that may occurred for co-firing inside the combustion chamber.

On the other hand, the fuel particles may be forced to go to the side walls, if the feeder flow pointed to it rather than to the centre of the combustion chamber.

To solve these problems, an overnight starting-up of the combustion rig was necessary to achieve target combustor chamber temperature.

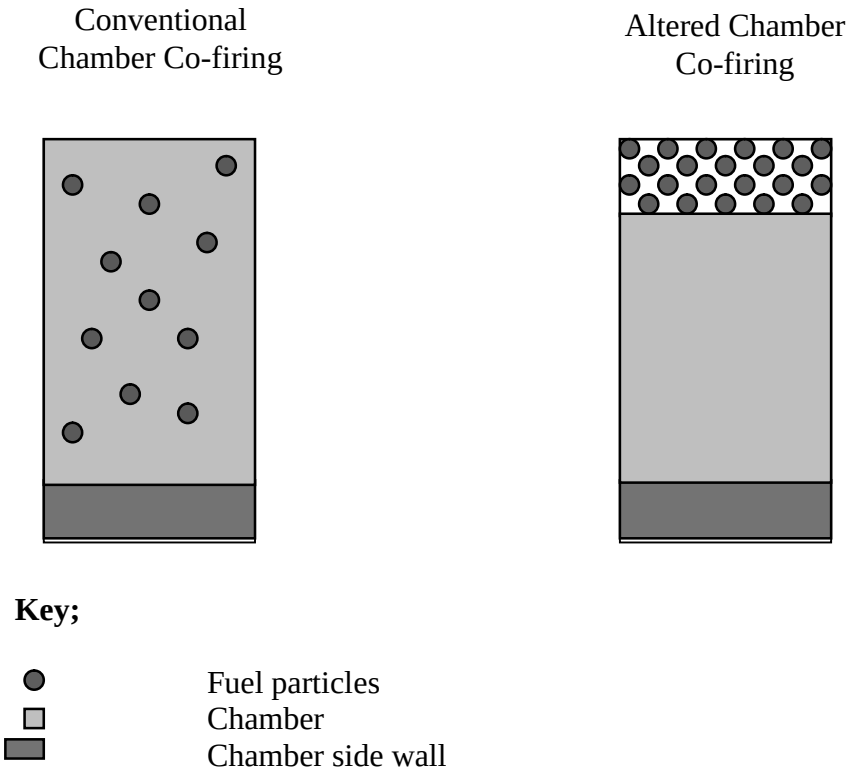

Figure 3.30 Cross section of combustion chamber body showing conventional and altered fuel particles at co-firing

For experimental run, it was found that a natural gas flow of ~ 40 l/min, coupled with an air flow of within a range ~ 1300-1750 l/min, was optimum for a high temperature in the fluidised bed during pre-heating. Also, improved combustion could be achieved at

excess (combusted gas stream output) oxygen content of around 4 volume % (in an acceptable of air/fuel ratio).

The ceramic deposit collector fitted to the probe and its position inside the combustion chamber was also found to be an issue of concern. Attempts were made to adjust the deposit probe (i.e. ceramic type, positions) to enable better deposit collection (i.e. minimise sample losses) during combustion/co-firing. Figure 3.31 shows a broken ceramic deposit collector after extraction (extraction takes place after the combustion rig has cooled down) due to a poorly fitting and type of ceramic collector. This was solved by using another type of ceramic purchased from Multi-Lab Ltd [Tynevale Works, Newcastle Upon Tyne, UK] with higher specification (such as maximum working temperature ~ 1700 °C, good thermal shock resistance) than the initial ceramic used. The full material specification of the ceramic is given in Appendix C (C.1).

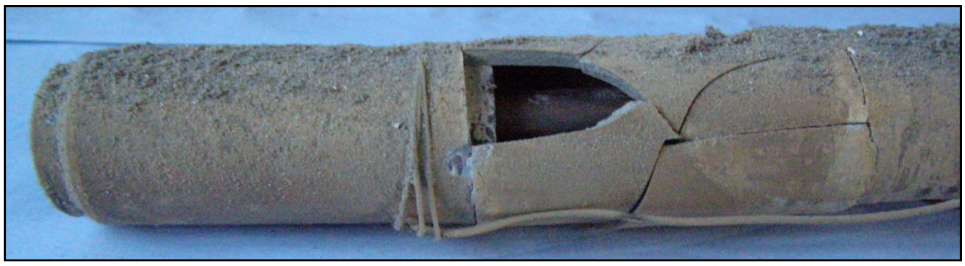

Figure 3.31 Broken deposit ceramic sample after extraction under wrong fitting/type

The deposition probes were located at variable places/ports in the combustion rig to study the effects of the location on the deposition flux. An initial tests run took ~ 1 hour and 30 minutes for co-firing 20 % CCP with El-cerrejon coal. Three deposit probes were exposed in the combustion chamber with nominal target surface temperatures of ~ 600 °C. The results proved that the location of the probe in the combustion chamber had no effect on the deposit layer thickness at the same probe surface temperature.

A major obstacle to be overcome during running of several tests in bio-oil combustion was that it was believed that nozzle feeder blockage may occur if it was kept inside the combustion chamber without cooling (see Figure 3.32). Therefore air should be flowed through the nozzle all the times even when starting to heat the rig, as well as the nozzle having to be withdrawn from the heat after completion of a test. After each use, it was

found to be a necessary routine to clean nozzle components (with Decon 90) in an ultrasonic bath for ~ 1 hour. The feeding tank and connecting pipe-work were soaked internally with hot water to remove any remain bio-oil. All of the components were then rinsed/dried and coated with dry film lubricant.

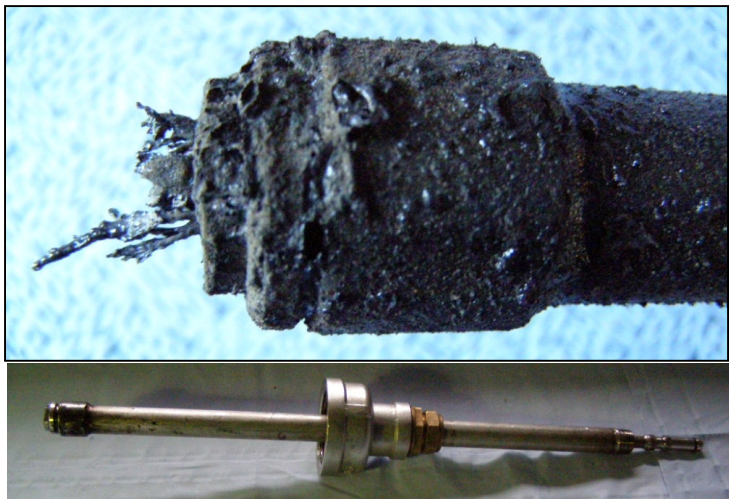

Figure 3.32 Bio-oil nozzle feeder (burner) after extraction under wrong fitting/treatment

Typical operation run

From the results of the preliminary work, a typical run (refer to as the standard) for combustion/co-firing tests of the pilot-scale combustion rig was carried out as follows:

Start-up procedure:

- Install deposit probe inside combustion chamber in a suitable position
- Turn on all water lines
- Turn on compressed air and extracted fan
- Set fluidising air, primary and secondary for the fluidised bed at 1050 l/min
- Set permanent burner at 110 l/min air and 10 l/min gas
- Set main pilot burner at 160 l/min air and 55 l/min gas
- Make sure the combustor is operating under a negative pressure (digital fan speed controller and the differential pressure gauge (difference between the combustor pressure and atmospheric pressure) control the combustor pressure accurately)

- Leave air/gas flow rate for overnight running
- Observe fluidised bed and vertical chamber (pulverised fuel combustion zone) temperatures via thermocouples connected to a monitor display
- When the temperature reaches the desired temperature (i.e. 900 °C) around deposition probe area, start feeding solid or liquid fuel at a typical feed rate
- Decrease the gas and air flow of the main pilot burner until zero, as main burner used to warming up the vertical chamber only (i.e. fuel feeder replaces gas/air feed to combustor)
- The fuel flow rates are adjusted to achieve ~ 4 % oxygen (in the exhaust), which is measured by a FTIR gas analyser
- Keep an eye on flame in the combustion chamber by windows port; do look at it regularly during the test
- Start recording data for the vertical chamber temperature, deposit probe temperature, air inlet (primary and secondary) and flue gas as a function of time.

After the completion of an experimental run, the rig shut-down procedure in a following order is outlined below:

Shut-down procedure:

- Stop feeding solid or liquid fuel
- Turn off gas flow of the permanent burner
- Make sure combustion/co-firing flame had gone away
- Allow air and water to cool down the combustion rig
- When temperature read by thermocouples along the rig reached ~ 100 °C, both water supplied and air were turned off.
- Check that everything is in safety status
- Extract deposit probe for analysis (e.g. SEM analysis) after the combustion rig has cooled down
- At steady state, the fly ash collection device is inserted through sample port (applied in some combustion exposures)

3.3 Test matrix/combustion conditions

Table 3.17 summarise the test matrix of the research experimental and modelling work carried out. Table 3.18 lists the operational combustion conditions used in the study.

Table 3.17 matrix for experimental & modelling testing

Test No.	Experimental Coal:Biomass Co-firing, Pellets & Liquid Combustion			Modelling Coal:Biomass Co-firing, Pellets & Liquid Combustion		
	Materials	**Analysis Gas (FTIR)**	**Analysis SEM, XRD**	**CP**	**HP**	**MTDATA calculation**
1	El-cerrejon Coal (100, % wt)	✔	✔	✔	✔	✔
2	CCP Biomass (100, % wt)	✔	✔	✔	✔	✔
3	El-cerrejon:CCP (20:80, % wt)	✔	✔	✔	✔	✔
4	El-cerrejon:CCP (40:60, % wt)	✔	✔	✔	✔	✔
5	El-cerrejon:CCP (60:40, % wt)	✔	✔	✔	✔	✔
6	El-cerrejon:CCP (80:20, % wt)	✔	✔	✔	✔	✔
7	Daw Mill Coal (100, % wt)	✔	✔	✔	✔	✔
8	Daw Mill:CCP (20:80, % wt)	✔	+	✔	✔	✔
9	Daw Mill:CCP (40:60, % wt)	✔	✔	✔	✔	✔
10	Daw Mill:CCP (60:40, % wt)	✔	+	✔	✔	✔
11	Daw Mill:CCP (80:20, % wt)	✔	+	✔	✔	✔
12	Daw Mill:Miscanth. (20:80, % wt)	✔	+	✔	✔	✔
13	Daw mill:Miscanth. (40:60, % wt)	✔	✔	✔	✔	✔
14	Daw mill:Miscanth. (60:40, % wt)	✔	+	✔	✔	✔
15	Daw mill:Miscanth. (80:20, % wt)	✔	+	✔	✔	✔
16	El-cerrejon:Miscanth. (40:60, % wt)	✔	✔	✔	✔	✔
17	Miscanthus pf (100, % wt)	✔	✔	✔	✔	✔
21	OSR Straw, Pellets (100, % wt) *** 4 Exposures**	✔	+	✔	✔	✔
22	Miscanthus Pellt (100, % wt)	✔	+	✔	✔	✔
23	Coppiced Willow (100, % wt)	✔	✔	✔	✔	✔
24	Bio-oil (100, % wt)	✔	✔	✔	✔	✔

Key;

(✔): Complete investigation done. For deposition analysis using SEM and XRD technique up to around 40 samples (each test) were carried out.

(+): Investigation done using SEM and XRD for high significant samples (~ 18 samples)

Table 3.18 Combustion operating conditions

Feeding	
Solid fuels (pulverised & pellets/lump)	
Solid feeding rate, kg/hr	Calibrate range (1.2-18.0)
Feeding N_2 (pf only) flow rate, l/min	30
Liquid fuels	
Bio-oil feeding rate, l/min	Calibrate range (0.03-0.3)
Bio-oil trace heated, °C	35
Feeding air flow rate, l/min	55
FBC process parameter	
Bed m aterial mass, kg	25
Bed materialtype:	
bed material A (100 %, wt)	Silica sand
bed material B (50:50 %, wt)	Silica sand:limestone
Bed temperature, °C	750-820
PF & FBC combustion process	
Pre-heated air temperature, °C	350
Natural gas flow rate, l/min	40
Total air flow rate, l/min	1730
Total air flow rate (bio-oil combustion), l/min	1325
Water flow rate, l/min	50
Combustor chamber temperature, °C	1200
Deposition probe temperature, °C	~ 500, 600 & 700
Combustor gas temperature at deposition probes, °C	~ 820-1100
Average deposit probes exhaust temperature, °C	~ 132
Combustor run time, hr	~ 3-4

There are a number of areas of experimental uncertainty in the combustion trials, which include errors in the levels of delivered fuels from the feeding systems. This was examined by comparing results from repeated feeding experiments conducted under identical conditions. These repeats showed the relative variability (or relative deviation) to be less than ~ 3 % for pulverised, solid and liquid feeding (Relative variability is defined here as 100 × standard deviation / mean determined from a group of experiments/samples [Miller and Miller, 2000] using the same fuel).

Data from repeated pilot-scale combustion experiments were only available for a limited set of fuels (either used alone or as a blend), due to the expense and scale of

PF/FBC operations. However, from measurements carried out the relative variability in the deposition fluxes calculated for miscanthus pellets, fast pyrolysis bio-oil and CCP:El-Cerrejon coal mixes (at 20, 40 and 60 %, wt) was less than 10 %. The analytical procedures (SEM-EDX, XRD) used for deposit composition identification appeared to have experimental variability of SEM-EDX of ± 0.1 % resolution and ± 1.0 % accuracy of measurements, whereas XRD detection above ~ 5.0 % by volume (except SiO_2). The FTIR gas analyser used in the present work had a high resolution (e.g. CO_2 resolution, % to seven decimal place) and calibrated range of 0-40 %, vol (H_2O), 0-65 %, vol (CO_2), 0-20.9 %, vol (O_2), 0-1500 ppm (NO), 0-1000 ppm (NO_2), 0-100 ppm (N_2O), 0-10000 ppm (SO_2) and 0-2500 ppm (HCl), which this work within these ranges. Therefore, a claim to be able to interpolate within high accuracy division can be justified. However, the slight uncertainties in the combustion efficiencies, flue gas component levels (e.g. NO_x) of the repeated experiments could come from the flue gas composition (i.e. the variation of the CO_2 concentration in the flue gas) and the fractional excess air. The uncertainties of the individual instruments, such as the balance used to weigh the fuels, the rotameter for reading the gas or air flow rates, will also contribute to the overall uncertainty. For example, a 5 % increase in air flow has the effect volume of ~ 0.5 % decrease in CO_2, 0.3 % decrease in H_2O, 0004 % decrease in HCl, 0.002 % decrease in SO_2, 0.1 % increase in N_2 and 0.7 % increase in O_2. Wet chemical analysis of the fuel properties were carried out by E.ON or TES Bretby (both of whom hold UK accreditation for this type of analysis) indicated good precision and repeatability of methods used (in a coverage factor of set of samples). For example, precision for coal analysis determined ± 0.65 % of C, ± 0.05 % of H, ± 0.05 % of N, whereas precision for bio-fuels were ± 0.36 % of C, ± 0.05 % of H and ± 0.08 % of N. Repeatability for coal analysis indicated 0.92 % (C), 0.07 % (H), 0.07 % (N), while bio-fuels gave 0.51 % (C), 0.06 % (H) and 0.11 % (N).

The uncertainty in the modelling of phase equilibria (using MTDATA) was examined by comparing results from repeated runs using the same input data which showed identical (i.e. any errors may come from relating input data), except for the modelling of the 17 elements system. However, an error message may appear during an MTDATA run forcing the need for a re-run to avoid different results. This can be explained as

stated in the NPL manual that the thermodynamic data in the SGTE source database had assembled from a large number of original sources and in some cases properties for individual species had been assumed from those of known species. Therefore, it was impractical to estimate the errors inherent in the predictions, other than those due to the input data.

3.4 Summary

The experimental investigations led to developments of improved solid (in the forms of pulverised fuel and pellets/lumps) and oil firing feeding systems which readily satisfied the experimental requirements (e.g. constant feeding rate) and gave combustion conditions favourable for high combustion efficiencies (using robust/control rig, i.e. under a typical operating run).

The modelling investigations have led to the use of a manage spreadsheet (which was modified to include data collected during the combustion trials) for combustion product and heat generation predictions. MTDATA under “15 elements system” lead to realistic model outputs.

CHAPTER 4 PULVERISED FUELS STUDIES RESULTS & DISCUSSION

4.1 Introduction

This chapter describes the modelling predictions and experimental data based on the combustion of pulverised fuels (two fossil fuels and two biomass; and a mid range of mixtures using the PF combustor. The fuels studied were as follows;

- Pure pulverised fuels (100 %, wt):
  - El-cerrejon coal
  - Daw Mill coal
  - CCP
  - Miscanthus
- Mixtures of pulverised fuels:
  - CCP: El-cerrejon coal (at 20, 40, 60 and 80 %, wt)
  - CCP: Daw Mill coal (at 20, 40, 60 and 80 %, wt)
  - Miscanthus: Daw Mill coal (at 20, 40, 60 and 80 %, wt)
  - Miscanthus: El-cerrejon coal (60:40 %, wt)

Parameters modelled (including combustion product and heat generation predictions, thermodynamic predictions) and experimental measurements (including combustion behaviour, gaseous emissions and depositions) are reported studied and discussed.

Part of this work has already presented (oral and poster papers) and a journal article published (see list of publication in Appendix E):

[1] Ala Khodier, Nigel Simms, Paul Kilgallon and Nigel Legrave. Investigation of gaseous emissions and ash deposition in a pilot-scale PF combustor co-firing cereal co-product biomass with coal. Renewable Energies and Power Quality

Journal, No. 8, Paper 368, April 2010**.** Available at: http://www.icrepq.com/rev-papers-10.html

[2] *Reviewed and accepted in Bioten Proceeding (CPL Press*), A.H.M. Khodier, N.J. Simms, J. E. Oakey and P.J. Kilgallon. Co-firing Daw Mill coal with cereal co-product biomass: ash deposition and gaseous emissions. Bioten Conference, 21-23 September 2010, Birmingham, UK.

[3] *Submitted to Fuel Journal*, A.H.M. Khodier, N.J. Simms, J. E. Oakey and P.J. Kilgallon. Co-firing Daw Mill coal with miscanthus biomass: a comparison of pilot-scale experimental data with predictions of a thermodynamic equilibrium model. The 8th European Conference on Coal Research & Its Applications (ECCRIA8), 6-8 September 2010, Leeds, UK.

4.2 Modelling

4.2.1 Pure fuels

4.2.1.1 El-cerrejon coal

Combustion product prediction

A constant coal feed rate of ~ 7.5 kg/hr and combustor air feed rate of ~ 1670 l/min combined with natural gas feeding rate of 40 l/min were applied for pure El-cerrejon coal combustion test runs. Combustion product predictions were calculated from the fuels compositions listed in Table 3.5 (Chapter 3). Table 4.1 shows the percent volume concentration of CO_2, H_2O, N_2, O_2, HCl and SO_2 calculated (the description of the calculations made is shown in Appendix A2 (spreadsheet example)).

Heat generation prediction

From the heat generation prediction (calculated from Eq. 3.12, Chapter 3), the heat losses of the system was 16.59 % for the combustion of pure El-cerrejon coal. This shows that heat losses were within the expected range when using this scale of combustion units.

MTDATA Calculations

The behaviour of the elements C, H, N, O, S, Cl, Na, K, Fe, Ca, Mg,Ti, Ba, Mn, P ("15 elements system") during combustion of pure El-cerrejon coal were calculated using MTDATA. Figure 4.1 show the percent (by volume) of the major gaseous species, whereas major/minor gaseous and condensed species (moles) are shown in Figure 4.2.

Predicted data of the major gaseous (i.e. CO_2, H_2O, N_2 and O_2) and minor gaseous (HCl and SO_2) at temperature around 1200 ºC (combustion zone temperature) are summarised in Table 4.1. This shows that the MTDATA results were almost identical to the CP results.

Table 4.1 Modelling of pure El-cerrejon coal combustion tests

	Pure El-cerrejon coal	
(%, vol.)	**CP[a]**	**MTDATA[b]** (at 1200 ^{o}C)
CO_2	11.95	11.94
H_2O	8.68	8.68
N_2	75.31	75.30
O_2	4.03	4.00
HCl	0.0010	0.0001
SO_2	0.0305	0.0303

Keys;
(a): Combustion product prediction
(b): Thermodynamic calculations

Also, the equilibrium combustion calculation indicated that the flue gas composition (~ 1200 ºC) of pure El-cerrejon in terms of NO, NO_2, N_2O (Fig. 4.1) were 456.69, 1.17 and 0.0279 ppm, respectively. HCl and SO_3 concentrations became lower at temperature ~ 800 ºC and 380 ºC, respectively. NO_x (NO and NO_2) showed a tendency to increase in the temperature range 200-1300 ºC. N_2O emissions started at around 480 ºC to follow NO_x behavior of increase trend.

The condensed species predicted indicated (Fig. 4.2) mainly sulfates (such as K_2SO_4, $CaSO_4$, Na_2SO_4, $MgSO_4$, $FeSO_4$), oxides (e.g. Fe_2O_3) and phosphate (e.g. K_3PO_4).

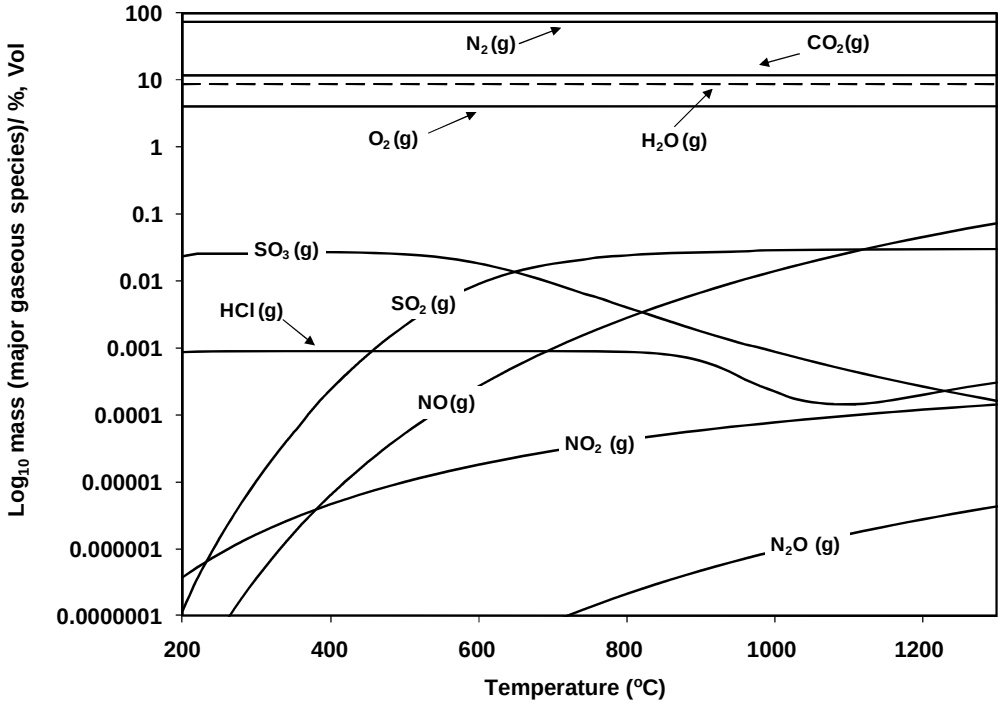

Figure 4.1 Calculated (MTDATA) major gaseous from pure El-cerrejon coal combustion

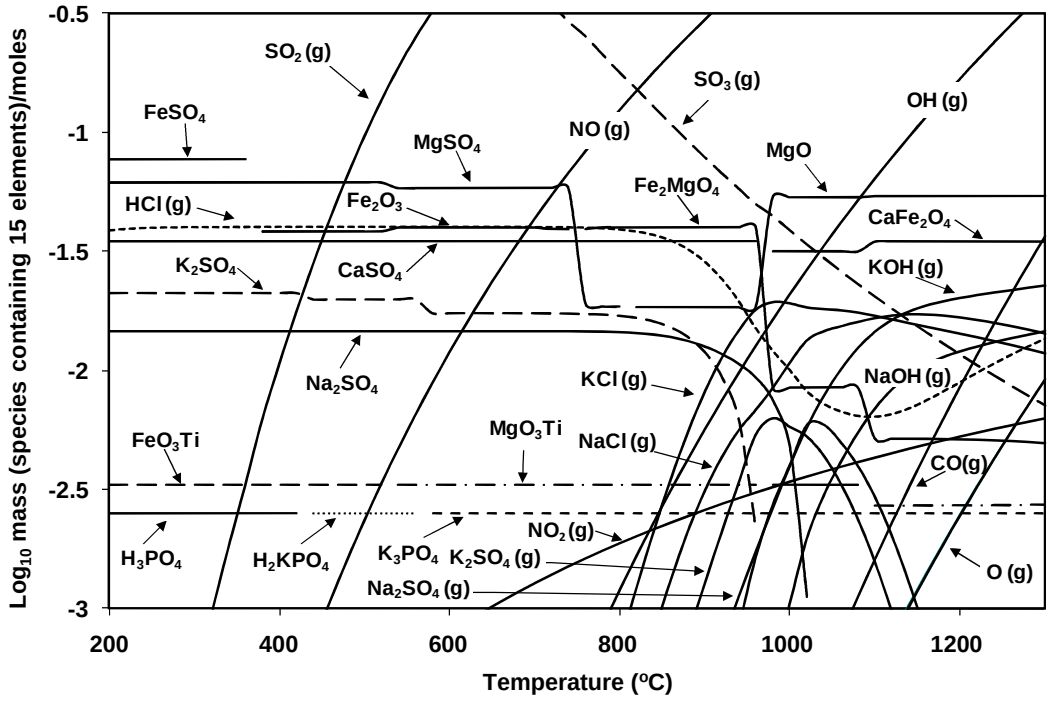

Figure 4.2 Calculated (MTDATA) gaseous & condensed species from pure El-cerrejon coal combustion

4.2.1.2 Daw Mill coal

Combustion product prediction

A constant coal feed rate of ~ 7.4 kg/hr and combustor air feed rate of ~ 1730 l/min combined with natural gas feeding rate of 40 l/min were applied for the pure Daw Mill coal combustion test runs. Combustion product predictions were calculated from the fuel composition listed in Table 3.5 (Chapter 3). Table 4.2 shows the percent (by volume) concentration of CO_2, H_2O, N_2, O_2, HCl and SO_2 calculated (full description of the calculations made are shown in Appendix A3).

Heat generation prediction

From the HP (see Appendix A4), the heat losses of the system was 8.06 % for the combustion of pure Daw Mill coal. This shows that heat losses in the PF using pure Daw Mill were in line with expectations from this scale combustion rig.

MTDATA Calculations

The behaviour of the elements ("15 elements system") during combustion of pure Daw Mill coal was calculated using MTDATA. Figure 4.3 show the percent (by volume) of the major gaseous species, whereas major/minor gaseous and condensed species (moles) are shown in Figure 4.4.

The predicted data of the major gaseous (i.e. CO_2, H_2O, N_2 and O_2) and minor gaseous (HCl and SO_2) at ~ 1180 ºC (combustion zone temperature) are summarised in Table 4.2. This shows that MTDATA results were almost identical to CP results.

The equilibrium combustion calculation indicated that the flue gas composition (~ 1180 ºC) of pure Daw Mill coal in terms of NO, NO_2, N_2O (Fig. 4.3) were 411.22, 1.12 and 0.0253 ppm, respectively. HCl remains almost constant all temperatures, whereas, NO_x

(NO and NO_2, started at 200 ºC) and N_2O emissions (started at 420 ºC) tend to increase with temperature.

Table 4.2 Modelling of pure Daw Mill coal combustion tests

	Pure Daw Mill coal	
(%, vol.)	**CP[a]**	**MTDATA[b]** (at 1180 °C)
CO_2	12.17	12.18
H_2O	8.25	8.25
N_2	75.50	75.55
O_2	4.00	3.97
HCl	0.0092	0.0085
SO_2	0.0646	0.0634

Keys;
(a): Combustion product prediction
(b): Thermodynamic calculations

The condensed species formed from the combustion of pure Daw Mill coal indicated possible similarities to those of pure El-cerrejon coal. However, concentrations and temperature ranges were varied (e.g. Ca_2SO_4 with concentration of ~ log -1.05 (200-1180 °C) of pure Daw Mill compared to concentration of ~ log -1.46 (200-960 °C) of pure El-cerrejon coal). Manganese sulfates ($MnSO_4$) concentrations from Daw Mill were higher than El-cerrejon coal (not shown in Fig. 4.2 of El-cerrejon, as it below the scale fraction 10^{-3}), whereas magnesium sulfates ($MgSO_4$) reported higher in El-cerrejon compared to Daw Mill coal. This can be related to fuel compositions of more Mn and less Mg in Daw Mill compared to El-cerrejon coal (see Table 3.5, Chapter 3). Phosphate (e.g. K_3PO_4) was not predicted in Daw Mill, this may be due to the missing data of P_2O_5 in ash composition (see Table 3.5, Chapter 3) being below the detection limit of analysis. However, P was confirmed to be condensed on probe deposition of Daw Mill coal combustion (see below Sec. 4.3.3 and Fig. 4.42.a)

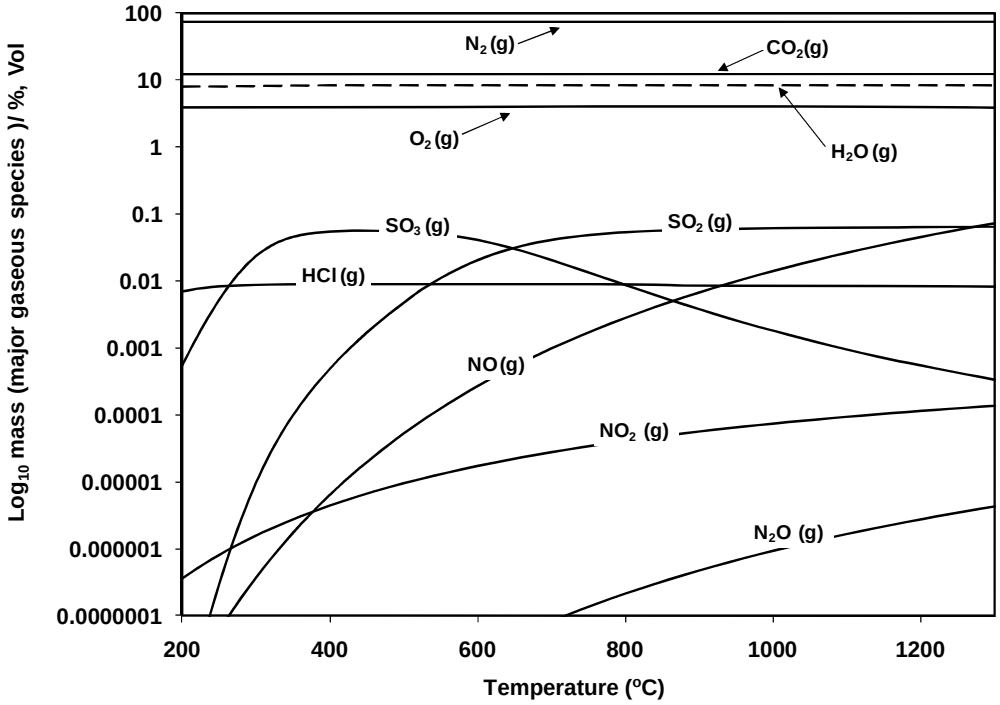

Figure 4.3 Calculated (MTDATA) major gaseous species from pure Daw Mill coal combustion

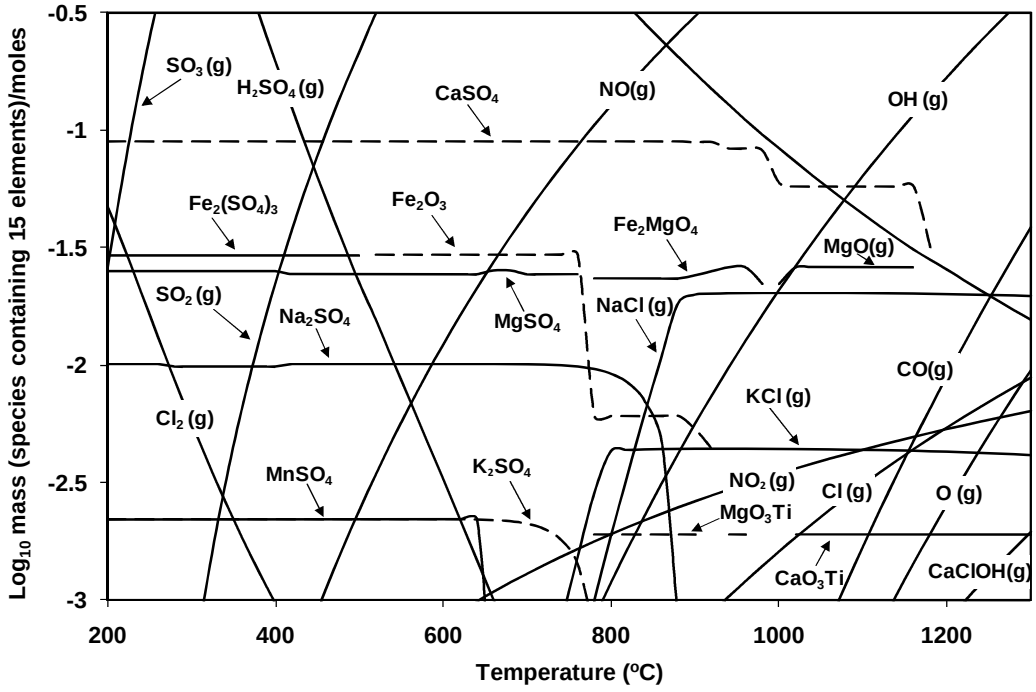

Figure 4.4 Calculated (MTDATA) gaseous & condensed species from pure Daw Mill coal combustion

4.2.1.3 CCP biomass

Combustion product prediction

A constant CCP feed rate of ~ 9.2 kg/hr and combustor air feed rate of ~ 1380 l/min combined with natural gas feeding rate of 40 l/min were applied for pure CCP biomass combustion test runs. Combustion product predictions were calculated from the fuels compositions listed in Table 3.6 (Chapter 3). Table 4.3 shows the percent (by volume) concentration of CO_2, H_2O, N_2, O_2, HCl and SO_2 calculated.

Heat generation prediction

From the HP (calculated from Eq. 3.12, Chapter 3), the heat losses of the system was 10.08 % for the combustion of pure CCP.

MTDATA Calculations

Figure 4.5 and Figure 4.6 show the percent (by volume) of the major gaseous species, major/minor gaseous and condensed species (moles), respectively. Predicted data of the major gaseous (i.e. CO_2, H_2O, N_2 and O_2) and minor gaseous (HCl and SO_2) at ~ 1200 ºC (combustion zone temperature) are summarised in Table 4.3. The results revealed very similar MTDATA predictions to CP calculations.

For NO_x emissions, the equilibrium combustion calculation indicated that the flue gas composition (~ 1200 ºC) of pure CCP of NO, NO_2, N_2O (Fig. 4.5) were 448.36, 1.16 and 0.0267 ppm, respectively.

The condensed species formed from the combustion of pure CCP includes, in addition to condensed species from coals (i.e. sulfates, oxides and phosphates), an alkali chloride (Fig. 4.6). Potassium chloride (KCl) was predicted with concentration range of ~ log -2.17 to log -2.99 and temperature range of 200-680 °C.

Generally, hematite (Fe_2O_3) showed lower concentrations (~ log -2.20) compared to El-cerrejon (~ log -1.42) and Daw Mill (~ log -1.53), whereas potassium phosphate (K_3PO_4) reveled higher concentration of ~ log -1.53 compared to El-cerrejon of ~ log -2.60.

Table 4.3 Modelling of pure CCP biomass combustion tests

	Pure CCP biomass	
(%, vol.)	**CP[a]**	**MTDATA[b]** (at 1200 ^oC)
CO_2	11.10	11.10
H_2O	12.99	12.98
N_2	71.81	71.80
O_2	4.08	4.04
HCl	0.0114	0.0108
SO_2	0.0118	0.0117

Keys;
(a): combustion product prediction
(b): Thermodynamic calculations

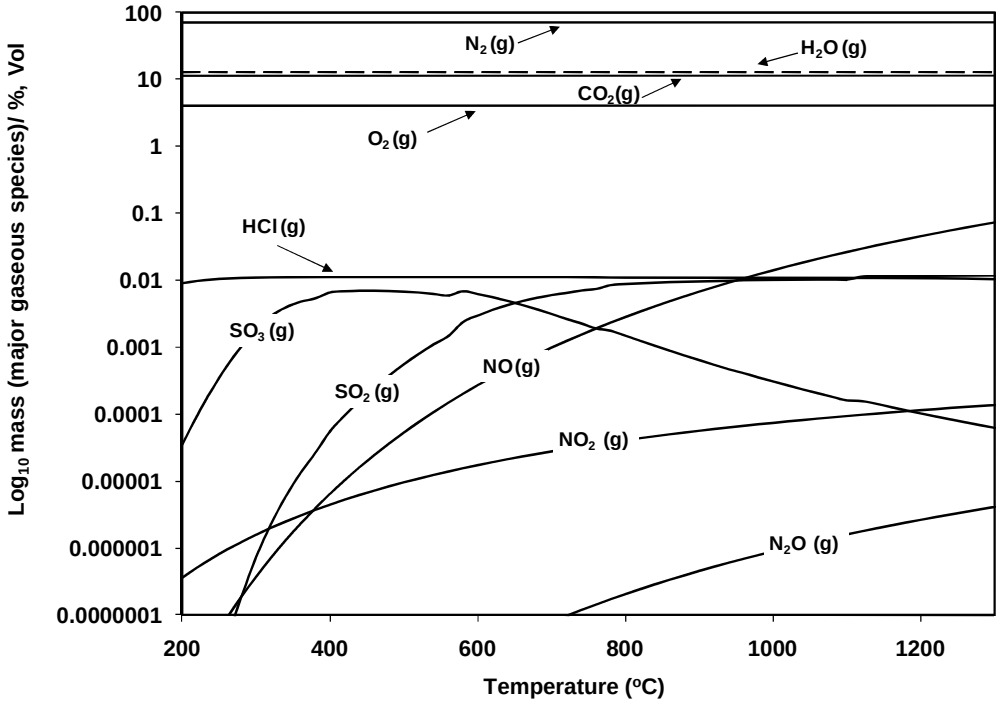

Figure 4.5 Calculated (MTDATA) major gaseous species from pure CCP biomass combustion

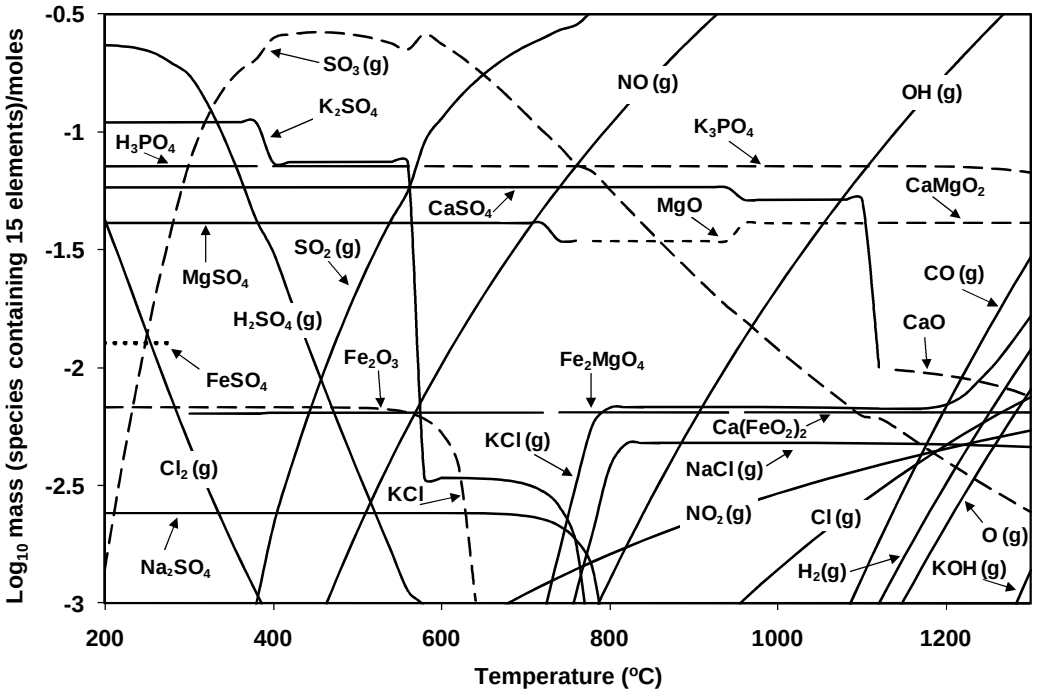

Figure 4.6 Calculated (MTDATA) gaseous & condensed species from pure CCP biomass combustion

4.2.1.4 Miscanthus biomass

Combustion product prediction

A constant miscanthus feed rate of ~ 13.68 kg/hr and combustor air feed rate of ~ 1730 l/min combined with natural gas feeding rate of 40 l/min were applied for pure miscanthus biomass combustion test runs. Combustion product predictions were calculated from the fuels compositions listed in Table 3.6 (Chapter 3). Table 4.4 shows the percent volume concentration of CO_2, H_2O, N_2, O_2, HCl and SO_2 calculated (the description of the calculations made is shown in Appendix A2 (spreadsheet example)).

Heat generation prediction

From the HP (calculated from Eq. 3.12, Chapter 3), the heat losses of the system was 9.70 % for the combustion of pure miscanthus.

MTDATA Calculations

Figures 4.7 and 4.8 present the percent (by volume) of the major gaseous species, major/minor gaseous and condensed species (moles), respectively. Predicted data for the major gaseous (i.e. CO_2, H_2O, N_2 and O_2) and minor gaseous (HCl and SO_2) at ~ 1180 ^oC (combustion zone temperature) are summarised in Table 4.4. The results showed that the MTDATA predictions were similar to the CP calculations.

The equilibrium combustion calculation of NO_x emissions indicated that the flue gas composition of pure miscanthus at ~ 1180 ^oC for NO, NO_2, N_2O (Fig. 4.5) were 399.34, 1.09 and 0.0239 ppm, respectively.

Condensed KCl was predicted with concentration range of ~ log -1.30 to log -2.07 at temperature range of 200-580 °C along with others (such as K_2SO_4, $CaSO_4$, Na_2SO_4, $MgSO_4$, $Fe_2(SO_4)_3$, Fe_2O_3, K_3PO_4, etc., (Fig. 4.8)). It should pointed out that the most significant condensed Na species was sodium phosphate (Na_3PO_4) as predicted almost in all temperatures range (at 260-1300 °C), while, condensed Na_2SO_4 was at 200-240 °C. This was not the case in other pure biomass CCP studied, as condensed Na_2SO_4 was the dominant species with no formation of Na_3PO_4. This may be explained by the S, Na, P ratio in the fuel composition (Table 3.6, Chapter 3).

Table 4.4 Modelling of pure miscanthus biomass combustion tests

	Pure miscanthus biomass	
(%, vol.)	**CP[a]**	**MTDATA[b]** (at 1180 ^oC)
CO_2	12.25	12.25
H_2O	12.46	12.46
N_2	71.27	71.26
O_2	4.00	3.97
HCl	0.0071	0.0070
SO_2	0.0097	0.0093

Keys;
(a): Combustion product prediction
(b): Thermodynamic calculations

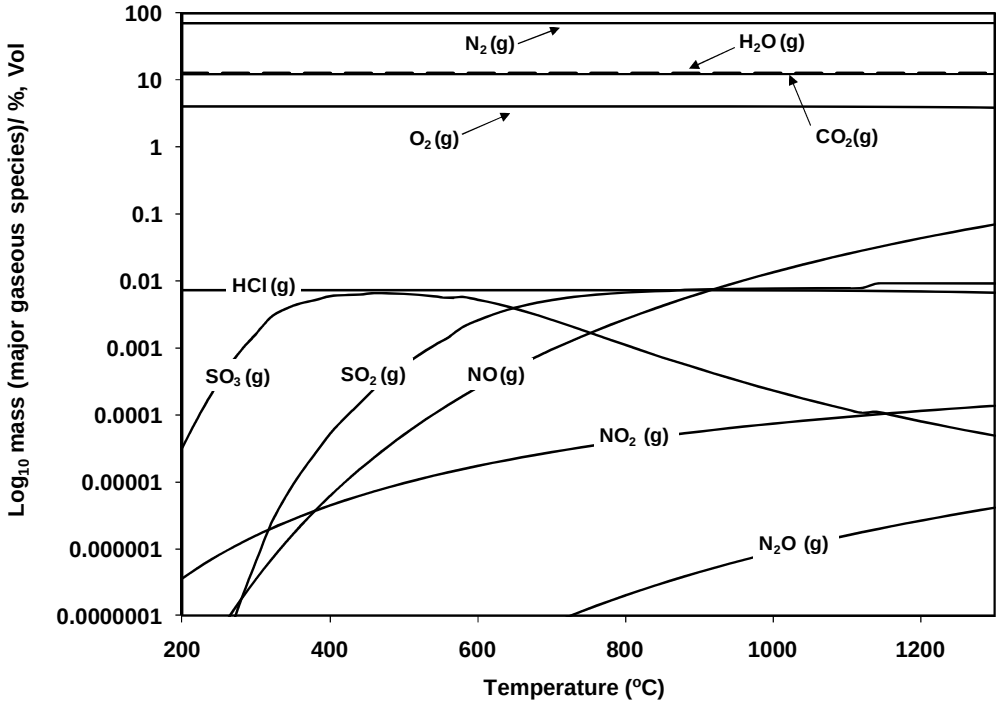

Figure 4.7 Calculated (MTDATA) major gaseous species from pure miscanthus biomass combustion

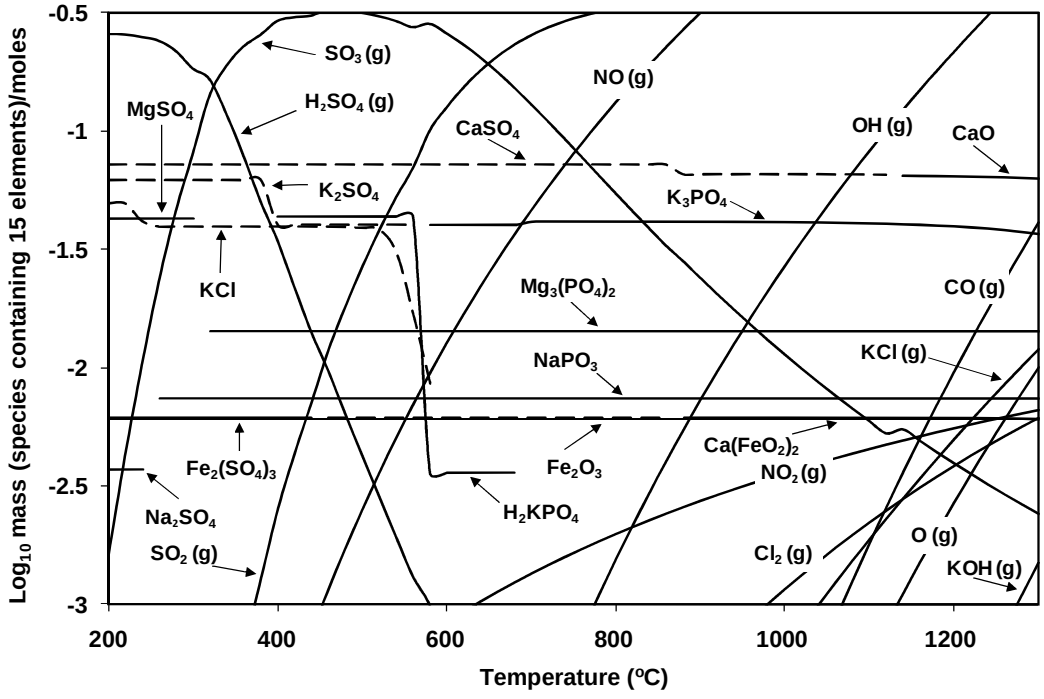

Figure 4.8 Calculated (MTDATA) gaseous & condensed species from pure miscanthus biomass combustion

4.2.2 Blend mixtures fuels

4.2.2.1 Co-firing CCP: El-cerrejon coal (20, 40, 60 and 80 %, wt)

Combustion product prediction

Constant fuel feed rates of about 7.9, 8.5, 9.0 and 9.6 kg/hr were applied for mixed fuel CCP:El-cerrejon , 20:80 %, wt, CCP:El-cerrejon, 40:60 %, wt, CCP:El-cerrejon, 60:40 %, wt) and CCP:El-cerrejon, 80:20 %, wt, co-firing test runs, respectively. Table 4.5 shows the percent (by volume) concentration of CO_2, H_2O, N_2, O_2, HCl and SO_2 calculated for co-firing CCP:El-cerrejon mixed fuels.

Heat generation prediction

From the HP (calculated from Eq. 3.12, Chapter 3), the heat losses of the system was 14.51, 12.62, 9.76, 12.49 % for co-firing El-cerrejon coal with 20 % CCP, 40 % CCP, 60 % CCP and 80 % CCP, respectively. These losses are in the range expected for this scale of combustion test rig.

MTDATA Calculations

Calculated data of the major and minor gaseous emissions by the equilibrium model (using “15 elements system”) of co-firing El-cerrejon coal with 20 % CCP, 40 % CCP, 60 % CCP and 80 % CCP are shown in Figures 4.9.a, 4.9.b, 4.9.c and 4.9.d, respectively. Predicted data of the major gaseous (i.e. CO_2, H_2O, N_2 and O_2) and minor gaseous (HCl and SO_2) at ~ 1200 ºC (combustion zone temperatures) are summarised in Table 4.5. These show that combustion product predictions were consistent with the MTDATA predictions. They also suggests decrease tendency of CO_2 and SO_2 with increase trend of moisture and HCl gaseous emissions.

The NO emissions predicted (at ~ 1200 ºC, Fig. 4.9.(a-d)) were 456.94, 453.30, 453.06 and 446.96 ppm for co-firing El-cerrejon coal with 20 % CCP, 40 % CCP, 60 % CCP

and 80 % CCP, respectively. This may suggested no variation impact of co-firing coal with biomass on NO emissions under combustion conditions.

The behaviour of condensed species (combined with minor gaseous species) during co-firing El-cerrejon coal with 20 % CCP, 40 % CCP, 60 % CCP and 80 % CCP are shown in Figures 4.10.a, 4.10.b, 4.10.c and 4.10.d, respectively. This shows that the condensed species formed in all mixed fuels were $CaSO_4$, $CaFe_2O_4$, K_2SO_4, Na_2SO_4, Fe_2MgO_4, Fe_2O_3, $FeSO_4$, K_3PO_4, MgO and MgO_3Ti. Also, it showed that Ca (e.g. $CaSO_4$) and P (e.g. K_3PO_4) species increased, while Fe species (e.g. Fe_2O_3) decreased as CCP biomass share increased. Condensed $NaPO_3$ was predicted to start at co-firing El-cerrejon with 40 % CCP with concentrations decreased as CCP share increased.

Condensed KCl was not predicted for the co-firing mixed fuels. It is obvious that Cl was predicted in gaseous species such as HCl, Cl, Cl_2 and KCl with increase tendency as CCP share increased.

Table 4.5 Modelling of co-firing mixed fuel of CCP:El-cerrejon tests

	CCP:El-cerj. mix 1[a]		**CCP:El-cerj. mix 2[b]**		**CCP:El-cerj. mix 3[c]**		**CCP:El-cerj. mix 4[d]**	
(%, vol.)	**CP[e]**	**MTDATA[f]** (at 1200 ^oC)	**CP**	**MTDATA** (at 1200 ^oC)	**CP**	**MTDATA** (at 1200 ^oC)	**CP**	**MTDATA** (at 1200 ^oC)
CO_2	11.82	11.82	11.76	11.76	11.60	11.60	11.49	11.49
H_2O	9.29	9.29	10.01	10.00	10.82	10.82	11.84	11.83
N_2	74.79	74.78	74.18	74.18	73.48	73.49	72.64	72.64
O_2	4.07	4.03	4.03	4.00	4.07	4.04	4.00	3.97
HCl	0.0025	0.0014	0.0044	0.0028	0.0065	0.0052	0.0090	0.0080
SO_2	0.0278	0.0274	0.0249	0.0246	0.0213	0.0211	0.0173	0.0211

Keys;
(a): CCP: El-cerrejon coal, 20:80 %
(b): CCP: El-cerrejon coal, 40:60 %
(c): CCP: El-cerrejon coal, 60:40 %
(d): CCP: El-cerrejon coal, 80:20 %
(e): Combustion product prediction
(f): Thermodynamic calculations

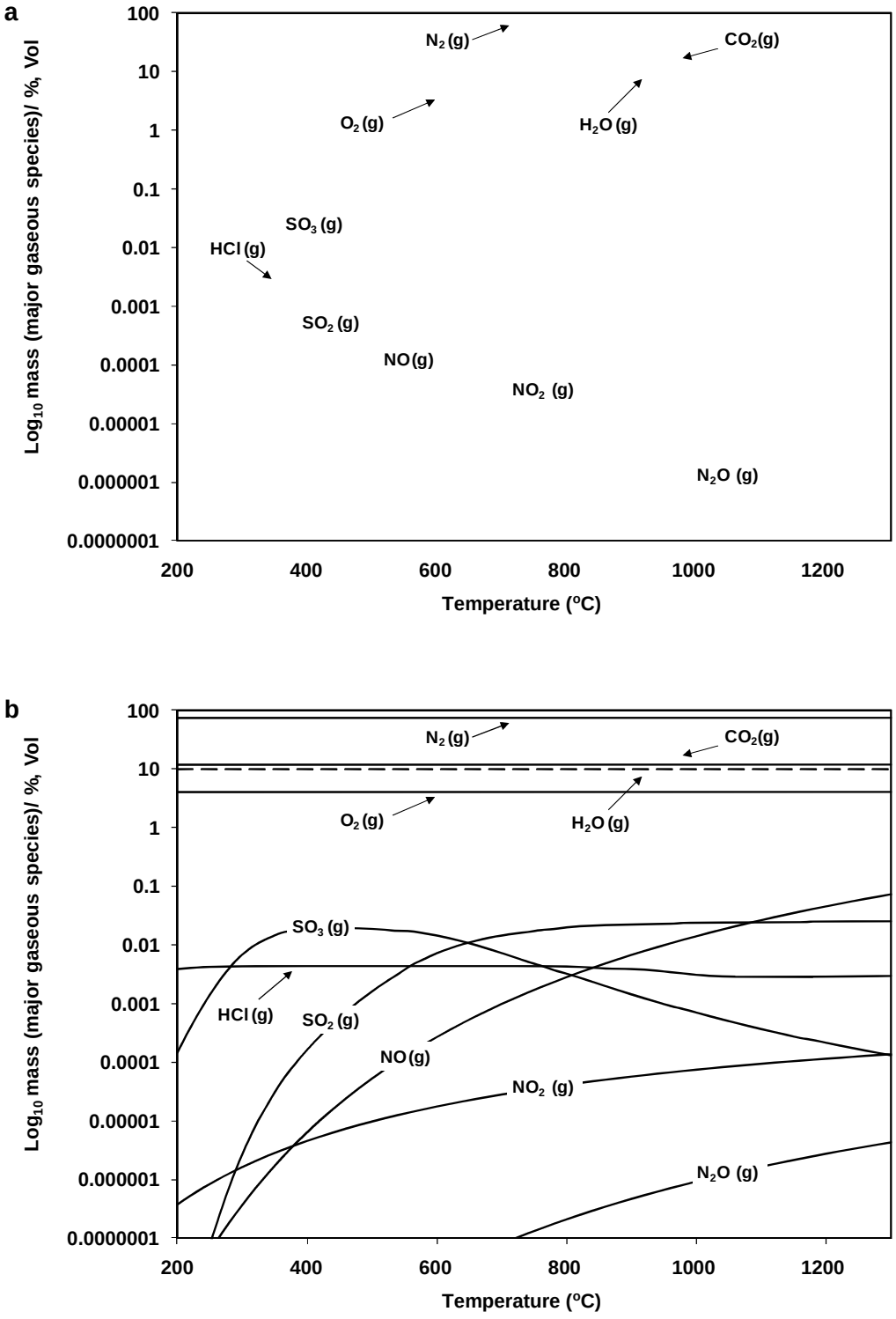

Figure 4.9 Calculated (MTDATA) major gaseous species from co-firing mixed fuels of a) CCP:El-cerrejon coal (20:80 %, wt) and b) CCP:El-cerrejon coal (40:60 %, wt**)**

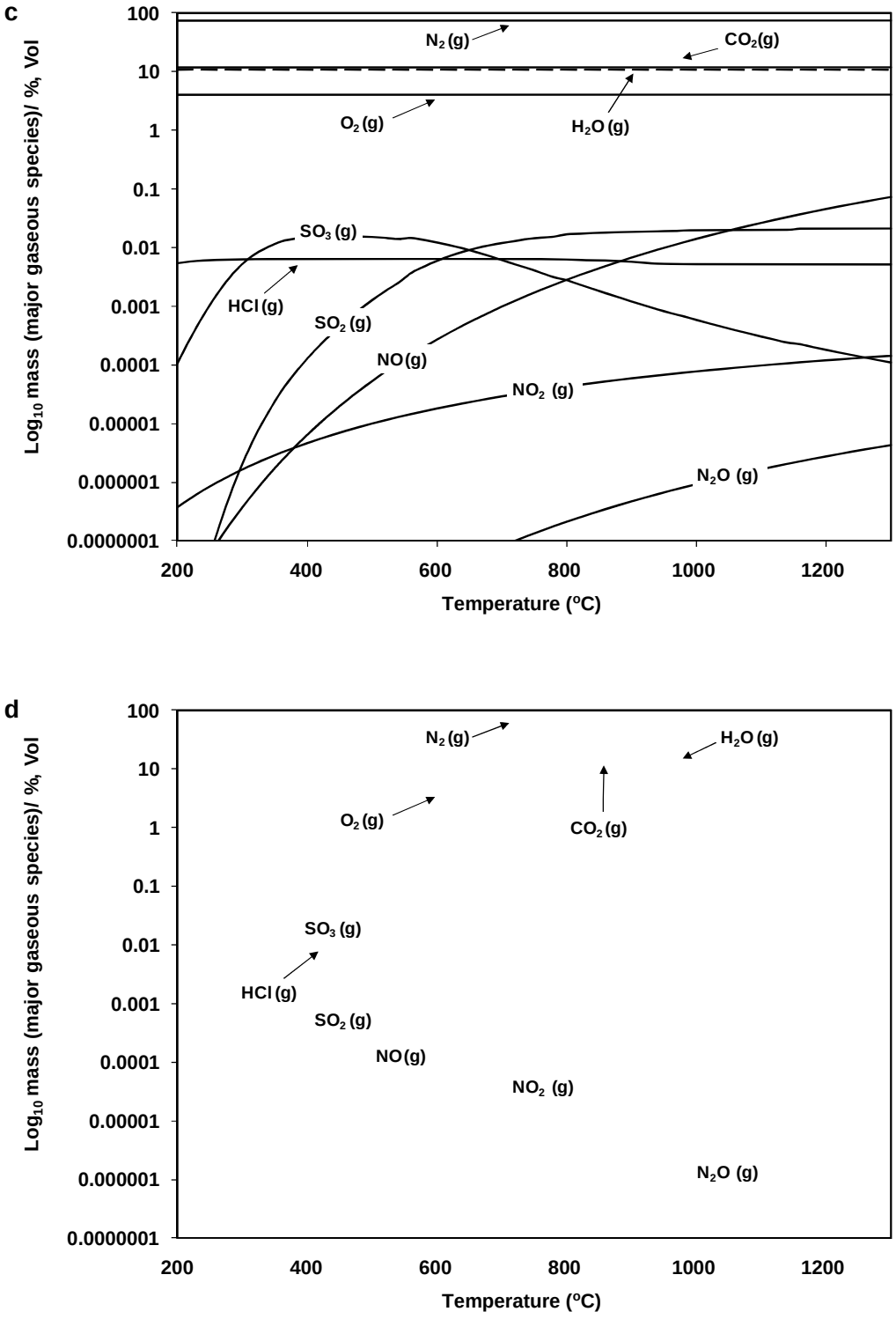

Figure 4.9 Calculated (MTDATA) major gaseous species from co-firing mixed fuels of c) CCP:El-cerrejon coal (60:40 %, wt) and d) CCP:El-cerrejon coal (80:20 %, wt)

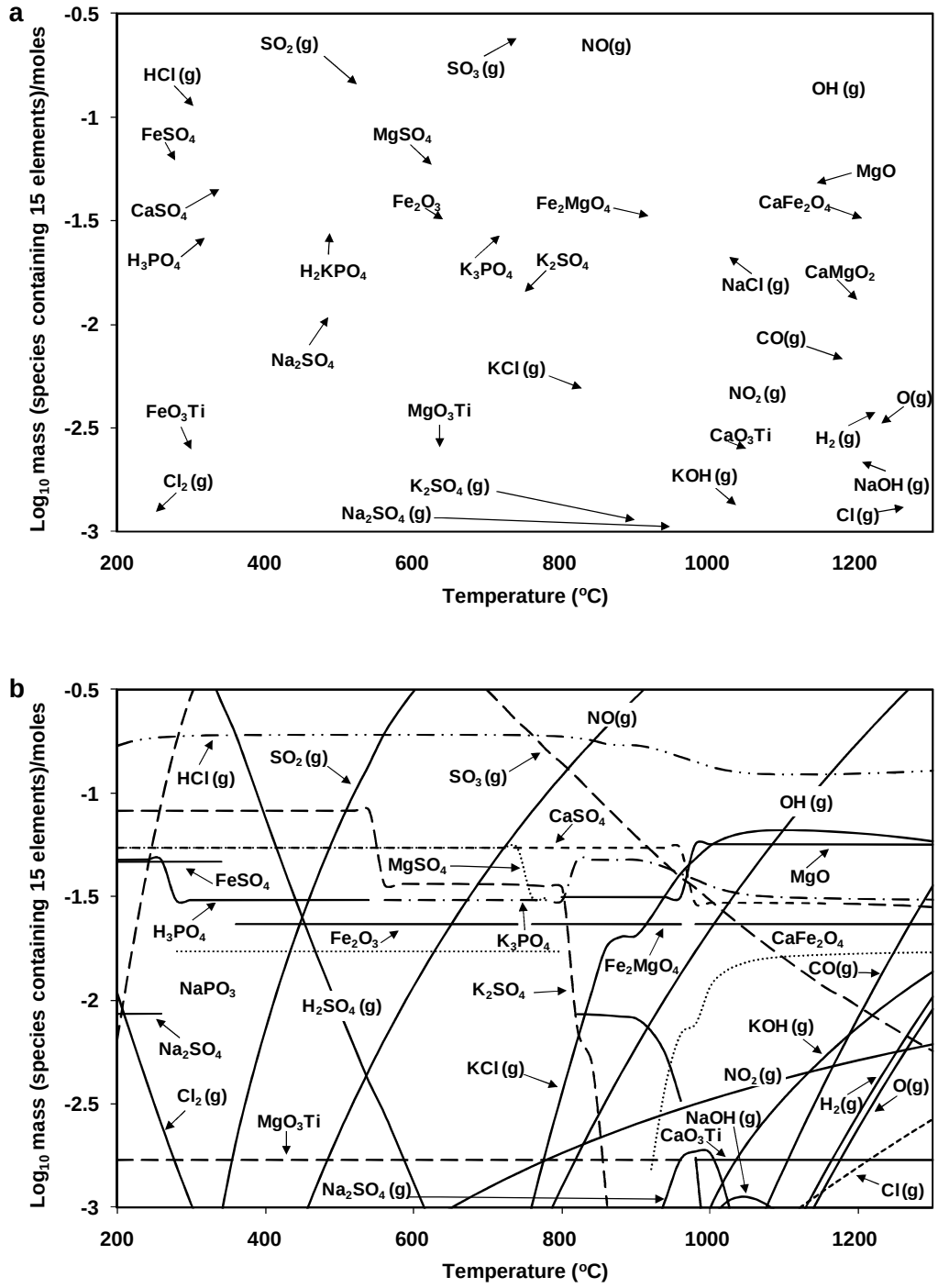

Figure 4.10 Calculated (MTDATA) gaseous & condensed species from co-firing mixed fuels of a) CCP:El-cerrejon coal (20:80 %, wt) and b) CCP:El-cerrejon coal (40:60 %, wt)

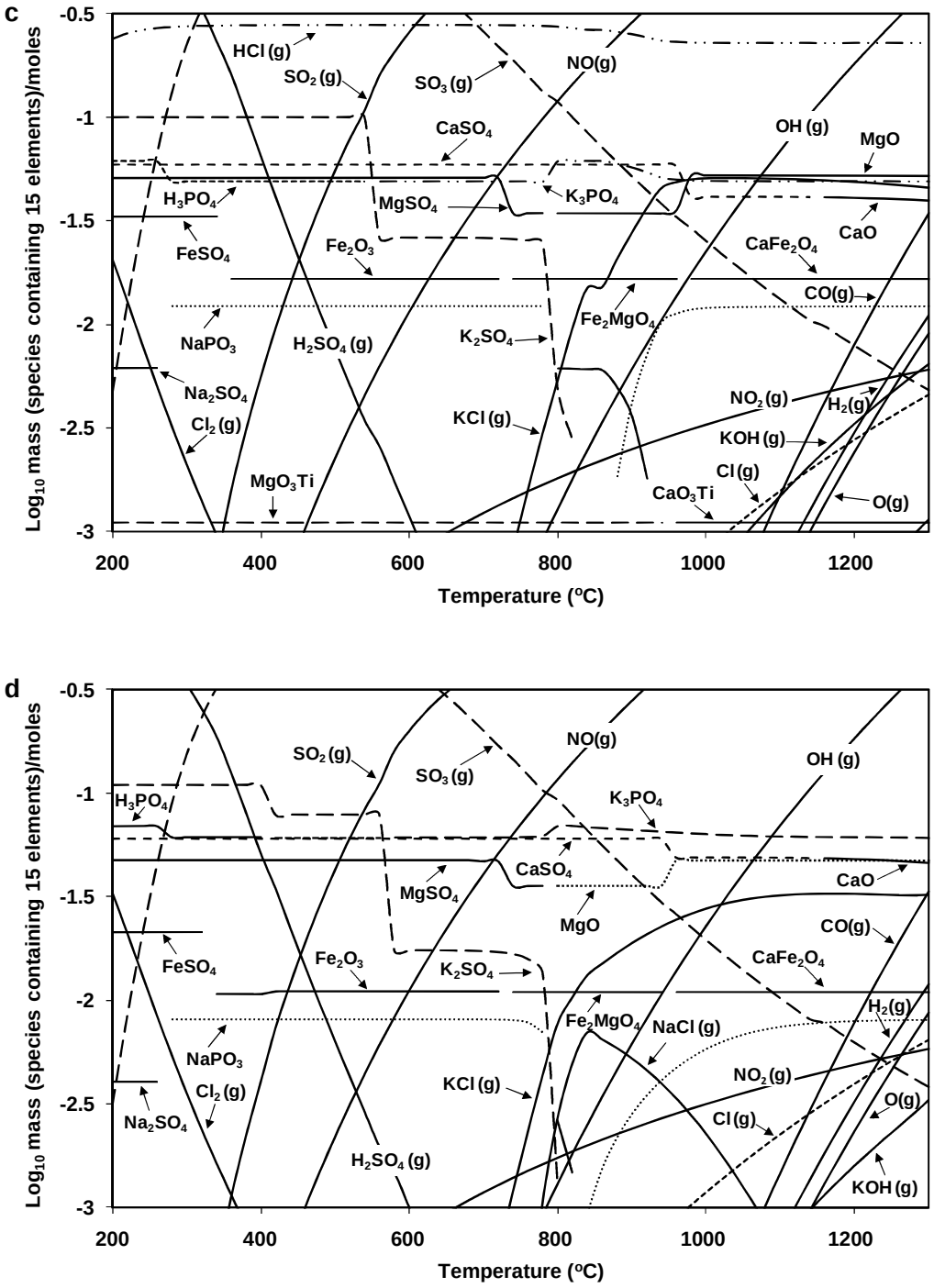

Figure 4.10 Calculated (MTDATA) gaseous & condensed species from co-firing mixed fuels of c) CCP:El-cerrejon coal (60:40 %, wt) and d) CCP:El-cerrejon coal (80:20 %, wt)

4.2.2.2 Co-firing CCP: Daw Mill coal (20, 40, 60 and 80 %, wt)

Combustion product prediction

Constant fuel feed rates of about 8.1, 8.9, 9.9 and 11.2 kg/hr were applied for mixed fuel CCP:Daw Mill , 20:80 %, wt, CCP:Daw Mill, 40:60 %, wt, CCP:Daw Mill, 60:40 %, wt, and CCP:Daw Mill, 80:20 %, wt, co-firing test runs, respectively. Table 4.6 shows the percent (by volume) concentration of CO_2, H_2O, N_2, O_2, HCl and SO_2 calculated for co-firing CCP:Daw Mill mixed fuels (full description of the calculations mad for CCP:Daw Mill , 20:80 %, wt, (as an example) are shown in Appendix A3).

Heat generation prediction

From the HP (calculated from Eq. 3.12, Chapter 3), the heat losses of the system was 7.84, 7.41, 6.91, 6.31 % for co-firing Daw Mill coal with 20 % CCP, 40 % CCP, 60 % CCP and 80 % CCP, respectively. These losses are in the range expected for this scale of combustion test rig.

MTDATA Calculations

Calculated data of the major and minor gaseous emissions by the equilibrium model (using “15 elements systems”) of co-firing Daw Mill coal with 20 % CCP, 40 % CCP, 60 % CCP and 80 % CCP are shown in Figures 4.11.a, 4.11.b, 4.11.c and 4.11.d, respectively. Predicted data of the major gaseous (i.e. CO_2, H_2O, N_2 and O_2) and minor gaseous (HCl and SO_2) at ~ 1200 ºC (combustion zone temperatures) are summarised in Table 4.6. These show that the combustion product predictions were almost identical with the MTDATA predictions. They also showed a decrease tendency of CO_2 and SO_2 with increase trend of moisture and HCl gaseous emissions. Moreover, Co-firing CCP mixed with Daw Mill suggested slight higher concentrations of CO_2, HCl and SO_2 emissions with lower concentrations of H_2O compared to Co-firing CCP mixed with El-cerrejon coal (see Table 4.5 & 4.6).

The NO emissions predicted (at ~ 1200 ºC, Fig. 4.11.(a-d)) were 454.32, 452.26, 449.68 and 446.67 ppm for co-firing Daw Mill coal with 20 % CCP, 40 % CCP, 60 % CCP and 80 % CCP, respectively. This showed the NO concentrations of co-firing CCP mixed with Daw Mill were close to CCP:El-cerrejon co-firing with similar behaviour trend.

The behaviour of condensed species (combined with minor gaseous species) during co-firing Daw Mill coal with 20 % CCP, 40 % CCP, 60 % CCP and 80 % CCP are shown in Figures 4.12.a, 4.12.b, 4.12.c and 4.12.d, respectively. This shows that the condensed species formed in all mixed fuels were $CaSO_4$, K_2SO_4, Fe_2MgO_4, Fe_2O_3, $FeSO_4$, K_3PO_4, MgO, and $NaPO_3$. Also, it suggested that $CaSO_4$, K_3PO_4 and $NaPO_3$ species increase, with a slight K_2SO_4 decrease as CCP biomass share increases. Condensed Na_2SO_4 predicted up to co-firing Daw Mill with 40 % CCP, while $MnSO_4$ (combined with other Mn species (e.g. MnO) started at 40 % CCP and increased as CCP share increased.

Condensed KCl was not predicted for the co-firing mixed fuels. It noticeable that Cl was predicted in gaseous species such as HCl, Cl, Cl_2, NaCl and KCl (Fig. 4.12.a-d).

Table 4.6 Modelling of co-firing mixed fuel of CCP:Daw Mill tests

	CCP:Daw M. mix 1[a]		**CCP:Daw M. mix 2[b]**		**CCP:Daw M. mix 3[c]**		**CCP:Daw M. mix 4[d]**	
(%, vol.)	**CP[e]**	**MTDATA[f]** (at 1200 °C)	**CP**	**MTDATA** (at 1200 °C)	**CP**	**MTDATA** (at 1200 °C)	**CP**	**MTDATA** (at 1200 °C)
CO_2	12.09	12.10	12.01	12.01	11.90	11.91	11.78	11.78
H_2O	8.86	8.87	9.59	9.59	10.47	10.47	11.55	11.55
N_2	74.97	75.01	74.34	74.37	73.57	73.59	72.64	72.64
O_2	4.00	3.97	4.00	3.97	4.00	3.97	4.00	3.97
HCl	0.0096	0.0058	0.0102	0.0091	0.0109	0.0098	0.0117	0.0105
SO_2	0.0578	0.0572	0.0497	0.0493	0.0400	0.0397	0.0282	0.0280

Keys;
(a): CCP: Daw Mill coal, 20:80 %
(b): CCP: Daw Mill coal, 40:60 %
(c): CCP: Daw Mill coal, 60:40 %
(d): CCP: Daw Mill coal, 80:20 %
(e): Combustion product prediction
(f): Thermodynamic calculations

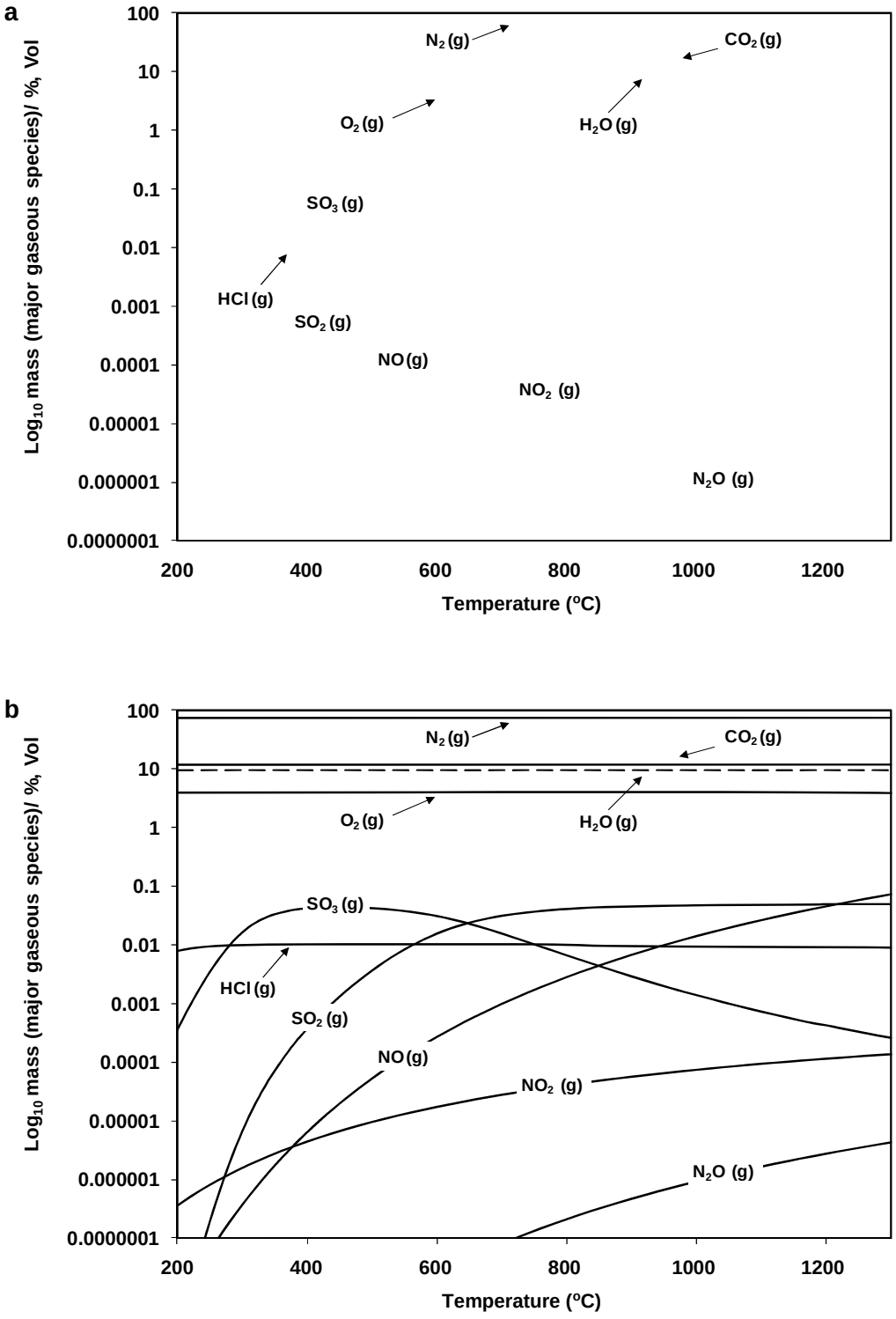

Figure 4.11 Calculated (MTDATA) major gaseous species from co-firing mixed fuels of a) CCP:Daw Mill coal (20:80 %, wt) and b) CCP:Daw Mill coal (40:60 %, wt)

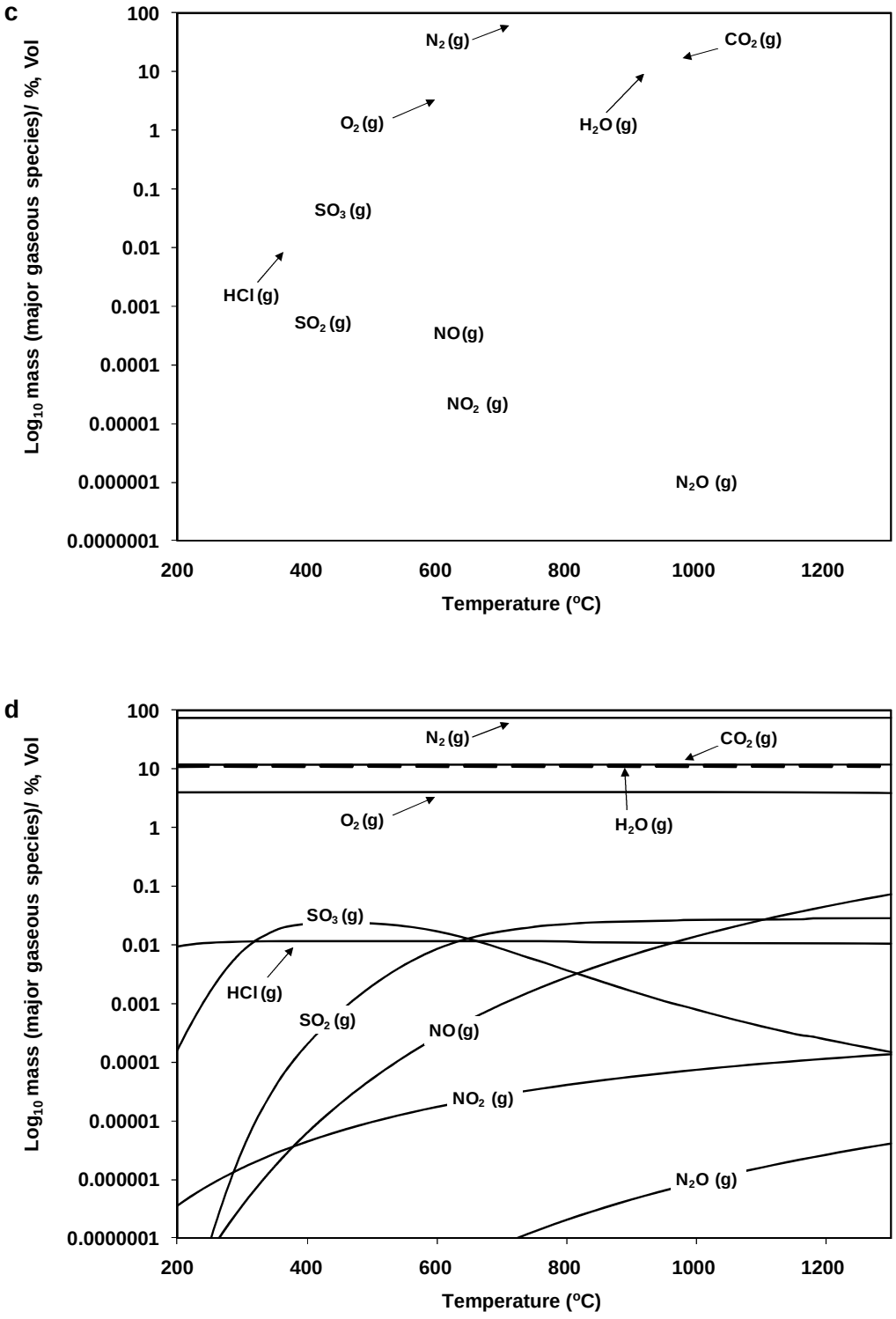

Figure 4.11 Calculated (MTDATA) major gaseous species from co-firing mixed fuels of c) CCP:Daw Mill coal (60:40 %, wt) and d) CCP:Daw Mill coal (80:20 %, wt)

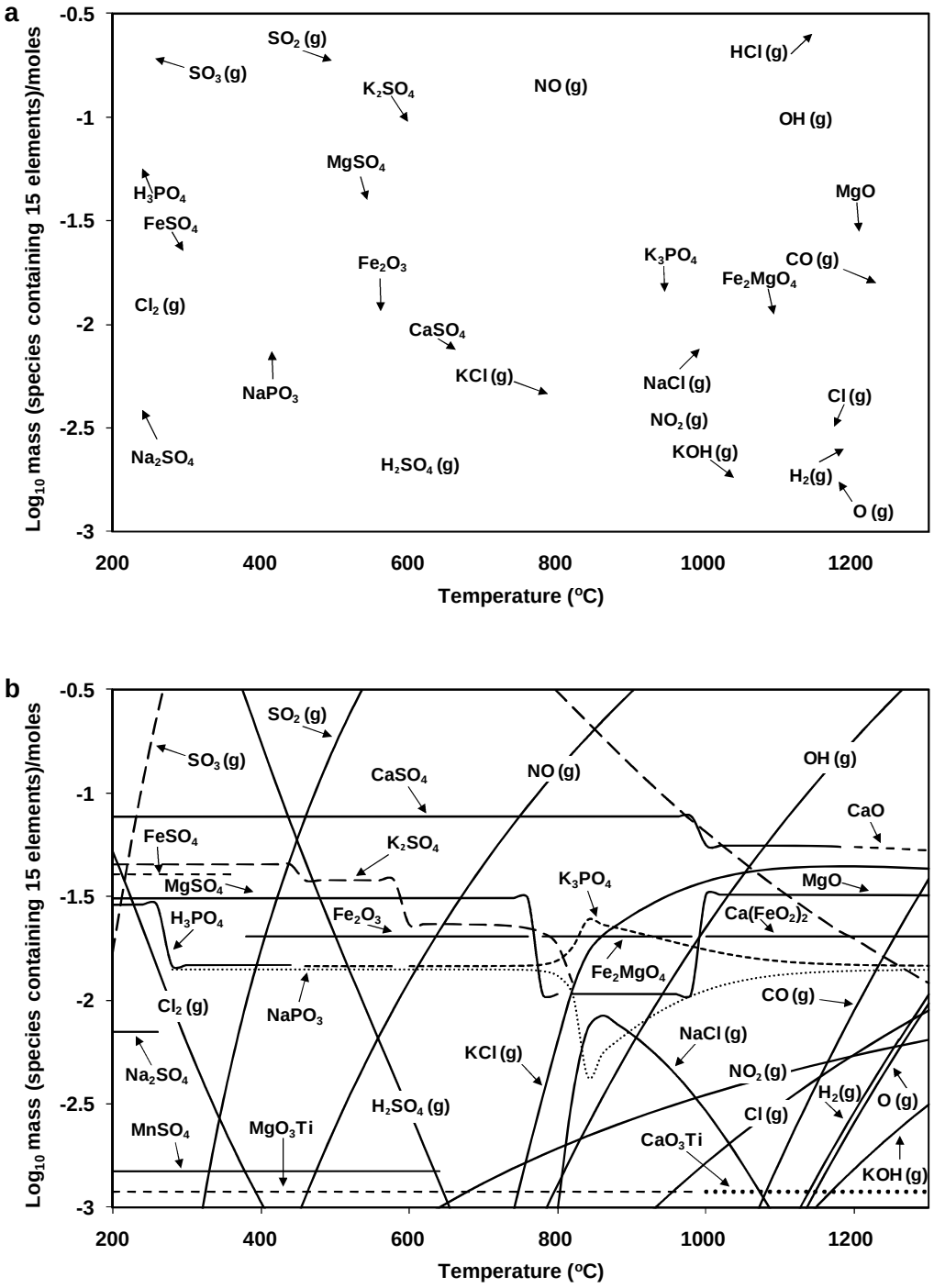

Figure 4.12 Calculated (MTDATA) gaseous & condensed species from co-firing mixed fuels of a) CCP:Daw Mill coal (20:80 %, wt) and b) CCP:Daw Mill coal (40:60 %, wt)

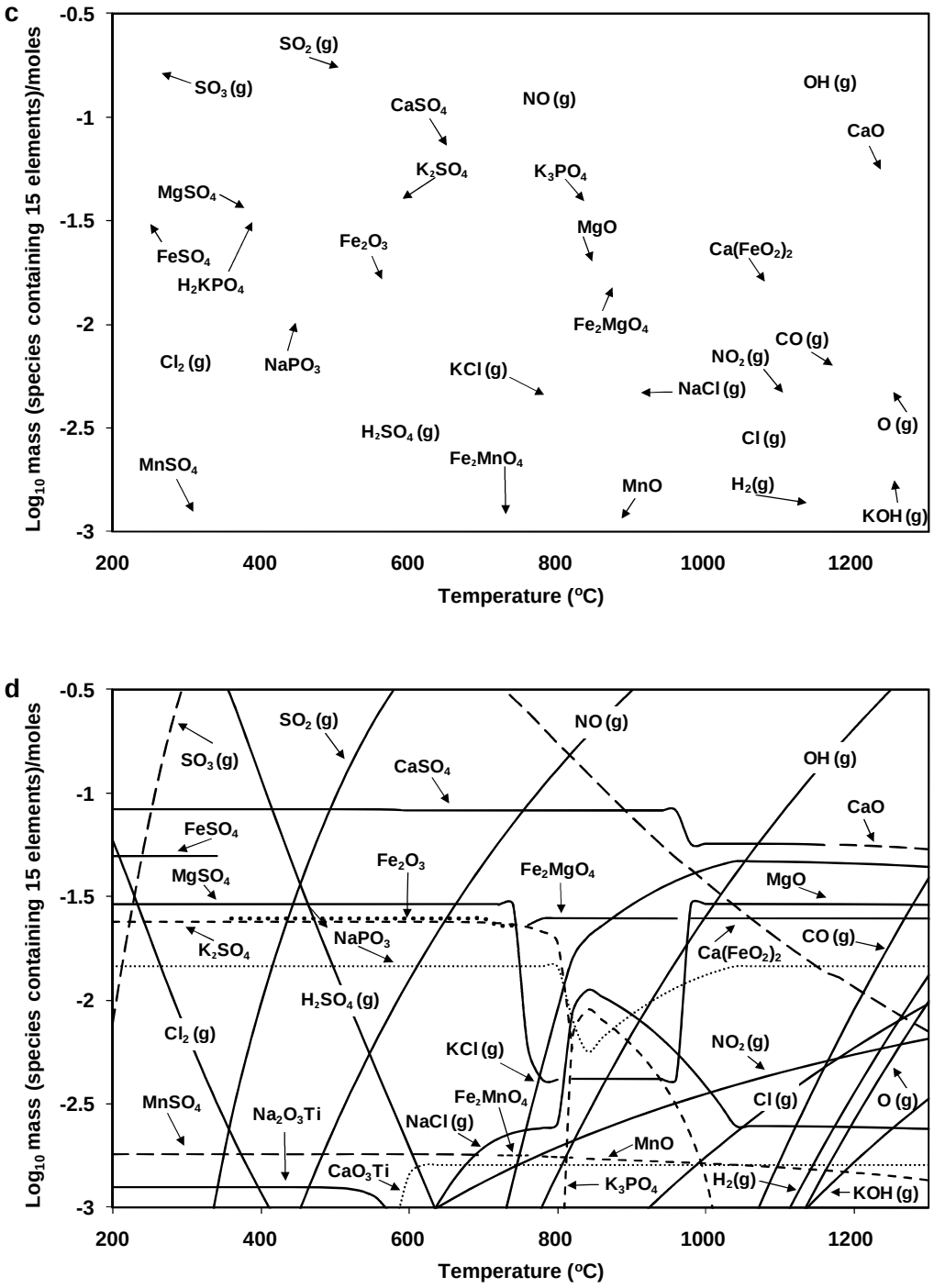

Figure 4.12 Calculated (MTDATA) gaseous & condensed species from co-firing mixed fuels of c) CCP:Daw Mill coal (60:40 %, wt) and d) CCP:Daw Mill coal (80:20 %, wt)

4.2.2.3 Co-firing Miscanthus: Daw Mill coal (20, 40, 60 and 80 %, wt)

Combustion product prediction

Constant fuel feed rates of about 8.1, 9.1, 10.2 and 11.7 kg/hr were applied for mixed fuel Miscanthus:Daw Mill, 20:80 %, wt, Miscanthus:Daw Mill, 40:60 %, wt, Miscanthus:Daw Mill, 60:40 %, wt), Miscanthus:Daw Mill, 80:20 %, wt, co-firing test runs, respectively. Table 4.7 shows the percent (by volume) concentration of CO_2, H_2O, N_2, O_2, HCl and SO_2 calculated for co-firing Miscanthus:Daw Mill mixed fuels.

Heat generation prediction

From the HP (see Appendix A4 (an example of Miscanthus:Daw Mill (60:40 %, wt)), the heat losses of the system was 8.62, 9.05, 9.63, 10.27 % for co-firing Daw Mill coal with 20 % miscanthus, 40 % miscanthus, 60 % miscanthus and 80 % miscanthus, respectively. These losses are in the range expected for this scale of combustion test rig.

MTDATA Calculations

Calculated data of the major and minor gaseous emissions by the equilibrium model (using “15 elements system”) of co-firing Daw Mill coal with 20 % miscanthus, 40 % miscanthus, 60 % miscanthus and 80 % miscanthus are shown in Figures 4.13.a, 4.13.b, 4.13.c and 4.13.d, respectively. Predicted data for the major gaseous (i.e. CO_2, H_2O, N_2 and O_2) and minor gaseous (HCl and SO_2) at ~ 1180 ºC (combustion zone temperatures) are summarised in Table 4.7. This proves once again that combustion product predictions were in line with the MTDATA predictions. Also, it showed little increase tendency of CO_2 and H_2O with decrease trend of SO_2 and HCl gaseous emissions. This is possibly a significant point to highlight when comparing the co-firing behaviour of miscanthus to CCP mixed with Daw Mill coal (in particular to HCl emissions behaviour).

The NO emissions predicted (at ~ 1180 ºC, Fig. 4.13.(a-d)) were 409.89, 408.32, 405.65 and 401.80 ppm for co-firing Daw Mill coal with 20 % miscanthus, 40 % miscanthus, 60 % miscanthus and 80 % miscanthus, respectively. This shows tiny variation with decreased tendency behaviour as miscanthus share increased.

The behaviour of condensed species (combined with minor gaseous species) during co-firing Daw Mill coal with 20 % miscanthus, 40 % miscanthus, 60 % miscanthus and 80 % miscanthus are shown in Figures 4.14.a, 4.14.b, 4.14.c and 4.14.d, respectively. This shows that the condensed species formed in all mixed fuels were $CaSO_4$, K_2SO_4, $Fe_2(SO_4)_3$, Fe_2O_3, CaO, $MgSO_4$ and Na_2SO_4 with slight decrease in their concentrations as miscanthus share increased. Condensed $NaPO_3$ predicted up to co-firing Daw Mill with 40 % miscanthus, while K_3PO_4 started at 40 % miscanthus and increased as miscanthus share increased.

Condensed KCl was not predicted for the co-firing mixed fuels. It obvious that Cl was predicted in gaseous species such as HCl, Cl, NaCl and KCl (Fig. 4.14.(a-d)).

Table 4.7 Modelling of co-firing mixed fuel of Miscanthus:Daw Mill tests

	Misc:Daw M. mix 1[a]		**Misc:Daw M. mix 2[b]**		**Misc:Daw M. mix 3[c]**		**Misc:Daw M. mix 4[d]**	
(%, vol.)	**CP[e]**	**MTDATA[f]** (at 1180 °C)	**CP**	**MTDATA** (at 1180 °C)	**CP**	**MTDATA** (at 1180 °C)	**CP**	**MTDATA** (at 1180 °C)
CO_2	12.18	12.19	12.19	12.19	12.21	12.21	12.23	12.22
H_2O	8.78	8.78	9.42	9.42	10.20	10.20	11.19	11.17
N_2	74.97	75.01	74.33	74.36	73.54	73.56	72.55	72.40
O_2	4.00	3.97	4.01	3.98	4.00	3.97	4.00	3.97
HCl	0.0089	0.0078	0.0086	0.0073	0.0082	0.0072	0.0078	0.0072
SO_2	0.0577	0.0561	0.0493	0.0476	0.0391	0.0386	0.0263	0.0261

Keys;
(a): Miscanthus: Daw Mill coal, 20:80 %
(b): Miscanthus: Daw Mill coal, 40:60 %
(c): Miscanthus: Daw Mill coal, 60:40 %
(d): Miscanthus: Daw Mill coal, 80:20 %
(e): Combustion product prediction
(f): Thermodynamic calculations

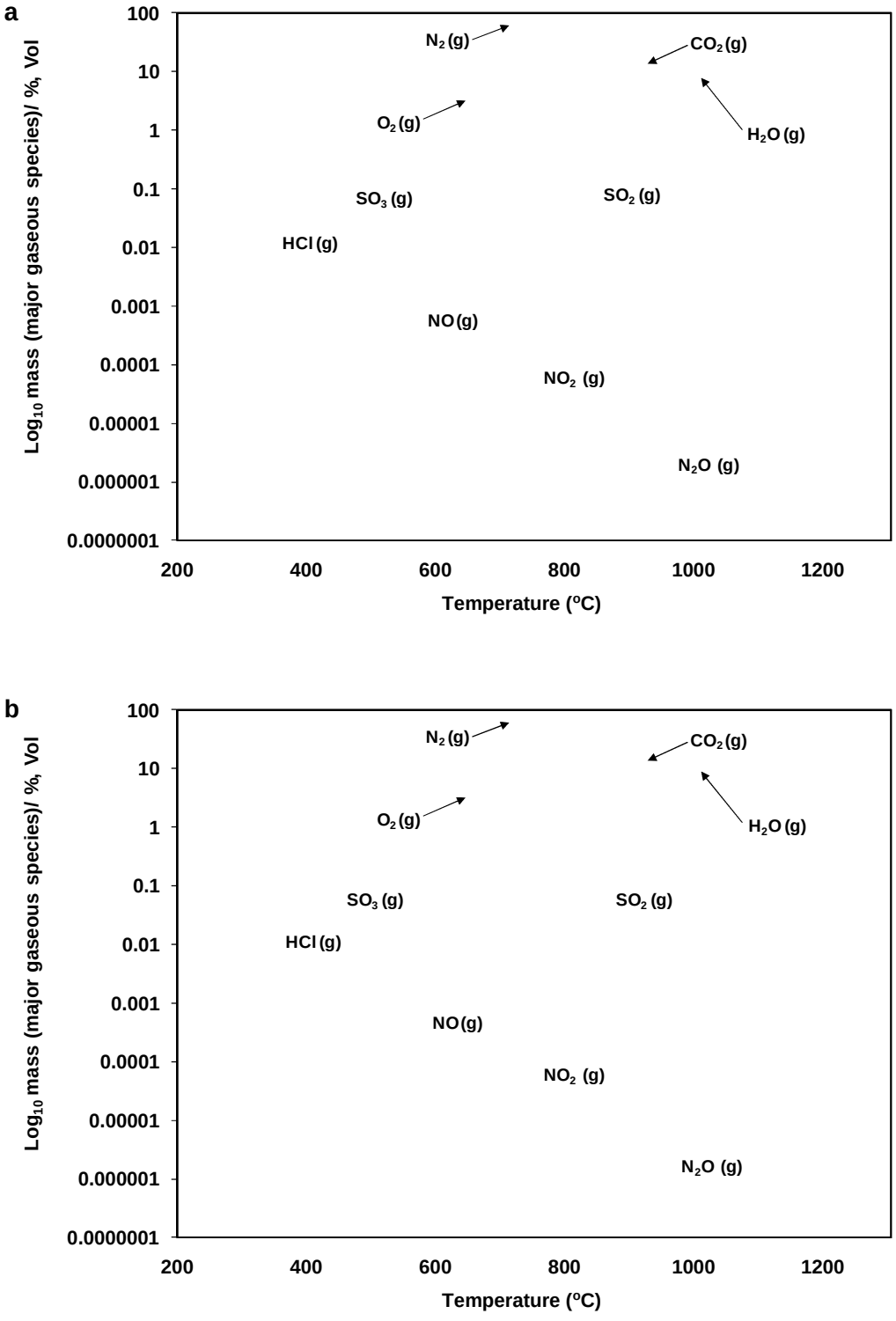

Figure 4.13 Calculated (MTDATA) major gaseous species from co-firing mixed fuels of a) Miscanthus:Daw Mill coal (20:80 %, wt) and b) Miscanthus:Daw Mill coal (40:60 %, wt)

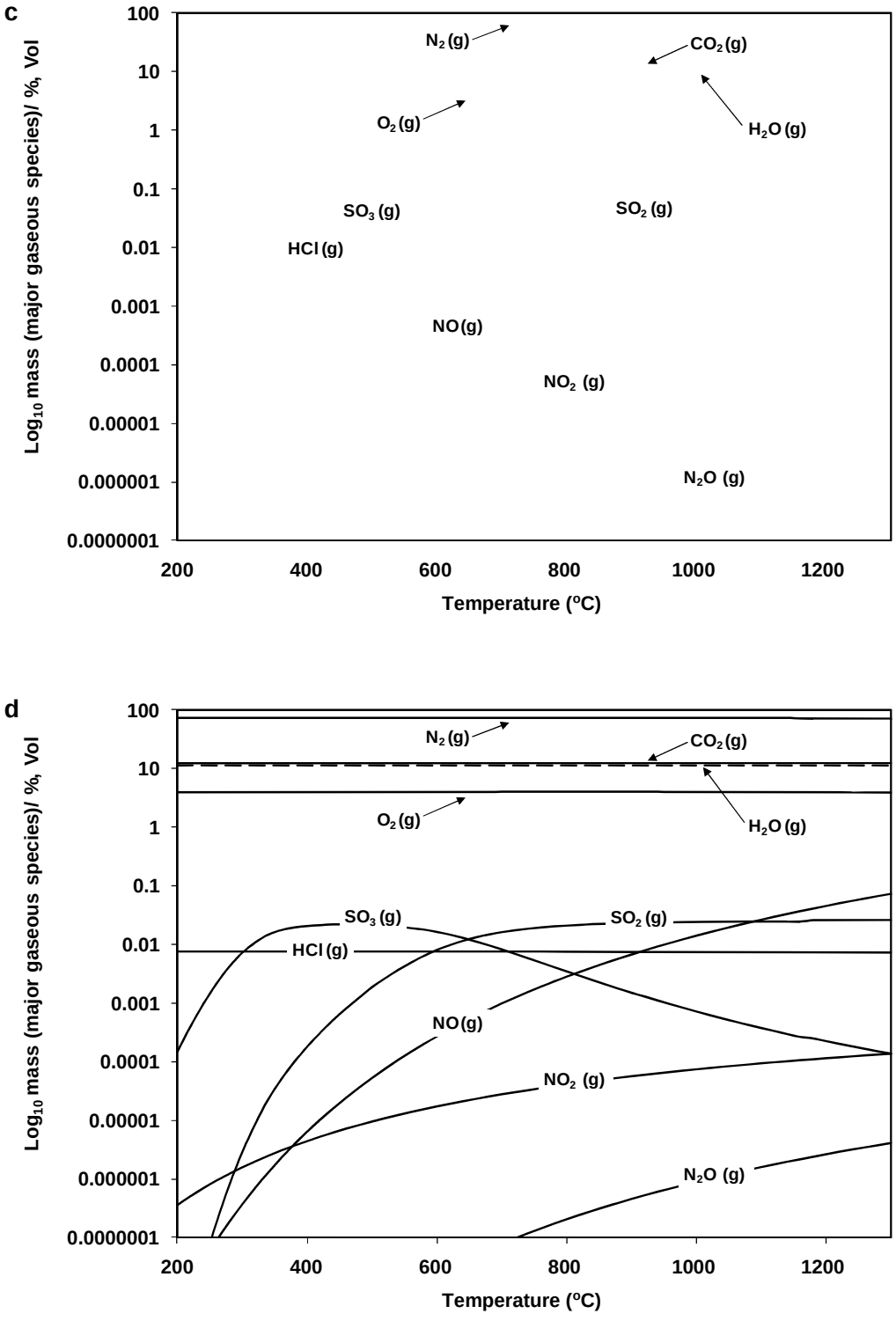

Figure 4.13 Calculated (MTDATA) major gaseous species from co-firing mixed fuels of c) Miscanthus:Daw Mill coal (60:40 %, wt) and d) Miscanthus:Daw Mill coal (80:20 %, wt)

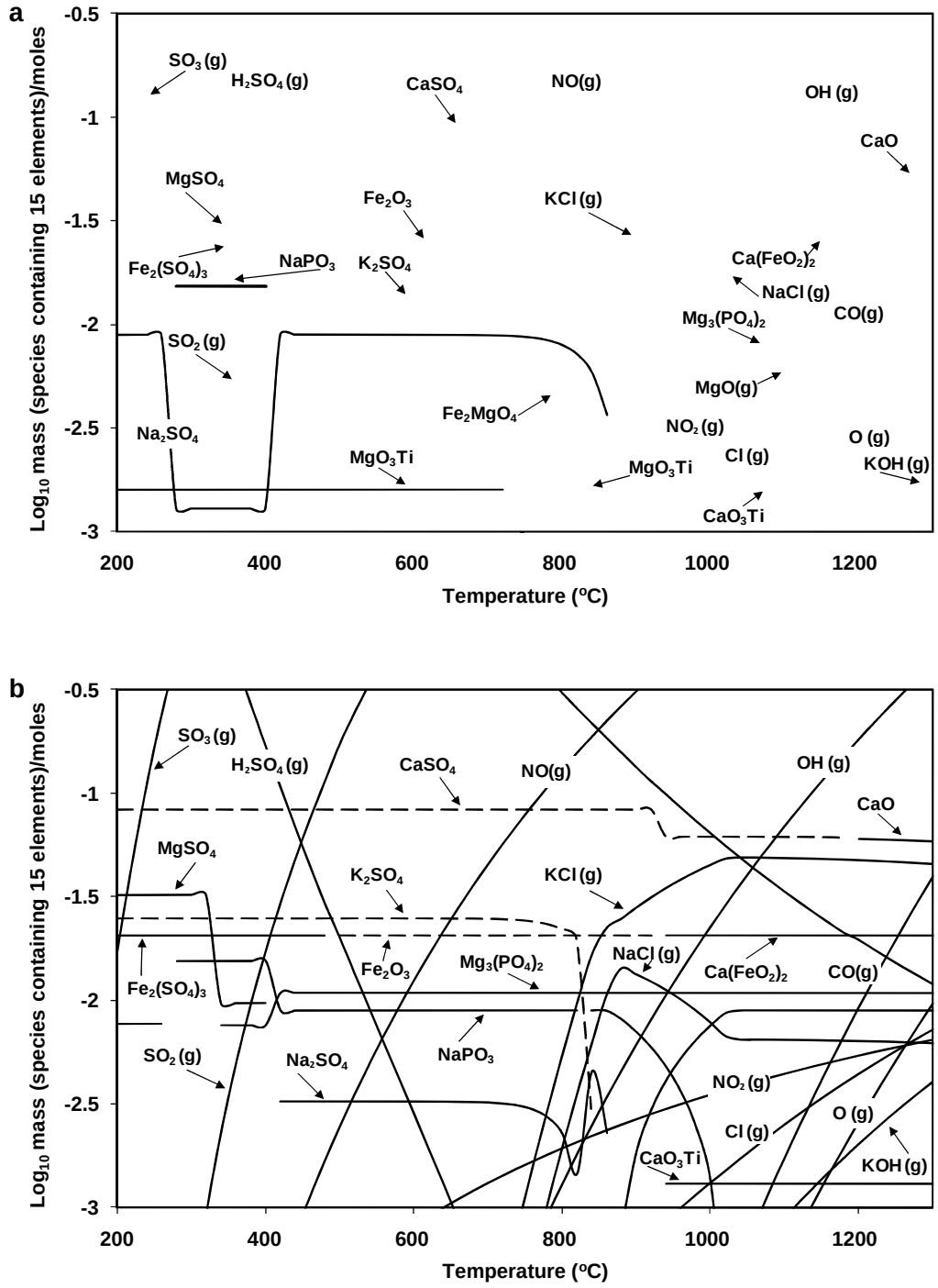

Figure 4.14 Calculated (MTDATA) gaseous & condensed species from co-firing mixed fuels of a) Miscanthus:Daw Mill coal (20:80 %, wt) and b) Miscanthus:Daw Mill coal (40:60 %, wt)

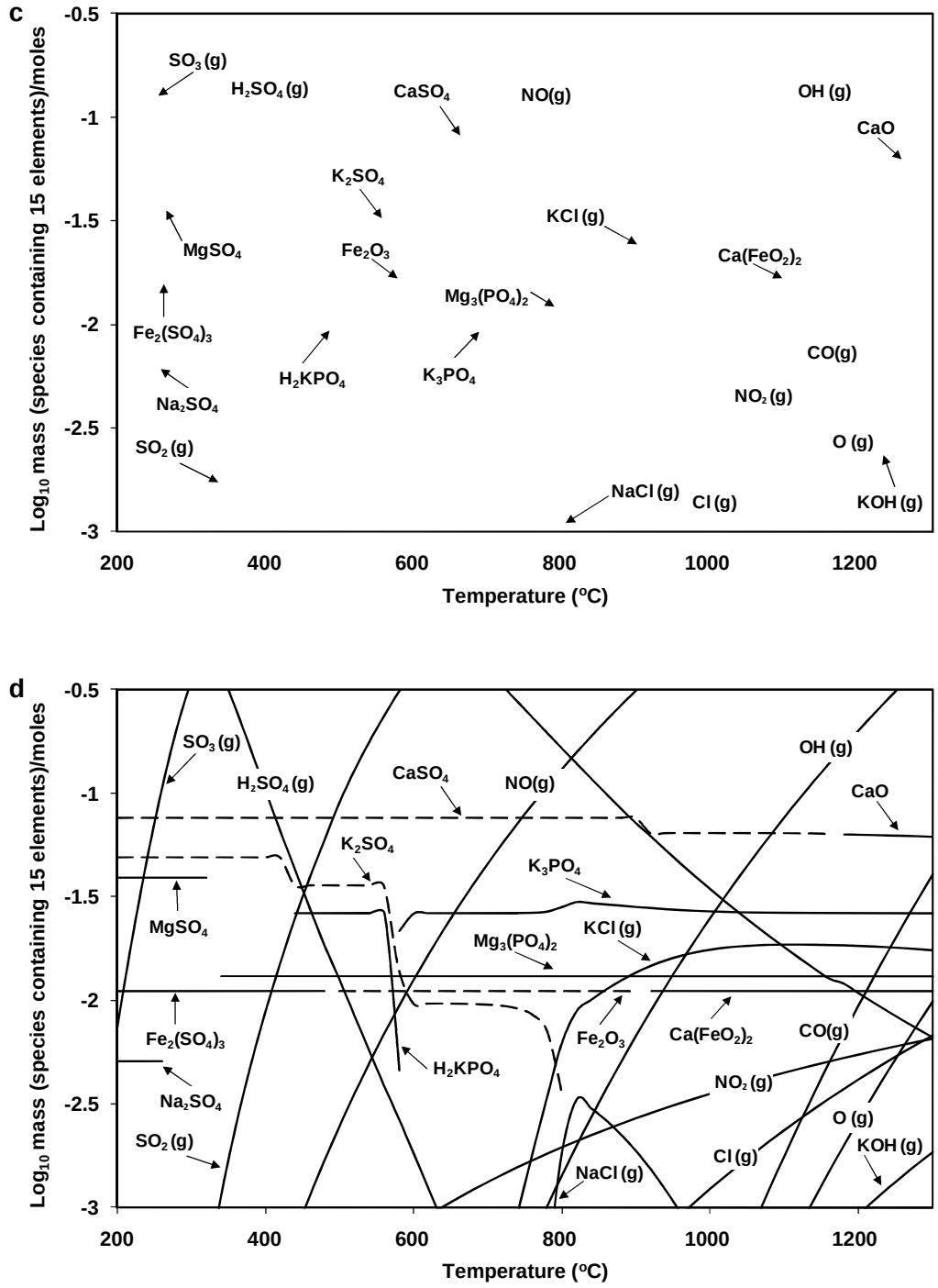

Figure 4.14 Calculated (MTDATA) gaseous & condensed species from co-firing mixed fuels of c) Miscanthus:Daw Mill coal (60:40 %, wt) and d) Miscanthus:Daw Mill coal (80:20 %, wt)

4.2.2.4 Co-firing Miscanthus: El-cerrejon coal (60:40 %, wt)

Combustion product prediction

A constant fuel feed rate of ~ 13.1 kg/hr and combustor air feed rate of ~ 1730 l/min combined with natural gas feeding rate of 40 l/min were applied for co-firing Miscanthus:El-cerrejon coal (60:40 %, wt) test runs. Table 4.8 shows the percent (by volume) concentration of CO_2, H_2O, N_2, O_2, HCl and SO_2 calculated.

Heat generation prediction

From the HP (calculated from Eq. 3.12, Chapter 3), the heat losses of the system was 15.21 % for the co-firing Miscanthus:El-cerrejon coal (60:40 %, wt). This shows that heat losses were within the expected range when using this scale of combustion unit.

MTDATA Calculations

Calculated data of the major and minor gaseous emissions by the equilibrium model (using "15 elements system") of co-firing El-cerrejon coal with 60 % miscanthus are shown in Figure 4.15. Predicted data of the major gaseous (i.e. CO_2, H_2O, N_2 and O_2) and minor gaseous (HCl and SO_2) at ~ 1200 ºC (combustion zone temperatures) are summarised in Table 4.8. High matching between combustion product predictions and MTDATA predictions were achieved.

For NO_x emissions, the equilibrium combustion calculation indicated that the flue gas composition (~ 1200 ºC) of Miscanthus:El-cerrejon coal (60:40 %, wt) of NO, NO_2, N_2O (Fig. 4.15) were 447.91, 1.15 and 0.0269 ppm, respectively.

For evaluation of mixed miscanthus with El-cerrejon coal compared to Daw Mill coal at this ratio (i.e. 60 %, wt), indicated that the predicted gaseous emissions concentrations were higher in CO_2 and NO_x and lower in H_2O, HCl and SO_2. This shows an important

of an experience (on combustion/deposition) to carry out of mixed such particular biomass with wide range of coals.

The predicted behaviour of condensed species (combined with minor gaseous species) during co-firing El-cerrejon coal with 60 % miscanthus is shown in Figure 4.16. This shows that the condensed species expected were $CaSO_4$, CaO, $CaMgO_2$, $Ca(FeO_2)_2$, $MgSO_4$, MgO, $Fe(H_2PO_3)_2$, Fe_2O_3, Fe_2MgO_4, MnO, MnO_2, K_2SO_4, Na_2SO_4 and K_3PO_4. Some of these condensed species presented in higher concentrations (in particular, $CaSO_4$), while other not much disparity (e.g. Fe_2O_3) with respect to temperatures range and dew points compared to Miscanthus:Daw Mill (60:40 %, wt).

Table 4.8 Modelling of co-firing mixed fuel of Miscanthus:El-cerrejon coal tests

	Miscanthus:El-cerrejon (60:40 %, wt)	
(%, vol.)	**CP[a]**	**MTDATA[b]** (at 1200 ^oC)
CO_2	13.48	13.47
H_2O	9.56	9.60
N_2	72.94	72.90
O_2	4.00	3.98
HCl	0.0049	0.0006
SO_2	0.0262	0.0221

Keys;
(a): Combustion product prediction
(b): Thermodynamic calculations

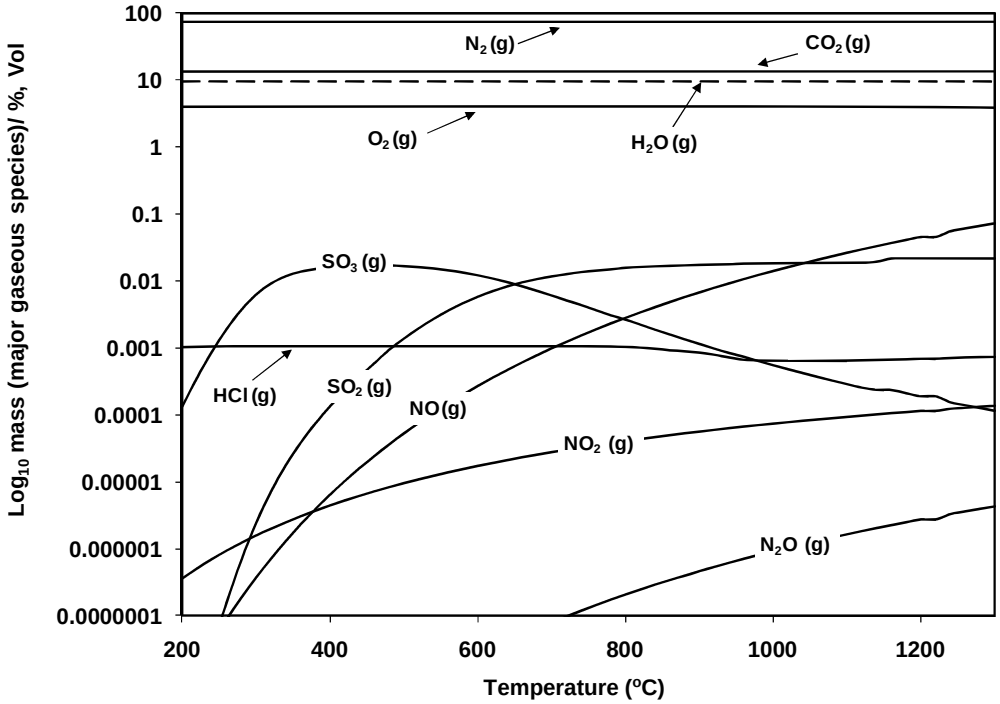

Figure 4.15 Calculated (MTDATA) major gaseous species from co-firing mixed fuels of Miscanthus:El-cerrejon coal (60:40 %, wt)

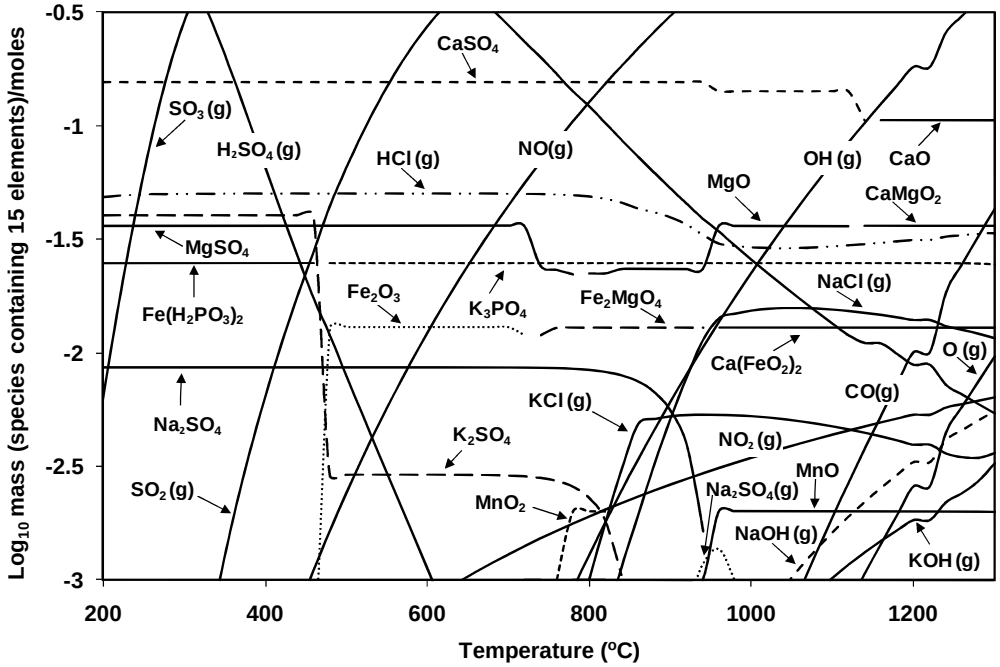

Figure 4.16 Calculated (MTDATA) gaseous & condensed species from co-firing mixed fuels of Miscanthus:El-cerrejon coal (60:40 %, wt)

4.3 Experimental pilot-scale combustion rig exposures

4.3.1 Co-firing CCP: El-cerrejon coal (0, 20, 40, 60 and 80 %, wt)

Combustion behaviour/efficiency & gaseous emissions

Figures 4.17 and 4.18 show the major flue gas and minor gaseous species, respectively, produced during two hours of stable combustion/co-firing of three of fuels (as examples) of pure El-cerrejon coal (100 %, wt), pure CCP biomass (100 %, wt) and high mixed fuel of biomass share (CCP:El-cerrejon coal, 80:20 %, wt).

Low CO emissions were achieved for all mixed fuel combustion. For example, CO emissions with averages of 324, 232 and 152 ppm for El-cerrejon coal (100 %, wt), CCP biomass (100 %, wt) and CCP:El-cerrejon coal (80:20 %, wt), respectively (Fig. 4.18), imply that most of the burnt carbon was converted to CO_2 (i.e. high combustion efficiency). This result would be expected from pulverised coal combustion, but is a significant data record for a high blend mixture of biomass (i.e. 80 %, wt) with coal.

Pilot-scale combustion gave the compositions of the major flue gases for El-cerrejon coal (100 %, wt) with an average of 9.2 % CO_2, 13.3 % H_2O, CCP (100 %, wt) with an average of 11.6 % CO_2, 13.4 % H_2O (Fig. 4.17). For the mixed fuel combustion (CCP:El-cerrejon coal, 80:20 %, wt), the flue gas compositions resulted an average of 11.5 % CO_2 and 14.3 % H_2O. The CO_2 volume outcomes of the experimental study match closely with the CP and MTDATA predictions calculations of El-cerrejon coal (11.9 %), CCP (11.1 % CO_2) and CCP:El-cerrejon coal mixtures (11.4 % CO_2). The H_2O volume outcomes of the experimental study showed a variations with the CP calculations which were 8.6, 12.9 and 11.8 % H_2O for El-cerrejon coal, CCP and CCP:El-cerrejon coal mixtures, respectively. Conceptually the cause is CP and MTDATA calculations were adopted to have the percent volumes of oxygen output of 4.0 %. Whereas, the oxygen output of the experimental combustion study of El-cerrejon coal, CCP and CCP:El-cerrejon coal mixtures (80:20 %, wt) were in the range of 5-9, 6-8, 3.9-7 %, respectively. Also, other factors, such as fuel moisture content could have changed during storage, proper mixing of solid fuels particles, residence time,

combustion zone temperature, type of feeding and the cooling effects of excess air should also be taken into consideration [Van Loo and Koppejan, 2008].

Examining the minor gaseous species SO_2 indicates that the SO_2 concentration is high in El-cerrejon coal (range of 396-452 ppm) compared with CCP biomass of average of 28.5 ppm, which is expected for coal and biomass based fuels. The combined effects of the low share mixed fuel (i.e. CCP:El-cerrejon coal, 20:80 %, wt) showed that SO_2 concentration dropped to an average of 220.1 ppm (measured data are close with those made by predictions data, see Table 4.5). For the high share mixed fuel (i.e. CCP:El-cerrejon coal, 80:20 %, wt), the average SO_2 was 152 ppm which indicates the significance of co-firing on SO_2 emissions. NO_x (NO and NO_2) concentrations show averages of 231.1, 479.5, 479.3 ppm, whereas the N_2O emissions were 25.8, 8.7, 5.4 ppm for El-cerrejon coal, CCP biomass and the mixed fuel (CCP:El-cerrejon coal, 80:20 %, wt), respectively. The NO_x concentrations of the intermediate mixed fuel (i.e. CCP 20, 40 and 60 %, wt) all had averages of ~ 400 ppm. This suggests that the major source of NO_x in flue gas is from fuel-N [Van Loo and Koppejan, 2008; Hall and Overend, 1987], which explains the similar outcome between CCP (100 %, wt) and high biomass mixed fuel (i.e. CCP of 80 %, wt). Leckner and Karlsson, 1993 also indicated that NO_x formation is dependence on the N content of the wood from combustion of wood and coal mixtures. Other possible reasons are that biomass produces greater volatile yields than coals and this can create larger fuel rich regions in the burner region, which are able to enhance the performance of low NO_x burners [Van Loo and Koppejan, 2008]. The HCl had averages of 79.8, 58.6, 111.2, 108.4, 90.1, 77.2 ppm for 100 % El-cerrejon coal, 100 % CCP and the mixed fuels 20 % CCP, 40 % CCP, 60 % CCP, 80 % CCP, respectively; indicated higher HCl released in low share biomass coal combustions. Also, revealed that higher emissions of gaseous HCl in co-firing mixed fuels compared to the combustion of pure fuels. Similar finding reported by Spliethoff et al., 2001 that higher HCl emissions during co-firing straw and coal mixtures (with straw thermal input of 60 %) in FB boiler compared to pure fuel combustion.

It is obvious that the minor gaseous species emissions (Fig. 4.18) remained almost constant during combustion runs and no significant drops have been noted.

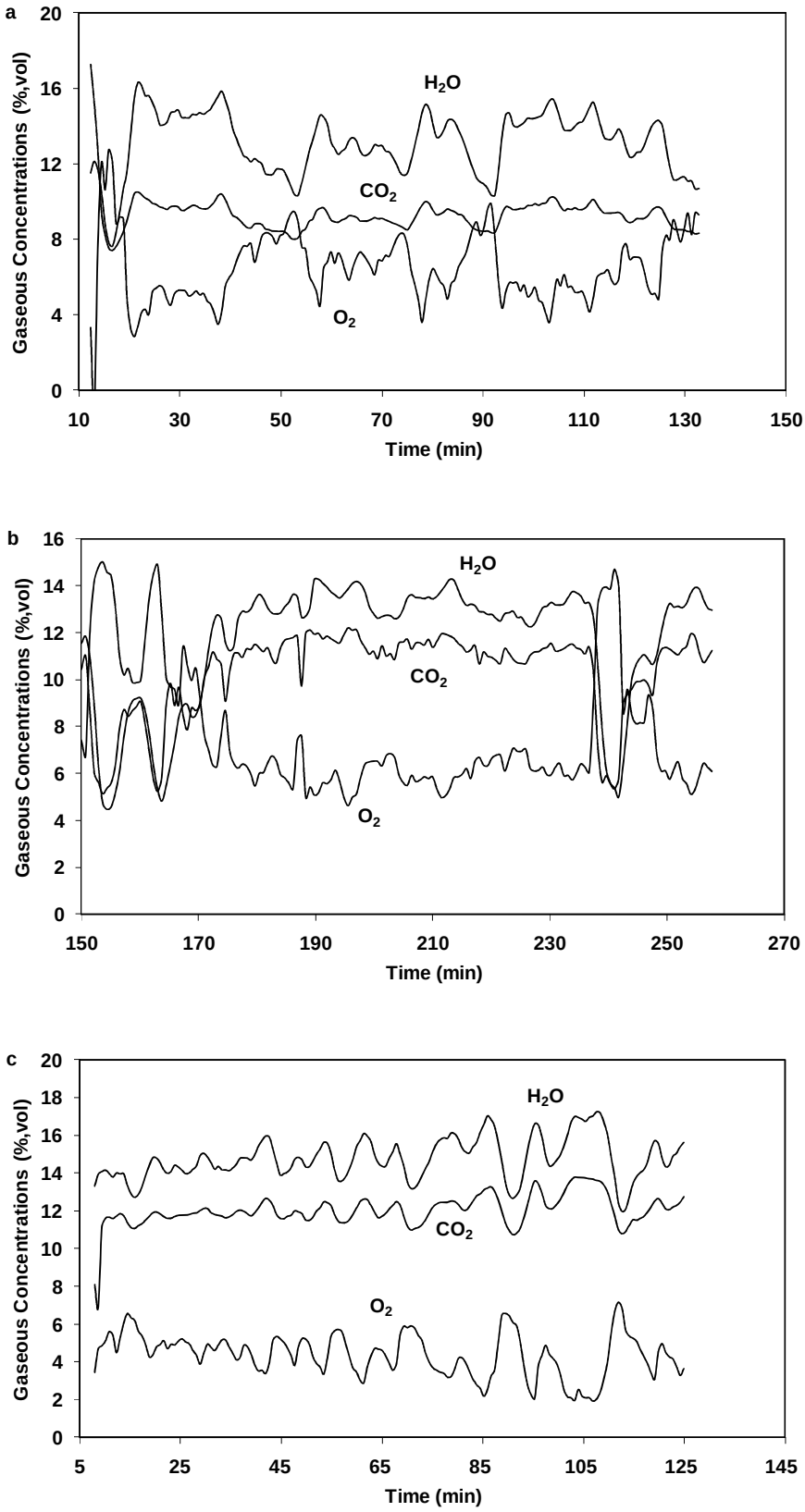

Figure 4.17 Major gaseous emissions from combustion of a) pure El-cerrejon coal (100 %, wt), b) pure CCP (100 %, wt) and c) CCP: El-cerrejon coal (80:20 %, wt)

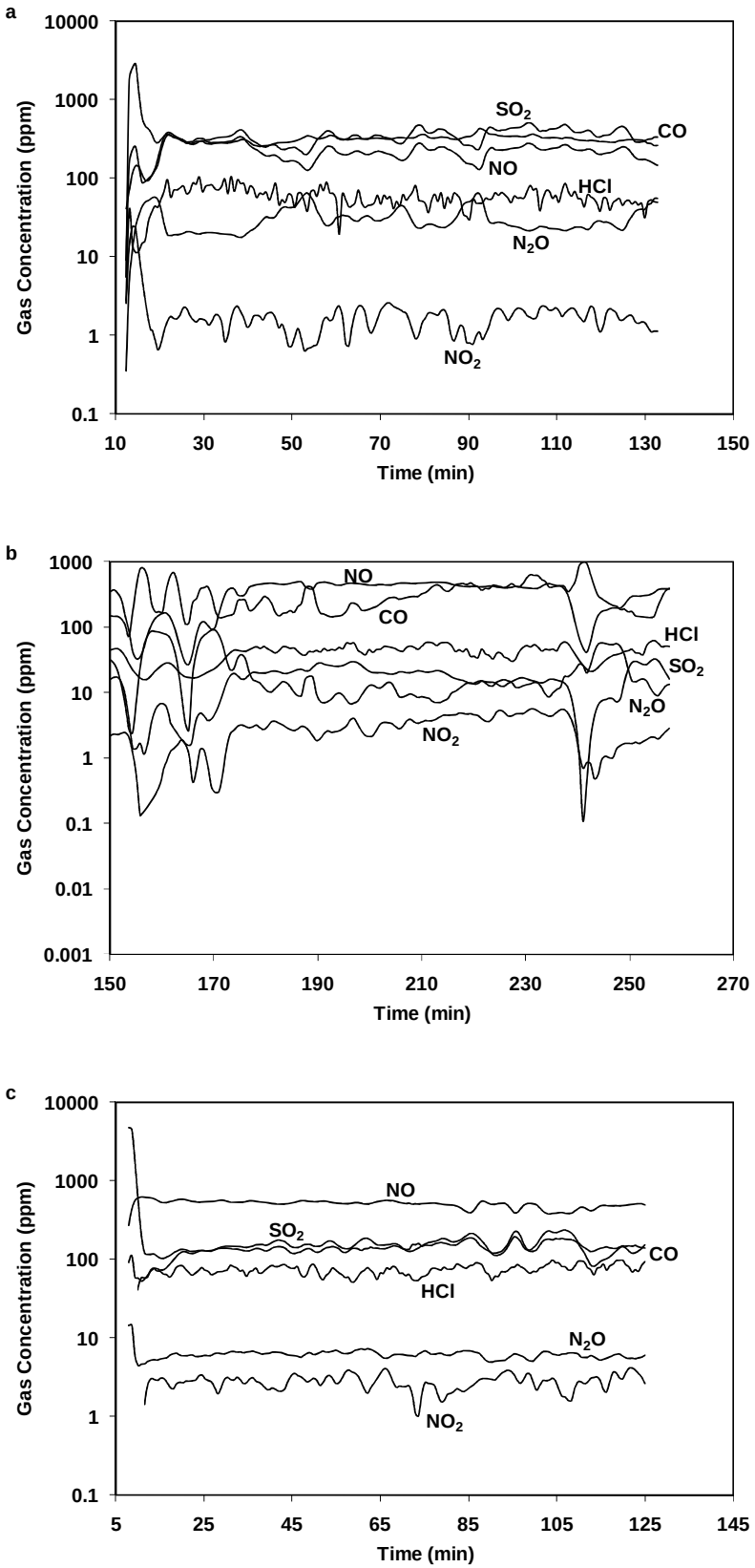

Figure 4.18 Minor gaseous emissions from combustion of a) pure El-cerrejon coal (100 %, wt), b) pure CCP (100 %, wt) and c) CCP: El-cerrejon coal (80:20 %, wt)

Deposition fluxes, compositions and analysis

Deposits from the ceramic sections of the three deposition probes with surface temperatures of ~ 700 °C (probe 1), ~ 600 °C (probe 2) and ~ 500 °C (probe 3) were collected after pulverised combustions runs. Figure 4.19 shows the deposition fluxes formed on each of the three probes (which represented upstream, side-stream and downstream of the deposit build up) for three of the fuel mixtures. This showed that the highest deposition flux was at surface temperature of ~ 500 ^{o}C (probe 3) for combustion CCP (100 %, wt) and the co-firing mixed fuel (CCP:El-cerrejon coal, 80:20 %, wt).

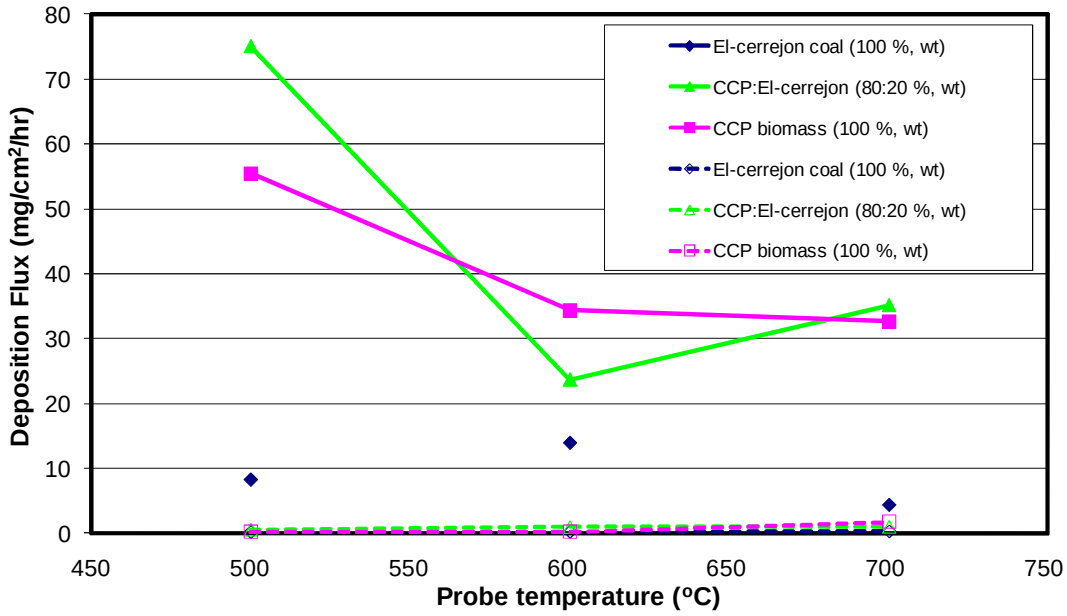

Figure 4.19 Deposition rates on the surface temperatures of the three probes (on each side) for three of the fuels mixtures

Figure 4.20 illustrates the deposition fluxes of all selected fuels from probe 3 (~ 500 °C), given as mass of deposits per square centimetre of surface area of the probe side per hour of feed. The results revealed higher deposition fluxes with higher shares of biomass in the fuel blend. This agrees with Gogebakan et al., 2009. Co-firing mixed fuel (CCP:El-cerrejon coal, 80:20 %, wt) exhibits the highest upstream deposit formation compared with the other fuel mixtures (with a deposition flux of 75.0 mg/cm^2/hr), in particular to CCP biomass (100 %, wt) of a deposition flux of 55.4 mg/cm^2/hr. This making it obvious that the different species in the mixed fuel interact with one another. Also, it can be seen that, little deposit is formed (below 1.0

mg/cm^2/hr) on side of the probes and none on the bottom of the probes for all the selected fuels.

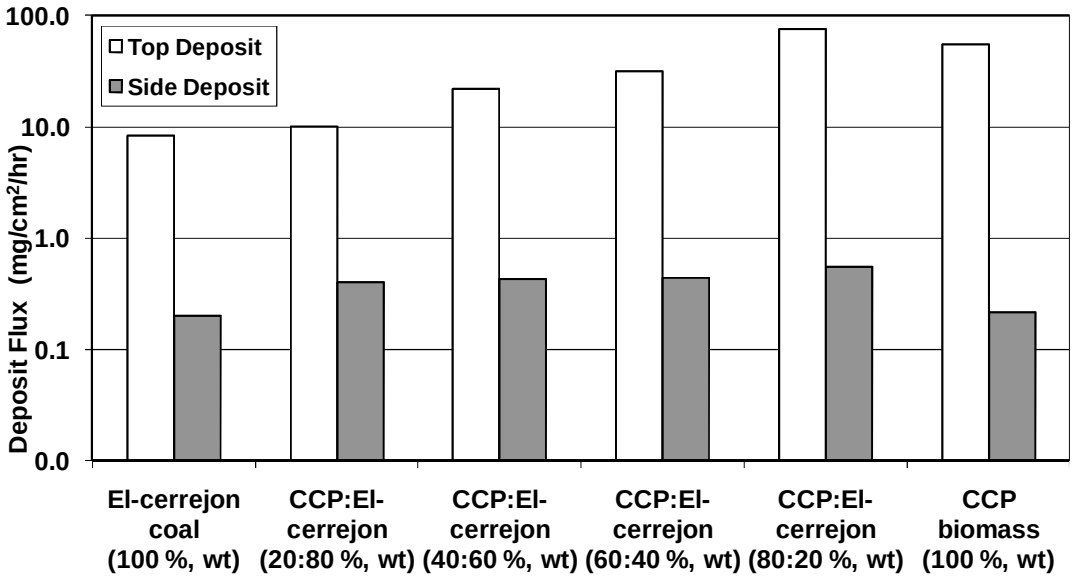

Figure 4.20 Deposition fluxes for probe 3 (~ 500 °C) on top and side deposits from CCP:El-cerrejon coal (pure and mixed) pulverised fuels combustion

The appearance of the deposits (on probe 3, as an example) after an average of ~ 3 hours feed of CCP:El-cerrejon pure and mixed fuels are shown in Figure D.1 (Appendix D). This shows that the deposits were coarse with less fibrous and more porous texture for co-firing this mixed fuel when compared to 100 % CCP. Indications from these photographs were in line with observations by SEM analysis. Also, it can be seen from the SEM images of the top deposits (Figure D.2, Appendix D) that the particles are much larger for pure CCP (100 %, wt) and mixed fuel (CCP:El-cerrejon coal, 80:20 %, wt) combustion when compared to 100 % El-cerrejon coal and low ratio of mixed biomass fuel of 20, 40 and 60 % CCP.

It should be pointed out that the dark colour of the particles was not due to unburned carbon as the carbon contents of the pure and mixed fuels deposit were ~ 0.1 % on a mass basis. Similar deposit colours were noticed by Robinson et al., 2002 after combustion of imperial wheat straw.

The elemental compositions of the deposits formed on the tops and sides of all three probes for combustion El-cerrejon coal (100 %, wt), CCP (100 %, wt) and high ratio biomass co-firing mixed fuel (CCP:El-cerrejon coal, 80:20 %, wt) analysed by EDX are shown in Figure 4.21.

Inspection of the figure 4.21 reveals varying concentrations of silicon, calcium, sulphur, potassium, iron and aluminium in the deposits of all probes. Silicon and aluminium combined are coal derived with high melting point compounds that can tie up alkalis. High concentrations of potassium and sulphur suggest formation of potassium sulfates in the deposits. Potassium concentration in the deposits of probe 3 (side ash) is found to be higher than potassium content in the other probe deposits with 23.2, 23.1, 23.6 % moles of El-cerrejon coal (100 %, wt), CCP biomass (100 %, wt) and CCP:El-cerrejon coal (80:20 %, wt), respectively. Sulfur concentrations behaved in a similar way (i.e. high concentration on probe 3) with concentrations of 7.1 % moles of El-cerrejon coal and CCP biomass tests, except CCP:El-cerrejon fuel mixtures which resulted in a higher sulfur concentration on probe 1 with 11.3 % moles. On the other hand, chlorine concentrations are formed in all probes of 100 % CCP biomass test (as expected) and none for El-cerrejon coal. Whereas, the deposits for the mixed fuel (CCP:El-cerrejon coal, 80:20 %, wt) showed chlorine formed only in the side deposits of probe 2 and probe 3 with concentrations of 5.5 and 4.0 % moles, respectively. Potassium and chlorine in the deposits form potassium chloride which is a highly fouling compound leading to corrosion of boiler components [Montgomery and Larsen, 2002; Obernberger et al., 1997; Van Loo and Koppejan, 2008]. The appearance of KCl in the deposit was confirmed by XRD results (seen in Figure D.3, Appendix D). These findings show that the Cl content of the deposits formed from the CCP:El-cerrejon coal (80:20 %, wt) mix is intermediate between the behaviour of the two pure fuels.

Co-firing mixed fuels 20 %, 40 %, 60 % CCP with coal showed a linear increase of Cl in side deposit of probe 3 (500 °C) with a concentration of 0.1, 0.4 and 1.9 % moles, respectively (seen in Figure 4.22). Also, 60 % CCP tests showed chlorine formation in the side deposit of probe 2 (~ 600 °C) with concentrations of 4.6 % moles. This outcome explains the fact pointed out earlier that HCl concentrations were higher in

combustion gases of low share biomass with coal (experimental study). This has been noticed by Bartolome et al., 2009 with no chlorine content in the deposit samples studied and suggested that the majority of the Cl was released as HCl gas when burning cynara biomass with coal (at shares of 15 %).

It is clear that compounds confirmed by XRD results (Figure D.3) such as sylvite (KCl), K_2SO_4 on pure CCP and condensed species like $CaSO_4$ and Fe_2O_3 on all mixed fuels were already predicted by MTDATA calculations (Fig. 4.6 and Fig. 4.10.a-d).

However, other compounds predicted, such as Na_2SO_4 and K_3PO_4, were not identified by XRD, but the SEM-EDX data (Fig. 4.21 & 4.22) indicated of formation. Figure D.4 (Appendix D) shows the SEM map images of top deposits (~ 500 ^oC) of pure El-cerrejon coal, CCP and fuel mixed (CCP:El-cerrejon (80:20 %, wt) as an example. It is obvious from the white dots (existence of the elements) of K and P in CCP:El-cerrejon (80:20 %, wt) were matched indicating K_3PO_4 presence. Also, the predicted fact (mentioned above, Sec., 4.2.2.1) that Ca (e.g. $CaSO_4$) and P (e.g. K_3PO_4) species increased, while Fe species (e.g. Fe_2O_3) decreased as CCP biomass share increased were in line with SEM-EDX results.

On the other hand, prediction of increase trend of HCl emissions (as CCP biomass share increased) disagreed with measured values. The most likely explanation for the difference between the predicted and measured values is that some species has been formed (experimentally) or interfere and/or kinetic constraints. Although, no thermodynamic basis could be found to support the hypothesis, this remains the most likely explanation.

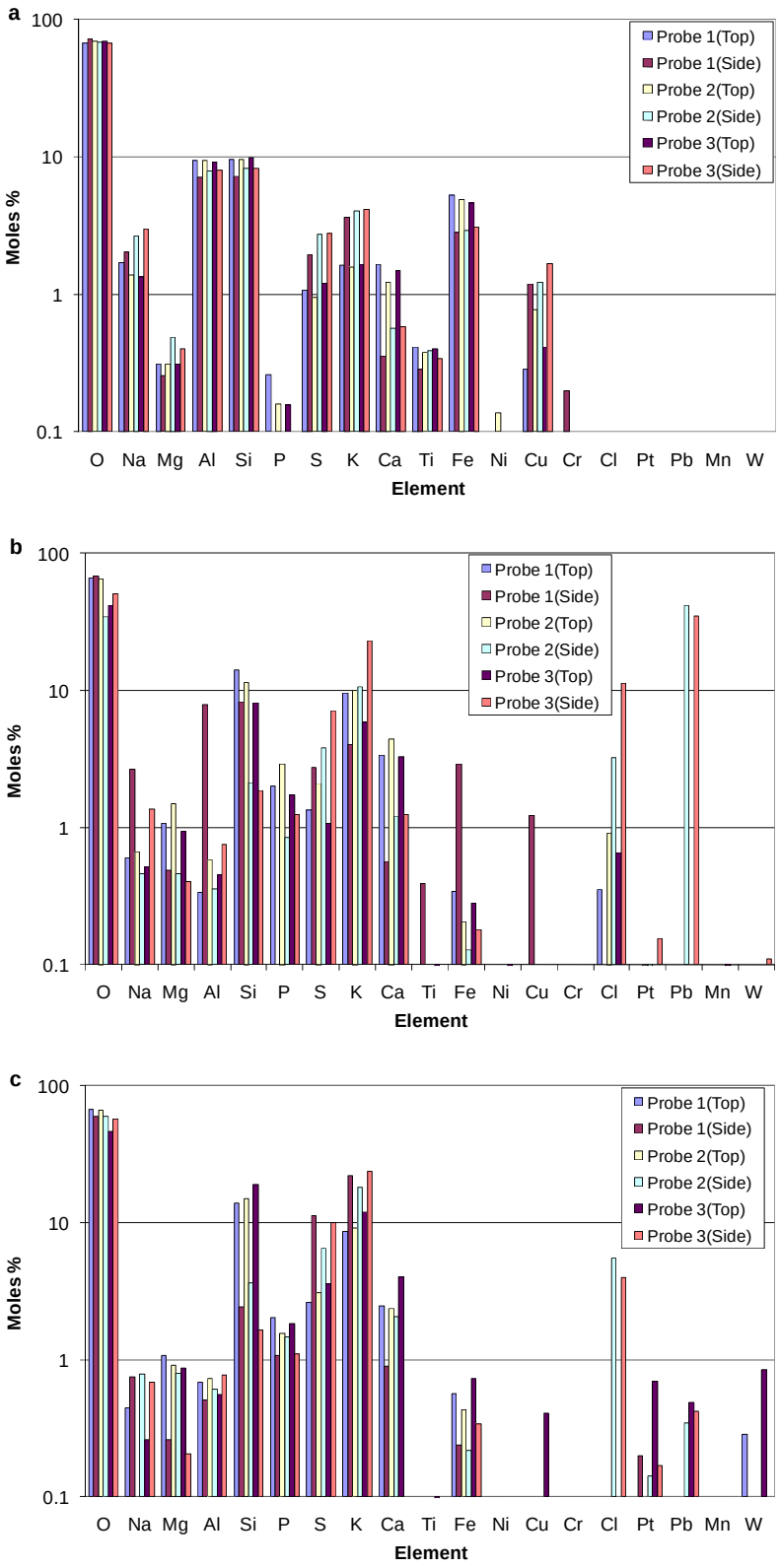

Figure 4.21 Elemental concentrations of the three probes deposits (top & side) from a) pure El-cerrejon coal (100 %, wt), b) pure CCP (100 %, wt) and c) CCP:El-cerrejon coal (80:20 %, wt)

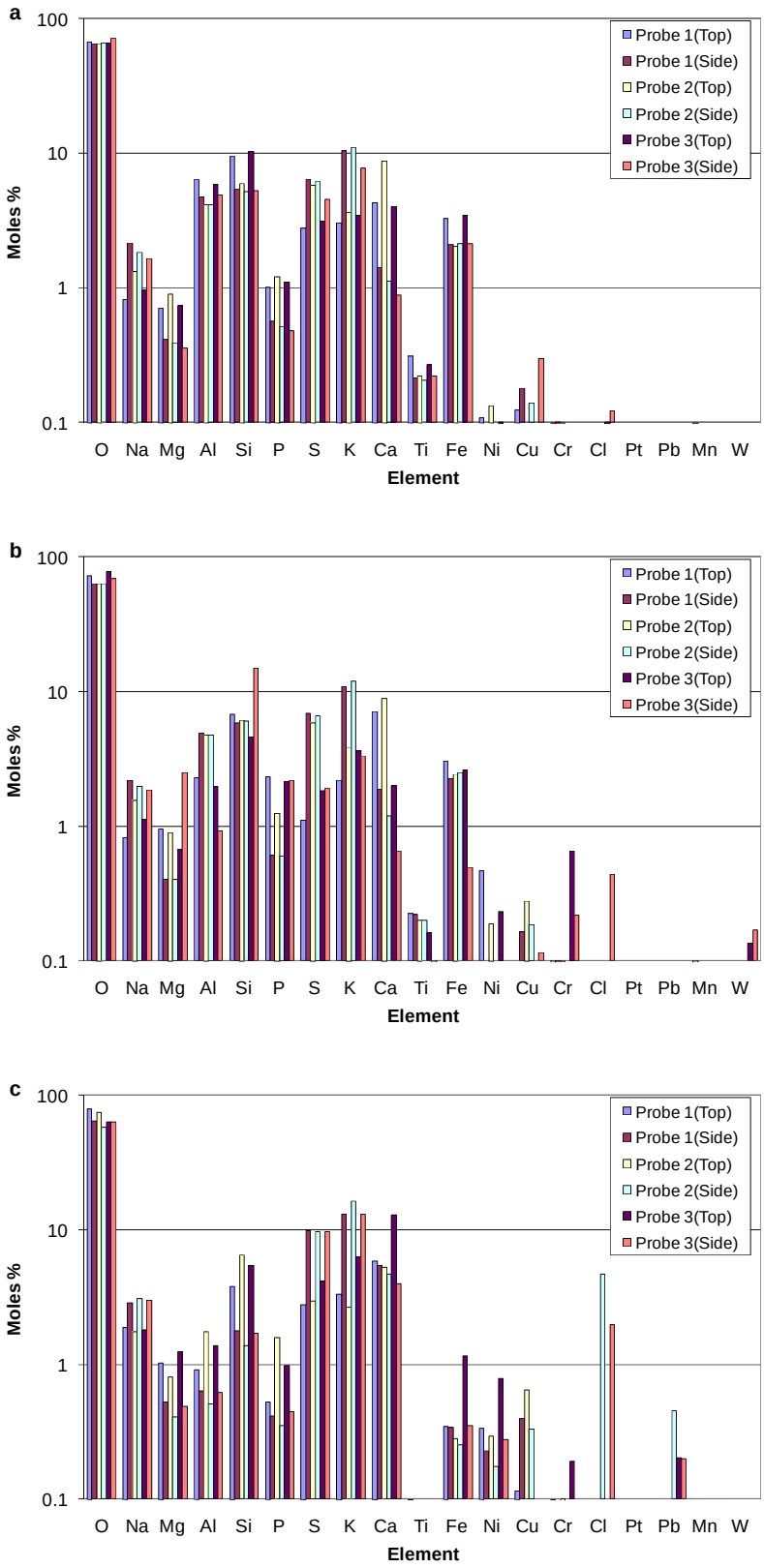

Figure 4.22 Elemental concentrations of the three probes deposits (top & side) from a) CCP:El-cerrejon coal (20:80 %, wt), b) CCP:El-cerrejon coal (40:60 %, wt) and c) CCP:El-cerrejon coal (60:40 %, wt)

4.3.2 Co-firing CCP: Daw Mill coal (0, 20, 40, 60 and 80 %, wt)

Combustion behaviour/efficiency & gaseous emissions

Figures 4.23 and 4.24 show the major and minor flue gas species, respectively, produced over three hours of stable combustion of four of the fuels mixtures (as examples of combustion behaviour) of pure Daw Mill coal (100 %, wt), CCP:Daw Mill (20:80 %, wt), CCP:Daw Mill (40:60 %, wt) and CCP:Daw Mill (80:20 %, wt). Furthermore, Figure 4.25 summerised the average of the gaseous emissions (major and minor) produced from pure and all the mixed fuel combustion. As an example, full temperatures measurements around the whole PF rig and around the deposits probes during CCP:Daw Mill (80:20 %, wt) co-firing are shown in Appendix D (D.5 & D.6, respectively, which display stable/control run).

Low CO emissions were achieved for all mixed fuel combustion. For example, CO emissions with averages of 242, 232, 87, 101 and 143 ppm for Daw Mill coal (100 %, wt), CCP biomass (100 %, wt) and CCP:Daw Mill (20:80 %, wt), CCP:Daw Mill (40:60 %, wt), CCP:Daw Mill (80:20 %, wt), respectively, imply that most of the carbon in the fuels was converted to CO_2 (i.e. high combustion efficiency).

The CO_2 emissions gave an average of 15.1 % for all co-fired mixed fuels compared to an average 14.8 % of coal firing alone. The H_2O emissions increases from 8.2 % at low share biomass to 11.5 % at high share mixed fuel.

Examining the minor gaseous species; the SO_2 concentration is high with Daw Mill coal (average of 453 ppm) compared with CCP biomass of average of 28.5 ppm, which is expected for coal and biomass based fuels. The combined effects of the low biomass share mixed fuel (i.e. CCP:Daw Mill, 20:80 %, wt) showed that SO_2 concentration dropped to an average of 357.6 ppm. For the high share mixed fuel (i.e. CCP:Daw Mill coal, 80:20 %, wt), the average SO_2 was 216.1 ppm which indicates the significance of co-firing on SO_2 emissions. The trend of lower SO_2 with increasing CCP in the fuel mix is in line with MTDATA predictions.

NO_x (NO and NO_2) concentrations show averages of 398.9, 479.5, 508.7, 485.4, 565.6 ppm, whereas the N_2O emissions were 2.5, 8.7, 2.6, 2.7, 2.9 ppm for Daw Mill coal, CCP biomass and the mixed fuels CCP:Daw Mill (20:80 %, wt), CCP:Daw Mill (40:60 %, wt), CCP:Daw Mill (80:20 %, wt), respectively. The NO_x concentrations of the intermediate mixed fuel (i.e. CCP 20, 40 and 60 %, wt) all had averages of ~ 490 ppm. This suggests that the major source of NO_x in flue gas is from fuel-N. The HCl had averages of 89.6, 58.6, 87.3, 69.1, 68.2, 71.6 ppm for 100 % Daw Mill, 100 % CCP and the mixed fuels 20 % CCP, 40 % CCP, 60 % CCP, 80 % CCP, respectively; indicated possibility of higher HCl released in low share biomass coal combustions.

It is obvious that the minor gaseous species emissions (Figure 4.24) remained almost constant during combustion runs and no significant drops or drastic increases have been noted (except for the case of feeding stopping due to blockage of dirt/stones in the fuels).

It is clear that all the measured data of major and minor gaseous were matched the calculated data (CP and MTDATA). For example, the gaseous emissions (Fig. 4.25) measured data of H_2O, O_2, CO_2 and HCl were an average of 9.7 %, 4.8 %, 14.9 % and 71.1 ppm, respectively, compared to the predicted calculated MTDATA data (Table 4.6) at ~ 1200 ºC which were 10.4 %, 3.9 %, 11.91 % and 98.0 ppm, for H_2O, O_2, CO_2 and HCl, respectively.

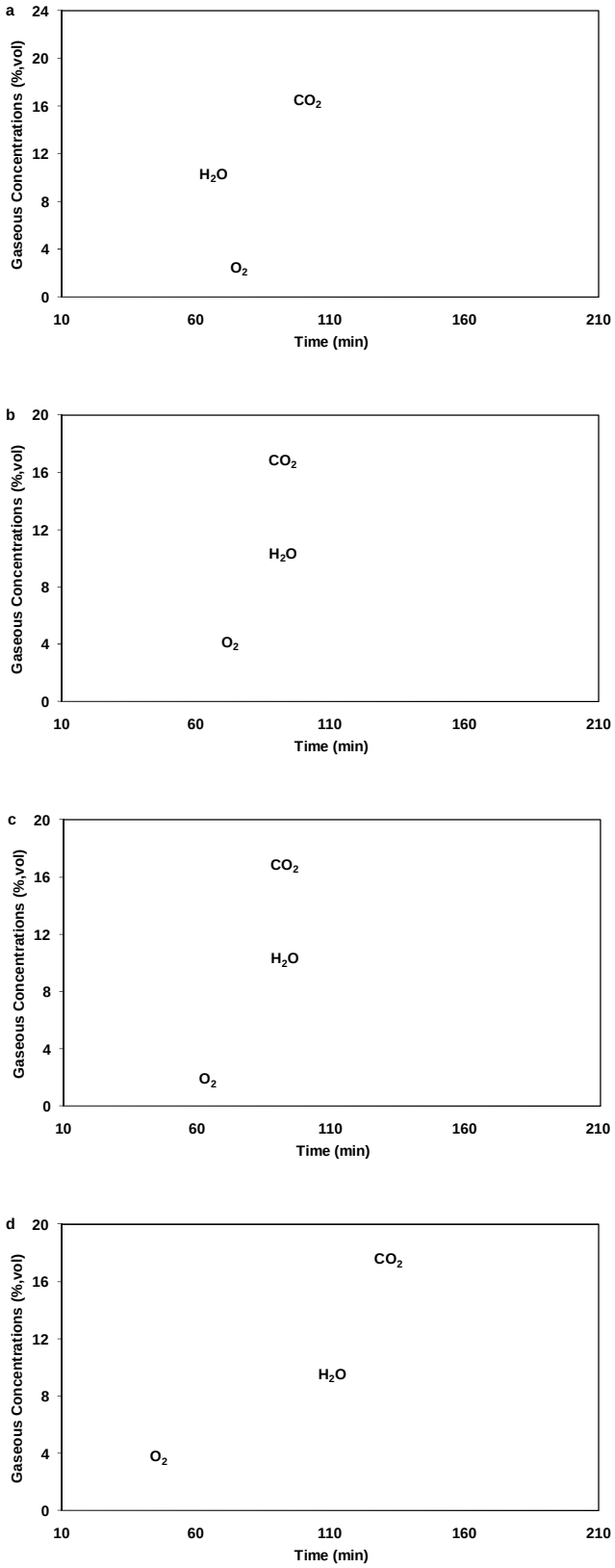

Figure 4.23 Major gaseous emissions from combustion of a) pure Daw Mill coal (100 %, wt), b) CCP:Daw Mill (20:80 %, wt), c) CCP:Daw Mill (40:60 %, wt) and d) CCP:Daw Mill (80:20 %, wt)

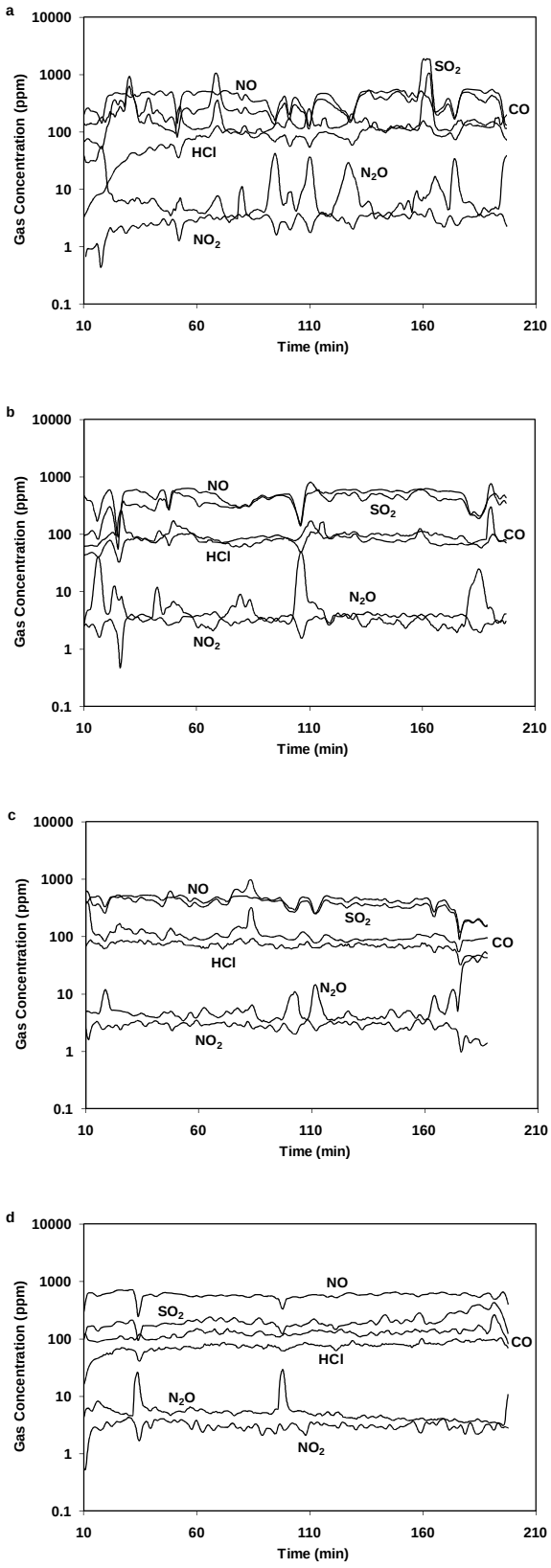

Figure 4.24 Minor gaseous emissions from combustion of a) pure Daw Mill coal (100 %, wt), b) CCP:Daw Mill (20:80 %, wt), c) CCP:Daw Mill (40:60 %, wt) and d) CCP:Daw Mill (80:20 %, wt)

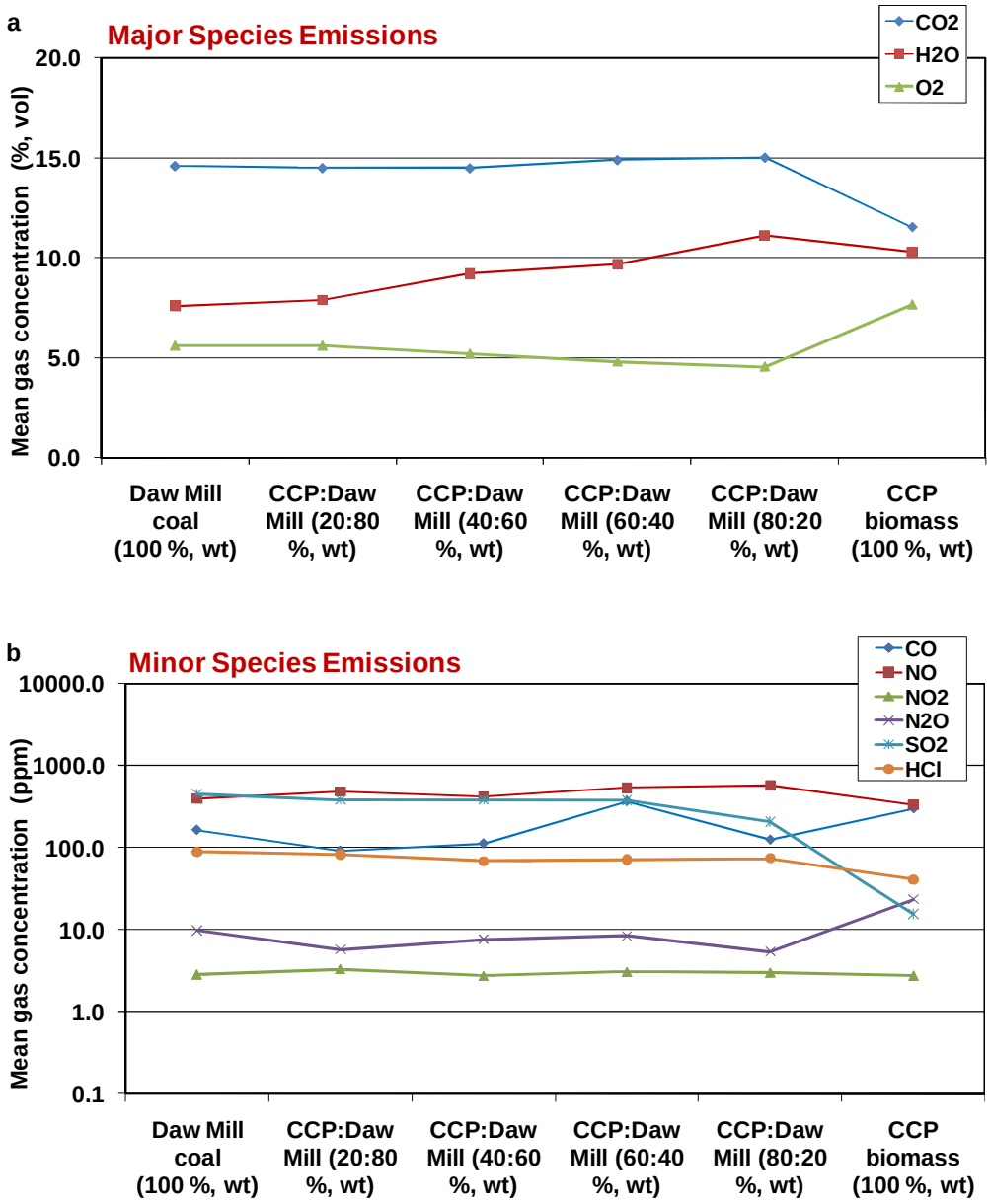

Figure 4.25 Mean concentrations of gaseous emissions (major & minor) from CCP:Daw Mill mixed fuels combustion

Deposition fluxes, compositions and analysis

Figure 4.26 shows the deposition fluxes formed on each of the three probes for all of the fuel mixtures. This showed that the highest deposition fluxes were found at surface temperatures of ~ 500 ^{o}C (probe 3) on the top of the probes for the co-firing mixed fuels. Little deposit was formed (below 1.0 mg/cm^2/hr) on side of the probes and on

underside of the probes for all the selected fuels, with none measureable on the underside of up to 40 % CCP mixed fuel at ~ 700 ^{o}C probe surface temperature.

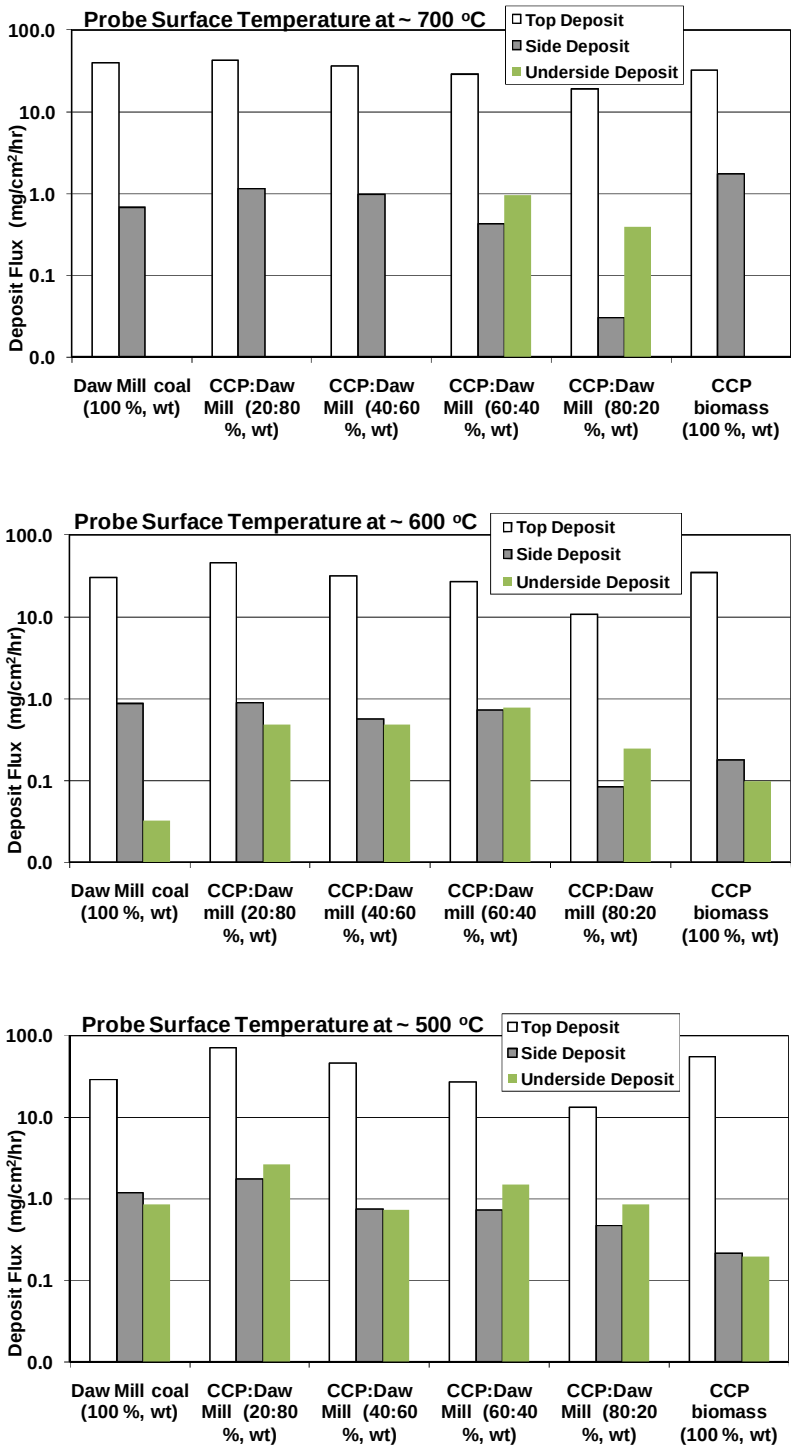

Figure 4.26 Deposition rate from probes 1, 2 and 3 (~ 700, 600, 500 ^{o} C, surface temperature) with deposits formed on top, side and underside from CCP:Daw Mill mixed fuels combustion

The results also revealed lower deposition fluxes with the higher shares of biomass in the fuel blend on the top surface (i.e. representing the upstream deposit formation). Co-firing mixed fuel (CCP:Daw Mill, 20:80 %, wt) exhibits the highest upstream deposit formation at ~ 500 ^{o}C surface temperature compared with the other fuel mixtures (with a deposition flux of 71.1 mg/cm^{2}/hr). This outcome is the opposite of the deposition fluxes formed in CCP:El-cerrejon coal mixed fuels.

The appearance, the SEM images on top and SEM images on side of the deposits on the lowest temperature probes after about 3 hours and 20 minutes of feed fuels mixtures are shown in Figure D.7, D.8 and D.9, respectively (Appendix D). This shows that the deposits were coarse with less fibrous and more porous texture for co-firing the mixed fuel when compared to 100 % CCP.

It can be seen from the SEM images that the deposit particles on the top surfaces are much larger for CCP (100 %, wt) and high share mixed fuel (i.e. 60 % CCP and 80 CCP %, wt) co-firing when compared to 100 % Daw Mill and low ratio of mixed biomass fuel of 20 % and 40 % CCP (Fig. D.8). Whereas, the SEM images of the side deposits shows a somewhat porous structure on the 100 % CCP and high mixed fuels.

A significant point to make (as can be seen in Fig. D.7, Appendix D) is that the colour of deposits was different to CCP:El-cerrejon coal mixed fuels. Furthermore, examining the elemental concentrations of the deposits indicates an increase in Si, Al, Mg, P, Ca, Ti and a decrease in Fe, K and Na of pure Daw Mill compared to El-cerrejon coal. Sulfur levels observed of variation, which either was higher or lower in the top and/or side deposits of probes temperatures (~ 700, 600, 500 ^{o}C) studied. Almost the trend behaviour of these elements were observed in the mixed fuels CCP:Daw Mill compared to CCP:El-cerrejon coal (at 20, 40, 60 and 80 %, wt).

The elemental compositions of the deposits formed on the top, side and underside of all three probes for co-firing mixed fuel CCP:Daw Mill (20:80 %, wt), CCP:Daw Mill (60:40 %, wt), CCP:Daw Mill (60:40 %, wt) and CCP:Daw Mill (80:20 %, wt) analysed by EDX are shown in Figure 4.27.

The results reveal varying concentrations of silicon, calcium, sulphur, potassium, iron and aluminium in the deposits of all probes. Potassium and sulphur concentrations in the deposits of all probes (on each side) of co-firing mixed fuels increased with increasing the share of CCP. For example, K content on the deposits with concentrations of 8.7, 22.3, 12.2 % moles of CCP:Daw Mill (80:20 %, wt) compared to CCP:Daw Mill (60:40 %, wt) of 5.7, 15.9, 8.6 % moles at probe 3 (~ 500 ^{o}C) on top, side and underside, respectively. Chlorine concentrations are formed in all probes of 100 % CCP biomass test (as expected) and only on the higher share of the mixed fuels CCP:Daw Mill (80:20 %, wt) in the side deposit of probe 2 (~ 600 ^{o}C) with 0.4 % moles, and in the side and underside of probe 3 (~ 500 ^{o}C) with concentrations of 6.0 and 1.5 % moles, respectively.

Calcium concentrations showed no significant variation, whereas iron results a linear decreases with increasing the share of biomass on all the probes surface temperatures of the studied conditions.

The mineral phases contained in the deposits from the coal and CCP co-firing were identified with X-ray diffraction. Figure D.10 (Appendix D) shows the XRD patterns of deposits from mixed fuel CCP:Daw Mill, 20:80 %, wt and CCP:Daw Mill, 80:20 %, wt formed (all around) on probes with surface temperatures of ~ 500 ^{o}C (as examples).

In high share mixed fuels with biomass (i.e. CCP:Daw Mill, 80:20 %, wt), the XRD patterns reveal that sylvite (KCl) and arcanite (K_2SO_4) were the main mineral phases on the side and underside deposits formed on the probes. According to Baxter et al., 1998 the presence of potassium chlorides and sulphates are responsible for low melting point deposits from combustion processes. For the other fuel mixtures, the mineral phases detected were quite different; anhydrite ($CaSO_4$) was the primary components with presence of quartz (SiO_2). With high levels of stable mineral phases with high melting points, deposits from these mixed fuels have much higher melting temperatures than CCP:Daw Mill (80:20 %, wt) and CCP (100 %, wt).

These compounds confirmed by XRD results (e.g. $CaSO_4$, Fe_2O_3, $FeSO_4$, K_2SO_4) were in line with the predictions made by MTDATA (Fig. 4.12.a-d). However, other compounds predicted, such as Na_2SO_4 were not identified by XRD, but the SEM-EDX data (Fig. 4.27) indicated of formation. Figure D.11 (Appendix D) shows the EDX maps of top surface deposits (~ 500 ^oC) of mixed fuel CCP:Daw Mill (20:80 %, wt), CCP:Daw Mill (60:40 %, wt) and CCP:Daw Mill (80:20 %, wt) as an example. It is obvious from the white dots (existence of the elements) of Na and S in CCP:Daw Mill (20:80 %, wt) were matched, indicating Na_2SO_4 presence. Also shows that the predicted fact (mentioned above, Sec., 4.2.2.2) of condensed Na_2SO_4 predicted up to co-firing Daw Mill with 40 % CCP was consistent with measured data from Na map of CCP:Daw Mill (60:40 %, wt) and CCP:Daw Mill (80:20 %, wt) of no bright areas appear with S map, indicating no Na_2SO_4 presence.

The predictions of no condensed KCl for co-firing CCP:Daw Mill mixed fuels were in agreement with experimental study up to co-firing Daw Mill with 60 % CCP. Formation of condensed KCl in the side and underside deposit of the higher share of mixed fuels CCP:Daw Mill (80:20 %, wt) suggested of available Cl in the system influenced by condensation and/or thermophoresis mechanisms (see literature review Chapter 2), which were not predicted by the model. Other hypothesis, the amount of condensed phase is quite sensitive to the amount of S in the system which makes condensed K_2SO_4 the dominant condensed species to form. Since K_2SO_4 has a lower vapour pressure than KCl, it leads to condensation and deposition at high temperatures. There is an ongoing discussion [Nielsen et al., 2000] whether sulfation reaction with KCl and K_2SO_4 take place in the gas phase or after condensation in the molten solid phase. Examination carried out by Anderson, 1998; Nielsen et al., 2000; Baxter 1993; Baxter et al., 1998 based on observation at different combustion units indicated that the deposits formation process for KCl and K_2SO_4 compounds was mainly characterised by condensation and thermophoresis mechanisms which form the first sticky, inner layer of the deposits. Whereas the outer deposit layer is dominated by K, Si and Ca which build up generally by inertial impaction mechanisms and consists mainly of the individual ash particles.

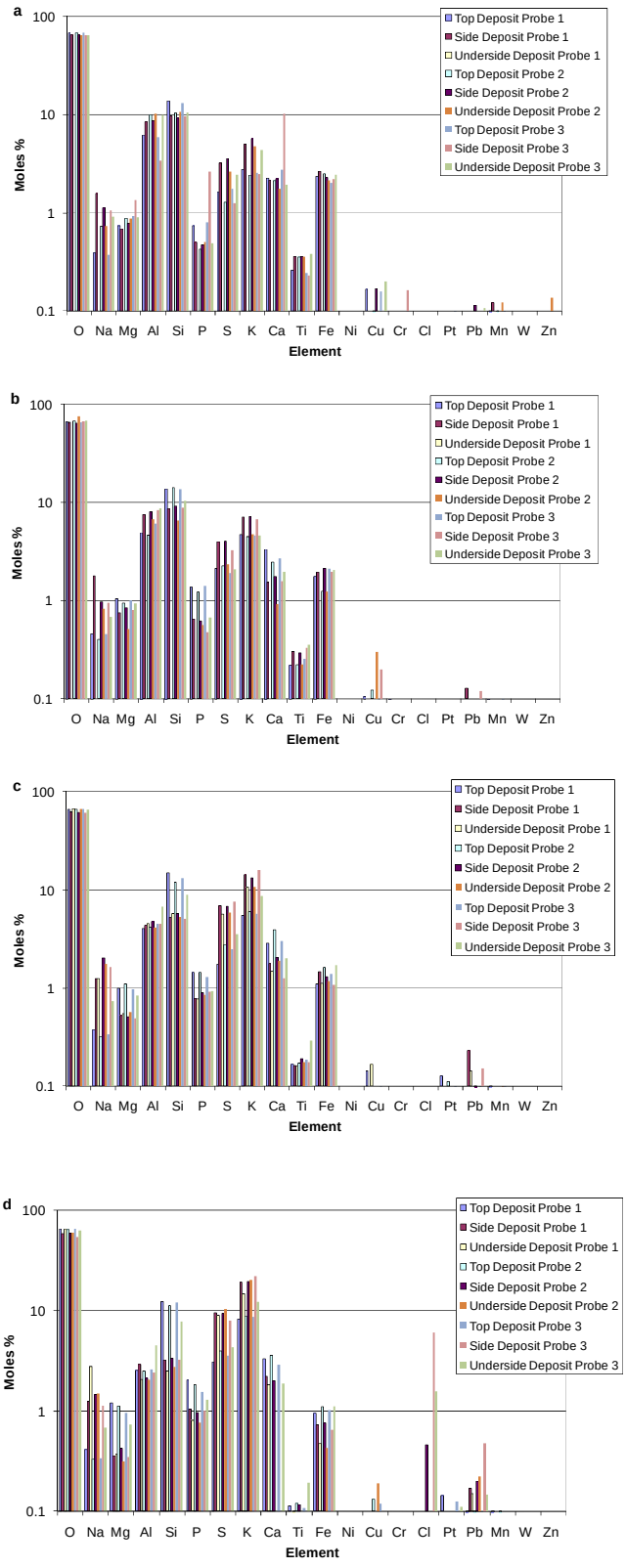

Figure 4.27 Elemental concentrations of the three probes (1, 2 and 3, ~ 700, 600, 500 ^{o}C) deposits (on top, side and underside) from co-firing of a) CCP: Daw Mill (20:80 %, wt), b) CCP: Daw Mill (40:60 %, wt), c) CCP: Daw Mill (60:40 %, wt) and d) CCP: Daw Mill (80:20 %, wt)

4.3.3 Co-firing Miscanthus: Daw Mill coal (0, 20, 40, 60 and 80 %, wt)

Combustion behaviour/efficiency & gaseous emissions

The major and minor flue gas species produced over two hours of stable combustion of four of the fuels mixtures (as examples) of mixed Miscanthus:Daw Mill (40:60 %, wt), Miscanthus:Daw Mill (60:40 %, wt), Miscanthus:Daw Mill (80:20 %, wt) and pure miscanthus (100 %, wt), are shown in Figures 4.28 and 4.29, respectively.

High combustion efficiencies were achieved for all fuel mixes as 'shown by' the low CO emissions (shown in Fig. 4.29). The CO emissions recorded with mean values of 242, 384, 254, 150, 58 and 263 ppm for pure Daw Mill coal, miscanthus and mixed fuels Miscanthus:Daw Mill (20:80 %, wt), Miscanthus:Daw Mill (40:60 %, wt), Miscanthus:Daw Mill (60:40 %, wt), Miscanthus:Daw Mill (80:20 %, wt), respectively. The CO_2 emissions gave a mean value of 14.8 % for all co-fired mixed fuels compared to a mean of 13.6 % for miscanthus firing alone. The H_2O emission increases from an average of 8.3 % at 20 % biomass to 11.1 % with 80 % biomass, whereas an average of 12.7 % was recorded for 100 % miscanthus combustion.

Investigating the minor gaseous species showed that the SO_2 concentration was the highest level for Daw Mill with a mean value of 453 ppm, whereas miscanthus resulted the lowest levels of SO_2 and HCl (mean values of 10.9 and 9.7 ppm). For the fuel mixes used the SO_2, NO and HCl concentrations decreased as the miscanthus share of the fuel mix increased. For example, from Fig. 4.29 the SO_2 concentrations had mean values of 393.4, 337.5, 218.8, 10.9 ppm, whereas the NO emissions were 386.1, 368.9, 276.3, 233.8 ppm for co-firing 40 % miscanthus, 60 % miscanthus, 80 % miscanthus and 100 % miscanthus, respectively. It should also be noted that the major and minor gaseous species remained almost constant during combustion runs, except for when the feeding stopped due to blockages of dirt/stones in the fuels.

Generally, the combustion gas measurement data (from pilot-scale experiments) for all fuels used (mixed and pure) were largely consistent with the thermodynamic equilibrium calculations. For example, the equilibrium model predicted H_2O at 9.4 %,

SO_2 at 474 ppm and NO at 408 ppm around ~ 1180 ^oC (section 4.2.2.3) compared to the experimental data (Fig. 4.29.a) were measured with an average of H_2O (8.5 %), SO_2 (393 ppm) and NO (386 ppm) for co-firing blended Miscanthus:Daw Mill (40:60 %, wt). However, it should be pointed out that the slight differences in the experimental data compared to the prediction data to the fact that these data were a mean values. Also, considering the oxygen content of the combusted gas stream was targeted at 4 volume % for prediction study, whereas the oxygen volume outcomes of the experimental study were in range of 4.3-5.6 % for all fuels mixes. The trend of lower SO_2, NO, HCl and of higher H_2O with increasing miscanthus in the fuel mix that was noted in the experimental results were in line with the model prediction data (as can be seen in Table 4.7 and Fig. 4.13.a-d)

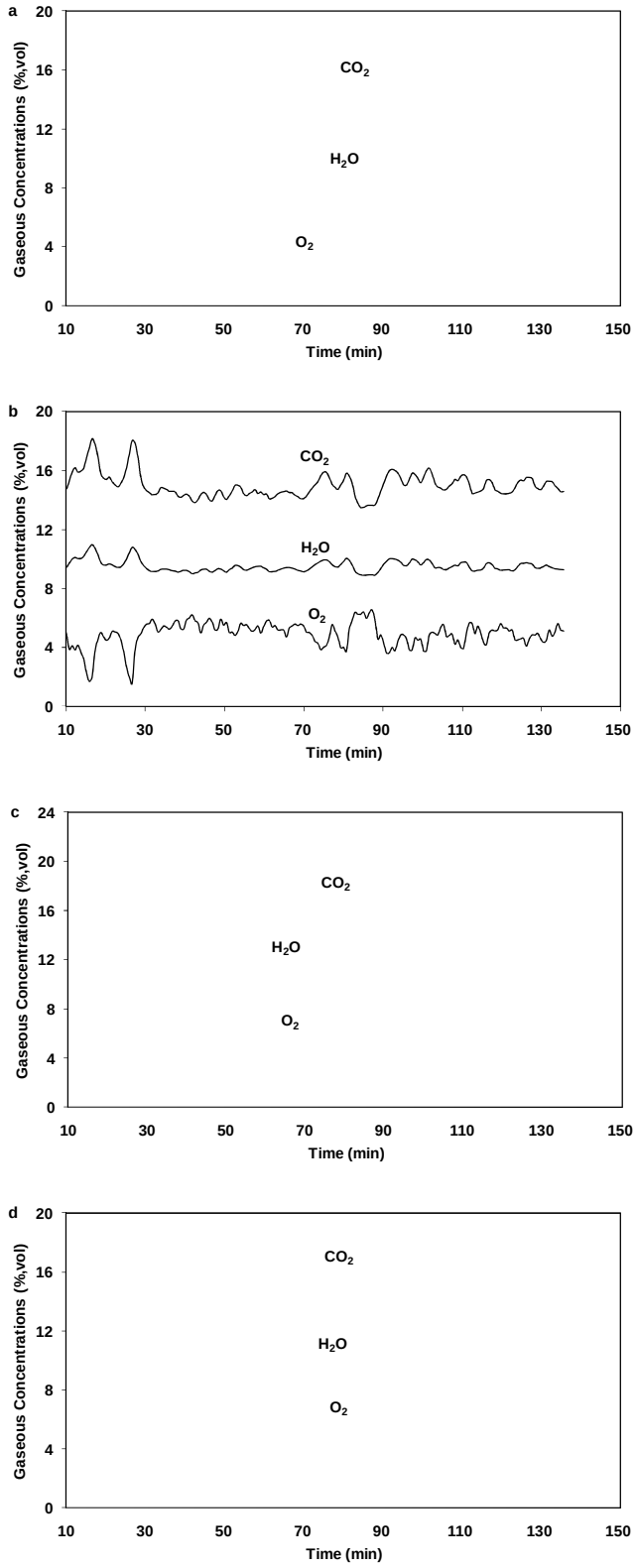

Figure 4.28 Major gaseous emissions from combustion of a) Miscanthus:Daw Mill (40:60 %, wt), b) Miscanthus:Daw Mill (60:40 %, wt), c) Miscanthus:Daw Mill (80:20 %, wt) and d) pure Miscanthus (100 %, wt**)**

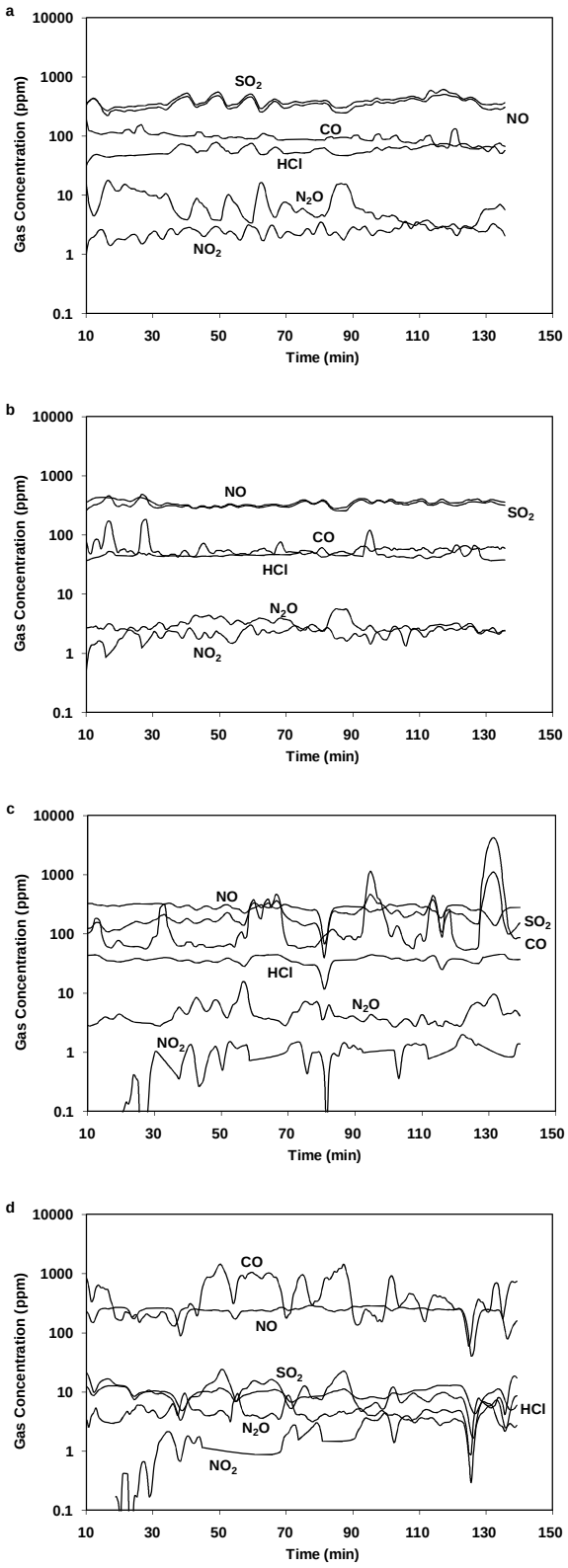

Figure 4.29 Minor gaseous emissions from combustion of a) Miscanthus:Daw Mill (40:60 %, wt), b) Miscanthus:Daw Mill (60:40 %, wt), c) Miscanthus:Daw Mill (80:20 %, wt) and d) pure Miscanthus (100 %, wt)

Deposition fluxes, compositions and analysis

Figure 4.30 shows the deposition fluxes formed on each of the three probes for all of the fuel mixtures. This showed that the highest deposition fluxes were found at surface temperatures of ~ 500 ^{o}C (probe 3) on the top of the probes for the co-firing mixed fuels (Miscanthus:Daw Mill, 20:80 %, wt) with a deposition flux of 51.0 mg/cm^2/hr. Also, underside deposits (i.e. representing underside-stream deposit formation) were formed on the surface temperatures of ~ 500 ^{o}C for all the fuel mixtures and only started to form at Daw Mill mixed with 40 % miscanthus and upwards on probes surface temperatures of ~ 600 and 700 ^{o}C. Pure miscanthus exhibits the highest upstream, side and underside deposit formation at ~ 500 ^{o}C surface temperature (compared with other probe temperatures) with a deposition flux of 1.4, 0.1 and 0.3 mg/cm^2/hr, respectively.

There is no specific trend to be drawn, however it can be said approximately that the top and side deposits (i.e. representing the upstream and sidestream deposit formation) decreased while underside deposits increased as miscanthus share with Daw Mill increased.

Figure D.12 (Appendix D) shows the appearance of the deposits (on top, side and bottom surfaces) formed over ~ 3-hour exposure periods on probe 3 (~ 500 ^{o}C surface temperature) for all fuel mixtures. This shows that the deposits on the upstream and sidestream (top and side surfaces) decreased with increasing biomass, but increased on the downstream (underside) surface. The SEM images (Fig. D.13, Appendix D) of the underside deposits (probe 3) showed that the particles size increases and they appear more agglomerated with less porous textures as the biomass ratio increases. This supports Baxter and Desoallar, 1993 study that the large particle size increases the deposition impaction rates because inertial impaction efficiencies on probes depend on the square of the particle diameter.

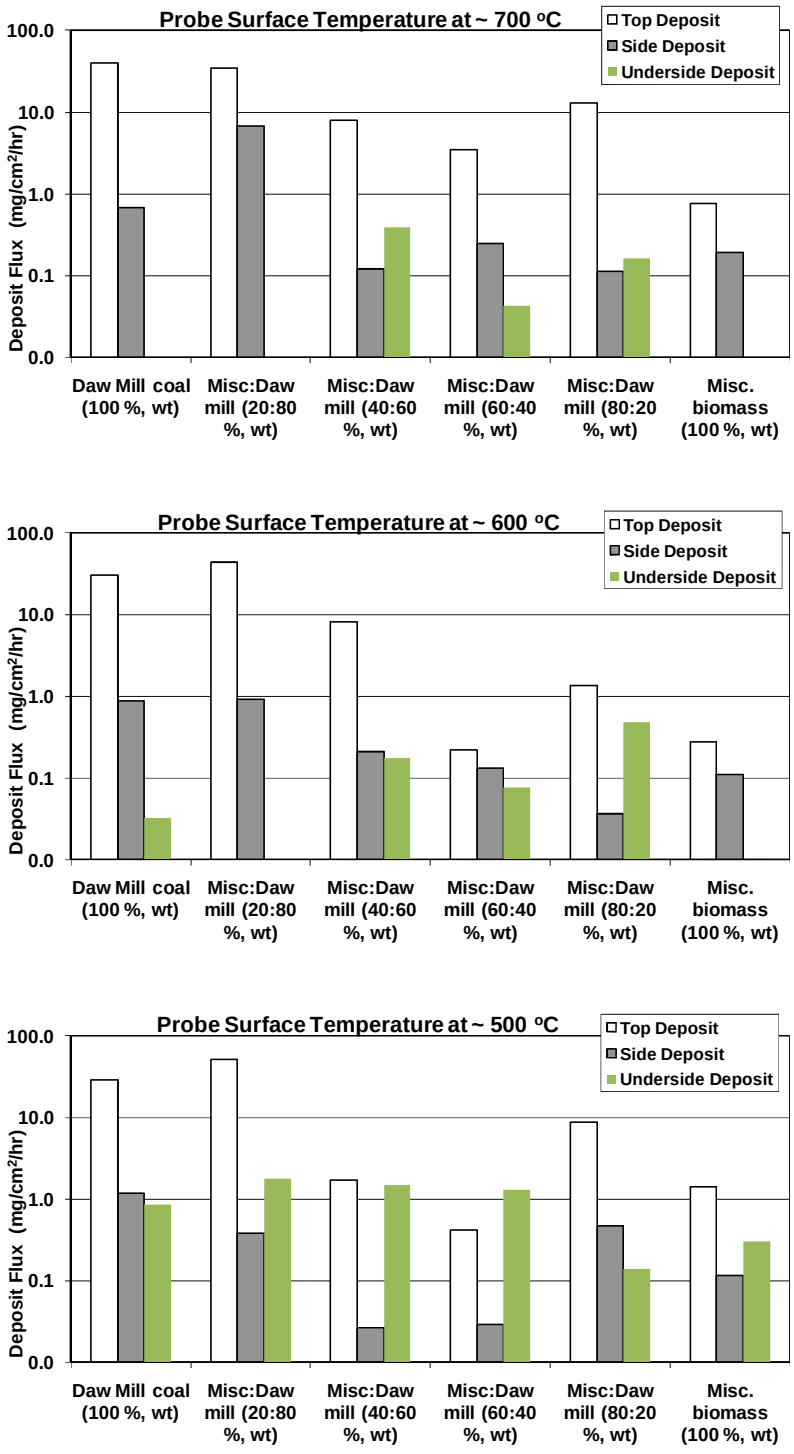

Figure 4.30 Deposition rate from probes 1, 2 and 3 (~ 700, 600, 500 ^{o}C, surface temperature) with deposits formed on top, side and underside from Miscanthus:Daw Mill mixed fuels combustion

The elemental compositions of the deposits formed on the top, side and underside of all three probes exposed during combustion exposures were analysed by SEM-EDX.

Results from runs using pure Daw Mill coal, Miscanthus:Daw Mill (20:80 %, wt), Miscanthus:Daw Mill (40:60 %, wt), Miscanthus:Daw Mill (60:40 %, wt), Miscanthus:Daw Mill (80:20 %, wt) and 100 % miscanthus (pure) are shown in Figure 4.31. The results revealed that Si, Al, Ca and Fe concentrations in the deposits on of all probes (on each side) showed no significant variation up to 60 % miscanthus co-firing, above which all decreased. For example, the Fe content in the deposits collected from probe 3 (~ 500 ^{o}C) had concentrations of 2.8 (top), 2.4 (side), 3.1 (underside) % moles from the combustion of Miscanthus:Daw Mill (40:60 %, wt) and 2.9, 2.3, 3.2 % moles from Miscanthus:Daw Mill (60:40 %, wt), compared values from Miscanthus:Daw Mill (80:20 %, wt) of 1.5, 1.7, 1.7 % moles. Following the opposite trend, K and S concentrations in the deposits of all probes (all sides) increased slightly up to 60 % miscanthus co-firing, and then showed the highest concentration level at 100 % miscanthus combustion. Chlorine concentrations were none in all probes up to 60 % miscanthus co-firing and then at low levels for the higher share of the mixed fuels; Miscanthus:Daw Mill (80:20 %, wt) in the underside deposit of probe 3 (~ 500 ^{o}C) with 0.1 % moles (Fig. 4.31.e). Whereas, Cl was found in deposits on all probes (all sides) from the 100 % miscanthus test with highest concentrations level at the side (5.0 % moles) and underside (3.4 % moles) of the coolest probe surface temperature (probe 3, ~ 500 ^{o}C), (Fig. 4.31.f).

XRD was used to identify the mineral phases with the higher concentrations contained in the deposits from the coal and miscanthus co-firing runs. Figure D.14 (Appendix D) shows the XRD patterns of deposits from mixed fuel Miscanthus:Daw Mill, 20:80 %, wt and Miscanthus:Daw Mill, 60:40 %, wt formed on the top of probes with surface temperatures of ~ 500 ^{o}C (as examples). The main compounds identified by X-ray diffraction include: quartz (SiO_2), anhydrite ($CaSO_4$), iron sulfite ($FeSO_3$) and hematite (Fe_2O_3) for all miscanthus/Daw Mill blends (at 0, 20, 40, 60 and 80 weight %). The presence of sylvite (KCl) and sodium silicate (Na_2SiO_3) as additional mineral phases were only detected in deposits from the gas phase during 100 % miscanthus combustion (Fig. D.14.c). This suggest that alkali species in 100 % miscanthus exposures were more mobile than in co-firing exposures, which was consistent with results from chemical fractionation analysis [Baxter et al., 1996]. Gas phase alkali mainly contributes to

deposit formation by vapour condensation reactions [Robinson et al., 2002]. Alkali species can react with silicon to form alkali silicates either via residual alkali in fly ash particles (condensed-phase reaction) or between gas-phase, alkali-bearing species and condensed-phase silica or silicate. The formation of alkali silicates that have relatively low melting temperatures (which increases the probability that a particle impacting the probe surface will stick [Baxter et al., 1996]) and KCl (which has often been identified as being associated with high levels of fouling and corrosion [Van Loo and Koppejan, 2008]) in 100 % miscanthus deposits indicates that there are significant changes in the balance of processes that form the deposits on cooled surfaces as the % of miscanthus increases.

It is clear that the pilot-scale experimental data were consistent with the prediction data for the probe deposits in the temperature range ~ 500-700 °C for all the fuels mixtures (e.g. for the compounds identified by X-ray diffraction, Fig. D.14 (Appendix D)). For example it was predicted, (Fig. 4.14 & Fig. 4.8) that $CaSO_4$ is stable over the temperature range 200-1180 °C, 200-1160 °C, 200-1100 °C, whereas Fe_2O_3 is stable over the temperature range 520-920 °C, 500-900 °C, 460-860 °C, for co-firing 20 % miscanthus, 60 % miscanthus and 100 % miscanthus firing, respectively. Also, condensed sylvites (KCl) have been predicted only for 100 % miscanthus (200-580 °C) combustion (as shown in Fig. 4.8).

On the other hand, XRD did not identify predicted K_2SO_4 (Fig. 4.14 & Fig. 4.8), but the SEM-EDX data indicated that the K and S content of the deposits were in a range ~ 3.3-7.3 % for the fuel mixes. As a result the % of K_2SO_4 would be less than the detection limit of the XRD. Also, XRD needs crystalline deposits and whether submicron aerosol particles (from the flue gas) produce crystalline deposits is debateable. Figure D.15 (Appendix D) shows the EDX map images of top deposits (~ 500 ^oC) of pure Daw Mill coal, miscanthus and mixed fuel Miscanthus:Daw Mill (60:40 %, wt) as an example. This can suggested the presence of K_2SO_4.

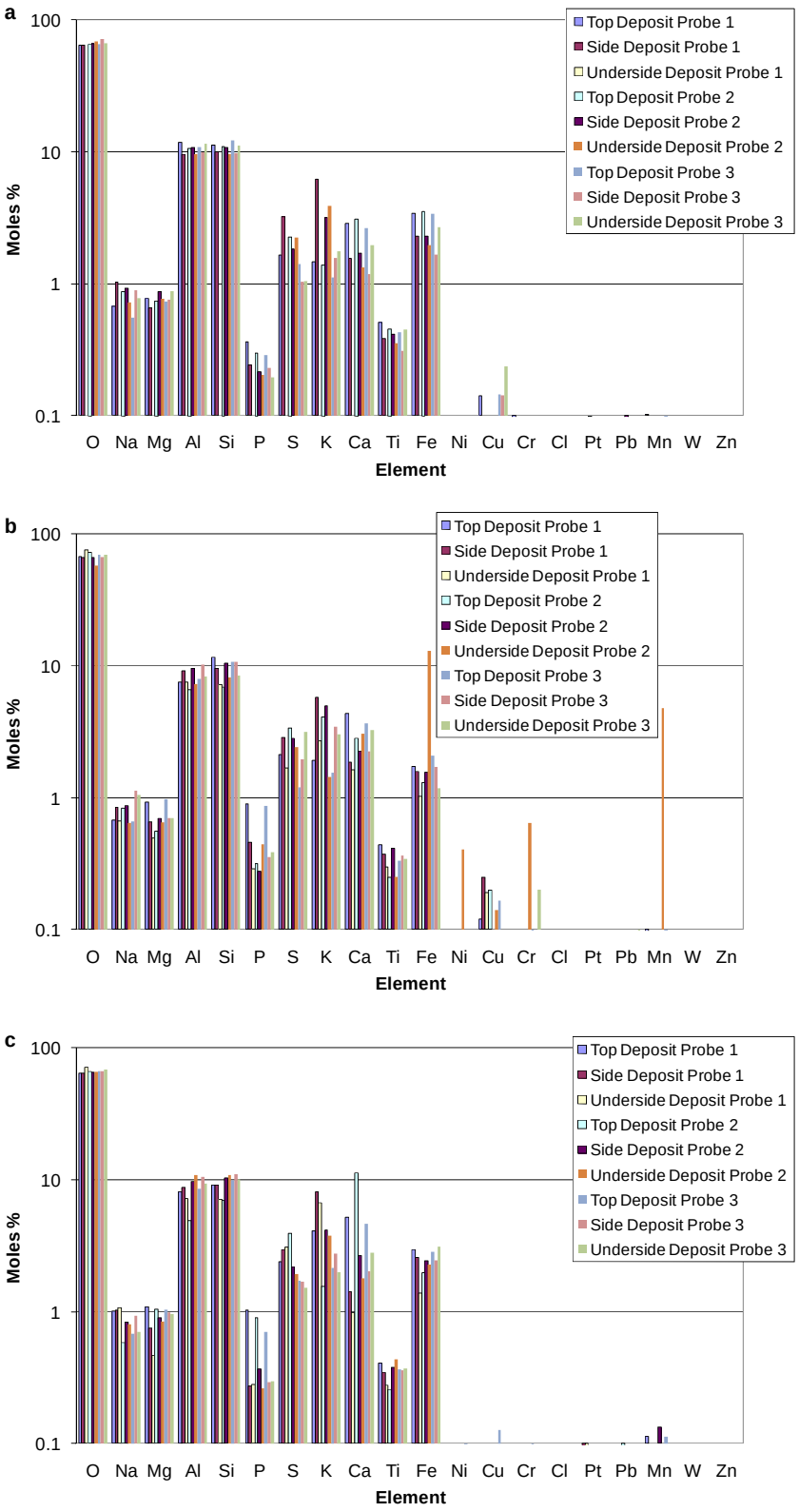

Figure 4.31 Elemental concentrations of the three probes deposits (1, 2 and 3, ~ 700, 600, 500 ^{o}C) deposits (on top, side and underside) from co-firing of a) pure Daw Mill coal (100 %, wt), b) Miscanthus:Daw Mill (20:80 %, wt) and c) Miscanthus:Daw Mill (40:60 %, wt)

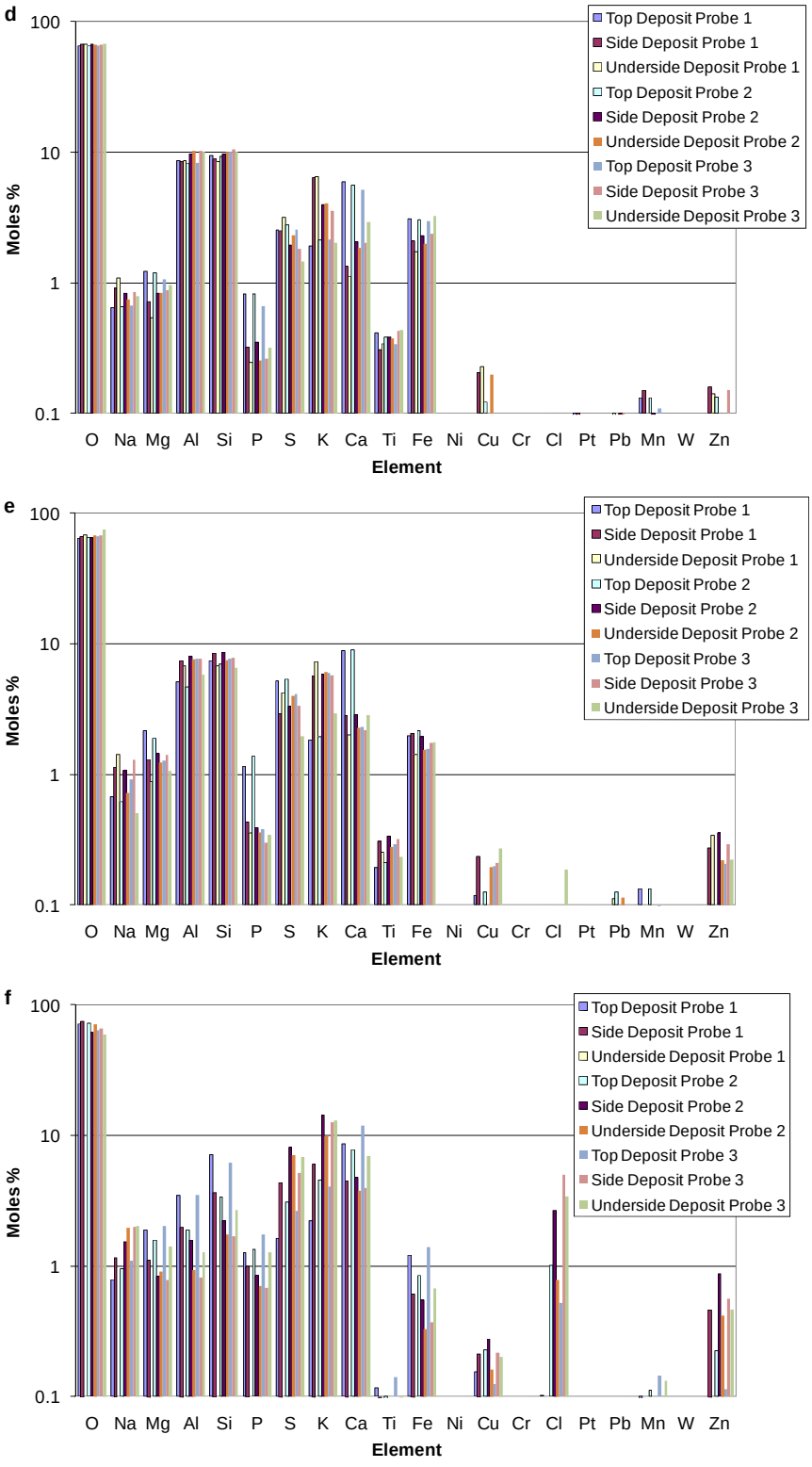

Figure 4.31 Elemental concentrations of the three probes deposits (1, 2 and 3, ~ 700, 600, 500 ^{o}C) deposits (on top, side and underside) from co-firing of d) Miscanthus:Daw Mill (60:40 %, wt), e) Miscanthus:Daw Mill (80:20 %, wt) and f) pure Miscanthus (100 %, wt)

4.3.4 Co-firing Miscanthus: El-cerrejon coal (60:40 %, wt)

Combustion behaviour/efficiency & gaseous emissions

Figure 4.32 shows the major and minor flue gas components produced over ~ 2 hours of stable co-firing of mixed Miscanthus:El-cerrejon coal (60:40 %, wt). The minor gas compositions (Fig. 4.32.b) resulted an average of 300.6 ppm SO_2, 52.7 HCl and 218.7 ppm NO. The CO concentration of an average of 635.4 ppm representing high combustion efficiency performed.

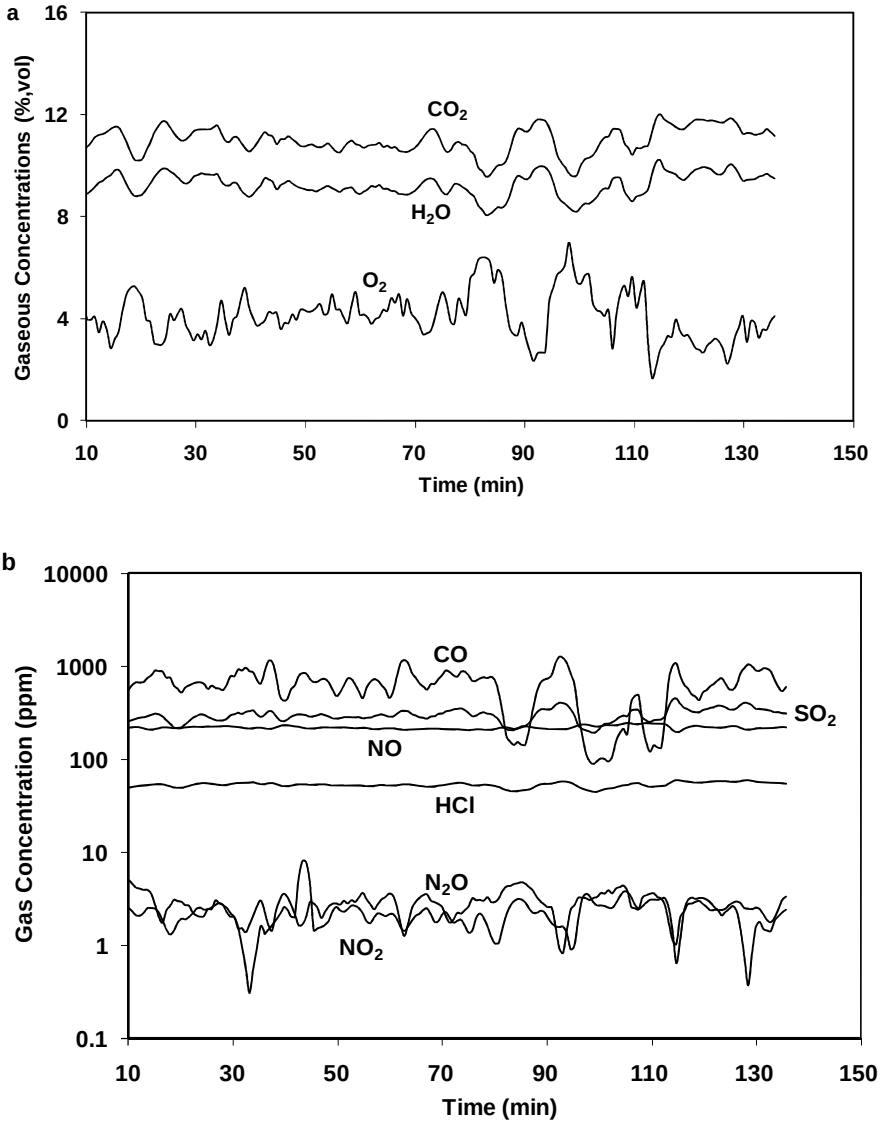

Figure 4.32 Gaseous species emissions from co-firing of Miscanthus:El-cerrejon (60:40 %, wt) of a) major species and b) minor species

It is obvious that all the measured data of major and minor gaseous (mentioned above) were matched the calculated data (Table 4.8). For example, the gaseous emissions (Fig. 4.32) measured data of H_2O, O_2, CO_2 and NO_2 were an average of 9.2 %, 4.0 %, 11.0 % and 2.2 ppm, respectively, compared to the predicted calculated MTDATA data at ~ 1200 ^oC which were 9.6 %, 3.9 %, 13.4 % and 1.15 ppm, for H_2O, O_2, CO_2 and NO_2, respectively. MTDATA predicted HCl emissions ~ 6.7 ppm, but CP calculated HCl 49.0 ppm (Table 4.8) which in consistent with measured data average of 52.7 ppm HCl.

Deposition fluxes, compositions and analysis

Figure D.16 (Appendix D) shows the photograph of the three probes deposit (~ 700, 600 and 500 ^oC surface temperatures), whereas the SEM images of the deposit formed on the top and underside surface of these probe are presented in Figure D.17 (Appendix D). This shows that overall deposition was low with higher deposition fluxes formed at surface temperature of ~ 500 ^oC. Closer examination also, showed a few impacted particles on the sidestream (side deposit) and downstream (underside deposits) of the probes surface temperature of ~ 700 and 600 ^oC as almost shiny ceramic section can be seen. The SEM images suggested that the particle sizes were fine textures with a possible of less porous on deposits (top and underside) formed on surface temperature of ~ 700 and 600 ^oC.

The deposition fluxes formed on each of the three probes are shown in Figure 4.33. The deposition rates of top deposits were 1.15, 0.31, 0.73 mg/cm^2/hr and underside deposits of 0.11, 0.07, 0.96 mg/cm^2/hr on ~ 700, 600 and 500 ^oC surface temperatures, respectively. The little higher flux of the top deposits formed on probe of ~ 700 ^oC surface temperatures is believed to be due to a few large particles found compared to other probes. Similar trend of deposition fluxes on top deposits were already found for co-firing 60 % miscanthus with Daw Mill coal (Fig. 4.30) with 3.43, 0.22 and 0.41 mg/cm^2/hr on ~ 700, 600 and 500 ^oC surface temperatures, respectively. Other possible comparison in particular on coolest probe (~ 500 ^oC) indicated higher concentration on top deposits with lower level on side and underside deposits for co-firing 60 % miscanthus with El-cerrejon coal compared to 60 % miscanthus with Daw Mill coal (as

can be seen in Fig. 4.33 compared to Fig. 4.30). Note that the deposition fluxes present at low levels, the comparison outcome results of mixed 60 % miscanthus with two different coals are often uncertain. However, by examining the photographs and SEM images between co-firing 60 % miscanthus with El-cerrejon coal compared to 60 % miscanthus with Daw Mill coal still can support the outcome hypothesis.

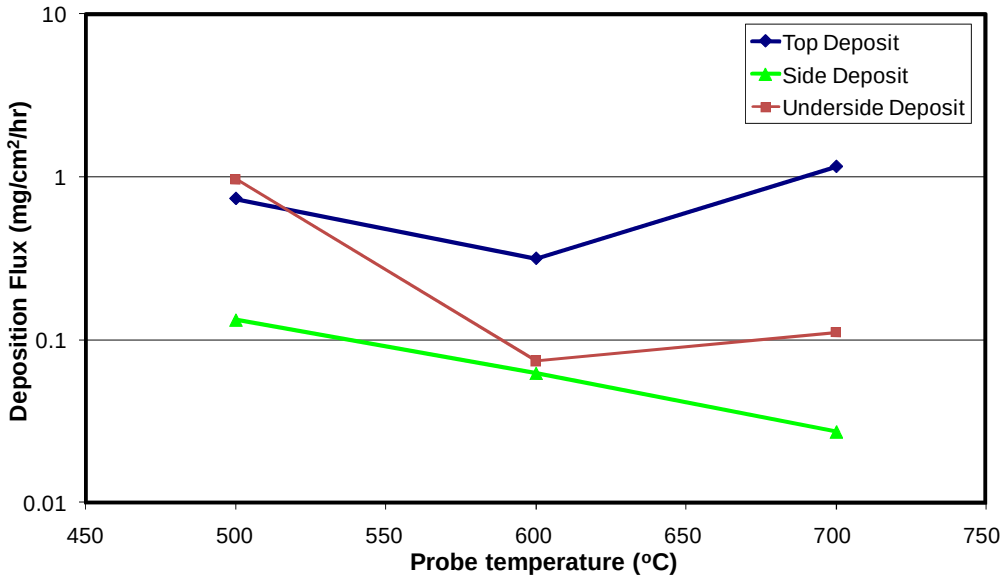

Figure 4.33 Deposition rates of the probes (top, side & underside) with surface temperatures of ~ 700, 600 and 500 ^{o}C from co-firing Miscanthus: El-cerrejon coal (60:40 %, wt)

The elemental compositions of the top, side and underside deposits for the three probes for co-firing Miscanthus:El-cerrejon coal (60:40 %, wt) analysed by EDX are shown in Figure 4.34. The results revealed a disparity in elemental compositions (with respect to concentrations and appearance of other elements (e.g. Cl)) compared to Miscanthus:Daw Mill coal (60:40 %, wt) shown in Figure 4.31.d. The elemental concentrations of the deposits indicates higher in Si (≤ 10.51 %, moles), Al (≤ 8.05 %, moles), Mg (≤ 1.22 %, moles), P (≤ 1.39 %, moles), Ca (≤ 5.91 %, moles), Ti (≤ 0.43 %, moles) of Miscanthus:Daw Mill coal (60:40 %, wt, Fig. 4.31.d) compared to Miscanthus:El-cerejon coal (60:40 %, wt, Fig. 4.34) of Si (≤ 6.89 %, moles), Al (≤ 5.56 %, moles), Mg (≤ 0.93 %, moles), P (≤ 1.19 %, moles), Ca (≤ 5.03 %, moles), Ti (≤ 0.27 %, moles) and a lower in Fe (≤ 3.22 %, moles), K (≤ 6.47 %, moles) and Na (≤

1.08 %, moles) of Miscanthus:Daw Mill coal (60:40 %, wt, Fig. 4.31.d) compared to Miscanthus:El-cerejon coal (60:40 %, wt, Fig. 4.34) of Fe (≤ 3.23 %, moles), K (≤ 10.78 %, moles) and Na (≤ 2.64 %, moles). Similar trend behaviour already found when compared CCP:El-cerrejon blend mixtures to CCP:Daw Mill mixed fuels (see Sec. 4.3.2).

Furthermore, Cl found in the top deposit of probe 3 (~ 500 ^{o}C) of Miscanthus:El-cerejon coal (60:40 %, wt, Fig. 4.34) with small concentrations of about 0.13 %, moles. Trace elements such as Zn and Cu were formed on all probes (all around sides) with concentrations of ≤ 0.40 and ≤ 0.25 %, moles, respectively of Miscanthus:El-cerejon coal (60:40 %, wt) compared be deposited on some probes of Miscanthus:Daw Mill coal (60:40 %, wt) of highest concentrations found on probe 1 (side deposit, ~ 700 ^{o}C) with 0.16 %, moles of Zn and on underside deposit of probe 1 with 0.22 %, moles of Cu.

On the other hand, the formation of $CaSO_4$, Fe_2O_3 and K_2SO_4 predicted by thermodynamic calculation (Fig. 4.16) is confirmed by XRD (Fig. D.18 (Appendix D), an example of XRD patterns of probe 3 top deposits) results of Miscanthus:El-cerejon coal (60:40 %, wt). Other main compounds predicted by MTDATA (e.g. K_3PO_4 (480-1300 °C), Na_2SO_4 (200-940 °C)) may also can be confirmed by the EDX maps (Fig. D.19, Appendix D) of probe 3 (~ 500 ^{o}C) top deposits.

Finally, the comparison of co-firing 60 %, wt miscanthus with El-cerrejon coal to Daw Mill coal (experimentally and predictions data) confirmed disparity and suggested careful consideration of fuel properties must be made for both coal and biomass.

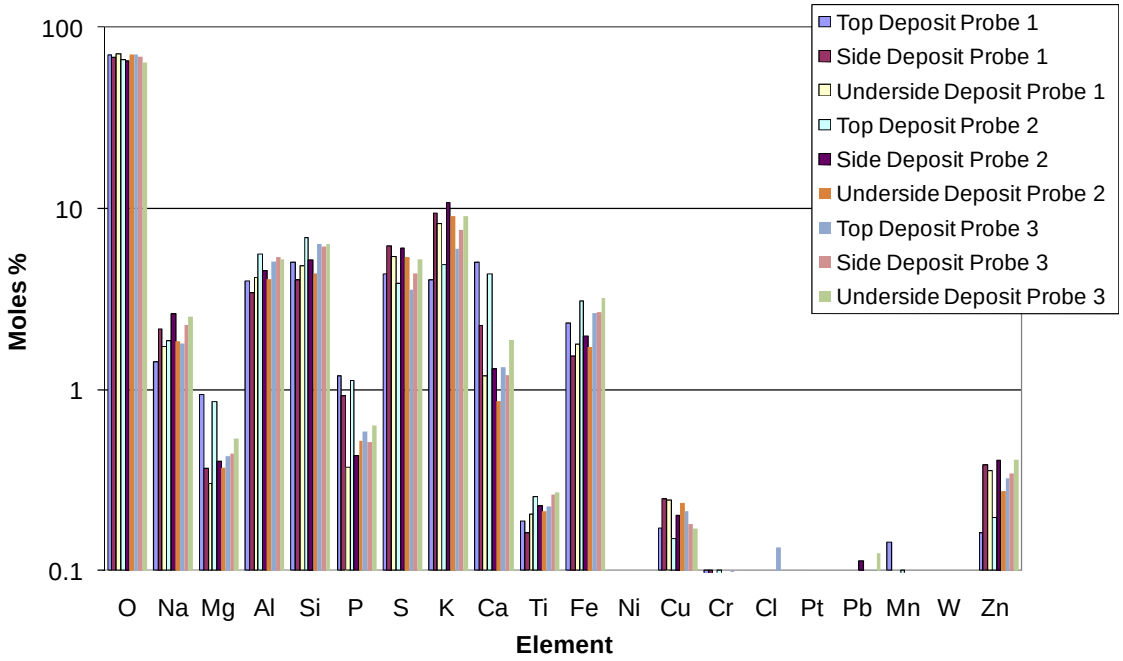

Figure 4.34 Elemental concentrations of the three probes deposits (1, 2 and 3, ~ 700, 600, 500 oC) deposits (on top, side and underside) from co-firing Miscanthus: El-cerrejon coal (60:40 %, wt)

4.4 General comments

Pilot-scale experiments and modeling (using heat generation prediction, CP and MTDATA) were performed using pulverised pure El-cerrejon and Daw Mill coals, CCP and miscanthus biomass and blends of CCP:El-cerrejon (at 20, 40, 60 and 80 weight %), CCP: Daw Mill (at 20, 40, 60 and 80 weight %), Miscanthus:Daw Mill (at 20, 40, 60 and 80 weight %) and Miscanthus:El-cerrejon (60:40 weight %) to examine the effect of co-firing on combustion behavior, gaseous emissions and deposit composition. Air-cooled probes were used to simulate heat exchanger surfaces operating with surface temperatures of ~ 500, 600 and 700 °C. The main conclusions can be drawn from this work are:

- In general the CP prediction data were almost identical to the MTDATA predictive of CO_2, H_2O, N_2, O_2, HCl and SO_2 species, whereas HP data shows that heat losses were within the expected range when using this scale of combustion unit. Both sets of data helped to confirm the combustion behaviour of these selected fuels.

- No operational/feeding problems and high combustion efficiency were found for all fuel mixes (due to low CO emissions and significant low energy heat losses).
- SO_2 levels decreased as the biomass fraction of the fuel increased, but the NO_x output remained stable (except for Miscanthus:Daw Mill mixtures with a suggestion of small decreasing in NO as the biomass share increased) .
- Higher HCl levels were released in low share biomass coal co-firing.
- The deposition flux was highest on the coolest probes for each fuel mix.
- The deposition rate was found to increase (for the top and side deposits) with increasing levels of CCP mixed with El-cerrejon coal, but the opposite was found for the deposition rate on the upstream surface which decreased with increasing CCP and miscanthus biomass mixed with Daw Mill coal (less ash particle deposition) and increased on the side and downstream surfaces (increase in vapour deposition).
- Generally, low variation in deposition rate and elemental concentration in deposits from co-firing up to 60 %, wt (in particular for the miscanthus mixes) may suggest that this biomass is unlikely to cause a deposition problem.
- The presence of Cl in the deposit was found on all probes for pure CCP and miscanthus biomass and was only detected at higher shares (≥ 80 %) for both biomass co-firing (mixed with the two coals) on coolest probe (~ 500 ^{o}C), however, mixed biomass with El-cerrejon may suggested very small Cl content at lower share level.
- Combining pilot-experiments with careful analysis and modelling has proved to be a successful approach.
- Due to composition differences between different available coals and biomass (i.e. the alkali and chlorine levels in biomass fuels often depend on the agricultural practices (e.g. harvest time [Robinson et al., 2002; Baxter et al., 2009]) and can vary between fuels identified with the same name), it is important to carry out such combustion/deposition evaluations for mixes of each specific fuel (e.g. as can be seen the variation results of co-firing Miscanthus:El-cerejon coal (60:40 %, wt) compared to Miscanthus:Daw Mill coal (60:40 %, wt)).

CHAPTER 5 PELLETISED/LUMP FUELS STUDIES RESULTS & DISCUSSION

5.1 Introduction

This chapter describes the modelling predictions and experimental data based on the combustions of pelletised/lump fuels (oil seed rape straw, miscanthus, coppiced willow) using a fluidised bed combustor. The parameters for modeling included: combustion product and heat generation prediction; thermodynamic predictions. The experimental results generated included: combustion and fluidised bed behavior; gaseous emissions; deposit flux and compositions. The modeling and experiment results are compared and discussed.

Part of this work has already been presented (oral and poster) and article published (see list of publications in Appendix E) as following;

Article: A.H.M. Khodier, N.J. Simms, J.E. Oakey and P.J. Kilgallon. Characterisation of ash from pilot-scale fluidised bed combustion of miscanthus and willow. Proceeding of 18th European Biomass Conference and Exhibition, 3-7 May 2010, Lyon, France, p 1360-1366.

5.2 Modelling

5.2.1 Oil seed rape straw (OSR) pellets

Canola straw pellets, with a diameter of 16 mm, were produced by Alchemy Technologies Ltd (Swansea, UK) from canola straw bales harvested in 2008 and stored for 10 months. Canola Straw (cv Excalibur) bales used to produce the pellets were harvested and collected from Church Farm (Lat. N 52:01:56 Long W 0:13:55) (Astwick, Stotfold, Hitchin, Herts, UK) in 2008. Canola straw collected in 2008 was swathed on the 7th July 2008, harvested on the 21st July 2008, baled on the 25th July

2008 and stored outdoors and uncovered until the 22nd August 2008. The canola straw was delivered to Harper Adams University College (HAUC) (Newport, Shropshire, UK) on 26th September 2008 and subsequently stored under cover in a shed (with roof and three open sides) at HAUC Farm.

Canola straw was milled using a Christy Norris 24 x 12 hammer mill (Christy and Norris Ltd., Chelmsford, UK) and pelletised using a California Pellet Mill 2000 (CPM:California Pellet Mill Co, Crawfordsville, USA). Calcium lignosulfate (Borregard-Lignotech, Sarpsborg, Norway) was added to milled straw prior to pelletisation at a concentration of 5 % (w/w) as lubricant/binder.

Canola straw pellets were stored as 10 kg ± 0.5 kg lots in plastic airtight zip bags (305*405 mm) (Harrison Packaging, Lancashire, UK) in an enclosed shed at Harper Adams University College for 1, 3, 6 and 12 months, subsequent delivered to Cranfield University for combustion trials.

Combustion product prediction

Fuel feed rates of 6.4, 6.6, 6.4, 6.4 kg/hr and air feed rates of 950, 1700, 1300 and 1700 l/min combined with natural gas feeding rate of 40 l/min were applied for OSR straw pellets stored for 1, 3, 6 and 12 months combustion test runs, respectively. Combustion product predictions were calculated from the fuels compositions listed in Table 3.7 (Chapter 3). Table 5.1 shows the percent volume concentration of CO_2, H_2O, N_2, O_2, HCl and SO_2 calculated for all OSR pellets stored fuels selected.

Heat generation prediction

The temperatures were measured at different points of the FBC system (during the combustion trials) with the main purpose of performing a system heat prediction. From the HP (see Appendix A4, an example for OSR 3 combustion), the heat losses of the system were: 13.83, 11.02, 13.89 and 13.01 % for the combustion of the pellets stored for 1, 3, 6 and 12 months respectively. The heat losses found in the combustion of these

OSR straw pellets were higher than the losses found by Permchart and Kouprianov, 2004 when combusting sawdust or bagasse (around 4 % losses); same authors have found heat losses of around 18 % when combusting rice husks. However, according to Baxter, 2005 losses in biomass combustion can be expected in the range of 0 to 10 % in addition to heat losses of coal combustion. Therefore, it can be concluded that heat losses during OSR straw stored pellets using FBC were in significant low.

MTDATA Calculations

Calculated data of the major and minor gases emissions by the equilibrium model (using "15 elements system") of the combustion of OSR pellets stored for 1, 3, 6 and 12 months is shown in Figures 5.1.a, 5.1.b, 5.1.c and 5.1.d, respectively. Predicted data of the major gaseous (i.e. CO_2, H_2O, N_2 and O_2) and minor gaseous (HCl and SO_2) at temperature around 800 º C (where about the experimental combustion takes place) and calculated combustion product prediction (from CP spreadsheet assuming full combustion) are summarised in Table 5.1. This shows that CP calculations were consistent with the MTDATA predictions.

The behaviour of nine minor elements (Na, K, Fe, Ca, Mg,Ti, Ba, Mn, P) with all major elements (C, H, N, O, S, Cl) for gaseous and condensed species during the combustion of pellet stored for 1, 3, 6 and 12 months is shown in Figures 5.2.a, 5.2.b, 5.2.c and 5.2.d, respectively. This shows that the predictions produced from the fifteen element system gave the possible condensed species for Ca and Cl elements (as an example) were $CaCO_3$, $CaSO_4$, $CaMgO_2$, CaO, $Ca(FeO_2)_2$, NaCl and KCl for all OSR pellets stored for 1, 3, 6 and 12 months combustions. However, temperatures and concentrations of these condensed species were varied between the different of OSR fuels selected. For example, the $CaCO_3$ temperature range within 200-760 °C and levels of ~ $\log_{10}$ 0.31-0.27 moles for the pellets stored for 1 month, compared to condensed $CaCO_3$ temperature range within 200-720 °C and levels of $\log_{10}$ 0.18 moles for the pellets stored for 12 month.

Also, the predictions made of stored pellets for the combustion show that condensed species such as H_3PO_4 were formed only for pellets stored for 1, 3 months (Fig. 5.2.a & 5.2.b) and $NaPO_3$ were formed pellets stored for 6 and 12 months (Fig. 5.2.c & 5.2.d). Other gases species like KCl and KOH revealed slightly higher concentrations for pellets stored for 6 and 12 months than pellets stored for 1 and 3 months combustions. From the fuel compositions (Table 3.7, Chapter 3) an obvious of minor increase of K and Cl concentrations for pellets stored for 6 and 12 months than pellets stored for shorter periods can also seen. This backup the hypothesis by Mojtahedi and Backman, 1989; Bander et al., 2001; Furimsky and Zheng, 2003, about the importance of chlorine in forming the gas phase potassium compounds indicating the fuel with highest chlorine and potassium contents (i.e. K/Cl ratio), the chemical equilibrium calculations predict the highest share of KCl and KOH in the combustion systems.

Table 5.1 Modelling of OSR stored pellets for pelletised/lump combustion tests

	OSR 1[a]		**OSR 2[b]**		**OSR 3[c]**		**OSR 4[d]**	
(%, vol.)	**CP[e]**	**MTDATA[f]** (at 800 ^oC)	**CP**	**MTDATA** (at 800 ^oC)	**CP**	**MTDATA** (at 800 ^oC)	**CP**	**MTDATA** (at 800 ^oC)
CO_2	12.39	12.39	7.52	7.52	9.54	9.54	7.47	7.46
H_2O	14.91	14.92	9.24	9.24	10.84	10.84	8.60	8.60
N_2	70.60	70.64	73.90	73.92	72.85	72.88	74.14	74.16
O_2	2.05	2.03	9.31	9.30	6.47	6.72	9.76	9.75
HCl	0.011	0.010	0.007	0.006	0.010	0.010	0.008	0.007
SO_2	0.032	0.013	0.016	0.005	0.025	0.010	0.019	0.008

Keys;
(a): OSR raw material 10 month storage, pellets 1 month storage
(b): OSR raw material 10 month storage, pellets 3 month storage
(c): OSR raw material 10 month storage, pellets 6 month storage
(d): OSR raw material 10 month storage, pellets 12 month storage
(e): Combustion product prediction
(f): Thermodynamic calculations

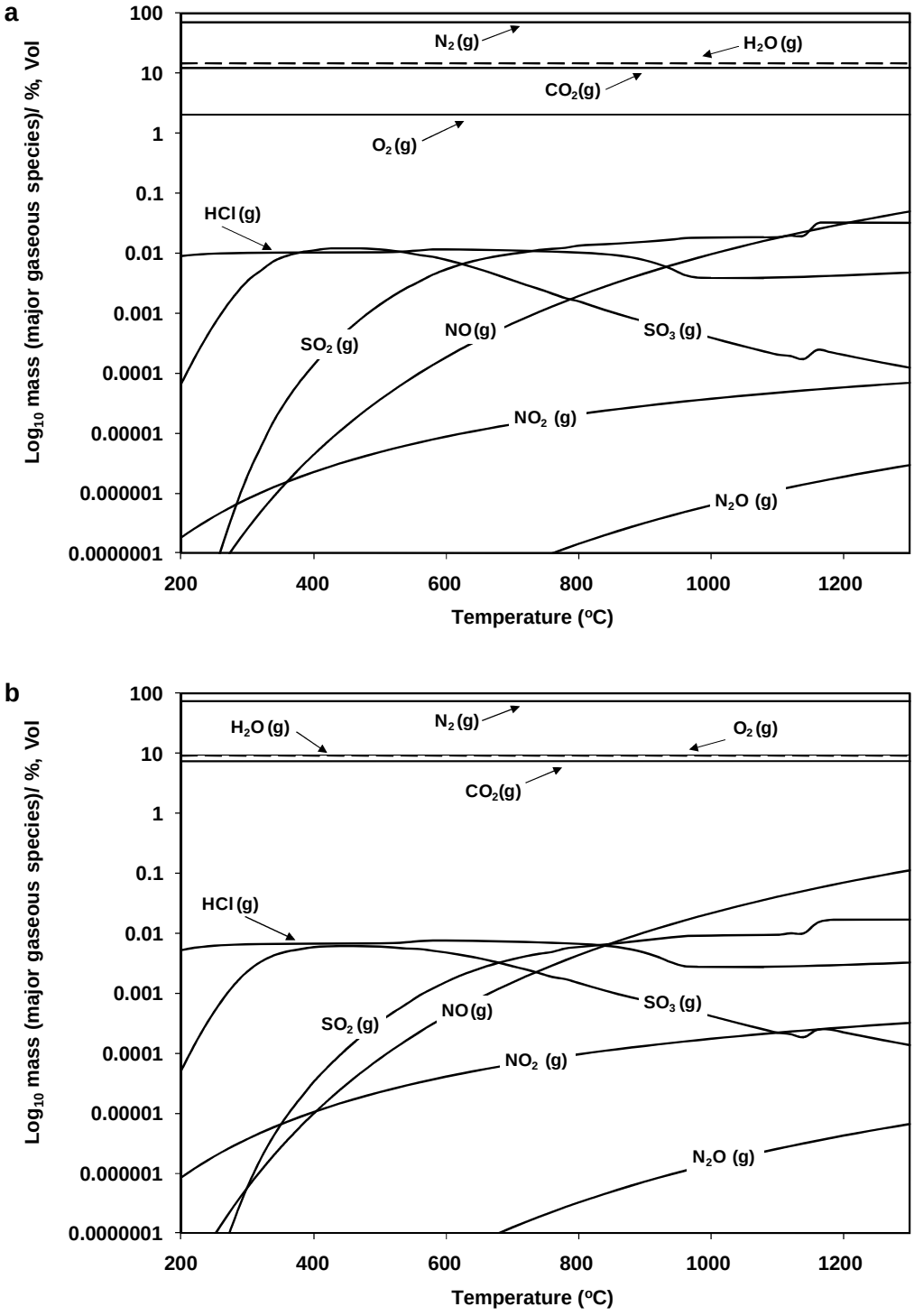

Figure 5.1 Calculated (MTDATA) major gaseous species from OSR combustion of a) 1 months of pellets storage, b) 3 months of pellets storage

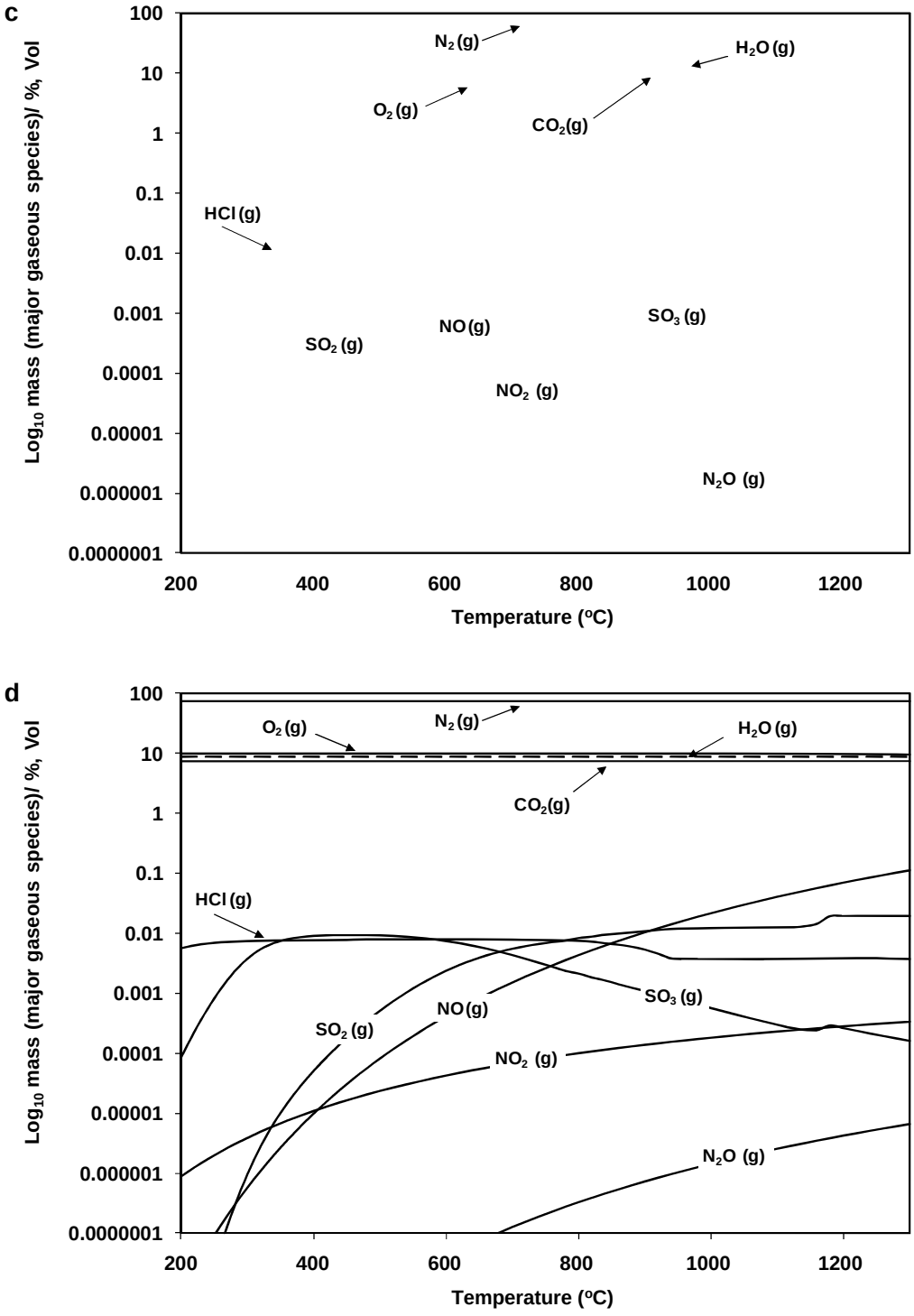

Figure 5.1 Calculated (MTDATA) major gaseous species from OSR combustion of c) 6 months of pellets storage, d) 12 months of pellets storage

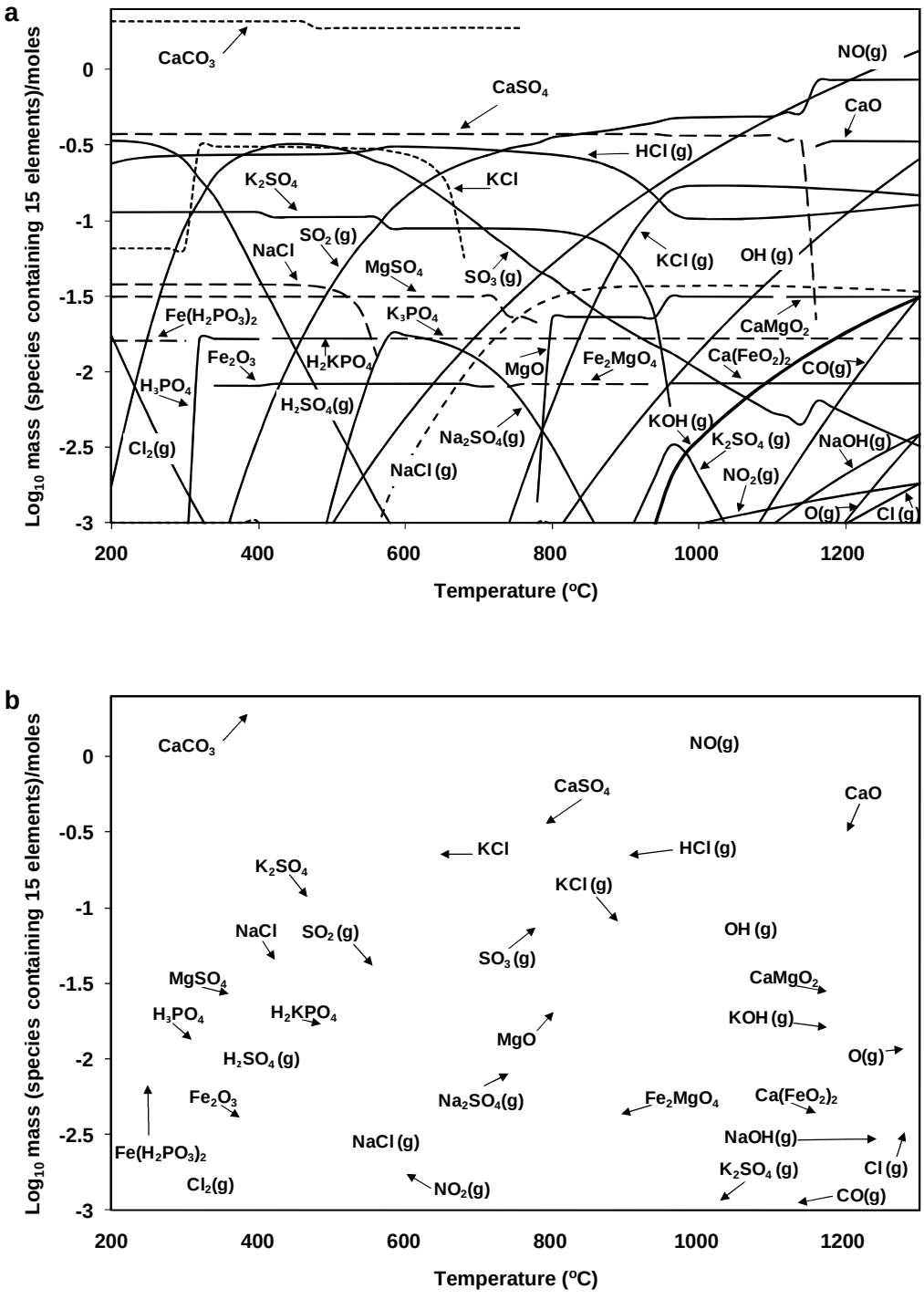

Figure 5.2 Calculated (MTDATA) gaseous & condensed species from OSR combustion of a) 1 months of pellets storage, b) 3 months of pellets storage

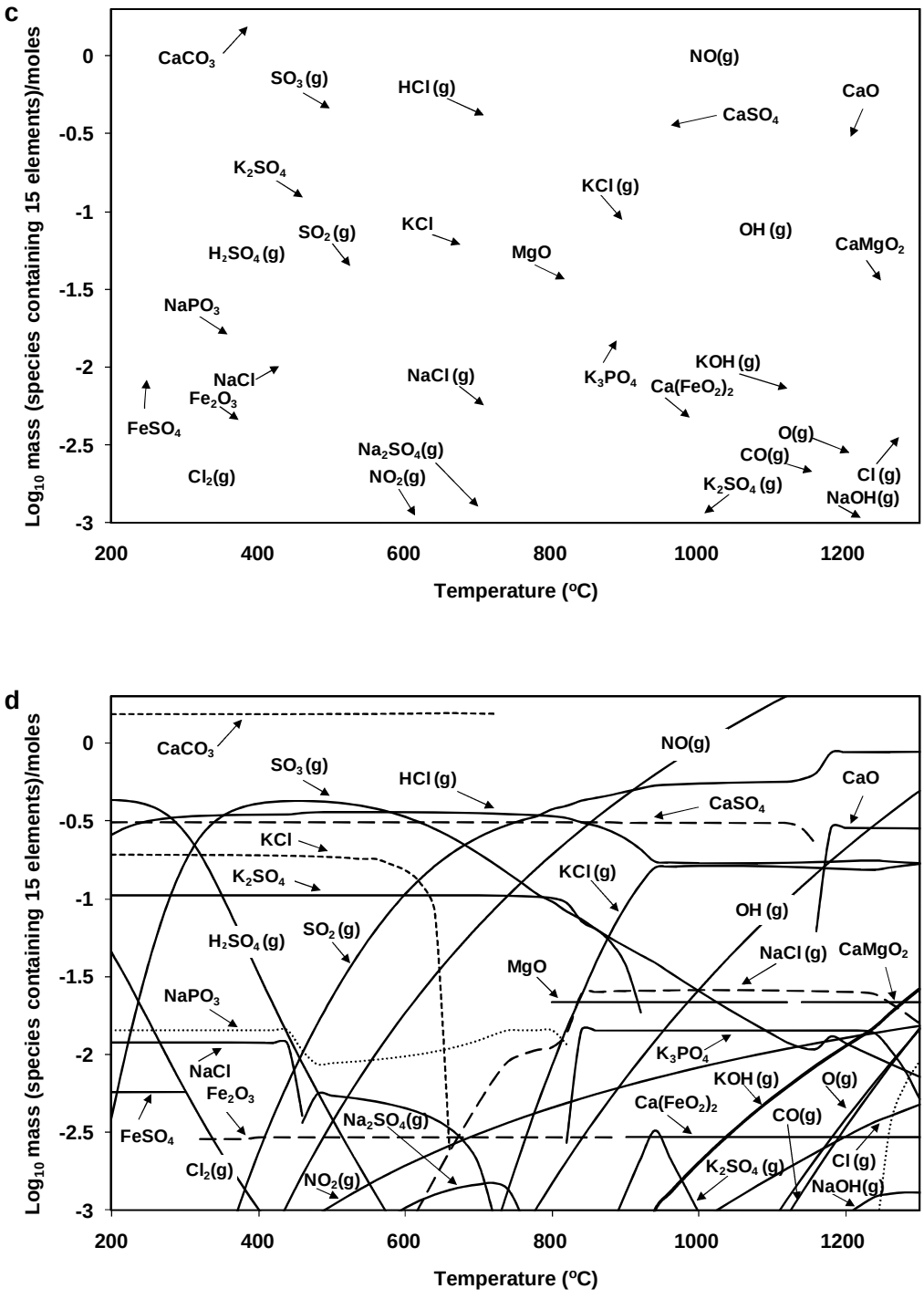

Figure 5.2 Calculated (MTDATA) gaseous & condensed species from OSR combustion of c) 6 months of pellets storage, d) 12 months of pellets storage

5.2.2 Miscanthus pellets

Combustion product prediction

Consistent fuel feed rates of ~ 6.5 kg/hr and air feed rates of ~ 970 l/min combined with natural gas feeding rates of 40 l/min under standard combustions conditions (listed in Table 3.18, Chapter 3) were applied for miscanthus combustion exposures. Combustion product predictions were calculated from the fuels compositions listed in Table 3.8 (Chapter 3). Table 5.2 shows the percent volume concentration of CO_2, H_2O, N_2, O_2, HCl and SO_2 calculated for miscanthus pellets combustions.

Heat generation prediction

From the HP (calculated from Eq. 3.12, Chapter 3), the heat losses of the system was 8.43 % for the combustion of the miscanthus. This shows a similar to OSR trials and level expected for small combustion test rig.

MTDATA Calculations

Calculated data of the major and minor gaseous emissions by the equilibrium model (using "15 elements system") of miscanthus pellets combustion is shown in Figure 5.3. The data for the major gaseous (i.e. CO_2, H_2O, N_2 and O_2) and minor gaseous (HCl and SO_2) at 750 ºC (experimental combustion zone) are summarised in Table 5.2. It is clear that SO_2 gas concentration (%, vol.) was nil in MTDATA calculations for firing miscanthus. Also, SO_3 gas was not predicted by MTDATA within all the range of temperatures studied (see Fig. 5.3). This may be to the low S in the fuel composition and possibly the amount of S in the flue gas was controlled by the equilibrium of the condensed species. Generally, a consistent result between the combustion product prediction and MTDATA predictions were achieved.

The behaviour of 15 elements (C, H, N, O, S, Cl, Na, K, Fe, Ca, Mg, Ti, Ba, Mn, P) for gaseous and condensed species during the combustion of miscanthus is shown in

Figures 5.4. This shows that the condensed species were $CaFe_2O_4$ (560-880 °C), $CaSO_4$ (200-1300 °C), KCl (320-640 °C), NaCl (200-600 °C), Fe_2MgO_4 (280-540 °C), K_3PO_4 (360-1120 °C), MgO (> 340 °C), $MgSO_4$ (200-340 °C), MnO_2 (200-400 °C), Mn_2O_3 (420-1240 °C), MnO (1260-1300 °C). Also, it can be seen that higher levels of condensed species were NaCl (minus $\log_{10}$ 0.65-2.22 moles), KCl (minus $\log_{10}$ 0.73-0.96 moles) and $CaSO_4$ (minus $\log_{10}$ 1.16-1.19 moles).

Table 5.2 Modelling of miscanthus pellets for pelletised/lump combustion tests

	Miscanthus pellets	
(%, vol.)	**CP[a]**	**MTDATA[b]** (at 750 ^oC)
CO_2	11.78	13.14
H_2O	14.70	14.15
N_2	70.37	69.55
O_2	3.14	3.14
HCl	0.0041	0.0029
SO_2	0.0045	0.0000

Keys;
(a): Combustion product prediction
(b): Thermodynamic calculations

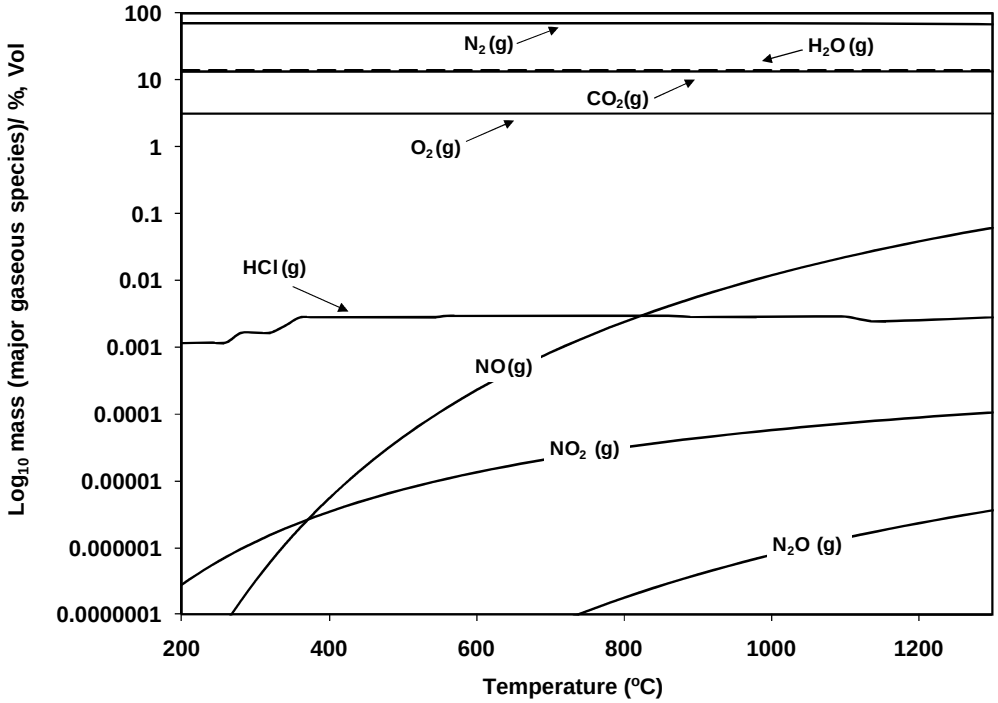

Figure 5.3 Calculated (MTDATA) major gaseous from miscanthus pellet combustion

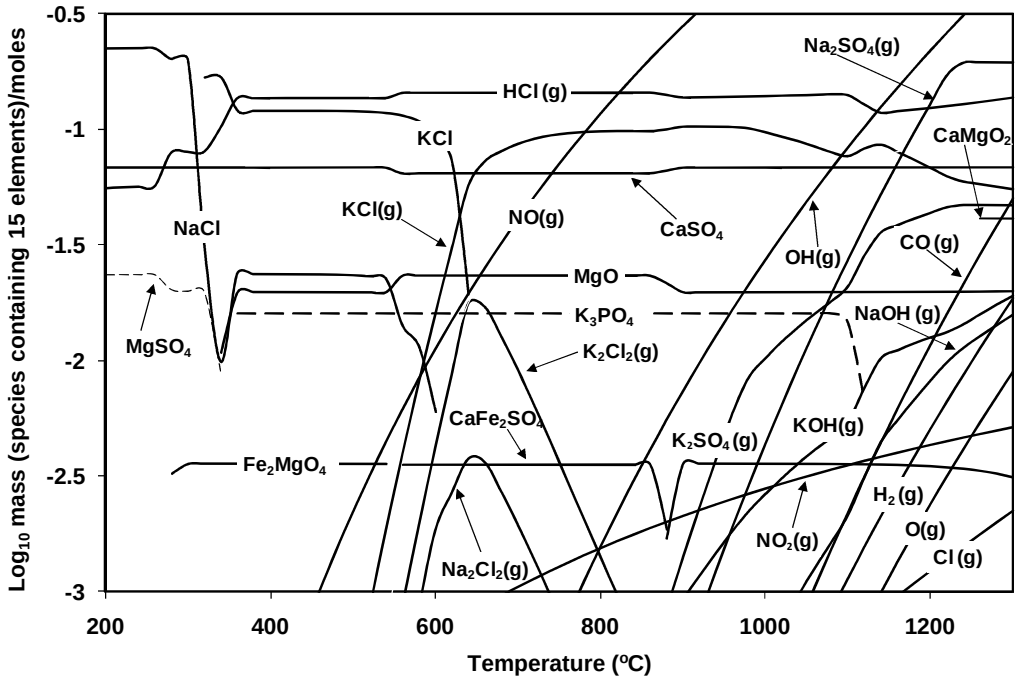

Figure 5.4 Calculated (MTDATA) gaseous & condensed species from miscanthus pellet combustion

5.2.3 Coppiced willow

Combustion product prediction

Consistent fuel feed rates of ~ 5.9 kg/hr and air feed rates of 1200 l/min combined with natural gas feeding rates of 40 L/min under standard combustions conditions (listed in Table 3.18, Chapter 3) were applied for willow combustion exposures. Combustion product predictions were calculated from the fuel compositions listed in Table 3.8 (Chapter 3). Table 5.3 shows the percent volume concentration of CO_2, H_2O, N_2, O_2, HCl and SO_2 calculated for coppiced willow combustions (full descriptions of the calculations made are shown in Appendix A3).

Heat generation prediction

From the HP (calculated from Eq. 3.12, Chapter 3), the heat losses of the system was 5.76 % for the combustion of the coppiced willow. This shows that the heat losses during willow combustion are in the range expected for this scale of combustion test rig.

MTDATA Calculations

Calculated data of the major and minor gaseous emissions by the equilibrium model (using "15 elements system") of coppiced willow combustion is shown in Figure 5.5. The data for the major gaseous (i.e. CO_2, H_2O, N_2 and O_2) and minor gaseous (HCl and SO_2) species at 800 ºC (experimental combustion zone) are summarised in Table 5.3. CP calculation of SO_2 and HCl gases showed close matching value with the MTDATA predictions (with clear suggestion of tiny values of MTDATA lower than CP). It can be seen from Figure 5.5 that SO_2 is not stable below ~ 680 °C and has a maximum of ~ 16.40 ppm at a temperature of about 1100 °C. The SO_2 and SO_3 gases were predicted with concentrations of 0.038 ppm and 0.01 ppm at 800 °C, respectively, and with concentrations of 0.23 ppm and 0.04 ppm at 840 °C, respectively. The higher HCl concentrations of about 4.42 ppm were predicted at 540 °C and 1.88 ppm at 800 °C. For

NO, NO_2 and N_2O the concentrations were 43.35 ppm, 1.14 ppm and 0.0034 ppm at 800 °C, respectively, and with concentrations of 129.91 ppm, 1.67 ppm and 0.00089 at 920 °C, respectively. For the major gaseous species, concentrations were in line between CP and MTDATA calculations as can be in Table 5.3.

Figures 5.6 explain the behaviour of 15 elements for gaseous and condensed species during the combustion of coppiced willow. This shows that the condensed species were $CaFe_2O_4$ (320-1300 °C), $CaSO_4$ (200-1080 °C), KCl (200-520 °C), NaCl (200-300 °C), K_2SO_4 (200-960 °C), Na_2SO_4 (320-980 °C) and CaO (1060- 1300 °C). This indicated (as expected) that the possibility of condensed compounds deposited while firing willow was much less than OSR straw and miscanthus pellets. However, the temperature range and concentrations of each compound are considered to be significant. For example, condensed KCl was predicted to be form below 520 °C with tiny levels of ~ negative $\log_{10}$ 2.39-1.71 moles. A comparison of the predicted condensed KCl with measured deposition probe with surface temperature of ~ 500 °C can be seen in Section 5.3.3.

Table 5.3 Modelling of coppiced willow for pelletised/lump combustion tests

	Coppiced Willow	
(%, vol.)	**CP[a]**	**MTDATA[b]** (at 800 ^oC)
CO_2	7.47	7.64
H_2O	7.82	7.76
N_2	73.63	73.52
O_2	11.08	11.06
HCl	0.0005	0.0002
SO_2	0.0017	0.00001

Keys;
(a): Combustion product prediction
(b): Thermodynamic calculations

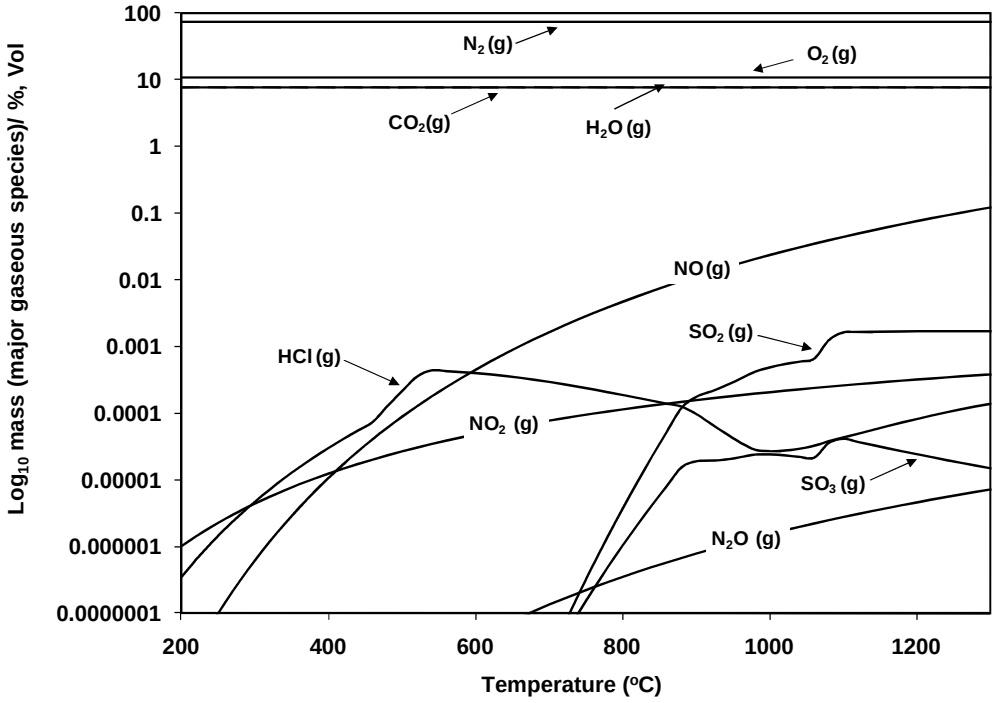

Figure 5.5 Calculated (MTDATA) major gaseous from coppiced willow combustion

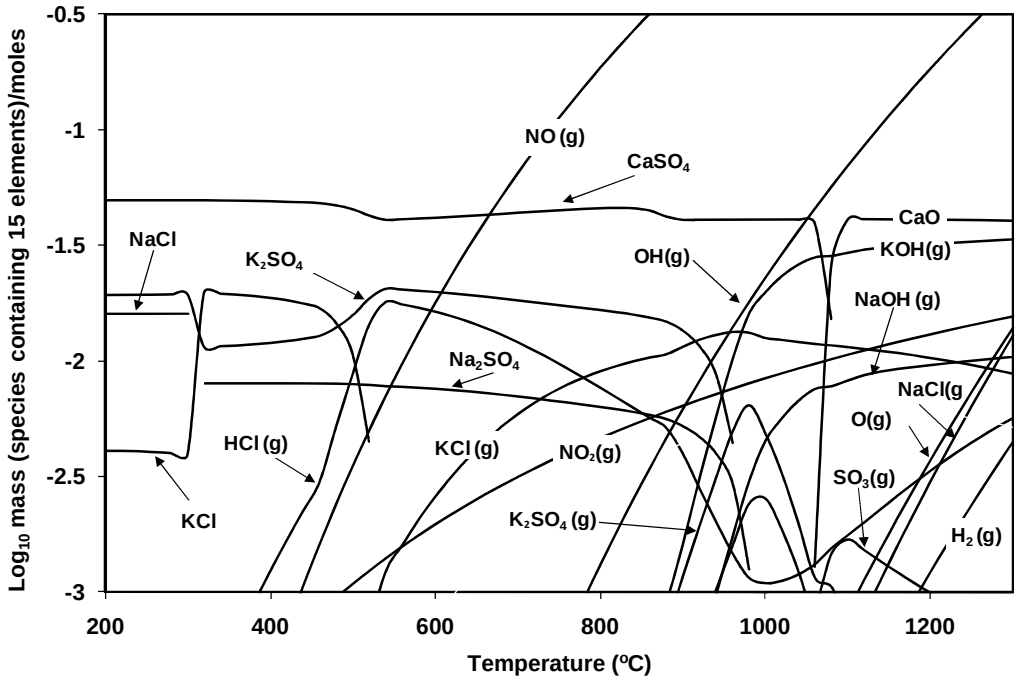

Figure 5.6 Calculated (MTDATA) gaseous & condensed species from coppiced willow combustion

5.3 Experimental pilot-scale combustion rig exposures

5.3.1 Oil seed rape straw (OSR) pellets

Fluidised bed combustion behaviour

The experimental results of the bed behaviour during continuous four hours periods of combustion of OSR straw pellets (stored for 1, 3, 6 and 12 months) are presented in Figure 5.7. This shows that stable combustion was achieved for all the tests performed, with fluidised bed temperatures of around 750-820 ºC. The temperatures achieved in the test performed with OSR straw pellets stored for 1 month were lower than the temperatures achieved in the other three tests. The reason for this was that the air feeding in the fluidised bed was ~ 950 l/min compared to the average of ~ 1700 l/min fed in the other three tests (i.e. the amount of excess air was less). Increasing the excess air in FBC technology means not only increasing the availability of fuel to react with oxygen in the air supplied, but also better heat transfer and increasing gas velocity which increases the turbulence in the bed leading to better solid mixing and gas-solid contacting and hence improves the carbon combustion efficiency [Van Loo and Koppejan, 2008]. However, the variation in air feeding and consequently the variations in temperatures of the test carried out after 1 month pellet storage compared to the other tests, were not considered to have an impact on the behaviour of the fluidised bed. Thus, high combustion efficiency was equally achieved for all the four tests as a result of low CO emissions (as described in gaseous emissions section).

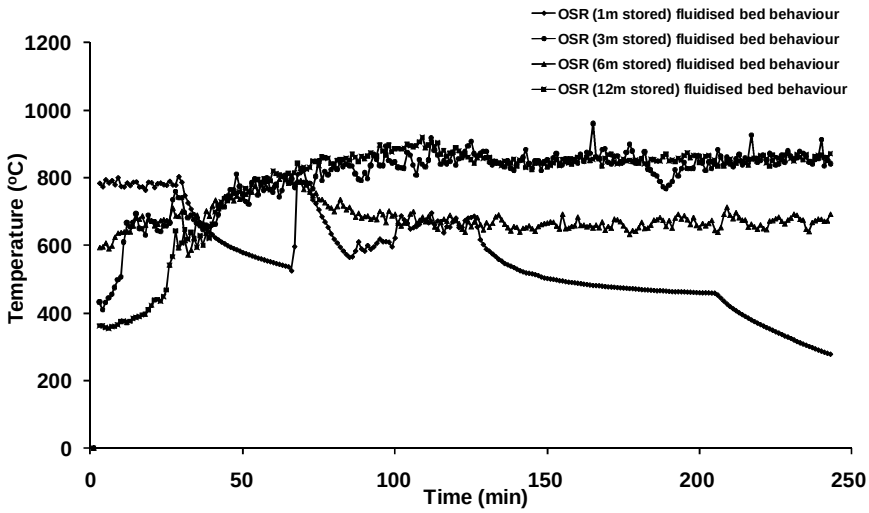

Figure 5.7 Fluidised bed behaviour during the combustion of OSR straw pellets after 1, 3, 6 and 12 months storage

Gaseous emissions

The mean values of the major (i.e. CO_2, H_2O and O_2) and minor (i.e. CO, NO, NO_2, N_2O, HCl and SO_2) gaseous species produced from the combustion of OSR straw pellets stored are presented in Figure 5.8 and Figure 5.9, respectively. These were measured during combustion periods of approximately 4 hours for each fuel.

The CO_2 emissions (Fig. 5.8) were shown to be very stable when the pellets were stored for 3, 6 and 12 months with concentrations of 10.58 % and standard deviations (SD) ± 0.027 %, 10.82 % ± 0.016 % and 9.65 % ± 0.051 %, respectively. However, the CO_2 concentration from the combustion of the pellets produced after 1 month of storage was 13.82 % ± 0.01 %. This higher value of CO_2 emissions compared with the other tests is mainly due to a lower excess air (i.e. O_2 concentration) used in the test carried out with the OSR straw pellets stored for 1 month, and not as a consequence of the storage impact.

The H_2O concentrations were 17.04 % ± 0.015 %, 10.21 ± 0.020, %, 13.65 ± 0.0150 % and 9.28 ± 0.032 % for the combustion of the pellets stored for 1, 3, 6 and 12 months, respectively. The variations found in the H_2O do not follow a particular trend and no evidences have been found to support it, however, they may originated from the variations in the fuel composition (Table 3.7, Chapter 3), which can be explained by the fact that when the water content of biomass increased, devoltilisation time will be greater and delayed the gas evolution from the fuel during devoltilisation process [Lai and Krieger-Brockett, 1992] and/or possibly matter biomass producing steam.

Low CO (Fig. 5.9) emissions were achieved for all the tests, regarding the storage period, with averages of 0.60 ppm ± 0.301 ppm, 7.89 ppm ± 0.072 ppm, 0.003 ppm ± 0.0014 ppm and 23.19 ppm ± 0.33 ppm for the pellets stored for 1, 3, 6 and 12 months. This means that most of the carbon in the OSR straw pellets was converted to CO_2 (i.e. high combustion efficiency).

The NO_x emissions (i.e. NO and NO_2) showed variations with storage with no clear trend (e.g. the NO emissions were 157.75 ppm ± 0.22 ppm, 118.79 ppm ± 0.27 ppm and

186.89 ppm ±0.54 ppm from the pellets stored for 1, 6 and 12 months storage; the NO_2 emissions were 2.50 ppm ± 0.02 ppm, 0.91 ppm ± 0.04 ppm and 9.869 ppm ± 0.12 ppm from the pellets stored for 1, 6 and 12 months storage). However, this variation on the NO_x in the flue gas is considered to be sourced from the fuel- N [Hall and Overend, 1987] (See Table 3.7). The SO_2 emissions presented in all the OSR straw pellet combustion tests are very low, ranging from 2.90 ppm ± 0.09 ppm to 5.04 ppm ± 0.13 ppm, which is expected from biomass burning fuels compared to fossil fuels. However, after 6 months storage the values of SO_2 were decreasing. Furthermore, the concentration of HCl emissions (ppm) has shown a decreasing linear trend with storage (from 30.03 ppm ± 0.35 ppm after 1 month storage to 8.33 ppm ± 0.18 ppm after 12 months).

It can be seen from the calculated data (CP and MTDATA shown in Table 5.1) that the major gaseous emissions were consistent with the experimental data. For example, the predicted calculated MTDATA data at 800 ºC of H_2O, O_2 and CO_2 for the pellets stored for 1 month was 14.92 %, 2.03 % and 12.39 % respectively, compared to the measured data (Fig. 5.8) which were 17.04 % ± 0.015 %, 1.99 % ± 0.024 % and 13.82 % ± 0.01 %, for H_2O, O_2 and CO_2, respectively.

The predicted data of the minor gaseous emissions were higher than the measured data. For example, the SO_2 and HCl emissions at 800 ºC after 1 month storage (Fig. 5.1.a) were 135.19 ppm and 103.20 ppm, respectively and for the pellets stored for 12 month (Fig.5.1.c) were 83.30 ppm and 75.47 ppm, respectively. However, the most significant finding was that HCl emissions had a linear decreasing tendency with storage, SO_2 emissions had a higher decreasing tendency after 6 months storage, NO_x emissions had variations within the pellets storage period as previously mentioned in the experimental data.

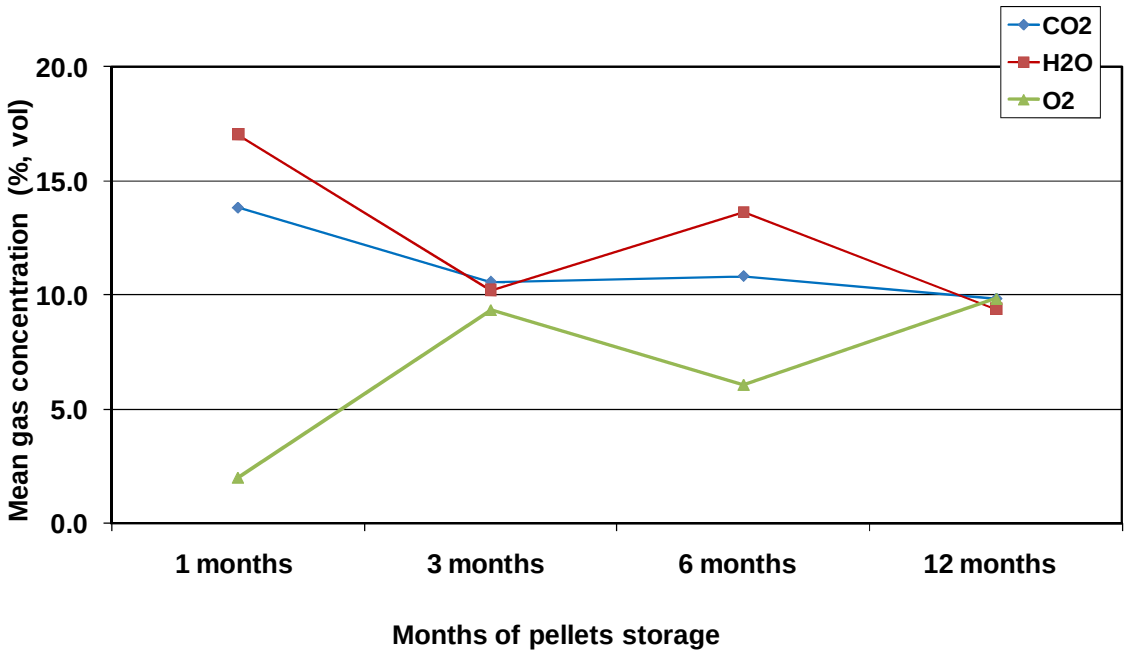

Figure 5.8 Figure 5.8 Major gaseous emissions species from the combustion of OSR straw pellets after 1, 3, 6 and 12 months storage

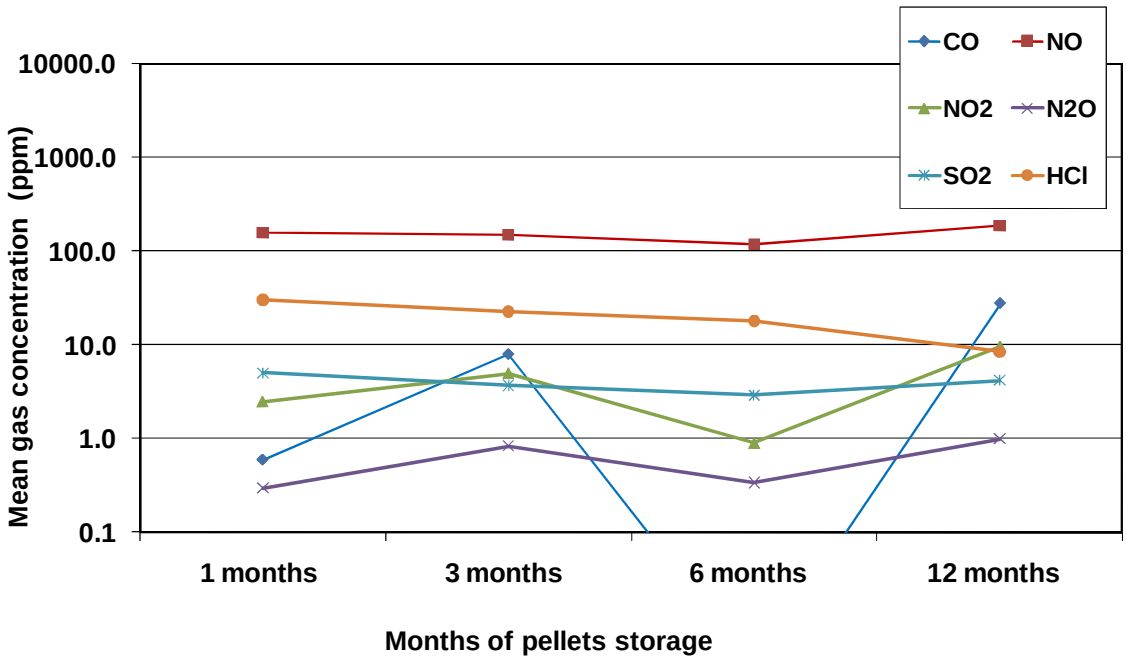

Figure 5.9 Minor gaseous emissions species from the combustion of OSR straw pellets after 1, 3, 6 and 12 months storage

Deposition fluxes, deposit compositions and analysis

Deposition fluxes for deposits formed on probes with surface temperatures of ~ 500 ^{o}C after ~ 4 hours of feed OSR straw pellets stored fuels are shown in Figure 5.10. It can be seen from the graph that a linear increase of deposits formed in the top (upstream surface) of the probes as the OSR pellets storage increased. OSR pellets stored for 12 months exhibit the highest deposition fluxes on the top and side of the probes with 43.55 and 0.10 mg/cm^2/hr, respectively.

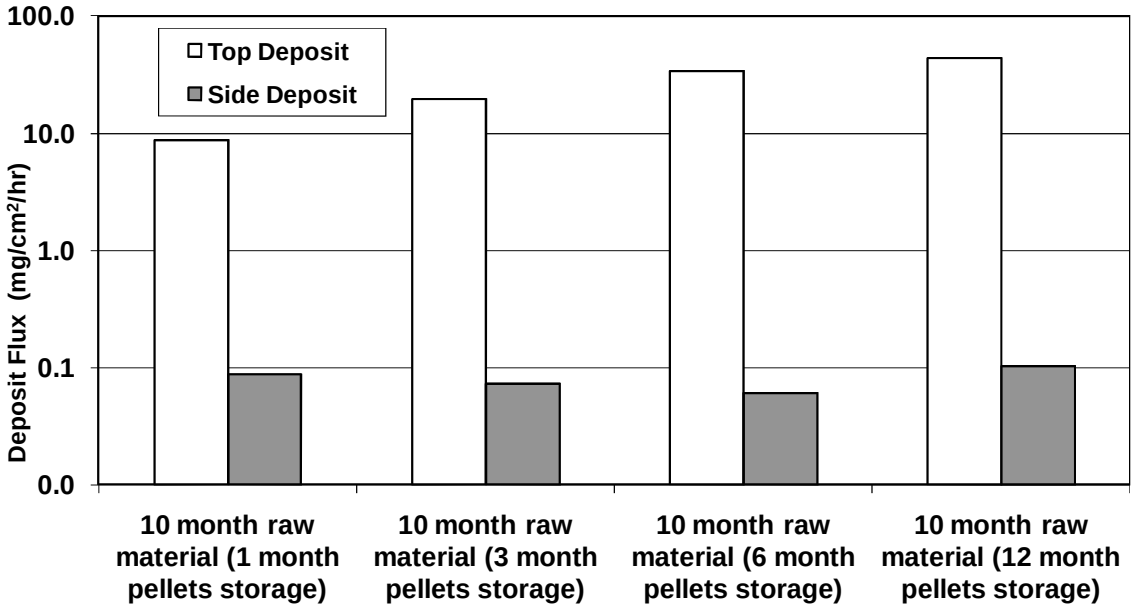

Figure 5.10 Deposition rates of the probes (top & side) with surface temperatures of ~ 500 ^{o}C from the combustion of OSR straw pellets after 1, 3, 6 and 12 months storage

The measurements of deposition fluxes were in accordance with the observations of the probes after removal from the FBC. Figure 5.11 shows the photographs of the probe deposits (~ 500 ^{o}C surface temperature), whereas the SEM images of the deposits formed on the top and side surface of the probes are presented in Figures 5.12 and 5.13, respectively. This shows that the deposits were coarse with a columnar, boxy structure (due to the stickiness of the straw fly ash particles) on the upstream side (top) of the probe. A thick white layer can clearly be seen increasing on the side and downstream (bottom) of the probes as the OSR pellets storage increases. This white material is alkali chloride salts that have condensed onto the cool probe surface, according to Robinson et

al., [2002]. They noticed that during the initial stages of the deposit formation while firing wheat straw this white layer covers the entire probe. In addition to condensing, these salts can also nucleate to form submicron aerosol particles that can be transported to the probe surface by thermophoresis mechanisms as described in literature review chapter 2 (Sec. 2.7.3). Also, it can be seen from the SEM images that the deposit particles sizes on the top surfaces (Fig. 5.8) are larger in OSR pellets stored for 1 month and decrease as the OSR pellets storage increases. SEM images on the side surfaces (Fig. 5.13) revealed that particles in the OSR straw deposits were bonded together creating an interconnected structure (which forms large flakes of material) and this increased as the OSR pellets storage increased.

OSR Pellets Storage 1 month (100 %, wt)

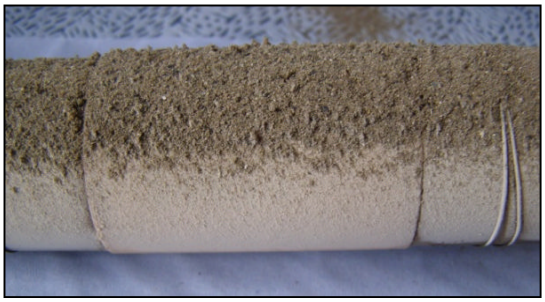

OSR Pellets Storage 3 month (100 %, wt)

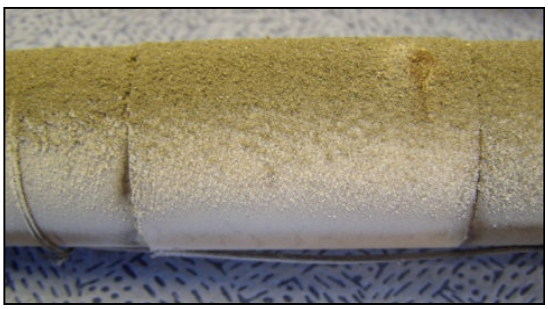

OSR Pellets Storage 6 month (100 %, wt)

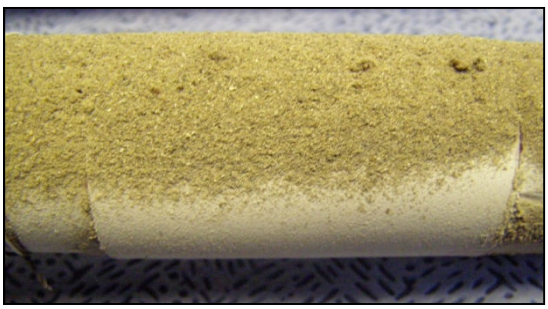

OSR Pellets Storage 12 month (100 %, wt)

Figure 5.11 Photographs of the deposits formed on probes with surface temperatures of ~ 500 ^{o}C from the combustion of OSR straw pellets after 1, 3, 6 and 12 months storage

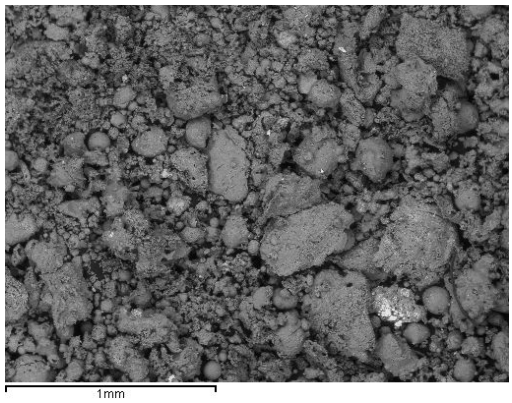

OSR Pellets Storage 1 month (100 %, wt)

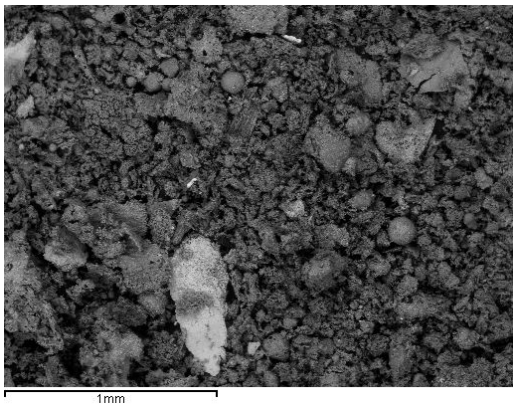

OSR Pellets Storage 3 month (100 %, wt)

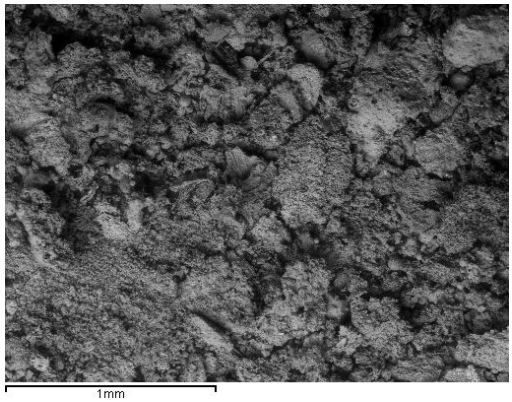

OSR Pellets Storage 6 month (100 %, wt)

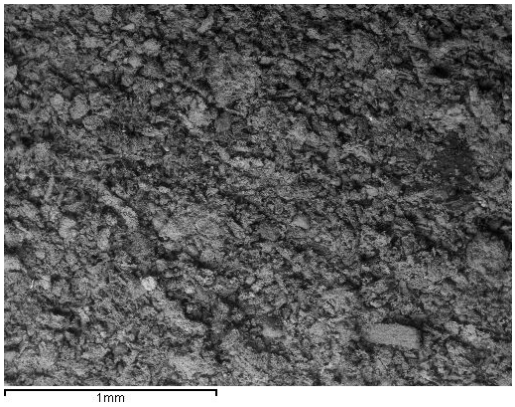

OSR Pellets Storage 12 month (100 %, wt)

Figure 5.12 SEM images of the top deposits from probes with surface temperatures of ~ 500 ^{o}C from the combustion of OSR straw pellets after 1, 3, 6 and 12 months storage

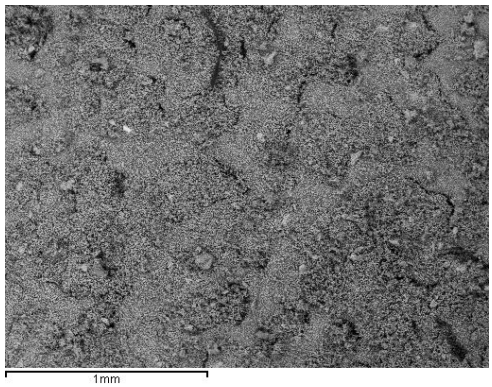

OSR Pellets Storage 1 month (100 %, wt)

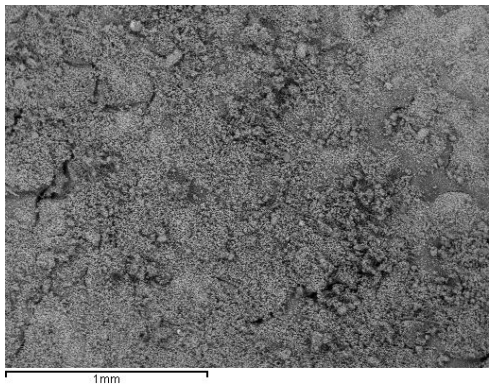

OSR Pellets Storage 3 month (100 %, wt)

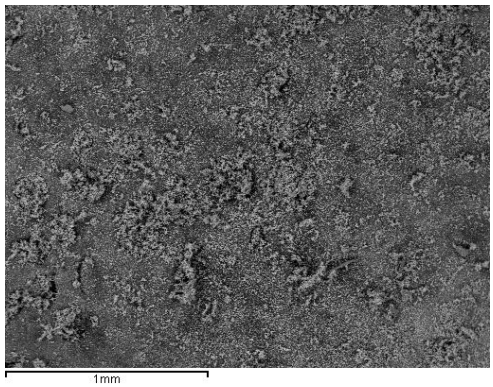

OSR Pellets Storage 6 month (100 %, wt)

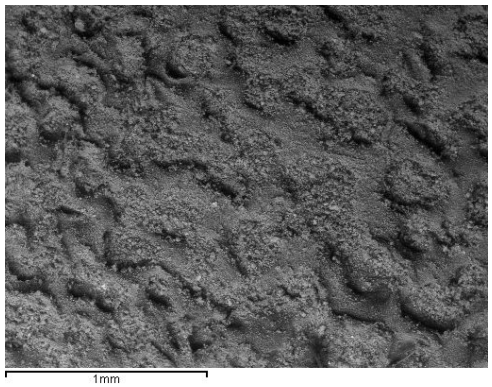

OSR Pellets Storage 12 month (100 %, wt)

Figure 5.13 SEM images of the side deposits from probes with surface temperatures of ~ 500 ^{o}C from the combustion of OSR straw pellets after 1, 3, 6 and 12 months storage

The elemental compositions of the deposits formed on the tops and sides of the probe (~ 500 ^{o}C surface temperature) for combustion OSR stored fuels analysed by EDX are shown in Figure 5.14. The results demonstrate varying concentrations of silicon, sulphur, potassium, iron and aluminium in the deposits. The calcium level ranged within 10.41-15.84 % moles on the top surface deposits and within 1.74-15.41 % moles on the side surface deposits. The chlorine concentrations deposited on the probes from OSR pellets shown an increase with pellets storage. For example, concentrations of top and side deposits were 0.23 and 0.63 % moles, respectively, for the pellets stored 1 month, compared to concentrations of top and side deposits of 6.88 and 3.81 % moles

respectively, for the pellets stored 12 months. Whereas, iron levels suggest a slight decrease after OSR pellets are stored for 3 months.

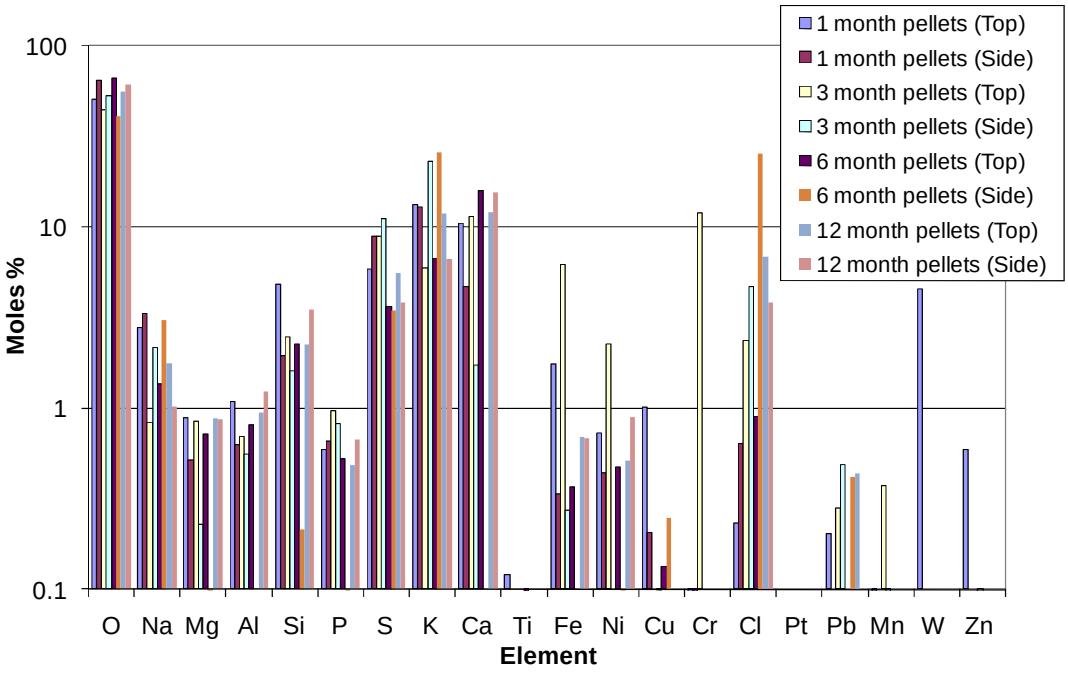

Figure 5.14 EDX analysis of deposits (top & side) from probes with surface temperature of ~ 500 ^{o}C exposed to combustion gases from combustion of OSR straw pellets after 1, 3, 6 and 12 months storage

Figure 5.15 illustrate the XRD patterns of the top surface deposits formed on probes (~ 500 ^{o}C surface temperature) for all the combusted OSR pellets. This shows that the sylvite (KCl) and calcite ($CaCO_3$) were the main mineral phases with presence of quartz (SiO_2), calcium silicate (Ca_2SiO_4) and lower levels of sodium phosphide (NaP). Hematite (Fe_2O_3) showed variation after OSR stored 6 months. Anhydrite ($CaSO_4$) was identified (by X-ray diffraction) only on the top surface of the probe for OSR stored 3 months, However, it may still presents for all other OSR stored fuels which may be less than the detection limit of the XRD.

Furthermore, it should be pointed out that jasmundite ($Ca_{11}(SiO_4)_4O_2S$) deposited from OSR combusted after 1 and 3 months storage was replaced by aphthitalite ($K_3Na(SO_4)_2$) for OSR combusted after 6 and 12 months storage. This possibly will suggests a distinction of deposition from combusted OSR after 6 months storage. However with

experimental uncertainty, the enrichment factors for compounds present at low level are debateable.

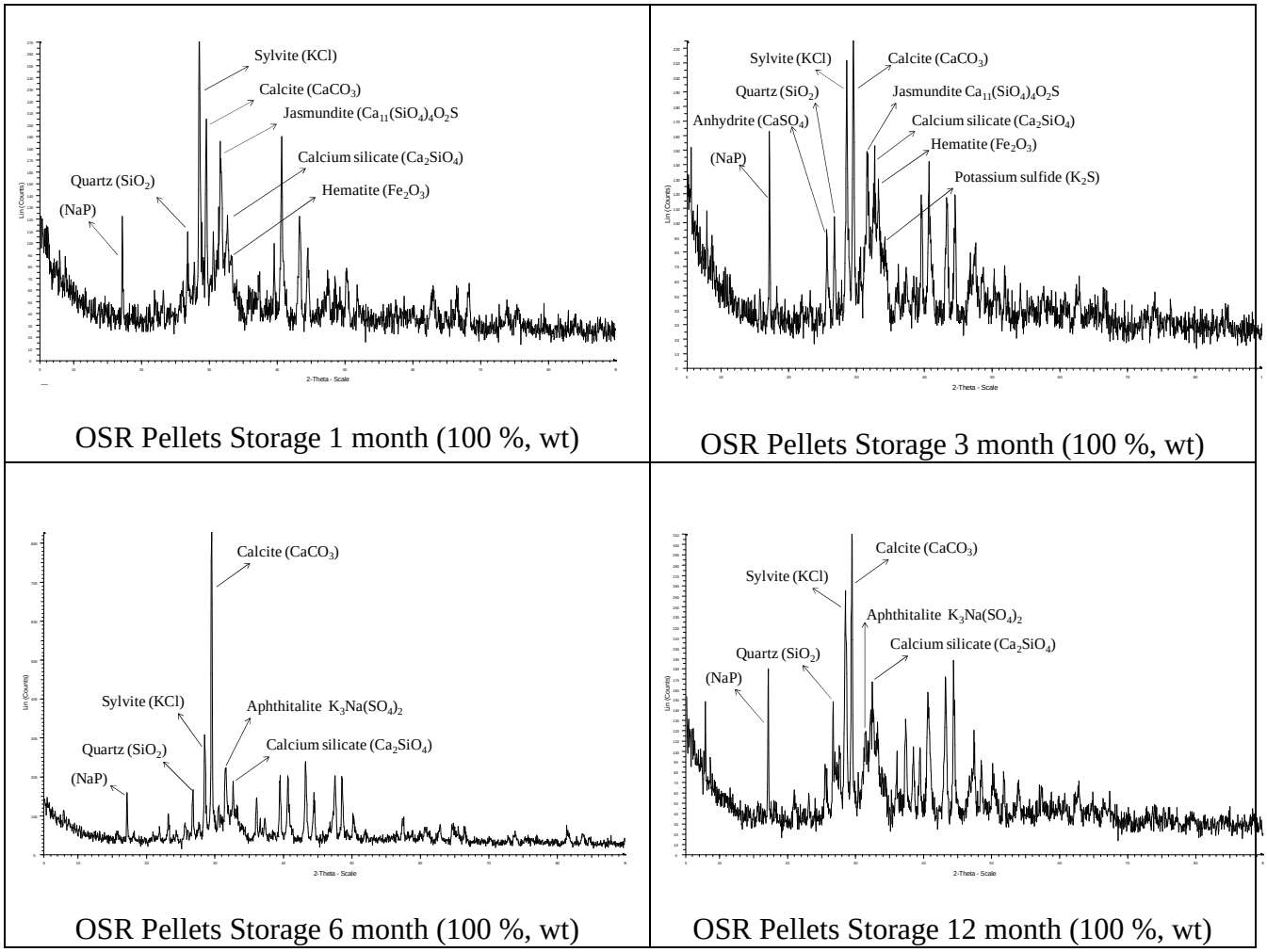

Figure 5.15 XRD patterns of the top deposits from probes with surface temperatures of ~ 500 ^{o}C exposed to combustion gases from combustion of OSR straw pellets after 1, 3, 6 and 12 months storage

The XRD identification for the side and underside deposits of all OSR stored combustions showed identical phases. Figure 5.16 demonstrate the XRD patterns of the side deposits formed on probes (~ 500 ^{o}C) for OSR pellets combusted after 6 months storage (as an example). This showed a high level of sylvite (KCl) and a low level of calcite ($CaCO_3$), which is consistent with white layer in the picture (Fig. 5.11).

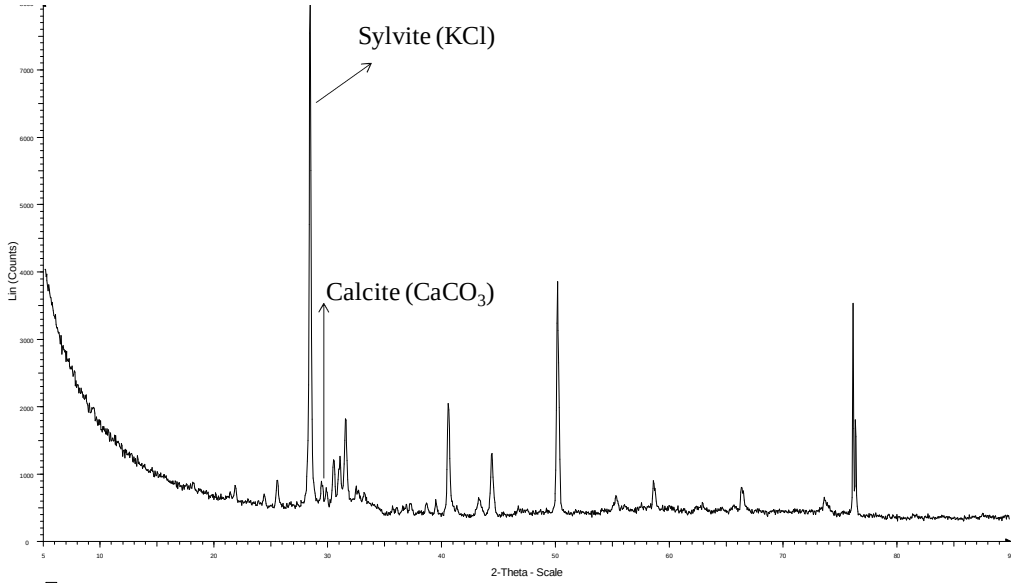

Figure 5.16 XRD patterns of the side deposits from probes with surface temperatures of ~ 500 ^{o}C exposed to combustion gases from combustion of OSR straw pellets after 6 months storage

It is clear that the major compounds confirmed by XRD results, such as sylvite (KCl) and calcite ($CaCO_3$), were already predicted by MTDATA calculations (Fig. 5.2.(a-d)). As mentioned above, calculated condensed $CaCO_3$ temperature range within 200-720 °C and condensed KCl temperature range within 200-680 °C, which were within the probe temperature study of ~ 500 ^{o}C. The predicted condensed K_2SO_4 was not identified by XRD. The reason for this could be that the concentrations level is less than the detection limit of the XRD. However, the formation K_2SO_4 was defined in all OSR deposits by the relative distribution of the respective elements (K, S and O) on the SEM map images. Figure 5.17 shows SEM map images of top surface deposits (~ 500 ^{o}C) from combusted OSR stored for 1 month (as an example). It is obvious from the white dots (existence of the elements) of K and S plus O matching. The lower than expected concentrations of K_2SO_4 can be explained, as suggested by Furimsky and Zheng, [2003] by the formation of potassium sulfates in the condensed phase being kinetically inhibited, or because of the residence time of particles in the FBC [Lisa et al., 1999; Wolf et al., 2005].

The predicted data of hematite (Fe_2O_3) showed slight variation in concentration, which were in consistent with the measured data. For example, the Fe_2O_3 stable temperature

range (340-720 °C) and concentrations of $\log_{10}$ -2.10 moles from the combusted pellets after storage for 1 month, compared to condensed Fe_2O_3 temperature range (320-880 °C) and concentrations of $\log_{10}$ -2.53 moles from the combusted after storage pellets for 12 month. This suggests another variation between the OSR stored fuels, which can be relate to the change in fuel compositions (see Table 3.7).

Other possible variations could be that other condensed compounds identified by MTDATTA like $Fe(H_2PO_3)$, H_3PO_4, H_2KPO_4 and Fe_2MgO_4 were formed only from the OSR pellets stored for 1 and 3 months (Fig. 5.2.a and Fig. 5.2.b), whereas condensed compound $NaPO_3$ deposited only from the OSR pellets stored for 6 and 12 months (Fig. 5.2.c and Fig. 5.2.d).

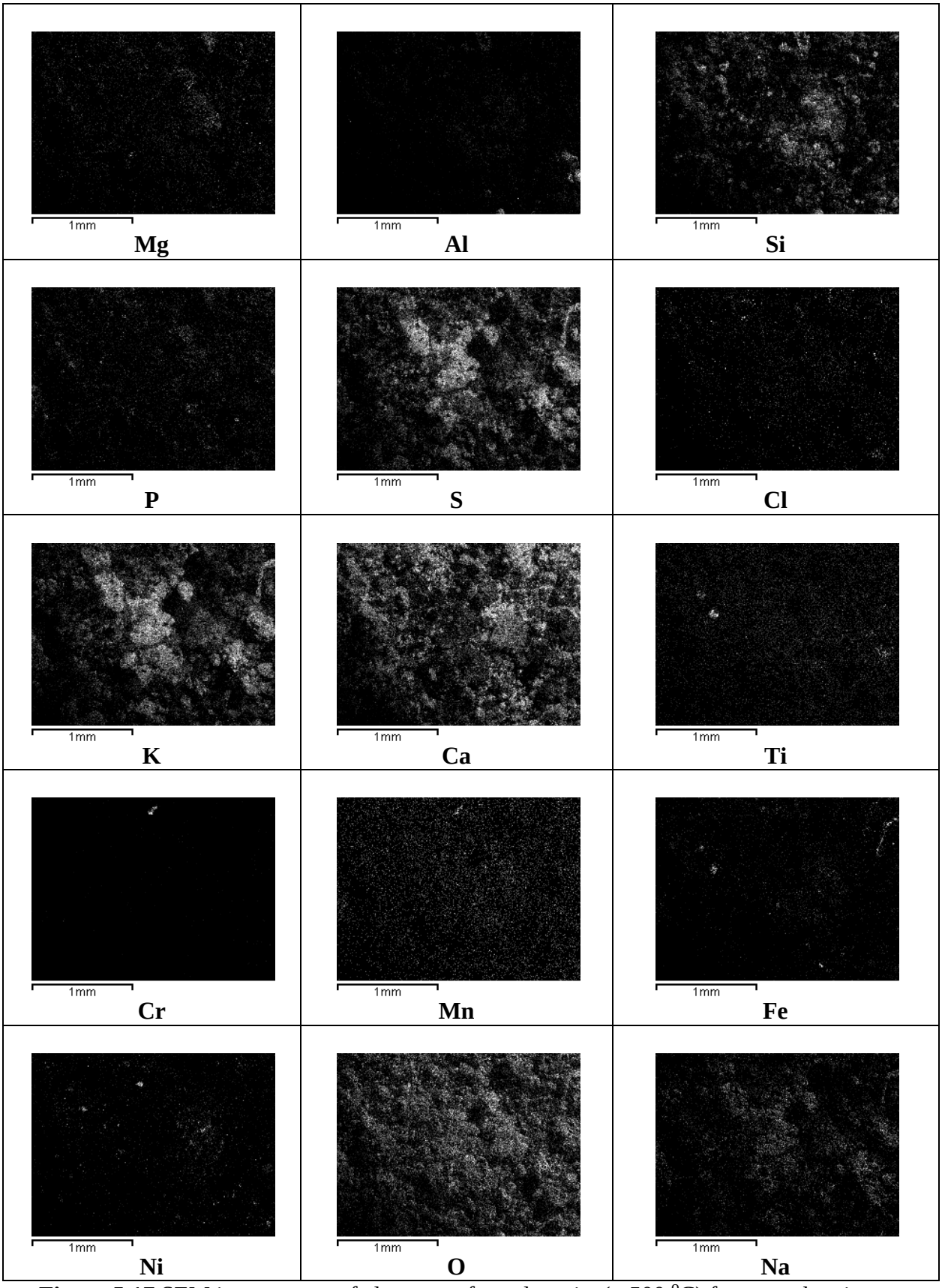

Figure 5.17 SEM images map of elements of top deposits (~ 500 ^{o}C) from combustion of OSR straw after 1 month storage

Bed materials and fly ash investigation

Fluidised bed materials and fly ash samples generated by the combustion of all the stored OSR straw pellets were also investigated. Figure 5.18 shows a photograph of bed materials extracted from the FBC after the combustion trials of two selected OSR straw pellets (stored for 1 & 12 months, as an example). Investigation of the bed materials weight revealed mass increase of ~ 0.3 kg from the original bed material (see 3.18, Chapter 3) for all the fuels selected. Small amounts of sand and ash particles with possible agglomerate/sintering structures were observed. However, these investigations showed similarities for all the stored OSR pellets fuels.

OSR Pellets Storage 1 month (100 %, wt)

OSR Pellets Storage 12 month (100 %, wt)

Figure 5.18 Close-up view of bed material after subtracted from FBC from the combustion of OSR straw pellets after 1 and 12 months storage

An SEM image (with varying magnification) of the bed material from the combustion of OSR straw pellets stored for 12 months (as an example) is shown in Figure 5.19. It is visible from the image that the sand is covered with all kind of elements derived from the combusted fuel. A higher magnification image shows the diverse shapes of the smaller attached particles. It was difficult to specify the exact composition (using EDX spot analysis) of the particle because of the variability of the interface.

Figure 5.20 illustrates the appearance of fly ash (see sample taken ports in Chapter 3). This revealed how complicated the structure of the particles were, which may then be relate to the varied structures formed on the surface of the bed materials. EDX analysis

of the fly ash from combusted (OSR pellets after storage for 12 months) and bed materials (for all the OSR stored fuels) are shown in Figure 5.21. The bed materials reveal presence of sulfur, calcium, aluminium, potassium in higher concentrations than for clean sand (see C.2, Appendix C). Chlorine was present on the bed materials and fly ash particles with different concentrations and was highest from combusted OSR straw pellets after storage for 12 months (Fig. 5.21). This means that some compounds were absorbed at the surface of the bed material, but it may also means that they could be released back to the system (i.e. fly ash) when the conditions inside the FBC change.

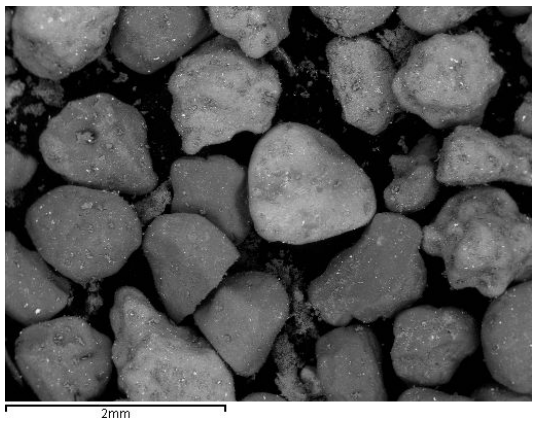

OSR Pellets Storage 12 month (100 %, wt)

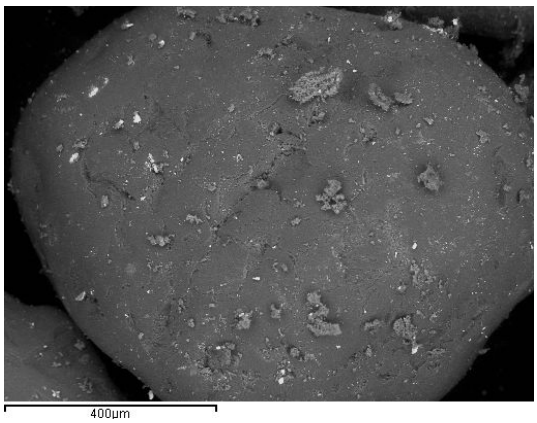

OSR Pellets Storage 12 month (100 %, wt) (higher magnification)

Figure 5.19 SEM images (with varying magnification) of bed material after subtracted from FBC from the combustion of OSR straw pellets after 12 months storage

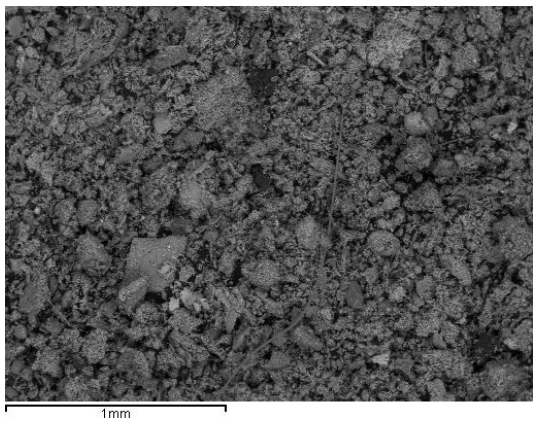

Figure 5.20 SEM images of fly ash from the combustion of OSR straw pellets after 12 months storage

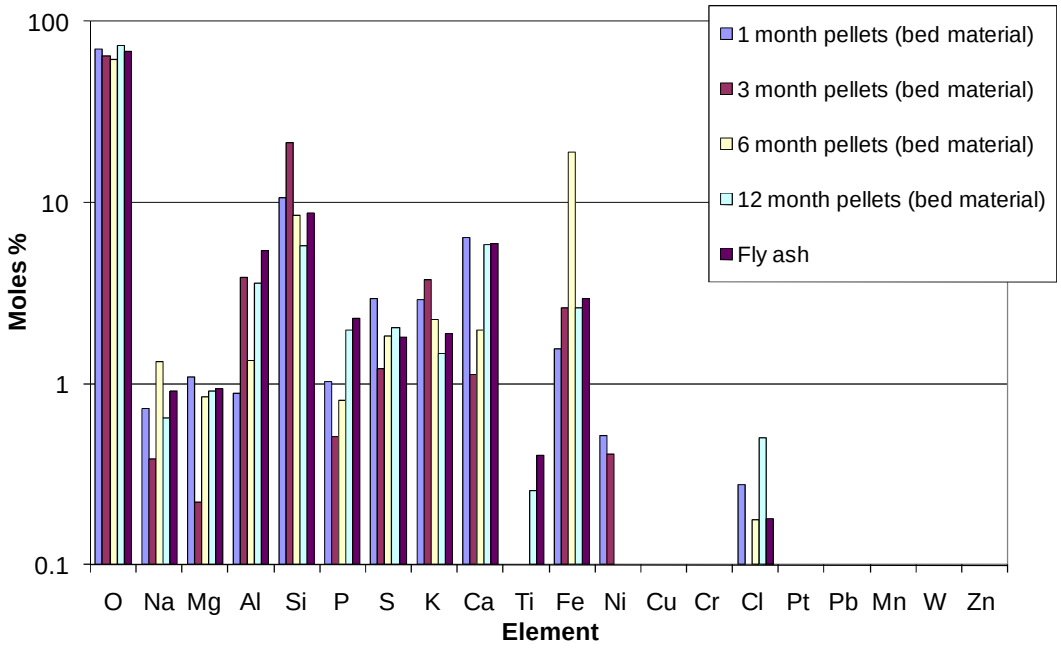

Figure 5.21 EDX analysis of bed materials (from the combustion of OSR straw pellets after 1, 3, 6 and 12 months storage) and fly ash (from the combustion of OSR straw pellets after 12 months storage)

5.3.2 Miscanthus pellets

Fluidised bed combustion behaviour

Agglomeration gradually leading to bed defluidisation was found in miscanthus combustion trials using fluidised bed material of silica sand (here called Bed A, see standard combustions conditions listed in Table 3.18, Chapter 3). The use of limestone (calcium carbonate, $CaCO_3$) as an additive mixed with silica sand to mass ratio 50 % (i.e. fluidised bed composition, SiO_2- $CaCO_3$, 50:50, wt %, Bed B) to inhibit the formation of bed agglomerates was shown to be effective. The experimental behaviour of Bed A and Bed B during continuous ~ 2 hr periods of miscanthus pellet combustion are presented in Figure 5.22. This shows Bed A behaviour once fuel feed started at ~ 520 ºC, slightly decreased and then increased linearly to around 910 ºC where the bed defluidised. Whereas, at the start of fuel feeding, the Bed B temperature shifted from ~ 501 ºC to around 760 ºC and continued with a stable behaviour to reach a maximum of ~ 826 ºC. Thus, stable combustion was achieved for miscanthus using Bed material B (see below gaseous emissions section).

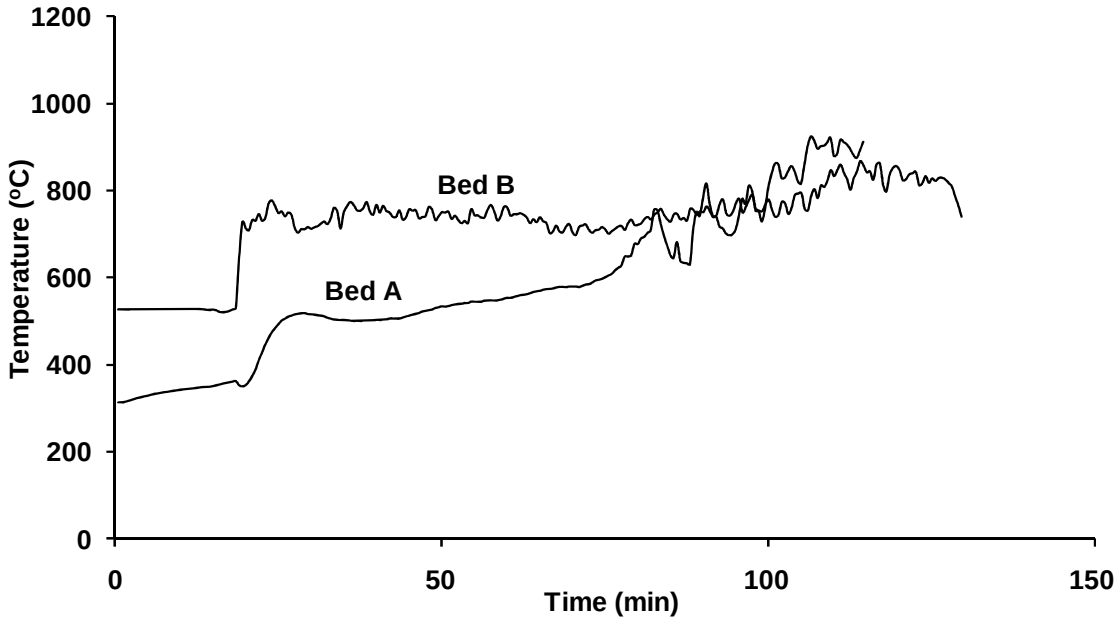

Figure 5.22 Fluidised bed behaviour during the combustion of miscanthus pellets using Bed mater A (silica sand) and Bed material B(silica sand: limestone, 50:50, wt %)

Gaseous emissions

Figure 5.23 shows the major flue gas components produced and Figure 5.24 the minor gaseous species during around two hours of combustion using Bed A and Bed B. It can be seen that the combustion efficiency of miscanthus was quite high in using bed material B as the levels of CO in the flue gas are dropped almost zero (see Fig. 5.24.b) compared to miscanthus combustion using bed material A with a high CO level (average of 2862 ppm, for about one hour feeding). The temperature and fluidisation using Bed A showed instability during the runs, indicating the formation of agglomerates, which can be seen in the abnormal behaviour of major and minor gaseous emissions (Fig. 5.23.a and Fig. 5.24.a). As described in Lind, [1999] the presence of agglomerates in the bed leads to poor fluidisation which causes differences in temperature in different parts of the bed. Whereas, the behaviour of major and minor gaseous emissions using Bed B showing steady production due to temperature and fuel distributions being maintained during the operation run.

With Bed B the minor gas species from miscanthus combustion were very low, with SO_2 concentration averaging 2.12 ppm but dropping at some points to ~ 0.87 ppm, HCl concentration averaging 26.90 ppm, NO_x (NO and NO_2) concentration averaging 118.4 ppm. This indicates the significance of stable miscanthus combustion on gaseous emissions. These values were lower than reported literature values [Collura, et al., 2006] of NO_x (170 ppm) and SO_2 (50 ppm); possibility due to the lower nitrogen and sulfur contents of the raw material and/or the type of the combustion rig, but more likely to be a result of using the large limestone addition in the bed to stop agglomeration.

For comparison between the measured data (using Bed B) and the calculated data (CP and MTDATA shown in Table 5.2) the results match well. For example, the major gaseous emissions measured data of H_2O, O_2 and CO_2 were an average of 16.51 %, 3.12 % and 13.22 % respectively, compared to the predicted calculated MTDATA data at ~ 760 ºC which were 14.15 %, 3.14 % and 13.14 % for H_2O, O_2 and CO_2, respectively. Minor gases also match well except NO_x emissions. HCl and NO emissions predicted of 29.29 and 16.17 ppm at 760 ºC, compared to measured data of an average of 26.90 and

114.94 ppm, respectively. According to MTDATA calculations (Fig. 5.3) NO concentration level increase to 29.01 ppm at ~ 820 ºC (which is reached by the combustion bed zone temperature) and to 104.74 at ~ 980 ºC (a temperature never reached by the combustion zone measurements). This can be explained by the fact that emissions of NO and N_2O have proved to be very much influenced by operating conditions and char particles in the bed [Johnsson and Dam-Johansen, 1991]. Also, as described by Gavin (1993), that addition of limestone or dolomite to the bed of sand increases the fuel-N conversion to NO, while N_2O is decreased (as both limestone and dolomite are catalysts for the heterogeneous oxidation of HCN and NH_3 (volatile-N), which has a high selectivity for the formation of NO and catalyse the decomposition of N_2O).

It should be noted that the SO_2 gas concentration calculated (by CP and MTDATA) was close to zero (as mentioned above) and this is very close to the measured data. This may be related to low sulfur in the fuel composition (0.06 %, wt. AR, see Table 3.8 Chapter 3) which gave the limestone ($CaCO_3$) addition to the bed only a little to do as an adsorbent for SO_2.

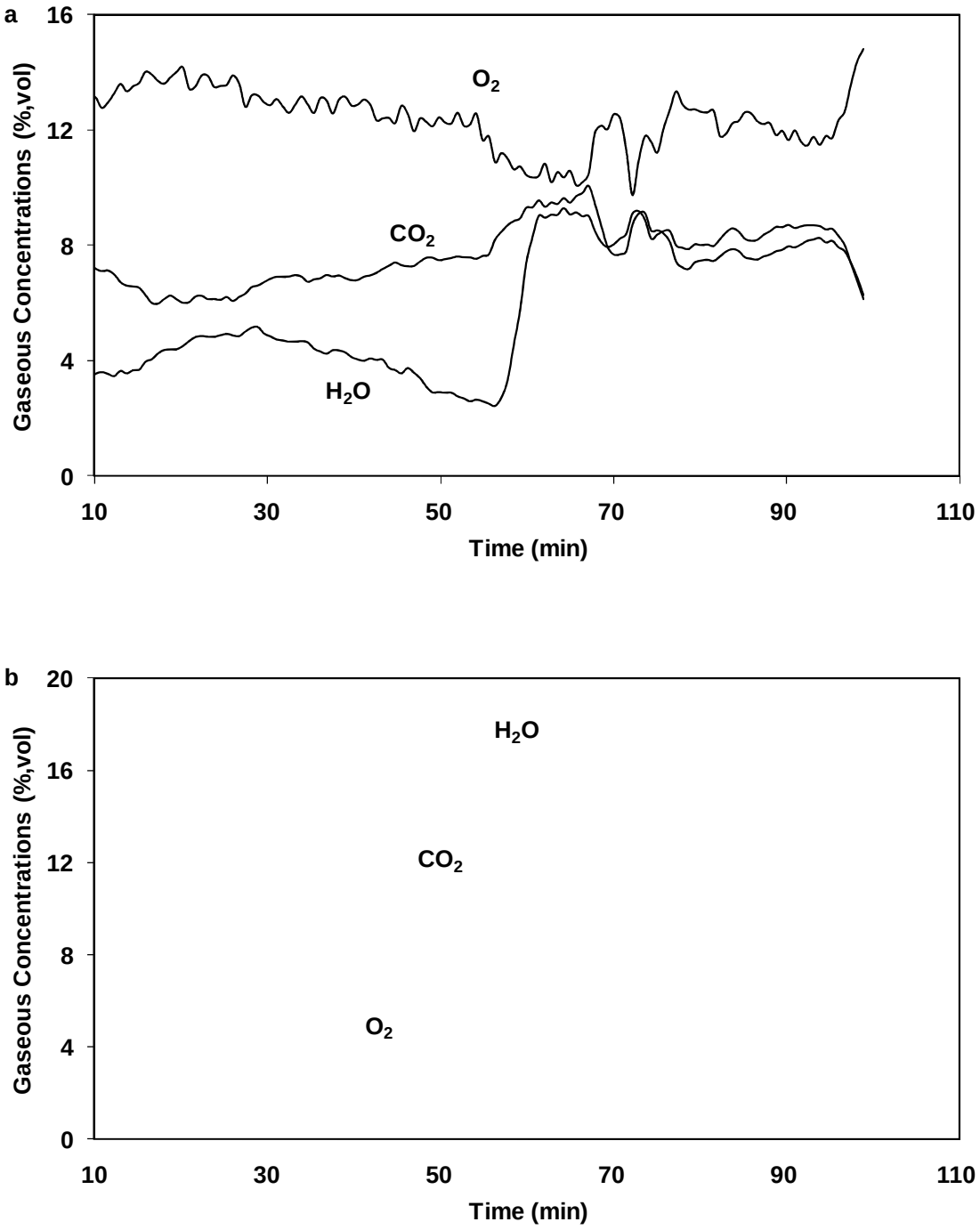

Figure 5.23 Major gaseous emissions from combustion of (a) miscanthus using Bed material A and (b) miscanthus using Bed material B

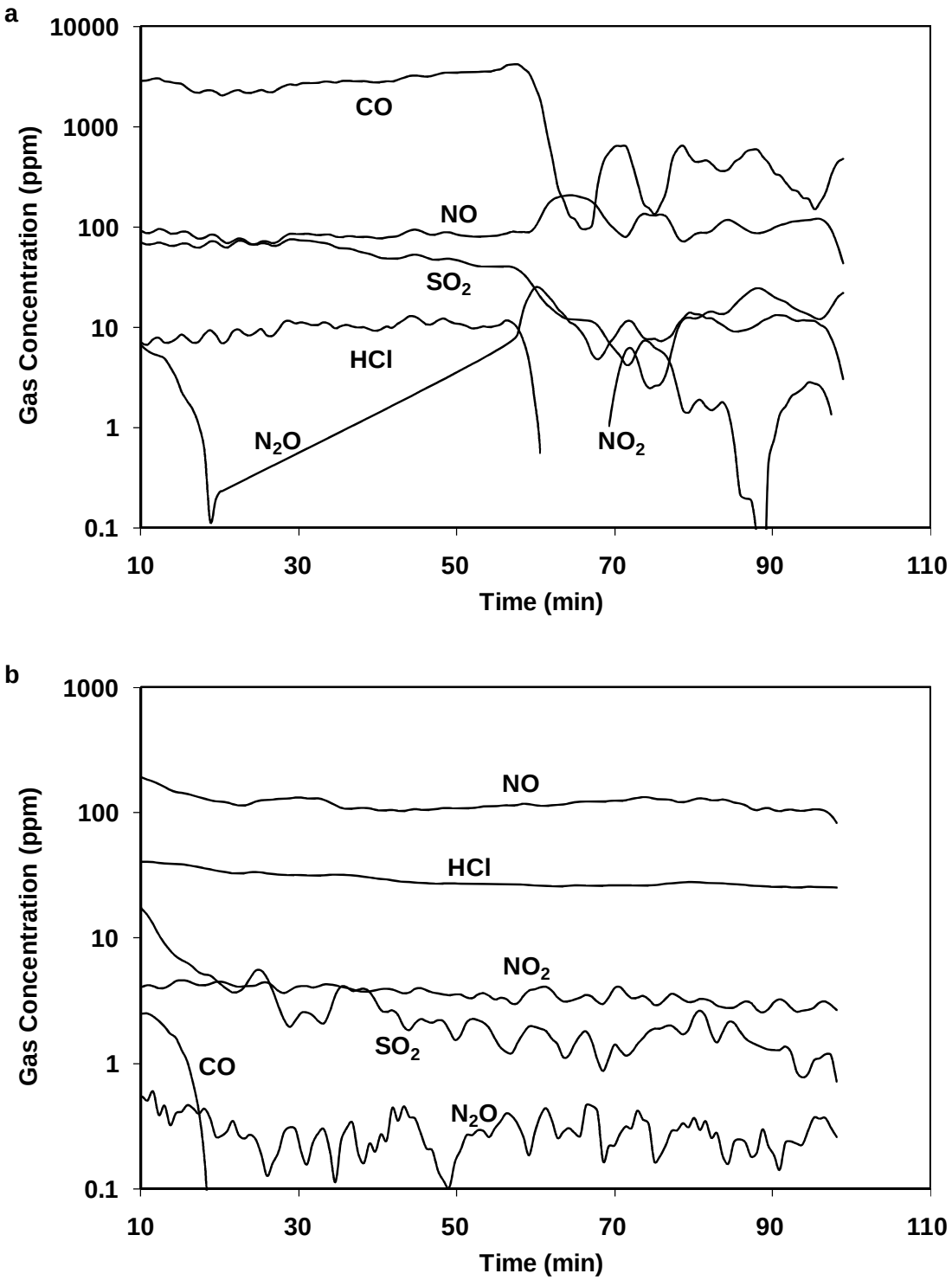

Figure 5.24 Minor gaseous emissions from combustion of (a) miscanthus using Bed material A and (b) miscanthus using Bed material B

Deposition fluxes, deposit compositions and analysis

The appearance of the deposit probe with a surface temperature of ~ 500 °C after 2 hours of feeding miscanthus using Bed A and Bed B compositions, respectively, are shown in Figure 5.25. This shows that the deposits were coarse on both with less fibrous and more porous texture and brighter colour from miscanthus combustion using Bed B when compared miscanthus combustion using silica sand (Bed A). This indicates more uniform miscanthus combustion using Bed B. Indications from these optical photographs were in line with observations by SEM analysis. It can be seen from the SEM images (Fig. 5.26) that the deposit particles are much larger for miscanthus combustion using Bed A when compared to Bed B.

(a) **(b)**

Figure 5.25 Photographs of the deposits formed on probes with surface temperatures of ~ 500 ^{o}C from a) miscanthus combustion using Bed A and b) miscanthus combustion using Bed B

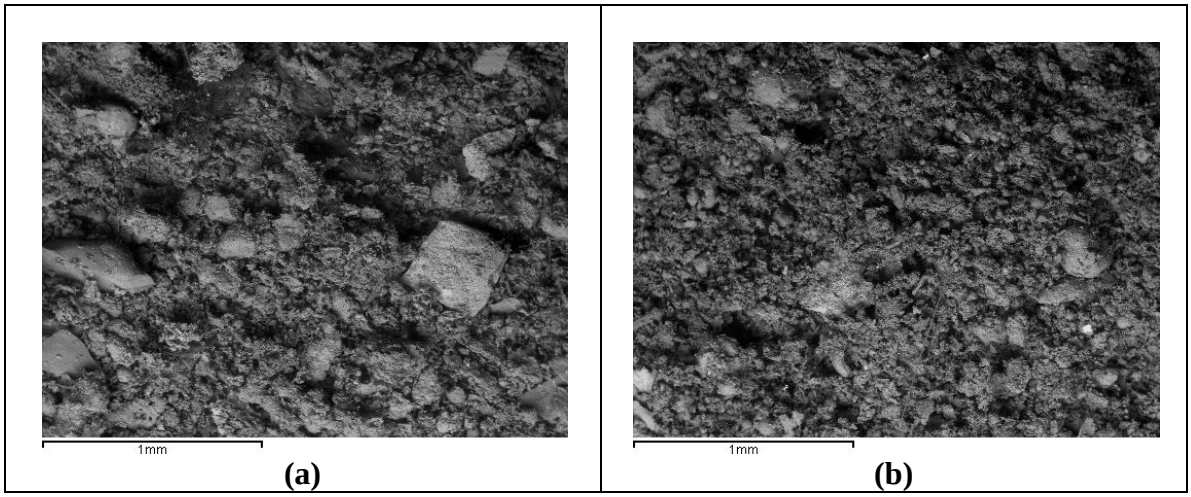

(a) **(b)**

Figure 5.26 SEM images of the top deposits formed on probes with surface temperatures of ~ 500 ^{o}C from a) miscanthus combustion using Bed A and b) miscanthus combustion using Bed B

Deposition fluxes formed on probes with surface temperature of ~ 700, 600 and 500 ^{o}C after ~ 2 hours of feed miscanthus pellets using Bed B are shown in Figure 5.27. This shows that highest rate of formation of the top surface deposits was on the probe surface of ~ 700 ^{o}C with 10.81 mg/cm^2/hr, whereas, side deposits formed at up to 0.045 mg/cm^2/hr on the probe surface of ~ 500 ^{o}C. Deposition fluxes on the probes using Bed A were almost double these amounts with bed materials and/or sintering materials observed.

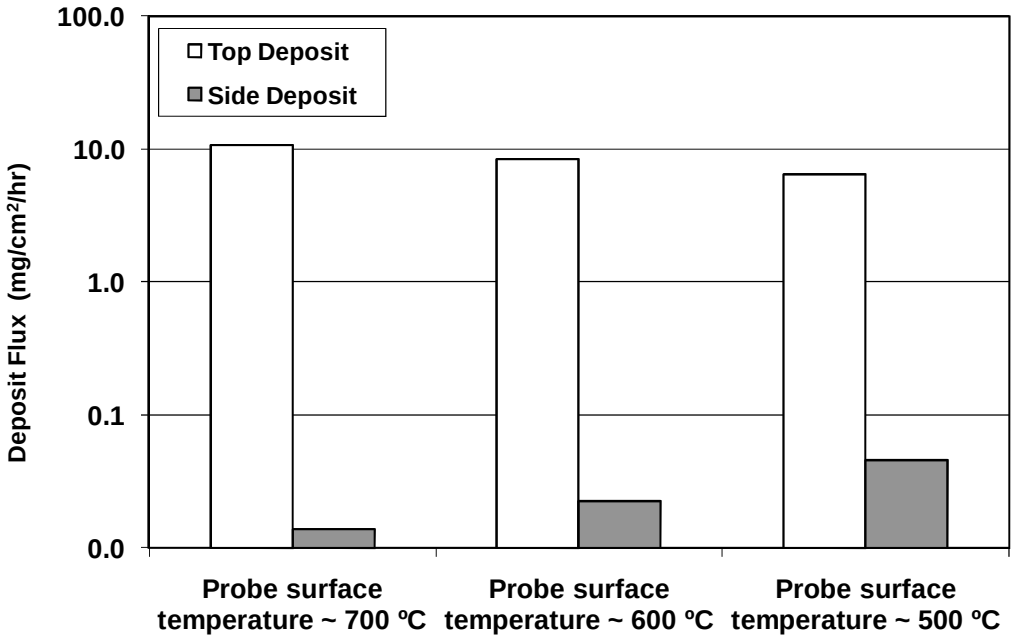

Figure 5.27 Deposition rates of the probes (top & side) with surface temperatures of ~ 700, 600 and 500 ^{o}C from the combustion miscanthus pellets using Bed B

The elemental compositions of the deposits formed on the top and side surfaces of the probes for miscanthus combustion using Bed B and the top surface of the probe using Bed A analysed by EDX are shown in Figure 5.28. Inspection of the figure for Bed B results reveals varying concentrations of silicon, calcium, sulfur, potassium, iron and aluminium in the deposits. Potassium, chlorine and sulfur concentrations in the side surface deposits of the probe were found to be higher than the top surface deposit formed on the probe with 14.6, 10.8, 4.7 % moles compared to 8.0, 0.4 and 2.1 % moles, respectively. Potassium and chlorine in the deposits form potassium chloride which is a highly fouling compound leading to corrosion of boiler components [Van

Loo and Koppejan, 2008]. The appearance of KCl in the top and side surface deposits was not detected by XRD results (Figure 5.29) but confirmed by SEM map images (Figure 5.30) results. Other main compounds identified by X-ray diffraction included: qaurtz (SiO_2), anhydrite ($CaSO_4$), potassium calcium phosphate ($KCaPO_4$), sodium calcium sulphate $(NaCa)_2SO_4$, calcium phosphate ($Ca_2P_2O_7$) and calcite ($CaCO_3$) as can be seen in Figure 5.28. Some of these results were been predicted (shown in Fig. 5.4) by the MTDATA equilibrium calculations (e.g. $CaSO_4$). However, the peaks of some of these compounds were detected in very low, the identification of these are uncertain.

On the other hand, the elemental concentrations of Ca, Si formed on the top surface probe deposit using Bed A were higher compared to Bed B (Fig. 5.28). Alonso-Herranz and Spliethoff [2009] indicated that the composition of the homogeneous agglomerates for rye straw combustion were similar to the fly ash includes high Si and Ca, whereas hetrogeneous agglomerates almost only silicon found.

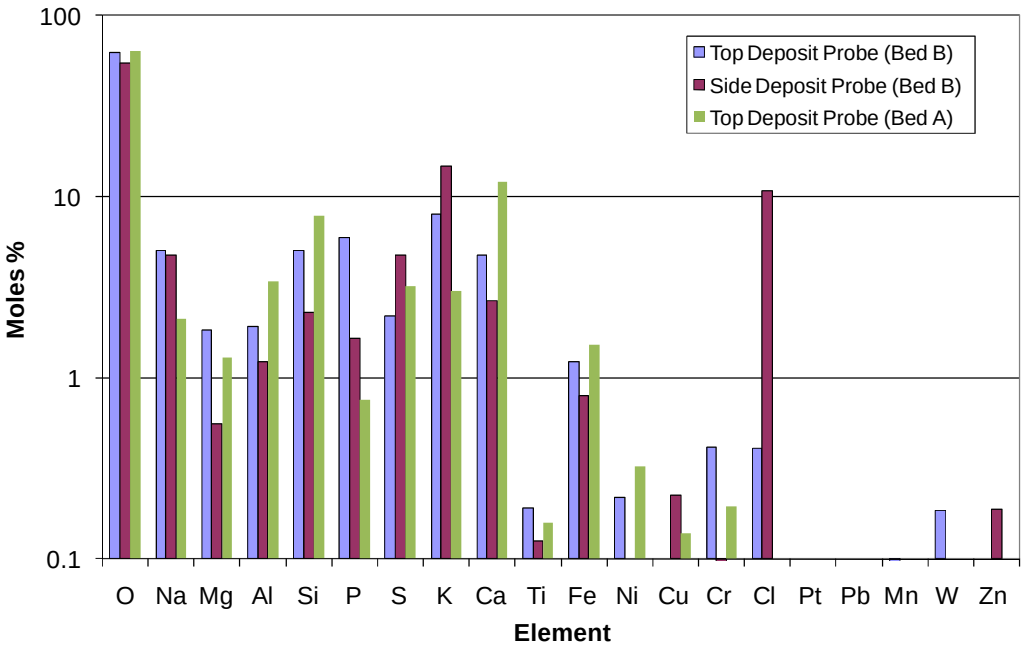

Figure 5.28 EDX analysis of the top surface deposits (using Bed A), top and side surface deposits (using Bed B) formed on probes with surface temperatures of ~ 500 ^{o}C from miscanthus pellet combustion

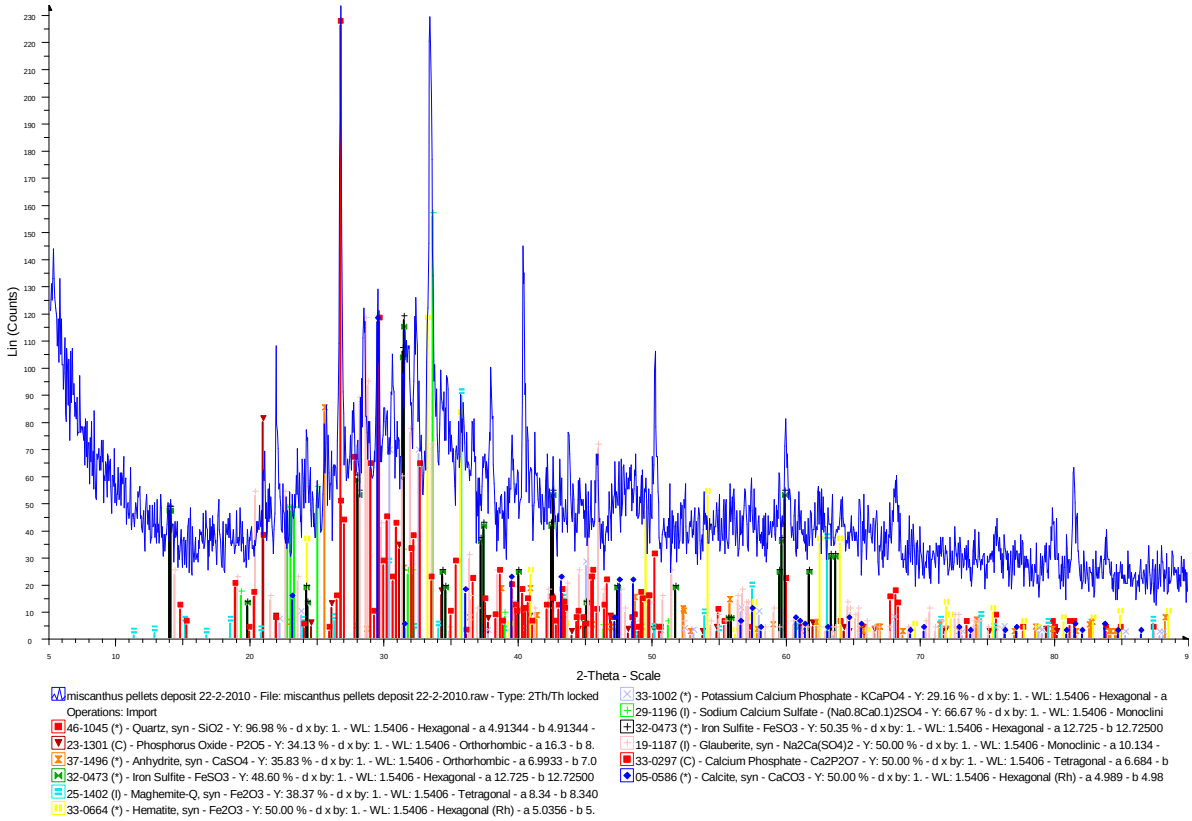

Figure 5.29 XRD patterns of the top deposits from probes with surface temperatures of ~ 500 ^{o}C exposed to gases from combustion of miscanthus using Bed B

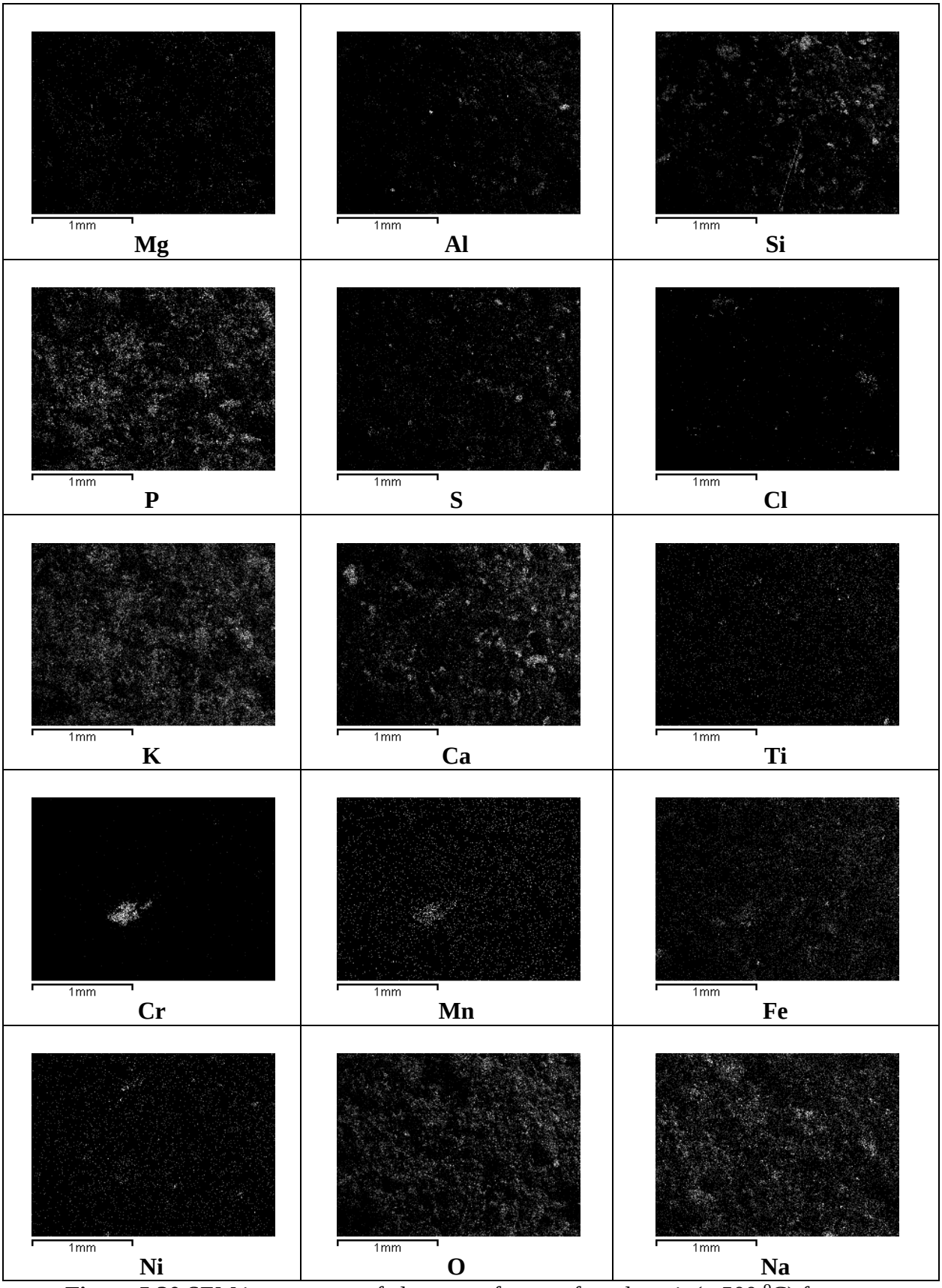

Figure 5.30 SEM images map of elements of top surface deposit (~ 500 ^{o}C) from combustion of miscanthus pellets using Bed B

Bed materials and fly ash investigation

Photographs of fluidised bed materials A and B extracted from the FBC after miscanthus pellet combustion are shown in Figure 5.31. It is obvious that the diversity of Bed A with possibility of both homogeneous agglomeration (in which particles of small and uniform size were formed with some of them being glasslike) and heterogeneous agglomeration (involving clusters formation of large and irregular particles) (homogeneous and heterogeneous agglomeration as described by Olofsson et al., [2002]) compared to plain Bed B. The SEM images (Fig. 5.32) of the two bed materials confirmed the diversity between them in which the sand grains of Bed A were covered or, "glued", by a thin layer of molten and clustered particles. Agglomeration of these two types is believed to be initiated by hot spots (in which grains of the bed material become covered by a layer of molten phase to form particle clumps, see example found in Bed A in Fig. 5.33). The resulting defluidisation increased the local temperature so that the bed then became totally blocked by the agglomerates. Generally, the formation of hot spots is not clear [Olofsson et al., 2002], however disturbances in the fluidisation around the feeding point, and/or temporary channelling of the carrier gas through the bed can lead to hot spots.

Investigation of bed material weight revealed a mass increase of ~ 0.7 kg from the original bed material (see 3.18, Chapter 3) for Bed B compared to ~ 1.8 kg for Bed A. This variation can be assumed to be done to the various alkali silicates agglomerating Bed A particles and/or additional unburn fuel entering the combustor bed during the defluidisation process.

Bed Material A

Bed Material B

Figure 5.31 Close-up view of bed materials after subtracted from FBC from the combustion of miscanthus pellets

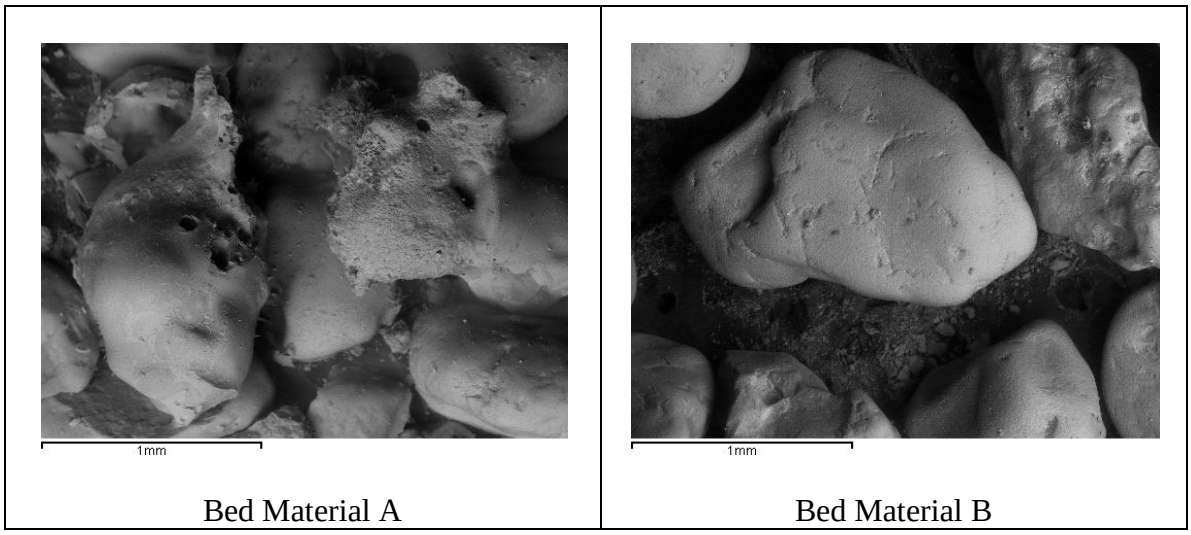

Figure 5.32 SEM images of bed materials after subtracted from FBC from the combustion of miscanthus pellets

Figure 5.33 Particle clump of hot spot of bed material A found after subtracted from FBC from the combustion of miscanthus pellets

To explain the different performances of the two beds in the combustion of miscanths, it is necessary to consider the interaction of the bed material and ashes from the fuel. According to Wang et al. 2009, the presence of high contents of potassium, sodium and silicon in biomass ash will lead to agglomeration. It can be observed in the results of chemical analysis of ashed miscanthus (Table 3.8, Chapter 3) that the concentrations of sodium were quiet high. The use of limestone (Bed B) or other additives [Van Loo and Koppejan, 2008] can be a necessary bed material base for some biomass fuels. Bed B

has a lower SiO_2 content than bed A and the use of limestone will reduce the formation of low melting point compounds needed for the formation of agglomerations.

EDX analysis of bed material A samples (after extraction from the FBC) taken from two different sections found in the bed (one has crystal shape and other like fine ash shape (both analysed as they were)) are presented in Figure 5.34. This showed a possible molten phase rich in Si, Na, K and Ca were found in both samples. This may explain that the agglomeration formed were $K_2O•nSiO_2$ that have melting point of 976 ^oC= $K_2O•SiO_2$, 1015 ^oC= $K_2O•2SiO_2$ [Weast, 1975], 740 ^oC= $K_2O•3SiO_2$ [Moilanen et al, 1999], 740 ^oC= $K_2O•4SiO_2$ [Grubor, 1995] and $Na_2O•nSiO_2$ of melting point of 1088 ^oC= $Na_2O•SiO_2$, 874 ^oC= $Na_2O•2SiO_2$ [West, 1975], 793 ^oC= $3Na_2O•8SiO_2$ [Roth et al., 1981]. Also, another possibility as described by Olofsson et al., [2002] was that the agglomeration resulted from the fusion of straw ash and sand, and so was related to the distribution of the atomic ratios of Si/Ca/K. They suggested that in the presence of large amount of Si (from bed material and fuel), potassium silicates to melt first and then stick the surrounding calcium silicates.

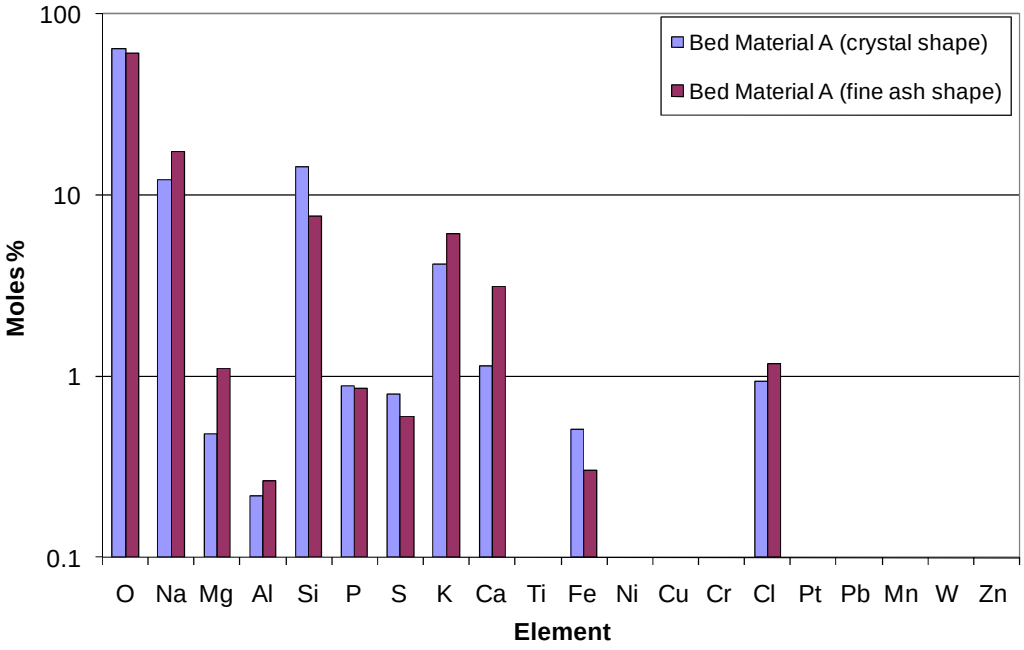

Figure 5.34 EDX analysis of bed materials A of two bulk samples found after subtracted from FBC from the combustion of miscanthus pellets

5.3.3 Coppiced willow

Fluidised bed combustion behaviour

Fluidised bed behaviour during a continuous ~ 4 hr period of combustion of coppiced willow is presented in Figure 5.35. Full temperatures measurements around the whole FBC rig during willow combustion were recorded. A stable combustion was achieved with fluidised bed temperatures of an average of ~ 801 ^{o}C.

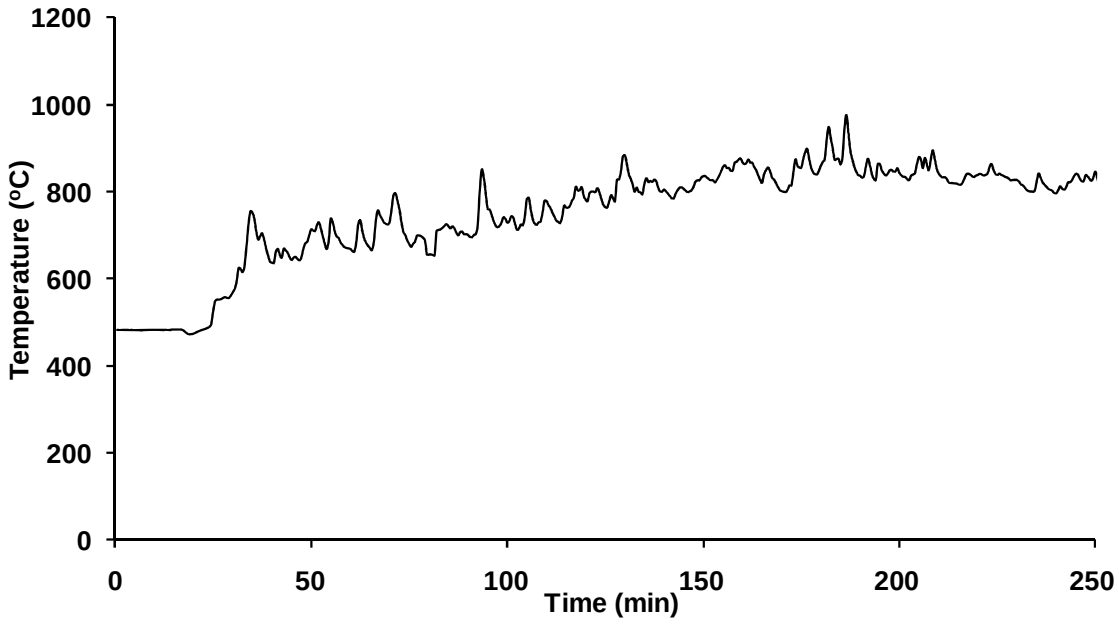

Figure 5.35 Fluidised bed behaviour during the combustion of coppiced willow

Gaseous emissions

Figure 5.36 shows the major and minor flue gas components produced by willow combustion. It is obvious that the gaseous species levels remained almost constant during combustion and no significant drops or drastic increases have been noted (except in the case of stopping feeding due to blockage of dirt/stones in the fuels (taken place at ~ minute 80 during the run)). The minor gas compositions (Fig. 5.36.b) resulted an average of 0.81 ppm SO_2, 1.13 HCl and 138 ppm NO. The CO concentration at an average of 80.09 ppm represents high combustion efficiency.

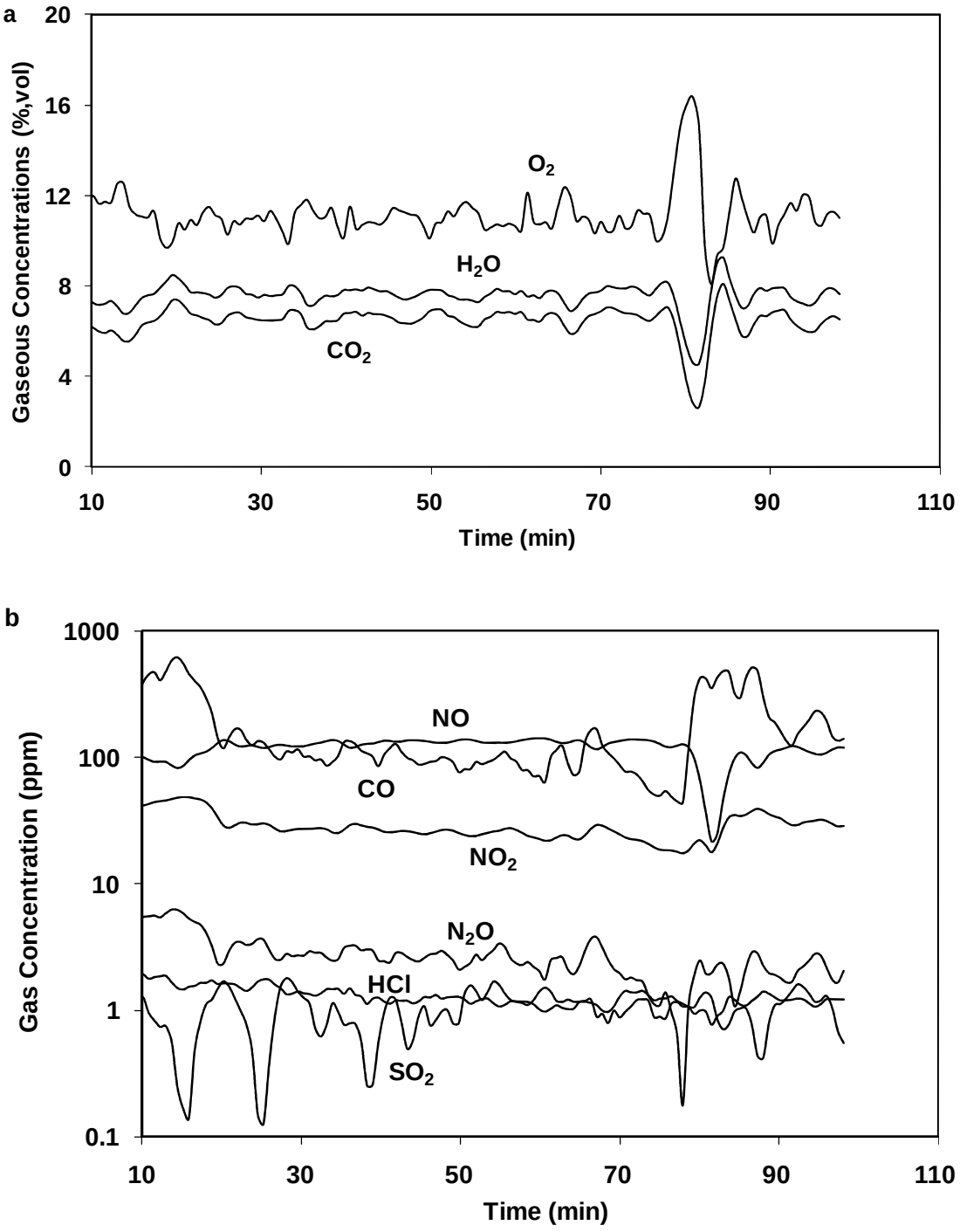

Figure 5.36 Gaseous species emissions from combustion of willow a) major species and b) minor species

All the measured data of major and minor gaseous matched well with the calculated data (CP and MTDATA). For example, the gaseous emissions (Fig. 5.36) measured data of H_2O, O_2, CO_2 and HCl were an average of 7.57 %, 11.13 %, 6.42 % and 1.13 ppm, respectively, compared to the predicted calculated MTDATA data at ~ 800 ºC

which were 7.76 %, 11.06 %, 7.64 % and 1.88 ppm, for H_2O, O_2, CO_2 and HCl, respectively.

As mentioned above, the predicted NO concentration was 129.91 ppm at 920 °C but lower at 800 °C with 43.35 ppm. It is believed that below of these temperatures should be considered when comparing to experimental measured NO concentration of 138 ppm. The reason being that NO_x emissions are particularly sensitive to changes in temperature, whereas the other species are not in this range, combined with the fact that the temperature measurements was for an average in bed temperature.

Deposition fluxes, deposit compositions and analysis

Figure 5.37 shows the photograph of probe deposit (~ 500 ^oC surface temperature), with the SEM images of the deposit formed on the top and side surfaces of this probe being presented in Figure 5.38. This shows that the deposits were fine particles with porous texture. The SEM images revealed that particle sizes in the top surface were larger than the side particles. This indicates that the inertial impaction mechanism dominated the formation of the deposit on the top surface of the probe, while condensation and/or thermophoresis mechanisms dominated the formation of the side deposits (see literature review Chapter 2).

Figure 5.37 Close-up view of the deposits formed on probes with surface temperatures of ~ 500 ^oC from combustion of willow

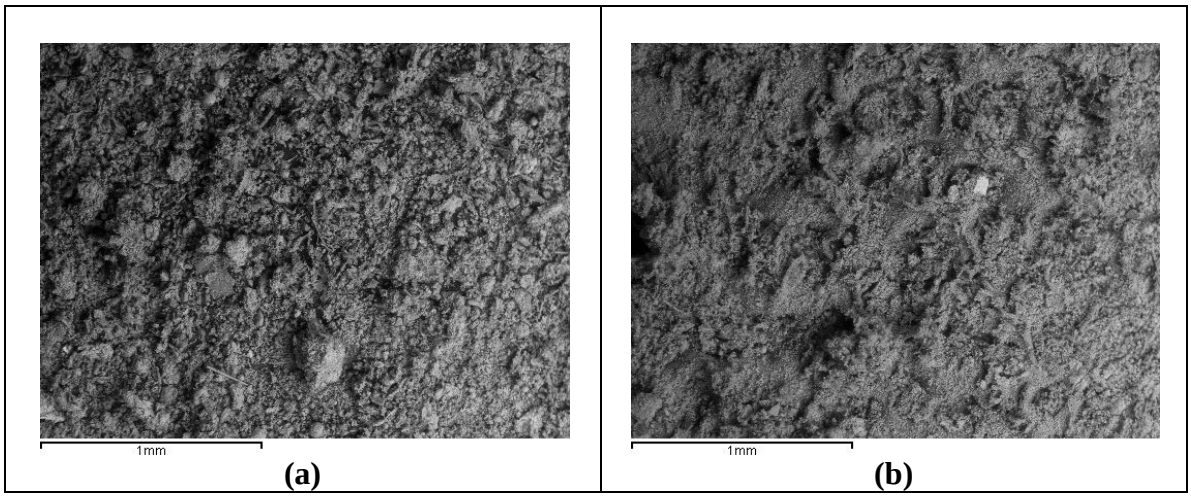

Figure 5.38 SEM images of deposits formed on probes with surface temperatures of ~ 500 ^{o}C of a) top deposits and b) side deposits from combustion of willow

Deposition fluxes formed on probes with surface temperatures of ~ 700, 600 and 500 ^{o}C during willow combustion are shown in Figure 5.39. This shows that deposition fluxes formed from willow fuel are among the lowest studied in this thesis. Also, it can be seen that there is not much distinction between the probe temperatures studied, with a suggestion of the highest fluxes being formed on the probe surface of ~ 500 ^{o}C with 3.46 and 0.012 mg/cm^2/hr on top and side, respectively. The very low deposition fluxes of the coppiced willow fuel suggests it is unlikely to cause deposition problems, which is consistent with previous experience of Red Oak wood [Robinson et al., 2002] and clean wood wastes [Tillman, 2002].

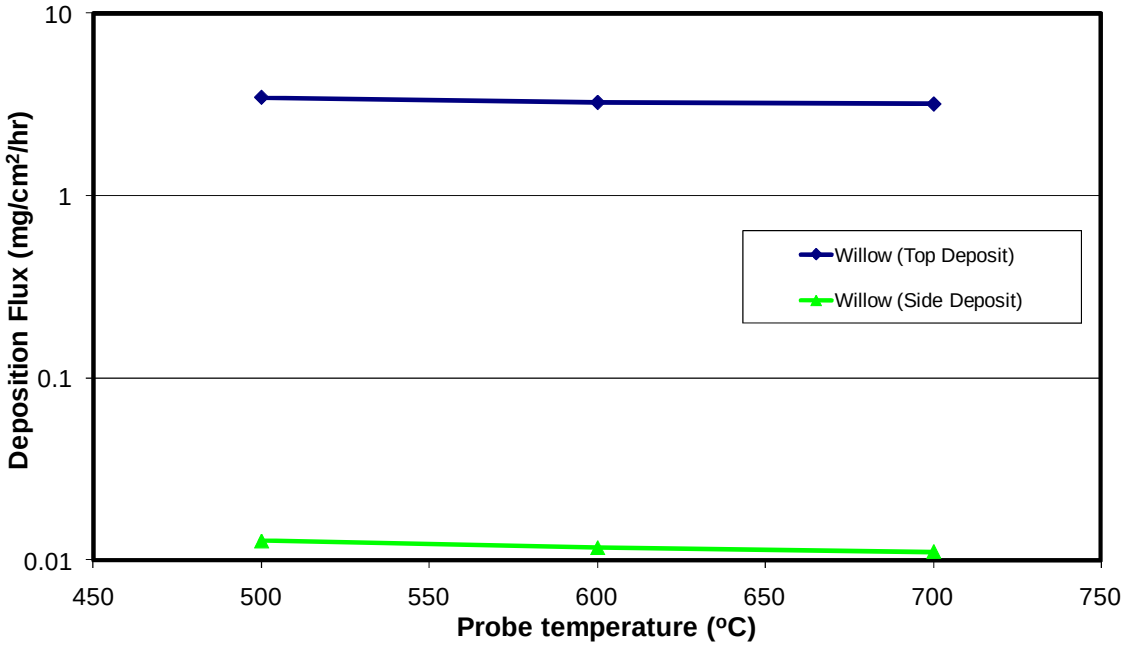

Figure 5.39 Deposition rates of the probes (top & side) with surface temperatures of ~ 700, 600 and 500 ^{o}C from the combustion coppiced willow

The elemental compositions of the top and side surface deposits analysed by EDX are shown in Figure 5.40. The results revealed a similar behaviour to miscanthus combustion (in respect to stable condition run using Bed B) with K, Cl and S concentrations in the side surface deposits of the probe being found to be higher than the top surface deposit formed on the probe with 13.0, 7.7, 3.1 % moles compared to 6.4, 2.8 and 2.2 % moles, respectively. The formation of Cl in the deposits of willow combustion agreed with Maenhaut et al., [1999] in that the composition of the fly ash (taken from different surface temperatures) were similar because of their identical structures (i.e. fine mode ash), and Valmari et al., [1998] indicate that Cl was found on the fine ash and not detected in the coarse fly ash.

The formation of KCl in the deposits was predicted by thermodynamic calculation at dew-points of 520 °C (Fig. 5.6) and confirmed by XRD (Fig. 5.41) results. Other main compounds predicted by MTDATA (e.g. K_2SO_4 (200-960 °C), Na_2SO_4 (320-980 °C)) can be confirmed by the SEM map images (Fig. 5.42) of probe top surface deposits (~ 500 ^{o}C).

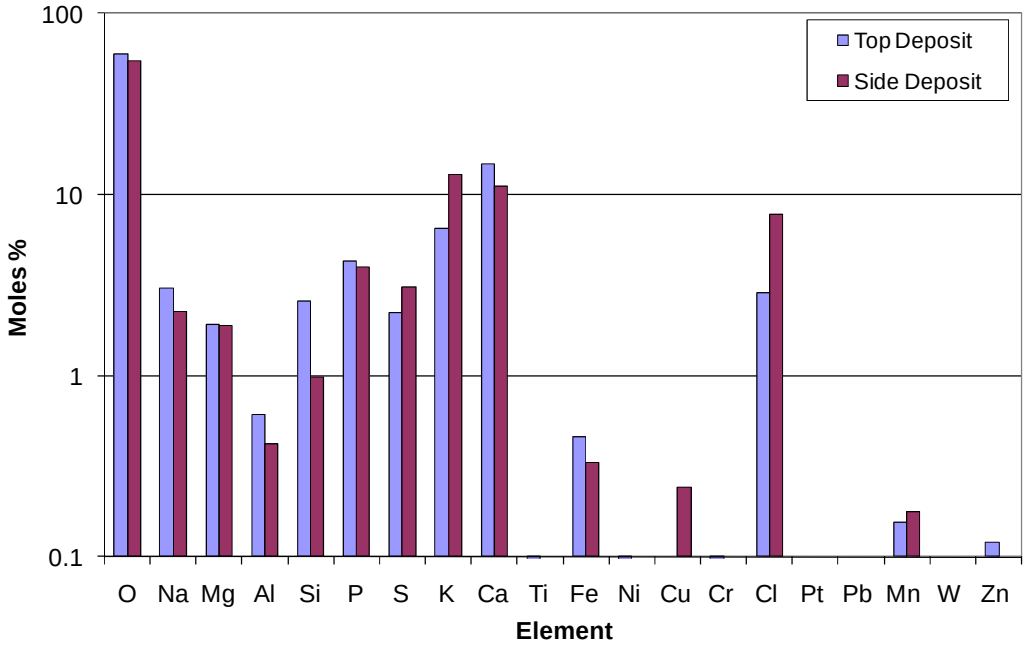

Figure 5.40 EDX analysis of the top and side deposits formed on probe with surface temperature of ~ 500 ^{o}C from willow combustion

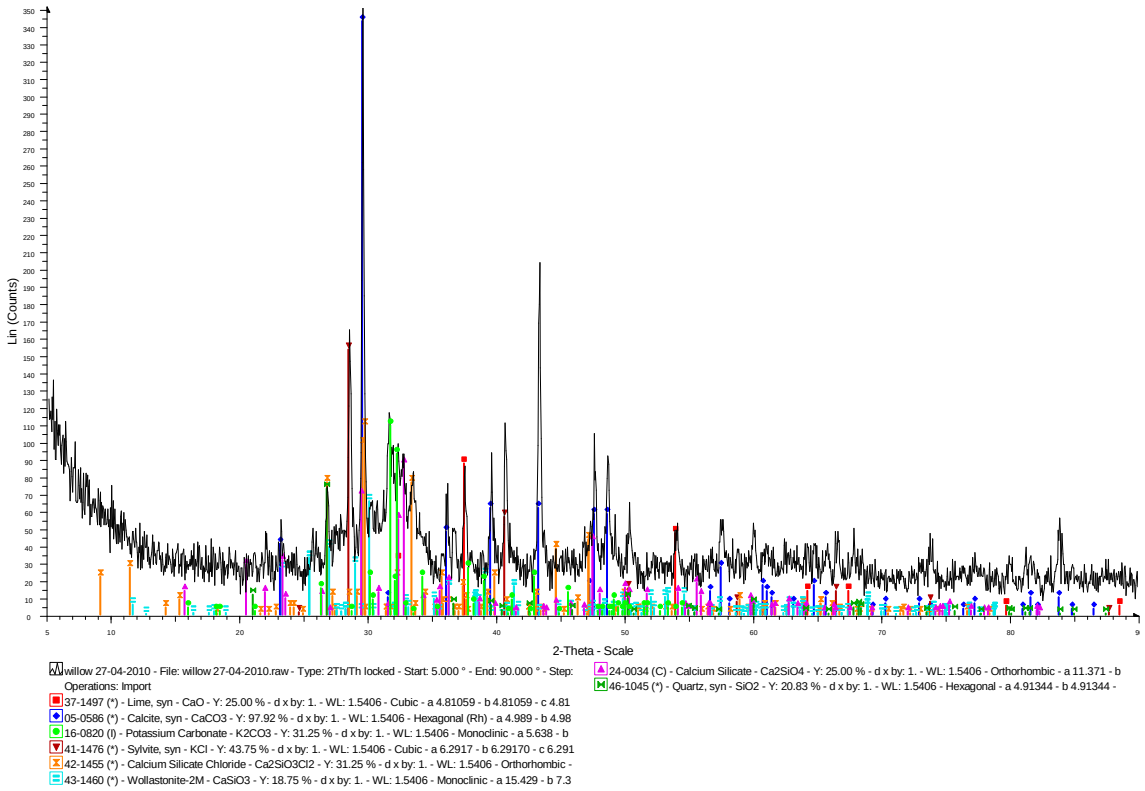

Figure 5.41 XRD patterns of the top deposits from probes with surface temperatures of ~ 500 ^{o}C exposed to gases from combustion of willow

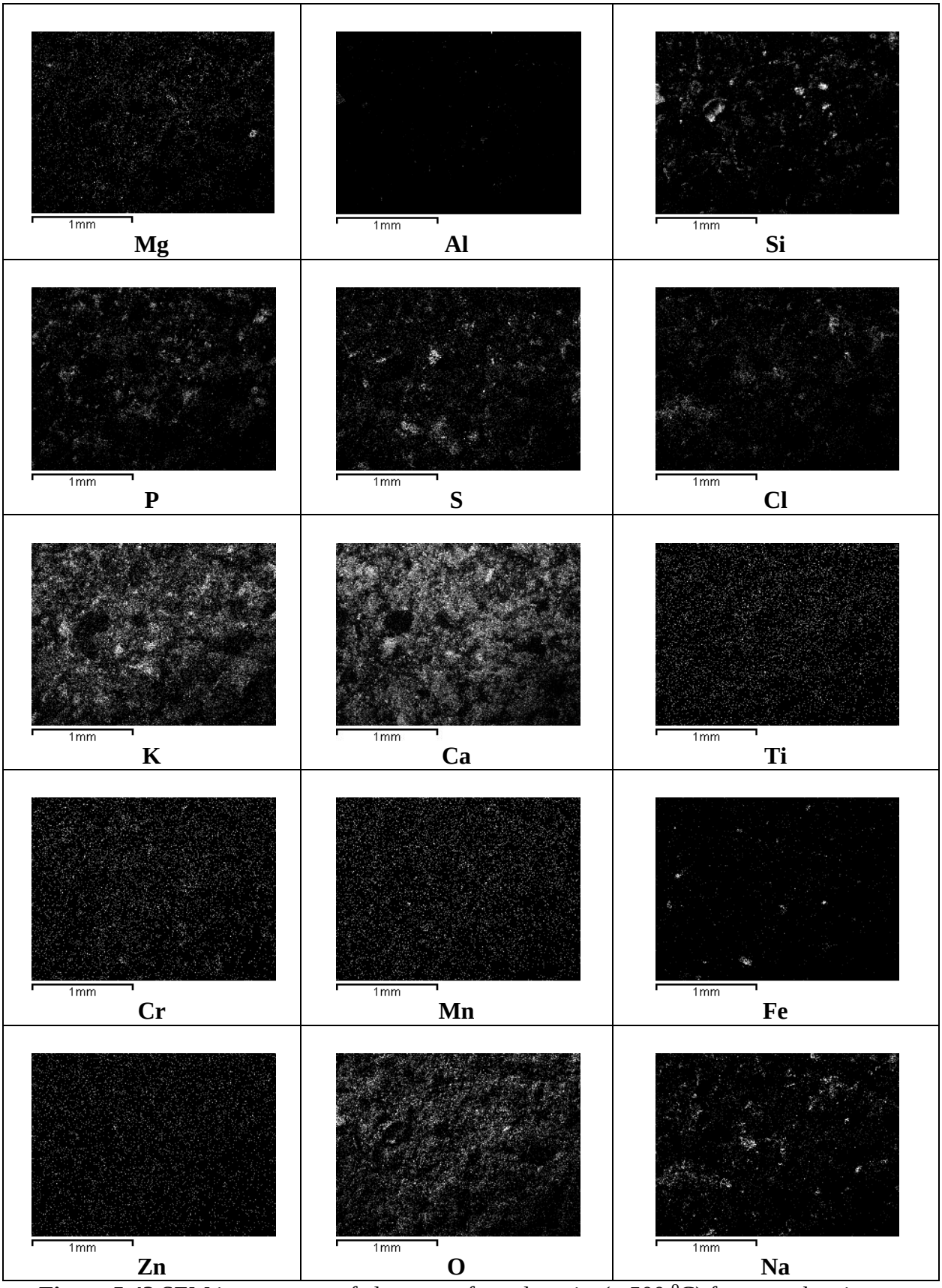

Figure 5.42 SEM images map of elements of top deposits (~ 500 ^{o}C) from combustion of coppiced willow

Bed materials and fly ash investigation

Close-up view and SEM image of fluidised bed materials after coppiced willow combustion are shown in Figure 5.43. These show little change during the combustion trials. Investigation of the bed materials weight revealed almost of negligible mass increase of ~ 0.09 kg from the bed material originated (excluding the stone seen in Fig. 5.43.a entering wrong during feeding). The EDX analysis (Fig. 5.44) illustrated a high concentration of Si (23.57 % moles) combined with tiny concentrations of only Al (0.40 % moles), S (0.13 % moles), K (0.06 % moles), Ca (0.14 % moles) and Fe (0.96 % moles) elements. This result and XRD analysis (Fig. 5.45, showed only Quartz (SiO_2)) confirmed no ash related problems during willow combustion. It can be observed in the results of the proximate analysis of willow that the ash is very low (1.30 %, wt. AR, Table 3.8 Chapter 3) compared to other biomass fuels (e.g. miscanthus pellets, 6.30 %, wt. AR, Table 3.8 Chapter 3), which suggests that this amount of ash in biomass has a very low impact in the fluidised bed (in respect to ash related problems).

(a)

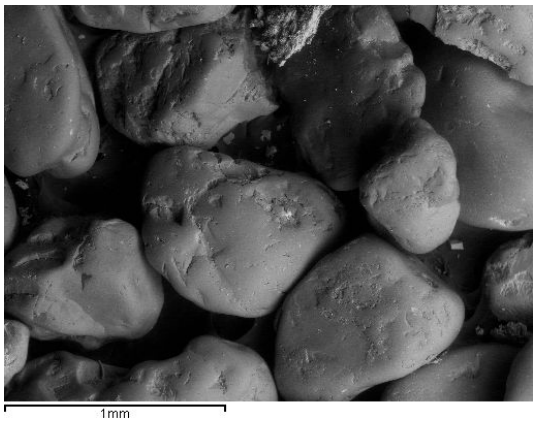

(b)

Figure 5.43 Close-up view of bed materials (a) and SEM images of the bed materials (b) after subtracted from FBC from the combustion of coppiced willow

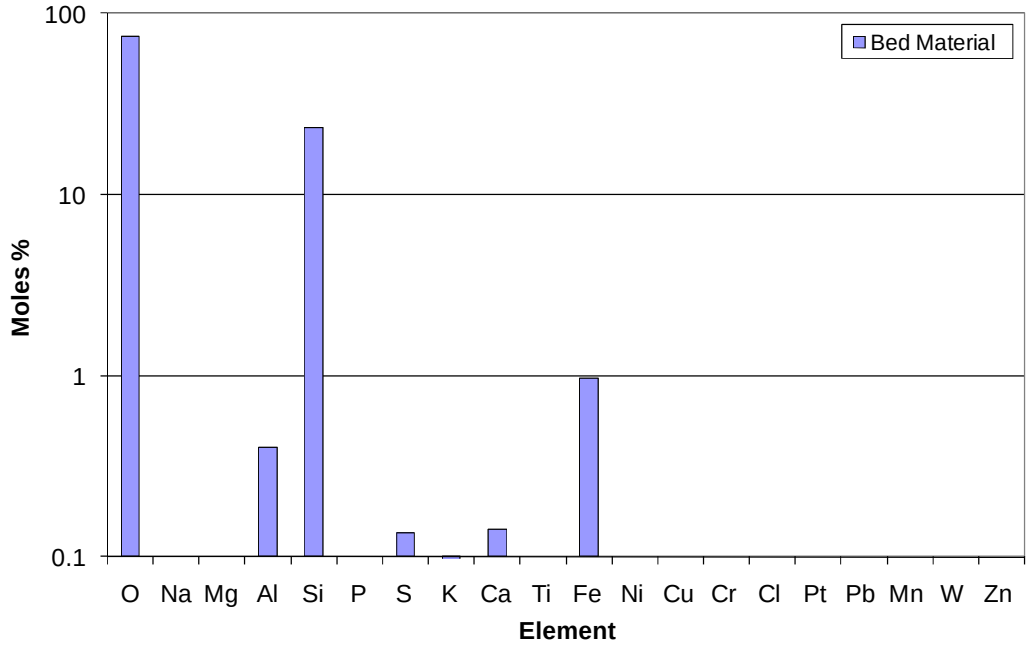

Figure 5.44 EDX analysis of bed materials after subtracted from FBC from the combustion of coppiced willow

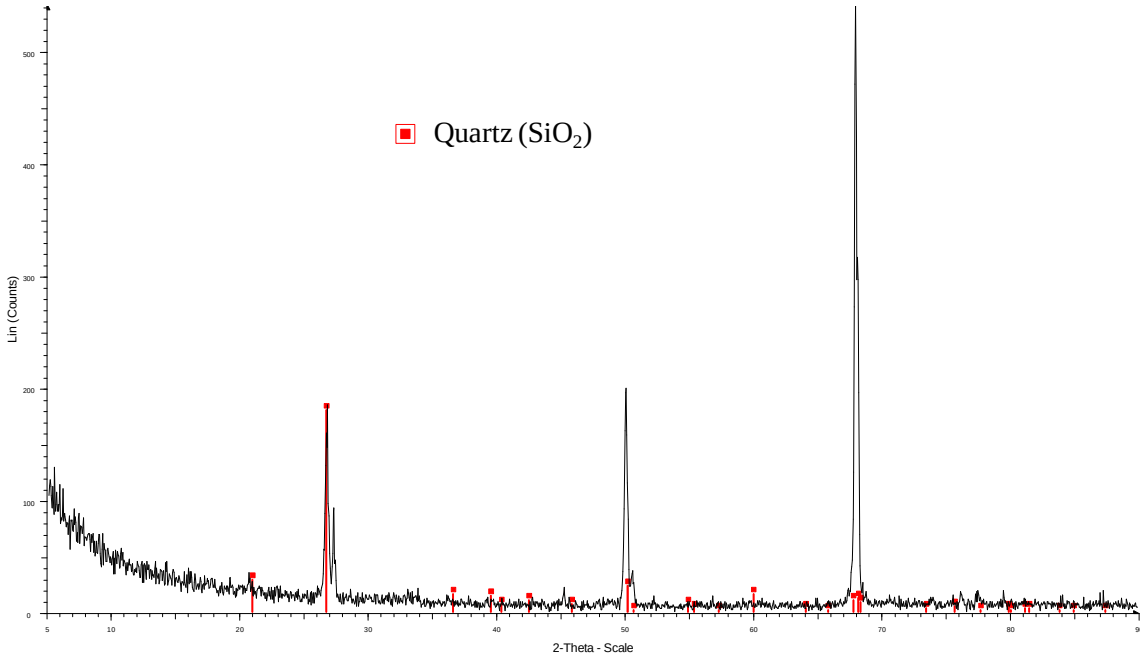

Figure 5.45 XRD patterns of bed material after subtracted from FBC from the combustion of coppiced willow

5.4 General comments

Oil seed rape pellets storage study

The storage of biomass has shown to be one of the process steps affecting its combustion behaviour as a result of the possible variations in biomass properties during storage. A series of combustion tests (in a fluidised bed combustor) and thermodynamic modelling runs (using MTDATA software) were carried out to investigate the emissions produced from the combustion of OSR straw pellets stored for 1, 3, 6 and 12 months. The main conclusions drawn from this work are:

- High combustion efficiency was achieved for all the tests performed after different storage periods due to low CO emissions.
- The emissions of H_2O and NO_x showed variations with the storage of OSR straw pellets. This may suggest that the storage of OSR straw pellets does not have any significant effects on these emissions.
- The HCl and SO_2 gas concentrations were shown to decrease as the storage of the pellets increased.
- OSR pellets stored for 12 months display the highest deposit formation on the top and side of the probes with surface temperature of ~ 500 °C.
- Analysis of the deposits compositions suggest that OSR stored for 6 and 12 months were comparable and different to OSR stored for 1 and 3 months.
- Fluidised bed materials after combustion revealed a slight mass increase with a similar compositions/behaviour for all OSR fuels selected.
- In general, the predicted data from the modelling work has closely matched the measured experimental data, helping to verify the modelling work carried out.

Miscanthus pellets and coppiced willow studies

A series of combustion tests have been carried out in a fluidised bed combustor to investigate different combinations of biomass fuels (miscanthus pellets and coppiced willow) and bed materials. The important experimental/modeling conclusions are:

- The combustion system performed well with willow using silica sand bed, producing stable combustion, no agglomeration and little change to bed material.
- The performance of miscanthus pellets varied with bed material used. The use of a bed of silica sand resulted in agglomeration and variable combustion performance, whereas a bed of silica sand mixed with 50 wt % limestone produced stable performance and no agglomeration, but the use of limestone also affected the behavior of certain fuel elements, in particular sulphur.
- Probes installed to investigate deposition on heat exchanger surfaces showed higher fluxes with miscanthus than coppiced willow, and a more even distribution of ash formation (around the rig and/or on the bed material) for the miscanthus.
- Equilibrium calculation software (MTDATA) was shown to be a useful first step in predicting flue gas emissions and deposit formation (e.g. KCl) from miscanthus and willow combustion

In general the most significant finding of using these different fuels (miscanthus pellets, coppiced willow and OSR straw stored pellets) in FBC is that small variations in biomass properties/composition may influence the gaseous emissions, deposition flux and deposit compositions.

CHAPTER 6 BIO-OIL FUEL STUDIES RESULTS & DISCUSSION

6.1 Introduction

This chapter describes the modelling predictions and experimental data based on the combustion of liquid fuel (fast pyrolysis bio-oil) using PF combustor technique. Parameters of modelling (including combustion product and heat generation prediction, thermodynamic predictions) and experimental measurements (including combustion behaviour, gaseous emissions and depositions) are reported and discussed.

Most of this work has already been published in a journal (see list of publication in Appendix E):
Ala Khodier, Paul Kilgallon, Nigel Legrave, Nigel Simms, John Oakey and Tony Bridgwater. (2009). Pilot-scale combustion of fast pyrolysis bio-oil: ash deposition and gaseous emissions. Environmental Progress & Sustainable Energy Journal, 28 (3), 397-403.

6.2 Modelling

6.2.1 Combustion product prediction

A constant bio-oil feed rate of 0.23 l/min and combustor air feed rate of ~ 1325 l/min were applied for all these fast pyrolysis bio-oil combustion test runs. Combustion product predictions were calculated from the fuel compositions listed in Table 3.9 (Chapter 3). Table 6.1 shows the percent volume concentration of CO_2, H_2O, N_2, O_2, HCl and SO_2 calculated (full description of the calculations made are shown in Appendix A3).

6.2.2 Heat generation prediction

From the HP (calculated from Eq. 3.12, Chapter 3), the heat losses of the combustion system was 4.11 % for the combustion of the bio-oil. These heat loses are in the range expected for the pulverised fuel combustion unit in this test rig (Chapter 3).

6.2.3 MTDATA calculations

The behaviour of the elements C, H, N, O, S, Cl, Na, K, Fe, Ca, Mg,Ti, Ba, Mn, P ("15 elements systems") during combustion of fast pyrolysis bio-oil were calculated using MTDATA. In order to discuss the behaviour of these elements for given combustion conditions, results have been analysed in terms of dominant species in gaseous and condensed forms (if present) with respect to temperature. Figure 6.1 shows the percent (by volume) of the major gaseous species, whereas major/minor gaseous and condensed species (moles) within wider range of fraction (i.e. fraction of 10^{-4} and 10^{-8}) are shown in Figures 6.2.

The predicted levels of the major gaseous (i.e. CO_2, H_2O, N_2 and O_2) and minor gaseous (HCl and SO_2) at ~ 1100 ºC are summarised in Table 6.1. It is clear that the MTDATA results were similar to the MB results.

Table 6.1 Modelling of bio-oil combustion tests

	Bio-oil	
(%, vol.)	**CP[a]**	**MTDATA[b]** (at 1100 °C)
CO_2	11.53	11.53
H_2O	16.71	16.71
N_2	66.72	66.77
O_2	4.97	4.97
HCl	0.0001	0.0001
SO_2	0.0030	0.0001

Keys;
(a): Combustion product prediction
(b): Thermodynamic calculations

The equilibrium combustion calculation indicated that the flue gas composition of bio-oil was 11.53 % CO_2, 16.71 % H_2O, 66.78 % N_2, 4.97 % O_2, 1.5 ppm (vol.) HCl, 1.4 ppm (vol.) SO_2, 35.72 ppm (vol.) NO, 0.52 ppm (vol.) NO_2 and 0.0025 ppm (vol.) N_2O at 820 °C. Also, MTDATA results showed that the concentration of CO_2, H_2O, N_2, O_2 and HCl did not significantly change in the range 200-1300 °C, but the concentration of

SO_2 becomes lower below ~ 840 °C and NO becomes higher above ~ 240 °C gradually (Fig. 6.1).

The condensed species form indicated that the higher concentrations species were $CaCO_3$ (200-740 °C) and CaO calculated to (760-1300 °C) (Fig. 6.2.a, fraction of 10^{-4}), whereas the lower concentrations identified were Ba_2O_4Ti (980-1300 °C), Mn_2O_4 (440-1260 °C) and KCl (200-560 °C) (Fig. 6.2.b, fraction of 10^{-8}).

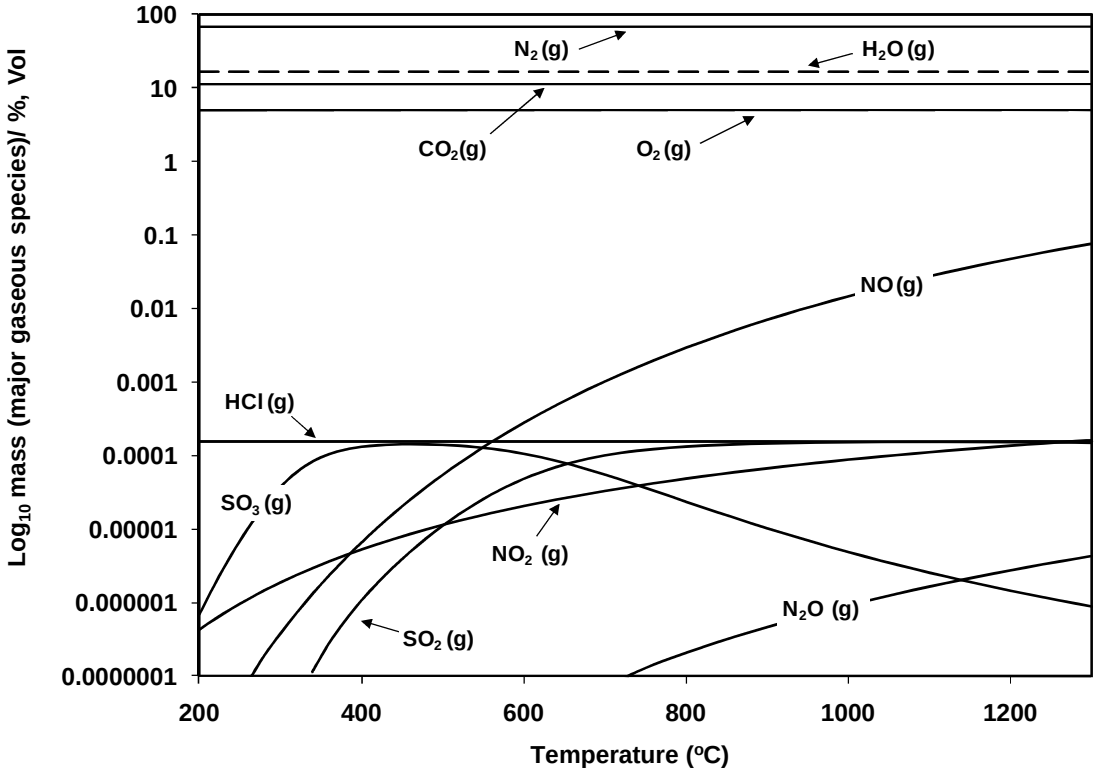

Figure 6.1 Calculated (MTDATA) major gaseous species from fast pyrolysis bio-oil combustion

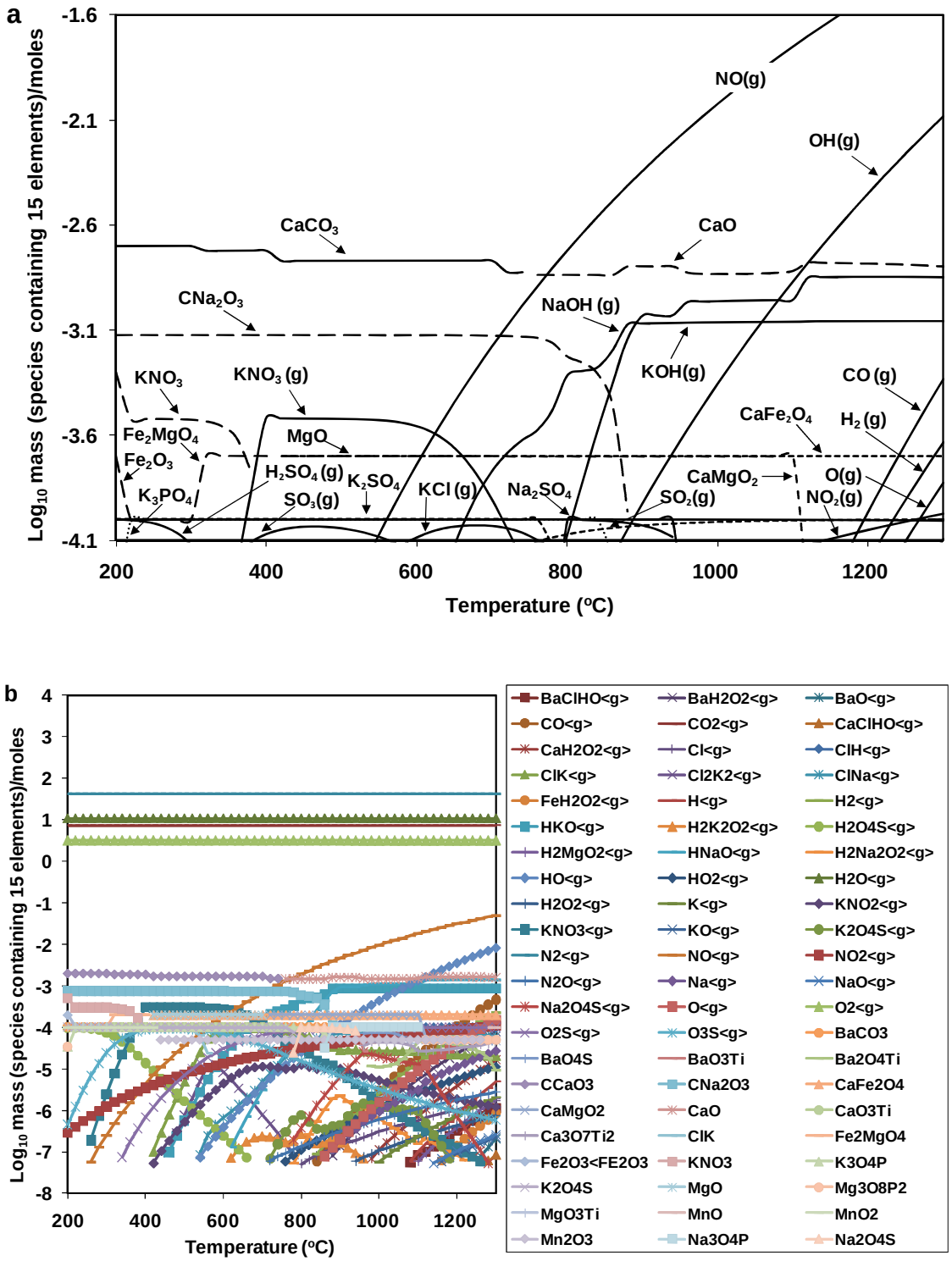

Figure 6.2 Calculated (MTDATA) from fast pyrolysis bio-oil combustion of a) minor gaseous and condensed species (at fraction of 10^{-4}) and b) major, minor gaseous and condensed species (at fraction of 10^{-8})

6.3 Experimental pilot-scale combustion rig exposures

6.3.1 Combustion behaviour/efficiency

Figures 6.3 shows the major flue gas components produced and Figure 6.4 the minor gaseous species (e.g. CO, NO_x, HCl, SO_2) under continuous bio-oil feeding rate (~ 0.23 l/min). It can be seen that the combustion efficiency was quite high as the levels of CO in the flue gas are small (average of 0.35 ppm). The levels of SO_2 initially peaked at 12.24 ppm but quickly dropped to an average level of 2.53 ppm. The level of HCl increased throughout the test but did not reach significant levels. The NO_x concentration remained almost constant around a level of 43.11 ppm (Fig. 6.4). Other minor gaseous species such as HF was found to be below 0.01 ppm. These low levels are expected given the low levels of sulphur and chlorine in the bio-oil.

To study the effect of the bio-oil feed rates on flue gas composition, a range of 0.03-0.3 l/min were also tested. The major gaseous combustion products and the minor gaseous emissions at various feed rate are shown in Figure 6.5 and Figure 6.6, respectively. The combustor air flow rate was kept constant at 1325 l/min, while the fuel feeding rate was increased in steps. The results showed a gradually increasing level of CO_2 and H_2O and decreasing O_2 as feeding rate increased, as would be expected. For the minor gaseous species, the results show no real influence due to the variation in feeding rate apart from a gradual increase. For example, bio-oil feeding rate at 0.24 l/min the NO_x emission was 44.35 ppm, whereas it measured of 45.81 ppm at 0.3 l/min feeding rate. This suggests that the major source of NO_x in flue gas is from fuel-N.

CO emissions tended to be a lot higher during the feed rate study compared to the continuous feed rate study. There are two possible reasons to explain the drop of combustion efficiency. Firstly, when considering combustion at constant air flow (i.e. 1325 l/min), increasing fuel feed rate means increasing the amount of combustion. The higher the fuel feed rate, the higher the amount of unburn combustibles in flue gas. Secondly, as pointed out by Artos et al., 1999 the carbon loss associated with elutriation rate is proportional to the carbon load. Increase of carbon loading (i.e. fuel feed rate) enhances the rate of particle attrition resulting in greater elutriation loss, which causes the carbon utilisation efficiency to decrease. It would be expected that if greater time

was allowed between changes in feeding rate that the CO levels would have dropped closer to levels found with the constant feed rate.

The results of pilot-scale experimental study of the bio-oil continuous feeding combustion match closely with the predicted MTDATA (e.g. O_2 and NO volume outcome were 4.68 % and 41.27 ppm, respectively (experimental study), compared to 4.97 % and 35.72 ppm, respectively (MTDATA study)).

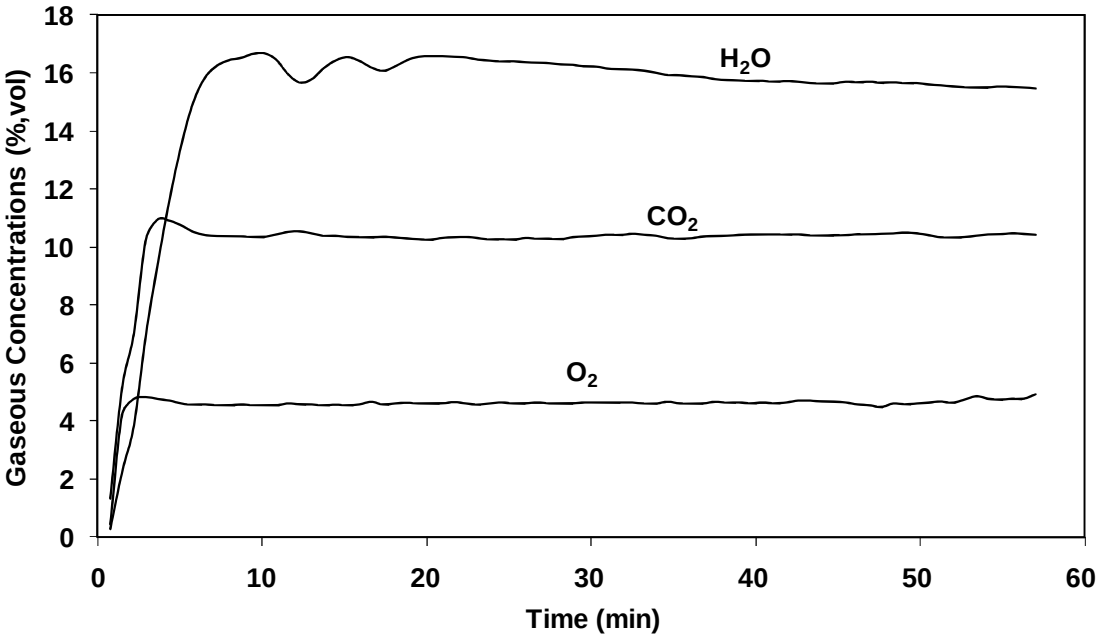

Figure 6.3 Major gaseous species emissions from bio-oil combustion continuously feeding at 0.23 l/min

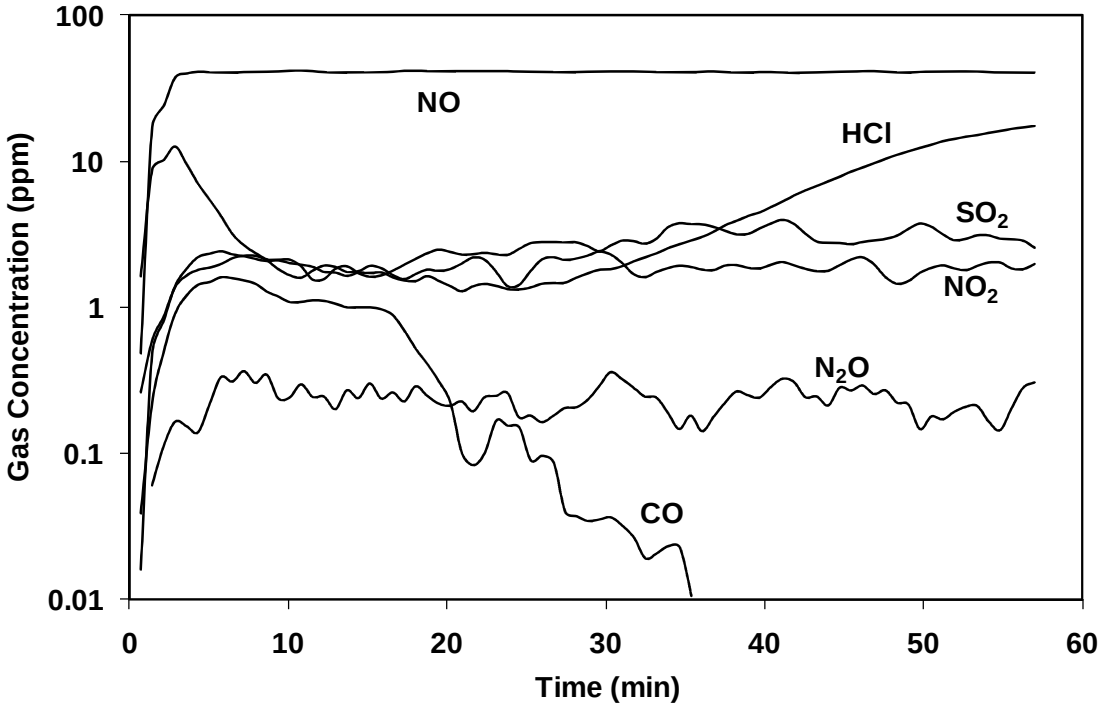

Figure 6.4 Minor gaseous species emissions from bio-oil combustion continuously feeding at 0.23 l/min

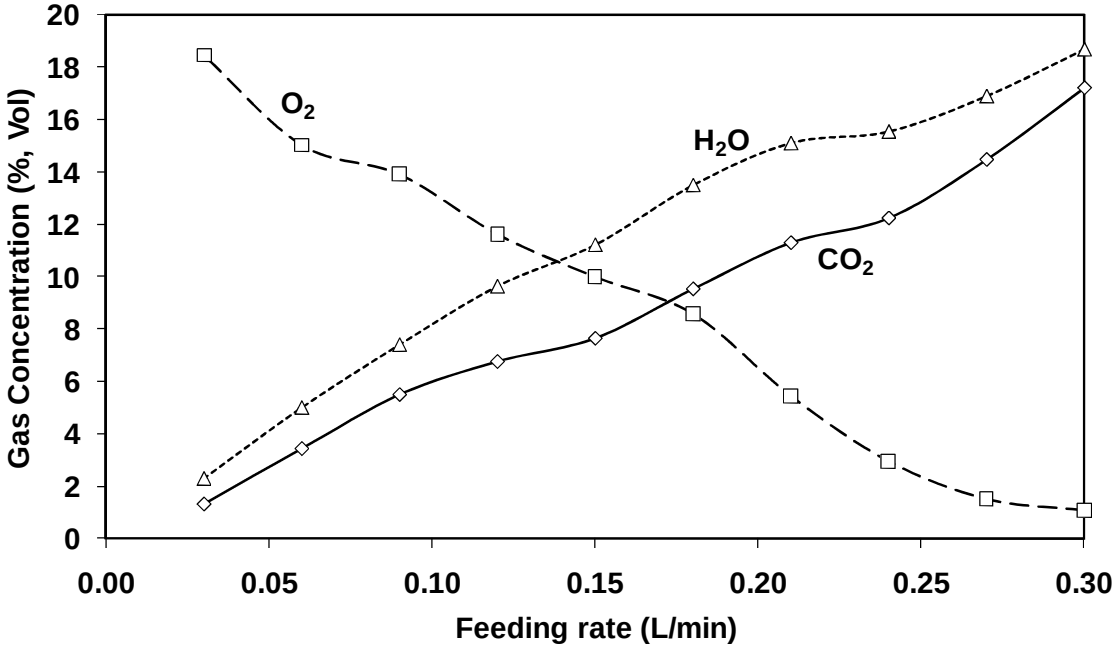

Figure 6.5 Major gaseous species emissions from bio-oil combustion continuously at various feeding rate

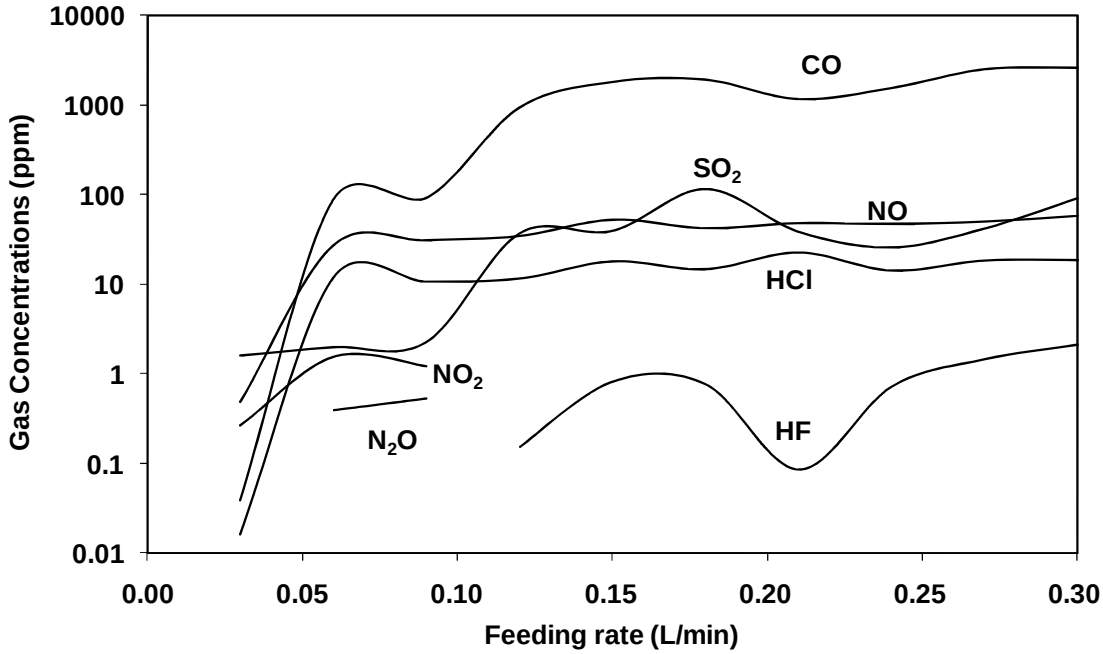

Figure 6.6 Minor gaseous species emissions from bio-oil combustion continuously at various feeding rate

6.3.2 Deposition fluxes, compositions and analysis

Deposits from the ceramic sections of the three deposit probes (probes 1 (~ 700 ^{o}C), probes 2 (~ 600 ^{o}C), probes 3 (~ 500 ^{o}C)) were collected after bio-oil combustion. Figure 6.7 shows ash deposition observed on each of the three probes after exposure.

It can be seen that the deposits formed on all probes had a wide range of particle sizes and had a porous structure. Also, it was observed that the majority of the ash deposit formed on the top surface with little on the sides and none on the bottom of the probes which implies a low risk for fouling. Figure 6.8 shows the SEM images of top and side deposits of the three probes; it can be seen from these SEM images that no agglomerated or molten particles were observed. The deposits have a powdery soft bubbles structure (as can be identified by the SEM images and photographs on top and side deposits) and could be easily blown off the probe.

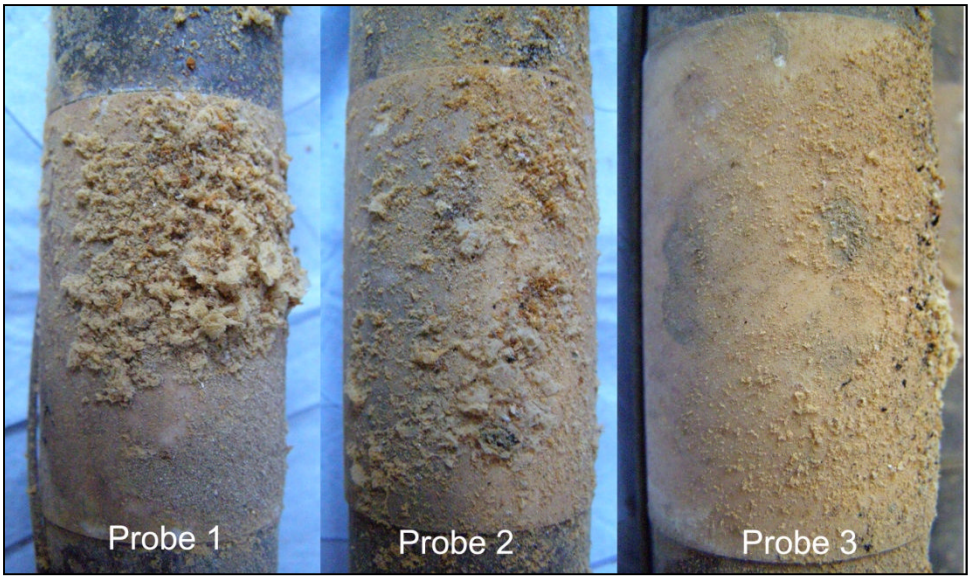

Figure 6.7 Close-up view of the deposits formed on probes (with various surface temperatures of ~ 700, 600 and 500 ^{o}C) from bio-oil combustion

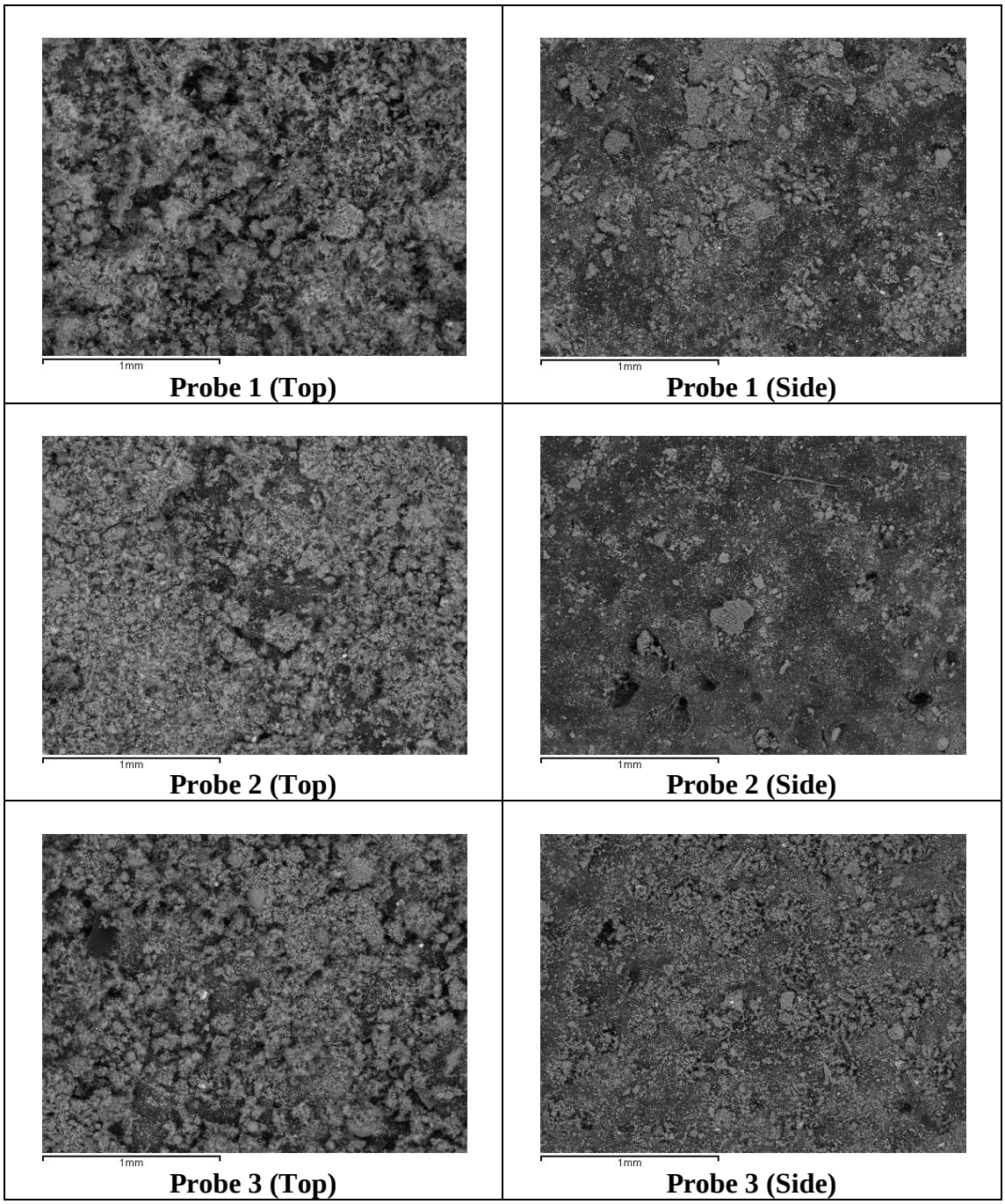

Figure 6.8 SEM images of the top and side deposits formed on probes (with various surface temperatures of ~ 700, 600 and 500 ^{o}C) from bio-oil combustion

The deposit rate of bio-oil combustion for probes 1, 2 and 3 from the top were calculated as 2.89, 2.17 and 2.76 mg/cm^2 h, respectively (shown in Figure 6.9). This showed that the deposit layer thickness did not vary dramatically with probe temperature.

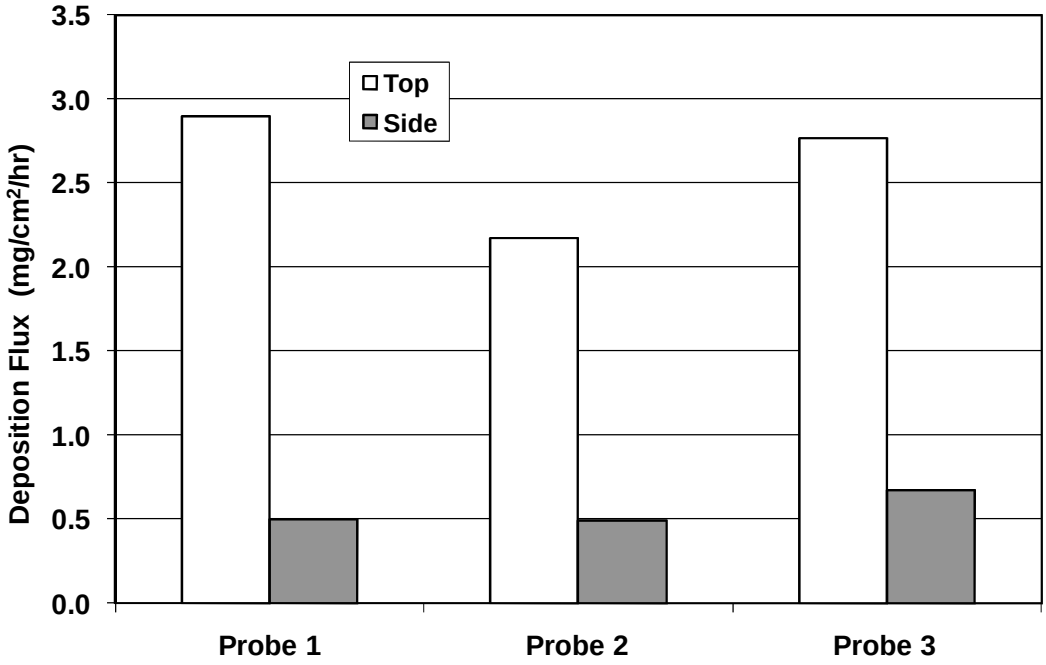

Figure 6.9 Deposition rate of the probes (with various surface temperatures of ~ 700, 600 and 500 ^{o}C) from bio-oil combustion

The elemental compositions of the deposits formed on the tops and sides of all three probes analysed by EDX are shown in Figure 6.10. It can be seen that Si, Al, K, and Ca were higher than the other elements. Also, chlorine concentrations are very low in all deposits indicating little formation of alkali chlorides. Therefore, the potassium in the deposits most likely is in the form of potassium sulfate, oxide or hydroxide compounds instead of potassium chloride which is a highly fouling compound leading to corrosion. Speigel et al., 2003 concluded that chlorine is the major contributor to corrosion in biomass fired boilers as it can be present in various forms; HCl gas, solid KCl and NaCl or in eutectic melts such as KCl-$ZnCl_2$.

The SEM-EDX findings were also confirmed with XRD analysis. Figure 6.11 and Figure 6.12 demonstrate the XRD patterns of the top deposits formed on probe 3 (~ 500 ^{o}C) and probe 1 (~ 700 ^{o}C), respectively. Potassium sodium sulphate $K_3Na(SO_4)_2$ as a minor phase, quartz (SiO_2) and calcium aluminium silicate ($Ca_2Al_2SiO_7$) as a major phase were observed. An overnight XRD run of the deposits formed on the probes (see Fig. 6.13, XRD of top deposits probe 1 (~ 700 ^{o}C), as an example) showed a similar

diffractogram to those run under ~ 45 minutes. This technique used to certify if any alkali sulfates and/or chloride can be detected during this longer scan time. Extra phases may have been detected (Fig. 6.13), such as potassium sulphide (K_2S_3) and hematite (Fe_2O_3), but at low levels and with the peak compare/match procedure (used in the XRD control computer) identification is very uncertain.

The EDX map images of top deposits of probe 1 (~ 700 ^oC) and probe 3 (~ 500 ^oC) are presented in Figures 6.14 and 6.15, respectively. This shows an absence of Cl element of map in deposits of probe 1 (Fig. 6.14), whereas it is not clear if Cl map presented in the deposits of probe 3 (Fig. 6.15) follow a match map of other element (i.e. no bright areas appear, indicating no or very little chlorine presence). The EDX map images suggested that O, Si, Ca, K, S, P and Na have produced fairly uniform mapping (e.g. top edge of the bright area in the Ca map is in consistent with O map (Fig. 6.14) or Ca map with S map (Fig. 6.15)). As chlorine is not detected in both SEM-EDX and XRD analyses of the deposits, the bio-oil can be denoted to have low fouling and corrosion propensity.

XRD data could not be compared with the MTDATA results (in respect to the condensed species) because the outcome showed mostly silicate phases, which MTDATA run under “15 elements system” excluding Si. But the SEM-EDX data indicated that the Ca, K, S, Fe, Na and possibly Mg were in a range for formation of possible predicted condensed compounds (Fig. 6.2) such as $CaCO_3$, CaO, MgO, $CaFe_2O_4$ and/or K_2SO_4.

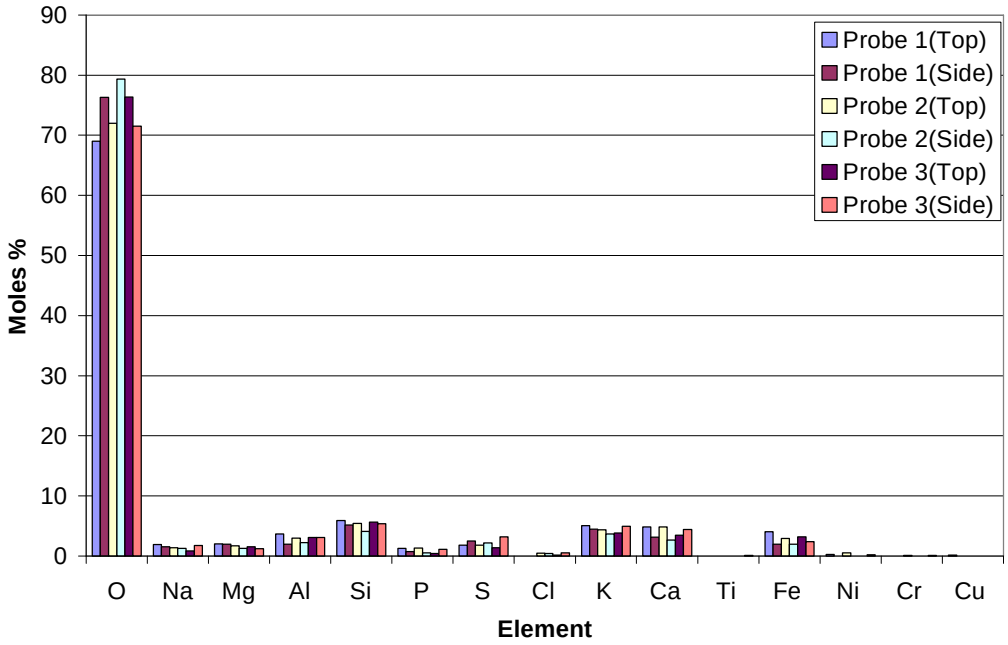

Figure 6.10 EDX analysis of deposits of the deposits produced from bio-oil combustion on the top and side of air cooled probes studied

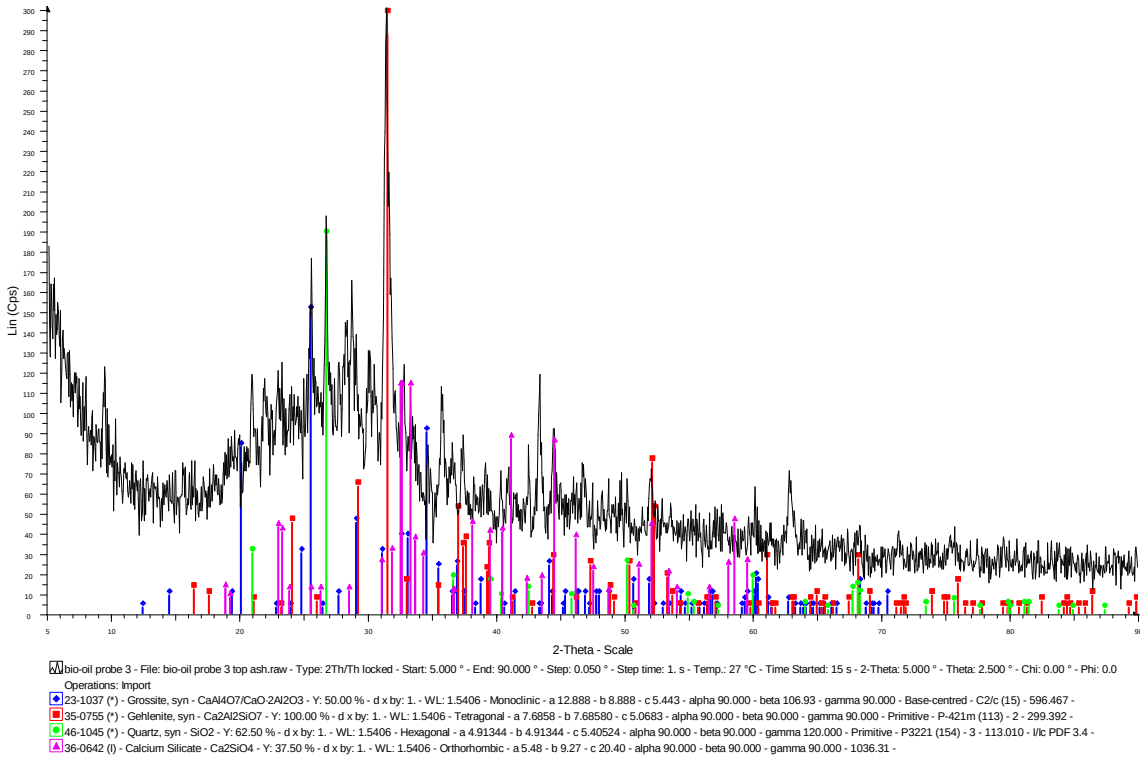

Figure 6.11 XRD patterns of the top deposits from probe 3 with surface temperatures of ~ 500 ^{o}C exposed to combusted bio-oil flue gas stream

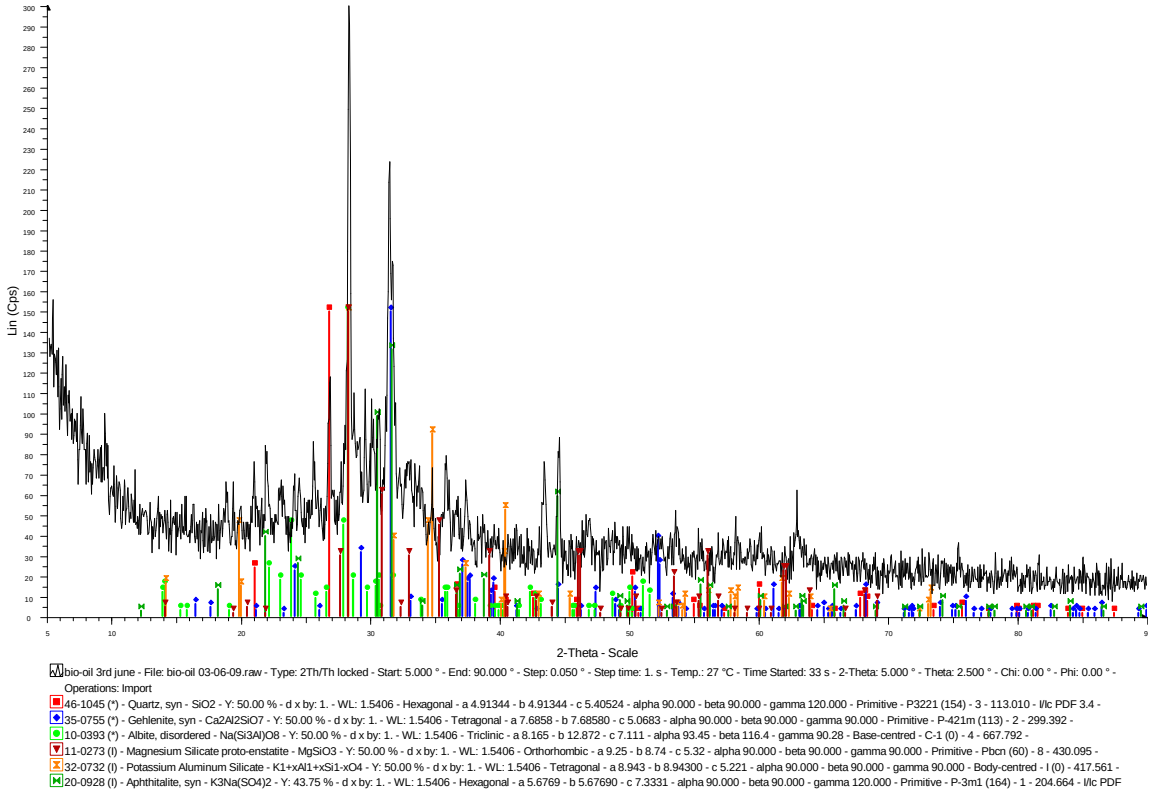

Figure 6.12 XRD patterns of the top deposits from probe 1 with surface temperatures of ~ 700 ^{o}C exposed to combusted bio-oil flue gas stream

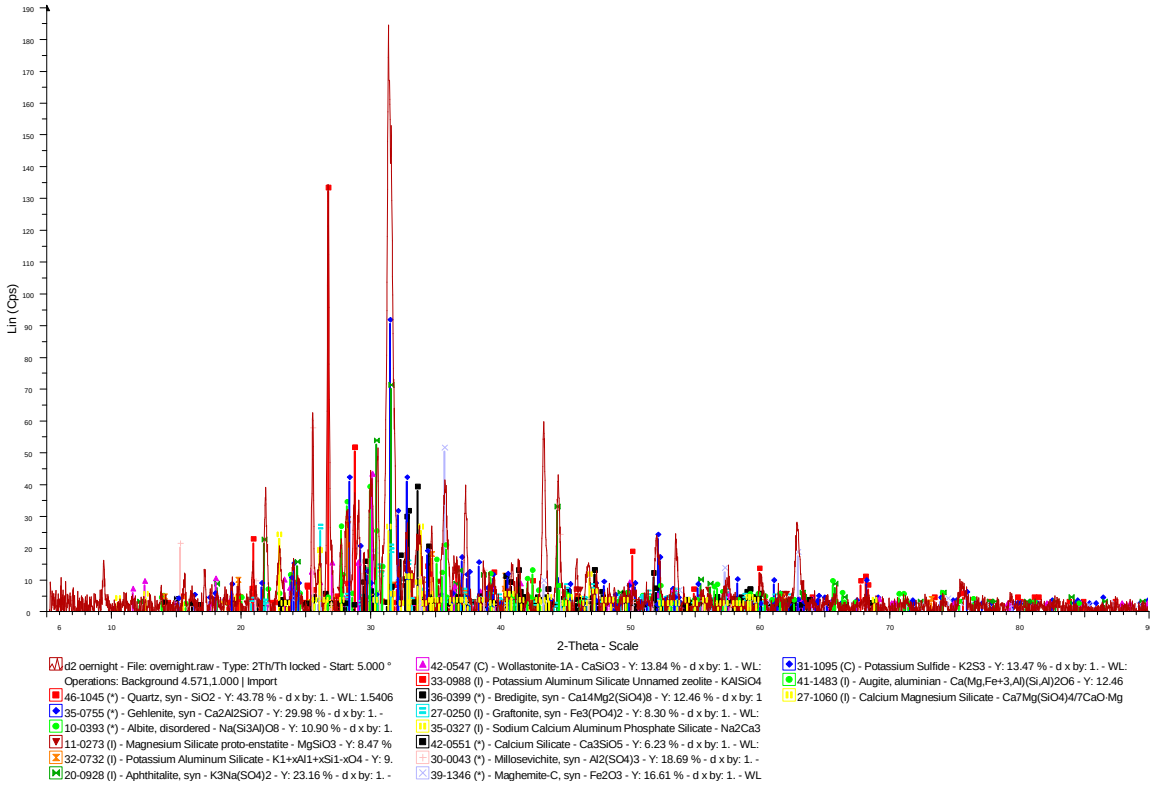

Figure 6.13 XRD patterns (overnight run) of the top deposits from probe 1 with surface temperatures of ~ 700 ^{o}C exposed to combusted bio-oil bio-oil flue gas stream

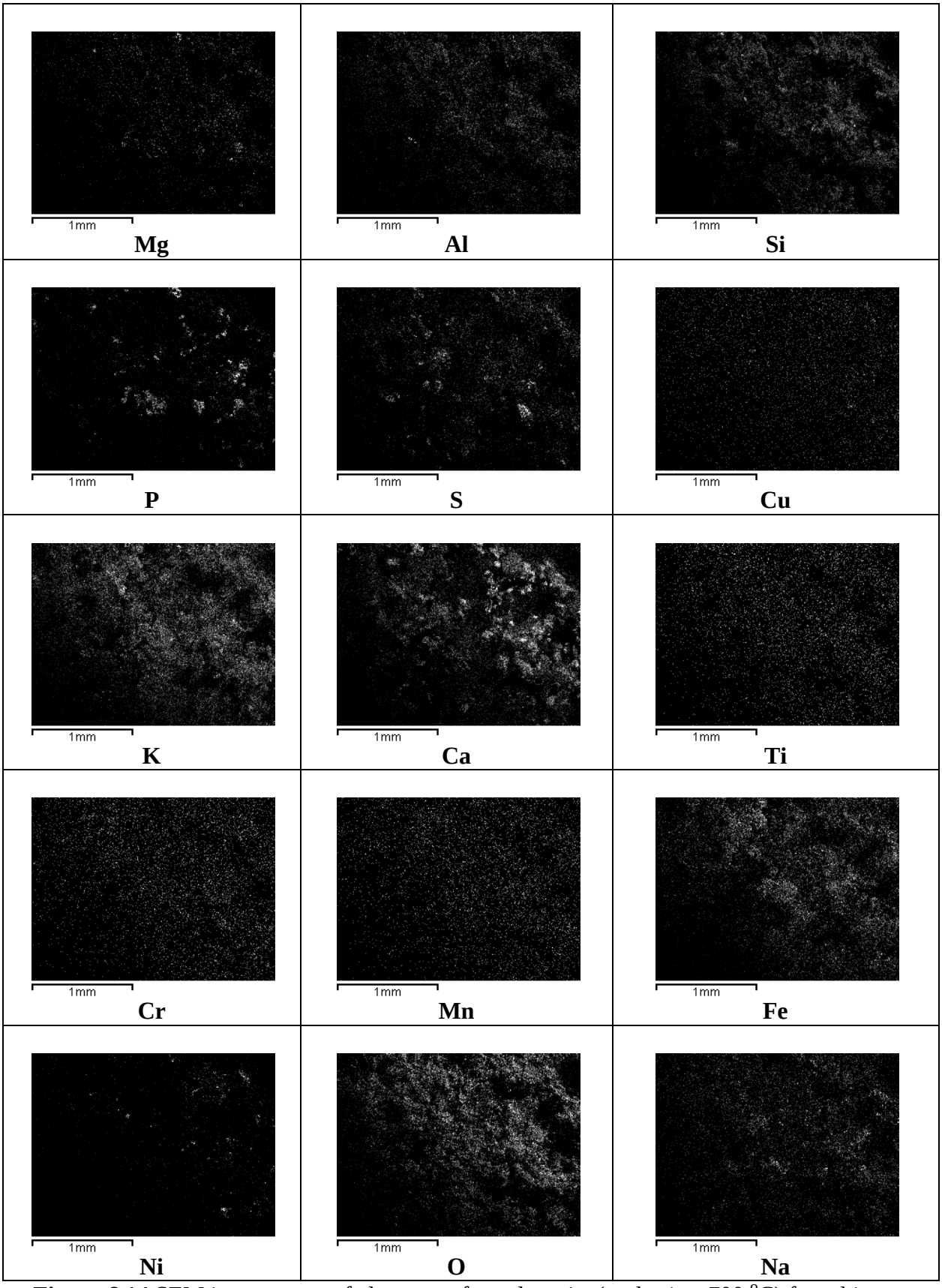

Figure 6.14 SEM images map of elements of top deposits (probe 1, ~ 700 ^{o}C) from bio-oil combustion

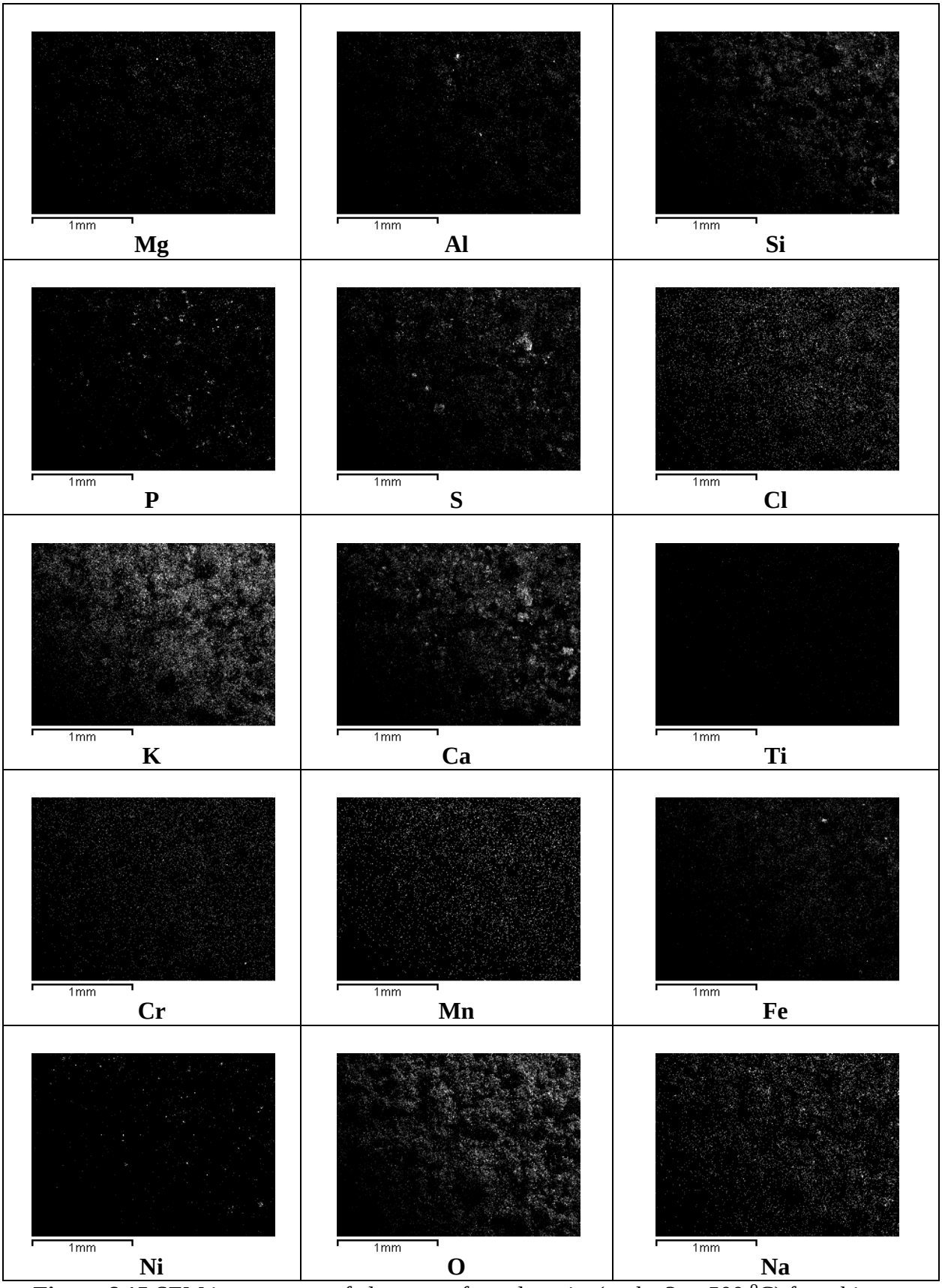

Figure 6.15 SEM images map of elements of top deposits (probe 3, ~ 500 ^{o}C) from bio-oil combustion

6.4 General comments

Combustion of fast pyrolysis bio-oil was carried out in a pilot-scale combustor test rig. The work addressed flue gas emissions and ash deposition as two main issues to study the effect of bio-oil combustion. Both of these issues are important in the area of combustion of biomass for power generation.

The gaseous emissions and deposit compositions collected on an air cooled probes at 500, 600 and 700 °C were assessed. The experimental results compared well with the calculated thermodynamic modeling data.

High combustion efficiency and relatively low ash deposition rates were found during combustion of bio-oil (under continuous feeding rate) and friable deposits were formed that were easy to remove. SEM-EDX indicated that the deposits were mainly Si, Al, K, and Ca with very low Cl levels. XRD analysis showed no formation of alkali chlorides. The experimental work and thermodynamic predictions indicate that the deposits formed have a low corrosion potential.

CHAPTER 7 GENERAL DISCUSSION

7.1 Introduction

In this chapter general trends are identified and discussed for the composition between experimental measurements and modeling predictions for all the fuels and combustions used in this study. General trends between research selected fuels of gaseous and depositions emissions (e.g. evaluation of mixed miscanthus (60 %, wt) with El-cerrejon coal compared to Daw Mill coal and/or miscanthus versus willow combustions) are covered in its related chapters.

7.2 Gaseous emissions model validation

The differences between MTDATA model predictions and experimental data for major gaseous (CO_2, H_2O), minor gaseous (SO_2, HCl, NO) and minor gaseous (NO_2, N_2O) from all combustion/co-firing tests (using PF and FBC) are summarised in Figures 7.1, 7.2 and 7.3, respectively.

The model predictions generally match the experimental trends very well (as mentioned previously, in the results for each fuel). However the model predictions differ from the measured values more for some fuels than others. For pelletised/lump fuels (miscanthus pellets (T19), coppiced willow (T20) and stored pellets OSR (T21-T24)) the difference in predicted and measured gaseous emissions of SO_2, NO, NO_2 and N_2O (see Figures 7.2 and 7.3) are more significant than the difference between the model and experimental data for pulverised and bio-oil fuels combustions. Also, it can be seen that the NO_2 and N_2O are predicted to be lower gaseous level than the measured data for all tests (see Fig. 7.3) with much lower levels of pelletised/lump fuels (using FBC). The possible explanation of this difference between the predicted and measured values could be that the FTIR system in same place in combustion rig, but different combustions being used, PF combustion is much lower than FBC. FBC is further from gas sampling point and gas has longer time to react before getting there, but is hundreds of degrees

cooler. Also, predictions are based on fuel analysis and impossible to estimate accuracy. Moreover, MTDATA calculations were adopted to have the percent volumes of oxygen output of 4.0 %.

The predicted HCl levels were more than the measured values for tests of pure CCP (T3), pure pf miscanthus (T4), stored pellets OSR (T21-T24), whereas predicted levels fall below the measured values for pure El-cerrejon (T1), CCP:El-cerrejon, 20:80 %, wt (T6), CCP:El-cerrejon, 40:60 %, wt (T7), CCP:El-cerrejon, 60:40 %, wt, (T8) and Miscanthus:El-cerrejon, 60:40 %, wt, (T18). For pure Daw Mill (T2), fast pyrolysis bio-oil (T5), miscanthus pellets (T19), coppiced willow (T20), CCP:El-cerrejon, 80:20 %, wt, (T9), blends CCP: Daw Mill (at 20 (T10), 40 (T11), 60 (T12) and 80 (T13) weight %) and blends Miscanthus: Daw Mill (at 20 (T14), 40 (T15), 60 (T16) and 80 (T17) weight %) suggested measurements not affected by predictions. Therefore, from the HCl gaseous emissions investigation, it can be said that the HCl maybe over-predicted when use a pure biomass (in form of pulverised and/or effected by stored conditions) or under-predicted or not be separate when using pure coal and blend mixtures with biomass.

For H_2O and CO_2, a common prediction for all fuels was that the concentration of these gases remained virtually the same between 200-1300 ^oC. Comparing the predictions with the measurements indicates higher levels of CO_2 and lower levels of H_2O for El-cerrejon, blend mixed El-cerrejon with CCP (CCP:El-cerrejon, at 20, 40, 60 and 80 weight %) and Miscanthus:El-cerrejon (60:40 %, wt). However, the prediction model indicated a lower level of CO_2 and higher level of H_2O for Daw Mill, blend mixed Daw Mill with CCP and Miscanthus (CCP:Daw Mill, Miscanthus:Daw Mill, at 20, 40, 60 and 80 weight %) in comparison to measured data (i.e. the opposite trend).

For all pure biomass in form of pellets and pulverised fuels (i.e. except fast pyrolysis bio-oil and coppiced willow) the difference between predicted and measured CO_2 and H_2O levels shows significant trends (Fig. 7.1). These gases were predicted at lower levels for pure fuels of CCP, miscanthus (pf), miscanthus (pellets) and OSR stored pellets, whereas not much differences (with a possibility of small increase of prediction

levels) of CO_2 and H_2O for bio-oil (T5) and coppiced willow (T20) compared to measured values.

For the major gas species a range of factors could have influenced these differences, such as: fuel moisture content could have changed during storage (e.g. OSR pellets and El-cerrejon coal (as author believed that El-cerrejon was stored in different environment for along period, whereas Daw Mill been fired after short period from supplier delivery)); proper mixing of solid fuels particles; residence time; and combustion zone temperature for various combustions technologies [Van Loo and Koppejan, 2008] can expect that the model predictions data levels to be lower than the measured values.

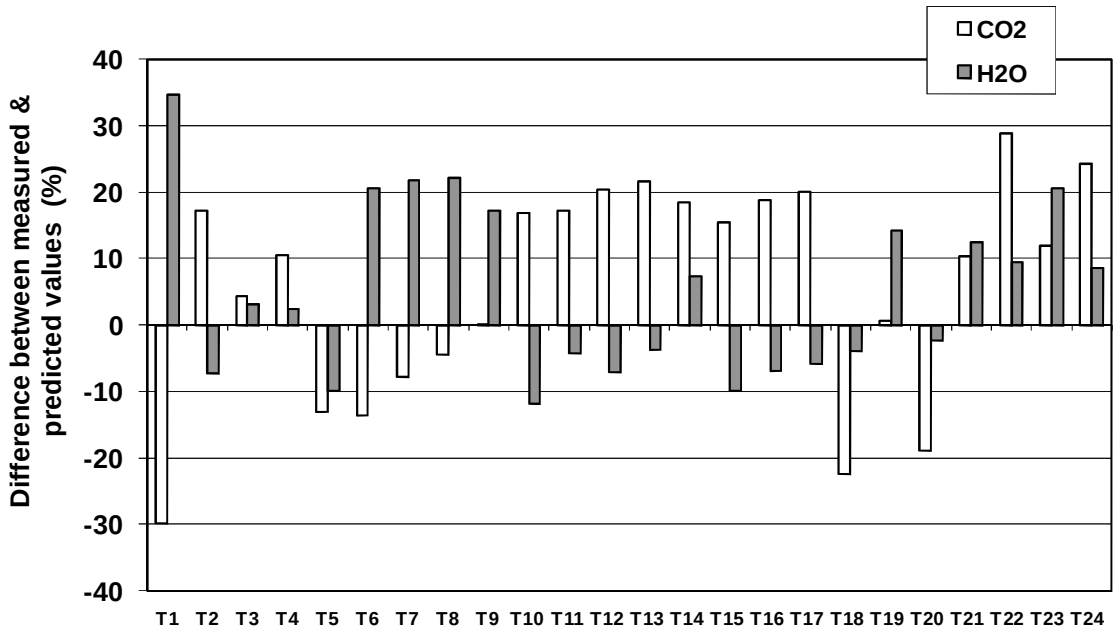

Figure 7.1 Major gaseous emissions for T-series fuels combustions/co-firing: Model predictions and experimental data

Where; T1 (pure El-cerrejon coal), T2 (pure Daw Mill coal), T3 (pure CCP), T4 (pure Miscanthus pf), T5 (pure fast pyrolysis bio-oil), T6 (CCP:El-cerrejon, 20:80 %, wt), T7 (CCP:El-cerrejon, 40:60 %, wt), T8 (CCP:El-cerrejon, 60:40 %, wt), T9 (CCP:El-cerrejon, 80:20 %, wt), T10 (CCP:Daw Mill, 20:80 %, wt), T11 (CCP:Daw Mill, 40:60 %, wt), T12 (CCP:Daw Mill, 60:40 %, wt), T13 (CCP:Daw Mill, 80:20 %, wt), T14 (Miscanthus:Daw mill, 20:80 %, wt), T15 (Miscanthus:Daw mill, 40:60 %, wt), T16 (Miscanthus:Daw mill, 60:40 %, wt), T17 (Miscanthus:Daw mill, 80:20 %, wt), T18 (Miscanthus:El-cerrejon, 60:40 %, wt), T19 (pure miscanthus pellets), T20 (coppiced willow), T21 (OSR 1), T22 (OSR 2), T23 (OSR 3) and T24 (OSR 4)

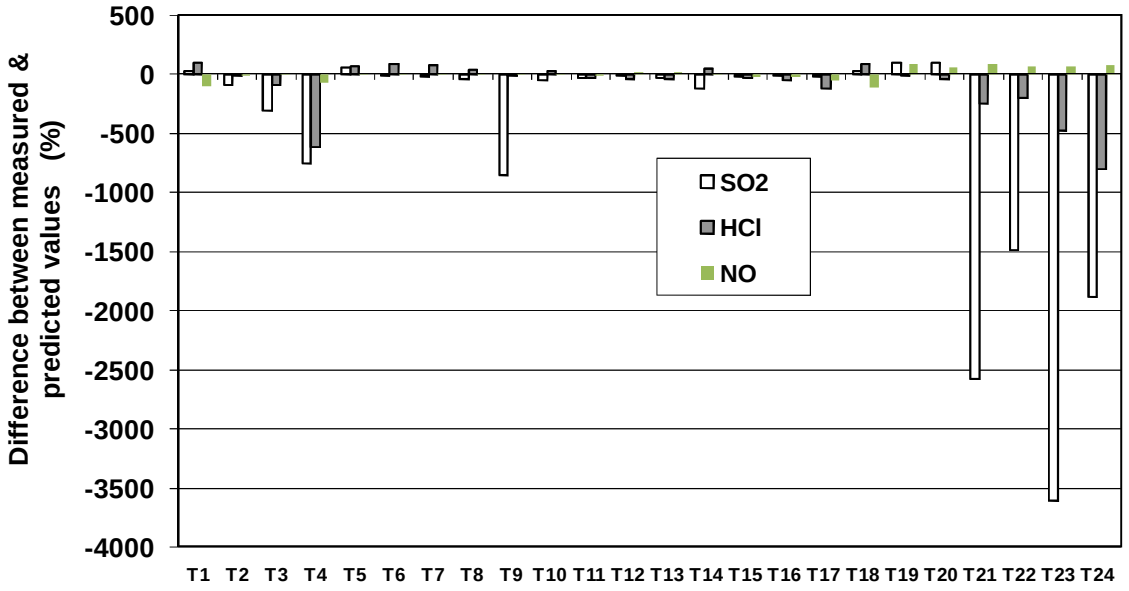

Figure 7.2 Minor gaseous emissions for T-series fuels combustions/co-firing: Model predictions and experimental data

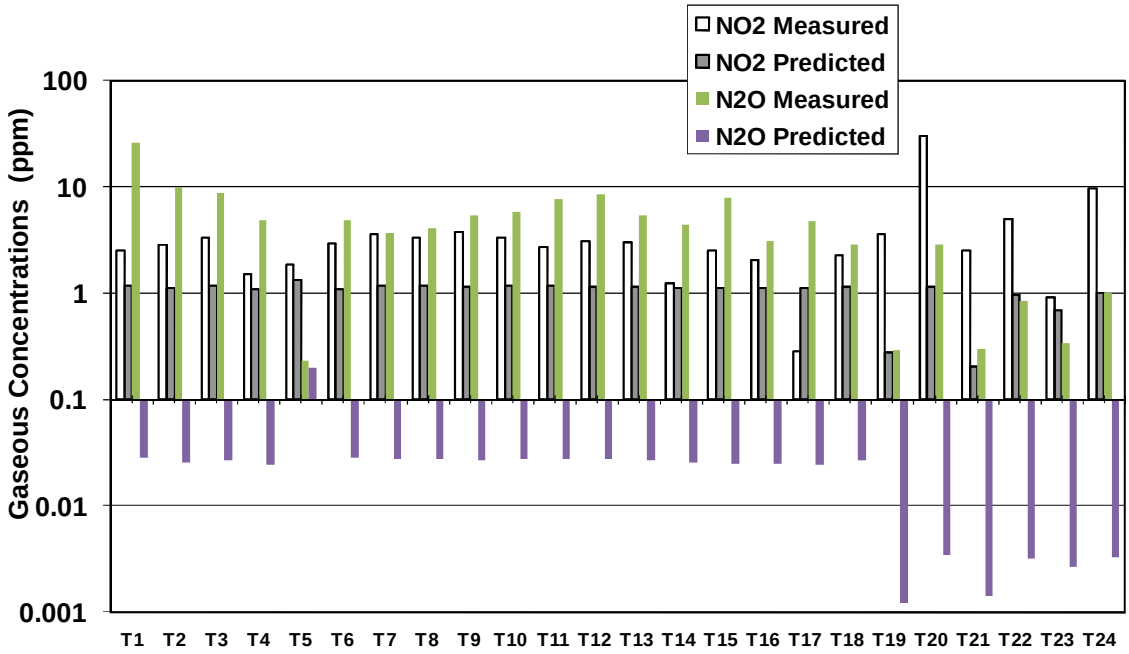

Figure 7.3 NO_2 and N_2O gaseous emissions for T-series fuels combustions/co-firing: Model predictions and experimental data

7.3 Deposition model validation

This section presents general trends observed for the predicted condensed species for the elements C, H, N, O, S, Cl, Na, K, Fe, Ca, Mg, Ti, Ba, Mn, P (listed in Table 3.1, Chapter 3, "15 elements system") compared to the experimental results of deposit compositions. For Ba element, the measured level in PF and FBC for all fuels tests did not exceed any detection limit in any test (as can be seen from SEM-EDX and XRD analysis), so Ba predicted condensed species can be totally validated. Since predicted carbon and nitrogen content of selected condensed species were almost none (see Table 3.1, Chapter 3), so a meaningful comparison/validation could not be made.

Generally the model follows the experimental results well for all fuels (as described in results and discussion chapters). However it was noted that there was a difference between pellet fuels (using FBC) compared to pulverised fuels (using PF). The preferred condensed species predicted for elements S, Cl, Na, K, Fe, Ca, Mg, Ti, Mn, P interactions behaviour were KCl, K_2SO_4, $CaSO_4$, Fe_2O_3, $FeSO_4$, $FeSO_3$, MgO, $MgSO_4$, MnO, $MnSO_4$, Na_2SO_4, K_3PO_4, $NaPO_3$, $CaCO_3$, CaO, $CaFe_2O_4$ and possibly NaCl (dependent on the elements level in the system for various fuels) and these were in agreement with the measured data from deposits collected (as analysed by SEM-EDX, SEM map images and/or XRD). The data can therefore be regarded as partially validating of selected condensed species (Table 3.1, Chapter 3) such as NaOH, H_2SO_4, STi, FeClO, Cl_2H_2MgO, Fe_2MnO_4, CaO_3Ti, MgS, K_2O, KNO_3, MnS_2, P_2S_3, etc., as these no were measured in the fuels combustion flue gas.

Nevertheless, the predictions and measured levels for some element (e.g. Cl) from pelletised/lump fuels were higher compared to pulverised fuels combustion (with respect to element concentrations). For example, pulverised miscanthus, which is categorised as high-K, high-Cl, than miscanthus pellets (see Table 3.6 & 3.8, Chapter 3), the higher concentrations of these elements were condensed on the side surface deposits of the coolest probe (~ 500 ^oC) were 12.6, 5.0 % moles of pulverised miscnathus, respectively, compared to 14.6, 10.8 % moles of miscanthus pellets combustion, respectively. Also, the prediction data indicated higher level of KCl (320-

640 °C) from miscanthus pellets with level of minus $\log_{10}$ 0.73-0.96 moles, compared to condensed KCl (200-580 °C) with level of minus $\log_{10}$ 1.30-2.07 moles, from pulverised miscanthus combustion. Therefore, even with this slight different, it is unlikely that the low predicted and measured values seen in PF compared to FBC for such element, limited the results and/or the model can be validated between these combustion technologies.

7.4 General comments

The outcome of the general comparison between predictions and measurements for gaseous emissions and deposition can be summarised as follows;

- Generally the model follows the experimental results very well for all fuels, both alone and when co-fired.
- Major gaseous emissions of H_2O and CO_2 from fuels will be affected by changes in fuel composition (e.g. during storage); this will mean that the model prediction levels presented will be lower than the measured values.
- The difference between predicted and measured gaseous emissions of SO_2 and HCl for pelletised/lump fuels combustion (in FBC) are more significant than the difference between model and measured data for pulverised and bio-oil fuels combustion.
- NO_2 and N_2O levels are predicted at lower gaseous levels than the measured values for all fuels combustion, with this difference being greatest for the pelletised/lump fuels in FB combustion.
- No significant amount of volatile Ba species was predicted under combustion/co-firing conditions, and none of this element was measured in the flue gases.
- No trends can be classified between deposit model predictions and measurements with fuel compositions or combustion technologies.
- Many of the condensed species available in the database used (e.g. STi, FeClO, Cl_2H_2MgO, etc.) could be omitted from the calculations without affecting the

quality of the predictions as they were only predicted to occur at very low levels and were not detected in the analysis of the deposits.

CHAPTER 8 CONCLUSIONS AND SUGGESTIONS FOR FURTHER WORK

8.1 Conclusions

A series of experiments have been carried out to investigate the combustion/co-firing of a range of fuels. Experimental observations have generated a large amount of data from these fuels in terms of flue gas combustions, deposition fluxes and deposit compositions. These data have been compared to the predictions of fundamental models. The fuels selected are either currently being used in UK power stations (e.g. El-cerrejon coal, Daw Mill coal, CCP), or being promoted by the UK government as energy (e.g. Miscanthus). The ranges of fuel mixes were selected to cover current use through to novel mixes (e.g. co-firing at high levels of biomass).

This project has extended the knowledge base for the behaviour of coal/biomass fuels in co-fired combustion systems. There is no doubt that new energy resources/technologies will have to be developed. The approach of combining model predictions with robust experimental studies has delivered new information on the fuel mixes used in the project and improved understands of their combustion behaviour, gas compositions, deposit compositions and deposition fluxes in such systems.

The most significant conclusions derived from this work presented below.

8.1.1 Experimental

- Preliminary studies led to design and construction of pulverised and liquid feeding systems. These feeding systems (and that for feeding for pellets/lumps fuels) were optimised with respect to precision and repeatability. Replicated combustion/co-firing preliminary tests for both solid and liquid fuels identified

outstanding issues/errors and provided a typical operating procedure for robust control of the combustion rigs (PF and FBC).

- The two main analytical methods were studied using:
  (a) FTIR for gaseous emissions (CO_2, O_2, H_2O, SO_2, CO, NO, NO_2, N_2O, HCl, HF)
  (b) SEM-EDX and XRD for analysis the deposits samples collected from the flue gas stream on air cooled probes with surface temperature set to 500 °C, 600 °C and 700 °C,

  allowed the study of this two main issues of the experimental concern during combustion/co-firing of the selected fuels.
- No operational/feeding problems were found for most of the fuels. The exception was miscanthus pellets where performance varied with bed composition. A bed of silica sand resulted in agglomeration and variable combustion performance, whereas a bed of silica sand mixed with 50 wt % limestone produced stable performance and no agglomeration.
- High combustion efficiency were found for all fuels (pure and mixes) combustions due to low CO measurements.
- Overall, the major gaseous emissions of H_2O and CO_2 from the combustion of all the fuels were consistent with the predictive calculations from CP and MTDATA. However, the outcomes of some experiments (e.g. CCP:El-cerrejon coal mixtures) showed a variations from which the most likely explanations are:
  (a) Fuel moisture content may affected/changed during storage,
  (b) Residence time and/or combustion zone temperature,
  (c) The cooling effects of excess air.
- The measured minor gaseous species of SO_2, HCl and NO_x were also consistent with the prediction made using the models. The data obtained in this study highlights the following:
  - The SO_2 concentrations are high in pure coal combustions compared with pure biomass (which is expected for coal and biomass based fuels) and showed that the levels decreased as the biomass share with coal increased. Also, SO_2 gas concentrations were shown to decrease as the oil seed rape storage of the pellets increased.

- Higher HCl released in low share biomass coal co-firing. For oil seed rape pellets storage study, the HCl concentrations were shown to decrease as the storage of the pellets increased.
- The NO_x output suggests that the major source of NOx in flue gas is from fuel-N and remained stable during fuels combustion/co-firing, except:
  (a) Miscanthus:Daw Mill mixtures, which suggested a small decrease in NO as the biomass share increased; and, (b) OSR stored pellets combustion which showed variations with no particular trend.

- Generally, the highest deposition fluxes formed at surface temperatures of ~ 500 ^{o}C for all combusted fuels. Analyses and observations proved that larger particle sizes were found in the top surface deposits (i.e. represented upstream deposit build up); which support their arrival by the direct inertial impaction mechanism. Analyses is of the side-stream and downstream deposits suggested more condensation and/or thermophoresis mechanisms, as reported by previous authors. Observations of the deposition fluxes of the selected fuels combustion enable the following conclusions:
  - Deposition from fast pyrolysis bio-oil and coppiced willow combustion formed at the lowest fluxes compared to other fuels, so it is suggested that these are unlikely to cause deposition problems.
  - Deposition fluxes were found to vary between El-cerrejon coal and Daw Mill coal mixed with CCP and/or miscanthus, this shows that it is important to carry out such combustion/deposition evaluations for mixes of each specific fuel.
- Deposit compositions in general reveal varying concentrations of silicon, calcium, sulphur, potassium, phosphorus, sodium, iron and aluminium in the deposits from all probes. For example, high concentrations of potassium or calcium and sulphur suggest formation of potassium or calcium sulfates. The EDX analyses maps of elements were more successful in identify these types of compounds and others than XRD analysis (as they may be present in amounts that were below the detection limits of this equipment). Observations of deposit compositions and Cl distrbution (as this is a highly fouling element leading to corrosion of boiler components) enable the following conclusions:

  - The presence of Cl in the deposits was found on probes (in particular at ~ 500 ^{o}C) for all pure biomass combustion with the lowest levels suggested in fast pyrolysis bio-oil combustion.
  - CCP or miscanthus co-fired with Daw Mill coal, the Cl was only detected at higher shares (≥ 80 %) whereas, mixed biomass with El-cerrejon coal may suggest small Cl contents at lower % share of biomass.
  - Analysis of the deposits compositions suggest that OSR stored for 6 and 12 months were similar to each other but different to deposits from OSR stored for 1 and 3 months.
- Technology relevance: comparing PF with FBC conditions (related to deposition flux), for example miscanthus produced higher deposition fluxes in FBC conditions. However, it is believed that in this effect will be fuel composition specific. This will have an effect on other aspects of plant operation (e.g. corrosion, heat transfer) but these are beyond the scope of this project.

8.1.2 Modelling

- Combustion product and heat generation prediction models were evaluated for all the fuels and mixes tested. A spreadsheet was constructed and information such as fuel composition, air and gas compositions, feeding rate were used to make predictions. These were compared to measurements obtained from the experiments carried out.
- Preliminary studies of thermodynamic calculations (MTDATA) led to the creation of lists of potential compounds in both the gaseous and condensed states for each element included in the calculations. This was a necessary first step as the software databases contain many possible compounds that are unlikely to form, and so would require MTDATA to effectively calculate zero values for and hence run for very long periods. Therefore, the compounds that were found not to form in initial trial runs were eliminated as potential outputs from subsequent calculations.

- Preliminary studies of MTDATA, also revealed that the model under "15 elements system" of elements C, H, N, O, S, Cl, Na, K, Fe, Ca, Mg, Ti, Ba, Mn and P lead to more realistic model outputs compared to an "8 elements system" (C, H, N, O, S, Cl, Na, K) and "17 elements system" (C, H, N, O, S, Cl, Na, K, Fe, Ca, Mg, Ti, Ba, Mn, P, Al, Si).
- Preliminary studies of the sensitivity of the MTDATA calculations to excess air with combustion process showed that the compound outputs were identical with excess air variation (with respect to the levels of these compounds).
- The heat losses (from HP spreadsheet) from all fuels combustion were in the range expected for experimental scale of the combustion test rigs used.
- NO_2 and N_2O levels are predicted at lower gaseous levels than the measured values for all fuels combustion with much lower levels of pelletised/lump fuels (FBC combustions).
- No significant amount of volatile Ba species was predicted at the combustion/co-firing conditions, and none of this element was measured in the flue gas.
- Many of the condensed species available in the database used (e.g. STi, FeClO, Cl_2H_2MgO, etc.) could be omitted from the calculations without affecting the quality of the predictions (as well as compounds eliminated initially from calculations under MTDATA preliminary study investigations), as they were only predicted to occur at very low levels and were not detected in the analyses of the deposits.

8.2 Technological implications

- Could limit co-firing by considering:
  (a) Total deposition flux as it will reduce heat transfer;
  (b) Alkali deposition (especially Cl) due to effect on corrosion
  The detailed data in this thesis shows that these effects are coal and biomass mix specific.
- Experimental testing will is needed to determine the optimum operating conditions (using PF and/or FBC) for any particular fuel mixes.

- The choice of the feeding method may often to be a key factor in the design of PF to handle biomass as a fuel. The biomass material (alone or high blends with coal) must be capable of being fed in such way (in respect to the appreciate sizing of the fuel) for its combustion to be completed to an acceptable degree.
- Such materials (e.g. miscanthus) which classified vary enormously in their properties either naturally (i.e. harvest) or manufactured (e.g. using pellets with varies binders) can be difficult to burn in FBC. Possible causes might be agglomeration or sintering of the bed particles.
- When PF is equipped for bio-oil firing (as one of the multi-fuel firing options), a flow of bio-oil transport air must be maintained during operating period irrespective of whether the fuel actually is fired or not. This provision is necessary to keep the oil feed nozzles cool at all times and to prevent their blockage.
- Where the top of the bio-oil nozzles protrude slightly into the hot zone of a combustor, good operation and maintenance will be needed to avoid conditions where the bio-oil can become either immobile or over heated.
- Trace heating of the bio-oil supply tube, temperature to ~ 35 ^{o}C should be used as a method for controlling the fast pyrolysis bio-oil viscosity.
- The absorption of minor elements by combustor gas path materials of construction may be significant (e.g. Ca & P condensed species), and must be considered when applying MTDATA modelling and experimentally-derived measurements for scale up to a commercial plant that will accumulate extended periods of operation.

8.3 Suggestions for further work

- Biomass materials that might be considered as combustion feedstocks (with careful consideration of fuel properties, in particular fuel alkali and chlorine levels, when extending the results of this study to other fuels) with potential of co-firing with high share of biomass with coal should be one area of investigation.

- An essential of accuracy calibrated test facilities with known repeatability and control feeding systems, sample preparation requirement for satisfactory combustions/analysis in any new feedstock.
- The promising studies on OSR stored pellet combustion should be extended to investigate the effects of longer or shorter periods for either raw material storage and/or pellet storage on gaseous and depositions emissions.
- Combustion of energy crops (miscanthus, willow) of various fuel properties (e.g. affected by agricultural practices) are recommended due to varying alkali absorption.
- To further investigate of gaseous emissions and deposition of the selected fuels in pilot scale PF and FBC under a variety of significant conditions such as oxyfuel firing and/or combustion of biomass with additives.
- The MTDATA software and the SGTE database has been used to predict the levels of 17 elements (C, H, N, O, S, Cl, Na, K, Fe, Ca, Mg, Ti, Ba, Mn, P, Al, Si) after combustion by the creation of lists of potential compounds (in gaseous and condensed states) for each of the elements in the selected fuels. The validity of this approach should be confirmed for other biomass fuels; this would determine any missing compounds, the significant levels of the elements involved and the sensitivity of the method on wide range of fuels.
- A further search should be made for the thermodynamic data on the species include extra trace elements in particular Ni, Cu, Cr, Pt, Pb, W and Zn as these were found on deposits for some selected fuels combustions. This may provide information on reactions between the flue gas stream and the materials of construction of the combustion rigs, as well as MTDATA model validation.
- The development of a model for the systematic prediction of deposition fluxes based on selected fuels and combustion conditions for comparison with the experimental deposition flux measurement made in this thesis would be useful for modelling validation.
- Experimental methods of identifying the formation of the species predicted by thermodynamic equilibrium calculations should be explored. The application of deposits probes set at wide range surface temperatures and/or fly ash collected

from different positions on the combustor rig (with improved sampling protocol). Studies on cyclone deposits/ash may be useful in this respect.

- The technique for collecting probe deposits technique could be an area of investigation. Collecting samples using a fine brush occasionally makes it difficult to control (in particular if the amount of deposits very little) which may effect the depositions flux calculations. Alternative methods of deposit collection should be investigated. In addition, investigation of deposits build-up during combustion (e.g. using CCD camera to take pictures) could be a useful identification of deposition formation around the probe (e.g. condensation mechanisms).
- Further study should be carried out of the economics of using the biomass fuels selected for this project. The process starts with reception of biomass fuel and ends with delivery of an end product (such as electricity). This will suggests challenges and/or benefits facing the fuels selected that relate to combustion technology and its applications.

REFERENCES

Allan, S. E., Erickson, T. A., McCollar, D.P. (1996). "Modelling of ash deposition in the convective pass of a coal-fired boiler", in Benson, S. A. (Editor), Applications of Advanced Technology to Ash-Related Problems in Boilers at Waterville Valley, NH; Plenum Press, New York, NY, pp. 451-470.

Alonso-Herranz, E., Spliethoff, H. (2009). Investigation of agglomeration behaviour of rye and wheat straw during FBC combustion. Proceedings of the 17th European Biomass Conference and Exhibition, pp. 1282-1287.

Andersen, K. (1998). Deposit formation during coal-straw co-combustion in a utility PF-boiler. PhD thesis, Technical University of Denmark.

Artos, V., Pis, J.J., Fuertes, A.B., Hoffman, J., Marban, G., Canibano, J. (1991). Fluidised bed combustion of high ash Spanish coals. Clean Energy for the World: Proceedings of the 11th International Conference on Fluidised Bed Combustion, Montreal, Canada, pp. 1407-1413.

Backreedy, R.I., Jones, J.M., Pourkashanian, M., Williams, A. (2004). Burn-out of pulverised coal and biomass chars. Fuel, V., 82, 2097-2105.

Bain, R.L., Overend, R.P., Craig, K.R. (1998). Biomass-fired power generation. Fuel Processing Technology, V., 54, 1-16.

Bapat, D.W, Kulkarni, S.V, Bhandarkar, V.P. (1997). "Design and operating experience on fluidised bed boiler burning biomass fuels with high alkali ash, In: Proceedings of the 14th International Conference on Fluidised Bed Combustion, Preto, F.D.S. (Editor), Vancouver, New York, pp. 165-74.

Baronet, J.M. (1983). ALEX Software, Laboratoire de Chimie des Plasmas, University of Limoges, France.

Barry, T.I., Chart, T.G. (1989). "New approach to materials design: calculated phase equilibria for composition and structure control", in: Bullock, E. (Editor), R & D of High Temperature Materials for Industry, Elsevier, Barking, pp. 565-592.

Bartolome, C., Ramos, I., Gil., A. (2009). "Ash deposition in co-firing using cynara biomass residues with coal in a PF pilot plant", in Proceedings of the 17th European Biomass Conference and Exhibition, Hamburg, Germany, pp.1230-1237.

Baxter, L.L. (1993). Ash deposition during biomass and coal combustion: a mechanistic approach. Biomass and Bioenergy, V., 4, 85-102.

Baxter, L.L. (1995). Biomass coal co-combustion: opportunity for affordable renewable energy. Fuel, V., 84, 1295-1302.

Baxter, X.C, Gudka, B., Gao, Y., Darvell, L.I., Jones, J.M, Barraclough, T., Yates, N.E., Shield, I. (2009). The influence of inorganic constituents in miscanthus combustion. Proceedings of the 17th European Biomass Conference & Exhibition, pp. 1288-1293.

Baxter, L.L, Desollar, R.W. (1993). A mechanistic description of ash deposition during pulverised coal combustion: predictions compared with observations. Fuel, V., 72, 1411-1418.

Baxter, L.L., Miles, T.R., Jenkins, B.M., Milne, T., Dayton, D., Bryers, R.W., Oden, L.L. (1998). The behaviour of inorganic material in biomass-fired power boilers: field and laboratory experiences. Fuel Processing Technology, V., 54, 47-78.

Baxter, L.L, Miles, T.R, Miles, T.R.J., Jenkins, B.M., Dayton, D.C., Milne, T.A., "et al". (1996). Alkali deposits found in biomass boilers: the behaviour of inorganic material in biomass-fired boilers- field and laboratory experience. Sandia National Laboratories, Report SAND96-8225 Vol. II.

Baxter, L.L., Tree, D., Fonseca, F., Lucas, W. (2003). Biomass combustion and co-firing issues overview: alkali deposits fly ash, NO_x/SCR impacts, presented at the: International Conference on Co-utilisation of Domestic Fuels, Gainesville, FL, USA.

Beer, J.M., Sarofim, A.F., Barta, L.E. (1992). "From coal mineral matter properties to fly ash deposition tendencies: a modelling route", in: Benson, S. A. (Editor), Inorganic Transformations and Ash Deposition During Combustion Engineering Foundation Press, New York, NY, 71-87.

BERR, (Department of Business, Enterprise and Regulatory Reform). (2007). UK Energy in Brief: A national statistics publication (at:http://www.dti.gov.uk /energy/sources/renewables/index.html), "accessed on 16/05/2009".

Benson, S.A., Hurley, J.P., Zygarlicke, C.J., Steadman, E.N., Erickson, T.A. (1993). Predicting ash behaviour in utility boilers. Energy and Fuels, V., 7, 746-754.

Blander, M., Milne, T., Dayton, D., Backman, R., Blake, D., Kuhnel, V., Linak, W., Nordin, A., Ljung, A. (2001). Equilibrium chemistry of biomass combustion: a round-robin set of calculations using available computer programs and databases. Energy and

Fuels, V., 15, 344 – 349.

Boylan, D., Bush, V., Bransby, D.I. (2000). Switchgrass co-firing: pilot-scale and field evaluation. Biomass and Bioenergy, V., 19, 411-417.

Bradshaw, A., Simms, N.J., Nicholls, J.R. (2008). Passage of trace metal contaminants through hot gas paths of gas turbines burning biomass and waste-fuels. Fuel, V., 87, 3529-3536.

Bridgwater, A.V. (2009). "Fast pyrolysis of biomass", in: Bridgwater, A.V., Hofbauer, H., Van Loo, S., (Editor), Thermal Biomass Conversion, CPL Prees, Newbury, Berks, UK.

Bridgwater, A.V., Kuester, J.L. (1991). Research in thermochemical biomass conversion. Elsevier Science Publishers, London.

Bridgwater, A.V., Peacock, G.V.C. (2000). Fast pyrolysis process for biomass. Renewable and Sustainable energy Reviews, V., 4, 1-73.

Brunner, T., Obernberger, I., Brouwers, J.J.H., Preveden, Z. (1998). Efficient and economic dust separation from flue gas by the rotational particle separator as an innovative technology for biomass combustion and gasification plants. Proceedings of the 10th European Bioenergy Conference, Würzburg, Germany, CARMEN, Rimpar, Germany.

CCC, (Committee on Climate Change). (2008). Building a low-carbon economy - the UK's contribution to tackling climate change. "accessed on 11/07/2010". (at:http://www.theccc.org.uk/reports/building-a-low-carbon-economy).

Christensen, K.A. (1995). The formation of submicron particles from the combustion of straw. PhD thesis, Department of Chemical Engineering, Technical University of Denmark.

Cleve, K. (1999). Latest developments and status of long term experience in CFB technology. Proceeding 15th ASME Conference on Fluidised Bed Combustion.

Collura, S., Azambre, B., Finqueneisel, G., Zimny, T., Weber, J.V. (2006). Miscanthus-Giganteus straw and pellets as sustainable fuels a combustion and emission tests, Environmental Chemistry Letters, V., 4, 75-78.

Daniel, P.L. (1991). "Corrosive species in RDF-fired boilers", Paper No.1, in: Leavy, A.V. (Editor), Corrosion-Erosion-Wear of Materials at Elevated Temperatures, NACE.

Davies, R.H., Dinsdale, A.T., Gisby, J.A. (2002). MTDATA – Thermodynamic and

phase equilibrium software from the national physical laboratory. Calphad, V., 26, 229-271.

Davies, R.H., Dinsdale, A.T., Gisby, J.A., Robinson, J.A.J. (2005). MTDATA-Application interface programming guide. National Physical Laboratory, Teddington, Middlesex, UK.

DECC, (Department of energy and climate change). (2009). Heat and energy saving strategy. Available at: http:decc.gov.uk/consultations/., "accessed on 06/12/2009".

Defra online website. Energy Crops Scheme. Available at: http://www.naturalengland.org.uk/ourwork/farming/funding/ecs/default.aspx, "accessed 17/08/ 2010".

De Jong, W. (2005). Nitrogen compounds in pressurised fluidised bed gasification of biomass and fossil fuels. PhD Thesis, Delft University of Technology.

Demirbas, A. (2003). Combustion characteristics of different biomass fuels. Progress in Energy and Combustion Science, V., 30, 219-230.

Demirbas, A.H., Demirbas, I. (2007). Importance of rural bioenergy for developing countries. Energy Conversion and Management, V., 48, 2386-2398.

Dinsdale, A.T., Hodson, S.M., Barry, T.I., Taylor, J.R. (1989). Computer software in chemical and extractive metallurgy. Pergamon Press, Oxford, 59-74.

Easterly, J.L., Burnham, M. (1996). Overview of biomass and waste fuel resources for power production. Biomass Bioenergy, V., 10, (2-3), 79-92.

EBA, (European Biomass Association). (2000). Wood pellets in Europe. State of the Art, Technologies, Activities, Market. Thermie B DIS/2043/98-AT, Industrial Network on Wood Pellets. Available at: http://www.energyagency.at/(en)/puble/pdf/pellets_net_en.pdf, "accessed 09/10/ 2009".

Ekmann, J.M, Smouse, S.M, Winslow, J.C, Ramezan, M., Harding, N.S. (1996). Co-firing of coal and waste. IEA Coal Research Report, IEACR/90, London.

European Bioenergy Networks (EUBIONET). (2005). Biomass co-firing – an efficient way to reduce greenhouse gas emissions. Available at:http://ec.europa.eu/ energy/res/sectors/doc/bioenergy/cofiring_eu_bionet.pdf), "accessed 05/06 2008

European Commission (EC). (2006). Co-firing of biomass with coal: constraints and role of biomass pre-treatment. Available at:http://ie.jrc.ec.europa.eu/publications

/scientific_publications/2006/EUR22461EN.pdf, “accessed 12/08/ 2007”.

(EREC), (European Renewable Energy Council). (2000). Renewable energy target for Europe.

Frandsen, F., Dam-Johansen, K., Rasmussen, P. (1994). Trace Elements from combustion and gasification of coal an equilibrium approach. Progress Energy Combustion Science, V., 20, 115-138.

Frontline Bio-energy Inc. What is biomass. Available at:http://www.frontlinebioenergy.com/id15.html. “accessed 14/03/ 2010”.

Fryda, L., Panopoulos, K., Vourliotis, P., Pavlidou, E., Kakaras, E. (2006). Experimental investigation of fluidised bed co-combustion of meat and bone meal with coals and olive bagasse. Fuel, V., 85, 1685-1699.

Furimsky, E., Zheng, L. (2003). Qualification of chlorine and alkali emissions from fluid bed combsution of coal by equilibrium calculation. Fuel Processing Technology, V., 83, 7–21.

Gavin, D.G. (1993). NO_x: basic mechanisms of formation and destruction and their application to emission control technologies. Proceedings; Imperial College of Science, London, UK.

Gibbs, B.M, Thompson, D., Argent, B.B. (2008). Mobilisation of trace elements from as-supplied and additionally cleaned coal: Predictions for Ba, Be, Cd, Co, Mo, Nb, Sb, V and W. Fuel, V., 87, 1217-1229.

Granada, E., Lareo, G., Miguez, J.L., Moran, J., Porteiro, J., Ortiz, L. (2006). Feasibility study of forest residue use as fuel through co-firing with Pellet. Biomass and Bioenergy, V., 30, 238-246.

Green, J.H. (1994). Trends and outlook for biomass energy. Energy engineering, V., 91(5), 18-28.

Grubor, B.D., Oka, S.N., Ilic, M.S., Dakic, D.V, Arsic, B.T. (1995). Biomass FBC combustions bed agglomeration problems. Proceedings 13th International Conference Fluidised Bed Combustion, V., 1, 515-522.

Gogebakan, Z., Gogebakan, Y., Selcuk, N., Selcuk, E. (2009). Investigation of ash deposition in a pilot-scale fluidised bed combustor co-firing with lignite. Bioresource Technology, V., 100, 1033-1036.

Goni, Ch., Helle, S., Garcia, X., Gordon, A., Parra, R., Kelm, U., Jimenez, R., Alfaro, G. (2003). Coal blend combustion: fusibility ranking from mineral matter

composition. Fuel, V., 82, 2087-2095

Gottwald, U., Monkhouse, P., Wulgaris, N., Bonn, B. (2002). In-situ study of the effect of operating conditions and additives on alkali emissions in fluidised bed combustion. Fuel Processing Technology, 75, 215–226

Gulyurtlu, I., Crujeira, A.T., Abelha, P., Cabrita, I. (2007). Measurements of dioxin emissions during co-firing in a fluidised bed. Fuel, V., 86, 2090-2100.

Hald, P. (1994). Alkali metals at combustion and gasification equlibrium calculations and gas phase measurements. PhD thesis, Technical University of Denmark.

Hall, D.O., Overend, R.P. (1987). Biomass Regenerable Energy. John Wiley & Sons Ltd. Chichester, UK.

Hansen, P.F.B., Andersen, K.H., Wieck-Hansen, K., Overgaard, P., Rasmussen, I., Frandsen, F.J., Hansen, L.A., Dam-Johansen, K. (1998). Co-firing straw and coal in a 150-MWe utility boiler: in-situ measurements. Fuel Processing Technology, V., 54, 207-225.

Hein, K.R.G., Bemtgen, J. M. (1998). EU clean coal technology: co-combustion of coal and biomass. Fuel Process Technology, V., 54, 159-169

Henderson, P., Szakalos, P., Pettersson, R., Anderson, C., Hogberg, J. (2006). Reducing superheater corrosion in wood-fired boilers. Materials and Corrosion, V., 57, 128-134.

Hernandez-Atonal, F.S., Ryu, C., Sharifi, V.N., Swithenbank, J. (2007). Combustion of refuse-derived fuel in a fluidized bed. Chemical Engineering Science, V., 62, 627-635.

Hossain, A.K.M.S. (2005). A Model for sustainable biomass electricity generation in Bangladesh. PhD thesis, Cranfield University, UK.

Howard, J.R. (1983). Fluidised beds combustion and application. Applied Science Publishers Ltd. London, UK.

Howe, W.C., Divilio R.J. (1993). Fluidised bed combustion experience with alternative fuels. Proceedings of Strategic Benefits of Biomass and Waste Fuels, Electric Power Research Institute (EPRI-TR), California, pp. 103-146.

Huang, Z., Conway, P.P., Thomson, R.C., Dinsdale, A.T., Robinson J.A.J. A. (2008). Computational interface for thermodynamic calculations software MTDATA. Computer Coupling of Phase Diagrams and Thermochemistry, V., 32, 129-134.

Huang, L.Y., Norman, J.S., Pourkashanian, M., Williams, A. (1996). Prediction of ash deposition on superheater tubes from pulverised coal combustion. Fuel, V., 75, 271-279.

Hughes, E. E., Tillman D.A. (1998). Biomass co-firing: status and prospects. Fuel Process Technology, V., 54, 127-142.

IEA, (International Energy Agency). (2003). Biogas upgrading and utilisation. IEA Bioenergy (b), Task 24, Available at: http://www.iea.org.

IEA, (International Energy Agency). (2007). Bio-energy project development and biomass supply. Available at: http://www.iea.org.

IWM, (Institute of Wastes Management). (1998). Anaerobic digestion. UK.

Japanese Society of Thermo-heat Measurement, Thermodynamic data base MALT 2. (1992). The Japanese Society of Thermo-heat Measurement. Kagakugijutsusha.

Jensen, P.A., Sander, B., Dam-Johansen, K. (2001). Pretreatment of straw for power production by pyrolysis and char wash. Biomass & Bioenergy, V., 20, 431-446.

Johnsson, J. E., Dam-Johansen, K. (1991). Formation and redection of NO_x in a fluidised bed combustor. Proceedings of the 11th International Conference on Fluidised Bed Combustion (Montreal, Canada); ASME: New York, 1991; p 1389-1396.

Kagaku Gijutsu-Sha, K. (1992). Thermodynamic data base MALT 2. The Japanese Society of Thermo-heat Measurement.

KaKauppinen, E., Lind, T., Kurkela, J., Latva-Somppi, J., and Jokiniemi, J. (1998). “Ash particle formation mechanisms during pulverised and fluidised bed combustion of solid fuels”, in Ashes and Particulate Emissions from Biomass Combustion, V., 3 of Thermal Biomass Utilization series, BIOS, Graz, Austria.

Kaufmann, H., Nussbaumer, Th., Baxter, L., Yang, N. (2000). Deposit formation on a single cylinder during combustion of herbaceous biomass. Fuel, V., 79, 141-151.

Karlsvik, E., Hustad, J.E., Skreiberg, O., Sonju, O.K. (1993). Greenhouse gas and NO_x emissions from wood-stoves. Energy, Combustion and the Environment, Gordon and Breach, V., 2, 539-550.

Klass, D.L. (1998). Biomass for renewable energy. Fuels and Chemicals, Academic Press, London, UK.

Krumdieck, S.P., Daily, J.W. (1998). Evaluating the feasibility of biomass pyrolysis oil

for spray combustion applications. Combustion Science and Technology, V., 134, 351-365.

Lai, W.C., Krieger-Brockett, B. (1992). Volatiles release rate and temperatures during large particle refuse derived fuel-Municipal solid waste devolatilisation. Combustion Science Technology, V., 85, 133-149.

Larkin, S., Ramage, J., Surlock, J. (2004). "Bioenergy", in: Renewable Energy Power for a Sustainable Future, Boyle, G., (Editor), Oxford University Press, UK, pp. 105-146.

Leckner, B., Karlsson, M. (1993). Gaseous emissions from circulating fluidised bed combustion of wood. Biomass and Bioenergy, V., 4, 379-389.

Lee, F.C.C., Riley, G.S., Lockwood, F.C. (1996). "Prediction of ash deposition in pulverised coal combustion systems", in: Benson, S. A. (Editor), Applications of Advanced Technology to Ash-Related Problems in Boilers at Waterville Valley, NH, Plenum Press, New York, NY, pp. 637-667.

Lind, T. (1999). Ash formation in circulating fluidised bed combustion of coal and solid biomass. VTT Publication, V., 387, 1-166.

Lind, T., Valmari, T., Kauppinen, E., Maenhaut, W., Huggins, F. (1998). "Ash formation and heavy metal transformations during fluidised bed combustion of biomass", in: Ashes and Particulate Emissions from Biomass Combustion, V., 3 of Thermal Biomass Utilization series, BIOS, Graz, Austria.

Lisa, K., Salmenoja, K., Baxter, L. (1999). Sulfation of potassium at combustion conditions. Energy and Fuels, V., 13, 1184-1190.

Livingston, W.R. (2005). A review of the recent experience in Britain with the co-firing of biomass with coal in large pulverised coal-fired boilers. Mitsui Babcock, Renfrew, Scotland, Presented at IEA Exco Workshop on Biomass Co-firing, Copenhagen.

Livingston, W.R. (2009). Fouling, corrosion and erosion, in: Bridgwater, A.V., Hofbauer, H., and Van Loo, S. (Editor), Thermal Biomass Conversion, CPL Prees, Newbury, Berks, UK.

Livingston, W.R., Morris, K.W. (2009). Experience with co-firing in PC boilers to reduce CO_2 emissions. Power-Gen International, Fossil Technologies II.

Lokare, S.S. (2008). Mechanistic investigation of ash deposition in pulverised coal and biomass combustion. PhD thesis, Department of chemical engineering, Brigham Young University, Provo, USA.

Lu, G., Yan, Y., Cornwell, S., Whitehouse, M., Riley, G. (2008). Impact of co-firing coal and biomass on flame characteristics and stability. Fuel, V., 87, 1133-1140.

Ma, L., Jones, J.M., Pourkashanian, M., Williams, A. (2007). Modelling of the combustion of Pulverised biomass in an industrial combustion test furnace. Fuel, V., 86, 1959-1965.

Maenhaut, W., Fernandez-Jimenez, M.T., Lind, T., Kauppinen, E. I., Valmari, T., Sfiris, G., Nilsson, K. (1999). In-stack particle size and composition transformations during circulating fluidised bed combustion of willow and forest residue, Nuclear Instruments and Methods in Physics Research Section B: Beam Interations with Materials and Atoms, V., 150, pp. 417-421.

Mann, M., Spath, P. (2001) A life cycle assessment of biomass co-firing in a coal-fired power plant. Clean Products and Processes, V., 3, 81-91.

Mcgowin, C.R., Wiltsee, G.A. (1996). Strategic analysis of biomass and waste fuels for electric power generation. Biomass and Bioenergy, V., 10, 167-175.

McKendry, P. (2002a). Energy production from biomass (part1): overview of biomass. Bioresource Technology, V., 83, 37-46.

McKendry, P. (2002b). Energy Production from Biomass (part2): Conversion Technologies. Bioresource Technology, V., 83, 47-54.

McMullan, J. (2004). Fossil fuel power generation. state-of-the-art. Technical Report, PowerClean Thematic Network.

Maschio, G., Koufopanos, C., Lucchesi, A. (1992). Pyrloysis, a promising rout for biomass utilisation. Bioresource Technology, V., 42, 219-231.

Meijer, R. (2005). Biomass co-firing: status in the Netherlands. Presented at the workshop “biomass co-firing-current trends and future challenges” organised by the International Energy Agency Bioenergy Agreement Task 32 Biomass Combustion & Co-firing in the Framework of the 2nd World Conference & Exhibition on Biomass for Energy, Industry & Climate Protection, Amsterdam. Available at www.ieabee.nl., “accessed 04/09/2010”.

Miles, T. R. (1996). Alkali deposits found in biomass boilers the behaviour of inorganic material in biomass fired power boilers field and laboratory experiments. Technical Report, Sandia National Laboratory.

Miles, T.R., Miles, T.R. Jr., Baxter, L.L, Bryers, R.W., Jenkines, B.M., Oden, L.L. (1995). Alkali deposits found in biomass power plants. National renewable Energy Laboratory, USA.

Miller, B.B, Kandiyoti, R, Dugwell, D.R. (2002). Trace element emissions from co-combustion of secondary fuels with coal: a comparison of bench-scale experimental data with predictions of a thermodynamic equilibrium model. Energy and Fuels, V., 16, 956-963.

Miller, B.B, Kandiyoti, R., Dugwell, D.R. (2004). Trace element behaviour during co-combustion of sewage sludge with polish coal. Energy and Fuels, V., 18, 1093-1103.

Miller, J.N., Miller, J.C. (2000). Statistics and chemometrics for analaytical chemistry. 4th Ed. Person Education Ltd., England, UK.

Moilanen, A., Kurkela, E., Laatikainen-Luntama, J. (1999). In Impact of Mineral Impurities on Solid Fuel Combustion, Gupta, R. P., Wall, T. F., Baxter, L., (Editor), Kluwer Academic/Plenum Publishers: New York, pp. 555-567.

Mojtahedi, W., Backman, R. (1989). The fate of sodium and potassium in the pressurised fluidised-bed combustion and gasification of peat. Journal of the Institute of Energy, 189-196.

Montgomery, M., Larsen, O.H. (2002). Field test corrosion experiments in Denmark with biomass fuels, Part 2: co-firing of straw and coal. Materials and Corrosion, V., 53, 185–194.

NERL, (National Renewable Energy Laboratory). (2005). HOMER Report. US Department of Energy. Available at:http://www.nrel.gov/homer, “accessed 10/06/2008”.

NPL, (National Physical Laboratory). (1994). MTDATA handbook general introduction. Documentation for NPL databank for metallurgical thermochemistry., Teddington, Middlesex, UK.

Nielsen, H., Frandsen, F., Dam-Johansen, K., Baxter, L. (2000). Deposition of potassium salts on heat transfer surfaces in straw-fired boilers: pilot-scale study. Fuel, V., 79, 1-139.

Obernberger, I. (1998). Decentralised biomass combustion: state of the art and future developments. Biomass and Bioenergy, V., 14, 33-56.

Obernberger, I., Biedermann, F. (1998). Fractionated heavy metal separation in Austrian biomass grate-fired combustion plants approach, experiences, results, in: Ashes and Particulate Emissions from Biomass Combustion, V., 3 of Thermal Biomass Utilization series, BIOS, Graz, Austria.

Obernberger, I., Dahl, J., Brunnert, A. (1999). Formation, composition and particle size

distribution of fly ashes from biomass combustion plants. Proceedings of the 4th Biomass Conference of the Americas, Oakland, CA, Elsevier Science Ltd., Oxford, UK, 377-1385.

Obernberger, I., Biedermann, F., Kohlbach, W., (1995). FRACTIO (Fraktionierte Schwermetallabscheidung in Biomasseheizwerken), Annual report, Institute of Chemical Engineering, Graz University of Technology, Austria.

OloFsson, G., Ye, Z., Bjerl, I., Andersson, A. (2002). Bed agglomeration problems in fluidised bed biomass combustion. Industrial and Engineering Chemistry Research, V., 41, 2888-2894.

Onizk-Poplawska, A., Rogulska, M., Wisniewski, G. (2003). Renewable energy developments in Poland 2020. Applied Energy, V., 76, 803-816.

Otsuka, N. (2002). Effects of fuel impurities on the fireside corrosion of boiler tubes in advanced power generating systems: a thermodynamic calculation of deposit chemistry. Corrosion Science, V., 44, 256-283.

Pahl, G. (2005). Biodiesel: growing a new energy economy. Chelsea Green Publishing Company. Canada.

Palz, W., Chartier, P. 1980. Energy from biomass in Europe. Applied Science Publishers, London, UK.

Permchart, W., Kouprianov, V.I. (2004). Emission performance and combustion efficiency of a conical fluidised bed combustor firing various biomass fuels. Biomass Technology, V., 92, 83-91.

PyNe. (2005). Overview biomass pyrolysis network. IEA Bioenergy. Available at:http://www.pyne.co.uk, “accessed 10/06/2008”.

Raask, E. (1985). Mineral impurities in coal combustion: behavior, problems, and remedial measures. Hemisphere Publishing, New York.

Ratafia-Brown, J.A. (1994). Overview of trace element partitioning in flames and furnaces of utility coal fired boilers. Fuel Processing Technology, V., 93(1-3), 139-157.

Robinson, A.L, Junker H, Baxter L.L. (2002). Pilot-scale investigation of the influence of coal-biomass co-firing on ash deposition. Energy Fuels, V., 220, 343-355.

Rosner, D.E., Tandon, P. (1995). Rational prediction of inertially induced particle deposition rates for a cylindrical target in a dust-laden Stream, Chemical Engineering Science, V., 50, 3409-3431.

Roth, R. S., Negas, T., Cook, L.P. (1981). Phase diagram for ceramists. The American Ceramic Society, Inc.: Columbus, OH, Vol. IV.

Ruichang, Y., Ruolei, L., Tao, Z., Lei, Z. (2008). Kinematic characteristics and thermophorestic deposition of inhalable particles in turbulent duct flow. Chineses Journal of Chemical Engineering, V., 16, 192-197.

Rushdi, A., Gupta, R., Sharma, A., Holcombe, D. (2005). Mechanistic approach of ash deposition in a pilot scale furnace. Fuel, V., 84, 1246-1258.

Sami, M., Annamalai, K., Wooldridge, M. (2001). Co-firing of coal and biomass fuel blends. Progress in Energy and Combustion Sciences, V., 27, 171-214.

Savolainen, K. (2003). Co-firing of biomass in coal-fired utility boilers. Applied Energy, V., 74, 369-381.

Shinya, Y., Yukihiko, M. (2008). The Asian biomass handbook: a guide for biomass production and utilisation. The Japan Institute of Energy.

Simms, N.J. (2009). Quantification of complex corrosion conditions for biomass fired power plant. Presented in High Temperature Corrosion, Gordon Researches Conference, July 26-31, Colby Sawyer College, New London, NH.

Simms, N.J., Encinas-Opropesa, A., Nicholls, J.R. (2008). Hot corrosion of coated and uncoated single crystal gas turbine materials. Materials and Corrosion, V., 59 (6), 476-483.

Skrifvars, B.J., Lauren, T., Hupa, M., Korbee, R., Ljung, P. (2004). Ash behaviour in a pulverised wood fired boiler -a case study. Fuel, V., 83, 1371-1379.

Skrifvars, B.J., Sfiris, G., Backman, R., Widegrin-Dafgard, K., Hup, A. M. (1996). Ash behaviour in a CFB boiler during combustion of Salix. Proceedings of the IEA Conference on Biomass Utilisation, Banff.

Smith, K.L., Smoot, L.D., Fletcher, T.H., Pugmire, R.J. (1994). The structure and reaction processes of coal. New York, Plenum Press.

Speigel, M., Zahs, A., Grabke, H. J. (2003). Fundamental aspects of chlorine induced corrosion in power plants. Material High Temperature, V., 20, 153-159.

Spliethoff, H., Unterberger, S., Hein, K. (2001). Status of co-combustion of coal and biomass in Europe. Proceedings of the Sixth International Conference on Technologies and Combustion for a Clean Environment, Porto, Portugal.

Tchobanoglous, G., Theisen, H., Eljassen, R. (1977). Solid waste: engineering

principles and management Issues. McGraw-Hili Book Company, New York, USA.

Tillman, D.A. (2000). Biomass co-firing: the technology, the experience, the combustion consequences. Biomass and Bioenergy, V., 19, 365-384.

Tomeczek, J., Palugniok, H. (2002). Kinetics of mineral matter transformation during coal combustion. Fuel, V., 81, 1251-1258.

Tomeczek, J., Palugniok, H., Ochman, J. (2004). Modelling of deposits formation on heating tubes in pulverised coal boilers. Fuel, V., 83, 213-221.

UN, (United Nations). (1997). United Nations framework convention on climate change-Kyoto Protocol.

Valmari, T., Kauppinen, E.I., Kurkela, J., Jokiniemi, J.K., Sfiris, G., Revitzer, H. (1998). Fly ash formation and deposition during fluidised bed combustion of willow. Journal of Aerosol Science, V., 29, 445-459.

Van Loo, S., Koppejan, J. (2008). The handbook of biomass combustion and co-firing. Earthscan publisher, London, UK.

Wang, H., Harb J.N. (1997). Modelling of ash deposition in large-scale combustion facilities burning pulverised coal. Progress in Energy and Combustion Sciences, V., 23, 267-282.

Wang, L., Hustad, J.E., Gronli, M. (2009). Influence of addtives on biomass ash characteristics. Proceedings of the 17th European Biomass Conference and Exhibition, pp. 1206-1211.

Warren Spring Laboratory. (1993). Fundamental research on the thermal treatment of wastes and biomass: literature review of part research on thermal treatment of niomass and wastes. ETSU, B/T1/00208/Rep/1.

Weast, R.C. (1975). Handbook of Chemistry and Physics, 56th ed. CRC Press, Cleveland, OH.

Weather, J., Seanger, M., Hartage, E.U., Ogada, T. Siagi, Z. (2000). Combustion of agricultural residues. Progress in Energy and Combustion, Science, V., 26, 1-27.

Wereko-Brobby, C.Y., Hagan, E.B. (1996). Biomass conversion and technology. UNESCO Energy Engineering Series. John Wiley and Sons, UK.

Wessel, R.A., Righi, J. (1988). Generalised correlations for interial impaction of particles on a circular cylinder. Aerosol Science and Technology, V., 9, 29-60.

White, L.P. Plaskett, L.G. (1981). Biomass as fuel. Academic Press, London, UK.

Wilemski, G., Srinivasachar, S., Sarofim, A.F. (1992). “Modelling of mineral matter redistribution and ash formation in pulverised coal combustion”, in: Benson, S. A. (Editor), Inorganic Transformations and Ash Deposition During Combustion Engineering, Foundation Press, New York, NY, pp. 545-565.

Williams, A., Pourkashanian, M., Jones, J.M. (2001). Combustion of pulverised coal and biomass. Progress in Energy and Combustion Science, V., 27, 587-610.

Wolf, K., Smeda, A., Müler, M., Hilpert, K. (2005). Investigation on the influence of additives for sulfur dioxide reduction during high alkaline biomass combustion. Energy and Fuels, V., 19, 820-824.

Wood, N.B. (1981). The mass transfer of particles and acid vapour to cooled surfaces. Journal of Institute Energy, V., 76, 76-93.

Yan, R., Gauthier, D., Flamant, G., Badie, J.M. (1999). Thermodynamic study of the behaviour of minor coal elements and their affinities to sulphur during coal combustion. Fuel, V., 78, 1817-1829.

Yan, L., Gupta, R.P., Wall, T.F. (2001). The implication of mineral coalescence behaviour on ash formation and ash deposition during pulverised coal combustion. Fuel, V., 80, 333-1340.

Yang, Y.B., Ryu, C., Khor, A., Sharifi, V.N., Swithenbank, J. (2005). Fuel size effect on pinewood combustion in a packed bed. Fuel, V., 84, 2026-2038.

Zheng, Y., Jensen, P.A., Jensen, A.D., Sander, B., Junker, H. (2006). Ash transformation during co-firing coal and straw. Fuel, V., 86, 1008-1120.

Zhou, H., Jensen, P.A., Frandsen F.J. (2007). Dynamic mechanistic model of superheater deposit growth and shedding in a biomass fired grate boiler. Fuel, V., 86, 1519-1533.

Zulfiqar, M., Moghtaderi, B., Wall, T.F. (2006). Flow properties of biomass and coal blends. Fuel Processing Technologies, V., 87, 281-288.

APPENDICES

APPENDIX A

This appendix contains reported excess air, CP, HP, MTDATA calculations/predictions data from combustions/co-firing of some research selected fuels.

A.1 Reported excess air, O_2 and CO_2 in flue gas for fossil fuels combustions

Table A1.1 Approximate values for CO_2 and O_2 in the flue gas as result of excess air for different fossil fuels combustion, Source: [Van Loo and Koppejan, 2008]

Excess Air %	**Carbon Dioxide (CO_2) in flue gas output (%, Volume)**				**Oxygen (O_2) in flue gas output (%, Volume)**
	Natural Gas	**Fuel Oil**	**Bituminous Coal**	**Anthracite Coal**	
0	12	15.5	18	20	0
20	10.5	13.5	15.5	16.5	3
40	9	12	13.5	14	5
60	8	10	12	12.5	7.5
80	7	9	11	11.5	9
100	6	8	9.5	10	10

A.2 Prediction of combustion products & spreadsheet example

Step 1

Some of fuel compositions report (i.e. as analysed) with the weight percentage of moisture in term as received (ar), whereas ash weight percentage can be presented in dry or as received basis. Elements C, H, O, N, S and Cl reported in dry-ash-free basis (daf). Therefore, a conversion of reported fuel composition to actual composition (i.e. uniform unit, ar % wt) is necessary as 1st step for combustion product prediction (CP). Table and calculation below showing an example of converting fuel composition into a uniform as received basis (ar % wt).

Table A2.1 Conversion of reported fuel composition to actual composition

Reported Fuel Composition			Actual Fuel Composition		
Component	**Basis**	**%weight**	**Basis**	**Conversion factor**	**% weight**
Moisture (H_2O)	ar	25	ar	none	25
Ash	dry	16	ar	((100-25)* 16)/100	12
C	daf	53	ar	53 * (100-25-12)/100	33.39
H	daf	8	ar	8 * 63/100	5.04
N	daf	0.9	ar	0.9 * 63 /100	0.567
O	daf	36.8	ar	36.8 * 63/100	23.184
S	daf	0.4	ar	0.4 * 63/100	0.252
Cl	daf	0.8	ar	0.8 * 63/100	0.504

Weight percent on as received of ash

Ash content expressed in weight % on dry base & on as received through the water content is related;

Ash content (dry % wt) = ash content (ar % wt) * 100/ (100 - water content (% wt)),

Therefore,
16 = % ar * 100/ (100-25)
% ar ash = (75 * 16)/100
% ar ash = 12

Weight percent on as received of C, H, N, O, S and Cl

daf = C + H + N + O + S + Cl = 100

ar = C + H + N + O + S + Cl + ash + water content = 100

Therefore,

% ar C = % daf * (100 - ash - water content)/100
% ar C = 53 * 63/100
% ar C = 33.39

Same for the others (i.e. H, N, O, S, and Cl)

Step 2

For complete combustion process;

Molar Input = Molar Output

The combustion of fuel particles (in a mass flow rate) subjected to a continuous phase (i.e. air, natural gas and may be a carrier fuel gas (e.g. in pulverised fuels feeding)) will present the input. In input (as an example), Primary Air (PA) and Secondary Air (SA) were dry air with composition of 21% Oxygen and 79 % Nitrogen.

Generally, output is from the mass fractions of ash deposit and flue gases. Carbon dioxide (CO_2), water vapour (H_2O), Nitrogen (N_2), Oxygen (O_2), Hydrogen Chloride (HCl) and Sulphur dioxide (SO_2) will be produced as flue gases in the combustion process.

Therefore,
As an example, assuming that the air to fuel = 1730 l/min: 1 kg/hr and natural gas feed rate of 40 l/min combined with fuel carrier gas of 30 l/min; then the % volumes of output can be calculated. Knowing the atomic mass unit for the elements, the ultimate analysis of fuel, air and natural gas input include flue gases output in mole basis could be done. Excel spreadsheet (example created) below showed the results of quantitatively combustion product prediction (CP) (input = output) of combustion/co-firing.

A2.2 Combustion product prediction (CP), calculations spreadsheet example

Type — **Actual Fuel Composition**

Fuel	Ultimate Analysis (% weight, as reseived)	C	H	O	N	S	Cl	F	Br			
		33.39	5.04	23.184	0.567	0.252	0.5	--				
	Proximate Analysis (% weight, as reseived)	Ash	Moisture	Volatiles	Calorific value (KJ/kg)	HHV (KJ/kg)	LHV KJ/kg)					
		12.00	25.00									
	Ash Composition (%)	Al	Ba	Ca	Mn	Fe	K	Mg	Na	Si	P	Ti

Atomic Mass Unit of Elements

Carbon =	12.01	Ca =	40.08
Hydrogen =	1.008	Mg =	24.305
Oxygen =	16.00	Si =	28.086
Nitrogen =	14.01	Al =	26.982
Sulphure =	32.06	Ba =	137.34
Chlorine=	35.45	Mn =	54.938
		Na =	22.99
		P =	30.974
Fe =	55.85	Ti =	204.37
K =	39.10		
Cd =	112.40		

Assume Complete Comustion of the selected Fuel

INPUT =	Fuel + Air + Gas + Carrier fuel
OUTPUT =	Flue gases + Ash

24.2 L/mole @ NTP
22.4 L/mole @ STP

Fuel Feed Rate = 1 kg/hour

	Fuel Input	Kg/hr	g/hr	Mols/hr
Input Selected fuel	Carbon in (C)	0.3339	333.90	27.79952
	Hydrogen in (H)	0.08	78.18	77.56501
	Nitrogen in (N)	0.01	5.67	0.404798
	Chlorine in (Cl)	0.01	5.04	0.14
	Sulphur in (S)	0.00	2.52	0.08
	Oxygen in (O)	0.45	454.06	28.38066
	Ash	0.12		
	Total	1.00		

Air (Primary + Secondary) = 1730 L/min 103800 L/hr

			L/hr	Mols/hr
Air Input	Nitrogen in with air (N_2)	79.00	82002.00	3388.512
	Oxygen in with air (O_2)	21.00	21798.00	900.7438

Gas Typical natural gas compositions 40 L/min 2400 L/hr

			L/hr	Mols/hr
Gas Input	Methan (CH_4) 70-97 %	C	2400.00	99.17355
	ethan, propane, butan...	H_4	2400.00	99.17355

Carrier fuel input 30 L/min

			L/hr	Mols/hr
N_2 feeding Input	Nitrogen (N_2)	100.00	1800.00	74.38017

Total Input Fuel + Air	Mols/hr
C	126.9730708
H	474.259229
N	6926.189922
Cl	0.14
S	0.08
O	1829.868266

Output		Mols/hr	% vol
Flue Gases	C (CO_2)	126.97307	2.82
	H (H_2O)	237.05853	5.27
	N (N_2)	3463.095	77.01
	O (O_2)	669.353	14.89
	Cl (HCl)	0.14	0.00
	S (SO_2)	0.08	0.00
TOTAL		4496.7005	100.00

Keys

Yealow Areas : Input
Pink Areas : Outputs
White Areas : Results

% vol = (Output (Mols/hr, eg. CO2) / total) * 100

Fuel Input	C, N, Cl, S (Kg/hr)	<-- Percent as reseived * 1.0 (kg/hr) / 100
	C, N, Cl, S (Mols/hr)	<-- g/hr (each)/atomic masses (each)
	H (Kg/hr)	<-- Percent as reseived * 1.0 (Kg/hr) / 100 + percent moisture * 1.0 / 100 * 2 (16 + 2)
	O (Kg/hr)	<-- Percent as reseived * 1.0 (Kg/hr) / 100 + percent moisture * 1.0 / 100 * 16 (16 + 2)
	H, O (Mols/hr)	<-- g/hr (each)/atomic masses (each)
Air Input	N_2, O_2 (L/hr)	<-- Percent as sea level (air composition) * 103800 (L/hr) / 100
	N_2, O_2 (Mols/hr)	<-- L/hr (each) / 24.2 L/mole @ NTP
Gas Input	C, H_4 (L/hr)	<-- Gas flow in hr rate
	C, H_4 (Mols/hr)	<-- L/hr (each) / 24.2 L/mole @ NTP
Carrier fuel Input	N_2 (Mols/hr)	<-- L/hr of the carrier fuel flow / 24.2 L/mole @ NTP
Total Input	C, H, Cl, S (Mols/hr)	<-- Mols/hr fuel Input
	N, O (Mols/hr)	<-- Mols/hr Air Input + Mols/hr Fuel Input
Output	CO_2, HCl, SO_2, N_2	<-- Mols/hr Total Input for C, Cl, S and 1/2 N, respectively
	H_2O	<-- Total Input H - HCl Output (mols/hr) / 2
	O_2	<-- Total Input O - (CO_2 * 2 - H_2O - SO_2 * 2) Output (mols/hr) / 2

Chemical Reactions

Overall reaction for a fuel of mean composition <-->

$CxHyOz + (x+y/4-z/2) \rightarrow x\ CO_2 + (y/2)\ H_2O$

Complete oxidation <-->

$C + O_2 \rightarrow CO_2$

$H_2 + 0.5\ O_2 \rightarrow H_2O$

$N_2 + O_2 \rightarrow 2\ NO$

$S + O_2 \rightarrow SO_2$

Gaseous species released during combustion for many fuels <-->

$CH_4 + 1/2\ O_2 \rightarrow CO + 2H_2$

$CO + 1/4\ O_2 + 1/2\ H_2O \rightarrow CO_2 + 1/2\ H_2$

$H_2 + 1/2\ O_2 \rightarrow H_2O$

$H_2S + 1/2\ O_2 + H_2O \rightarrow SO_2 + 2H_2$

$NH_3 + 5/4\ O_2 \rightarrow NO + 3/2\ H_2O$

$NO + NH_3 + 1/4\ O_2 \rightarrow N_2 + 3/2\ H_2O$

$NO + CO \rightarrow \frac{1}{2}\ N_2 + CO_2$

A.3 Combustion product prediction of three fuels combustion/co-firing (using PF & FBC)

Table A3.1 CP spreadsheet for pure Daw Mill combustion (using PF)

TYPE		Material Composition					
	Ultimate Analysis (% by weight, as reseived)	C	H	O	N	S	Cl
		74.15	4.38	10.49	1.17	1.28	0.20
Daw Mill (100 ,% wt)	Proximate Analysis (% by weight, as reseived)	Ash	Moisture	Volatiles	Calorific value (KJ/kg)	HHV (KJ/kg)	LHV (KJ/kg)
		4.20	4.60				
	Ash Composition (%)	Al	Ba	Ca	Mn	Fe	K

1 kg/min
?

INPUT	Fuel + Air
OUTPUT	Flue gas + Ash

Assume Complete Comustion of the selected Fuel

Basis (of fuel as fired) = 7.446 kg/hour =

	Fuel Input 60 kg/houre	Kg/hr	g/hr	Mols/hr
Input Selected fuel	Carbon in (C)	5.52	5521.03	459.66
	Hydrogen in (H)	0.36	364.02	361.17
	Nitrogen in (N)	0.09	86.92	6.21
	Chlorine in (Cl)	0.01	14.94	0.42
	Sulphur in (S)	0.10	95.07	2.97
	Oxygen in (O)	1.09	1085.42	67.84
	Ash	0.31		
	Total	7.48		

Air (Primary + Secondary) = 1730 L/min 103800 L/hr

Air Input 1000 (L/min)			L/hr	Mols/hr
	Nitrogen in with air (N2)	79.00	82002.00	3388.512397
	Oxygen in with air (O2)	21.00	21798.00	900.7438017

Total Input Fuel + Air (mols/hr)					
		C		99.17355372	
		H4	96.20	99.17355372	
C	558.84				
H	757.86	30.00	L/min feeding	1800 L/hr	74.38016529
N	6931.990872				
Cl	0.42				
S	2.97				
O	1869.330325				

Output		Mols/hr	% vol
Flue Gas	C (CO2)	558.84	12.17
	H (H2O)	378.7207922	8.25
	N (N2)	3465.995436	75.50
	O (O2)	183.502	4.00
	Cl (HCl)	0.42	0.009180037
	S (SO2)	2.97	0.064601005
TOTAL		4590.442399	100.00
Ash			

24.2 L/mole @ NTP
22.4 L/mole @ STP

% vol = (mass unit/total)*100

Fuel Input	C, N, Cl, S (Kg/hr)
	C, N, Cl, S (Mols/hr)
	H (Kg/hr)
	O (Kg/hr)
	H, O (Mols/hr)
Air Input	N2, O2 (L/hr)
	N2, O2 (Mols/hr)
Total Input	C, H, Cl, S (Mole/hr)
	N, O (Mole/hr)
Output	CO2, HCl, SO2, N2
	H2O
	O2

Table A3.2 CP spreadsheet for mixed Daw Mill with CCP (80:20 %, wt) co-firing (using PF)

TYPE		Material Composition					
	Ultimate Analysis (% by weight, as reseived)	C 67.98	H 4.66	O 15.50	N 1.47	S 1.05	Cl 0.19
Daw Mill + CCP (80:20 ,% wt)	**Proximate Analysis** (% by weight, as reseived)	Ash 4.20	Moisture 5.30	Volatiles	Calorific value (KJ/kg)	HHV (KJ/kg)	LHV (KJ/kg)
	Ash Composition (%)	Al	Ba	Ca	Mn	Fe	K

1 kg/min	
?	

INPUT	Fuel + Air
OUTPUT	Flue gas + Ash

Assume Complete Comustion of the selected Fuel

Basis (of fuel as fired) = 8.13 kg/hour =

	Fuel Input 60 kg/houre	Kg/hr	g/hr	Mols/hr
Input Selected fuel	Carbon in (C)	5.53	5526.61	460.13
	Hydrogen in (H)	0.43	426.91	423.57
	Nitrogen in (N)	0.12	119.83	8.55
	Chlorine in (Cl)	0.02	15.81	0.45
	Sulphur in (S)	0.09	85.65	2.67
	Oxygen in (O)	1.64	1643.54	102.73
	Ash	0.34		
	Total	8.16		

Air (Primary + Secondary) = 1730 L/min 103800 L/hr

Air Input 1000 (L/min)			L/hr	Mols/hr
	Nitrogen in with air (N2)	79.00	82002.00	3388.512397
	Oxygen in with air (O2)	21.00	21798.00	900.7438017

Total Input Fuel + Air (mols/hr)						
				96.20	99.17355372	
C	559.30					
H	820.26	30.00	L/min feeding	1800	L/hr	74.38016529
N	6934.340067					
Cl	0.45					
S	2.67					
O	1904.215212					

Output		Mols/hr	% vol
Flue Gas	C (CO2)	559.3029959	12.09
	H (H2O)	409.9066269	8.86
	N (N2)	3467.170034	74.97
	O (O2)	185.180	4.00
	Cl (HCl)	0.45	0.0096
	S (SO2)	2.67	0.0578
TOTAL		4624.677013	100.00
Ash			

24.2 L/mole @ NTP
22.4 L/mole @ STP

% vol = (mass unit/total)*100

Fuel Input	C, N, Cl, S (Kg/hr)
	C, N, Cl, S (Mols/hr)
	H (Kg/hr)
	O (Kg/hr)
	H, O (Mols/hr)
Air Input	N2, O2 (L/hr)
	N2, O2 (Mols/hr)
Total Input	C, H, Cl, S (Mole/hr)
	N, O (Mole/hr)
Output	CO2, HCl, SO2, N2
	H2O
	O2

Table A3.3 CP spreadsheet for coppiced willow combustion (using FBC)

TYPE		Material Composition					
	Ultimate Analysis (% by weight, as received)	C 42.02	H 4.75	O 36.20	N 0.56	S 0.03	Cl 0.01
Coppiced Willow (100,% wt)	**Proximate Analysis** (% by weight, as received)	Ash 1.30	Moisture 15.10	Volatiles	Calorific value (KJ/kg)	HHV (KJ/kg)	LHV (KJ/kg)
	Ash Composition (%)	Al	Ba	Ca	Mn	Fe	K

1 kg/min	
?	

INPUT	Fuel + Air
OUTPUT	Flue gas + Ash

Assume Complete Comustion of the selected Fuel

Basis (of fuel as fired) = 5.97 kg/hour =

	Fuel Input 60 kg/houre	Kg/hr	g/hr	Mols/hr
	Carbon in (C)	2.51	2508.59	208.86
Input	Hydrogen in (H)	0.38	383.74	380.73
Selected fuel	Nitrogen in (N)	0.03	33.43	2.39
	Chlorine in (Cl)	0.00	0.60	0.02
	Sulphur in (S)	0.00	1.79	0.06
	Oxygen in (O)	2.96	2962.45	185.16
	Ash	0.08		
	Total	5.97		

Air (Primary + Secondary) = 1200 L/min 72000 L/hr

Air Input			L/hr	Mols/hr
	Nitrogen in with air (N2)	79.00	56880.00	2350.413223
	Oxygen in with air (O2)	21.00	15120.00	624.7933884
		30.00 L/min	1800 L/hr	

Gas Input		40.00 %		
Typical Natural gas compostions	Methane (CH4) 70-97 % ethane, propane,butane….		L/hr	Mols/hr
		C	720.00	29.75206612
		H4	720.00	29.75206612

Total Input Fuel + Air (mols/hr)		0.00 L/min feeding	0 L/hr	0 Moles/hr
C	238.61			
H	499.74			
N	4703.213253			
Cl	0.02			
S	0.06			
O	1434.751266			

Output		Mols/hr	% vol
Flue Gas	C (CO2)	238.6101129	7.47
	H (H2O)	249.8609936	7.82
	N (N2)	2351.606626	73.63
	O (O2)	353.779	11.08
	Cl (HCl)	0.02	0.000527225
	S (SO2)	0.06	0.001749068
TOTAL		3193.929596	100.00
Ash			

24.2 L/mole @ NTP
22.4 L/mole @ STP

% vol = (mass unit/total)*100

Fuel Input	C, N, Cl, S (Kg/hr)
	C, N, Cl, S (Mols/hr)
	H (Kg/hr)
	O (Kg/hr)
	H, O (Mols/hr)
Air Input	N2, O2 (L/hr)
	N2, O2 (Mols/hr)
Total Input	C, H, Cl, S (Mole/hr)
	N, O (Mole/hr)
Output	CO2, HCl, SO2, N2
	H2O
	O2

A.4 Heat generation prediction (HP) spreadsheet example of three fuels combustion/co-firing

Table A4.1 HP spreadsheet for pure Daw Mill combustion (using PF)

ds	Daw Mill (kg/hr)	Moisture (%AR)	Ash (%)	C(%)		H (%)	O (%)	N (%)	S (%)	Cl (%)
7.09776	7.44	4.6	4.2		74.15	4.38	10.49	1.17	1.28	0.2
Feeding rate (kg/hr)		**dry basis (%)**	4.403	77.725		4.591	10.996	1.226	1.342	0.210
7.44		**kg/hr**	0.31248	5.51676		0.325872	0.7805	0.087048	0.0952	0.0149
	at 100 %	**kmol/hr**		0.4597		0.3259	0.0488	0.0062	0.0030	0.0004
	1									

				CO_2	H_2O	SO_2	NO	HCl	O_2	N_2	ash
air (l/min)	**N_2**	**O_2**	**kmol/hr**	0.4865	0.2353	0.0030	0.0062	0.0004	0.3873	3.6608	0.312
1730	**1366.7**	**363.3**	**kg/hr**	21.4067	4.2356	0.285696	0.286	0.0153	12.39	102.5	
kmol/hr	**3.660803571**	**0.973125**	**% vol**	**0.1018**	**0.0492**	**0.0006**	**0.0013**	**0.0001**	**0.0811**	**0.7659**	
			dry % vol	**10.70632**		**0.0654902**	**0.1368**	**0.0092**	**8.522**	**80.56**	
natural gas (l/min)	**10**		**dry at 6 O_2%**	**11.0015**		**0.0672958**	**0.1406**	**0.0095**	**6**	**82.781**	
kmol/hr	**0.026785714**		**measured**								
kg/hr	**0.428571429**										

Heat input
Net calorific value (kJ/kg)
49966.048
0.005948339

Heat balance

		Daw Mill (MW)	MW
	Heat input	**0.0498**	**55751**
			Cassing loss
	Gross calorific value KJ/kg	**25260**	**0.0631**
	Net Calorific value KJ/kg	**24107**	6690.1
	Daf calorific value kJ/kg		

	T bed	**900**		
	Heat output		**MW**	
	T	**1000**	**450**	**25**
Cp (J/g)	**air**	1136.20	936.99	1006.44
	ash	1068.23	81.331	787.98
	CO2	1123.32	6679.59	831.07
	H2Og	2135.47	2512.50	1858.98
	SO2	702.10	55.72	608.34
	NO	1088.19	86.46	984.78
	O2	1035.72	3565.26	912.54
	N2	1166.21	33205.52	1034.49
Latent heat vaporisation c	**H2O**	2135.47	583.46	1858.98
Enthalpy J/kg	**H2O**	4640982.00	5460.37	2539644.94
		Total heat with gases	**52235.20**	
	heat in sand (MW)	4.989875		

Heat input total	Fuel input	55751	
	air	1066.75	
Total		56817.7	
Heat output total	Flue gas	49052.9	
Heat losses		-13.666	
	radiation	1136.35	2
	C (unburned)	10.9087	0.019199433
Specific losses	CO	233.961	0.411774843
	H2O	835.408	1.47033021
	Ash	25.4142	0.044729341
		2242.05	4
		-9.7201	

Taking latent heat of water into account

(all gas)	**Total losses**	-8.0653

Table A4.2 HP spreadsheet for mixed Daw Mill with Miscanthus (40:60 %, wt) co-firing (using PF)

Fuel 1

ds	Daw Mill (kg/hr)	Moisture (%AR)	Ash (%)	C(%)	H (%)	O (%)	N (%)	S (%)	Cl (%)
3.9114		4.1	4.6	4.2	74.15	4.38	10.49	1.17	1.28	0.2
Feeding rate (kg/hr)			**dry basis (%)**	4.403	77.725	4.591	10.996	1.226	1.342	0.210
10.25			**kg/hr**	0.1722	3.04015	0.17958	0.43009	0.04797	0.0525	0.0082
	at 40 %		**kmol/hr**		0.2533	0.1796	0.0269	0.0034	0.0016	0.0002
		0.4								

Fuel 2

	Miscanthus PF (kg/hr)	Moisture (%AR)	Ash (%)	C(%)	H (%)	O (%)	N (%)	S (%)	Cl (%)
5.4858		6.15	10.8	4.6	43.59	4.8	35.52	0.58	0.11	0.09
			dry basis (%)	4.600	43.590	4.800	35.520	0.580	0.110	0.090
	at 60 %		**kg/hr**	0.2523468	2.39126022	0.2633184	1.94855616	0.03181764	0.006	0.00493722
		0.6	**kmol/hr**		0.1993	0.2633	0.1218	0.0023	0.0002	0.0001

				CO_2	H_2O	SO_2	NO	HCl	O_2	N_2	ash
air (l/min)	**N_2**	**O_2**	**kmol/hr**	0.5434	0.32221338	0.0018	0.0057	0.0004	0.338	3.6608	0.42
1730	**1366.7**	**363.3**	**kg/hr**	23.9117977	5.7998408	0.17554314	0.2622	0.0135	10.82	102.5	
kmol/hr	**3.660803571**	**0.973125**	**% vol**	**0.1115**	**0.0661**	**0.0004**	**0.0012**	**7.5948E-05**	**0.0695**	**0.7513**	
			dry % vol	**11.94297269**		**0.040185143**	**0.1252**	**0.008133235**	**7.433**	**80.451**	
natural gas (l/min)	**10**		**dry at 6 O_2%**	**12.12783962**		**0.040807174**	**0.1272**	**0.008259131**	**6**	**81.696**	
kmol/hr	**0.026785714**		**measured**								
kg/hr	**0.428571429**										

Heat input
Net calorific value (kJ/kg)
49966.048
0.005948339

Heat balance

		Daw Mill (MW)	Miscanthus PF (MW)	MW
	Heat input	**0.0274**	**0.0272**	**60554.1344**
				Cassing loss
	Gross calorific value KJ/kg	**25260**	**17824**	**0.08047544**
	Net Calorific value KJ/kg	**24107**	**16478**	7266.49613
	Daf calorific value kJ/kg			

	T bed	**900**		
	Heat output		**MW**	
	T	**1000**	**450**	**25**
Cp (J/g)	**air**	1136.20	936.99	1006.44
	ash	1068.23	65.679	787.98
	CO2	1123.32	7461.2647	831.07
	H2Og	2135.47	3440.3877	1858.98
	SO2	702.10	34.2357	608.34
	NO	1088.19	79.24	984.78
	O2	1035.72	3113.83	912.54
	N2	1166.21	33205.52	1034.49
Latent heat vaporisation cal/mol	**H2O**	2135.47	798.93	1858.98
Enthalpy J/kg	**H2O**	4640982.00	7476.93	2539644.94
		Total heat with gas	**55681.0138**	
	heat in sand (MW)	4.989875		

Heat input total	Fuel input	60554.1344		
	air	1066.75		
Total		61620.8815		
Heat output total	Flue gas	51371.0223		
Heat losses		-16.63374329		
	radiation	1232.41763	2	
	C (unburned)	6.011502	0.009755625	
Specific losses	CO	191.3367249	0.310506309	
	H2O	460.3726	0.747104859	
	Ash	27.88400064	0.045250895	
	Total	1918.022458	3	
		-13.5211256		
Taking latent heat of water into account (all gas)	**Total losses**	-9.6394		

Table A4.3 HP spreadsheet for OSR stored pellets (6 months storage) combustion (using FBC)

Fuel 1

ds	OSR 3 (kg/hr)	Moisture (%AR)	Ash (%)	C(%)	H (%)	O (%)	N (%)	S (%)	Cl (%)
5.70496		6.4	10.86	7.47	43.98	4.49	31.69	0.83	0.45	0.21
Feeding rate (kg/hr)		**dry basis (%)**	8.380	49.338	5.037	35.551	0.931	0.505	0.236
		kg/hr	0.47808	2.81472	0.28736	2.02816	0.05312	0.0288	0.01344
	at 100 %	**kmol/hr**		0.2346	0.2874	0.1268	0.0038	0.0009	0.0004
		1							

				CO_2	H_2O	SO_2	NO	HCl	O_2	N_2	ash
air (l/min)	**N_2**	**O_2**	**kmol/hr**	0.3417	0.396389752	0.0009	0.0038	0.0004	0.477	3.597321	0.48
1700	**1343**	**357**	**kg/hr**	15.034926	7.13501553	0.0864	0.1745	0.0138	15.26	100.725	
kmol/hr	**3.597321429**	**0.95625**	**% vol**	**0.0709**	**0.0823**	**0.0002**	**0.0008**	**7.8588E-05**	**0.0991**	**0.7467**	
			dry % vol	**7.72902876**		**0.0203572**	**0.0858**	**0.00856415**	**10.79**	**81.36836**	
natural gas (l/min)	**40**		**dry at 6 O_2%**	**8.14383298**		**0.0214498**	**0.0904**	**0.00902378**	**6**	**85.73526**	
kmol/hr	**0.107142857**		**measured**								
kg/hr	**1.714285714**										

Heat input
Net calorific value (kJ/kg)
49966.048
0.023793356

Heat balance

		OSR 3 (MW)	MW
	Heat input	**0.0272**	**51018.6931**
			Cassing loss
	Gross calorific value KJ/kg	**17180**	**0.121593115**
	Net Calorific value KJ/kg		6122.24317
	Daf calorific value kJ/kg		

	T bed	**900**		
	Heat output		**MW**	
	T	**800**	**450**	**25**
Cp (J/g)	**air**	1097.49	936.99	1006.44
	ash	1025.07	99.546	787.98
	CO2	1085.23	3625.8649	831.07
	H2Og	2071.07	3283.7963	1858.98
	SO2	681.93	13.0930	608.34
	NO	1071.15	41.55	984.78
	O2	1017.36	3450.41	912.54
	N2	1121.42	25101.14	1034.49
Latent heat vaporisation cal/mol	**H2O**	2071.07	953.21	1858.98
Enthalpy J/kg	**H2O**	4158317.66	8241.57	2539644.94
		Total heat with gases	**44815.1712**	
	heat in sand (MW)	4.989875		

Heat input total	Fuel input	51018.6931	
	air	1028.03	
Total		52046.7254	
Heat output total	Flue gas	40473.6264	
Heat losses		-22.235979	
	radiation	1040.93451	2
	C (unburned)	16.6897728	0.032066903
	CO	184.593583	0.354668966
Specific losses	H2O	1696.59264	3.259749056
	Ash	47.5907829	0.091438573
	Total	2986.40129	6
		-16.498056	

Taking latent heat of water into account

(all gas)	**Total losses**	-13.8943

A.5 Molar composition input in MTDATA for each fuel combustion/co-firing

Table A5.1 Total moles of major and minor elements total moles input in the equilibrium calculation for pure pulverised fuels

Molar numbers	Pulverised Pure Fuel			
	El-cerrejon Coal (100 %, wt)	**Daw Mill (100 %, wt)**	**CCP (100 %, wt)**	**Miscanthus (100 %, wt)**
C	531.27	558.83	430.83	595.70
H	772.06	757.86	1008.26	1212.28
O	1809.96	1869.33	1682.96	2187.35
N	6698.34	6931.99	5572.44	6931.53
S	1.3568	2.9654	0.4591	0.4693
Cl	0.0423	0.4214	0.4411	0.3472
Si	0.8686	0.2570	0.3100	0.4275
Al	0.3712	0.1967	0.0229	0.0283
Fe	0.0800	0.0588	0.0129	0.0122
Ca	0.0348	0.0898	0.0582	0.0719
Mg	0.0618	0.0260	0.0412	0.0429
K	0.0423	0.0044	0.2204	0.1239
Na	0.0294	0.0203	0.0048	0.0074
Ti	0.0033	0.0019	0.0002	0.0003
Ba	0.0006	0.0002	0.0001	8.99961E-05
Mn	0.0006	0.0022	0.0005	0.0009
P	0.0025	0.0005	0.0712	0.0797

Table A5.2 Total moles of major and minor elements total moles input in the equilibrium calculation for El-cerrejon coal: Cereal Co-product (CCP) blends

Molar numbers	Pulverised Blend Mixtures Fuel			
	CCP:El-cerrejon (20:80 %, wt)	**CCP:El-cerrejon (40:60 %, wt)**	**CCP:El-cerrejon (60:40 %, wt)**	**CCP:El-cerrejon (80:20 %, wt)**
C	520.25	515.57	501.25	487.06
H	818.03	877.95	935.83	1003.94
O	1809.79	1826.08	1823.70	1816.92
N	6582.67	6506.60	6352.24	6159.08
S	1.2222	1.0923	0.9207	0.7313
Cl	0.1114	0.1918	0.2792	0.3794
Si	0.7377	0.6165	0.5048	0.4026
Al	0.2750	0.1921	0.1224	0.0661
Fe	0.0622	0.0466	0.0332	0.0220
Ca	0.0464	0.0545	0.0592	0.0604
Mg	0.0596	0.0564	0.0522	0.0472
K	0.1114	0.1638	0.1994	0.2182
Na	0.0229	0.0172	0.0123	0.0081
Ti	0.0024	0.0017	0.0011	0.0006
Ba	0.0004	0.0003	0.0002	0.0002
Mn	0.0006	0.0006	0.0006	0.0006
P	0.0280	0.0476	0.0613	0.0692

Table A5.3 Total moles of major and minor elements total moles input in the equilibrium calculation for Daw Mill coal: Cereal Co-product (CCP) blends

Molar numbers	Pulverised Blend Mixtures Fuel			
	CCP:Daw Mill (20:80 %, wt)	**CCP:Daw Mill (40:60 %, wt)**	**CCP:Daw Mill (60:40 %, wt)**	**CCP:Daw Mill (80:20 %, wt)**
C	559.30	560.25	561.48	562.93
H	820.25	895.70	988.37	1104.73
O	1904.21	1946.28	1997.93	2062.81
N	6934.34	6937.17	6940.65	6945.02
S	2.6714	2.3199	1.8887	1.3464
Cl	0.4460	0.4761	0.5130	0.5593
Si	0.2676	0.2782	0.2888	0.2994
Al	0.1620	0.1272	0.0925	0.0577
Fe	0.0497	0.0405	0.0313	0.0221
Ca	0.0835	0.0772	0.0708	0.0645
Mg	0.0290	0.0321	0.0351	0.0382
K	0.0476	0.0908	0.1340	0.1772
Na	0.0172	0.0141	0.0110	0.0079
Ti	0.0016	0.0012	0.0009	0.0005
Ba	0.0002	0.0002	0.0001	0.0001
Mn	0.0018	0.0015	0.0012	0.0008
P	0.0147	0.0288	0.0429	0.0571

Table A5.4 Total moles of major and minor elements total moles input in the equilibrium calculation for Daw Mill coal: Miscanthus blends

Molar numbers	Pulverised Blend Mixtures Fuel			
	Misc:Daw Mill (20:80 %, wt)	**Misc:Daw Mill (40:60 %, wt)**	**Misc:Daw Mill (60:40 %, wt)**	**Misc:Daw Mill (80:20 %, wt)**
C	563.10	568.35	575.50	584.19
H	812.15	878.54	962.22	1069.38
O	1907.38	1953.90	2012.31	2087.31
N	6931.93	6931.86	6931.78	6931.68
S	2.6656	2.2994	1.8438	1.2552
Cl	0.4123	0.4014	0.3881	0.3706
Si	0.2891	0.3222	0.3563	0.3914
Al	0.1657	0.1333	0.0996	0.0646
Fe	0.0502	0.0413	0.0319	0.0222
Ca	0.0866	0.0832	0.0796	0.0758
Mg	0.0292	0.0324	0.0358	0.0393
K	0.0266	0.0497	0.0736	0.0983
Na	0.0179	0.0154	0.0128	0.0102
Ti	0.0016	0.0013	0.0010	0.0007
Ba	0.0002	0.0002	0.0001	0.0001
Mn	0.0019	0.0017	0.0014	0.0011
P	0.0153	0.0305	0.0464	0.0627

Table A5.5 Total moles of major and minor elements total moles input in the equilibrium calculation for OSR stored pellets for pelletised/lump combustion

Molar numbers	OSR stored pellets Fuel			
	OSR 1 (1 m storage)	**OSR 2 (3 m storage)**	**OSR 3 (6 m storage)**	**OSR 4 (12 m storage)**
C	326.75	338.97	333.51	335.43
H	786.99	833.82	758.42	773.45
O	1156.96	1936.14	1519.10	1936.44
N	3724.68	6663.46	5096.35	6663.02
S	0.8583	0.7616	0.8983	0.8783
Cl	0.3068	0.3537	0.3790	0.3610
Si	0.2140	0.2231	0.1541	0.0820
Al	0.0464	0.0283	0.0219	0.0172
Fe	0.0167	0.0080	0.0093	0.0059
Ca	0.3728	0.3350	0.3316	0.3093
Mg	0.0313	0.0259	0.0240	0.0217
K	0.2278	0.2386	0.2331	0.2092
Na	0.0381	0.0440	0.0265	0.0261
Ti	0.0006	0.0003	0.0003	0.0002
Ba	0.0000	0.0000	0.0000	0.0000
Mn	0.0010	0.0010	0.0009	0.0008
P	0.0166	0.0158	0.0157	0.01426

Table A5.6 Total moles of major and minor elements total moles input in the equilibrium calculation for El-cerrejon coal: Miscanthus blend, miscanthus pellets, coppiced willow and fast pyrolysis bio-oil

Molar numbers	Fuel			
	Misc:El-cerrejon (60:40 %, wt)	**Miscacthus pellets (100 %, wt)**	**Coppiced Willow (100 %, wt)**	**Bio-oil (100 %, wt)**
C	626.85	318.25	238.61	7.4715
H	889.54	794.51	499.73	21.658
O	2072.76	1203.90	1434.75	32.218
N	6785.64	3802.56	4703.21	86.529
S	1.2176	0.1233	0.0558	0.0019
Cl	0.2290	0.1115	0.0168	7.33083E-05
Si	0.5962	0.4424	0.0274	0.0077
Al	0.1299	0.0160	0.0063	0.0010
Fe	0.0329	0.0071	0.0019	0.0004
Ca	0.0682	0.0685	0.0607	0.0020
Mg	0.0525	0.0234	0.0145	0.0002
K	0.1124	0.1685	0.0427	0.0009
Na	0.0144	0.5061	0.0159	0.0015
Ti	0.0012	0.0002	5.49985E-05	1.14228E-05
Ba	0.0002	0.0004	8.47789E-05	0.0000
Mn	0.0009	0.0008	0.0010	1.18E-05
P	0.0652	0.0159	0.0183	0.0001

APPENDIX B

This appendix contains comparison results of biomass fuel compositions available on the Phyllis database (of Netherlands Energy Research Centre (ECN)).

Table B.1 Miscanthus compositions as recorded in phyllis, database for biomass and waste, (http://www.ecn.nl/phyllis)

Type	ID No.	Moisture ar, %wt	Ash ar, %wt	C daf, %wt	H daf, %wt	O daf, %wt	N daf, %wt	S daf, %wt	Cl daf, %wt
Miscanthus 1	568	40	2.9	50.3	5.8	43.0	0.57	0.12	0.189
Giganthus	948	14.2	1.3	49.1	6.4	43.9	0.30	0.10	0.132
Sinensis gracillimus, Oregon	898	12.5	2.9	49.3	5.9	44.1	0.47	0.05	0.083
Miscanthus fresh	1201	4.4	4.6	49.3	6.0	44.2	0.56	0.09	0.492
Miscanthus, high K	1991	9.8	1.4	48.8	5.9	42.5	0.30	0.10	0.162
Miscanthus, low K	1990	25.6	0.8	49.5	6.1	44.3	0.61	0.10	0.101
Miscanthus, silage	1203	2.8	4.9	49.6	6.1	44.0	0.47	0.08	0.066
Miscanthus, silage, dried	1204	2.6	4.6	49.6	6.1	44.0	0.45	0.07	0.498
Miscanthus, silberfeder, Oregon	897	14.5	2.6	48.8	5.9	44.8	0.34	0.06	0.062
Sorghastrum avenaceum, Oregon	899	11.3	3.7	49.3	6.3	44.0	0.33	0.04	0.042
Miscanthus leaf/fiber	2553	x[a]	x	x	x	x	x	x	x
Mean		13.77	2.97	49.36	6.05	43.88	0.44	0.08	0.18
SD		11.47	1.47	0.43	0.19	0.65	0.11	0.02	0.17
% RSD[b]		83.3	49.7	0.8	3.1	1.4	26.6	31.5	93.5

Keys;

(a): Missing data *Phyllis website*

(b): percentage relative deviation results high variation of miscanthus compositions on moisture, ash, S and Cl

Table B.2 Wheat compositions as recorded in phyllis, database for biomass and waste, (http://www.ecn.nl/phyllis)

Type	ID No.	Moisture ar, %wt	Ash ar, %wt	C daf, %wt	H daf, %wt	O daf, %wt	N daf, %wt	S daf, %wt	Cl daf, %wt
Wheat stalk	2788	6.2	7.1	49.4	5.9	43.7	0.78	0.24	x[a]
Wheat stems	714	15.8	5.0	49.3	6.0	43.4	0.73	0.10	0.467
Wheat straw	424	x[a]	x[a]	48.5	5.8	43.6	1.74	0.11	0.263
Wheat straw (Danish)	1129	10.3	4.2	49.6	6.2	43.4	0.61	0.07	0.179
Wheat straw (Danish, weathered)	1303	12.5	2.9	x[a]	x[a]	x[a]	x[a]	x[a]	0.134
Wheat straw (Dutch, pellets)	1304	7.6	9.3	48.3	4.7	44.9	0.71	0.19	1.268
Wheat straw Danish 1995	1891	10.5	4.3	49.9	6.2	43.3	0.63	x[a]	x[a]
Wheat straw pellets	2248	x[a]	x[a]	49.2	6.6	42.1	1.84	0.26	x[a]
Wheat straw waste	2039	9.7	20.6	47.7	6.2	42.8	1.32	0.35	1.499
Wheat straw waste (pellets)	2332	7.5	17.7	47.4	5.9	44.4	1.47	x[a]	x[a]
Mean		10.01	8.88	48.81	5.94	43.51	1.09	0.188	0.65
SD		3.08	6.67	0.87	0.52	0.81	0.49	0.10	0.59
% RSD[b]		30.8	75.1	1.7	8.8	1.8	45.7	53.8	93.7

Keys;

(a): Missing data from *Phyllis website*

(b): percentage relative deviation results high variation of miscanthus compositions on moisture, ash, S and Cl

APPENDIX C

This appendix contains a specification of some materials used in this project.

Table C.1 Material specification of the ceramic used for the deposits collection

Specifics	Units	Measurements
Al_2O_3	%	99.7
Alkali content	%	0.05
Type acc to DIN VDE 0335*	-	799
Water absorption	%	≤ 0.2
Leakage rate at 20˚C (Helium)	mbar	10^{-10}
Density-ρ	$g.cm^{-3}$	3.80-3.93
Flexural strength	MPa	300
Hardness (Mohs scale)	-	9
Thermal expansion	20-700 ˚C 20-1000 ˚C	7.8 8.6
Thermal Conductivity	20-100 ˚C ($W.m^{-1}.K^{-1}$	26.0
Maximum working temperature	˚C	1700
Permissible permanent temperature for temperature measurement	˚C	1600+/1800++
Dielectric strength related to 1.5mm wall thickness	$kV.mm^{-1}$	17
Volume resissitivity D.C @ 20 ˚C	Ω.cm	10 14
Thermal shock resistance	-	Good
Pore size	μm	-

Table C.2 Bed material specification (Bed A) for pelletised/lump fuels combustion

Clean sand	
Metal analysis – As analysed (mg/kg) – air dried	
Pb	2
Cu	7
Zn	28
As	4
Cd	<0.1
Mn	19
Cr	0.6
Na	<10
K	125
Tl	<1
Hg	0.05
Elemental oxide analysis (%) – as analysed	
SiO_2	95.4
Al_2O_3	0.1
Fe_2O_3	1.0
TiO_2	<0.1
CaO	<0.1
MgO	<0.1
Na_2O	<0.1
K_2O	<0.1
P_2O_5	<0.1

APPENDIX D

This appendix contains additional data explained/presented in Chapter 4. The appendix includes deposit probes photographs, SEM images/SEM maps and XRD analysis of deposit compositions for the PF trials. Also, an example of temperature measurements around the whole PF rig and probes deposits during combustion/co-firing is included.

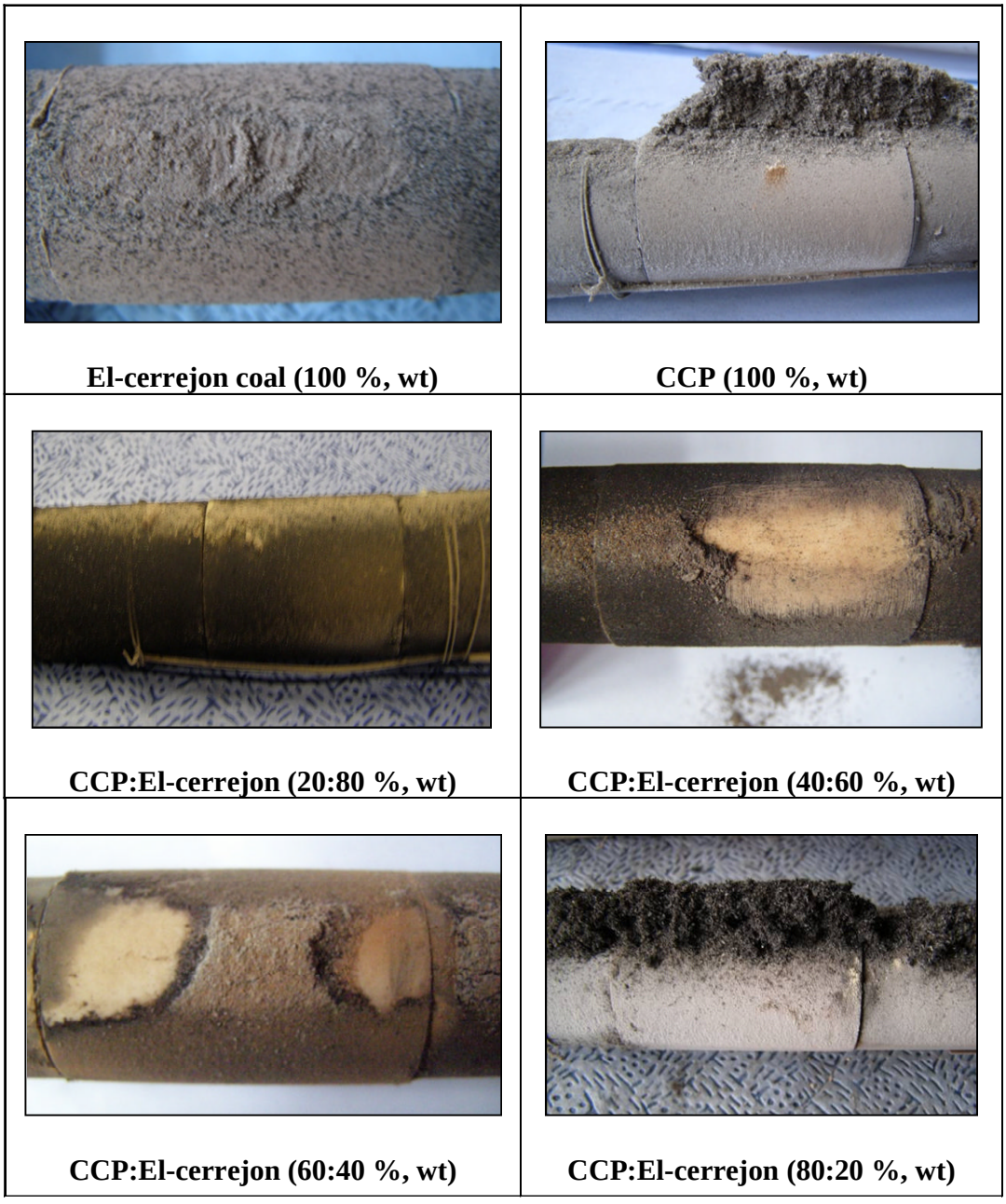

Figure D.1 Photographs of the deposits formed on probes with surface temperatures of ~ 500 ^{o}C from CCP:El-cerrejon coal (pure and mixed) pulverised fuel combustion

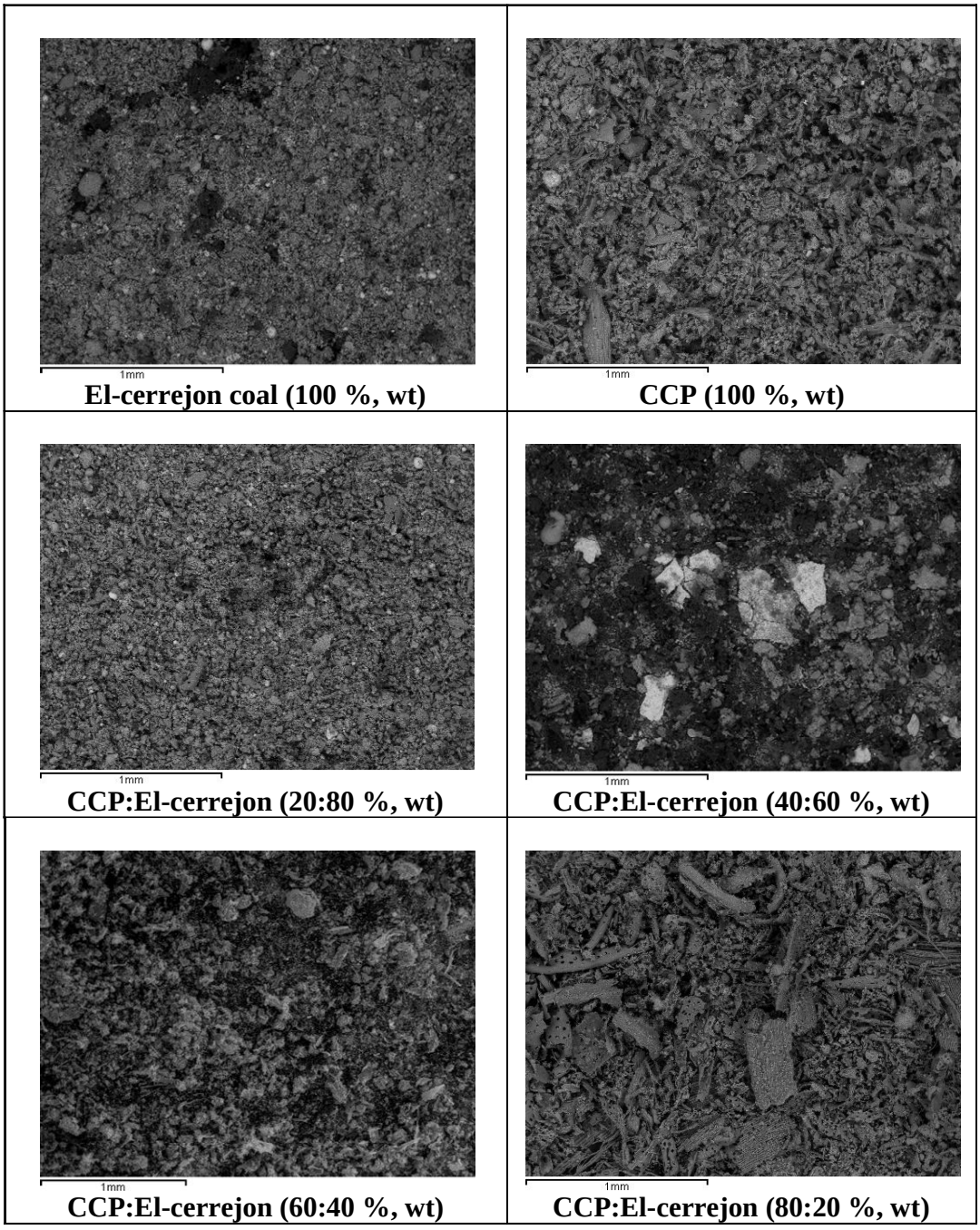

Figure D.2 SEM images of the top deposits from probes with surface temperatures of ~ 500 ^{o}C from CCP:El-cerrejon coal (pure and mixed) pulverised fuel combustion

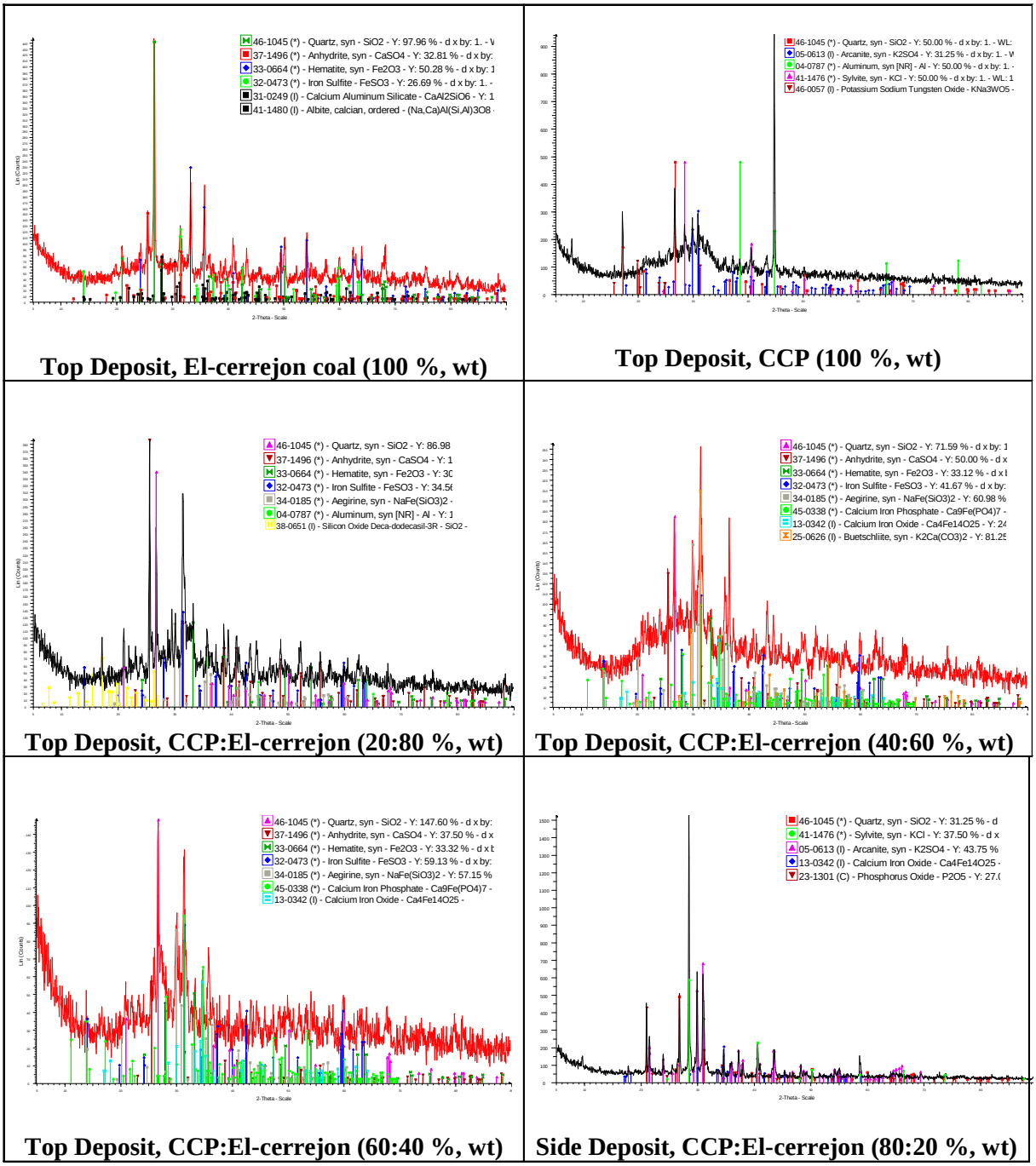

Figure D.3 XRD patterns of the deposits from probes with surface temperatures of ~ 500 ^{o}C from CCP:El-cerrejon coal (pure and mixed) pulverised fuels combustion

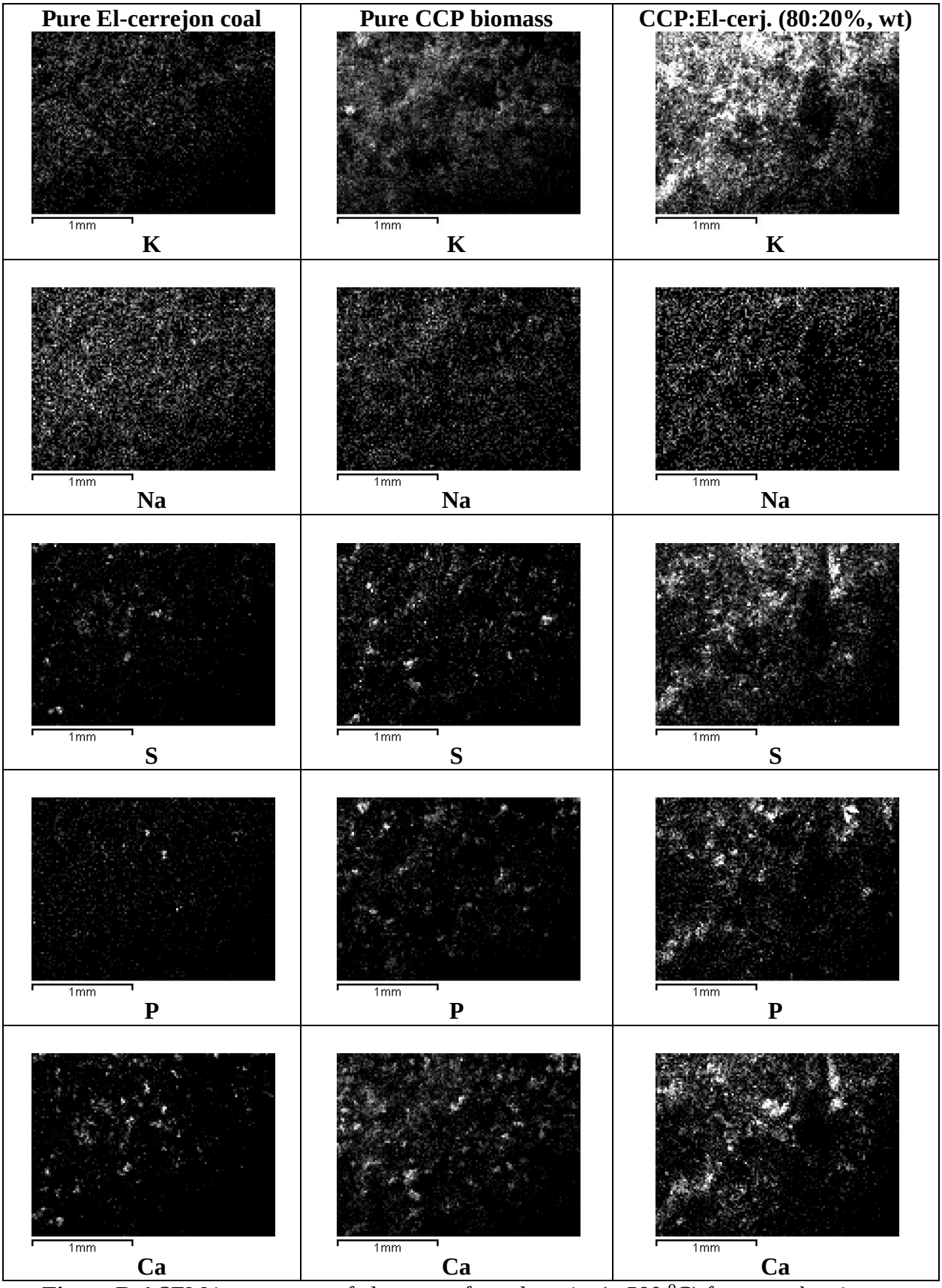

Figure D.4 SEM images map of elements of top deposits (~ 500 ^{o}C) from combustion of three of the CCP:El-cerrejon coal fuels mixtures

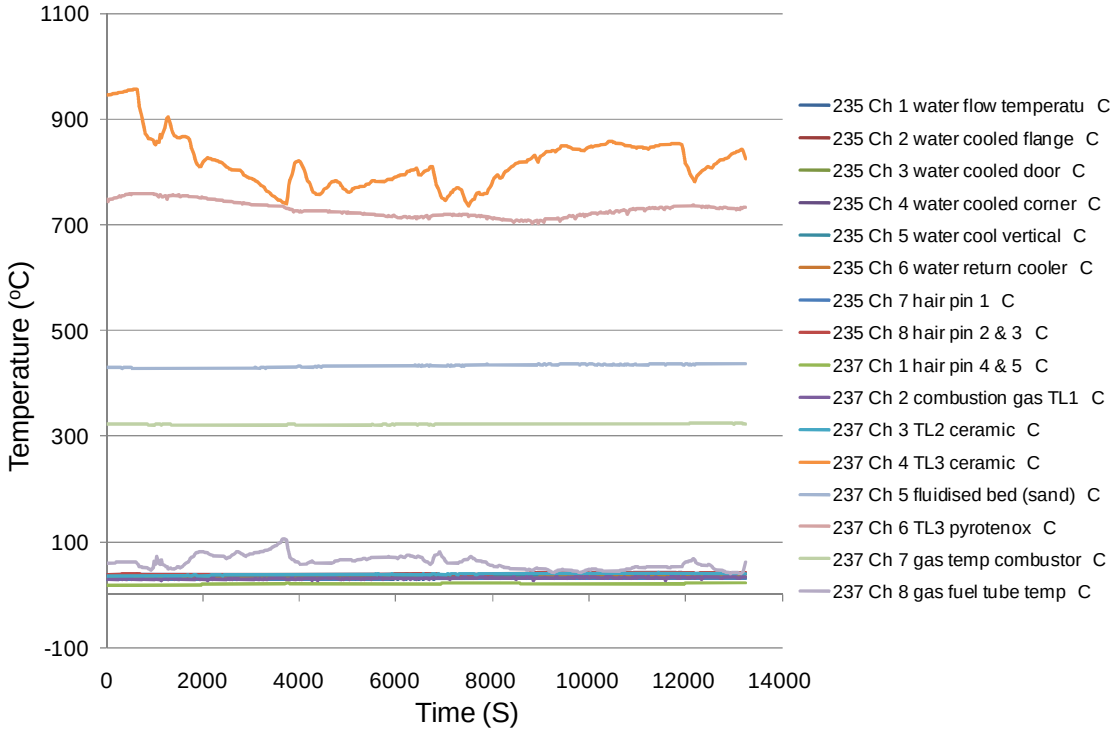

Figure D.5 Temperature profile/measurements around the PF rig during co-firing CCP:DawMill (80:20 %, wt)

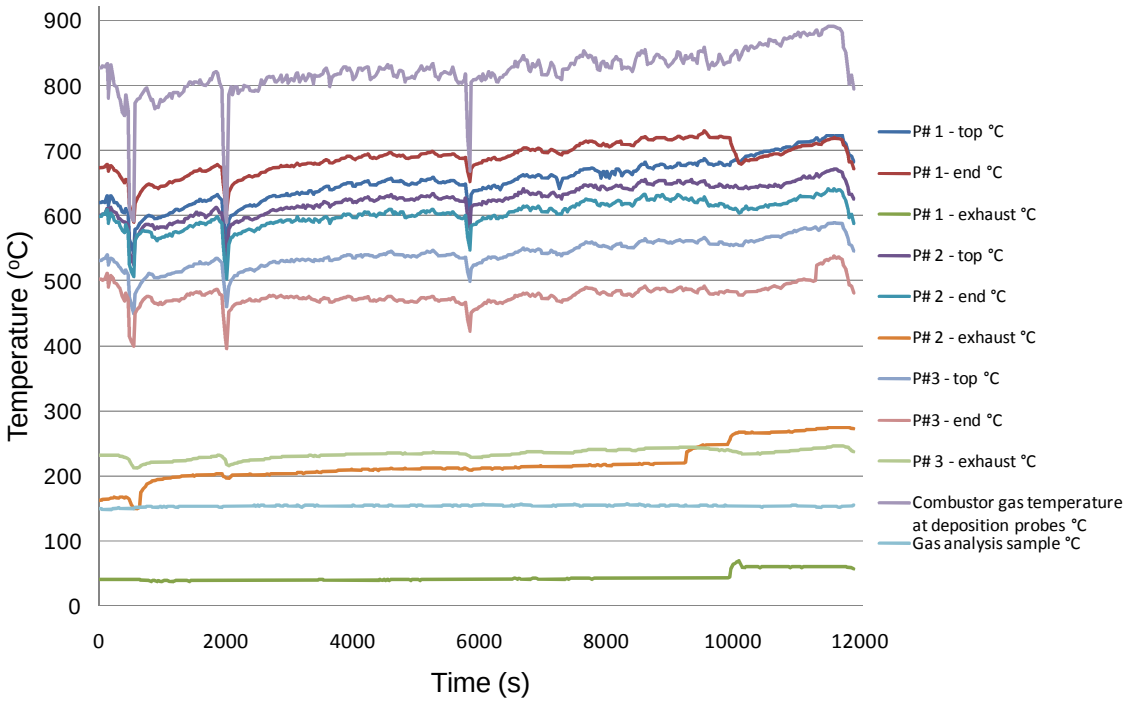

Figure D.6 Temperature profile/measurements around the deposits probes during co-firing CCP:DawMill (80:20 %, wt)

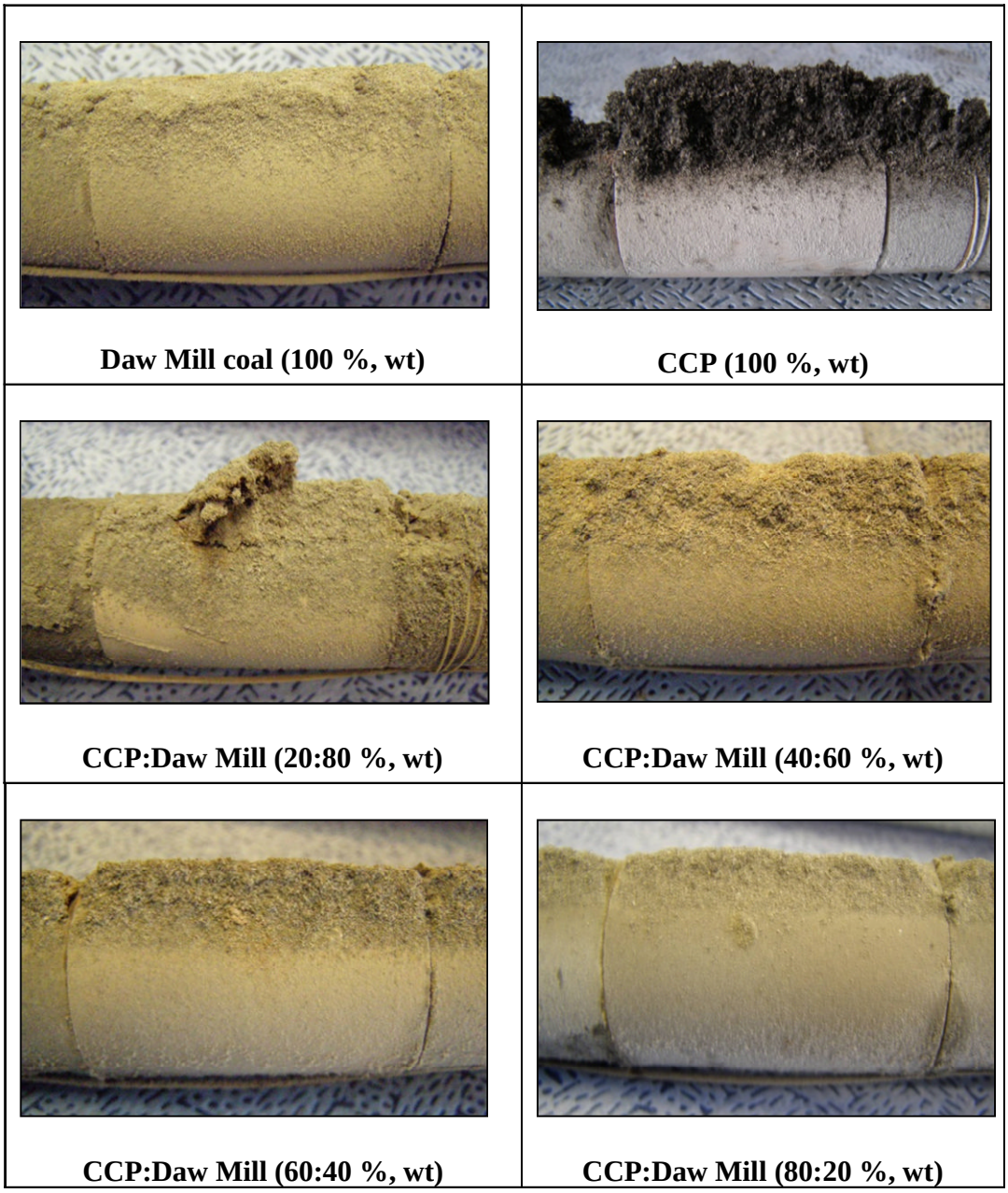

Figure D.7 Photographs of the deposits formed on probes with surface temperatures of ~ 500 ^{o}C from CCP:Daw Mill coal (pure and mixed) pulverised fuel combustion

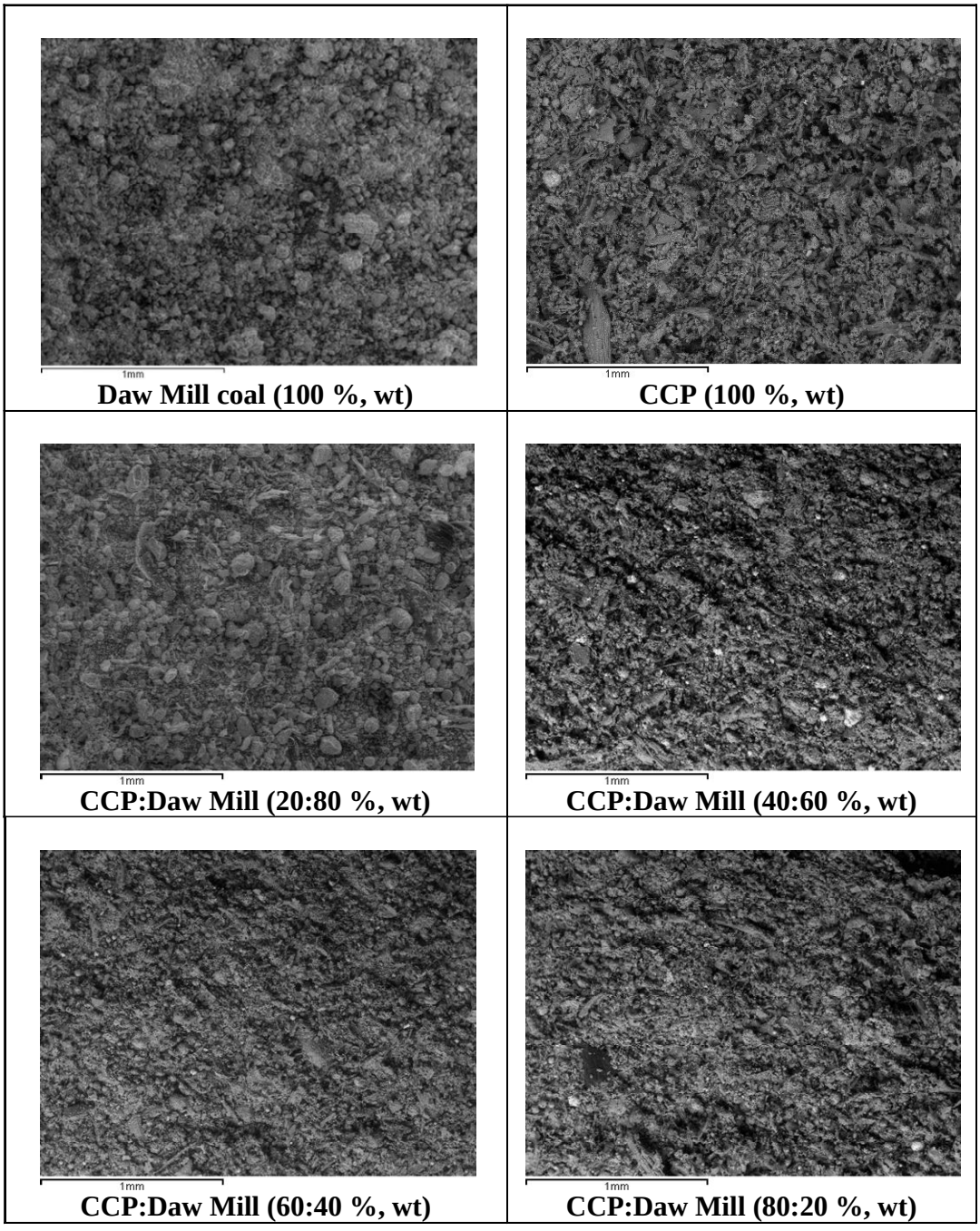

Figure D.8 SEM images of the top deposits from probes with surface temperatures of ~ 500 ^{o}C from CCP:Daw Mill coal (pure and mixed) pulverised fuel combustion

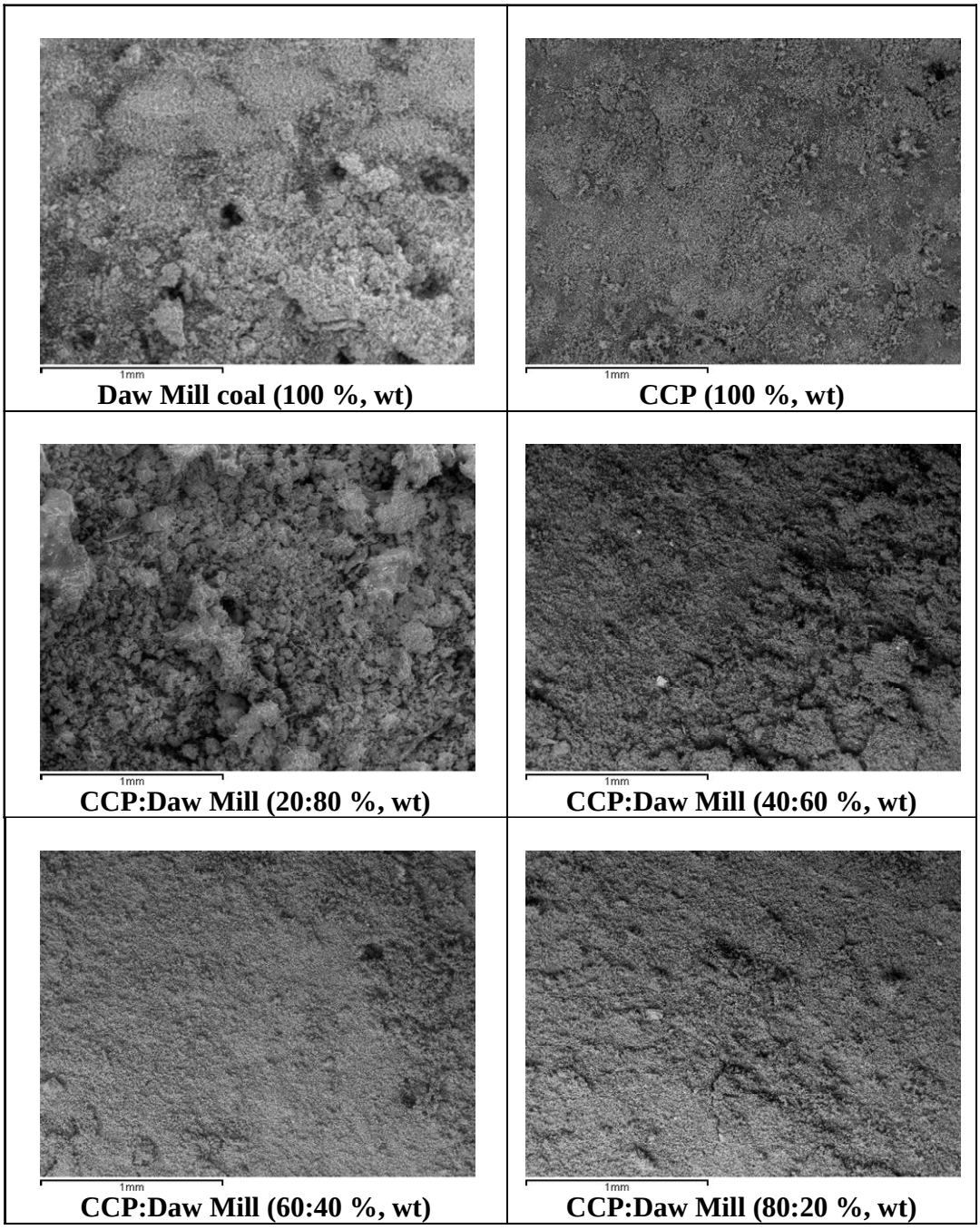

Figure D.9 SEM images of the side deposits from probes with surface temperatures of ~ 500 ^{o}C from CCP:Daw Mill coal (pure and mixed) pulverised fuel combustion

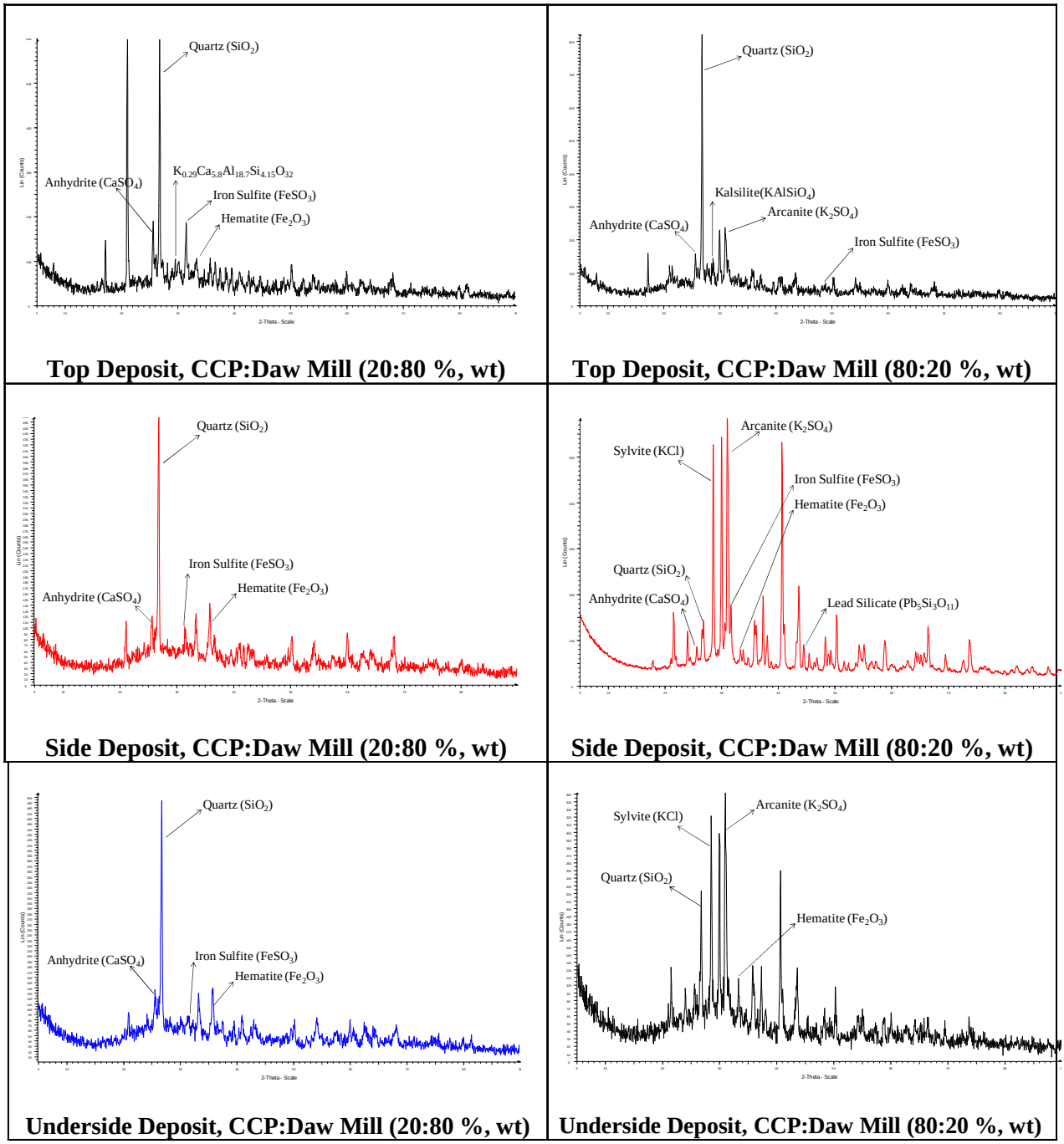

Figure D.10 XRD patterns of the deposits from probes with surface temperatures of ~ 500 ^{o}C exposed to combustion gases from (left) CCP: Daw Mill (20:80 %, wt) and (right) CCP: Daw Mill (80:20 %, wt)

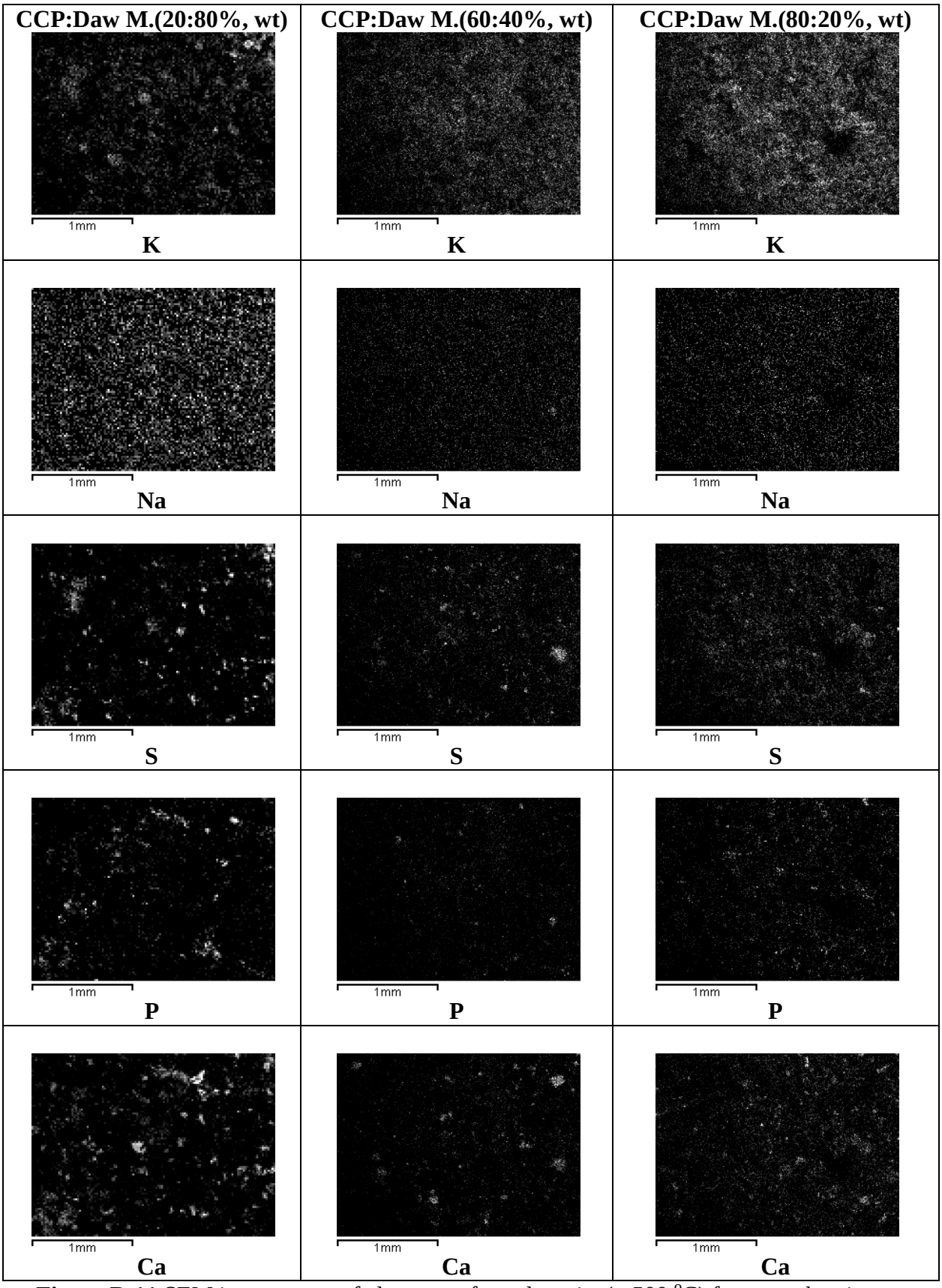

Figure D.11 SEM images map of elements of top deposits (~ 500 ^{o}C) from combustion of three of the CCP:Daw Mill coal fuels mixtures

(a) Top & Side Deposit
Miscanthus:Daw Mill (20:80 %, wt)

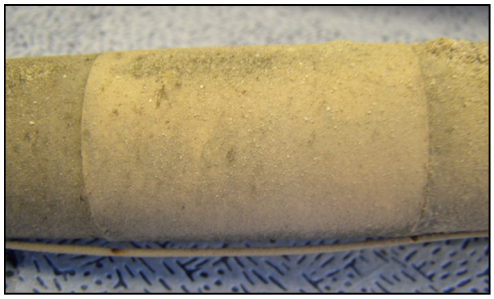

(b) Top & Side Deposit
Miscanthus:Daw Mill (40:60 %, wt)

(c) Top & Side Deposit
Miscanthus:Daw Mill (60:40 %, wt)

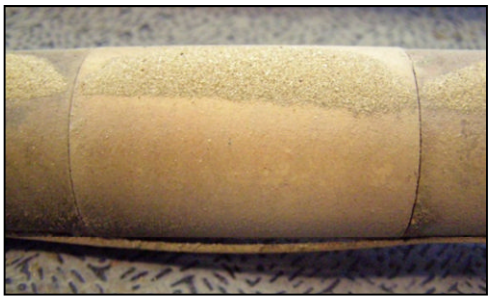

(d) Top & Side Deposit
Miscanthus:Daw Mill (80:20 %, wt)

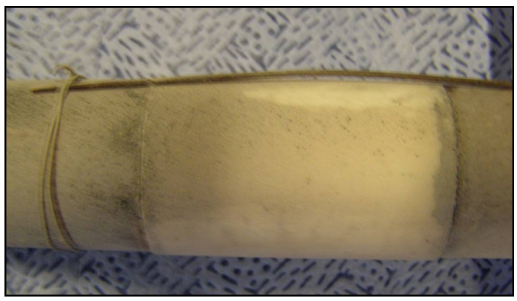

(e) Underside Deposit
Miscanthus:Daw Mill (20:80 %, wt)

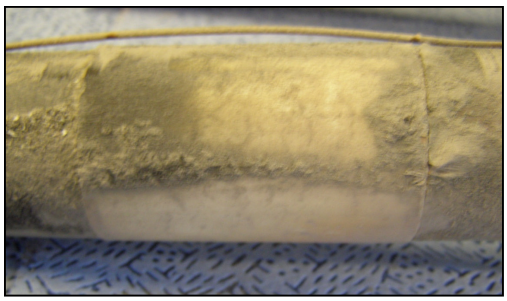

(f) Underside Deposit
Miscanthus:Daw Mill (40:60 %, wt)

(g) Underside Deposit
Miscanthus:Daw Mill (60:40 %, wt)

(h) Underside Deposit
Miscanthus:Daw Mill (80:20 %, wt)

Figure D.12 Photographs of the deposits formed on probes with surface temperatures of ~ 500 ^{o}C from Miscanthus:Daw Mill coal (mixed) pulverised fuels co-firing

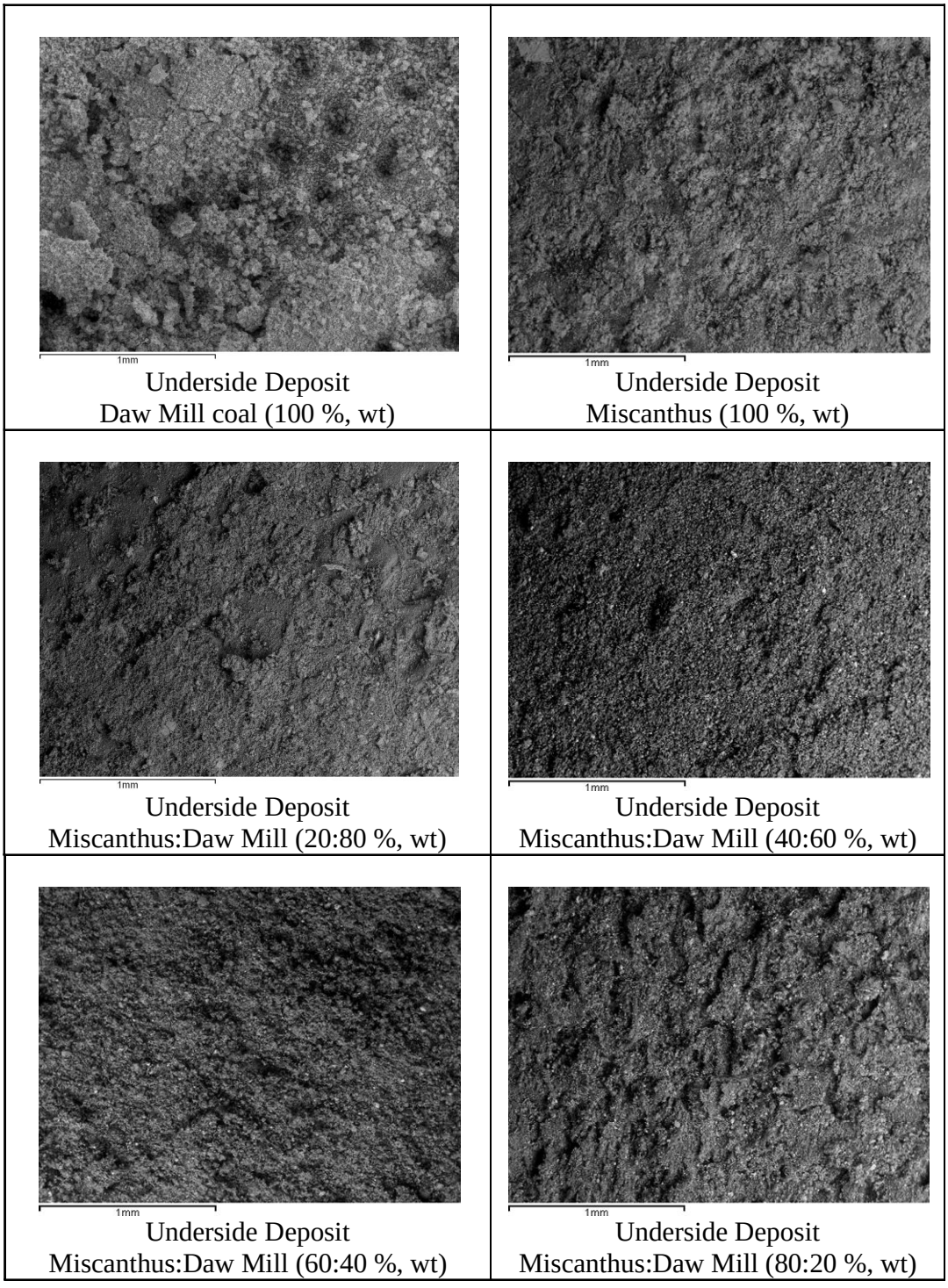

Figure D.13 SEM images of the underside deposits from probes with surface temperatures of ~ 500 ^{o}C from Miscanthus:Daw Mill coal (mixed) pulverised fuels co-firing

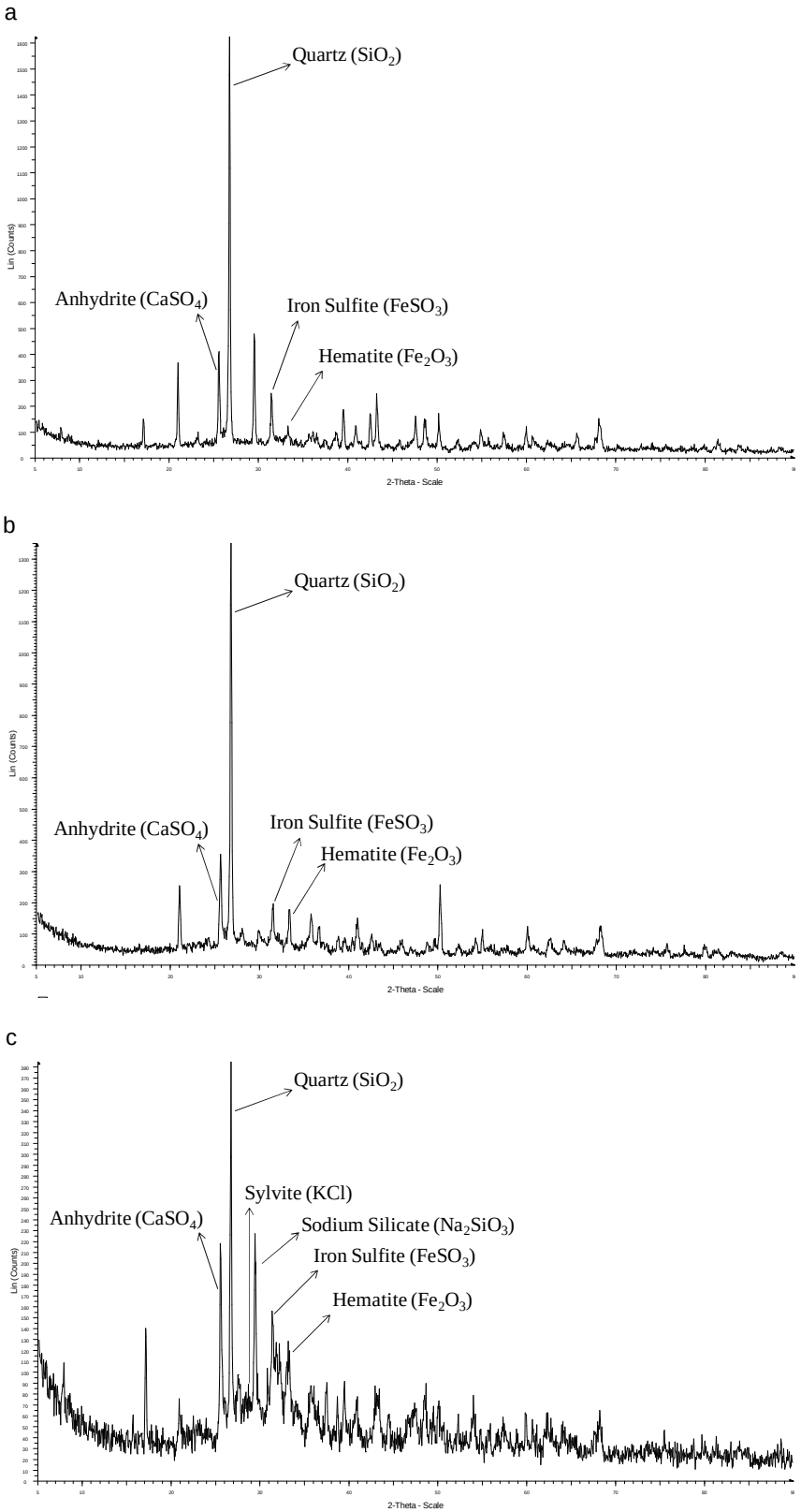

Figure D.14 XRD patterns of the top deposits from probes with surface temperatures of ~ 500 ^{o}C exposed to combustion gases from combustion of a) Miscanthus:Daw Mill (20:80 %, wt), b) Miscanthus:Daw Mill (60:40 %, wt) and c) pure Miscanthus (100 %, wt)

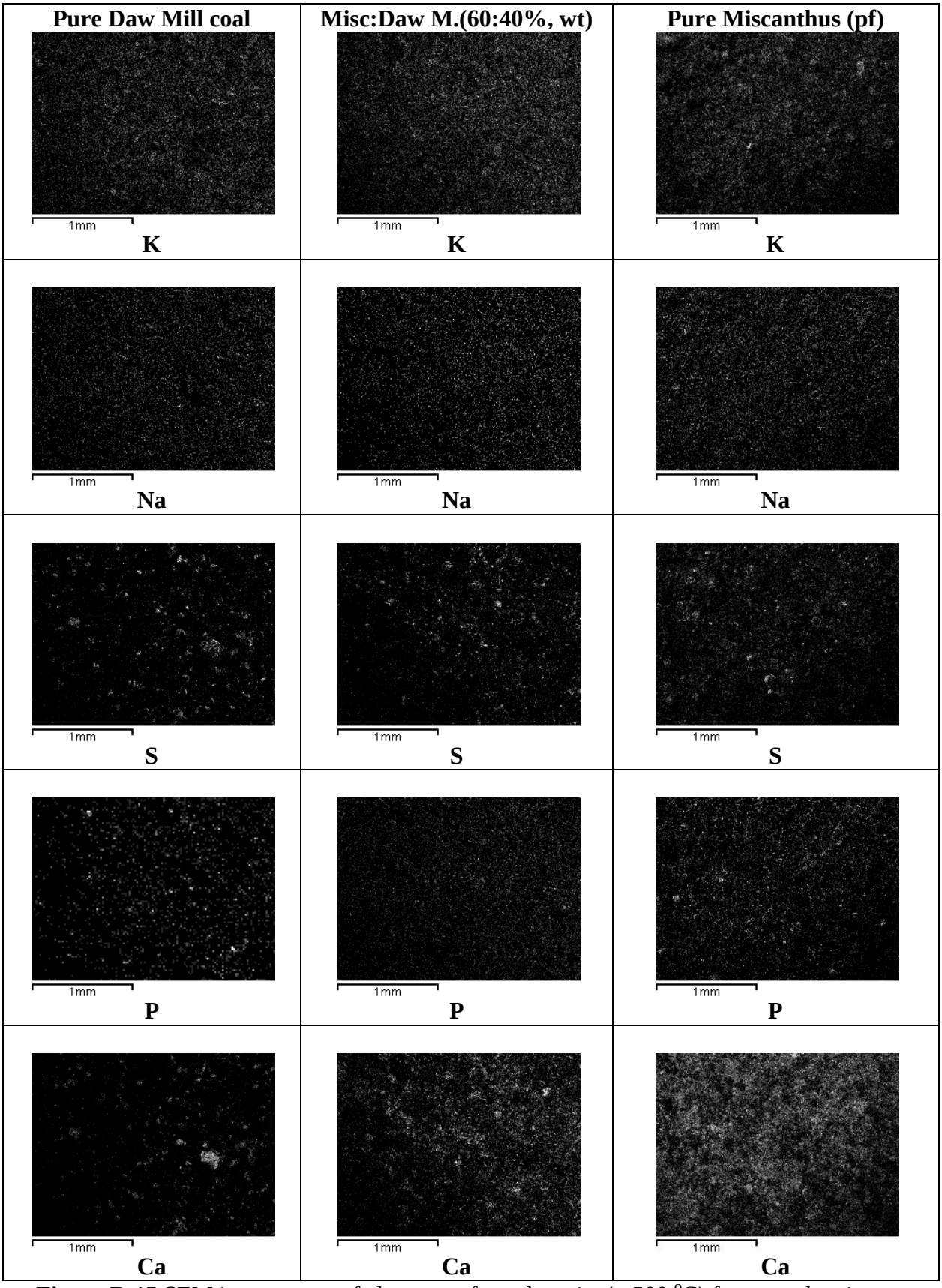

Figure D.15 SEM images map of elements of top deposits (~ 500 ^{o}C) from combustion of pure Daw Mill coal, miscanthus and one fuel mixtures

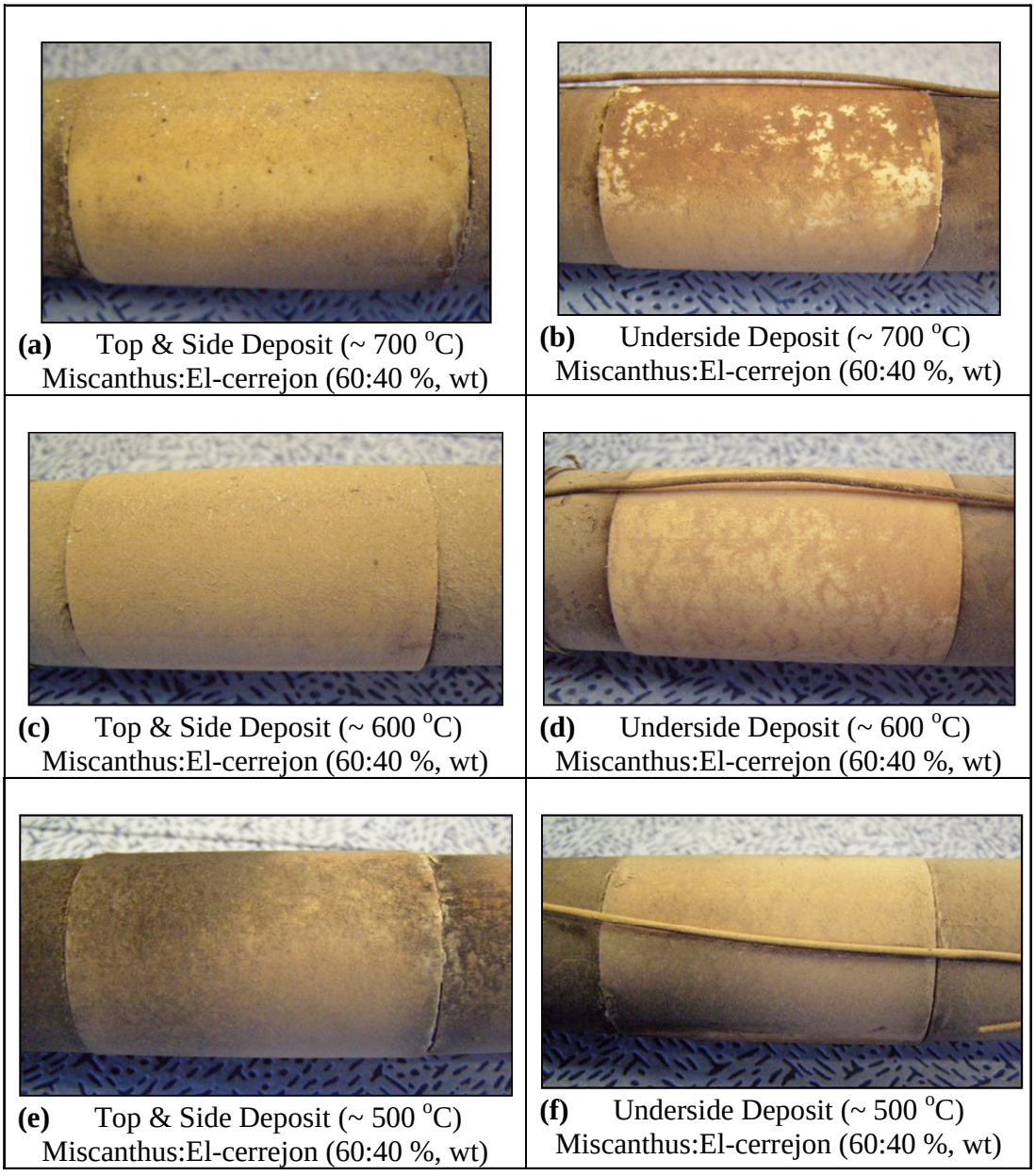

(a) Top & Side Deposit (~ 700 ^{o}C) Miscanthus:El-cerrejon (60:40 %, wt)

(b) Underside Deposit (~ 700 ^{o}C) Miscanthus:El-cerrejon (60:40 %, wt)

(c) Top & Side Deposit (~ 600 ^{o}C) Miscanthus:El-cerrejon (60:40 %, wt)

(d) Underside Deposit (~ 600 ^{o}C) Miscanthus:El-cerrejon (60:40 %, wt)

(e) Top & Side Deposit (~ 500 ^{o}C) Miscanthus:El-cerrejon (60:40 %, wt)

(f) Underside Deposit (~ 500 ^{o}C) Miscanthus:El-cerrejon (60:40 %, wt)

Figure D.16 Photographs of the deposits formed on three probes with surface temperatures of ~ 700, 600, 500 ^{o}C from co-firing Miscanthus: El-cerrejon coal (60:40 %, wt)

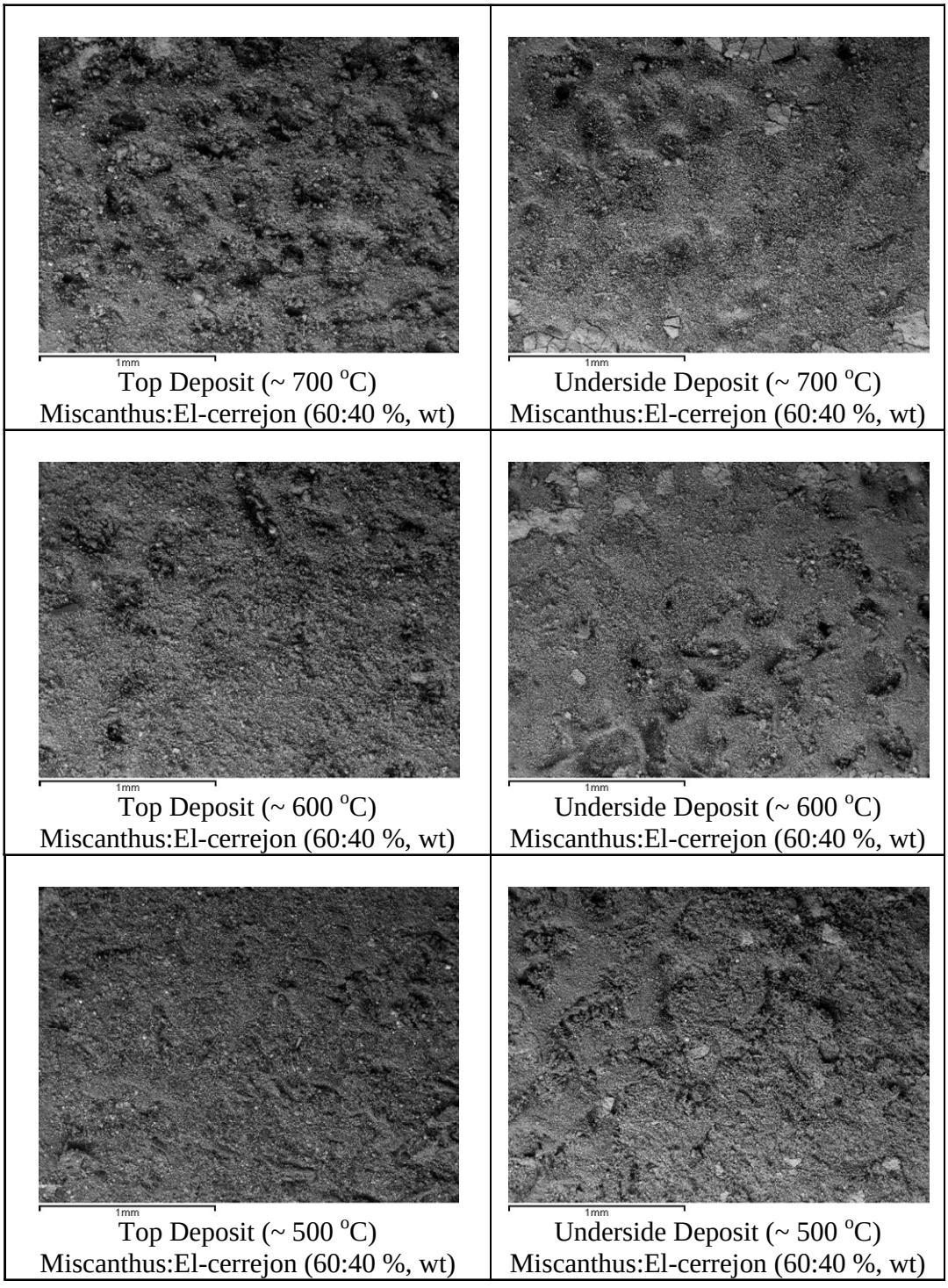

Figure D.17 SEM images of the top and underside deposits from probes with surface temperatures of ~ 700, 600, 500 °C from co-firing Miscanthus: El-cerrejon coal (60:40 %, wt)

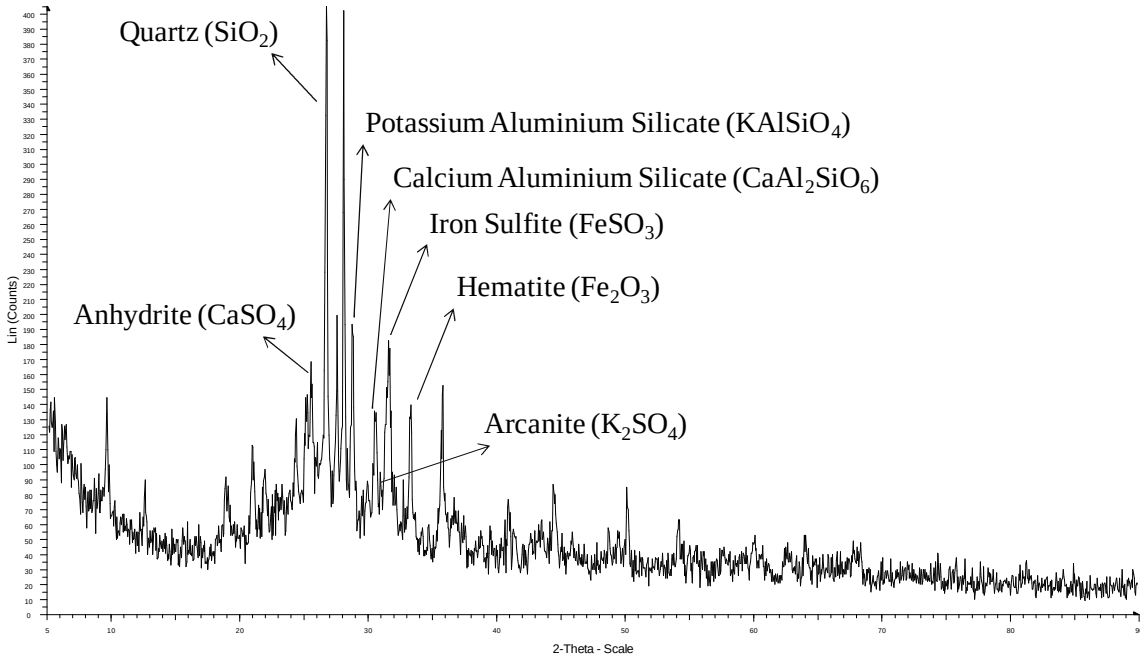

Figure D.18 XRD patterns of the top deposits from probe 3 with surface temperatures of ~ 500 ^{o}C exposed to combustion gases from co-firing Miscanthus: El-cerrejon coal (60:40 %, wt)

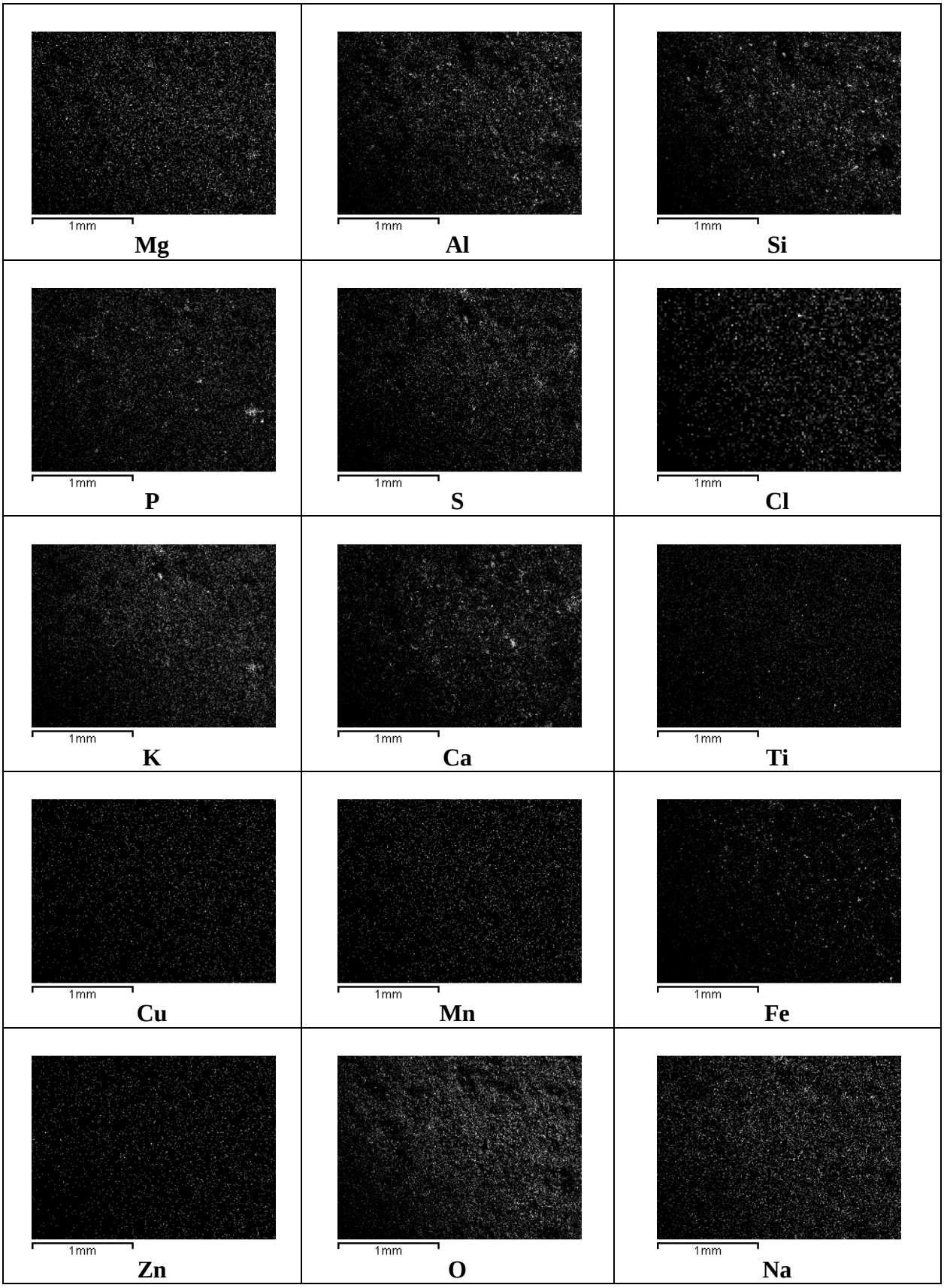

Figure D.19 SEM images map of elements of top deposits (~ 500 oC) co-firing Miscanthus: El-cerrejon coal (60:40 %, wt)

APPENDIX E

This appendix contains the lists of publications already published (article, oral, poster) and/or articles submitted to journals from this project.

ARTICLES

[1] Ala Khodier, Paul Kilgallon, Nigel Legrave, Nigel Simms, John Oakey and Tony Bridgwater. Pilot-scale combustion of fast pyrolysis bio-oil: ash deposition and gaseous emissions. Environmental Progress & Sustainable Energy Journal, October 2009, Vol. 28, No. 3, page 397-403.

[2] Ala Khodier, Nigel Simms, Paul Kilgallon and Nigel Legrave. Investigation of gaseous emissions and ash deposition in a pilot-scale PF combustor co-firing cereal co-product biomass with coal. Renewable Energies and Power Quality Journal, No. 8, Paper 368, April 2010**.** Available at: http://www.icrepq.com/rev-papers-10.html

[3] A.H.M. Khodier, N.J. Simms, J.E. Oakey and P.J. Kilgallon. Characterisation of ash from pilot-scale fluidised bed combustion of miscanthus and willow. Proceeding: 18th European Biomass Conference and Exhibition, 3-7 May 2010, Lyon, France, page 1360-1366

[4] *Accepted & reviewed in* Bioten Proceeding (CPL Press), A.H.M. Khodier, N.J. Simms, J. E. Oakey and P.J. Kilgallon. Pilot-scale co-firing of miscanthus with Daw Mill and El-cerrejon coals: A comparison of ash deposition and gaseous emissions. Bioten Conference, 21-23 September 2010, Birmingham, UK.

[5] *Submitted to Fuel Journal*, A.H.M. Khodier, N.J. Simms and P.J. Kilgallon. Co-firing Daw mill coal with miscanthus biomass: a comparison of pilot-scale experimental data with predictions of a thermodynamic equilibrium model. The 8th European Conference on Coal Research & Its Applications (ECCRIA8), 6-8 September 2010, Leeds, UK.

[6] *Due to submission to Fuel Journal*, A.H.M. Khodier, N.J. Simms and P.J. Kilgallon. Combustion of El-Cerrejon coal with cereal co-product: use of a thermodynamic software package to assess the fate of trace metals in the combustion gas path.

[7] *Due to submission in Biosystems Engineering Journal*, L. Chico-Santamarta, A.H.M. Khodier, N.J. Simms A.C. Humphries, J.E. Oakey, P.J. Kilgallon, K. Chaney, D.R. White, R.J. Godwin. The effect of on-farm storage of oilseed rape (canola) straw pellets on the combustion behaviour: gaseous emissions.

PRESENTAIONS

[1] Ash deposition studies using oilseed rape straw pellets in a pilot-scale combustor. **Ala Khodier**, Nigel Simms, Paul Kilgallon & John Oakey (Energy Technology Centre, Cranfield University, Beds MK43 0AL, UK). Leticia Chico Santamarta, Andrea Humphries & Dick Godwin (Harper Adams University College, Newport, Shropshire, TF10 8NB, UK). Energy from Biomass and Waste (EBW) Conference and Exhibition, 26-27 January 2010, London, UK.

[2] A.H.M. Khodier, N.J. Simms, J. E. Oakey and P.J. Kilgallon. Pilot-scale co-firing of miscanthus with Daw Mill and El-cerrejon coals: A comparison of ash deposition and gaseous emissions. Bioten Conference, 21-23 September 2010, Birmingham, UK.

[3] N.A. Legrave, A.H.M. Khodier, P.J. Kilgallon and N.J. Simms. Co-combustion of coal-biomass mixture in air and oxy-fired configurations: rate and composition of deposit formation on heat exchanger surfaces. The 8th European Conference on Coal Research & Its Applications (ECCRIA8), 6-8 September 2010, Leeds, UK.

[4] Co-firing biomass derived products in power generation systems. SUPERGEN Annual Meeting, 10-12 February 2009, Solihull, UK. Available at: http://www.supergen-bioenergy.net/?_id=416

[5] Co-firing biomass derived products in power generation systems. SUPERGEN Young Researcher's Meeting, 29-30 October 2008, Leeds, UK: 1st prize oral presentation.

POSTERS

[1] A.H.M. Khodier, N.J. Simms, J.Oakey and P.J. Kilgallon. Characterisation of ash from pilot-scale fluidised bed combustion of miscanthus and willow. The 18th European Biomass Conference and Exhibition, 3-7 May 2010, Lyon, France.

[2] Ala Khodier, Nigel Simms, Paul Kilgallon and Nigel Legrave. Investigation of gaseous emissions and ash deposition in a pilot-scale PF combustor co-firing cereal co-product biomass with coal. The 10th International Conference of Renewable Energies and Power Quality (ICREPQ'10), 23-25 March 2010**,** Granada, Spain.

[3] Pilot-scale combustion of fast pyrolysis bio-oil: ash deposition and gaseous emissions. The International Conference on Thermochemical Conversion Science (tcbiomass), 16-18 September 2009, Chicago, USA. Available at: http://www.gastechnology.org/webroot/app/xn/xd.aspx?it=enweb&xd=3TrainingConfer/conferences/tcbiomass2009posters.xml.

[4] Co-firing biomass in combustion systems. SUPERGEN Annual Meeting, 10-12 February 2009, Solihull, UK.

[5] Co-firing biomass derived products in power generation systems. SUPERGEN Young Researcher's Meeting, 29-30 October 2008, Leeds, UK.

[6] Pilot-scale combustion of fast pyrolysis bio-oil: ash deposition and gaseous emissions. SUPERGEN Annual Meeting, 25-26 March 2010, Solihull, UK.

[7] Co-firing biomass derived products in power generation systems. UK Energy Research Centre (UKERC), Energy Summer School 23-27 June 2008, Roehampton University, London, UK.

[8] The 8th European Conference on Coal Research & Its Applications (ECCRIA8), 6-8 September 2010, Leeds, UK. A.H.M. Khodier, N.J. Simms and P.J. Kilgallon. Co-firing Daw mill coal with miscanthus biomass: a comparison of pilot-scale experimental data with predictions of a thermodynamic equilibrium model.